UNIVERSITY OF NAPLES FEDERICO II

DEPARTMENT OF PHARMACY

PhD programme in Pharmaceutical Sciences

Title

Low carbon footprint routes to privileged scaffolds

PhD student
Antonella Ilenia Alfano

Coordinator
Prof.
ROSARIA MELI

Tutor
Prof.
MARGHERITA BRINDISI

XXXV CYCLE (2020-2022)

Abstract

This PhD thesis was focused on the development of greener and more sustainable organic reactions for the preparation of privileged scaffolds in medicinal chemistry. In most of the examples reported in the present thesis, the newly conceived protocols relied upon the use of flow chemistry in its sustainable declination. In particular, during these three years, I focused my attention on indoline-based structures, that have always deserved particular importance, being embedded in medicinally relevant compounds of natural and synthetic origins. Fischer indolisation and its variation (interrupted Fischer) still represent the preeminent methods for synthesizing the indole and the indolenine rings. In our quest towards the development of a reliable methodology avoiding or at least minimizing the issues associated to the synthesis of (spiro)indolenines, I reported a telescoped sustainable synthesis of 3,3-disubstituted indolenines through the use of flow chemistry. This newly developed protocol displayed the potential to turn into an effective coupling point for additional flow reactions for multistep syntheses. Accordingly, we sought to investigate the usefulness of (spiro)indolenines as substrates for the generation of peptidomimetic frameworks through a Joulliè-Ugi multicomponent reaction. A telescoped flow approach coupling interrupted Fischer reaction and subsequent Joulliè-Ugi was established, using small amounts of solvent and requiring limited reaction times. The generated peptidomimetic derivatives were evaluated as anti-biofilm agents, thus also fostering further scaffold diversification through the developed methodology.

Flow-based approaches are also amenable for organocatalytic applications. While many examples of catalytic asymmetric Strecker are

reported on acyclic imines, the same reaction is barely studied on cyclic imines. I applied asymmetric catalysis in flow to (spiro)indolenine substrates in order to develop a fast, sustainable and highly enantioselective Strecker synthesis of cyclic α-amino-nitriles. Furthermore, I recently developed indoline-based metallo-β-lactamase (MBL) inhibitors to be potentially used in synergy with beta-lactam antibiotics to overcome microbial resistance. Inspired by the structure of the drug Captopril, behaving as a weak MBL inhibitor,[4] we developed a flow protocol for the fast and diversity-oriented generation of new derivatives, in high yields and optical purities, thus guaranteeing fast structure-activity relationships studies and a focused optimization process. Furthermore, I spent a 6-month period working in the Noël research group, directed by Professor Timothy Noël, University of Amsterdam. I had the possibility to apply the flow chemistry world to the photocatalysis, studying a new methodology for the classic Giese reaction. The aim was the development of a simple and straightforward protocol for hydroalkylation of an electron poor olefin with unactivated alkyl bromides.

Abbreviation

HTS: high throughput screening

GWP: global warming potential

VOCS: volatile organic compounds

RME: reaction mass efficiency

PMI: process mass intensity

PEEK: polyether ether ketone

PTFE: polytetrafluoro ethylene

PFA: polyfluoroacetate

BPR: back pressure regulator

UV: ultraviolet

FT-IR: fourier transform infrared

BRCS: biologically relevant chemical space

RNA: ribonucleic acid

DNA: deoxyribonucleic acid

Ro5: rule of five

n-BuLi: *n*-butyllitihium

THF: tethrahydrofuran

MeCN: acetonitrile

NaOH: sodium hydroxide

CDI: 1,1'-Carbonyldiimidazole

PEG: polyethylene glycol

CCD: central composite design

DMF: *N,N*-dimethylformamide

MeOH: methanol

HIV: human immunodeficiency virus

CNS: central nervous system

ET: 7-ethyltryptophol

IL: ionic liquid

DCM: dichloromethane

AcOH: acetic acid

CHCl3: chloroform

QP-SA: quadrapure-sulfonic acid

QP-DMA: *N*,*N*—di-methylbenzylamine

EtOAc: ethyl acetate

DIPEA: *N*,*N*-Diisopropylethylamine

Fsp^3: fraction of saturated carbons

PLK: polo-like kinase

BOC: *tert*-butyloxycarbonyl protecting group

EtOH: ethanol

p-TsOH: paratoluensulfonic acid

HPLC: high performance liquid chromatography

GC-MS: gas chromatography mass

TRH: thyrotropin releasing hormone

SPPS: solid-phase peptide synthesis

FDA: food and drug administration

MCR: multicomponent reaction

Hpg: 4-hydroxyphenylglycine

Dpg: 3,5-dihydroxyphenylglycine

HATU: hexafluorophosphaye azabenzotriazole tetramethyl uronium

DOS: diversity-oriented synthesis

iMCRs: isocyanide-based multicomponent reaction

U-4CR: Ugi four component reaction

U-3CR: Ugi three component reaction

Cbz: benzyl choroformate

MIC: minimum inhibitory concentration

THIQ: tetrahydroisoquinoline

DPP-4: dipeptidyl peptidase-4

HCN: hydrogen cyanide

TMSCN: trimethylsilyl cyanide

MDM2: mouse double minute 2 homolog

DCE: dichloroethane

NMR: nuclear magnetic resonance

DMSO: dimethylsulfoxide

PBP: penicillin binding protein

COVID-19: coronavirus disease 2019

SBL: serine beta lactamase

MBL: metallo beta lactamase

IMP-1: imipenemase-1

VIM: verona integron-encoded MBL

NDM-1: new delhi MBL-1

PDB: protein data bank

ACE: angiotensin converting enzyme

XAT: halogen atom transfer

HAT: hydrogen atom transfer

AIBN: azobisisobutyronitrile

TTMS: tris(trimethylsilyl)silane

BDE: bond dissociation energy

HFIP: hexafluoro-2-propanol

HWE: Horner-Wadswoth-Emmons

Chapter 1

Introduction – Part 1: Privileged scaffolds in medicinal chemistry

1.1 Definition and importance of privileged scaffolds in medicinal chemistry

Paul Ehrlich and Emil Fischer contributed to set the bases for modern medicinal chemistry by introducing innovative concepts for the design of new biologically active compounds. In 1902, Fischer was the first organic chemist to win the Nobel Prize in Chemistry, thanks to his work based on carbohydrates moieties, which inspired the 'lock and key model' (also known as the Fisher's theory). The model assumes that the active site of the enzyme and the substrate are complementarily shaped: the substrate fits perfectly into the active site of the enzyme, like a lock only fits a specific key. The enzyme represents the lock and the substrate the key.[1]

In 1908, Ehrlich, the founder of chemotherapy, received the Nobel Prize for Physiology or Medicine, thanks to his 'magic bullet theory'.[2,3] He stated that drugs could be designed to hit a specific target, just like a bullet fired from a gun. The notion of ligand-receptor complementarity and molecular recognition opened the way to design new drugs in a rational fashion.

In 1958, Daniel Koshland proposed a more accurate and realistic description of the lock-and- key theory for ligand-target binding. According to its induced fit theory, the active site of an enzyme will undergo a conformational change when binding a substrate, in order to perfectly adapt to each other.[4]

Nowadays, supported by the steady advancement of computational technologies, researchers screen millions of compounds every day aiming at identifying biologically active compounds. In this context, the potential chemical space to be explored is huge. Identifying a biologic active compound is not that easy, it could be seen as a very challenging mission. Modern medicinal chemists can rely upon several computational techniques and enabling technologies, thus shrinking the search to the tiny part of the haystack around the needle, also called biologically relevant chemical space (BRCS).[5]

For small molecule drug discovery, the most important aspect is the molecular weight, which should be limited to 300–500 Da to guarantee acceptable bioavailability.[6] The chemical space of drug-like molecules has been estimated to contains at least 10^{60} molecules.[7] The limits of BRCS are defined by the specific binding interactions between small molecules and the three- dimensional molecular recognition patterns on biological molecules, such as proteins, RNA and DNA. It should be noted that not all molecules reported in BRCS can be considered drug-like compounds. Drug space contains bioactive molecules with favorable potency, selectivity, and pharmacokinetic properties (absorption, distribution, metabolism, and excretion) and is only a tiny part of all biologically relevant chemical space.[8] Currently, the researchers focus their attention especially on the modification of already existent lead-like structures, in order to improve their binding features and 'drug-likeness'. Drug-likeness assesses qualitatively the chance for a molecule to become an oral drug and is established by molecular properties, including hydrophobicity, molecule size and flexibility, electronic distribution, and pharmacokinetic features, such as metabolic stability, bioavailability, protein binding,

toxicity, transport properties. The definition of drug-likeness was proposed for the first time by Lipinski, in 1997, with the Rule of Five (Ro5), also known as Pfizer's rule of five, a kind of ‘guide’ for the design of small-molecule drugs.[9] Lipinski's rule states that, in general, an orally active drug has no more than one violation of the following criteria:

1. No more than 5 hydrogen bond donors (the total number of nitrogen–hydrogen and oxygen–hydrogen bonds)
2. No more than 10 hydrogen bond acceptors (all nitrogen or oxygen atoms)
3. A molecular mass less than 500 daltons
4. An octanol-water partition coefficient (log P) that does not exceed 5

Since this work, various definitions and methods to predict drug-likeness have been proposed.[10,11,12,13-18]

Despite different studies have demonstrated that some natural products break the Ro5, such as macrolides and peptipes, [19] most researcher still keep in mind the rule for driving their drug discovery trajectory.

Brent Stockwell, one of the most important figures in drug discovery, in an interview said:

‘‘*In 1957, during a cleanup of his lab at the pharmaceutical company Roche, Sternbach discovered an old flask containing a chemical he had synthesized previously, but discarded for lack of interest. On a lark, he decided to have it tested for its anti-anxiety potential, a therapeutic area he had become interested in. The chemical, of an unknown identity, had striking anti-anxiety activity that was superior to the existing marketed*

drugs of that era. Within three years, Sternbach was able to figure out the identity of the chemical and had it approved for use in patients – a remarkable success, considering that drug development nowadays takes 10 to 15 years. This chemical was the first of the benzodiazepines, a class of drugs with a specific shape and structure that is powerful for treating anxiety. Some years later, Ben Evans and his colleagues at Merck discovered that benzodiazepine derivatives were also effective in treating other diseases and in interacting with other types of proteins. He suggested that this class of molecules is privileged, in the sense that it is especially effective at interacting with proteins and altering the course of disease. Other privileged molecular structures have since been discovered, and these molecules might be the key to addressing the undruggable proteins. Since these privileged compounds are so effective at interacting with numerous classes of proteins, they may be an effective starting point to look for new drugs against the supposedly undruggable protein targets.''

As Stockwell explains in his interview, in 1988, Evans coined for the first time the term 'privileged scaffold' to describe simple templates containing common structures being embedded in numerous bioactive compounds, and thus functioning as ligands for different kinds of receptors.[20] The definition adopted by Evans is "privileged structures are capable of providing useful ligands for more than one receptor."

The decoration of these scaffolds paves the way to the development of novel receptor ligands and to the fine-tuning of their selectivity and potency towards a specific target. Over years, the first definition of 'privileged scaffold' was associated to different meanings as well as a huge number of synonymous, including 'molecular framework', 'molecular template', 'chemotype', 'substructure', 'molecular fragment',

and ‘molecular scaffold’, basically in parallel to the progress of medicinal and computational chemistry techniques.[21]

Privileged scaffolds are structures endowed with favorable properties for drug discovery purposes. They also represent useful starting points for structural morphing and decoration in order to shape ligands for the selected biological target.

Privileged scaffolds play a crucial role in the discovery of novel biologically active compounds. Among all privileged templates, heterocycles own a primary role: more than half of the approved drugs contain at least one heterocyclic component in their structure.[22]

Numerous privileged scaffolds are broadly embedded in pharmaceutically relevant compounds of natural and synthetic origins. As an example, medicinally relevant alkaloids contain a high variety of heterocycles such as quinolines, isoquinolines, indoles, pyrrolidines etc. Five and six-membered rings containing *N, O, S* and their fused derivatives, represent a huge portion of privileged templates incorporated into the synthetic drugs.[23] Since heterocyclic compounds contain one or more heteroatoms, they could also help to improve solubility, lipophilicity, polarity, and hydrogen bonding interaction with the biological target, thus optimizing pharmacokinetic and pharmacodynamic properties of drugs or drug candidates.[24]

Figures 1 and 2 show some examples of privileged scaffolds in marketed drugs and natural compounds, respectively.

Privileged scaffolds — ***Marketed drugs***

1
Indole

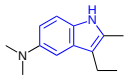

2
Medmain (Serotonin inhibitor)

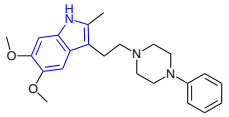

3
Oxypertine (Anti-depressant)

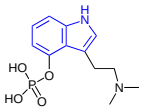

4
Psilocybin (Psychomimetic)

5
Quinoline

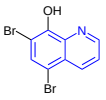

6
Broxyquinoline (Antiseptic)

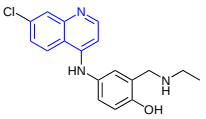

7
Amodiaquin (Antimalarial)

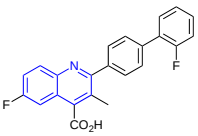

8
Brequinar (Immunosuppressant)

9
Benzoxazole

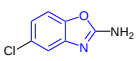

10
Zoxazolamine (Muscle relaxant)

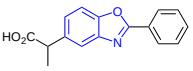

11
Benoxaprofen (Anti-inflammatory)

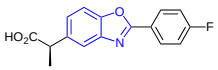

12
Flunoxaprofen (Anti-inflammatory)

13
Quinoxaline

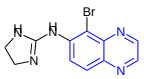

14
Brimonidine (Anti-glaucoma)

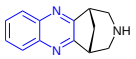

15
Varenicline (Smoking cessation)

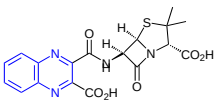

16
Quinacillin (Anti-bacterial)

Privileged scaffolds ——— ***Marketed drugs***

17
Purine

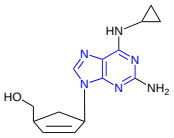

18
Abacavir (Anti-HIV)

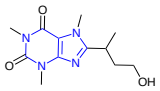

19
Cafaminol (Decongestant)

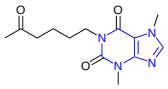

20
Pentoxifylline (Hemorheologic agent)

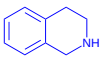

21
Tetrahydroisoquinoline

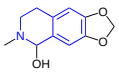

22
Hydrastinine (Hemostatic)

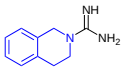

23
Debrisoquin (Anti-hypertensive)

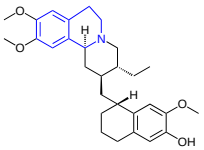

24
Cephaeline (Anti-amebic)

25
Benzofuran

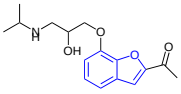

26
Befunolol (Anti-glaucoma)

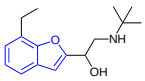

27
Buturalol (Anti-anginal)

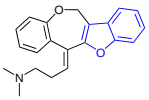

28
Oxetorone (Analgesic)

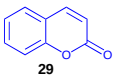

29
Coumarin

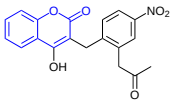

30
Acenocoumarol (Anti-coagulant)

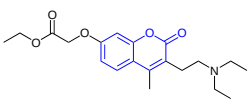

31
Chromonar (Vasodilator)

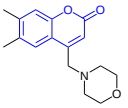

32
Folescutol (Capillary protectant)

Figure 1. Examples of privileged scaffolds retrieved in marketed drugs.[25]

Privileged scaffolds	*Marketed drugs*
 **1** **Indole**	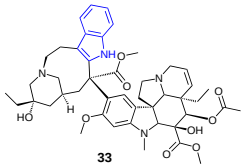 **33** Vinblastine (Anti-cancer)
 **5** **Quinoline**	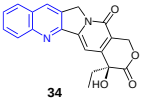 **34** Camptothecin (Anti-cancer)
 **9** **Benzoxazole**	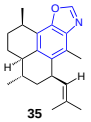 **35** Pseudopteroxazole (Anti-tubercolosis)
 **13** **Quinoxaline**	 **36** Pyocyanine (Antibiotic)
 **17** **Purine**	 **37** Caffeine (Stimulant)
 **21** **Tetrahydroisoquinoline**	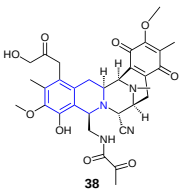 **38** Saframycin R (Anti-cancer)
 **25** **Benzofuran**	 **39** Cacalol (Anti-inflammatory)
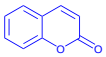 **29** **Coumarin**	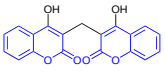 **40** Dicoumarol (Anti-coagulant)

Figure 2. Examples of privileged scaffolds in drugs of natural origin.[25]

1.1.1 Spirocompounds in medicinal chemistry

One of the current strategies for obtaining compounds with increased drug-like features, especially in terms of aqueous solubility, is limiting the number of aromatic rings and increasing the fraction of saturated carbons (defined by Fsp^3) in a drug candidate. The Fsp^3 is a measure of complexity of molecules defined as:

Fsp^3 = (Number of sp^3 hybridized carbons/Total carbon count) [26]

A suitable value of Fsp^3 is considered ≥ 0.42 and 84% of marketed drugs stays within this ideal value.[27] Furthermore, it was found that the Fsp^3 for enriched fragment library of Life Chemicals is increased to 0.36 for 2.2 million molecules in the drug discovery phase and is up to 0.47 for 1179 approved drugs. [28] Beyond the benefits in terms of increased solubility, increasing the sp^3 carbon fraction in a compound allows the possibility to have out-of-the plane substituents, thus helping a better tuning of receptor-ligand recognition, with a consequent increase in potency and selectivity. Nonetheless, increasing Fsp^3 in drug-like compounds also implies the development of new reactions and drug design strategies, due to the concomitant increase in structural complexity (*eg.* the introduction of carbon quaternary stereocenters).[29] In this frame, a particular relevance should be given to spirocyclic scaffolds.

Nowadays, the spirocyclic compounds play a relevant role in marketed drugs, as displayed in Figure 3.

Spirocompounds

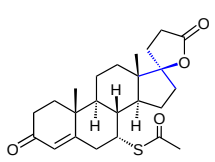

41
Spironolactone
(Aldosterone antagonist)

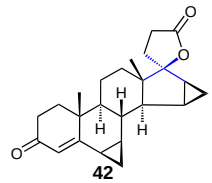

42
Drospirenone
(Corticoid receptor antagonist)

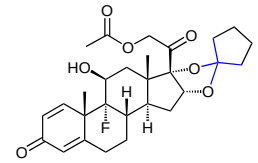

43
Amcinonide
(Anti-inflammatory)

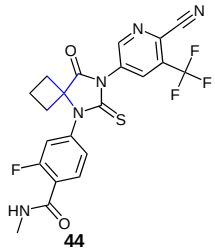

44
Apalutamide
(Anti-cancer)

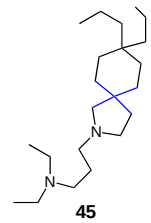

45
Atiprimod
(Anti-cancer)

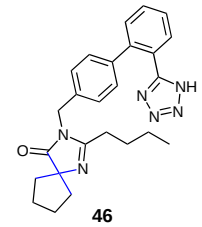

46
Irbesartan
(Angiotensin antagonist)

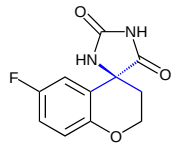

47
Sorbinil
(Aldose reductase inhibitor)

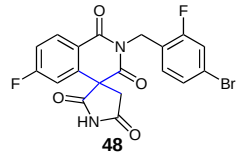

48
Minalrestat
(Aldose reductase inhibitor)

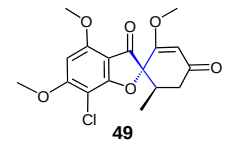

49
Griseofulvin
(Anti-fungal)

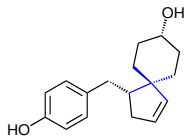

50
Sequosempervirin A
(Anti-fungal)

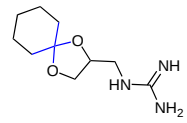

51
Guanadrel
(Anti-hypertesive)

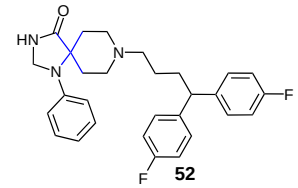

52
Fluspirilene
(Anti-cancer)

Spirocompounds

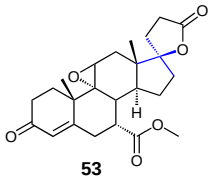

53
Eplerenone
(Aldosterone antagonist)

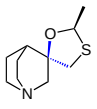

54
Cevimeline
(Muscarinic agonist)

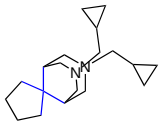

55
Tedisamil
(Potassium channel inhibitor)

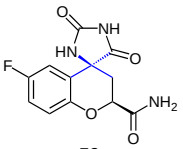

56
Fidarestat
(Aldose reductase inhibitor)

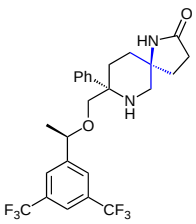

57
Rolapitant
(NK1 Antagonist)

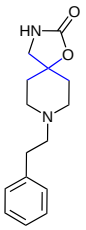

58
Fenspiride
(Anti-tussive)

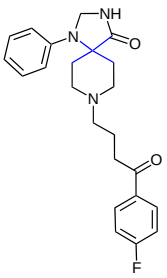

59
Spiperone
(Anti-dopamine)

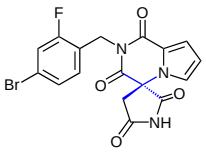

60
Ranirestat
(Aldose reductase inhibitor)

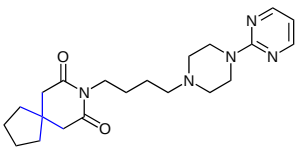

61
Buspirone
(Anti-anxiety)

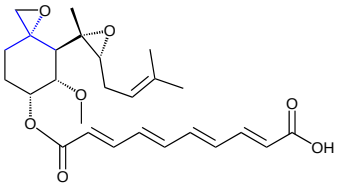

62
Fumagillin
(Aminopeptidasi inhibitor)

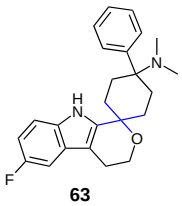

63
Cebranopadol
(NOP & opioid recpetor agonist)

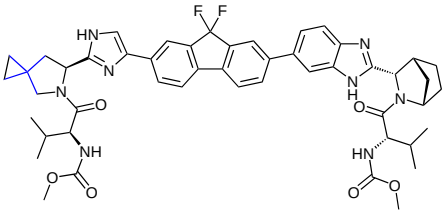

64
Ledipasvir
(Anti-HCV)

Figure 3. Marketed drugs containing spirocyclic moieties in their structures.[25]

The spirocyclic quaternary carbon offers structural complexity and conformational rigidity, reducing the penalty for conformational entropy and allowing the exploration of novel spatial regions, with the final aim of developing molecules with improved three-dimensionality.[30]

In addition, potentially flexible and highly entropic moieties of bioactive molecules, can be replaced with spirocyclic structural frameworks in order to gain affinity while reducing off-target liabilities.

The IUPAC defines spirocyclic systems as "systems that have two or more rings linked by one common atom".[31] Compared with monocyclic ring systems, spirocyclic systems with the same number of atoms contribute to reduce the lipophilicity of the ring system and its substituents. The number of publications in medicinal chemistry journals having spirocyclic compounds as their focus is highly rising, as described in the review of Krasavin *et al.*[32]

The introduction of a spirocyclic moiety, however cannot be considered a brand-new innovation of recent medicinal chemistry approaches. The first discovery of spirocyclic scaffolds dates back to 1957 with the introduction of the spironolactone into the progesterone structure, combining the anti-metallocorticoid activity with the cardiotonic effects of digitoxin, which carries a lactone ring; the resulting compound also showed oral bioavailability.[33]

The recent review published by Krasavin and co-workers[32] summarizes the role of spirocyclic scaffolds in medicinal chemistry, focusing the attention on their impact on potency, selectivity, stereochemistry and physicochemical properties compared to non-spiro compounds.

Among all examples presented in the review, some of them highlight the importance of replacing non-spiro moieties with spiro ones.

In term of selectivity improvement, Reilly *et al.*[34] replaced the piperazine with a spirocyclic moiety in compound **65** behaving as an antagonist of dopamine D3 and D2 receptors (Table 1). Even though the new compound **66** is 100-fold less active than the original compound, it exhibits 10-fold selectivity over D2 dopamine receptor. Adding a chain in the lead compound, the selectivity to D2 is increased to 905-fold (**66b**).

Table 1. Selectivity improvement by Reilly *et al.*[34]

	*K*i [nM]	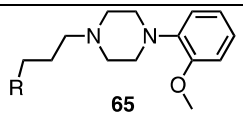 **65**	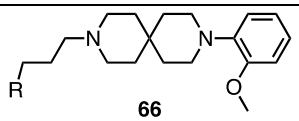 **66**
a R = H	D2	20.6	26,793
	D3	23	2,700
b	D2	260	10,895
	D3	6	12

R= 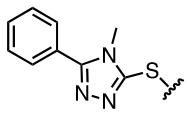			

In another reported example, Harada *et al.*[35] replaced the carbamate portion in compound **67**, an agonist of the G-protein-coupled receptor 119 (GPR119) with a spirocyclic moiety (**68**). The new compound **68** shows lower CYP inhibitory activity (EC50 < 10 μM against CYP1A2, 3A4, 2C8, 2C9, 2C19, and 2D6) compared with the non-spirocyclic agonist **68** (EC_{50} > 10 μM against CYP2C8, 2C9, and 2C19), and higher solubility in fed state simulated intestinal fluid (FeSSIF) (441.5 μM in **68** against 221.8 μM in **67**).

Table 2. Physicochemical improvement reported by Harada *et al.*[35]

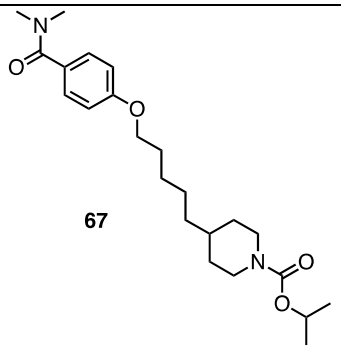 67	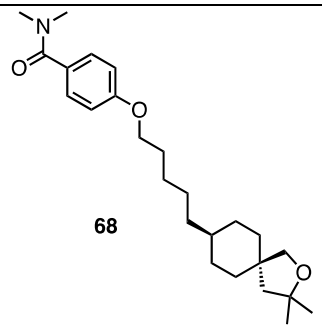 68
EC_{50} GPR119 = 10 nM	EC_{50} GPR119 = 4 nM
CYP 2C8, 2C9, 2C19 IC_{50} < 10 μM	CYP 1A2, 3A4, 2C8, 2C9, 2C19, 2D6 IC_{50} > 10 μM

Solubility = 221.8 μM in FeSSIF	Solubility = 441.5 μM in FeSSIF

Sampson *et al.*[36] replaced the double bond in compound **69** (Polo-like kinase 4 inhibitors PLK4) with a spiro cyclopropane as in compound **70**, in order to improve the physicochemical profile. Despite the potency decreased from 0.23 μM to 1.0 μM, the solubility improved more than 11-fold, due to the different crystal packing of the molecule. The selectivity was raised as well, due to the lower inhibitory activity on five CYP450 isoforms.

Table 3. Physicochemical improvement reported by Sampson *et al.*[36]

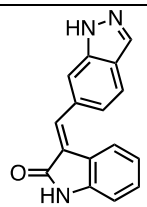 **69**	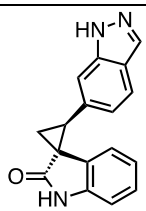 **70**
PLK4 IC_{50} = 0.23 μM	PLK4 IC_{50} = 1.0 μM
Solubility pH 7.4 = 0.7 μg/mL	Solubility pH 7.4 = 8.0 μg/mL

Pettus *et al.*[37] included a spirocyclic moiety in a pan-Pim kinase inhibitor, displaying a 2-aryl-6,7-dihydro-1*H*-pyrrolo[3,2-c]pyridin-4(5*H*)-one structure, namely inhibitor compound **71**. Although, the new inhibitor **72** shows similar clearance to **71**, it displays increased half-life and bioavailability.

Table 4. Pharmacokinetics improvement reported by Pettus *et al.*[37]

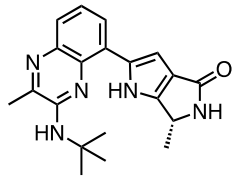 71	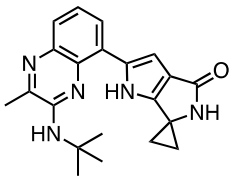 72
IC_{50} Pim-Pim-2 = 0.7/1.0 nM	IC_{50} Pim-Pim-2 = 0.4/0.5 nM
CL = 0.5 L/h/kg	CL = 0.6 L/h/kg
$t_{1/2}$ = 3.0 h	$t_{1/2}$ = 4.5 h
F = 62%	F = 100%

1.2 Spiroindolenines and spiroindolines: synthetic challenges

The importance of indole and indol(en)ine substructures in biologically relevant compounds, has been associated in recent years with the increase of Fsp3 in order to examine poorly explored regions of three-dimensional chemical space, to decrease the possibility of non-specific binding to molecular targets and, simultaneously, to improve key pharmacokinetic parameters, such as solubility, as detailed in the previous paragraphs.

In this regard, spiroindolines and spiroindolenines, attracted great attention because of their multiple therapeutic potential and their presence in a wide range of biologically active natural products (Figure 4).[38,39]

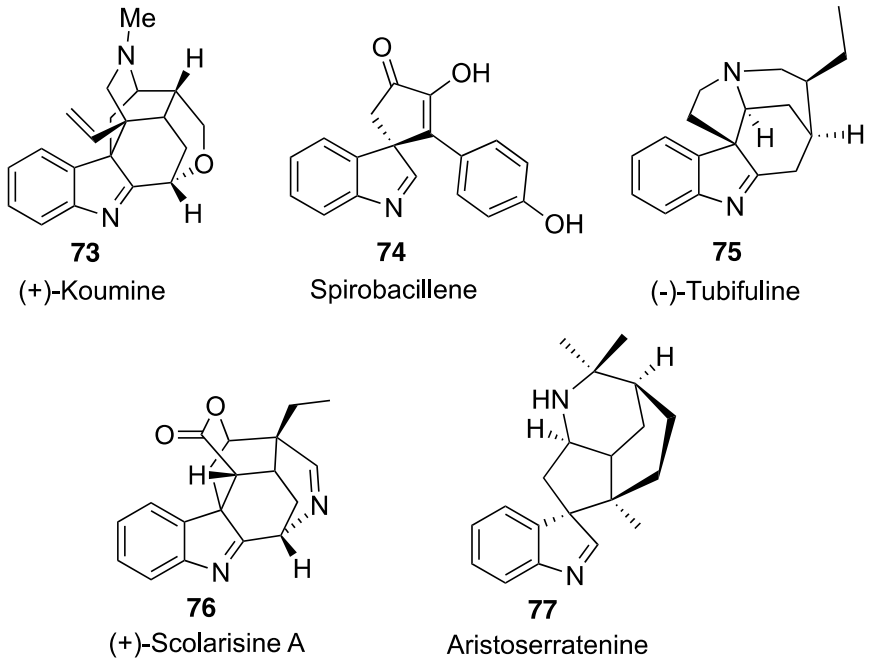

Figure 4. Structures of indoline- and indolenine-containing alkaloids and synthetic medicinally relevant compounds.[38,39]

Spiroindolines are known in the literature as inhibitors of Tankyrase-1, a poly-ADP- ribosyltransferase involved in various processes such as the Wnt signalling pathway, telomere length control and vesicle trafficking.[138] This scaffold has also been investigated for the generation of selective histone deacetylase inhibitors, which emerged as promising therapeutics for the treatment of neurodegeneration, cancer, and rare disorders. Spiroindolines have been known as potential anticancer agents, especially acting as kinase inhibitors.[40]

Besides the pharmacological importance of these privileged scaffolds, the particular reactivity of these compounds also allows to use them as precursors of other privileged heterocycles, including indolines, oxindoles, carbazoles, indoles and others (Figure 5).[41]

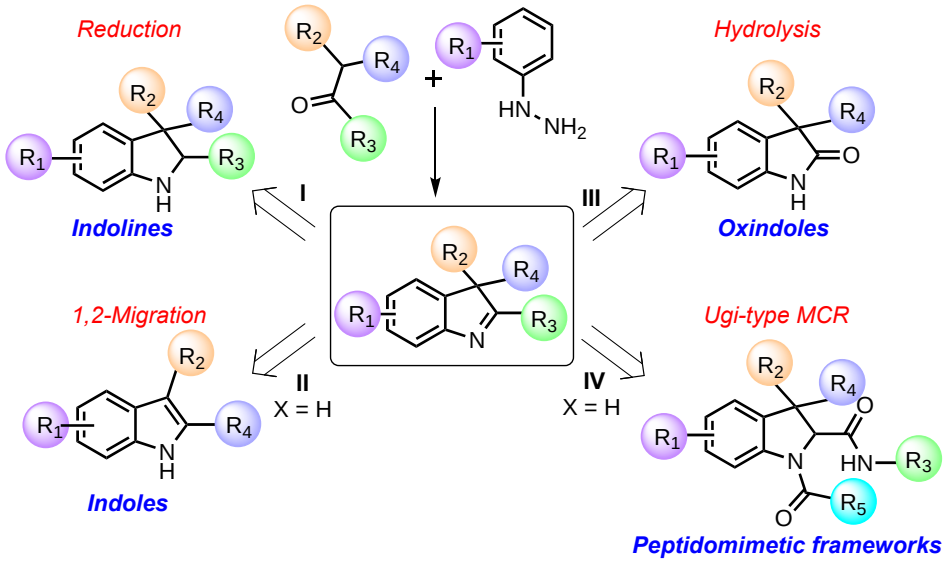

Figure 5. Utility of 3,3-disubstituted indolenines as precursors for other structural templates.[41]

Whit this in mind, the elaboration of efficient strategies for the direct synthesis of the spirocyclic indolenines could be pretty useful for both synthetic and pharmaceutical chemists. Many researchers focused their efforts to building up robust synthetic methods for spirocyclization of indoles and derivatives.[42] A valid approach is represented by the interrupted Fischer reaction (Scheme 1), that represents the oldest reported method for the synthesis of 3,3'disubstituted indolenines. (N.B.: "Interrupted" is used when an existing chemical process is redirected to a different final product).

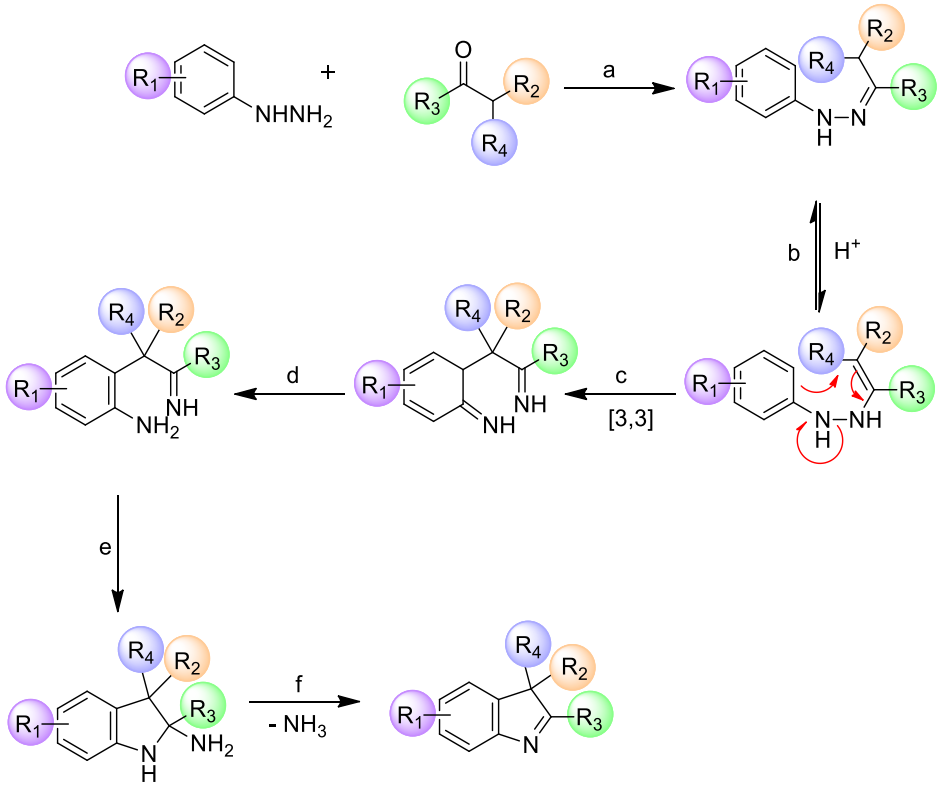

Scheme 1. Mechanism of interrupted Fischer synthesis: (a) The first step involves the reaction of the most nucleophilic nitrogen of phenylhydrazine with the carbon of carbonyl ketone. The reaction is chemoregioselective. There is dehydration and formation of imine; (b) The immine form is in tautomeric equilibrium with the form phenyldrazone-enamminon; (c) A sigmatropic 3,3 catalyzed by acid takes place; (d) Tautomerization reaction restores the aromaticity; (e) The amino group attacks the electrophilic carbon of the intermediate iminium; (f) 3,3-indolenin is formed by the loss of ammonia group.

In the synthetic protocols for the preparation of spiroindolenines or - more generally - of 3,3-disubstituted indolenines, there are several issues to be taken into account.

First of all, the tendency of metastable indolenines to undergo to 1,2-migrations under acidic conditions leading to the formation of the more thermodynamically stable indolic counterparts (Scheme 2). The acidic catalyst should then be rapidly removed from the reaction mixture in order to maintain the integrity of the indolenine ring system. Furthermore, 3,3'-disubstituted indolenines, just like other imines, exist in equilibrium with their tri-imminic form (Scheme 2).[43] This equilibrium could not represent an issue for consequent reactivity, due to the rapid collapse to the imine *in situ*, but could also represent a source of complexity in terms of chemical identification of the compounds, since the analytical data of the trimeric form are cumbersome to analyze. Indeed, the NMR of the indolenine moiety showed that they were in equilibrium mixtures with cyclic trimer in deuterated chloroform.[43]

Under acidic conditions the equilibrium can be altered to promote the imine species (protonated), but at the same time these conditions can trigger unwanted 1,2-migration towards the indole counterparts. In addition, steric, electronic, and chemical issues related to quaternary carbon generation must also be considered.

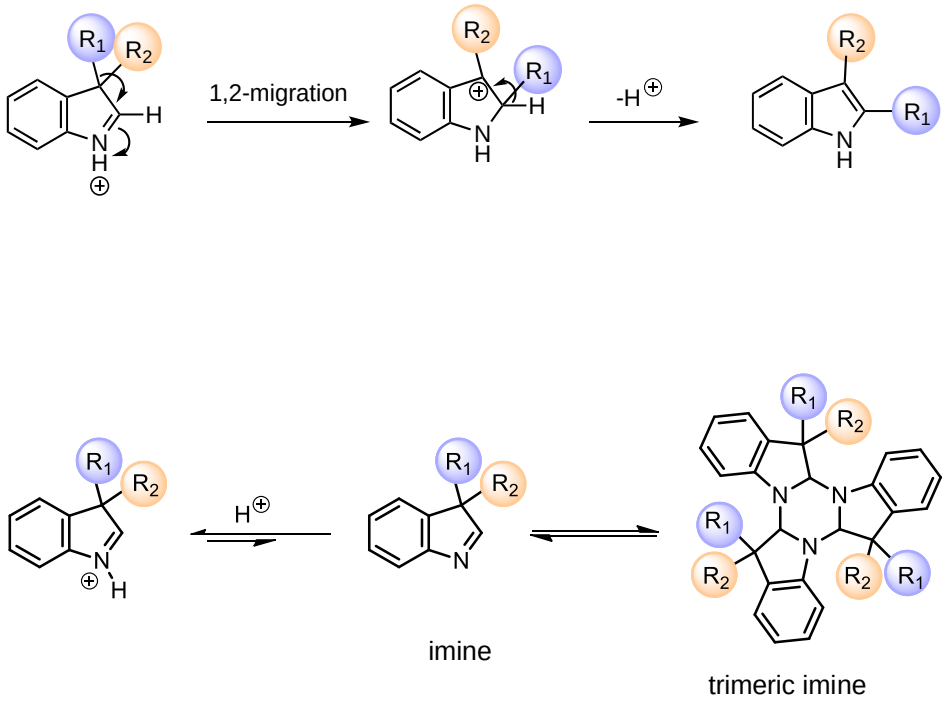

Scheme 2. Issues associated to 3,3-disubstituted indolenines.[43]

1.3 Peptidomimetics: medicinal chemistry relevance

Peptides are an important class of therapeutic agents and have deeply influenced the growth of pharmaceutical chemistry, with more than 60 peptide drugs on the market and over 350 in clinical and preclinical development.[44-46] Therapeutic peptides consist of several amino acids, usually with molecular weights of 500-5000 Da, breaking the rule of five.[47] Peptides have a primary role in diverse vital functions in human body, *i.e.* reproduction, respiration, metabolism and so on.[48]

The discovery of insulin, a peptide displaying 51 amino acid residues, represented one of the colossal medical breakthroughs in the history of drug discovery. Isolated by Frederick Banting in 1921, it was already

available for patients with diabetes mellitus just a year after its first isolation.[49]

Despite their pharmaceutical importance, unfortunately, peptides suffer from several drawbacks and limitations. First of all, the big dimensions and the high molecular weight represent key hurdles for their absorption, as well as the lack of specific transport systems for the excretion phase. That means poor absorption and rapid excretion through kidneys and liver. Another important limitation is associated to poor stability: the amide bond rapidly undergoes proteolysis by several peptidases in the human body, which severely limits the duration of their therapeutic effect.[50]

Moreover, the low selectivity due to the high number of rotatable bonds present in their structure, induce random interactions with multiple targets, often also involving also the binding site of antibodies, thus justifying antigenicity and immunogenicity often associated to peptides.[51]

In light of these considerations, the development of peptide-like structure could overcome all the drawbacks associated to peptides. In particular, peptidomimetics have been designed *ad hoc* to mimic as much as possible the parent peptides, by the introduction of chemical modifications on the parent peptide structure, while preserving the portions responsible for the activity. Conformational restriction is one of the main advantages that peptidomimetics can provide, in order to avoid the poor stability, low absorption and off-target liability.

Despite several classifications of peptidomimetics developed over the years, the one proposed by Grossmann[52] is currently the most commonly used. This classification clusters peptidomimetics into 4 classes, from A to D, based on the degree of peptide character.

- **Class A.** The first class contains peptidomimetics very similar to the parent peptide, displaying only small modifications with

respect to the original peptide structure, like the introduction of further lateral chain. The drug pentagastrin (Peptavlon) used as a diagnostic tool for the evaluation of gastric acid secretory function belongs this class, since it just contains modification on the bioactive region of endogenous gastrin.

- **Class B.** The second class involves further modified peptidomimetics resulting from the class A, containing unnatural amino acids or small-molecule building blocks.
- **Class C.** The third class includes peptidomimetics in which the backbone is completely replaced by a small molecule template. Somatostatin and TRH analogues belong to this class.
- **Class D.** The last class involves further modified peptidomimetics resulting from class C, with almost no similarity to the original peptide structure.

The development of new peptidomimetics involves different steps, based on what is already known about the target protein.[53] First of all, the minimal peptide sequence responsible for the interaction with the biological target needs to be identified. Then, through local modifications, or the use of secondary structure mimetics and restrictions, new optimized peptidomimetic hits can be achieved, and further modified avoiding the side effects associated to the starting hit compound.

The development of new protocols to synthetize peptidomimetic drugs besides the solid-phase peptide synthesis (SPPS),[54-55] has attracted the researchers, also due to the steady increase of marketed peptidomimetic drugs, as testified by the list of drugs approved by FDA in the past few years.[56]

Peptidomimetics represent already a good portion of approved drugs or compounds in late- stage phase of the clinical phases. Figure 1 shows some examples.

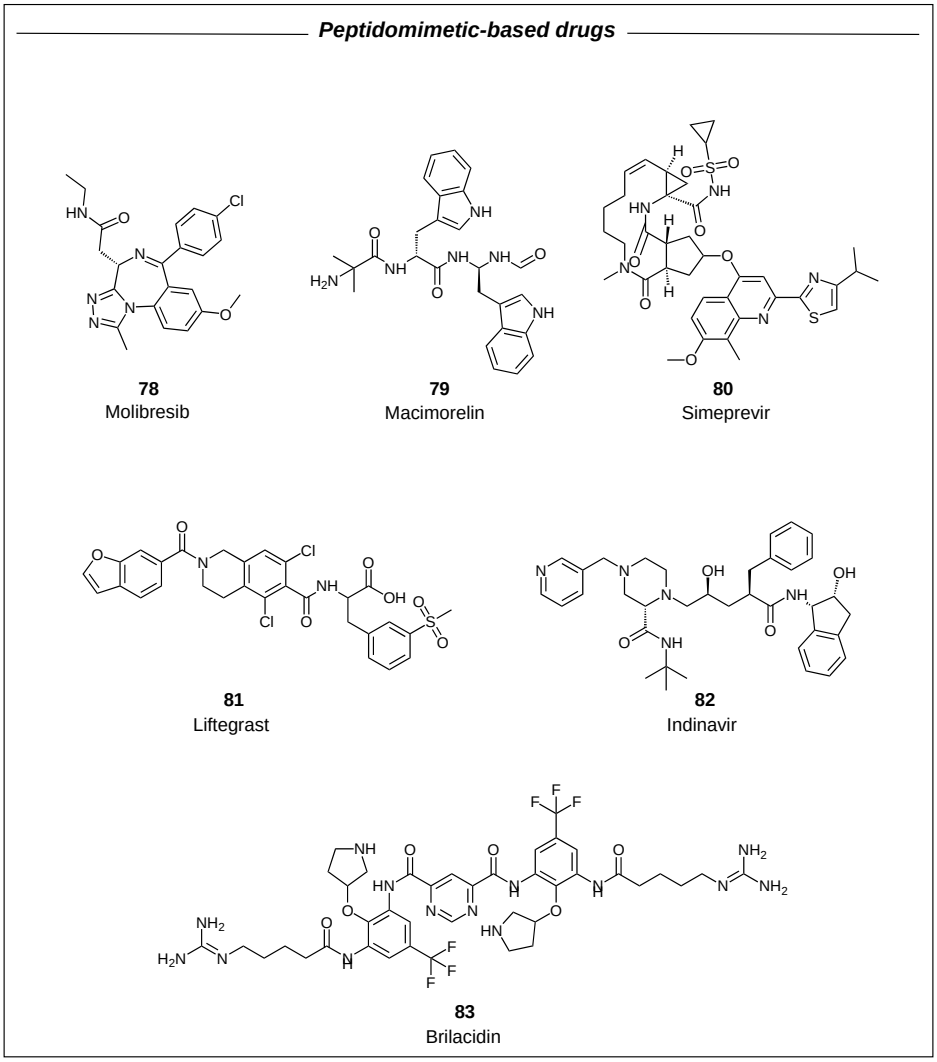

Figure 6. Peptidomimetic-based drugs.[45]

1.4 α-Amino nitriles: relevance in medicinal chemistry

Nitriles are a class of organic compound containing a -C ≡ N polarized bond, that is eight times smaller than a methyl group.[57] Nowadays, with the growing number of drugs containing nitrile functionalities, synthetic methods for the generation of nitriles are steadily developing, thus becoming one of the hottest topics in the organic chemistry field.[58]
In particular, since 1850, when Adolph Strecker discovered a condensation between amines, carbonyl compounds and hydrogen cyanide, basically unveiling a methodology for building amino acid precursors, the development of synthetic protocols for the preparation of α-aminonitriles has captured the attention of many research groups.[59]

From a merely chemical point of view, α-aminonitriles may be considered masked iminium ions or "cyanide-protected", that could easily undergo several subsequent reaction, like Opatz and co-workers,[60] reported in their paper in 2020 (Figure 7). Firstly, they may be subjected to acidic hydrolysis, replacing the cyano group with an amide functionality or the carboxylic acid counterpart, furnishing the corresponding α-amino acid derivative. Alternatively, in basic conditions the α-proton could be removed though α-deprotonation, with subsequent substitution or addition of other functional groups or easily converted into nitrile-stabilized ammonium ylides through quaternization. Moreover, hydrogenation leads to the correspondent amine, or a loss of cyano group, induced for example by Ag^{+} or Cu^{2+}, can provide the reductive decyanation. Finally, nitrile derivatives they could be subjected to retro-Strecker reaction.[61-64]

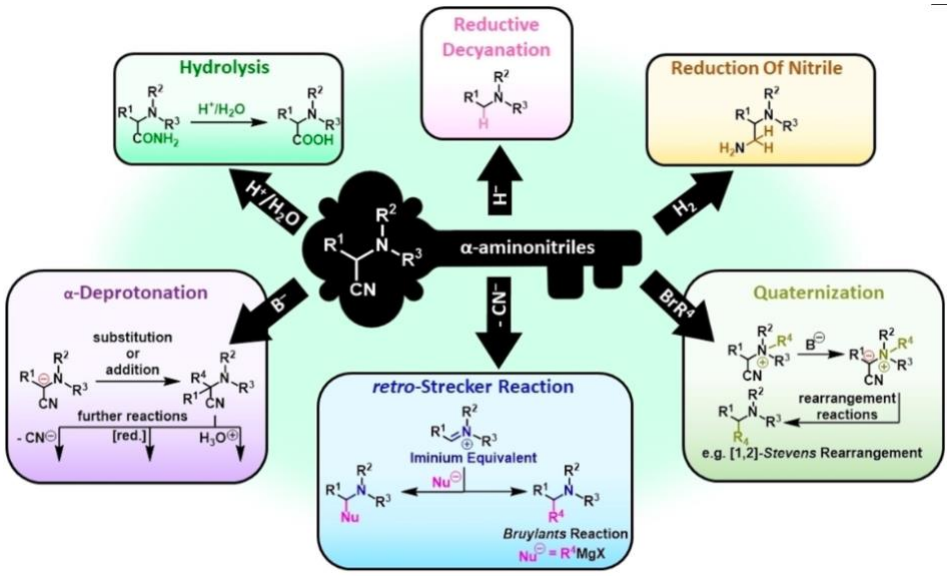

Figure 7. Reactivity of alfa amino nitriles.[60]

Due to the broad reactivity of these building blocks, they have also been considered highly useful and versatile in the synthesis of nitrogen-containing heterocycles, drugs and natural products.[65-69]

In addition to being important key intermediates in natural product synthesis, such as in the total synthesis of ecteinascidin 743,[70] as well as venenatine and alstovenine,[71] they can be embedded in the structures of complex bioactive products. Figure 8 shows some examples.

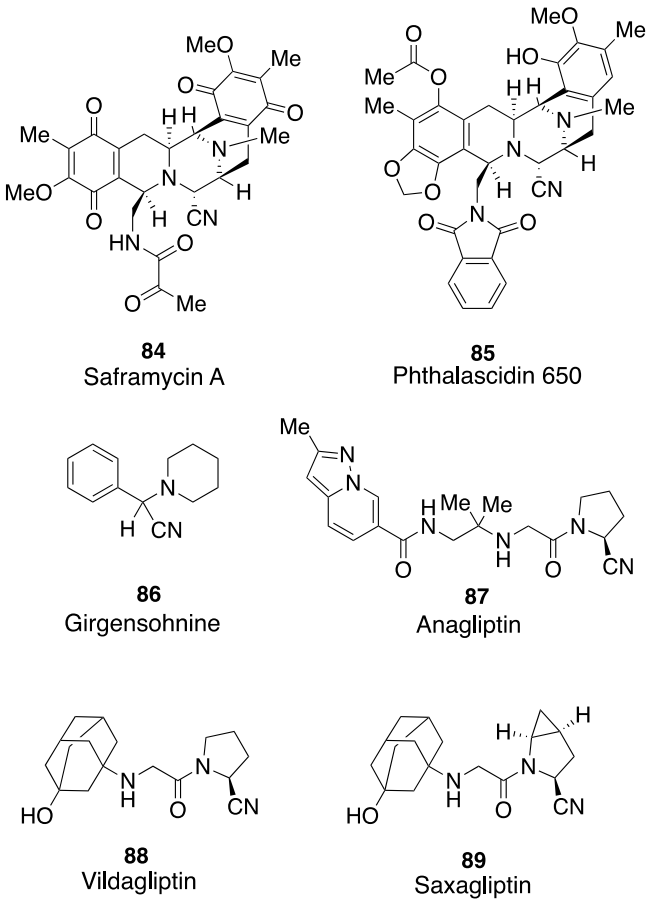

Figure 8. Representative biologically active α-amino nitrile-containing natural products and synthetic drugs.[72-77]

Saframycin A (SafA) is a member of the tetrahydroisoquinoline (THIQ) alkaloid family of natural products, and it was isolated for the first time in 1977. SafA displays potent antiproliferative effects in leukemia- and tumor-derived cells.[72,73]

Another example is Phtalascidin, a synthetic antitumor agent with the structure, the potency and mode of action comparable to ecteinascidin 743.[74,75]

A cyclic α-amino nitrile substructure is also included in the dipeptidyl peptidase-4 (DPP-4) inhibitor class of anti-hyperglycemic drugs like anagliptin, vildagliptin and saxagliptin.[76,77]

Furthermore, also different cathepsins inhibitors, used for the treatment of osteoporosis, contain aminoacetonitrile substructures.[78]

As mentioned above, Adolph Strecker discovered in 1850 a condensation between amines, carbonyl compounds and hydrocyanic acid furnishing α-aminonitriles. The reaction, known as "Strecker reaction" is the most straightforward and viable main method for the synthesis of natural and non-natural α-amino acids, such as hydantoins and polypeptides.[79,80]

Strecker protocols could be reasonably defined as multicomponent reactions (MCR).

The simple reaction protocol, together with the huge availability of starting materials under prebiotic conditions, rises the idea of the involvement of the cyanide group in the origins of life, like precursors of nicotinic acids and nucleic acids.[81-83]

Figure 9 shows some examples of drugs and natural products prepared by Strecker-type reactions or Strecker intermediates.

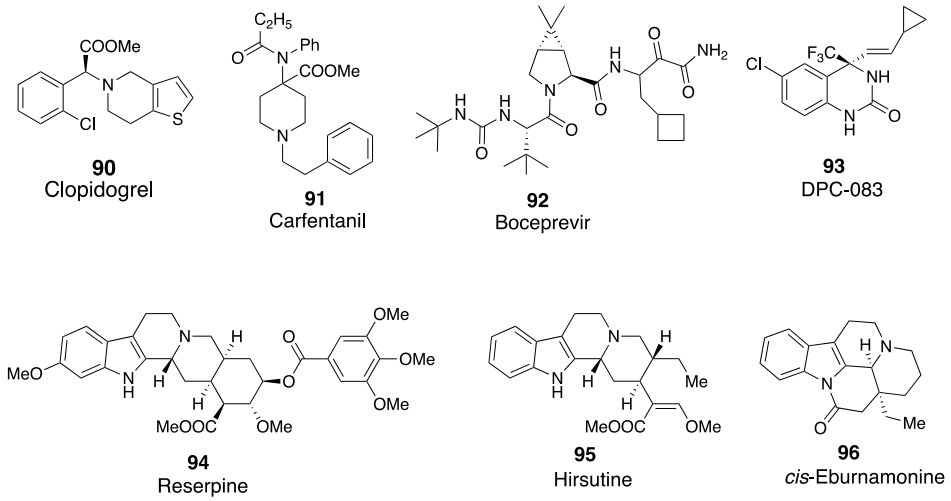

Figure 9. Selected drugs and natural products prepared by Strecker-type reactions or Strecker intermediates. [84-86]

From the mechanistic point of view, the reaction starts with the formation of the iminium ion by the addition of ammonia to the carbonyl compound (aldehyde or ketone), followed by the nucleophilic attack of the cyanide ion. The resulting α-amino nitrile then undergoes basic or acid hydrolysis leading to the corresponding amino acid (Scheme 3).

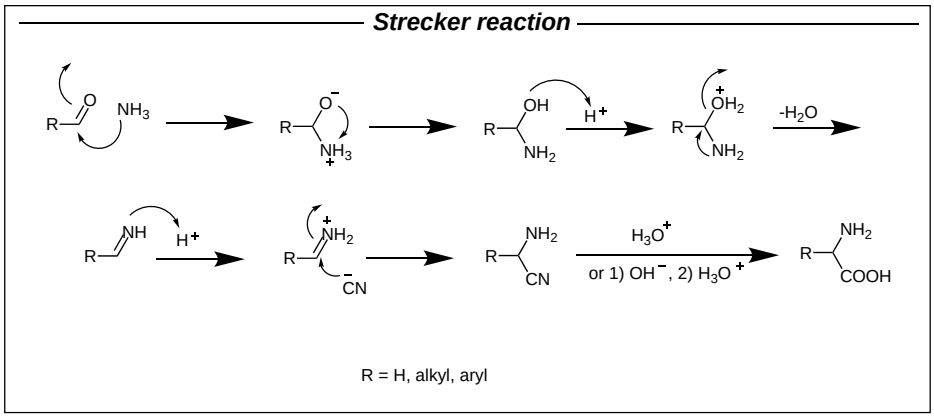

Scheme 3. Mechanism of the Strecker reaction.[58]

The classic Strecker reaction involves HCN as the cyanide source, but investigation of other sources like KCN, TMSCN, $(EtO)_2P(O)CN$, Et_2AlCN, Bu_3SnCN, MeCOCN, as well as greener and safer acetone cyanohydrin and ethyl cyanoformate or hexacyanoferrates are still ongoing in order to maximize the yield and improve the eco-sustainability of the reaction.

Since Strecker synthesis only provides amino nitrile compounds in form of their racemic mixtures, several protocols including chiral HPLC or enzymatic resolution, using hydrolytic enzymes like α- chymotrypsin and subtilisin have been implemented to obtain enantiomerically pure products.[87]

However, in the last three decades, prompted by the increasing request for enantioenriched α-amino acids, many researchers at both academic and industrial level, have found a huge interest in the development of enantioselective Strecker reaction protocols.

The first example of enantioselective Strecker reaction appeared in 1963, when Harada replaced the classic ammonia with enantiopure *(*S)-α-phenylethylamine, achieving the corresponding α-aminonitrile in a modest diastereoselective ratio of 3.3:1.[88]

However, this breakthrough opened the way for synthetizing enantioenriched amino acids with similar protocols.[89]

The real turning point has taken place in 1996, when the first catalytic enantioselective Strecker protocol has been discovered (Scheme 4).[90]

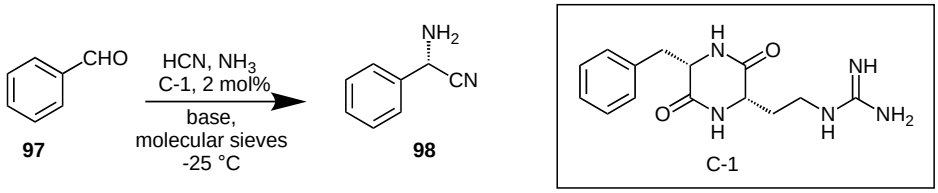

Scheme 4. First catalytic enantioselective Strecker.[90]

Over years, two main strategies have been increasingly followed for the achievement of enantiopure Strecker products:[91]

1) Nucleophilic addition of cyanide to chiral nonracemic imines;

2) Catalytic enantioselective cyanation of achiral imines.

In particular, the second approach, that employs substoichiometric amounts of chiral catalyst, currently represents the method of choice in the synthesis of chiral non racemic amino nitriles.

Among all the available chiral catalysts, including Zr (IV), Al (III) and Ti (IV) complexes, chiral organocatalysts played in the latest years the most significant role, also due to their potential for developing greener and sustainable Strecker protocols.

The 2021 Nobel Prize in Chemistry, awarded to Benjamin List and David MacMillan, recognizes the importance of pure enantiomers, accomplishing stereoselective synthesis through the use of asymmetric organocatalysis.[92]

Asymmetric organocatalysts represent currently a huge field of organic chemistry, that employs versatile small chiral organic catalysts in order to achieve enantiopure products. Amino acid derivatives, alkaloids, thioureas, Lewis and Brønsted acids are commonly used. Chiral organocatalysts are biodegradable, safe, cheap, eco-sustainable, easy to control, generally insensitive towards oxygen and moisture and available

from nature, with respect to the toxic and more expensive metal-based catalysts.[93]

Additionally, in most of the cases, they can be recovered and potentially reused. All these factors are undoubtedly in line with the twelve principles of green chemistry, and it is worth noticing that both green chemistry and asymmetric organocatalysis fields are growing side by side.

Regarding the involved reaction mechanisms, asymmetric organocatalysts[94] could have two different interactions with the substrate: covalent and non-covalent (Figure 10). Amines, *N*-heterocyclic carbenes and general Lewis bases act through the formation of a covalent bond;[95-98] thiourea, squaramide and phosphoric acid catalysts act through hydrogen bonding interaction.[99-101]

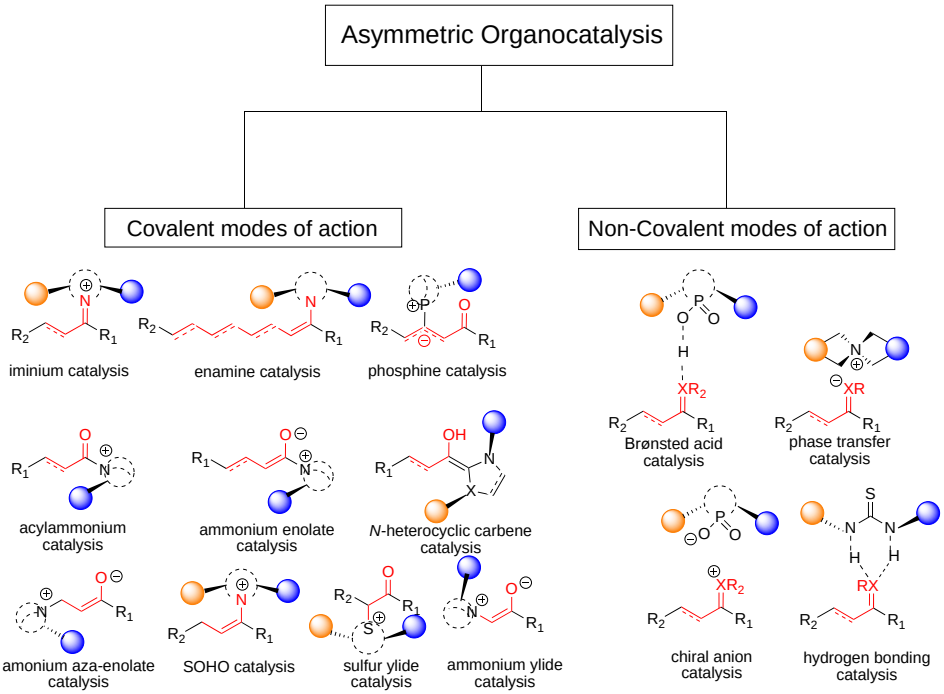

Figure 10. Asymmetric covalent and non-covalent organocatalysis.[94]

From the pharmaceutical point of view, having in hand a single enantiomer is preferable due the propensity of the majority of the biological targets to preferentially or uniquely interact with only one of the two enantiomers (eutomer). Furthermore, the less active or inactive enantiomer (distomer) could also be responsible of off-target or even toxic effects.[102]
Organocatalysis has been widely applied to medicinal chemistry fields, for generating drugs, lead compounds, fragrances, flavors and bioactive natural products.[103]

By taking advantage of asymmetric organocatalysis, medicinal chemists have made achievements in the asymmetric synthesis also of novel cardiovascular drugs, antiparasitic and anti-obesity agents.
The toolbox of asymmetric organocatalysis also in this case helped the synthesis of new antiviral agents for RNA retroviruses and DNA viruses.
One representative example dates back to 2009, when Hayashi and co-workers reported a total synthesis of Oseltamivir (Tamiflu®), involving an organocatalytic step.[104]
The synthetic strategy to reach enantiopure (-)-Oseltamivir envisaged nine steps, employing only 5 mol% of the chiral secondary amine catalyst diphenylprolinol silyl ether, with a final yield of 57%.

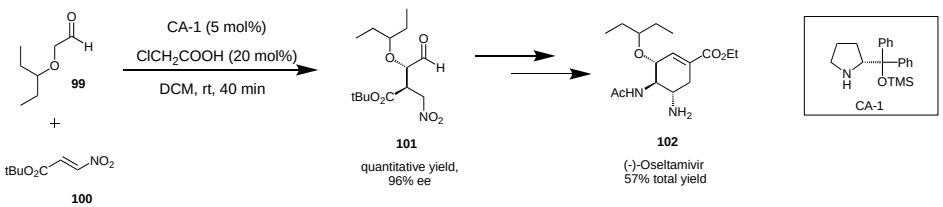

Scheme 5. Organocatalytic asymmetric Michael addition as a key reaction for the synthesis of Oseltamivir (Tamiflu®).[104]

The rising need for improved therapies for cancer diseases, in addition to surgery, chemo- and radio-therapy, has stimulated the researchers to take advantages from organocatalysis to synthetize new chemical libraries.
One representative case in this field, goes back to 2004. Roche developed (-)-nutlin-3, a new anti-cancer compound, able to inhibit the protein-protein interaction p53-MDM2. Despite the high efficiency, the synthetic procedure was quite expensive and furnished only a racemic mixture, sort it out later in pure enantiomers. Only few years later, in 2011, Davis and Johnston developed the first highly enantioselective synthesis of (-)-nutlin-3, in the presence of a bifunctional tertiary amine catalyst with 41% of yield and 91% of *ee*, decreasing the cost and undoubtedly improving the synthetic efficiency.[105]

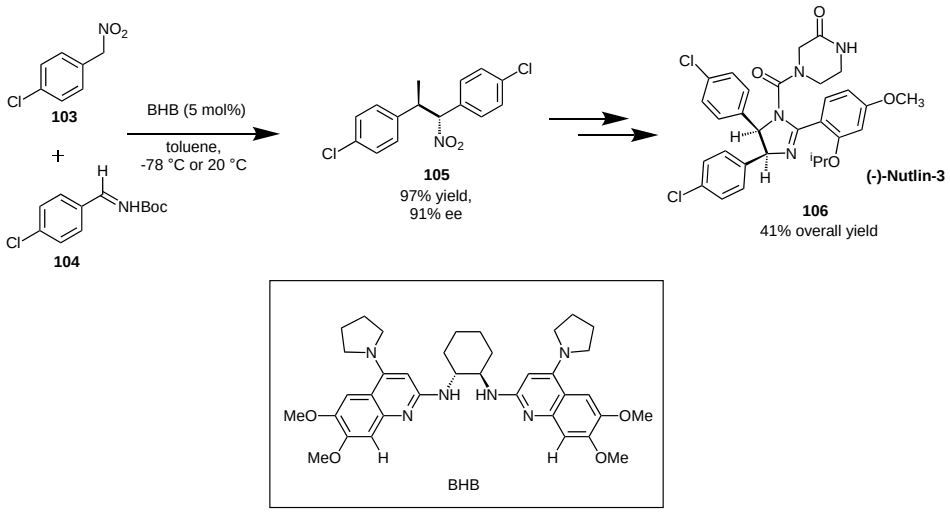

Scheme 6. Organocatalytic asymmetric aza-Henry reaction as a key step for the synthesis of (−)-Nutlin-3.[105]

1.5 Spiroindolines as privileged scaffolds for the identification of beta-lactamase inhibitors

β-lactam antibiotics are compounds containing the beta-lactam ring and represent the most important class of antibacterial agents.[106] Since the penicillin discovery (Fleming, 1928) and isolation (Florey and Chain, 1948), several other classes, like cefalosporine, carbapenemases and monobactam have been introduced into the clinic (Figure 11).[107]

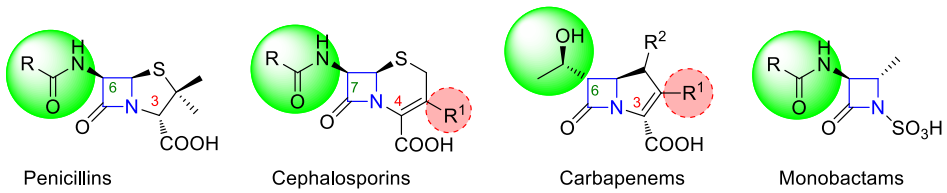

Figure 11. Classes of beta-lactam antibiotics.[108]

The mechanism of action relies upon the inhibition of the catalytic activity of bacterial transpeptidases, a series of enzymes also known as Penicillin Binding Proteins (PBP), displaying a crucial role in the synthesis of the peptidoglycan layer of the bacterial cells. The discovery of β-lactam antibiotics set out an essential revolution, in the treatment of bacterial infections previously considered lethal. Despite their well-known importance, the enormous and irresponsible use of antibiotics in the last years, worsened the already compromised situation in terms of antibiotic resistance, creating a major public health emergency.[109]

Several clinically-relevant Gram-negative pathogens (carbapenem-resistant *Klebsiella pneumoniae*, *Acinetobacter baumannii*, *Pseudomonas aeruginosa*, and *Enterobacter spp*.) – included among the acronymically

dubbed ‘‘ESKAPE pathogens’’ – have become highly-resistant to the most of available antibiotics.

The current COVID-19 pandemic accelerated the evolution of antibiotic resistance, since COVID-19 patients are routinely treated with broad-spectrum antibiotics, including expanded-spectrum cephalosporins (eg, ceftriaxone, ceftazidime, and cefepime), quinolones, and carbapenems. [110] Furthermore, infections with antibiotic-resistant *S. aureus*, *K. pneumoniae*, *P. aeruginosa*, or *A. baumannii* have been reported in patients with COVID-19 in intensive care units.

So far, two different types of microbial resistance are known:

1) Intrinsic: various specific strains of bacterial are resistant to a particular drug;

2) Acquired: several bacterial classes undergo to spontaneous genetic mutations or genetic recombination (transformation or conjugation phenomena), leading to the acquisition from the cell target of resistant genes derived from another resistant cell by means of mobile genetic elements, called transposons.[111]

Among all resistance mechanism, the synthesis of enzymes able to inactivate the antibiotics, called beta-lactamases, is one of the most troublesome.[112]

Based on the homology of the primary aminoacidic sequence (Ambler classification), the beta lactamases are clustered into 4 classes (Table 5).[113]

Table 5. Ambler classification.

Ambler classification	**Substrates**	**Enzymes**
A	Penicillins	PC1 da S. aureus

(penicillinases)	Penicillins, cephalosporins narrow spectrum	TEM-1, TEM-2, SHV-1
	Penicillins, cephalosporine narrow and broad spectrum	SHV-2/6, TEM-3/26, CTX-Ms
	Penicillins	TEM-30,SHV-72
	Penicillins,carbenicillins	PSE-1
	Cefalosporins broad spectrum	FEC-1, CepA
	Penicillins,cephalosporins, carbapenes	KPC-2, SME-1, NMC-A
B (metallo beta-lactamases)	Beta lactam antibiotics	NDM-1 IMP-1, VIM-1, CcrA, BcII(B1); CphA(B2); L1(B3)
C (cephalosporinases)	Cephalosporins	AmpC,CMY-2, ACT-1
D (oxacillinases)	Penicillins, cloxacillines	OXA-1, OXA-10

Carbapenems, also known as the “last resort” for antibiotic treatment, are outstanding for their broad spectrum activity against Gram + and Gram – bacteria. Despite carbapenems are pretty powerful from the clinical point of view, their common use generated significantly resistance mechanisms. The production of carbapenemases, enzyme able to hydrolyze carbapenemen as well as penicillins and cephalosporins, represent the most robust strategy of bacteria to become resistant.[114]

Carbapenemases are member of the four classes of beta lactamases, (A, B, C, D) based on the Ambler classification.

Classes A, C, D involve the serine beta lactamases (SBL), while the class B contains the metallo beta lactamases (MBL).[115]
The SBL are so-called because the nucleophilic serine residue in the active site enables the hydrolysis of the beta lactam ring. The MBL require one zinc ion or two zinc ions in the active site and the hydrolysis carry out through the attack of OH^-, coordinated and stabilized by zinc ion. MBLs have no mechanistic or structural relationship with the SBLs.

1) Class A contains enzymes chromosomally encoded or plasmid encoded. [116] Those coded in plasmids are the most clinically significant enzymes of this class, such as KPC and GES. They have been found in *Klebsiella pneuomoniae, Enterobacter, Salmonella, P.aeruginosa* and *A. baumannii;*[117-119]

2) Class B involves metallo beta lactamases, MBLs. These enzymes show the utmost carbapenemases activity[120] and they have been found in *P.aeruginosa, A. baumannii* and *Enterobacterales.*[121]

3) Class C contains only 5 enzymes able to hydrolyzing carbapenems (ACT-1, DHA-1, CMY-2, CMY-10 and ADC-68) because they have been recently identified.[122]

4) Class D contains oxacillinase OXAs, because of the oxacillin-hydrolyzing property. They have been found in *Enterobacterales* and *A. baumannii.*[118]

The relevance of the MBL has grown significantly in the last years for the followed reasons:
1) the ability to hydrolyze most of all beta-lactam antibiotics;
2) the increasing expression by pathogenic bacteria;

3) the unavailability of clinically useful MBL inhibitors;

4) the transferability of their encoding genes;

5) their ubiquity;

The MBLs are further clustered into three subclasses in B1, B2 and B3, based on overall homology and active site geometry (Table 6).[123]

Table 6. Subclasses of MBLs.[123]

Ambler subgroups	Bush-Jacoby-Medeiros subgroups	Action spectra	Enzymes	Zinc affinity
3a	B1	Broad spectrum	Bc II, IMP- I, CcrA, VIM, NDM-1, SPM-1	Active with just one or both zinc group in the active site
3b	B2	Carbapenem (above all)	Cph A, Sfh-1	Active with one zinc group
3c	B3	Cefalosporine (above all)	LI, FEZ-1, Gob-1, CAU-1	Active with both of zinc groups

A study of the enzyme BcII crystal (Bacillus cereus, subclass B1) confirmed the presence of two zinc ions within the active site, known as Zn1 and Zn2. The Zn1 binding site, also known as site 3H, contains three histidine residues (His 116, 118, 196), while the Zn2 site, or DCH, includes the residues Asp 120, Cys 221, and His 263. Zn1 is also preserved in all three subclasses, while Zn2 in subclasses B1 and B2 includes the residues mentioned above and in B3, instead, Cys 221 is replaced by His

121. The difference in the amino acid sequence between the diverse subclasses is reflected in the different catalytic properties of enzymes. For example, class B1 shows full catalytic activity with either one and two $Zn2^{+}$ ions, class B3 works with only both $Zn2^{+}$ bound ions in place, while subclass B2 is even inhibited by the binding of the second zinc ion. Therefore, the enzymes of subclasses B1 and B3 are defined as bi-nucleated enzymes, while those belonging to B2 are mononucleated enzymes.

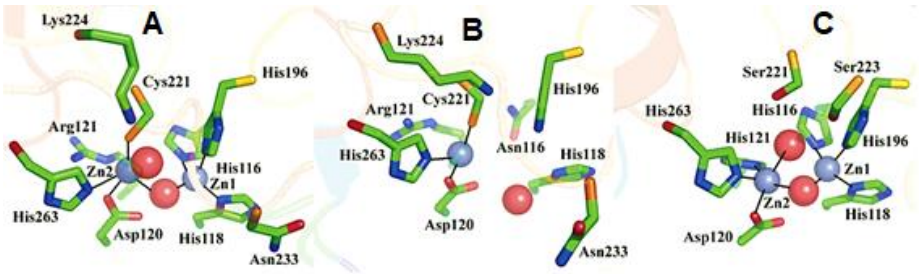

Figure 12. Active site of **A**: BcII (B_1), **B:** CphA (B_2), **C:** L1 (B_3). The grey spheres represent Zn^{2+} ions, while the red ones represent H_2O molecules. The black continuous lines show the coordination bonds.[124]

Among the B1 subfamily, Imipenemase-1 (IMP-1), Verona integron-encoded MBL (VIM), and New Delhi metallo-β-lactamase-1 (NDM-1) are the most relevant MBLs observed from a clinic point of view.[125]

The B1, together with B3 subfamily, catalyzes hydrolysis of a huge portion of beta lactamases, including the latest generations of cephalosporins and carbapenems.[126] On the other hand, B2 has a narrow spectrum, being active only against carbapenems.

The three subclasses have a different hydrolytic mechanism, guaranteed by a nucleophilic species that attacks the amide bond of the lactam ring, represented by a hydroxide ion bridged between the two metal ions for the dinucleate B1 and B3 MBL or by a water molecule for the mononucleated B2.

Having MBLs a common catalytic mechanism, despite several differences in structural homology, the identification of broad-spectrum inhibitors, to be employed in synergy with currently available antibiotics, is a challenging but feasible task. SBL inhibitors were introduced in the commerce already in the 1980s, while no clinically approved inhibitors of MBLs exist so far (Figure 13).

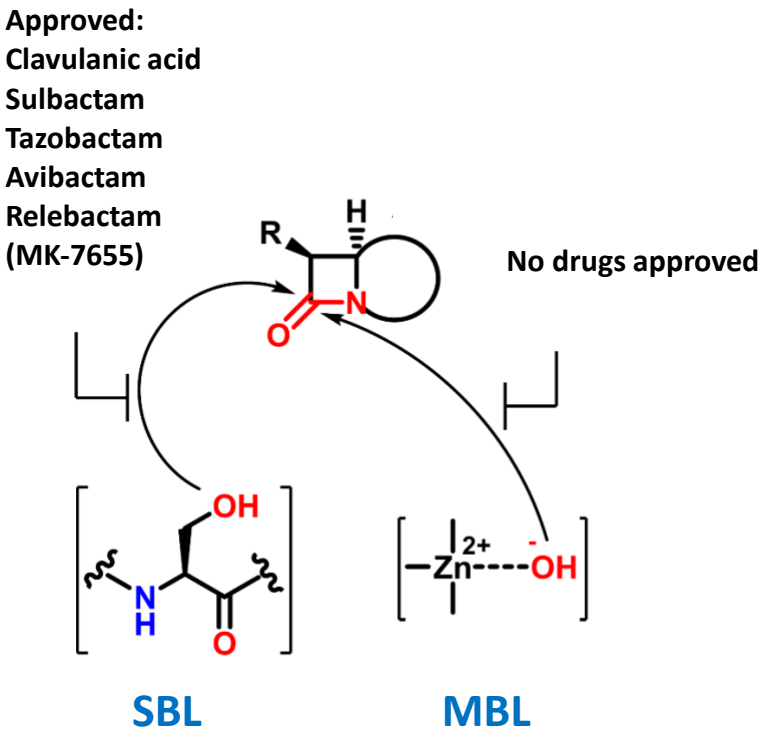

Figure 13. Approved beta-lactamases inhibitor drugs.

Although several compounds have been proposed as MBL inhibitors, poor sequence similarity among various members, selectivity issues towards human metalloenzymes and the presence of shallow active sites pose a relevant hurdle to the development of safe and effective broad-spectrum MBL inhibitors.

Two main strategies are currently used to counteract resistance due to β-lactamases. The first involves the synthesis of new β-lactam antibiotics resistant to hydrolysis by these enzymes, *e.g.* cefiderocol. The second strategy is the development of β-lactamase inhibitors, in order to be combined with available antibiotics and formulated as a single product.

The New Delhi metallo-β-lactamase 1 (NDM-1) enzyme, isolated for the first time in a patient coming from India in 2008, is currently one of the most dangerous MBL isoforms, due to its substrate promiscuity, prompt appearance of variants, broad spectrum of action and its global abundance.[127] Structurally, NDM-1 contains 12 β-sheets and 6 α-helices, arranged in a αβ/βα fold with two divalent zinc ions bridged by a hydroxide ion (Figure 14).

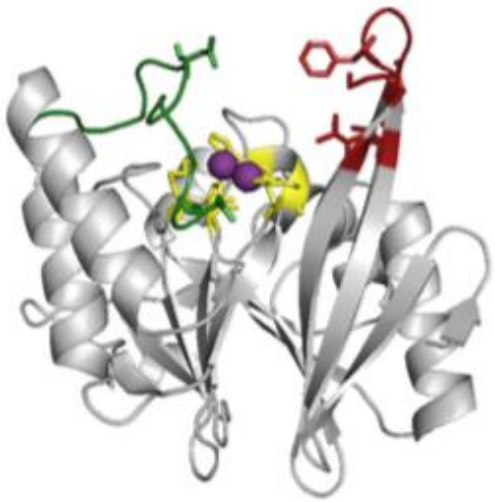

Figure 14. Secondary structure of NDM-1 with loop 3 (red), loop 10 (green), and the zinc ions (violet) and zinc-coordinating amino acids (yellow) being highlighted (PDB: 4hl2).[128]

About the hydrolytic activity of NDM-1, the OH^- attacks the carbonyl C, with the stabilization of the Zn ion, causing C-N cleavage. The dissociation is followed by the regeneration of the OH^-, in order to be ready for a new catalytic hydrolysis.[129]

After the product dissociation from the active site and the regeneration of the bridging hydroxide, the enzyme is reactivated for a new hydrolytic reaction (Figure 15).[130]

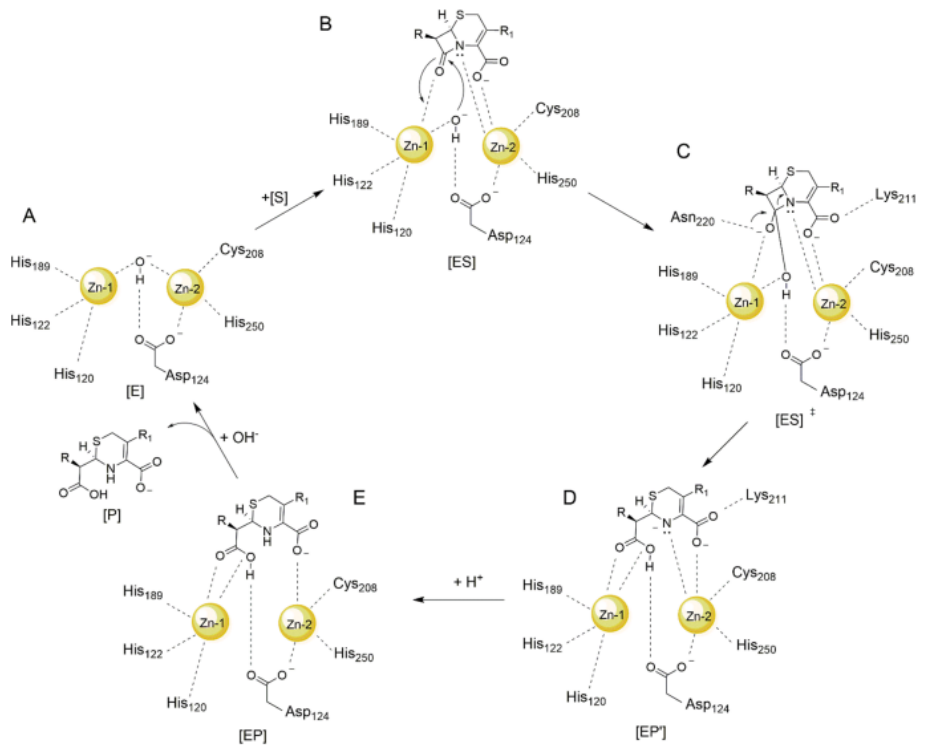

Figure 15. Hydrolytic activity of NDM-1 on a generic cephalosporin beta-lactam antibiotic.[130]

The gene coding for NDM-1 has been found on several types of plasmids and can be transferred between Gram- bacterial cells by conjugation. Despite the NDM-1 coding gene is not found on integrons, like IMP and VIM, has spread widely and rapidly.

The currently available small molecules acting as MBL inhibitors work by 3 different mechanisms:

1) zin ion sequestration;

2) coordination with the zinc ion(s);

3) covalent bond with the protein;

As reported above, despite a huge number of potential NDM-1 inhibitors have been synthetized, none of them have yet been clinically approved.
Specific MBL inhibitors are still missing in clinic, due to the structural variability among three classes, to the diversity of the loop arrangement and to the increasing presence of new NDM-1 variants.
In addition, the catalytic mechanism does not involve an enzyme-substrate covalent intermediate which may be the target of potential inhibitors, unlike SBL.[131]
In the present paragraph, inhibitors will be classified based on their structure, order to show recent trends in the design of NDM-1 inhibitors.

-Thiols

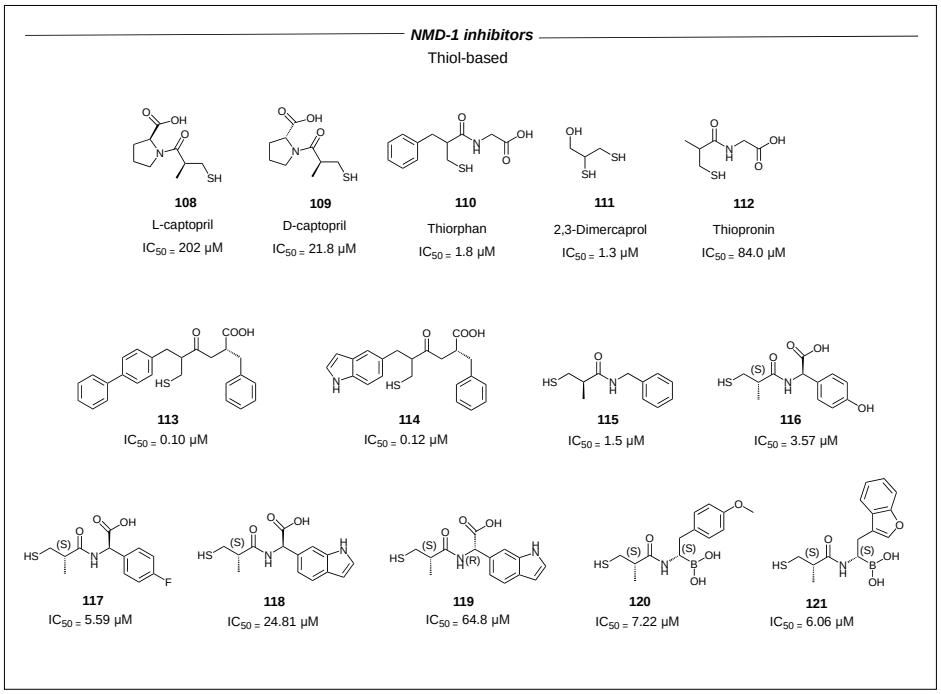

Figure 16. Thiol-based MBL inhibitors.[132-136]

The use of thiol group to inhibit MBL was inspired by an antihypertensive drug, captopril, having the thiol group that coordinates a zinc group in the angiotensin-converting enzyme (ACE). Due to the similarity of the zinc-containing active site of MBL and ACE, researchers hypothesized that Captopril (L-Captopril **108** and D-Captopril **109**) could also be able to inhibit NDM-1, although with the significant off-target effect related to their effect on ACE enzyme, with consequent reduction of blood pressure. Crystallization of captopril within the NDM-1 binding pocket revealed interactions between the thiol group and zinc in the active site. In addition, a hydrogen interaction between the carboxyl group on the captopril and Asn220 of NDM-1 was highlighted (PDB = 5ZIO and 5ZJ2 respectively for crystal structure of NMD in complex with -L and -D captopril.[132-134]

Other compounds containing thiol group are: thiorphan (**110**, an antidiarrheal agent), which binds the two zinc atoms with the thiol group at the active site of NDM-1. In addition, the phenyl ring in the thiorphan undergoes a π-stacking with the imidazole ring of His122, and the glycine portion engages hydrogen bond interaction within the active site. 2,3-Dimercaprol (**111**, used to treat toxic metal poisoning) contains two thiol groups, coordinating the two zinc ions. These two compounds showed the best inhibition against NDM-1, with IC_{50} values of 1.8 μM and 1.3 μM respectively. Finally, thiopronin (**112**, to treat toxic metal poisoning, liver disease and cystinuria) showed an IC_{50} value of 84 μM. It is also important to note that D-captopril, thiorphan, dimercaprol and thiopronin have the ability to reduce the minimum inhibitory concentration (MIC) of imipenem in *E. coli* and *K. pneumoniae* strains expressing NDM-1, thus

demonstrating their efficacy in synergy studies with beta-lactam antibiotics.[135,136]

Other approaches to the design of thiol NDM-1 inhibitors have been aimed at modifying the structure of captopril (compounds **113-121**, Figure 32), although with no significant improvement with respect to previously disclosed thiol-based compounds.

-Thioesters, azolilthioacetamides and carboxylic acids

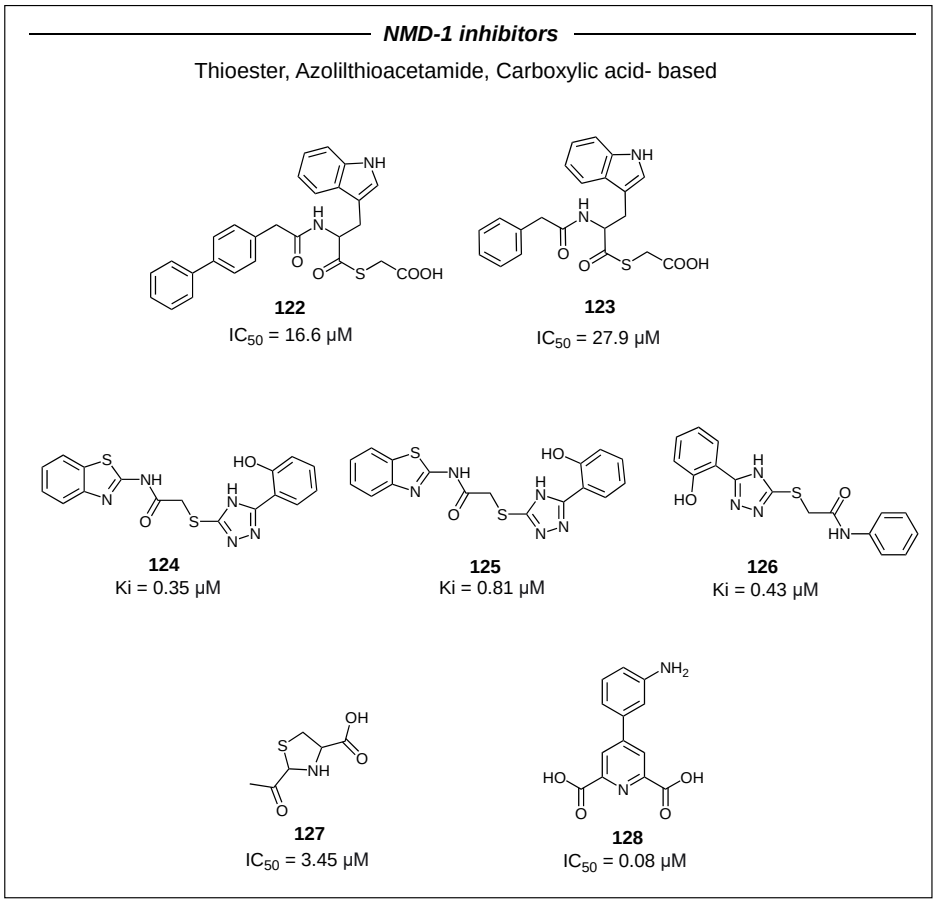

Figure 17. Thioester-, azolilthioacetamide-, and carboxylic acid-based MBL inhibitors.[137,138]

Thioesters show a unique mechanism of inhibition of MBL: the thioester hydrolysis product, mercaptoacetic acid, inhibits *B. Cereus II*, the hydrolytic reaction catalyzed by the enzyme facilitates the formation of a disulfide bridge between mercaptoacetic acid and the cysteine residue in the active site of the enzyme.[137]

Molecular modeling experiments have confirmed that the triazole part of azolythioacetamide coordinates the zinc atoms at the active site of NDM-1. The same coordination role is exerted by the carboxylic group in carboxylic acid-based compounds.[138]

-Boronic acids

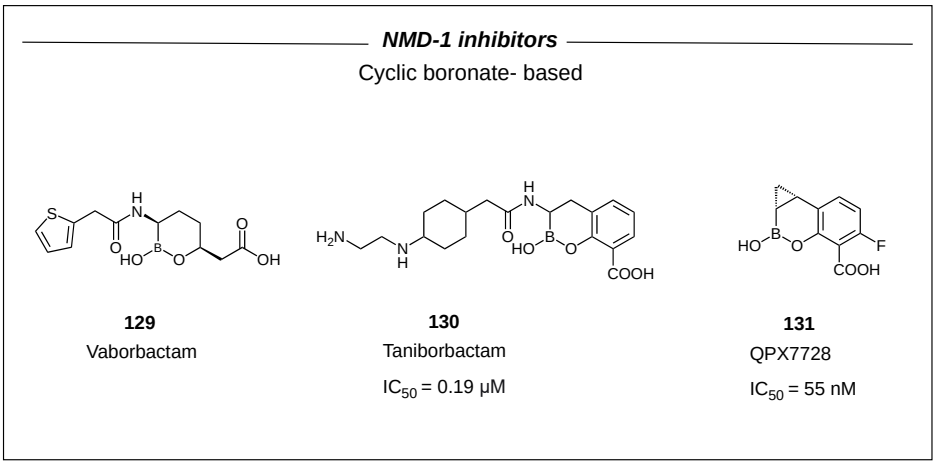

Figure 18. Boronic acid-based MBL inhibitors.[139.140]

Cyclic boronates, so far, are among the most promising inhibitors of NDM-1 because they have the potential to inhibit multiple classes of beta-lactamases. Vaborbactam (**129**), is the first cyclic boronate inhibitor of SBL to have been approved by the FDA.[139] Despite its inefficient against MBL, its structure inspired further research, leading to the development of

taniborbactam (**130**) and QPX7728 (**131**), two new boron containing compounds which are effective against most MBL belonging to B1 subclass and against SBL. [140]

-Heterocycles

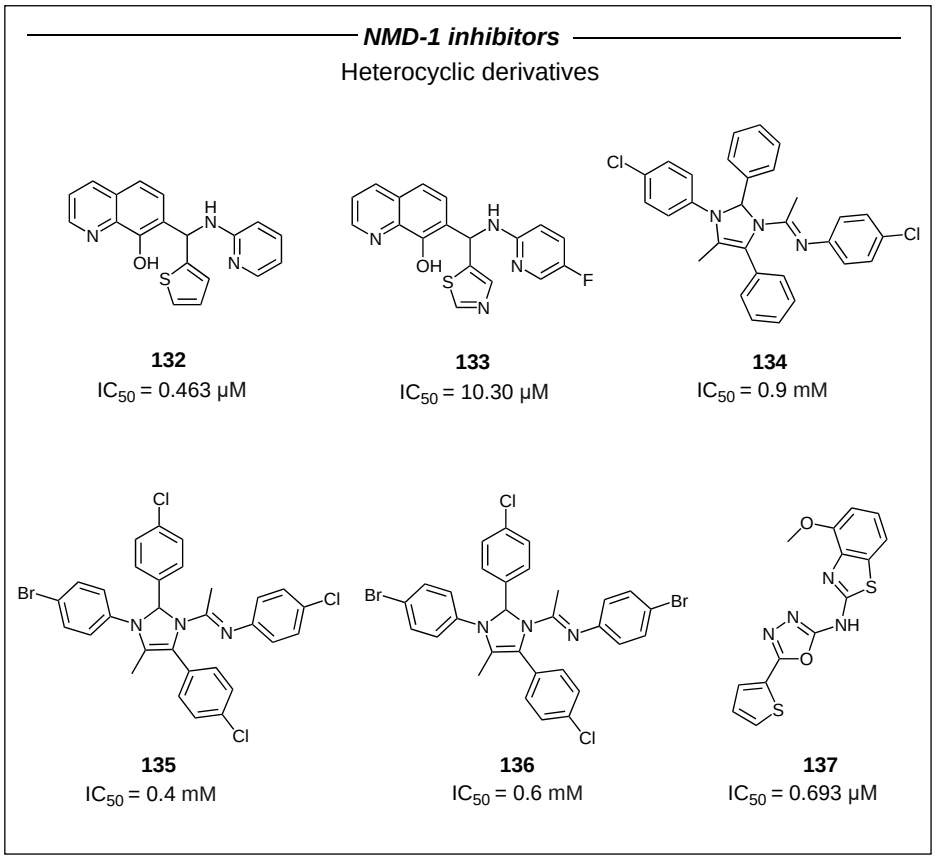

Figure 19. Heterocycles-based MBL inhibitors.[138]

Despite these structures show low activity against MBL, represent an important starting point to achieve other derivatives.

-Covalent inhibitors and bisthiazolidines

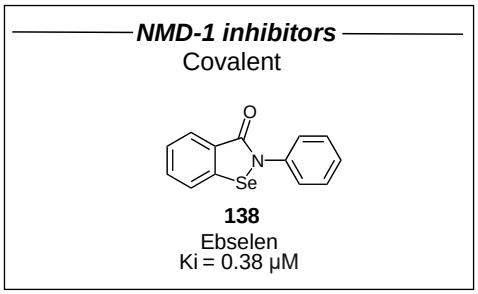

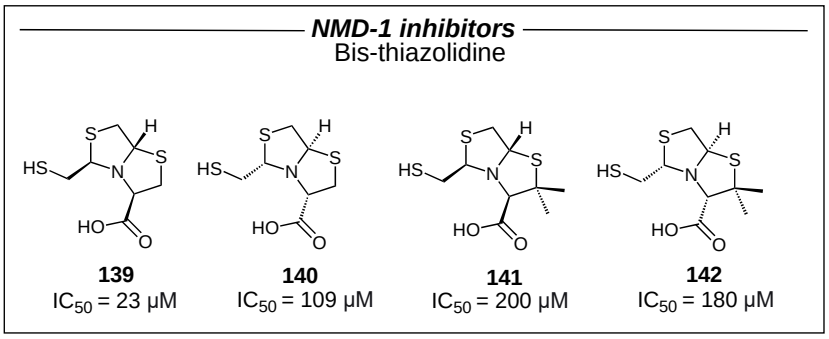

Figure 20. Covalent inhibitors and bisthiazolidine-based MBL inhibitors.[141-143]

Suitable structures can establish covalent interaction with two amino acids namely residues of Lys224 and Cys221, which are located near Zn2. This type of mechanism of action has been studied with ebselen (**138**). This compound is susceptible to nucleophilic attack by the Cys221 side chain, leading to the formation of a Se-S covalent bond. Although compound **138** is able to reduce MIC values for both meropenem and ampicillin in *E. coli*, the toxicity of selenium and the lack of selectivity limit the *in vivo* use of this compound. It has been observed that MBL more likely bind bicyclic structures with respect to monocyclic structural templates. Crystal structures have revealed that the thiol function in compounds **139-142** is responsible for binding NDM-1, coordinating both zinc atoms in the active

site. Furthermore, in vivo toxicity and selectivity studies show that these compounds are safe and effective.[141-143]

-Natural compounds

NMD-1 inhibitors

Natural compounds

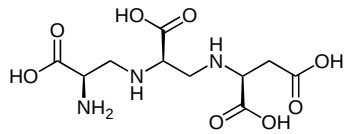

143

Aspergillomarasmine A

IC_{50} = 4.0 μM

Figure 21. Natural compounds MBL inhibitors.[144]

MBL can also be inactivated by zinc chelating compounds, in this context, an inhibitory action against MBL has been identified by a natural compound extracted from a fungus, namely aspergillomarasmin A, (**143**) which appears to be more selective and less toxic when assessed in animal infections models in comparison with other chelators.[144]

Introduction – Part 2: Sustainable routes to privileged scaffolds

1.6 Green chemistry: general definitions and metrics

Drug discovery process represents a crucial issue in the pharmaceutical industry, since it involves several steps taking 10-15 years from the beginning to the marketing approval and involving more than 1 billion US$ of investments.[145]

Drug discovery process is significantly evolving during the years and not only for the breakthrough of new targets and mechanisms of action, but also for the advancements in emerging technologies, such as combinatorial chemistry, high throughput screening (HTS), and modern molecular modeling techniques.[146,147] The aim, however, remained the same: to find a biological active chemical substance that leads to causing minimum undesired effects.

Over time, also the environmental impact of drug fabrication has become a serious worldwide issue, and the management of pharmaceutical wastes represents an important aspect for the pharmaceutical industries. Among all wastes, solvents play a crucial role, mainly ascribable to their wide use in chemistry operations. Consequently, the resulting high volumes of solvent wastes have to be disposed in a safe and environmentally benign way, thus increasing production costs.[148]

Regarding unused drugs, their disposal involves incineration, autoclaving, microwaving, chemical disinfection, secure landfilling, encapsulation and inertization, based on the features of the pharmaceuticals.[149.150]

For instance, solid organic wastes undergo incineration at 1.200 °C in dedicated incinerators; this technique is still one of the main methods for disposal, also described as “thermal method”. Despite its efficiency, this represents a disputable approach for waste disposal/management, due to issues associated to emission of gaseous pollutants and greenhouse gases.[151]

However, not only the waste disposal as such poses issues, but generally the amount of energy needed for the large-scale fabrication of actives as well as the widespread use of non-renewable, fossil-based starting materials, call for a paradigm change also in the pharmaceutical industries.

The pharmaceutical sector has received little attention from the ‘sustainability community’ in terms of its contribution to the global carbon footprint.[152]

A study revealed that the pharmaceutical industry is significantly more emission-intensive than the automotive industry.[153]

Carbon footprint is a measure in form of carbon dioxide equivalents, *i.e.* CO_2e, used to summarize the total greenhouse gas emissions directly or indirectly associated with a product, an organization or a service.

The term carbon footprint is a consequence of the previous known “ecological footprint” proposed by Wackernagel and Rees in 1996.[154]

Among all greenhouse gases, CO_2, methane (CH_4), nitrous oxide (N_2O), perfluorocarbons and hydrofluorocarbons represent the most dangerous from the sustainability point of view, since they are the most widely released into the atmosphere.

In particular, carbon dioxide equivalent expresses the “global warming potential” (GWP) of greenhouse effect. Kyoto gases, tropospheric ozone and black carbon are actively participating to increase the GWP.[155]

The tCO2*e*, *i.e.* tons of CO_2 equivalent, allows expressing the greenhouse effect produced by these gases with reference to the greenhouse effect produced by CO_2, considered equal to 1.
The robust increment of CO_2 emissions, general resource depletion, soil degradation, potentially irreversible climate change and biodiversity loss in flora and fauna, support the urgent need of new technologies to be implemented in order to guarantee a more sustainable future also to pharmaceutical industries.

The need for more sustainable research protocols as well as increased control in the pharmaceutical industry to reduce overall environment impact leads to the emerging importance of "green chemistry" concepts also from a drug discovery standpoint.
Green chemistry is an innovative science that currently represents a crucial point in process chemistry. The objective is the identification of creative synthetic solutions able to minimize the number of steps, replace problematic solvents and reactants and reduce consumption of energy, without significantly raising production costs.
The green chemistry movement started over two decades ago, when the rise of the industrial activities began to generate the first environmental issues.[156]
The term "Green chemistry" has been used for the first time by Cathcar in 1990 in a discussion on the development of the Irish chemical industry.[157] However, only in 1998, when Paul Anastas and John Warner published Theory and Practice (1998), Green Chemistry began to assume the currently known meaning. In particular, Anastas and Warner postulated the 12 Green Chemistry principles, still in use today, that helped to furnish a systematic vision for the new movement.[158]

These principles mostly focus on how to carry out chemical reactions and generate chemical products and to establish a synthetic chemistry in an eco-compatible fashion way.[159] Consequently, use of benign auxiliaries including solvents for reactions and separations, reduced number of steps, minimized wastes and improved atom economy, are crucial points of green chemistry. Figure 21 summarizes the 12 principles of Green Chemistry, according to Anastas and Warner.

Figure 21. The 12 principles of Green Chemistry.[157]

As represented in the Figure 21, these 12 principles are based on the atom and energy economies, as well as on the waste and by-product prevention, the employment of less hazardous chemicals and solvents, and the use of renewable sources. Furthermore, the use of selective catalytic reagents is preferred to the employment of reagents in stoichiometric amounts.

As mentioned in the previous paragraph, the first crucial point in the environmental impact related to chemical industry involves the toxicity of solvents, due to their huge presence and overall volumes in chemical operations.

In chemical manufacture, organic solvents, especially volatile organic compounds (VOCS), are widely used in several operations. VOCS show a high vapor pressure at room temperature and low water solubility, that means they can evaporate under ambient pressure and temperature, representing a huge problem for earth's ecosystems.

Figure 22 shows the relative contributions of materials commonly employed in the production of an active pharmaceutical ingredient (API).[160]

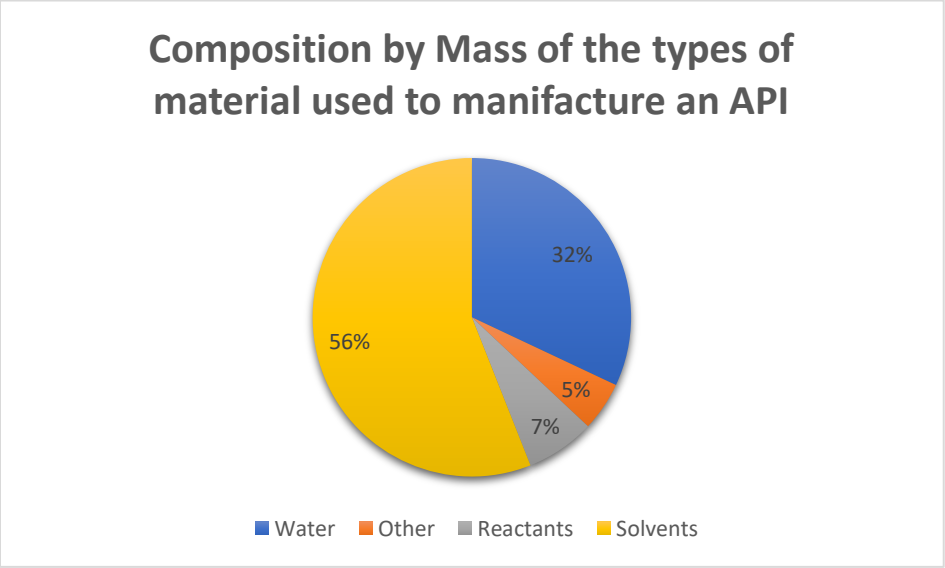

Figure 22. Composition by mass of the types of material used to manufacture an API.[160]

Regarding solvent toxicity, different companies and institutions have published solvent selection guides, in several formats, each of them reflecting the company's way of thinking.[161]

Pfizer was the first company to publish its colour-coded solvent selection guide for pharmaceutical chemists (Table 7).[162]

Table 7. Pfizer selection guide.[162]

Preferred	Usable	Undesirable
Water	Cyclohexane	Pentane
Acetone	Heptane	Hexane(s)
Ethanol	Toluene	Di-isopropyl ether
2-Propanol	Methylcyclohexane	Diethyl ether
1-Propanol	Methyl *t*-butyl ether	Dichloromethane
Ethyl acetate	Isooctane	Dichloroethane
Isopropyl acetate	Acetonitrile	Chloroform
Metahanol	2-Methyl THF	*N*-Methylpyrrolidone
Methyl ethyl ketone	Tetrahydrofuran	Pyridine
1-Butanol	Xylenes	Dimethyl acetate
t-Butanol	Dimethyl sulfoxide	Dioxane
	Acetic acid	Dimethoxyethane
	Ethylene glycol	Benzene
		Carbon tetrachloride

Furthermore, a solvent replacement table has been published for each solvent belonging to the red/undesirable category, in order to replace "undesirable" solvents with. "usable" or "preferred" ones. (Table 8)

Table 8. Solvent replacement table.

Undesirable solvents	Alternative
Pentane	**Heptane**
Hexanes(s)	**Heptane**
Di-isopropyl ether or diethyl ether	**2-MeTHF or *tert*-butyl methyl ether**
Dioxane or dimethoxyethane	**2-MeTHF or *tert*-butyl methyl ether**
Chloroform, dichloroethane or carbon tetrachloride	**Dichloromethane**
Dimethyl formamide, dimethyl acetamide or *N*-methylpyrrolidone	**Acetonitrile**
Pyridine	**Et_3N (if pyridine used as base)**
Dichloromethane (extractions)	**EtOAc, MTBE, toluene, 2-MeTHF**
Dichloromethane (chromatography)	**EtOAc/heptane**
Benzene	**Toluene**

In 2014, Prat *et al.* compared and integrated different guides to develop a comprehensive table including six categories of solvent types: 1) recommended; 2) recommended or problematic; 3) problematic; 4) problematic or hazardous; 5) hazardous; 6) highly hazardous (Table 9).[163]

Table 9. Solvent classification published by Prat *et al.*[163]

Recommended	Water, EtOH, i-PrOH, *n*-BuOH, EtOAc, i-PrOAc, n-BuOAc, anisole, sulfolane.
Recommended or problematic	MeOH, *t*-BuOH, benzyl alcohol, ethylene glycol, acetone, MEK, MIBK, cyclohexanone, MeOAc, AcOH, Ac_2O.
Problematic	Me-THF, heptane, Me-cyclohexane, toluene, xylenes, chlorobenzene, acetonitrile, DMPU, DMSO.
Problematic or hazardous	MTBE, THF, cyclohexane, DCM, formic acid, pyridine.
Hazardous	Diisopropyl ether, 1,4-dioxane, DME, pentane, hexane, DMF, DMAc, NMP, methoxy-ethanol, TEA.
Highly hazardous	Diethyl ether, benzene, chloroform, CCl_4, DCE, nitromethane.

Furthermore, since 1997 Food and Drug Administration (FDA) provides a classification of solvents into three different risk-based classes: class 1, class 2 and class 3, respectively (Table 10).[164]

Table 10. Solvent classification by FDA updated to 2017.[164]

Class 1	Benzene, carbon tetrachloride, 1,2-trichloroethane.

Class 2	Me-THF, Me-cyclohexane, toluene, xylenes, chlorobenzene, acetonitrile, 1,2-dichloroethane, DMSO, cyclohexane, cumene, 1,4-dioxane, ethylene glycol, formamide, methanol, pyridine.
Class 3	Acetone, 1-butanol, ethanol, ethyl acetate, pentane, formic acid.

Solvents belonging to class 1, such as benzene or carbon tetrachloride, should generally be avoided in drug discovery because of their huge toxicity. Class 2 includes solvents like acetonitrile, 1,2-dichloroethane, and hexane, that could instead be tolerated for a limited use in pharmaceutical research. Solvents belonging to class 3, such as acetone, ethyl acetate, are the preferred ones from the sustainable point of view, being less toxic and thus being related to a general lower risk for human health. Of course, it is of utmost importance a careful crosscheck between FDA and CHEM21 classification for a responsible solvent selection.

Besides solvents, the choice of starting materials represents another important point in the context of greener and more sustainable chemistries. Processes can be rendered more sustainable using renewable feedstocks, in form of chemicals derived from biological sources and biopolymers.
The reagent guide is more challenging than the solvent one, being them even more hazardous and causing additional environmental issues. Alfonsi *et al.* tried to develop a rational guide, classifying all the reagents in 6 different zones, based on their features in terms of utility, scalability and greenness. The ideal reagent should work providing good yields, be usable without any kind of issues for scaling up protocol and, finally, be as green as possible.[162]

One of the fundamental of green chemistry is the atom economy. Atom economy is quantification of how many atoms of reactants end up in the final product and how many in by-products or waste. The concept of atom economy was first proposed by Trost in 1991.[165]

Atom economy can be calculated as a percentage of the mass of all atoms in the desired product, divided by the mass of atoms in all reactants.

The greater the % of atom economy in a reaction, the more 'efficient' or 'economic' the process is.

$$Atom\ economy = \frac{Mass\ \ of\ atoms\ in\ desired\ product}{Mass\ of\ atoms\ in\ reactants}\ x\ 100$$

Atom economy does not take into consideration inorganic reagents, solvents and molar excess of reactants. Of course, there are a number of common reaction types inherently atom efficient, like rearrangements, additions, Diels-Alder and other concerted reactions, and other far away from atom economy, like substitutions, eliminations, Wittig and Grignard reactions.

To verify the greenness of a chemical reaction, the Reaction Mass Efficiency (RME) represents a reliable parameter.[166]

$$RME = \frac{Mass\ of\ isolated\ product}{Total\ mass\ of\ reactants}\ x\ 100$$

RME represents an evolution with respect to the atom economy concept, since it also takes into account the yield and the amounts of reactants.

Another important concept in green chemistry metrics is the so-called "E factor" (efficiency factor), proposed for the first time by Roger Sheldon in 1992.[167] It is defined as the ratio of waste produced in a process.

$$E - factor = \frac{1}{RME} - 1$$

It takes into consideration all reagents, solvents, and yields and can be calculated including or not process water.

E-factor plays a crucial role in the chemical industry, and, particularly, in the pharmaceutical sector, being the value of the actual amount of waste produced in a process. Table 11 shows the comparison of typical E-factors for the different types of industries.[168]

Table 11. Typical E-Factors for chemical industry sectors.[168]

Sector	Product tonnage	E-Factor (kg waste per kg product)
Oil refining	10^6-10^8	<0.1
Bulk chemicals	10^4-10^6	<1 to 5
Fine chemicals	10^2-10^4	5 to >50
Pharmaceuticals	10-10^2	25 to >100

Notwithstanding the ideal E-factor is equal to zero, higher E-factors are associated to waste generation during the process and negative environmental impact. Table 11 shows that different kinds of chemical industries impact on waste production and eco-compatibility to different extents, with oil refining being associated to the lower E-factor values, in contrast to the much higher E-factor values found for pharmaceutical industry. The reason for high E-factor in the pharmaceutical sector mainly resides in the high molecular complexity and the huge number of chemical steps involved in the synthesis of APIs.

The process mass intensity (PMI) is quite similar to E-factor, but it is based on 1 kg of API.[169] The ideal PMI is 1 when no waste is produced.

$$PMI = \frac{Mass\ of\ all\ materials\ used\ to\ make\ the\ product}{Mass\ of\ product}$$

The E-factor can be also derived from PMI.

$$E - factor = PMI - 1$$

In line with the green chemistry principles and metrics described so far, a huge number of methodologies, like combinatorial chemistry, the use of supported reagents and solid phase protocols have been increasingly implemented in the drug discovery process.

1.7 Flow chemistry: general setup and potential advantages

Innovative technologies exist to increase process efficiencies and reduce manufacturing footprint; examples are represented by the application to the chemical processes of microwave irradiation,[170] sonication,[171] nanotechnologies[172] and flow chemistry.[173,174]

Flow chemistry, in particular, involves the development of protocols for single chemical reactions or multi-step synthesis whereby reactants are combined in a continuous fashion in segmental flow setups of different scales, allowing for an accurate control of reaction conditions.[175]

The classic batch chemistry displays several advantages including durability, versatility and cost-efficiency; however, it suffers of significant problems related to reaction scale up. This hurdle becomes even more

relevant when dealing with unstable or extremely reactive starting materials or intermediates. In this context, flow chemistry principles and the basic approach of replacing reaction flasks with reactor tubes, increasingly spread among researchers in the field of organic synthesis.[176,177]

Flow chemistry represents an important chance for intertwining safety and efficiency of a given chemical process, to the development of greener and sustainable synthetic protocols.[178]

Nevertheless, the concepts of flow chemistry and green chemistry do not travel necessarily on the same binary. You can have a perfectly green and sustainable reaction in conventional batch mode, as well as a highly toxic reaction in flow. The advantages of flow chemistry have been demonstrated during the years for many active pharmaceutical ingredients (APIs)[179,180], like artemisin[181], imatinib[182], efavirenz[183], pregabalin[184] and so on.

A very recent review by Holtze and Boehling reported on the benefits of continuous flow chemistry when compared to classic batch approaches, discussed from an industrial point of view and considering the entire R&D workflow.[185] Figure 23 shows the proposed guidelines for a careful selection between batch or continuous flow protocols. This helps highlighting all the potential advantages of flow chemistry, although also focusing on the necessity of a careful and thorough assessment of reaction conditions before rashly embarking a flow-based approach.

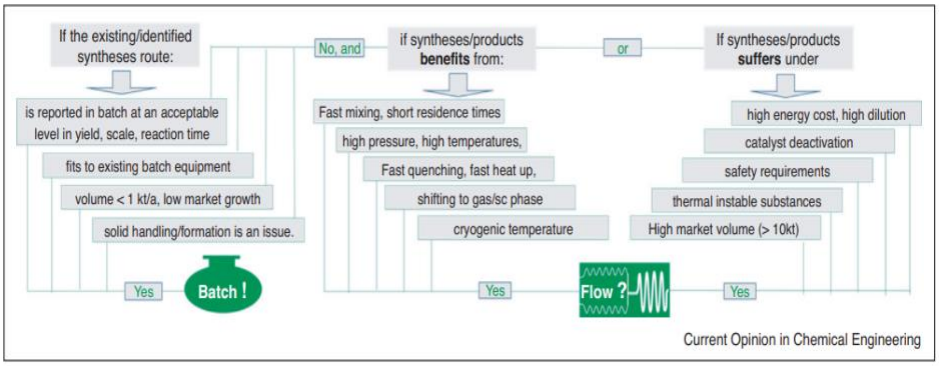

Figure 23. Guideline to select batch or continuous processing.[185]

First of all, to understand how chemical reactions proceed in flow chemistry reactors, residence time is a crucial parameter to be taken into account. Two or more starting materials are pumped in a first extremity of the tube; then, reaction takes places and the resulting products are released from the other end of the tube. The residence time is the total time that the solution spends inside the tube.[186] It could be easy calculated by the following formula:

$$Residence\ time\ = \frac{Reactor\ volume}{Flow\ rate}$$

The residence time represents a crucial point for flow chemical reactions.

Flow processes are generally run in the "microreactors", or' meso-scale' reactors. A typical batch reactor (Figure 24A) is characterized by internal dimensions of 10^4 µm and internal volumes ranging from mL to kL. Microreactors (Figure 24B) are usually characterized by tubes or channel, with a width ranging from 100 µm to 500 µm and internal volumes between µL and mL. The resulting surface area to volume ratio (20,000 m^2/m^3) increase heat and mass transfer, avoiding the resistance often found

in batch. However, mesoscale reactors (Figure 24C) have internal diameter up to 1000 µm and internal diameter up to several mL.[187] The reaction mixture is introduced in the reactors in small, controllable volumes in sequence under rigorously controlled conditions in a confined space.[188]

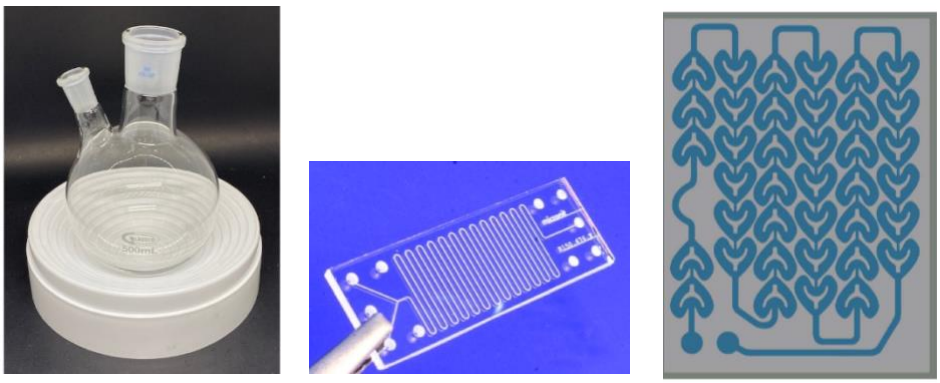

A) B) C)

Figure 24. A) Batch reactor; B) Microreactor; C) Mesoscale reactor.[187]

One of the most important advantages of flow chemistry protocols is represented by the most efficient mixing of reagents, that could reduce the time and increase the yield of the performed reaction. In a classic batch method, the stirring that generates eddies of different sizes, is the predominant mixing process. It could be considered a turbulent and chaotic mixing and lead to inhomogeneities. In flow microreactor, laminar flow is predominant. To understand how mixing proceeds in flow, we can take into consideration a reaction between two starting materials in flow followed by the introduction of scavenger resin or quenching reagent after a residence time of 10 minutes. The time for homogenization needs to be shorter than 10 minutes to guarantee the reaction. If the solution doesn't reach a quick homogenization in flow reactor, the reaction control based

on the kinetics is pointless. The power of flow chemistry is to be sought in the better mixing in the order of milliseconds with respect to seconds in batch reaction.

In addition to the most-efficient mixing, mass transfer is improved in flow reactors due to the small dimensions and the high interfacial surface. Let us to compare a classic liquid-liquid extraction in batch and in flow: while precise and rigorous shaking is needed in batch to improve the mass transfer between aqueous and organic phase, in flow the high internal surface allows rapid and effective mass transfer (Figure 25).[189]

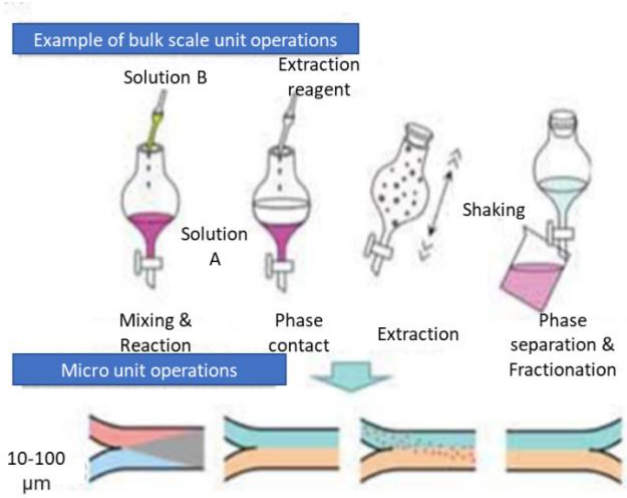

Figure 25. Comparison between the bulk scale operations and micro unit operations.[189]

In line with the improvement of mass transfer, in flow microreactor heat transfer is enhanced due to the high surface-to-volume ratio, particularly when employing steel- or silicon-based materials, due to their high thermal conductivity. Figure 26 shows the comparison between a microreactor (2.5

mL volume) and a batch reactor (630 mL volume). The first one reaches the desired temperature of 250 °C in only one minute; the second one requires 8 minutes to achieve the same temperature.[190]

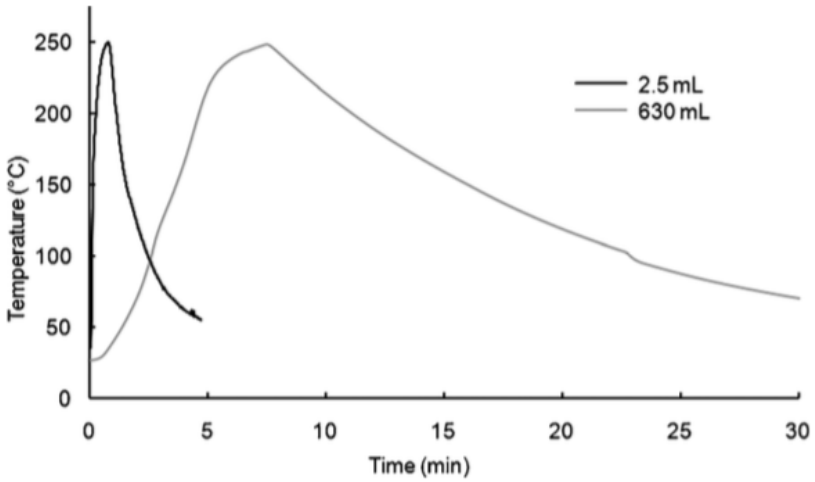

Figure 26. Temperature profile of a microreactor and batch reactor upon heating.[190]

Because of this, application or removal of a heating or cooling source is simpler, thus permitting a very precise temperature control along the microreactor.[190,191]

Flow processes are intrinsically safer with respect to batch counterparts, due to the lower reactor volume. Certainly, 1 mg of hazardous chemical used in flow is safer than 100 mg in batch; the risks are minimized in flow microreactor. In general, all chemicals possess high hazard potential, associated to handling by the researcher as well as their transportation and

site-storage. However, to overcome all these issues, hazarding chemicals could be synthetized *in situ* in a dedicated small reactor that "generate" substances from safe, cheap and benign precursors. Chemical generator concept was developed in Kappe's laboratories for the production of toxic, explosive and short-lived reagents. Figure 27 shows the concept of chemical generator with in-line purification to remove byproducts and with an in-line analysis (PAT: process analytical technologies).[192]

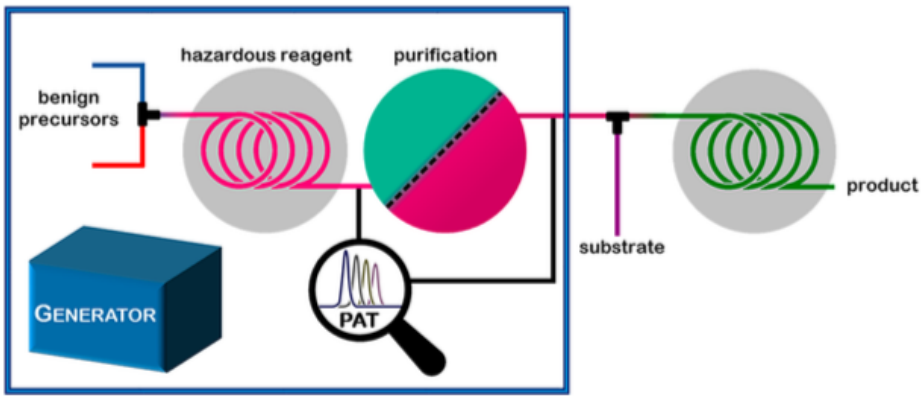

Figure 27. Chemical generator with subsequent in-line purification.[192]

Flow processes can also be used to perform a fast screening of the reaction conditions, and then, with the optimized conditions in hand, scale-up of the reaction can be planned. While the scale up could either require the use of harsh reaction conditions or cause a yield drop in batch, in flow flow chemistry allows the possibility to run the reaction for a longer time to increase product generation, thus minimizing the decrease in performance. Three main strategies can be considered for scaling up flow reaction (Figure 28): i) increase the number of reactors, ii) increase the channel length and iii) increase the channel diameter.[193]

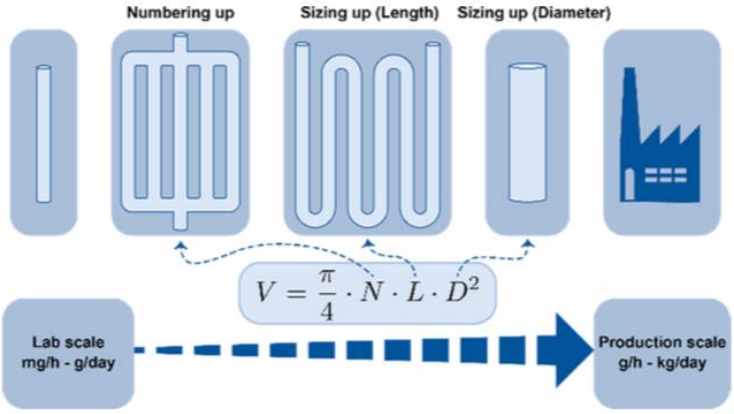

Figure 28. Scale up strategies for a tubular flow reactor.[193]

Having established the advantages that flow chemistry, the next section will analyze in more detail the instrumental part. The term flow chemistry refers nowadays to small laboratory scales as well as industrial settings involving much higher scales.[194-197] Many examples of both kind of application are nicely and comprehensively discussed in several recent reviews. In parallel to the growing interest in flow chemistry, a steadily increasing development of new compact commercial instruments has been registered. Although a basic and cheap homemade setup is in general sufficient for a significant amount of laboratory scale protocols, a huge variety of variations and additions are possible. Figure 29 shows a general scheme for continuous flow setup and figure 30 shows an overview of typical components in a flow set up.[196]

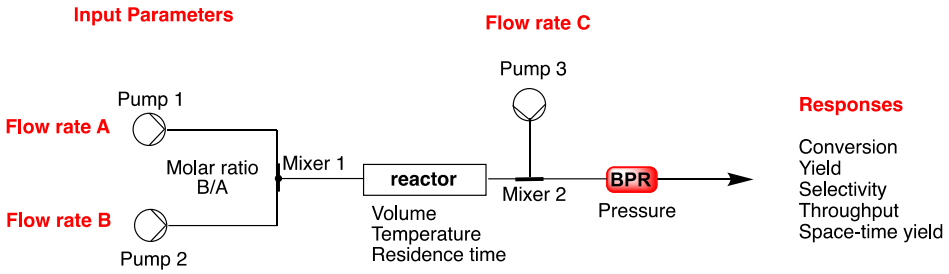

Figure 29. General scheme of continuous flow set up.

Figure 30. Overview of typical components in a flow set up.[196]

One or more pumps like syringe pumps, piston pumps, gear or peristaltic pumps are necessary to flow the reaction mixture into the reactor tubes. The pump should be calibrated before the use and can influence the reaction stoichiometry. The piston pump can overcome the issue of the single syringe pump associated to limited reservoir. Piston pump can be

made out of several materials, such as steel, stainless steel, nickel-molybdenum alloys or ceramics. Piston pumps allow an uninterrupted continuous when connected to a fluid containing reservoir. When the streams containing the starting materials are two or more, a mixer can be added, thus representing the first mixing point. The simplest type of mixer is the classic T-mixer or T-piece, so-called due to its typical "T" shape. However, in case of reactions involving biphasic solutions, this mixer is not the right choice, while structured static mixers or dynamic mixers represent a more suitable option.[194]

The core of flow process is the reactor, where the reactions are carried out.[198,199] The most used reactor types are: chip, coil and packed bed, chosen based on the type of transformation to be carried out (Figure 31).

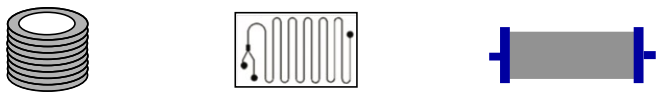

Figure 31. Reactor types for continuous flow chemistry: A) Reactor coil; B) Chip reactor; C) Packed bed reactor.

Chip reactors can be employed in reactions performed at room or low temperature and offer the best heat transfer due to the high surface-to-volume ratios. Based on the material, chip reactors can be used at high temperatures and pressure as well.[200] About the materials choice, silicon, glass or ceramic are the most commonly utilized.[201] Due to the small reactor volumes (1 µL up to several µL), a reaction optimization could be carried out using only a small amount of material. Despite the high surface

area, the researchers normally prefer the coil reactor, because the chip is in general quite expensive and suffers from significant clogging-related drawbacks.[194] he reactor coil consists of a tubing system, made up from polyether ether ketone (PEEK), polytetrafluoro ethylene (PTFE), polyfluoroacetate (PFA), copper, palladium alloys, stainless steel or Hastelloy. When the reaction envisages extreme temperature and pressure conditions (beyond 200 °C and few hundred bars), metal coils is the material of choice, while polymer tubing can be used when strong acidic or basic conditions are required. Coil reactors can also easily undergo shortening or elongation, which is an additional benefit when dealing with precipitation and subsequent clogging issues.[194] When the presence of heterogeneous catalysts or supported reagents is required, the reaction can be handled in packed bed reactors.[202,203] Packed bed consists in external columns or cartridges made up from stainless steel, plastic or glass containing the needed heterogeneous material. This type of reactor is the right choice for liquid-solid, gas-solid or gas-liquid-solid reactions. One of the main advantages of packed beds is the possibility of recycling the catalyst, and that is economical and environmentally-sound.
The last essential piece for a setup is a back pressure regulator (BPR), a one-way valve that allows a precise constant upstream pressure. The use of BPR is mandatory when the reaction produces volatile gaseous reagents or when the chosen temperature of the system is higher than the boiling point of the selected solvent. The selection of BPR is based on the pump properties, the reactor type, flow rate, temperature, and pressure.

Inline, at-line, off-line and on-line monitoring can be added to the basic flow set up (Figure 32).[204,205] Different chemical reactions requires different analytical techniques, like mass spectrometry, flame ion

detection, IR, NMR. The review of Morin *et al.* reported several examples of the process analytical technology (PAT) for real-time monitoring in a continous flow protocol.[206]

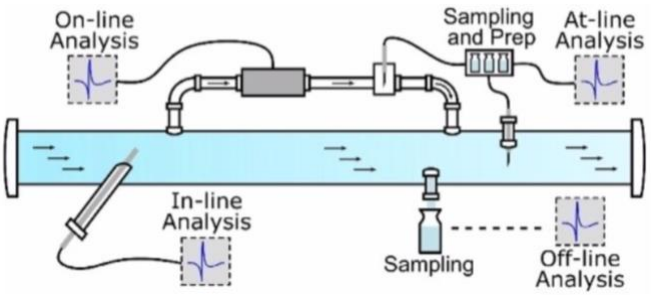

Figure 32. Real-time monitoring in continuous flow.[206]

The aim of continuous flow chemistry is to overcome the challenges and problems associated to classic synthesis in batch. Coupling flow chemistry to enabling fields, like organocatalysis or photochemistry, gives additional advantages to the reaction. The heterogeneous organocatalysis in flow attracted the researchers in the last few years, representing the main tool to creating new chiral bonds, without the use of enzyme and metals, with the possibility to easy regenerate and reuse the supported catalyst. Furthermore, the use of organocatalysis offers environmental advantages, since most of the catalysts can be prepared from renewable sources. [207,208]

Besides organocatalysis, flow chemistry represents also a great advantage in photochemistry, due to better and uniform irradiation and efficient scale up.

One of the most interesting aspect of photochemistry is the use of photons as “traceless and green reagents”, that responds to the principles of green chemistry.

The correct wavelength (λ) of the electromagnetic radiation that is required for the bond to be photocleaved can be calculated according to Planck’s equation reported below. In this equation, E is the energy (J), h is the Planck’s constant, (ν) is the frequency (Hz) and c is the constant of the speed of light (m/s).

$$E = h \cdot \nu = h \cdot \frac{c}{\lambda}$$

Proper and homogeneous irradiation is necessary in order to perform photochemical reactions with high yields and selectivity. The absorbance (A) indicates the right point in which molecules absorb photons of a particular energy. According to the Bouguer-Lambert-Beer Law [90] (see equation below), the molar absorption coefficient (ε), the concentration (c) and the path length of the beam into the sample (l) account for the absorbance. Furthermore, the absorbance (A) is also equal to either the logarithm of initial intensity of the light (I_0) by the intensity of the light after absorbance (I) or the logarithm of 1 divided by the transmittance (T). The transmittance is defined as the ratio of the light that has passed through an object (I) to the incident light (I_0):

$$A = \varepsilon \cdot c \cdot l = \log_{10} \frac{I_0}{I} = \log_{10} \frac{1}{T}$$

Figure 33. Graph showing the distance of light penetration is plotted against the transmittance of light.[209]

By plotting the relationship between absorption and reactor radius, it is possibile to know how the light intensity decreases when the distance increases (Figure 33).[209] In this way, when a reaction is performed in batch, only the external part of the flask is over-irradiated, thus hampering homogeneous irration, and also causing byproduct formation. In order to overcome this problem, but also the issues associated to prolungated times, harsh scale up, high photocatalyst loading, flow microreactors are increasily applied to photochemistry protocols.[210-211]

Indeed, flow chemistry guarantees proper irradiation of the entire solution, because of narrow diameter of tubes, homogeneously penetrable by the light. A higher amount of irradiated molecules can be obtained per time unit, leading to a smaller path length of the beam into the sample.

1.7.1 Flow chemistry applied to privileged scaffolds

As mentioned above, ‘privileged scaffolds’ represents a useful and robust tool for impacting the drug discovery process. Nonetheless the straightforward synthesis and decoration of privileged structures should be supported by new enabling technologies available to synthetic chemists. In particular, new technologies should render more effective the synthesis of large libraries for high-throughput screening protocols, but also the scale-up of key intermediates or active ingredients. More compounds in a shorter time, just like high-speed train containing as many passengers as possible: this is the main goal for medicinal chemists. Of course, as discussed above, flow chemistry approaches can help medicinal chemists to reach this objective, increasing- to use the same metaphor- the speed of the train and the quantity of the passengers inside.

The review by Alfano *et al.* lists and discusses the use of flow chemistry applied to privileged scaffolds.[175] Flow protocols were discussed trying to obtain a unified language for flow setup representations, such to facilitate effective comparison between chemical approaches and chosen technical solutions; the proposed unified representation is shown in Figure 34.

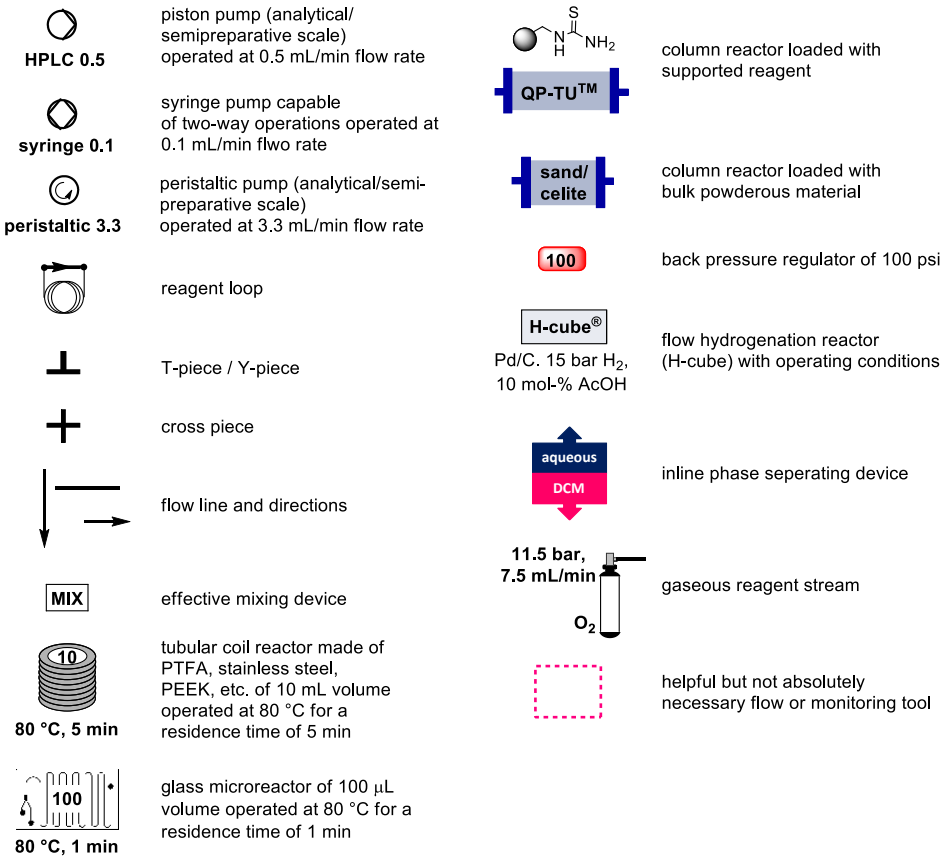

Figure 34. Unified symbol language introduced by Alfano *et al.* for reviewing activities in the field of flow-chemical formation of privileged scaffolds.[175]

Besides our symbol language, Kappe and co-workers in 2021 developed their own reference textbook for setting convention in flow chemistry.[212]

In addition to producing a current picture of the field, another purpose of this review was to encourage researchers to use ‘flow chemistry’ as a potentially useful tool, instead of seeing flow processes just as a nice but complex ornament to synthetic organic chemistry protocols.[213-215]

Selected examples from our review are reported in the present thesis, with a particular focus on those nicely intertwining flow chemistry protocols with greener and more sustainable chemical procedures.[216-217]

In the first example, Kim *et al.*[218] in 2015 developed a library of 9 thioquinazolinones target compounds, starting from *o*-bromophenyl isothiocyanate, with yields ranging from 75% to 98% (Scheme 7). Mixing with *n*-BuLi in a reactor coil at 25 °C, allows the bromine-lithium exchange in THF in only 0.016 seconds, in a kind of flash chemistry way. The subsequent addition of phenyl isocyanate derivatives furnishes the *S*-lithiated thioquinazoline scaffold in only 2.3 seconds and concomitantly plays a quenching reagent role for the aryllithium. The latter compound can be easily alkylated by the addition of different benzyl bromides in 5.9 seconds. The flow synthesis clearly outperformed the batch synthesis: reaction time decreased from 9 hours in batch to few seconds of residence time in the reactor, while the yield increased from 50% in batch to 98% in flow.

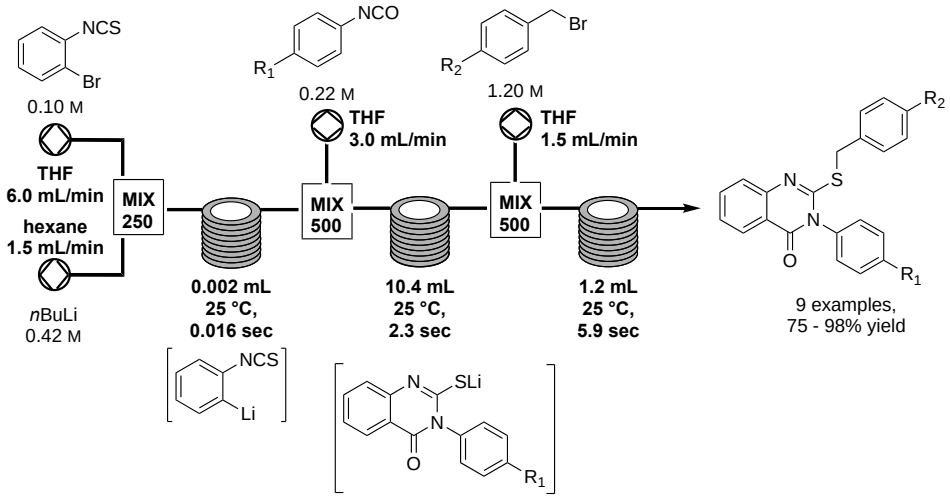

Scheme 7. Thioquinazolinones in flow according to Kim *et al.*[218]

The second example shows the work of Poh *et al.*[219] in 2016, based on the telescoped flow synthesis of pyrazole derivatives involving 4 different steps starting from anilines (Scheme 8). First of all, a solution of aniline in MeCN was mixed in a reactor coil with HCl for 5 min to give the chloride salt. Then, a flow diazotization with *tert-butyl* nitrite and subsequent reduction with L-ascorbic acid as green reducing agent were performed in other 2 reactor coils in 10 min. An in-line ReactIR following the exit of the third reactor, monitored the reactions and controlled the addition of pentan-2,4-dione to achieve the hydrolysis and cyclocondensation. After 28 min of residence time at 140 °C, a library of 13 compounds was obtained, with yields between 13-76%.

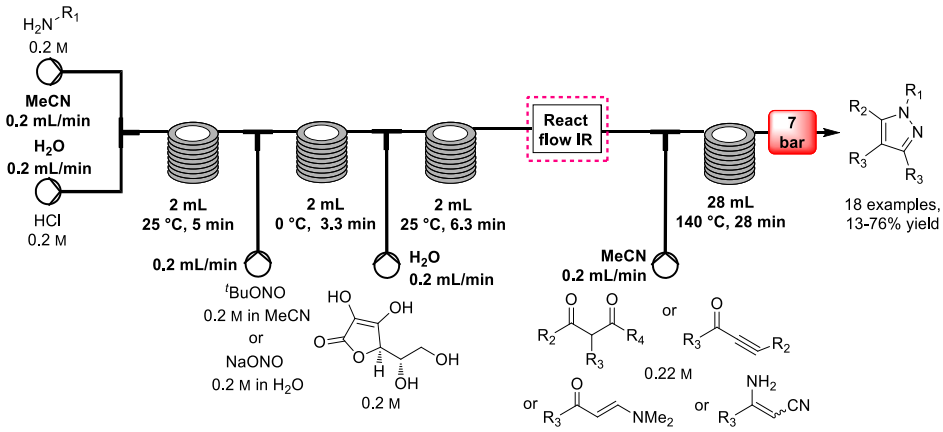

Scheme 8. Telescoped flow process yielding pyrazoles as proposed by Poh *et al.*[219]

Baumann and Baxendale,[220] in 2017, reported the continuous flow synthesis and derivatization of 1,2,4-thiadiazoles, to overcome the batch issues associated with trichloromethanesulfenylchloride that was planned to be used as the reagent (Scheme 9). Two different solutions of hydrated

benzamidine hydrochloride in NaOH and trichloromethanesulfenylchloride in EtOAc, were mixed before the flow entered in a tubular reactor pressurized at 75 psi at room temperature. After only 5 minutes of residence time, the target product 5-chloro-1,2,4-thiadiazole was achieved in 80% in yield. Even though the reaction gave high performance in 5 minutes, hazardous side products could be destroyed only when extending residence time to 30 min. To broaden the scope of 5-chloro-1,2,4-thiadiazoles, the authors added a bromide atom in various positions on the phenyl moiety, replacing the initial hydrate benzamidine hydrochloride with the corresponding bromophenylamidine hydrochloride.

In order to avoid any solubility issues, the first set-up was modified and the aqueous solution of NaOH was added *via* third stream. After 30 min of residence time, three bromo-containing products were obtained in 79-85% yield.

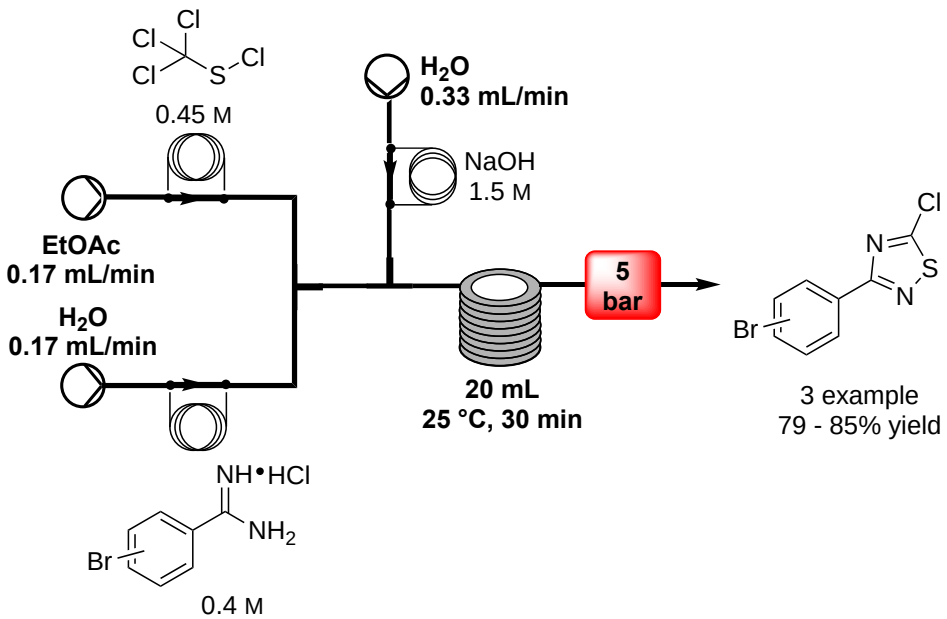

Scheme 9. Flow synthesis of bromo-substituted thiadiazoles according to Baxendale *et al.*[220]

In 2019, Movsisyan *et al.*[221] developed a telescoped flow synthesis aimed at functionalizing the phenothiazine moiety (Scheme 10). Two different solutions of 3-chloropropionyl chloride in DMF and of 10H-phenothiazine in DMF, respectively, were mixed in a reactor coil for 5 min at 100 °C, to give 3-chloro-1-(10H-phenothiazin-10-yl)propan-1-one with 97% conversion. A third stream containing a solution of 4-piperidineethanol in DMF and triethylamine in H_2O/MeOH 1:1 was combined with the first one. After 5 minutes of residence time in a second reactor coil at 100 °C, 3-(4-(2-hydroxyethyl)piperidin-1-yl)-1-(10H-phenothiazin-10-yl) propan-1-one was obtained in 73% yield, without further purification. The flow yield of 73% is higher with respect to the one obtained in batch mode, that is only 31%. Furthermore, the reaction time decreased from 2 days in classic batch mode to 10 min in flow, using temperature of 100 °C, instead of the 130 °C required in batch. Still, in terms of stoichiometry of reactants, equimolar amounts of all starting materials were sufficient to provide in flow the desired phenothiazine product, while the batch protocol required an excess of 3-chloropropionyl chloride (2.4 equivalents) and K_2CO_3 (3.8 equivalents).

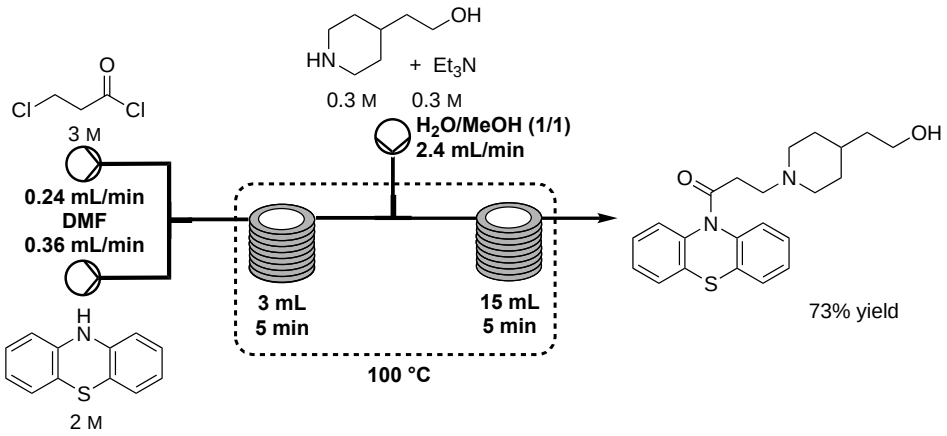

Scheme 10. Proof-of-principle study on phenothiazines in flow by Movsisyan *et al.*[221]

1.8 Indole and indoline-based privileged compounds in flow chemistry: state of art

Among all heterocycles, indoles have always attracted special attention as a privileged scaffold in drug discovery and development. Indole is a planar bicyclic compound, consisting of a six-membered benzene ring fused to a five-membered nitrogen pyrrole ring. Having 10 π-electrons, 8 from double bonds and 2 from nitrogen, indole can be considered an aromatic compound according to Huckel's rule.[222] Regarding the reactivity of the indole system, indoles readily undergo electrophilic substitution reactions as well as benzene ring, due to the delocalization of π-electrons, while they are also prone to undergo nucleophilic substitution on the nitrogen atom.

Several synthetic protocols for indole-based frameworks have been proposed overtime, that could be generally classified in metal-catalyzed and metal-free reactions. Scheme 11 and 12 show the most representative examples.

Synthesis of indoles

Metal catalyzed

A)

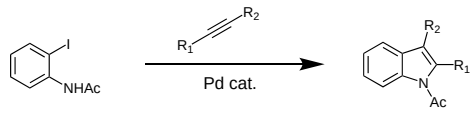

B)

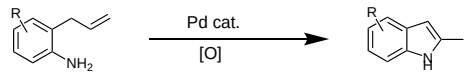

C)

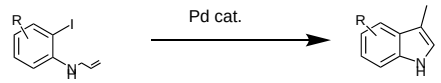

D)

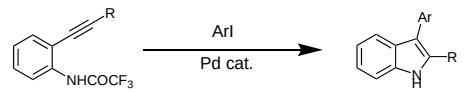

E)

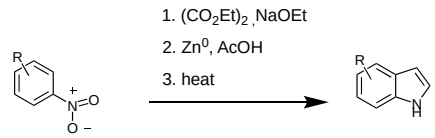

F)

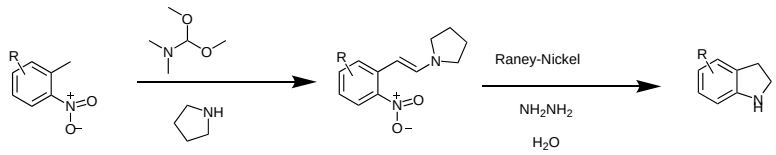

Scheme 11. Metal-catalyzed protocols for the synthesis of indoles. A) Larock reaction;[223] B) Hegedus reaction;[224]. C) Mori-Ban reaction;[225] D) Cacchi reaction;[226] E) Reissert reaction;[227] F) Leimgruber- Batcho reaction;.

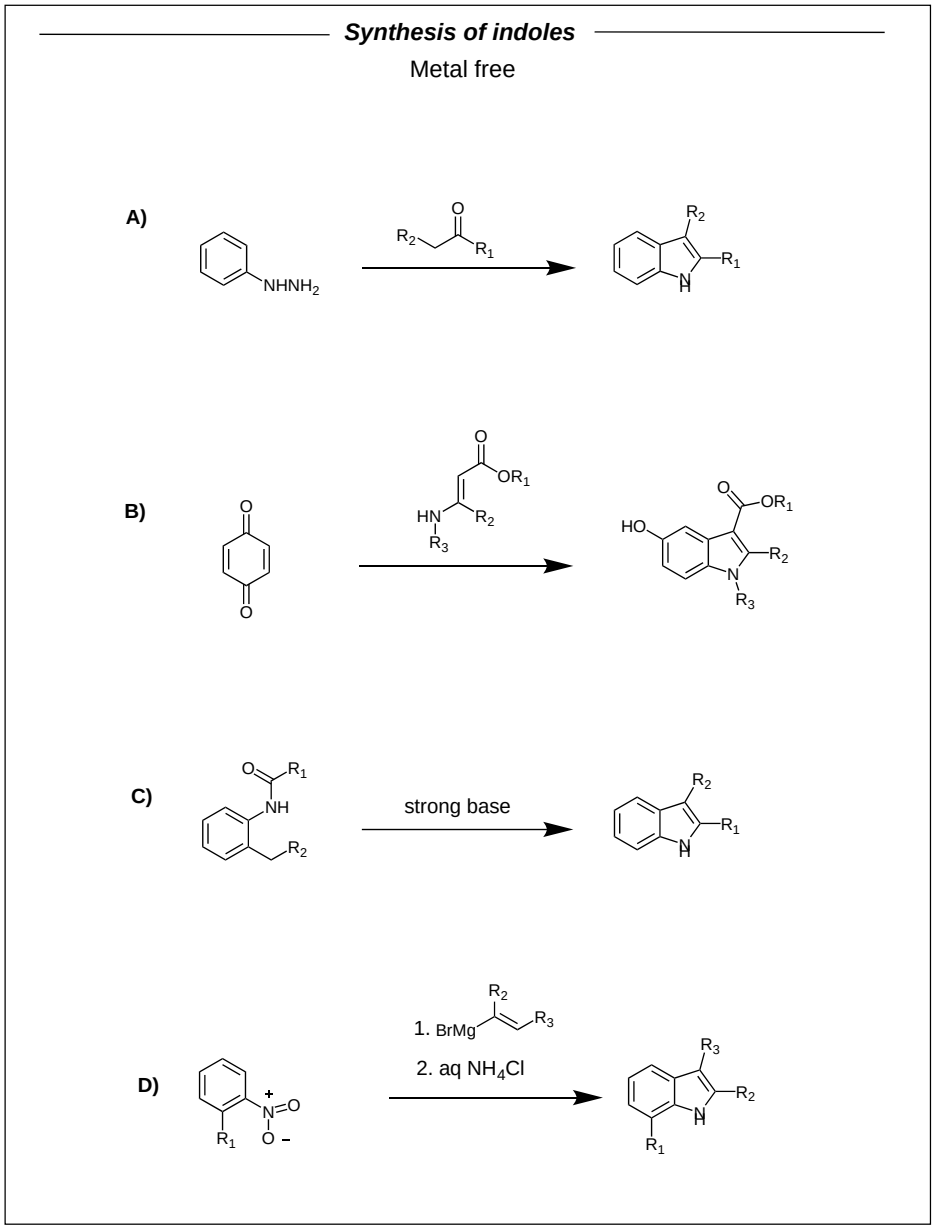

Scheme 12. Metal-free protocols for the synthesis of indoles. A) Fischer reaction;[228] B) Nenitzescu reaction;[229] C) Madelung reaction; [230] D) Bartoli reaction.[231]

Indoles substructures are present in several natural compounds like alkaloids, plants, hormones and so on and interact with different receptors,

like dopamine, serotonin and sigma receptors with high affinity (Figure 35). Indole derivatives have been applied in many human diseases, such as hypertension, HIV, inflammation central nervous system (CNS) diseases, cancers, inflammation and diabetes, to name a few.[232]

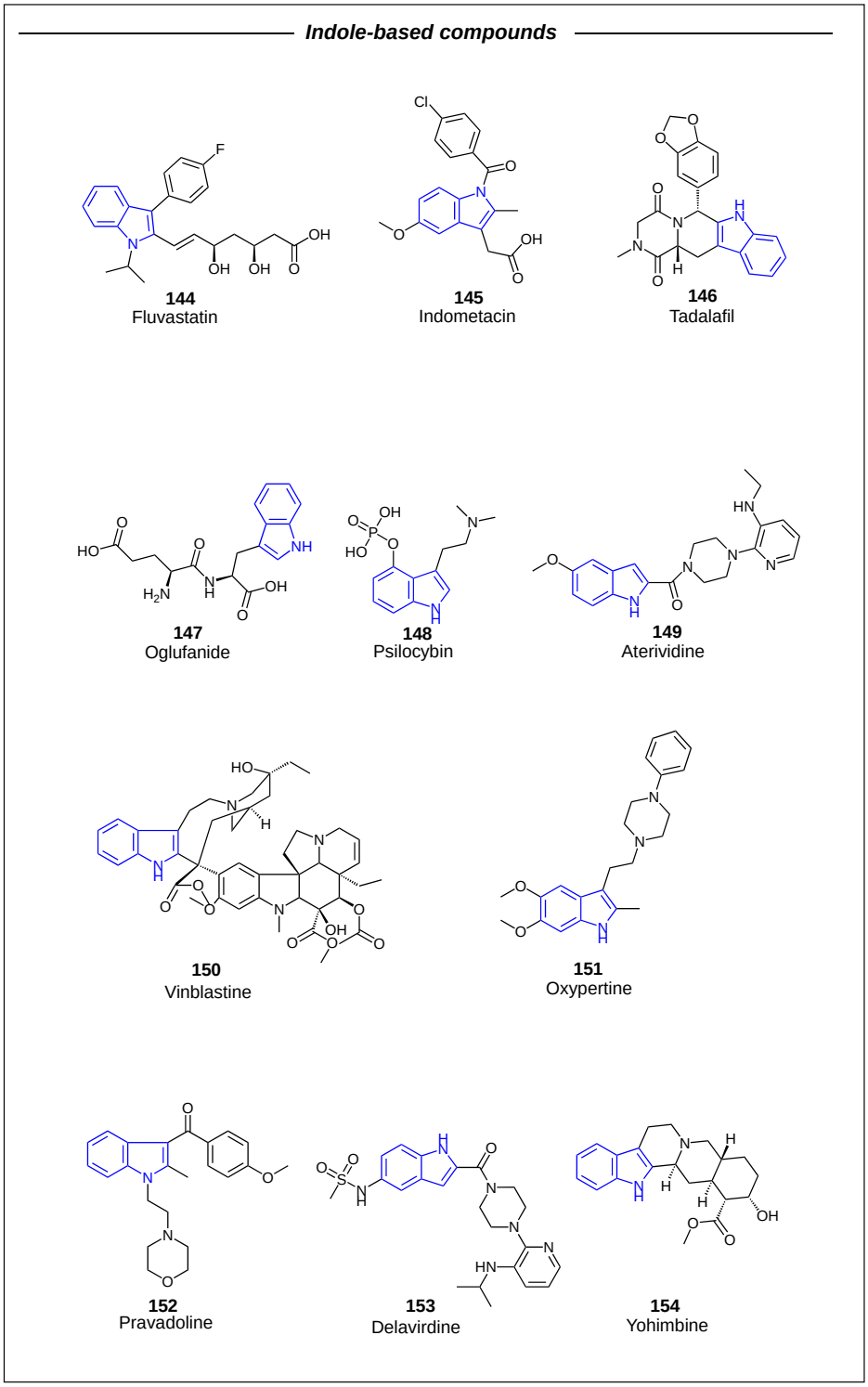

Figure 35. Indole-based compounds.[233]

Most of the flow-based protocols for the synthesis of indoles scaffolds envisage the use of the classical Fischer indole synthesis, discovered in 1883 by Emil Fischer. Starting from substituted or not phenylhydrazines and aldehydes or ketones under acidic conditions, *i.e.* Bronsted acid or Lewis acid, the corresponding indole templates are obtained as final products. Climbing out from Fischer reaction, only a limited number of innovative and differentiating approaches are available. A recent review sums up in more detail the efforts of indole synthesis in flow.[234] A few selected examples are reported below.

In 2010, Watts *et al.*[235] reported two different versions for the flow Fischer indole synthesis (Scheme 13). The first one is entirely carried out in solution mode: phenylhydrazine and the selected ketone were reacted in a reactor coil at 105 °C using acetic acid as the solvent and 10% sulfuric acid (v/v) as the catalyst. Whereas the acetic acid was useful for improving space-time yield, its use in telescoped approaches might represent an issue, due to the harsh conditions required for its elimination between the first and the second step.

The second approach was developed to solve this issue, replacing the acetic acid with ethanol as green solvent and the sulfuric acid with a heterogeneous acidic catalyst, such as Amberlyst IR-120H and decreasing the temperature from 105 °C to 70 °C. A small library of 3 compounds with conversion between 59% and 98% was achieved. No isolated yield was reported in this paper. The comparison between the first and second approach highlights the significant improvement ascribable to the heterogeneous conditions. As an example, one of the generated compounds, *i.e.* 2,3-dimethylindole, was produced at the rate of 17.1 mgh-

[1] through the heterogeneous protocols, in comparison to 8.3 mgh^{-1} generated by the homogeneous counterpart.

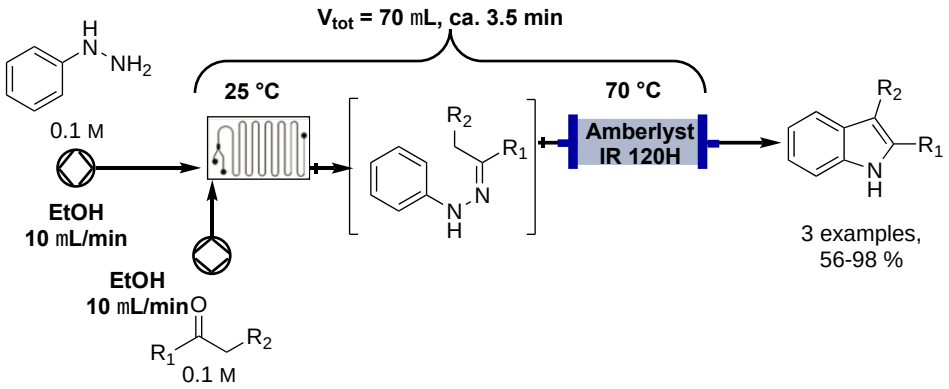

Scheme 13. Fischer indole synthesis in flow as proposed by Watts *et al.*[235]

Kappe *et al.*[236] applied in 2013 the flow Fischer indole synthesis to 7-ethyltryptophol (7-ET). In only 3 minutes 41% of 7-ET was obtained, mixing in a reactor coil at 150 °C phenylhydrazine hydrochloride and 2,3-dihydrofuran using MeOH/H_2O 2/1.

Another Fischer indole synthesis in flow was published by Yu *et al.*[237] in 2017. After the initial optimization in batch, the authors found the best conditions to achieve 3-methylindole in flow, using the ionic liquid (IL) 1-ethyl-3- methylimidazolium tetrafluoroborate ([emim]TFB) as solvent. Two solutions in the IL of phenylhydrazine and propanal respectively, were flowed in the first reactor coil heated to 60 °C, before reacting them with a solution of $ZnCl_2$ as Lewis acid catalyst in IL, added *via* a third incoming stream, in the second reactor coil at 200 °C. The final product

was obtained with 80% yield after dilution with water and work up with toluene.

Moving out from Fischer indole synthesis, in 2011, Colombo *et al.*[238] reported the Reissert indole synthesis in flow.
In only 8 minutes, the reduction of *o*-nitrophenylpyruvate is achieved to give the final product ethyl-1*H*-indole-2-carboxylate in 93% yield, using continuous flow hydrogenation. The same reaction in batch needs 7 hours affording the product in 88% yield, under the same temperature and pressure flow conditions (20 °C and 1 bar). It should, however, be pointed out the lower quantity of Pd/C (5%) used I batch, with respect to 10% Pd/C used with H-cube cartridges. A library of 9 compounds was synthetized with yields between 41% and 96%.

A Hemetsberger-Knittel synthesis in flow of indoles was published by Jones in 2013.[239] Flowing a solution of azidocinnamates in xylene as solvent though a glass chip at 165° C, a small library of 4 compounds was achieved with yields between 41% and 96%. The residence time is decreased by a factor 12 with respect to the same reaction in batch.

Kappe[240] and co-workers in 2017 developed a Cadogan- Sundberg type synthesis converting 16 *o*-vinilynitrobenzene derivatives into the correspondent indoles in only 15-30 minutes, with yields between 40% and 90%. The reaction involves the use of carbon monoxide to reduce *in situ* palladium (II) catalyst to palladium (0).

Baumann *et al.*[220] in 2017 applied the continuous flow to the synthesis of an auxin mimic-based herbicide 5-(6-(trifluoromethyl)-1*H*-indol-3-yl)-

1,3,4-oxadiazol- 2(3*H*)-one. A solution of 2-chloro-4-trifluoronitrobenzene and ethyl cyanoformate in DCM was reacted with a solution of 1,1,3,3-tetramethylguanidine in the first reactor coil at 50 °C. A subsequent glass chip reactor with an aqueous solution of HCl was added at the end of reactor coil to achieve the quenching. The isolation and the evaporation of the solvent of the crude product after in line work up gave the product ethyl 2-cyano-2-(2-nitro-4-(trifluoromethyl)phenyl)acetate with yield around 95%. Diluting in EtOH, the product was thus subjected to a reductive cyclisation with H-Cube (Pd/C and AcOH). After the isolation and the consequent re-dilution in THF, the latter compound was mixed with a hydrazine in THF and pumped in the second reactor coil at 100 °C before mixing, *via* additional stream, with 1,1′-carbonyldiimidazole (CDI) in THF or triphosgene in $CHCl_3$. The third and last reactor coil at 55 °C allowed the formation of oxadiazole in 3 position of indole with 82% or 91% yield (in case of the use of CDI or triphosgene respectively), after quenching through a cartridge filled with quadrapure-sulfonic acid (QP-SA) or polymeric *N*,*N*-di-methylbenzylamine (QP-DMA). The use of heterogeneous work up with polymer-supported scavengers could be a potential limitation since they must be efficiently regenerated, in order to avoid the generation of useless chemical waste.

Crifar *et al.*[241] in 2019 reported the continuous flow synthesis of indole through the Heumann reaction. A DMF solution of aniline and methyl bromoacetate was introduced into a tubular reactor at 110° C to quantitatively generate *N*-arylglycinate in only 90 minutes. The crude of the reaction underwent hydrolysis of the ester using NaOH in MeOH at 60 °C in 15 minutes, thus providing the free *N*-arylglycine quantitatively after

purification and isolation through an off-line work up. The Heumann cyclisation with acetic anhydride and triethylamine in EtOAc at 130 °C gave the product in 15 minutes. The overall yield of six desired products was higher in flow with respect to the batch counterpart in a shorter time. As a representative example, 1-acetyl-3-(but-3-enyl)indole, was obtained in flow with 90% yield over three steps in 135 minutes. The batch protocol for the same compound provided a 42% yield over three steps in 18 hours.

Among indole derivatives, indolines deserves a special role, especially due to their striking importance as privileged scaffolds in pharmaceutical chemistry, due to their ability to bind different biological targets. Accordingly, indoline-based compounds display anti-inflammatory, anti-cancer, anti-oxidant, antimicrobial and anti-obesity agents activity among others.

Different methods in batch have been developed for the synthesis of indolenine, as schematically shown, in scheme 8.

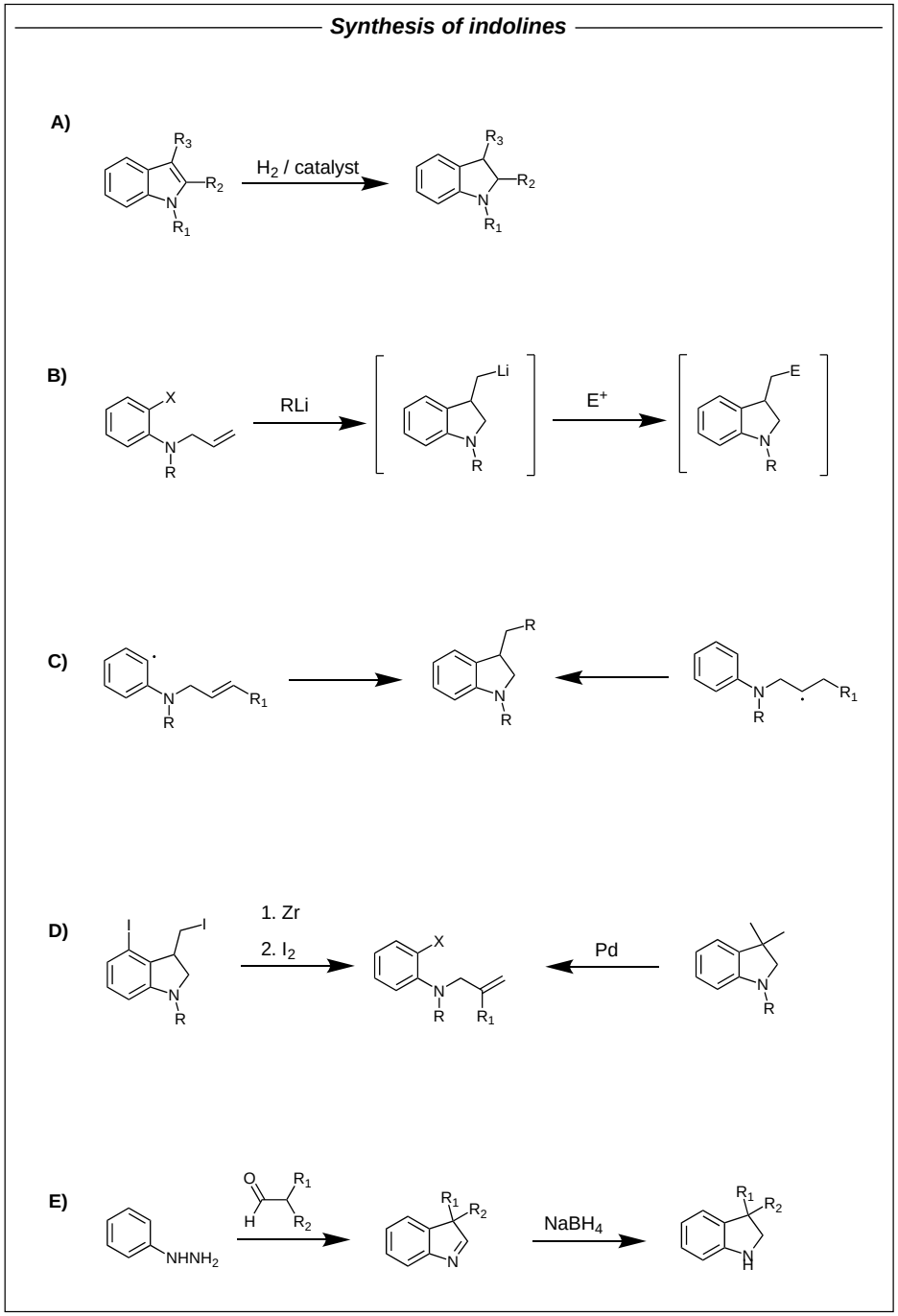

Scheme 14. Selected examples for indoline synthesis.

A) reduction of indoles; B) anionic cyclization; C) radical cyclization D) metal-mediated intramolecular cyclizations; E) interrupted Fischer reaction.

Indoline synthesis presents several issues, including the harsh reaction conditions for the reduction of *N*-unprotected indoles and chemical instability when employing the unsaturated indolenine precursors as synthetic intermediates.

In 2017, Örkényi *et al.*[242] developed the synthesis of indoline derivatives through the use of continuous flow chemistry. An H-cube filled with palladium catalyst on aluminum oxide, allowed the initial reductive cyclisation and *N*-alkylation reactions, using an excess of methanesulfonic acid as the catalyst and acetic acid as the solvent at an exercise temperature of 50 °C. The subsequent *N*-alkylation step with 7 equiv. of 1,2-dibromomethane and DIPEA provided the product with 95% conversion and 91% selectivity in less than 45 min. The productivity in flow was overall 200 times higher than in batch on the same scale.
A photochemical telescoped approach to synthetized *N*-diaminoalkylated 3-arylmethylene-2,3-dihydro-1*H*-isoindolin-1-ones was published by Oelgemöller *et al.*[243] in 2019 (Scheme 15). In a capillary photoreactor, *N*-(bromoalkyl) phthalimides and arylacetate were reacted for 30 min to achieve photodecarboxylation, before mixing with aqueous sulfuric acid, added *via* third stream, to generate dehydration in another coil immersed in an ultrasonic bath. The flow-born passed through a column packed with strongly basic Dowex 1-X8 ion exchange resin, in order to quench the excess of acid before adding the amine, *via* additional stream, to carry out

the final nucleophilic substitution in a reactor at 80 °C. A library of 5 examples was achieved with yield of 73-77%.

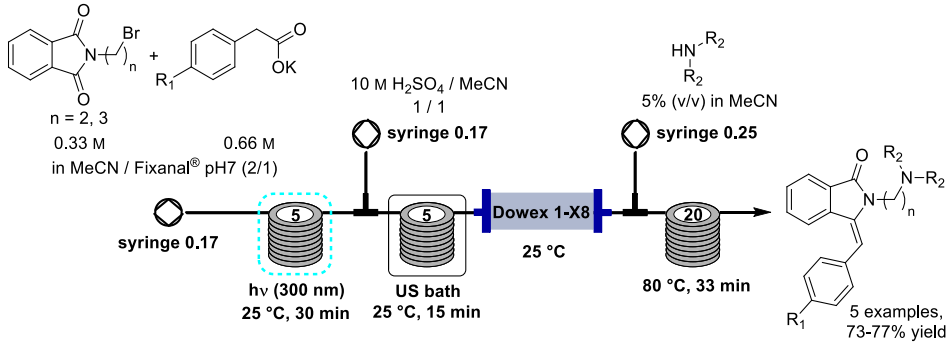

Scheme 15. Flow photosynthesis of isoindolinones as presented by Oelgemöller *et al.* [243]

1.9 Peptidomimetics in flow chemistry: state of art

The importance of peptidomimetic structures highlighted in the previous paragraph, justifies the growing research efforts in elaborating efficient strategies for their synthesis. However, most of the recent strategies for the synthesis of peptidomimetic templates are characterized by poor efficiency and high number of steps and, most importantly, the concomitant generation of considerable amount of waste. Therefore, no valid sustainable protocols for their synthesis are currently available in the chemists' toolbox.[243,244]

Intertwining flow-based approaches with the synthesis of peptidomimetics could represent an attractive perspective towards greener and more

sustainable approaches, despite the few examples so far reported. Some of the most relevant examples are shown in the Table 12.

Table 12. Peptidomimetics in flow.

Entry	Starting compound(s)	Coupling reagent(s) / catalysts	Targeted structural scope	Reactor
1[245]	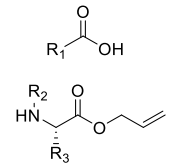	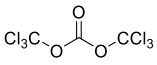 DIPEA	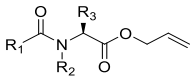	
2[a 246]	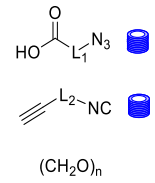	---	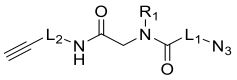	
3[247]	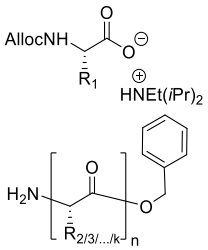	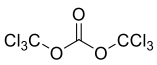 DMA	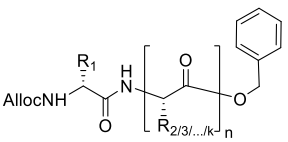	
4[248]	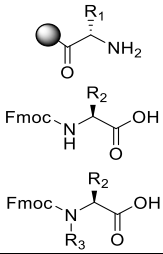	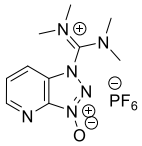 DIEA	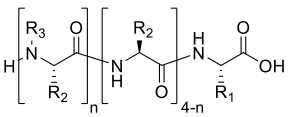	

[a] Small blue reactor symbols close to substances indicate their in-situ generation during the protocol.

Fuse *et al.*[245] reported in 2014 the rapid generation of peptidomimetics starting from various carboxylic acids and amines, employing triphosgene and DIPEA (Table 10, Entry 1). In just few seconds, two compounds were synthetized with 74% and 98% yield, with the further benefit of suppressing the epimerization events.

In the following year, 2015, Kappe and his research group[246] developed the method for the generation of peptoids through the use of isocyanide-based multicomponent reactions (MCR) (Table 10, Entry 2). Peptoids, belonging to class B according to Grossman, are oligomers of N-substituted glycines and contain the side chain connected to nitrogen of the peptide backbone instead of being connected to the α-carbon. Starting from amines, oxo building blocks, isocyanides and azides, a library of 8 linear peptoids was realized in telescoped flow mode in only 25 min, without requiring the isolation or purification of intermediates and with yields ranging between 80 and 95%. Due to the smell and the high reactivity of isocyanides precursors and the chemical risk associated to the use of azides, those two building blocks were prepared *in situ* via an upstream protocol. Furthermore, the reactor effluent gave 8 linear peptoides underwent subsequent macrocyclization step *via* copper catalyzed cycloadditions, to provide cyclic peptoids with yields ranging between 71% and 91% after purification.

Fuse and collaborators, in 2016, applied their foregoing work[247] to the total synthesis of oligopeptide containing non-proteinogenic amino acids, like 4-hydroxyphenylglycine (Hpg) and 3,5-dihydroxyphenylglycine (Dpg): feglymycin (Table 10, Entry 3). These unnatural aminoacids are pretty

susceptible to racemization; thus, the application of flow chemistry can help overcoming, or at least reducing, this issue due to the very short residence time.

In 2018, Fülöp[248] and co-workers, reported the sustainable flow synthesis of mono- and multiple-N-methylated peptides in solid phase, based on their previous work (Table 10, Entry 4). A reaction between Fmoc-protected amino acids, HATU as the coupling reagent, DIPEA in a column packed with Tentagel resin-bound alanine tetrapeptide, followed by deprotection step, provided the desired products. Due to the high yields obtained for the generation of 4 *N*-methylated oligoalanines, (>92%), the same method was tested on difficult sequences, including oligovalines; gratifyingly, also in this case final yields were comparable to those obtained with oligoalanines. This approach allowed the generation of the target compounds with limited solvent consumptions (only 4 mL of solvents used with respect to 66 mL in the batch counterpart), and significantly reduced reaction times (28 minutes against the 3 hours in the literature-reported batch method).

References

(1) F.Cramer *Pharm. Acta Helv.* **1995**, *69*, 193.
(2) Strebhardt, K.; Ullrich, A. *Nat. Rev. Cancer* **2008**, *8*, 473.
(3) Schwartz, R. S. *N Engl J Med* **2004**, *350*, 1079.
(4) Csermely, P.; Palotai, R.; Nussinov, R. *TIBS* **2010**, *35*, 539.
(5) Fink, T.; Bruggesser, H.; Reymond, J. L. *Angew. Chem. Int Ed. Engl.* **2005**, *44*, 1504.
(6) Lee, A. CL.; Harris, J. L.; Khanna, K. K.; Hong, *JH Int J Mol Sci.* **2019**, *20*, 2383.
(7) Reymond, J. L.; van Deursen, R.; Blum, L. C.; Ruddigkeit, L. *MedChemComm* **2010**, *1*, 30.
(8) Lipinski, C.; Hopkins, A. *Nature* **2004**, *432*, 855.
(9) Lipinski, C. A.; Lombardo, F.; Dominy, B. W.; Feeney, P. *Adv. Drug. Deliv. Rev.* **2001**, *46*, 3.
(10) Murcko, A. A. M.; Walters, W. P. *J. Med. Chem.* **1998**, *41*, 3314.
(11) Wang, J.; Ramnarayan, K. *J. Comb. Chem.* **1999**, *1*, 524.
(12) Walters, W. P.; Murcko, A. M. A. *Curr. Opin. Chem. Biol.* **1999**, *3*, 384.
(13) Lipinski, C. A. *J. Pharmacol. Toxicol Methods* **2000**, *44*, 235.
(14) Muegge, I.; Heald, S. L.; Brittelli, D. *J. Med. Chem.* **2001**, *44*, 1841.
(15) Veber, D. F.; Johnson, S. R.; Cheng, H. Y.; Smith, B. R.; Ward, K. W.; Kopple, K. D. *J. Med. Chem.* **2002**, *45*, 2615.
(16) Proudfoot, J. R. *Bioorg. Med. Chem. Lett.* **2002**, *12*, 1647.
(17) Walters, W. P.; Murcko, M. A. *Adv. Drug. Deliv. Rev.* **2002**, *54*, 255.
(18) Egan, W. J.; Walters, W. P.; Murcko, M. A. *Curr. Opin. Drug Discov. Devel.* **2002**, *5*, 540.
(19) Doak, B. C.; Kihlberg, J. *Expert Opin. Drug Discov.* **2017**, *12*, 115.
(20) Bohm, H. J.; Flohr, A.; Stahl, M. *Drug Discov. Today Technol.* **2004**, *1*, 217.
(21) Duarte, C. D.; Barreiro, E. J.; Fraga, C. A. *Mini Rev. Med. Chem.* **2007**, *7*, 1108.
(22) Taylor, R. D.; MacCoss, M.; Lawson, A. D. *J. Med. Chem.* **2014**, *57*, 5845.
(23) Bräse, S. **2015**.
(24) Rotella, D. P. *Adv. Heterocycl. Chem*, **2021**, 134, 149-183.
(25) Welsch, M. E.; Synder, S. A.; Stockwell, B. R. *Curr. Opin. Chem. Biol.*, **2010**, 14, 3, 347-361.
(26) Tajabadi, F. M.; Campitelli, M. R.; Quinn, R. J. *Springer Sci. Rev.* **2013**, *1*, 141.

(27) Kombo, D. C.; Tallapragada, K.; Jain, R.; Chewning, J.; Mazurov, A. A.; Speake, J. D.; Hauser, T. A.; Toler, S. *J. Chem. Inf. Model.* **2013**, *53*, 327.
(28) https://lifechemicals.com/screening-libraries/%20fragment-libraries, accessed November 14th 2022.
(29) Wei, W.; Cherukupalli, S.; Jing, L.; Liu, X.; Zhan, P. *Drug Discov.* **2020**, *25*, 1839.
(30) Talele, T. T. *J. Med. Chem.* **2020**, *63*, 13291.
(31) https://iupac.org, accessed November 14th 2022.
(32) Hiesinger, K.; Dar'in, D.; Proschak, E.; Krasavin, M. *J. Med. Chem.* **2021**, *64*, 150.
(33) Garthwaite, S. M.; McMahon, E. G. *Mol. Cell. Endocrinol.* **2004**, *217*, 27.
(34) Reilly, S. W.; Griffin, S.; Taylor, M.; Sahlholm, K.; Weng, C. C.; Xu, K.; Jacome, D. A.; Luedtke, R. R.; Mach, R. H. *J. Med. Chem.* **2017**, *60*, 9905.
(35) Harada, K.; Mizukami, J.; Kadowaki, S.; Matsuda, I.; Watanabe, T.; Oe, Y.; Kodama, Y.; Aoki, K.; Suwa, K.; Fukuda, S.; Yata, S.; Inaba, T. Bioorg. Med. Chem. Lett. **2018**, *28*, 1228−1233.
(36) Sampson, P. B.; Liu, Y.; Patel, N. K.; Feher, M.; Forrest, B.; Li, S. W.; Edwards, L.; Laufer, R.; Lang, Y.; Ban, F.; Awrey, D. E.; Mao, G.; Plotnikova, O.; Leung, G.; Hodgson, R.; Mason, J. M.; Wei, X.; Kiarash, R.; Green, E.; Qiu, W.; Chirgadze, N. Y.; Mak, T. W.; Pan, G.; Pauls, H. W. *J. Med. Chem.* **2015**, *58*, 130.
(37) Pettus, L. H.; Andrews, K. L.; Booker, S. K.; Chen, J.; Cee, V. J.; Chavez, F.; Chen, Y.; Eastwood, H.; Guerrero, N.; Herberich, B.; Hickman, D.; Lanman, B. A.; Laszlo, J.; Lee, M. R.; Lipford, J. R.; Mattson, B.; Mohr, C.; Nguyen, Y.; Norman, M. H.; Powers, D.; Reed, A. B.; Rex, K.; Sastri, C.; Tamayo, N.; Wang, P.; Winston, J. T.; Wu, B.; Wu, T.; Wurz, R. P.; Xu, Y.; Zhou, Y.; Tasker, A. S.; Wang, H.-L. *J. Med. Chem.* **2016**, *59*, 6407−6430.
(38) Dadashpour, S; Emami, S *Eur. J. Med. Chem*., **2018**, 150, 9–29.
(39) Thakur, A.; Singh, A.; Kaur, N.; Ojha, R.; Nepali, K. *Bioorg. Chem*., **2020**, *94*, 103436.
(40) Shirai, F.; Tsumura, T.; Yashiroda, Y.; Yuki, H.; Niwa, H.; Sato, S.; Chikada, T.; Koda, Y.; Washizuka, K.; Yoshimoto, N.; Abe, M.; Onuki, T.; Mazaki, Y.; Hirama, C.; Fukami, T.; Watanabe, H.; Honma, T.; Umehara, T.; Shirouzu, M.; Okue, M.; Kano, Y.; Watanabe, T.; Kitamura, K.; Shitara, E.; Muramatsu, Y.; Yoshida, H.; Mizutani, A.; Seimiya, H.; Yoshida, M.; Koyama, H. *J. Med. Chem*. **2019**, *62*, 3407.
(41) Welsch, M. E.; Snyder, S. A.; Stockwell, B. R. *Curr. Opin. Chem. Biol.* **2010**, *14*, 347.

(42) Bariwal, J.; Voskressensky, L. G.; Van der Eycken, E. V. *Chem. Soc. Rev.* **2018**, *47*, 3831.
(43) Liu, K. G.; Robichaud, A. J.; Lo, J. R.; Mattes, J. F.; Cai, Y. *Org. Lett.* **2006**, *8*, 5769.
(44) Mizuno, A.; Matsui, K.; Shuto, S. *Chem.* **2017**, *23*, 14394.
(45) Li Petri, G.; Di Martino, S.; De Rosa, M. *J. Med. Chem.* **2022**, *65*, 7438.
(46) Lenci, E.; Trabocchi, A. *Chem. Soc. Rev.* **2020**, *49*, 3262.
(47) Wang, L.; Wang, N.; Zhang, W.; Cheng, X.; Yan, Z.; Shao, G.; Wang, X.; Wang, R.; Fu, C. *Signal Transduct Target Ther* **2022**, *7*, 48.
(48) Fosgerau, K.; Hoffmann, T. *Drug Discov.* **2015**, *20*, 122.
(49) Lewis, G. F.; Brubaker, P. L. *J. Clin. Invest.* **2021**, *131*.
(50) Werner, H. M.; Cabalteja, C. C.; Horne, W. S. *ChemBioChem* **2016**, *17*, 712.
(51) Van Regenmortel, M. H. *Biologicals* **2001**, *29*, 209.
(52) Pelay-Gimeno, M.; Glas, A.; Koch, O.; Grossmann, T. N. *Angew. Chem. Int. Ed. Engl.* **2015**, *54*, 8896.
(53) Marshall, G. R. *Tetrahedron* **1993**, *49*, 3547.
(54) Abdildinova, A.; Kurth, M. J.; Gong, Y. D. *Asian J. Org. Chem.* **2021**, *10*, 2300.
(55) Merrifield, R. B. *Adv. Enzymol Relat. Areas Mol. Biol.* **1969**, *32*, 221.
(56) https://www.fda.gov/drugs/development-approval-process-drugs accessed November 14th 2022.
(57) Eliel, E. L.; Wilen, S. H. *Stereochemistry of Organic Compounds*, 1994.
(58) Fleming, F. F.; Yao, L.; Ravikumar, P. C.; Funk, L.; Shook, B. C. *J. Med. Chem.* **2010**, *53*, 7902.
(59) Strecker, A. *Justus Liebigs Annalen der Chemie* **1850**, *75*, 27.
(60) Grundke, C.; Vierengel, N.; Opatz, T. *Chem. Rec.* **2020**, *20*, 989.
(61) Enders, D.; Shilvock, J. P. *Chem. Soc. Rev.* **2000**, *29*, 359.
(62) Williams, R. M.; Hendrix, J. A. *Chem. Rev.* **1992**, *92*, 889.
(63) Enders, D.; Amaya, S. A.; Pierre, F. *NJC*, *23*, 261.
(64) Maldonado, L.; Stork, G. *J. Am. Chem. Soc.* **1971**, *93*, 5286.
(65) Orejarena Pacheco, J. C.; Lipp, A.; Nauth, A. M.; Acke, F.; Dietz, J. P.; Opatz, T. *Chemistry* **2016**, *22*, 5409.
(66) Groger, H. *Chem. Rev.* **2003**, *103*, 2795.
(67) Rommelmann, P.; Betke, T.; Gröger, H. *Org. Process Res. Dev.* **2017**, *21*, 1521.
(68) Opatz, T.; Ferenc, D. *Org. Lett.* **2006**, *8*, 4473.
(69) Lorenz, J. C.; Busacca, C. A.; Feng, X.; Grinberg, N.; Haddad, N.; Johnson, J.; Kapadia, S.; Lee, H.; Saha, A.; Sarvestani, M.; Spinelli, E. M.;

Varsolona, R.; Wei, X.; Zeng, X.; Senanayake, C. H. .*J Org. Chem.* **2010**, *75*, 1155.
(70) Endo, A.; Yanagisawa, A.; Abe, M.; Tohma, S.; Kan, T.; Fukuyama, T. *J. Am. Chem. Soc.* **2002**, *124*, 6552.
(71) Lebold, T. P.; Wood, J. L.; Deitch, J.; Lodewyk, M. W.; Tantillo, D. J.; Sarpong, R. *Nat. Chem.* **2013**, *5*, 126.
(72) Arai, T.; Takahashi, K.; Ishiguro, K.; Yazawa, K. *J Antibiot (Tokyo)* **1980**, *33*, 951.
(73) Dong, W.; Liu, W.; Liao, X.; Guan, B.; Chen, S.; Liu, Z. *J Org. Chem.* **2011**, *76*, 5363.
(74) Martinez, E. J.; Owa, T.; Schreiber, S. L.; Corey, E. J. *Proc Natl Acad Sci U S A* **1999**, *96*, 3496.
(75) Cuevas, C.; Perez, M.; Martin, M. J.; Chicharro, J. L.; Fernandez-Rivas, C.; Flores, M.; Francesch, A.; Gallego, P.; Zarzuelo, M.; de La Calle, F.; Garcia, J.; Polanco, C.; Rodriguez, I.; Manzanares, I. *Org. Lett.* **2000**, *2*, 2545.
(76) He, H.; Tran, P.; Yin, H.; Smith, H.; Batard, Y.; Wang, L.; Einolf, H.; Gu, H.; Mangold, J. B.; Fischer, V.; Howard, D. *Drug. Metab. Dispos.* **2009**, *37*, 536.
(77) Juillerat-Jeanneret, L. *J Med Chem* **2014**, *57*, 2197.
(78) Li, C. S.; Deschenes, D.; Desmarais, S.; Falgueyret, J. P.; Gauthier, J. Y.; Kimmel, D. B.; Leger, S.; Masse, F.; McGrath, M. E.; McKay, D. J.; Percival, M. D.; Riendeau, D.; Rodan, S. B.; Therien, M.; Truong, V. L.; Wesolowski, G.; Zamboni, R.; Black, W. C. *Bioorg Med Chem Lett* **2006**, *16*, 1985.
(79) Goncalves, P.; Peeraer, A.; Adriaenssens, Y.; Zonnekein, L.; Franck, P.; Maes, B. U. W.; Augustyns, K.; Van Der Veken, P. *ACS Omega* **2021**, *6*, 1328.
(80) Masamba, W. *Molecules* **2021**, *26*.
(81) Ashe, K.; Fernàndez-Garcìa, C.; Corpinot, M. K.; Coggins, A. J.; Bučar, DK.; Powner, M. P. *Communications Chemistry* **2019**, *2*.
(82) Cleaves, H. J.; Chalmers, J. H.; Lazcano, A.; Miller, S. L.; Bada, J. L. *Orig Life Evol Biosph* **2008**, *38*, 105.
(83) Parker, E. T.; Zhou, M.; Burton, A. S.; Glavin, D. P.; Dworkin, J. P.; Krishnamurthy, R.; Fernandez, F. M.; Bada, J. L. *Angew Chem Int Ed Engl* **2014**, *53*, 8132.
(84) Fukuyama, T.; Yang, L.; Ajeck, K. L.; Sachleben, R. *Journal of the American Chemical Society* **1990,** *112*, 9, 3712-3713.
(85) Dong, W.; Liu, W.; Liao, X.; Guan, B.; Chen, S.; Liu, Z. *J Org Chem* **2011,** *76*, 13, 5363-5368.
(86) Martinez, E. J.; Owa, T.; Schreiber, S. L.; Corey, E. J. *Proc Natl Acad Sci U S A* **1999,** *96*, 7, 3496-3501.

(87) Miyazawa, T. *Amino Acids* **1999**, *16*, 191.
(88) Harada, K. *Nature* **1963**, *200*, 1201.
(89) Stout, D. M.; Black, L. A.; Matier, W. L. *Journal of Organic Chemistry* **1983**, *48*, 5369.
(90) Iyer, M. S.; Gigstad, K. M.; Namdev, N. D.; Lipton, M. *Amino Acids* **1996**, *11*, 259.
(91) Wang, J.; Liu, X.; Feng, X. *Chem Rev* **2011**, *111*, 6947.
(92) Ahrendt, K. A.; Borths, C. J.; MacMillan, D. W. C. *J. Am. Chem. Soc.* **2000**, *122*, 4243.
(93) Antenucci, A.; Dughera, S.; Renzi, P. *ChemSusChem* **2021**, *14*, 2785.
(94) Abbasov, M. E.; Romo, D. *Nat. Prod. Rep*., **2014**, *31*, 1318-1327.
(95) Bugaut, X.; Glorius, F. *Chem Soc Rev* **2012**, *41*, 3511.
(96) Grossmann, A.; Enders, D. *Angew Chem Int Ed Engl* **2012**, *51*, 314.
(97) Mondal, S.; Yetra, S. R.; Mukherjee, S.; Biju, A. T. *Acc Chem Res* **2019**, *52*, 425.
(98) Guo, H.; Fan, Y. C.; Sun, Z.; Wu, Y.; Kwon, O. *Chem Rev* **2018**, *118*, 10049.
(99) Wei, Y.; Shi, M. *Chem Rev* **2013**, *113*, 6659.
(100) Narayanaperumal, S.; Rivera, D. G.; Silva, R. C.; Paixao, M. W. *Chemcatchem* **2013**, *5*, 2756.
(100) Fang, X.; Wang, C. J. *Chem Commun (Camb)* **2015**, *51*, 1185.
(101) Ivancova, I.; Pohl, R.; Hubalek, M.; Hocek, M. *Angew. Chem. Int. Ed. Engl* **2019**, *58*, 13345.
(102) Eichelbaum, M. *Toxicology in Transition*, **1995**, *17*, 514-21.
(103) Seki, M.; Mori, Y.; Hatsuda, M.; Yamada, S. *J. Org. Chem.* **2002**, *67*, 5527.
(104) Ishikawa, H.; Suzuki, T.; Hayashi, Y. *Angew Chem Int Ed Engl* **2009**, *48*, 1304.
(105) Han, B.; He, X. H.; Liu, Y. Q.; He, G.; Peng, C.; Li, J. L. *Chem. Soc. Rev.* **2021**, *50*, 1522.
(106) Chen, C.; Oelschlaeger, P.; Wang, D.; Xu, H.; Wang, Q.; Wang, C.; Zhao, A.; Yang, K. W. *J. Med. Chem.* **2022**, *65*, 5954.
(107) King, D. T.; Strynadka, N. C. *Future Med. Chem.* **2013**, *5*, 1243.
(108) Donowitz, G. R.; Mandell, G. L. *N Engl J Med* **1988**, *318*, 419-426.
(109) Zaman, S. B.; Hussain, M. A.; Nye, R.; Mehta, V.; Mamun, K. T.; Hossain, N. *Cureus* **2017**, *9*, e1403.
(110) Rawson, T. M.; Moore, L. S. P.; Zhu, N.; Ranganathan, N.; Skolimowska, K.; Gilchrist, M.; Satta, G.; Cooke, G.; Holmes, A. *Clin. Infect. Dis.* **2020**, *71*, 2459.
(111) Gupta, V. *Expert Opin. Investig. Drugs* **2008**, *17*, 131.

(112) Ambler, R. P.; Coulson, A. F.; Frere, J. M.; Ghuysen, J. M.; Joris, B.; Forsman, M.; Levesque, R. C.; Tiraby, G.; Waley, S. G. *Biochem. J* **1991**, *276*, 269.
(113) Crowder, M. W.; Spencer, J.; Vila, A. J. *Acc. Chem. Res.* **2006**, *39*, 721.
(114) Nordmann, P.; Poirel, L. *Clin. Infect. Dis.* **2019**, *69*, S521.
(115) Diene, S. M.; Rolain, J. M. *Clin. Microbiol. Infect.* **2014**, *20*, 831.
(116) Queenan, A. M.; Bush, K. *Clin. Microbiol. Rev.* **2007**, *20*, 440.
(117) Jeon, J. H.; Lee, J. H.; Lee, J. J.; Park, K. S.; Karim, A. M.; Lee, C. R.; Jeong, B. C.; Lee, S. H. *Int. J. Mol. Sci.* **2015**, *16*, 9654.
(118) Hammoudi Halat, D.; Ayoub Moubareck, C. *Antibiotics (Basel)* **2020**, *9*.
(119) Nordmann, P.; Gniadkowski, M.; Giske, C. G.; Poirel, L.; Woodford, N.; Miriagou, V.; European Network on, C. *Clin. Microbiol. Infect.* **2012**, *18*, 432.
(120) Boyd, S. E.; Livermore, D. M.; Hooper, D. C.; Hope, W. W. *Antimicrob. Agents. Chemother.* **2020**, *64*.
(121) Evans, B. A.; Amyes, S. G. *Clin. Microbiol. Rev.* **2014**, *27*, 241.
(122) Ghuysen, J. M. *Annu Rev Microbiol* **1991**, *45*, 37.
(123) Hou, C. D.; Liu, J. W.; Collyer, C.; Mitic, N.; Pedroso, M. M.; Schenk, G.; Ollis, D. L. *Sci Rep* **2017**, *7*, 40357.
(124) Daumann, L. J.; Schenk, G.; Gahan, L. R. *Eur JIC,* **2014**, *2014*, 18, 2869-2885.
(125) Chen, A. Y.; Thomas, P. W.; Stewart, A. C.; Bergstrom, A.; Cheng, Z.; Miller, C.; Bethel, C. R.; Marshall, S. H.; Credille, C. V.; Riley, C. L.; Page, R. C.; Bonomo, R. A.; Crowder, M. W.; Tierney, D. L.; Fast, W.; Cohen, S. M. *J Med Chem* **2017**, *60*, 7267.
(126) Walsh, T. R.; Toleman, M. A.; Poirel, L.; Nordmann, P. *Clin Microbiol Rev* **2005**, *18*, 306.
(127) Dalhoff, A. *Infection* **2021**, *49*, 569.
(128) Palica, K.; Voracova, M.; Skagseth, S.; Andersson Rasmussen, A.; Allander, L.; Hubert, M.; Sandegren, L.; Schroder Leiros, H. K.; Andersson, H.; Erdelyi, M. *ACS Omega* **2022**, *7*, 4550.
(129) Linciano, P.; Cendron, L.; Gianquinto, E.; Spyrakis, F.; Tondi, D. *ACS Infect. Dis.* **2019**, *5*, 9.
(130) Wu, S.; Xu, D.; Guo, H. *J. Am. Chem. Soc.* **2010**, *132*, 17986.
(131) Drawz, S. M.; Bonomo, R. A. *Clin. Microbiol. Rev.* **2010**, *23*, 160.
(132) Nagulapalli Venkata, K. C.; Ellebrecht, M.; Tripathi, S. K. *Eur J. Med. Chem.* **2021**, *225*, 113747.
(133) Tehrani, K.; Bruchle, N. C.; Wade, N.; Mashayekhi, V.; Pesce, D.; van Haren, M. J.; Martin, N. I. *ACS Infect. Dis.* **2020**, *6*, 1366.

(134) Ma, G.; Wang, S.; Wu, K.; Zhang, W.; Ahmad, A.; Hao, Q.; Lei, X.; Zhang, H. *Bioorg. Med. Chem.* **2021**, *29*, 115902.
(135) Everett, M.; Sprynski, N.; Coelho, A.; Castandet, J.; Bayet, M.; Bougnon, J.; Lozano, C.; Davies, D. T.; Leiris, S.; Zalacain, M.; Morrissey, I.; Magnet, S.; Holden, K.; Warn, P.; De Luca, F.; Docquier, J. D.; Lemonnier, M. *Antimicrob. Agents Chemother.* **2018**, *62*.
(136) Fullington, S.; Cheng, Z.; Thomas, C.; Miller, C.; Yang, K.; Ju, L. C.; Bergstrom, A.; Shurina, B. A.; Bretz, S. L.; Page, R. C.; Tierney, D. L.; Crowder, M. W. *J Biol. Inorg. Chem.* **2020**, *25*, 717.
(137) Payne, D. J.; Bateson, J. H.; Gasson, B. C.; Proctor, D.; Khushi, T.; Farmer, T. H.; Tolson, D. A.; Bell, D.; Skett, P. W.; Marshall, A. C.; Reid, R.; Ghosez, L.; Combret, Y.; Marchand-Brynaert, J. *Antimicrob. Agents Chemother.* **1997**, *41*, 135.
(138) Christopeit, T.; Yang, K. W.; Yang, S. K.; Leiros, H. K. *Acta Crystallogr F Struct Biol Commun* **2016**, *72*, 813.
(139) Yan, Y. H.; Chen, J.; Zhan, Z.; Yu, Z. J.; Li, G.; Guo, L.; Li, G. B.; Wu, Y.; Zheng, Y. *RSC Adv* **2020**, *10*, 31377.
(140) Tsivkovski, R.; Totrov, M.; Lomovskaya, O. *Antimicrob. Agents Chemother* **2020**, *64*.
(141) Chiou, J.; Wan, S.; Chan, K. F.; So, P. K.; He, D.; Chan, E. W.; Chan, T. H.; Wong, K. Y.; Tao, J.; Chen, S. *Chem. Commun. (Camb)* **2015**, *51*, 9543.
(142) Chen, C.; Yang, K. W. *Eur. J. Med. Chem.* **2020**, *203*, 112573.
(143) Palacios, A. R.; Mojica, M. F.; Giannini, E.; Taracila, M. A.; Bethel, C. R.; Alzari, P. M.; Otero, L. H.; Klinke, S.; Llarrull, L. I.; Bonomo, R. A.; Vila, A. J. *Antimicrob. Agents Chemother.* **2019**, *63*.
(144) King, A. M.; Reid-Yu, S. A.; Wang, W.; King, D. T.; De Pascale, G.; Strynadka, N. C.; Walsh, T. R.; Coombes, B. K.; Wright, G. D. *Nature* **2014**, *510*, 503.
(145) Jorgensen, W. L. *Science* **2004**, *303*, 1813.
(146) Parvathaneni, V.; Kulkarni, N. S.; Muth, A.; Gupta, V. *Drug Discov.* **2019**, *24*, 2076.
(147) Szymanski, P.; Markowicz, M.; Mikiciuk-Olasik, E. *Int. J. Mol. Sci.* **2012**, *13*, 427.
(148) Jaseem, M.; Kumar, P.; John, R. M. *The pharma innovation* **2017**, *6 (3)*, 158.
(149) Pratyusha K; Gaikwad, N. M.; Phatak, A.; Chaudhari, P.D. *Int. J Pharm. Sci. Rev. Res* **2012**, *16 (2)*, 121.
(150) Ngwuluka, N. C.; Ochekpe, N.; Odumosu, O.P. *AJB* **2011**, 11259.
(151) L. Wang, Y. H., H. Lo, and C. Yapijakis, Eds. **2004**.
(152) Pandey, D.; Agrawal, M.; Pandey, J. S. *Environ. Monit. Assess.* **2011**, *178*, 135.

(153) Belkhir, L.; Elmeligi, A. *J. Clean. Prod.* **2019**, *214*, 185.
(154) Wackernagel, M.; Rees, W. *Electron. Green J.* **1997**.
(155) Kerr, R. A. *Science* **2007**, *318*, 1230.
(156) de Marco, B. A.; Rechelo, B. S.; Totoli, E. G.; Kogawa, A. C.; Salgado, H. R. N. *SPJ* **2019**, *27*, 1.
(157) Cathcart, C. *SCI* **1990**, 684.
(158) Anastas, P. T.; Warner, J.C. *Green Chemistry: Theory and Practice.* ; Oxford University Press, New York, 1998.
(159) Tobiszewski, M.; Marc, M.; Galuszka, A.; Namiesnik, J. *Molecules* **2015**, *20*, 10928.
(160) Henderson, R. K.; Jimènez-Gonzàlez, C.; Constable, D. J. C.; Alston, S. R.; Inglis, G. G. A.; Fisher, G.; Sherwood, J.; Binks, S. P.; Curzons, A. D. *Green chem.* **2011**, *13*, 854.
(161) Curzons, A. D.; Constable, D. C.; Cunningham, V. L. *Clean Products and Processes* **1999**, *1*, 82.
(162) Alfonsi, K.; Colberg, J.; Dunn, P. J.; Fevig, T.; Jennings, S.; Johnson, T. A.; Kleine, H. P.; Knight, C.; Nagy, M. A.; Perry, D. A.; Stefaniak, M. *Green chem.* **2007**, *10*, 31.
(163) Prat, D.; Hayler, J.; Wells, A. *Green Chem.* **2014**, *16*, 4546.
(164) https://www.fda.gov accessed November 14th 2022.
(165) Trost, B. M. *Science* **1991**, *254*, 1471.
(166) Dicks, A. P.; Hent, A. *Atom Economy and Reaction Mass Efficiency*, 2014.
(167) Sheldon, R. A. *Green chem.* **2007**, *9*, 1273.
(168) Dunn, P. J. *Chem. Soc. Rev.* **2012**, *41*, 1452.
(169) Galema, S. A. *Chem. Soc. Rev.* **1997**, *26*, 233.
(170) Martinez, R. F.; Cravotto, G.; Cintas, P. *J Org Chem* **2021**, *86*, 13833.
(171) Whitesides, G. M. *Small* **2004**, *1*, 172.
(172) Plutschack, M. B.; Pieber, B.; Gilmore, K.; Seeberger, P. H. *Chem Rev* **2017**, *117*, 11796.
(173) Gérardy, R.; Emmanuel, N.; Toupy, T.; Kassin, V. E.; Tshibalonza, N. N.; Schmitz, M.; Monbaliu, JC. M. *EurJOC* **2018**, *2018*, 2101.
(174) Guidi, M.; Seeberger, P. H.; Gilmore, K. *Chem. Soc. Rev* **2020**, *49*, 8910-8932.
(175) Alfano, A.I.; Brindisi, M.; Lange, H. *Green chem* **2021**, *23*, 2233.
(176) Jensen, K. F. *AlChE Journal* **2017**, *63*, 858-869.
(177) Ley, S. V. *Chem Rec* **2012**, *12*, 378.
(178) Jiménez-González, C.; Poechlauer, P.; Broxterman, Q. B.; BS Yang, BS.; Ende, D.; Baird, J.; Bertsch, C.; Hannah, R. E.; Dell'Orco, P.; Noorman, H.; Yee, S.;Reintjens, R.; Wells, A.; Massonneau, V.; Manley, J.; *Org. Process Res. Dev.* **2011**, *15*, 900.

(179) Gautmann, B.; Cantillo, D.; Kappe, C. O. *Angew Chem Int Ed Engl.* **2015**, *54*, 6688-6728.
(180) Chen, Y.; Monbaliu, JC. M *Flow and Microreactor Technology in Medicinal Chemistry*, **2022**.
(181) Lèvesque, F.; Seeberger, P. H. *Angew Chem Int Ed Engl.* **2012**, *51*, 1706-1709.
(182) Hopkin, M. D.; Baxendale, I. R.; Ley, S. V. *Chem Commun.* **2010**, *46*, 2450-2452.
(183) Cooreia, C. A.; Gilmore, K.; McQuade, D. T.; Seeberger, P. H. *Angew Chem Int Ed Engl.* **2015**, *54*, 4945-4948.
(184) Ghislieri, D.; Gilmore, K.; Seeberger, P. H. *Angew Chem Int Ed Engl* **2014**, *54*, 678-682.
(185) Holtze, C.; Boehling, R. *Curr Opin Chem Eng*, **2022**, *36*, 100798.
(186) Mandity, I. M.; Otvos, S. B.; Fulop, F. *ChemistryOpen* **2015**, *4*, 212-223.
(187) Monbaliu, JC. M.; Emmanuel, N.; Gérardy, R.; *Chimie Nouvelle*: **2016**, 122, 18.
(188) Porta, R.; Benaglia, M.; Puglisi, A. *Org. Process Res. Dev.* **2016**, *20*, 2.
(189) Mawatari, K.; Kazoe, Y.; Aota, A.; Tsukahara, T.; Sato, K.; Kitamori, T. *J. Flow Chem.* **2011**, *1*, 3–12.
(190) Glasnov, T. N.; Kappe, C. O. *Chem Eur J*. **2011**, *17*, 11956-11968.
(191) Razzaq, T.; Kappe, C. O. *Chem Asian J* **2010**, *5*, 1274.
(192) Dallinger, D.; Gutmann, B.; Kappe, C. O. *Acc. Chem. Res*. **2020**, *53*, 1330−1341
(193) Buglioni, L.; Raymenants, F.; Slattery, A.; Zondag, S. D. A.; Noël, Timothy *Chem. Rev*. **2022**, *122*, 2752−2906.
(194) Plutschak, M. B.; Pieber, B.; Gilmore, K.; Seeberger, P. H. *Chem Rev*. **2017**,*117*,11796–11893.
(195) Movsisyan, M.; Delbeke, E. I. P.; Berton, J. K. E. T.; Battilocchio, C.; Ley, S. V. *Chem. Soc. Rev*. **2016**, *45*, 83–117.
(196) Britton, J.; Raston, C. L. *Chem. Soc. Rev*. **2017**, *46*, 1250–127.
(197) Gambacorta, G.; Sharley, J. S.; Baxendale, I. R. *Beilstein J Org Chem*. **2021**, *17*, 1181–1312.
(198) Wiles, C.; Watts, P. *Green chem*. **2011**, *14*, 38.
(199) Fanelli, F.; Parisi, G.; Degennaro, L.; Luisi, R. *Beilstein J. Org. Chem.* **2017**, *13*, 520.
(200) Jensen, K. F.; Reizman, B. J.; Newman, S. G. *Lab Chip* **2014**, *14*, 3206.
(201) Cambie, D.; Bottecchia, C.; Straathof, N. J.; Hessel, V.; Noel, T. *Chem Rev* **2016**, *116*, 10276.

(202) Frost, C. G.; Mutton, L. *Green chem.* **2010**, *12*, 1687.
(203) Munirathinam, R.; Huskens J.; Verboom, W. *Adv. Synth. Catal.* **2015**, *357*, 1093.
(204) Yoshida, J.; Kim, H.; Nagaki, A. *ChemSusChem* **2011**, *4*, 331.
(205) Vaccaro, L.; Lanari, D.; Marrocchi, A.; Strappaveccia, G. *Green Chem.* **2014**, *16*, 3680.
(206) Morin, M. A.; Zhang, W.; Mallik, D.; Organ, M. G. *Angew Chem Int Ed Engl*, **2021**, 60, 20606-20626.
(207) MacMillan, D. W. C. *Nature*, **2008**, 455, 304-308.
(208) De Risi, C.; Bortolini, O.; Brandolese, A.; Di Carmine, G.; Ragno, D.; Massi, A**.** *React. Chem. Eng.*, **2020**, *5*, 1017-1052.
(209) Mayerhofer, T. G.; Pahlow, S.; Popp, J. *Chemphyschem* **2020**, *21*, 2029.
(210) Cambie, D.; Bottecchia, C.; Straathof, N. J.; Hessel, V.; Noel, T. *Chem Rev* **2016**, *116*, 10276.
(211) Knowles, J. P.; Elliott, L. D.; Booker-Milburn, K. I. *Beilstein J Org Chem* **2012**, *8*, 2025.
(212) Hone, C. A.; Kappe, C. O. *Chemistry Methods*, **2021**, *1*, 11, 454-467.
(213) Garlets, Z. J.; Nguyen, J. D.; Stephenson, C. R. *Isr J Chem* **2014**, *54*, 351.
(214) Su, Y.; Straathof, N. J.; Hessel, V.; Noel, T. *Chemistry* **2014**, *20*, 10562
(215) Hartman, R. L. *Curr Opin Chem Eng*, **2020**, 29, 42-50.
(216) Wiles, C.; Watts, P. *Future Med. Chem*, **2009**, 1.
(217) Bogdan**,** A. R.; Dombrowski, A. W. *J. Med. Chem.* **2019**, 62, 14, 6422–6468.
(218) Kim, H.; Lee, H. J.; Kim, D. P. *Angew. Chem. Int. Ed Eng.l* **2015**, *54*, 1877.
(219) Poh, J. S.; Browne, D. L.; Ley, S. V. *React. Chem. Eng.* **2016**, *1*, 101.
(220) Baumann, M.; Baxendale, I. R. *Bioorg. Med. Chem.* **2017**, *25*, 6218.
(221) Movsisyan, M.; De Coen, L. M.; Heugebaert, T. S. A.; Verlee, A.; Roman, B. I.; Stevens, C. V. *Eur JOC* **2019**, 1350.
(222) Sravanthi, T. V.; Manju, S. L. *Eur J Pharm Sci* **2016**, *91*, 1.
(223) Larock, R. C.; Yum, E. K. *J. Am. Chem. Soc.* **1991**, *113*, 6689.
(224) Hegedus, L. S.; Allen, G. F.; Waterman, E. L. *J. Am. Chem. Soc.* **1976**, *98*, 2674.
(225) Mori, M.; Katsumi, C.; Ban, Y. *Tetrahedron Letters* **1977**.
(226) Cacchi, S.; Fabrizi, G. *Chem. Rev.* **2005**, *105*, 2873.
(227) Reissert, A. *Berichte der deutschen chemischen Gesellschaft* **1905**.

(228) Emil Fischer, F. J. *Berichte der deutschen chemischen Gesellschaft* **1883**.
(229) Du, F.; Zhou, Q.; Sun, W.; Yang, C.; Wu, C.; Wang, L.; Chen, G. *Molecules* **2020**, *25*.
(230) Houlihan, W. J.; Parrino, V. A.; Uike, Y. *JOC* **1981**, *46*, 4511.
(231) Bartoli, G.; Palmieri, G.; Bosco M.; Dalpozzo, M. *Tetrahedron Lett.* **1989**, *30*.
(232) Kumari, A.; Singh, R. K. *Bioorg. Chem.* **2019**, *89*, 103021.
(233) Barreiro, E. J. *Privileged Scaffolds in Medicinal Chemistry: Design, Synthesis, Evaluation*, **2015**, *1*, 1-15.
(234) Colella, M.; Degennaro, L.; Luisi, R. *Molecules* **2020**, *25*.
(235) Wahab, B.; Ellames, G.; Passey, S.; Watts, P. *Tetrahedron* **2010**, *66*, 3861.
(236) Gutmann, B.; Gottsponer, M.; Elsner, P.; Cantillo, D.; Roberge, D. M.; Kappe, C. O. *Org Process Res Dev*, **2013**, 17, 294-302.
(237) Xu, J.; Jin, Y.; Li, J.; Yu, Z.; Lv, Y. *Chem. Eng. and Process.* **2017**, *121*, 144.
(238) Colombo, E.; Ratel, P.; Mounier, L.; Guillier, F. *J. Flow Chem.* **2011**, *1*, 68.
(239) Ranasinghe, N.; Jones, G. B. *Bioorg. Med. Chem. Lett.* **2013**, *23*, 1740.
(240) Glotz, G.; Gutmann, B.; Hanselmann, P.; Kulesza, A.; Roberge, D.; Kappe, O. C. *RSC Advances* **2017**, *7*.
(241) Crifar, C.; Ducker, F. L.; Nguyen Thanh, S.; Kairouz, V.; Lubell, W. D. *J. Org. Chem.* **2019**, *84*, 10929.
(242) Örkényi, R.; Beke, G.; Riethmüller, E.; Szakács, Z.; Kóti, J.; Faigl, F.; Éles, J.; Greiner, I. *EurJOC* **2017**, *2017*, 6525.
(243) Freidinger, R. M. *J. Med. Chem.* **2003**, *46*, 5553.
(244) Reichelt, A.; Martin, S. F. *Acc. Chem. Res.* **2006**, *39*, 433.
(245) Fuse, S.; Mifune, Y.; Takahashi, T. *Angew. Chem. Int. Ed. Engl.* **2014**, *53*, 851.
(246) Salvador, C. E.; Pieber, B.; Neu, P. M.; Torvisco, A.; Kleber, Z. A. C.; Kappe, C. O. *J. Org. Chem.* **2015**, *80*, 4590.
(247) Fuse, S.; Mifune, Y.; Nakamura, H.; Tanaka, H. *Nature Comm* **2016**, *7*, 13491.
(248) Aliz Szloszár, I. M. M., Ferenc Fülöp *J. Flow Chem.* **2018**, *8*, 21.

Chapter 2

PhD work: General aims & methods

The aim of my PhD thesis is the rapid production of chemical libraries, boosted by flow chemistry protocols in a sustainable declination and employing green chemistry methodologies. Considering that my PhD project is at the edge between organic chemistry methodology and medicinal chemistry application, I wanted to utilize flow chemistry to develop a greener and sustainable synthesis of the privileged (spiro)indolenine and (spiro)indoline scaffolds and their derivatives. Our first goal has been to study a sustainable protocol for the synthesis of 3,3-disubstituted indolenine through interrupted Fisher indolisation reaction, in order to overcome the issues associated to the synthesis of spiroindolenine (Application 1). Capitalizing on this protocol, we investigate the use of spiroindolenine as substrate for the generation of peptidomimetic frameworks with potential antibiofilm activity (Application 2). Furthermore, fascinated by the efficiency and the elegance of organocatalytic approaches, the third goal was to explore an enantioselective Strecker reaction, starting from indolenine templates, in order to develop a fast, sustainable and highly enantioselective synthesis of cyclic α-amino nitriles (Application 3). Finally, the last goal was to develop a library of indolenine-based scaffolds as novel metallo beta lactamases inhibitors, inspired by the structure of the drug Captopril (Application 4).

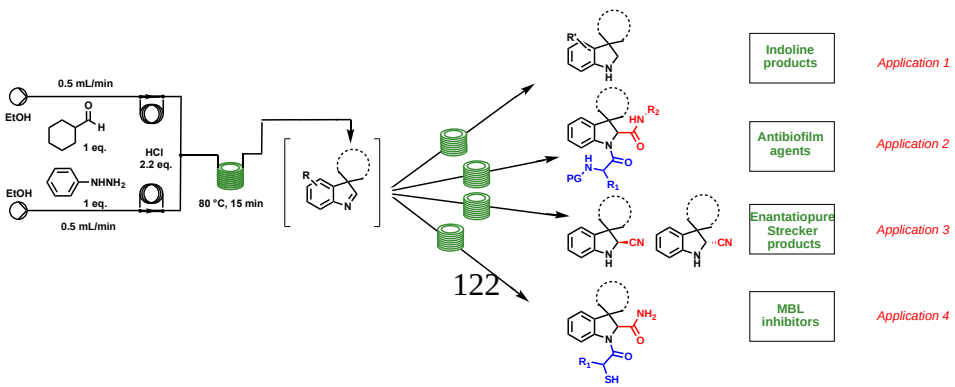

Figure 1. Applications of flow chemistry to indolenine privileged scaffolds.

All reagents and chemicals were purchased from Sigma Aldrich-Merck or Zentek and used without further purification. TLC analysis was conducted using aluminum foil supported thin-layer silica gel chromatography plates (F254 indicator). Column chromatography was performed using 230–400 mesh, 60 Å pore diameter silica gel using mixtures of ethyl acetate and hexane or petroleum ether. Preparative HPLC separations were achieved using a Waters 510 HPLC pump, a Rheodine injector and a Waters differential Refractometer model 401. Chemical transformations in flow were realized using a self-made flow reactor: 2 or 4 HPLC pumps were connected each to a Rheodyne 9010 injection valves, each equipped with a 1 or 2 mL sample loop made from PTFE tubing and an injection port for disposable syringes. The injection valves were further connected via a T-piece to a coiled PTFE tubing or Syrris. The tubular reactor finished into a back pressure regulator (BPR), which was either spring mechanism-based (6.7 bar) or simply a PEEK capillary of defined length (1.7 bar). The products were characterized using standard instrumental analyses: i) ^{1}H NMR and ^{13}C NMR; ii) UV-Vis spectroscopy; iii) gas-chromatography coupled to mass spectrometry (GC-MS); iv) liquid chromatography coupled to mass spectrometry (LC-MS); v) polarimeter.

Chapter 3

Spiroindolines and spiroindolenines in continuous flow

3.1 Interrupted Fischer reaction in continuous flow: sustainable synthesis of spiroindolenines and spiroindolines

As reported in the introduction, the tendency of metastable indolenines to undergo to 1,2- migrations under acidic conditions lead to the formation of the more thermodynamically stable indolic counterparts. Furthermore, 3,3'-disubstituted indolenines, just like other imines, exist in equilibrium with their tri-imine form. Our first aim was to develop an efficient, more reproducible and cost-effective synthesis for 3,3-indolenines to overcome synthetic hurdles associated to the classic interrupted Fischer indolisation. In this context, the Fischer indolisation in continuous flow has attracted the researchers in the last years.[1,2] Despite this, to the best of our knowledge, only few papers have been reported on its interrupted variation in batch and in flow.[3,4] We developed a green and sustainable flow-aided methodology for the generation of spiroindolenines, employing EtOH as green solvent, and avoiding the use excess of acetic acid in the dual role of catalyst and solvent. The developed protocol significantly reduced reaction times required minimum manual handling and allowed to avoid intermediate purification steps. Due to the intrinsic instability of most of the indolenines, we decided to couple the first step, namely the generation of the flow-born indolenine systems, to a subsequent reduction step to achieve the formation of their reduced counterparts, *i.e*. the corresponding indolines. Our method allows the formation of the spiroindoline products, avoiding the isolation of metastable indolenine and reducing the yield drop caused by degradation.

As a preliminary task, a first investigation in batch was performed in order to fine-tune and optimize reaction conditions before the transposition in continuous flow. [5]

Two different α,α′-disubstituted carbaldehydes were chosen as model compounds: 1-Boc-piperidine-4-carboxaldehyde **1a** and cyclohexylaldehyde **1b** and this choice was basically undertaken for two main reasons:i) being spiroindolenines more prone to the 1,2-migration path, a good result with these aldehydes, in principle, should guarantee an even better outcome when using acyclic aldehydes for the interrupted Fischer reaction; ii) the Boc protecting group could rapidly be removed under acid conditions. Its stability in our conceived reaction conditions could guarantee the mildness of the protocol, while opening up possibility for further telescoped functionalization of the substrates upon Boc-deprotection.

Table 1. Optimization of reaction conditions in batch for the preparation of 3,3-disubstituted indolenines.

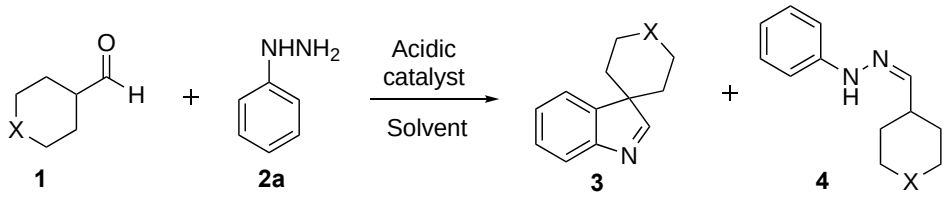

1 **2a** **3** **4**

	X	**PhNHNH$_2$**	**Acid**	**Solvent**	**Temp (°C)**	**Time (h)**	**Yield 3 (%)[a]**	**Yield 4 (%)[a]**
1	*N*-Boc **1a**	(free base)	AcOH	AcOH	80	2	73	n.d
2		(free base)	AcOH	iPrOH	80	12	n.d.	n.d.
3		(free base)	Amberlyst -15	iPrOH	80	12	n.d	85

4		(free base)	Amberlyst -15	EtOAc	25	12	n.d.	21
5		(free base)	*p*-TsOH	EtOAc	80	12	23	67
6		(HCl salt)	-	EtOH	50	4	45	32
7	CH_2 **1b**	(free base)	AcOH	AcOH	80	2	85	n.d.
8		(free base)	AcOH	AcOH	50	2	n.d.	n.d.
9		(free base)	Amberlyst -15	EtOH	80	4	16	n.d.
10		(free base)	Amberlyst -15	EtOH	50	2	n.d.	n.d.
11		(free base)	*p*-TsOH	EtOH	50	4	13	53
12		(HCl salt)	-	EtOH	50	2	90	n.d.
13		(HCl salt)	Amberlyst -15	EtOH	50	2	80	n.d.

[a] Determined by GC-MS. n.d.: not determined

First of all, after thoroughly screening the literature, we tried to reproduce the best reported batch conditions of Fischer indolisation. Starting from an equimolar mixture of 1-Boc-piperidine-4-carboxaldehyde (**1a)** and phenylhydrazine in form of free base (**2a)** and employing acetic acid with the dual role of catalyst and solvent, the complete consumption of starting materials was obtained after 2 hours at 80 °C, achieving a 73% yield of the desired product (Table 1, Entry 1).

On the basis of these reaction conditions, an exploration of key parameters allowed the identification of the reagent mixing mode, stoichiometry, and the optimum solvent, temperature and reaction time.

Disappointing results have been obtained when using isopropanol as green solvent and acetic acid in the unique role of catalyst (Table 1, Entry 2), as well as using Amberlyst 15 as heterogeneous acid catalyst, (Table 1, Entry 3). In the latter case, the opening form of the desired product, the phenylhydrazone precursor **4**, could be detected, (Table 1, Entries 4-5) when employing Amberlyst 15 or *p*-TsOH in EtOAc as sustainable

solvent. The use of *in situ* HCl provided by release from phenylhydrazine hydrochloride, employing EtOH as green solvent at 50 °C inverted the trend (Table 1, Entry 6). The phenylhydrazone precursor **4** was detected in only 32% and the product in 45% yield. The same behavior was observed using the other aldehyde **1b** (Table 1, Entries 7-13). The best result was achieved using phenylhydrazine hydrochloride in EtOH at 50 °C for 2 hours, giving the desired product in 90% yield.

With these batch results in hand, we shifted the reaction from the classical flask into a capillary reactor using a home-made flow system, consisted of two conventional HPLC pumps and two six-port Rheodyne injectors containing volume sample loops of 2 mL. A simple T-piece connected the two HPLC pumps to a 15 mL PTFE tubular reactor was immersed in a classic oil bath, followed thus by a BPR, an essential part of flow setup, consisting of different pressure to maintain the control of the system. Pressure control in flow chemistry is an important key component; when a general reaction involves high temperature, a reagent can reach boiling point, which negatively impacts the reaction. Controlling reaction pressure by adding a BPR at the end of the line can prevent reagent boiling.

EtOH was chosen as best compatible green solvent for the reaction. Table 6 shows the optimization of the reaction conditions in flow.

Table 2: Optimisation of reaction conditions in flow.

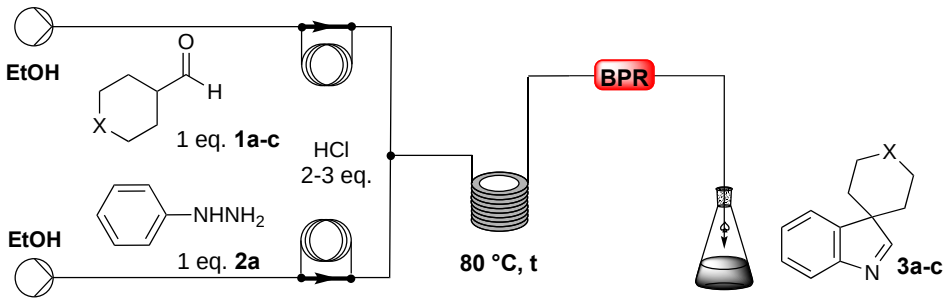

Entry	PhNHNH$_2$	X	eq. HCl	Solvent	Flow-Rate (mL/min)	Time (min)	GC yield (%) [e]
1[a]	free base	*N*-Boc	2.0	EtOH	1.0	15	51
2[a]	Free base		2.0	EtOH	0.7	21	31
3[a]	free base		2.0	EtOH	0.5	30	23
4[b]	free base		2.2	EtOH	1.0	15	86
5[d]	HCl salt		1.2	EtOH	1.0	15	87
6[c]	HCl salt		1.0	EtOH/AcOH 1:1	1.0	15	---
7[c]	HCl salt		1.0	n-PrOH/AcOH 1:1	0.7	21	23
8[c]	HCl salt		1.0	EtOH/H_2O 2:1	0.5	30	4
9[a]	free base	CH_2	2.0	EtOH	2.0	10[f,g]	39
10[a]	free base		2.0	EtOH	0.5	20[g]	18
11[a]	free base		2.0	EtOH	1.0	15	54
12[a]	free base		3.0	EtOH	1.0	15	10
13[b]	free base		2.0	EtOH	1.0	15	53
14[b]	free base		2.2	EtOH	1.0	15	74
15[d]	HCl salt	*N*-Cbz	1.2	EtOH	1.0	15	74

[a] Method A: Sample loop (SL) A: 0.5 mmol aldehyde + equiv. HCl in 2 mL of EtOH, SL B: 0.5 mmol $PhNHNH_2$ in 2 mL of EtOH; [b] Method B: SL A: 0.5 mmol aldehyde + 0.5 mmol $PhNHNH_2$ in 2 mL of EtOH, SL B: equiv. HCl in 2 mL of EtOH; [c] Method C: SL A: 0.5 mmol aldehyde + (equiv.$^{-1}$) HCl in 2 mL of EtOH, SL B: 0.5 mmol $PhNHNH_2$•HCl in 2 mL of EtOH; [d] Method D: 0.5 mmol aldehyde + 0.5 mmol $PhNHNH_2$•HCl in 2 mL of EtOH, heated to 50 ºC for 5 min prior to loading into the SL, SL B: (equiv.$^{-1}$) HCl in 2 mL of EtOH; [e] Determined by GC-MS; [f] 6.9 bar; [g] Reactor volume decreased to 10 mL.

We started to load two injection loops with two different solutions: (Table 2, Entry 1) 0.5 mmol of 1-Boc-piperidine-4-carboxaldehyde and 2 equiv. of HCl, added in form of 2 M ethanolic HCl solution, were premixed in 2 mL of EtOH and loaded in the first loop; another solution of 0.5 mmol of phenylhydrazine free base **2a** in 2 mL of EtOH was immediately injected into the second loop. The solutions were pumped simultaneously into the reactor coil heated to 80 °C, followed by 1.7 bar BPR, with a flow rate of 0.5 mL min^{-1} and 15 minutes of residence time. The crude product was directly analyzed through the GC-MS, that revealed complete consumption of the starting material and 51% yield of the final product. Phenylhydrazone **4** was detected in 12% yield and the formation of the diethyl acetal of the aldehyde **1a** as well. Increasing the residence time from 15 minutes to 21 (Table 2, Entry 2) or 30 (Table 2, Entry 3) minutes did not avoid the formation of by-products. Due to the major issue related to reagent preparation, with the undesired reaction between aldehyde and HCl before the T-piece, we decided to modify the injection modality. An equimolar solution of 0.5 mmol of 1-Boc-piperidine-4-carboxaldehyde and phenylhydrazine **2a** as free base were premixed in 2 mL of EtOH and injected in the first loop; another solution containing 2.2 equivalents of HCl, in form of 2 M ethanolic solution, was loaded in the second loop. After 15 minutes of residence time at 80 °C, the product was obtained with 86% GC yield (Table 2, Entry 4). This outcome has been verified when the phenylhydrazine **2a** was replaced with its hydrochloride salt and decreasing the equivalents of HCl from 2.2 to 1.2 (Table 2, Entry 5).

Since we did not obtain a clear solution while premixing aldehyde and phenylhydrazine in EtOH, we rapidly heated the mixture in a water bath at 50 °C before loading it in the loop, thus overcoming this insolubility

issue. Following this method, the product was achieved in 87% GC yield. When we tried to overcome the insolubility issue without using the pre-heating strategy, and instead adding water or AcOH as additives, the yield drastically decreased (Table 2, Entries 6-8). In principle, the same behavior was observed using both the selected aldehydes **1b** and **1c** reaching a final 74% GC yield for both of them (Table 2, Entries 9-15).

This simple set-up was then used to investigate reaction scope and versatility. The generation of a library of (spiro)indolenines was then planned, exploring various aldehydes and phenylhydrazines (Table 3). Due to the intrinsic instability of the indolenine system, we further coupled the indolenine flow synthesis to a subsequent reduction step providing the formation of corresponding indolines, without isolation of intermediates. Accordingly, we collected the flow stream exiting from the reactor coil in a classical flask containing a suspension of a molar excess of sodium borohydride in EtOH. After 15 minutes, a quenching with water, work-up with ethyl acetate and chromatography purification were performed furnishing the final products. A focused library of 9 compounds, exploring cyclic and acyclic aldehydes and different phenylhydrazines was generated with isolated yields ranging between 43% and 76% (Table 7).

Table 3. Continuous-flow synthesis of 3,3-disubstituted indolines.

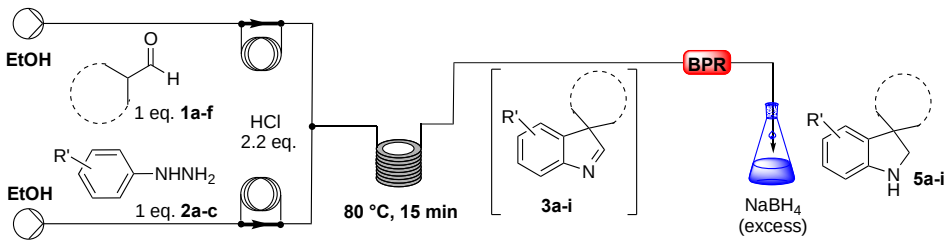

Entry	Ansatz reagents	Aldehyde/ Ketone	Hydrazine	Product	Yield (%)	Output (g/h)
1	D	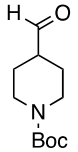 1a	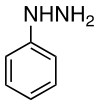 2a	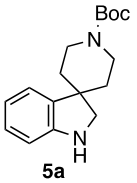 5a	92[a] 58[b]	0.170
2	D	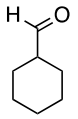 1b		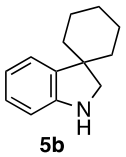 5b	87[a] 58[b]	0.110
3	D	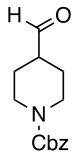 1c		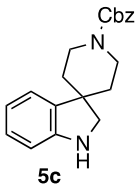 5c	79[a] 55[b]	0.180
4	D	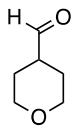 1d		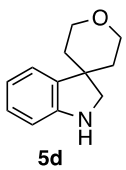 5d	61[a] 43[b]	0.08
5	B	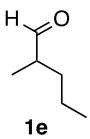 1e		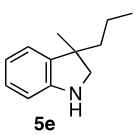 5e	37[a] 76[b]	0.136
6	B	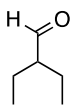 1f		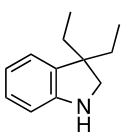 5f	58[a] 56[b]	0.100
7	B	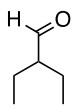 1f	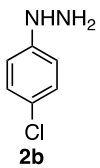 2b	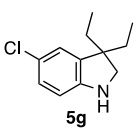 5g	44[b]	0.092
8	D	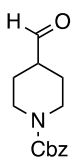 1c		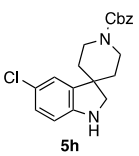 5h	50[b]	0.178

9	D	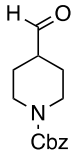 **1c**	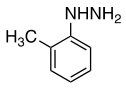 **2c**	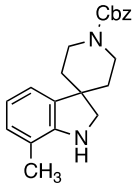 **5i**	46[b]	0.159

[a] Yield of the indolenine calculated via GC-MS; [b] Yield of the corresponding indoline after purification by column chromatography.

Finally, we developed a telescoped approach coupling both the interrupted indolisation and the reduction step that allowed generation of a library of indolenines and indolines with limited solvent consumption and manual intermediate work-up procedures. The telescoped sequence is shown in Scheme 1.

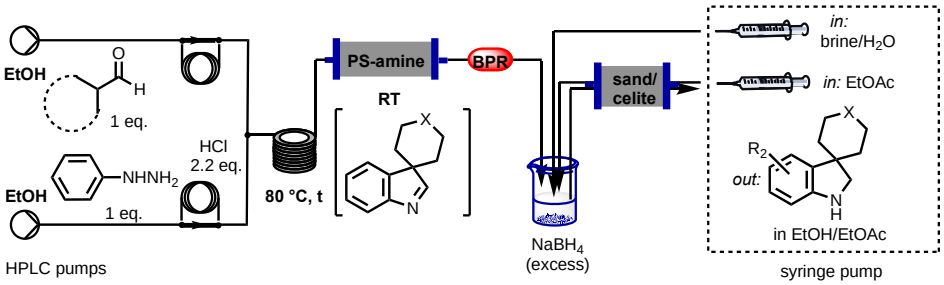

Scheme 1. Two-step flow process to indolines.

The 15 mL reactor coil was followed by a plastic column filled with an excess of polymeric tris(2-aminoethyl)amine in order to quench the excess of HCl and the unreacted aldehyde. Having eliminated the acid and aldehyde from the crude product, we also succeeded in decreasing the required sodium borohydride suspension amount in the flask by two third. Approximatively 5 minutes after indolenine collection, the reaction was quenched by addition of an aqueous phase consisting of 50% brine and an

organic phase represented by ethyl acetate as organic solvent, in a ratio of 1:0.5, respectively, using a classic syringe pump. Further, in order to dry the organic phase, a column filled with a 1:1 (m/m) mixture of dried celite and sand was added between the syringe and the tube leading to the vessel. In conclusion, the telescoped approach allowed generation of the target compounds consuming a total of only 12 mL ethanol and 5 mL of ethyl acetate as green solvents on a 0.5 mmol scale with minimum manual handling or intervention in only 30 minutes, which represents a valuable achievement with respect to the 5 hours required in batch.

3.2 Experimental part

General comments

All reagents and chemicals were purchased from Sigma Aldrich-Merck or Zentek and used without further purification. TLC analysis was conducted using aluminum foil supported thin-layer silica gel chromatography plates (F254 indicator). Column chromatography was performed using 230– 400 mesh, 60 Å pore diameter silica gel using mixtures of ethyl acetate (EA) and hexane (H) or petroleum ether (P).

Synthesis of indolenines in batch (general procedure (GP)-I)

tert-Butyl spiro[indole-3,4'-piperidine]-1'-carboxylate (**3a**). A stirred solution of 1-Boc-piperidine-4-carboxaldehyde **1a** (108 mg, 0.5 mmol) and phenylhydrazine **2a** (50 μL, 0.5 mmol) in AcOH (3 mL) was heated to 80 °C for 2 h. After completion of the reaction, AcOH was removed in

vacuo and the residue was diluted with EtOAc (5 mL) and a saturated solution of $NaHCO_3$ was added. The mixture was extracted with EtOAc (3 × 10 mL) and the combined organic layers were dried over Na_2SO_4, filtered and evaporated in vacuo. The crude material was purified by column chromatography on silica gel (EA/P 1 : 4) obtaining **3a** as a red oil. Yield: 104 mg (73%).

Reduction of indolenines in batch (GP-II)

tert-Butyl spiro[indoline-3,4'-piperidine]-1'-carboxylate (**5a**). To a solution of **1a** (45 mg, 0.16 mmol) in MeOH (3 mL), $NaBH_4$ (30 mg, 0.8 mmol) was added. The reaction was kept stirring for 3 h at 50 °C. Then the reaction was quenched with a saturated solution of $NaHCO_3$ (10 mL), MeOH was removed under reduced pressure and residue was dissolved with EtOAc and washed with dist. water (3 × 10 mL). The organic phase was dried over Na_2SO_4 and solvents removed in vacuo to give a residue which was purified by flash column chromatography on silica gel (EA/P 1:4) obtaining **5a** as orange solid. Yield: 37 mg (80%).

Synthesis of indolenines in flow (GP-III)

Chemical transformations in flow were realized using a self- made flow reactor: two Waters 510 HPLC pumps were connected each to a Rheodyne 9010 injection valves, each equipped with a 2 mL sample loop made from PTFE tubing and an injection port for disposable syringes. The injection valves were further connected via a T-piece to a coiled PTFE tubing of 15 mL volume. The coil was immersed in a silicone oil bath for controlling reaction temperatures. The tubular reactor finished into a back pressure regulator (BPR), which was either spring mechanism-based (6.7 bar) or simply a PEEK capillary of defined length (1.7 bar). Product containing

exiting streams were collected directly in a flask. An aliquot of the collected phase was used for analysis by GC-MS. Reagents were prepared for loading into the sample loops according to one of the following four methods: method A: sample loop (SL) A: 0.5 mmol aldehyde + equiv. HCl in 2 mL of EtOH, SL B: 0.5 mmol $PhNHNH_2$ in 2 mL of EtOH; method B: SL A: 0.5 mmol aldehyde + 0.5 mmol $PhNHNH_2$ in 2 mL of EtOH, SL B: equiv. HCl in 2 mL of EtOH; method C: SL A: 0.5 mmol aldehyde + (equiv. $^{-1}$) HCl in 2 mL of EtOH, SL B: 0.5 mmol $PhNHNH_2$·HCl in 2 mL of EtOH; method D: 0.5 mmol aldehyde + 0.5 mmol $PhNHNH_2$·HCl in 2 mL of EtOH, heated to 50 °C for 5 min prior to loading into the SL, SL B: (equiv. $^{-1}$) HCl in 2 mL of EtOH.

Synthesis of indolines in flow-batch combination (GP-IV)

Indolines were realized using the above-described flow set- up, collecting the exiting, indolenine-containing stream in a flask held at 0 °C and typically prepared with 142 mg (3.75 mmol, 7.5 equiv.) of $NaBH_4$ for a standard 0.5 mmol indolenine production in flow. 15 minutes after finishing collecting the indolenine product stream, the flask was allowed to gradually warm up to room temperature. Aqueous quench and work-up was achieved adding $NaHCO_3$ solution, followed by three-fold extraction of the aqueous phase with an equal volume of EtOAc. The organic phase was dried over $MgSO_4$ and concentrated in vacuo. Crude products were purified over silica gel.

Generation of indoline solutions in telescoped segmented continuous flow

Indolines were realized using the above described flow set-up with the following modifications: an Omnifit column (10 mm i.d. × 100 mm) filled with 1 g (3.5–5.0 mmol g^{-1} loading) of polymer-supported tris(2-

aminoethyl)amine was placed in-line between to the outlet of the PTFE reactor coil and the 1.7 bar BPR. The exiting stream was collected in a slim beaker kept at RT and equipped with 47 mg (1.25 mmol, 2.5 equiv.) $NaBH_4$ in 1 mL EtOH. 5 minutes after collection of indolenine-containing reaction mixture was finished, a NE-1000 programmable syringe pump was activated to deliver into the beaker 5 mL of EtOAc from a glass syringe equipped with activated 4 Å molecular sieve beads, and 10 mL of half- concentrated brine from a disposable syringe. A chromatography column charged with a 1:1 mixture (m/m) of sand and celite was placed in-line between the glass column and the capillary used for directing the organic solvent into the beaker and for aspiring the organic phase again: approx. 2 minutes after addition of these phases, magnetic agitation was stopped and phases were allowed to separate. The syringe pump was subsequently activated in reverse mode to aspire 90–95% of the organic phase.

NMR analyses

^{1}H NMR measurements. An accurately weighed amount of analyte (about 5.0–10.0 mg) was dissolved in 600 μL of deuterated chloroform ($CDCl_3$). The mixture was transferred into a 5 mm NMR tube. The spectra were acquired on a Bruker 400 MHz spectrometer using the standard Bruker zg sequence (32 scans at 20 °C). NMR data were processed with MestreNova (version 8.1.1, Mestrelab Research).

^{13}C NMR measurements. An accurately weighed amount of analyte (about 35.0 mg) was dissolved in 600 μL of deuterated chloroform ($CDCl_3$). The mixture was transferred into a 5 mm NMR tube. The spectra were acquired on a Bruker 400 MHz spectrometer using the standard Bruker zgpg30

sequence (3072 scans at 20 °C). NMR data were processed with MestreNova (version 8.1.1, Mestrelab Research).

GC-MS analysis

Purified samples were dissolved in EtOAc at concentrations between 0.5 and 1.0 mg mL^{-1}. Analysis of reaction mixtures were performed after a quick work-up of a 1 mL aliquot: the reaction mixture was brought to pH 8 by addition of conc. $NaHCO_3$ solution. The aqueous solution was subsequently extracted once with 1.0 to 1.5 mL of ethyl acetate. The organic phase was separated and dried over magnesium sulphate. Solids were pelleted by centrifuging, and a 0.5 mL aliquot of the organic phase was subjected to analysis gas chromatographic separation of the samples was achieved using an Agilent Technologies 5973 N GC/MS system equipped with 7683 ALS automatic liquid sampler autoinjector. A Supelco fused-silica capillary column SLBTM- 5 ms (30 m long, 0.25 mm thick, 0.25 μm diameter) was used as stationary phase, He (UHP grade) as mobile phase; the system was operated in 'linear velocity mode' with a starting pressure of 100 kPa, 280 °C injection temperature, and 200 °C interface temperature, running as temperature program: 50 °C start temperature for 1 min, 10 °C min^{-1} heating rate, 280 °C final temperature for 5 min. System control and analyses were realised using the Agilent Mass Hunter GC/MS soft- ware package (version B.07.06.2709).

Product characterization

tert-Butyl spiro[indoline-3,4'-piperidine]-1'-carboxylate (**5a**). According to GP-D, a mixture of phenylhydrazine salt **2a** (73 mg, 0.5 mmol) and 1-Boc-piperidine-4-carboxaldehyde **1a** (108 mg, 0.5 mmol) was treated with

HCl (300 μL, 0.6 mmol) before $NaBH_4$ (144 mg, 3.82 mmol) was added. Yield: 83 mg (58%); orange solid; Rf = 0.4 (H:E = 7:3). ^{1}H NMR (400 MHz, $CDCl_3$) δ 7.01–6.96 (m, 2H), 6.67 (td, *J* = 7.4, 1.0 Hz, 1H), 6.58 (dd, *J* = 7.3, 1.0 Hz, 1H), 4.07–3.92 (m, 2H), 3.41 (s, 2H), 2.92–2.80 (m, 2H), 1.77–1.69 (m, 2H), 1.67–1.60 (m, 2H), 1.42 (s, 9H). GC-MS (EI, 70 eV): m/z (%) = 286 $[M]^+$; tR = 20.87 min. NMR data are in agreement with reported data. [6]

Spiro[cyclohexane-1,3'-indoline] (**5b**). According to GP-D, a mixture of phenylhydrazine salt **2a** (73 mg, 0.5 mmol) and cyclohexanecarboxaldehyde **1b** (59 μL, 0.5 mmol) was treated with HCl (300 μL, 0.6 mmol) before $NaBH_4$ (144 mg, 3.82 mmol) was added. Yield: 54 mg (58%); yellow solid; Rf = 0.6 (H:E = 7:3). ^{1}H NMR (400 MHz, $CDCl_3$) δ 7.00–6.92 (m, 2H), 6.67 (td, *J* = 7.4, 1.0 Hz, 1H), 6.57 (dt, *J* = 7.7, 0.8 Hz, 1H), 3.35 (s, 2H), 1.70–1.61 (m, 5H), 1.55–1.47 (m, 2H), 1.37–1.25 (m, 3H). GC-MS (EI, 70 eV): m/z (%) = 187. $[M]^+$; tR = 14.94 min. NMR data are in agreement with reported data. [7]

Benzyl spiro[indoline-3,4'piperidine]-1'carboxylate (**5c**). According to GP-D, a mixture of phenylhydrazine salt **2a** (73 mg, 0.5 mmol) and 4-formyl-N-Cbz-piperidine **1c** (103 μL, 0.5 mmol) was treated with HCl (300 μL, 0.6 mmol) before $NaBH_4$ (144 mg, 3.82 mmol) was added. Yield: 88 mg (55%); yellowish solid; Rf = 0.25 (H:E = 7:3). ^{1}H NMR (400 MHz, $CDCl_3$) δ 7.33–7.25 (m, 5H), 7.01–6.95 (m, 2H), 6.68 (td, *J* = 7.4, 1.0 Hz, 1H), 6.58 (dd, *J* = 7.8, 0.8 Hz, 1H), 5.09 (s, 2H), 4.12–4.02 (m, 2H), 3.42 (s, 2H), 2.99–2.88 (m, 2H), 1.67–1.46 (m, 4H). GC-MS (EI, 70 eV): m/z (%) = 322 $[M]^+$; tR = 26.34 min. NMR data are in agreement with reported data. [6]

2',3',5',6'-Tetrahydrospiro[indoline-3,4'-pyran] (**5d**). According to GP-D, a mixture of phenylhydrazine **2a** (50 µL, 0.5 mmol) and tetrahydropyran-2H-4-carbaldehyde **1d** (54 µL, 0.5 mmol) was treated with HCl (600 µL, 1.2 mmol) before $NaBH_4$ (144 mg, 3.82 mmol) was added. Yield: 42 mg (43%); yellow solid; Rf = 0.4 (H:E = 7:3). ^{1}H NMR (400 MHz, $CDCl_3$) δ 7.03 (dd, *J* = 7.4, 1.3, 0.6 Hz, 1H), 6.98 (td, 1H), 6.70 (td, 1H), 6.59 (dd, 1H), 3.94–3.86 (m, 2H), 3.53–3.46 (m, 4H), 1.96–1.88 (m, 2H), 1.60 (dd, *J* = 13.7, 2.3 Hz, 2H). GC-MS (EI, 70 eV): m/z (%) = 189 $[M]^+$; tR = 15.39 min. NMR data are in agreement with reported data. [8]

3-Methyl-3-propylindoline (**5e**). According to GP-D, a mixture of phenylhydrazine **2a** (50 µL, 0.5 mmol) and 2-methyl- valeraldehyde **1e** (63 µL, 0.5 mmol) was treated with HCl (600 µL, 1.2 mmol) before $NaBH_4$ (144 mg, 3.82 mmol) was added. Yield: 46 mg (52%); yellowish liquid; Rf = 0.7 (H : E = 7 : 3). ^{1}H NMR (400 MHz, $CDCl_3$) δ 7.00–6.89 (m, 2H), 6.66 (dd, *J* = 7.4, 1.0 Hz, 1H), 6.56 (dt, *J* = 7.6, 0.9 Hz, 1H), 3.33 (d, *J* = 8.8 Hz, 1H), 3.17 (d, *J* = 8.8 Hz, 1H), 1.51 (t, 2H), 1.21 (s, 3H), 1.19– 1.12 (m, 2H), 0.81 (t, *J* = 7.3 Hz, 3H). GC-MS (EI, 70 eV): m/z (%) = 175 $[M]^+$; tR = 11.81 min. NMR data are in agreement with reported data.[7]

3,3-Diethylindoline (**5f**). According to GP-D, a mixture of phenylhydrazine **2a** (50 µL, 0.5 mmol) and 2-ethyl- butyraldehyde **1f** (64 µL, 0.5 mmol) was treated with HCl (600 µL, 1.2 mmol) before $NaBH_4$ (144 mg, 3.82 mmol) was added. Yield: 49 mg (56%); yellowish liquid; Rf = 0.6 (H:E = 7 : 3). ^{1}H NMR (400 MHz, $CDCl_3$) δ 6.95 (td, *J* = 7.6, 1.3 Hz, 1H), 6.89 (ddd, *J* = 7.4, 1.3, 0.6 Hz, 1H), 6.64 (td, *J* = 7.4, 1.0 Hz, 1H),

6.54 (dt, *J* = 7.7, 0.8 Hz, 1H), 3.27 (s, 2H), 1.71–1.59 (m, 2H), 1.59–1.48 (m, 2H), 0.75 (t, *J* = 7.5 Hz, 6H). GC-MS (EI, 70 eV): m/z (%) = 175 $[M]^+$; tR = 11.94 min. NMR data are in agreement with reported data.[7]

5-Chloro-3,3-diethylindoline (**5g**). According to GP-D, a mixture of 4-chloro-phenylhydrazine salt **2b** (91 mg, 0.5 mmol) and ethylbutyraldehyde **1f** (63 µL, 0.5 mmol) was treated with HCl (300 µL, 0.6 mmol) before $NaBH_4$ (144 mg, 3.82 mmol) was added. Yield: 46 mg (44%); yellow liquid; Rf = 0.6 (H:E = 7:3). ^1H NMR (400 MHz, $CDCl_3$) δ 6.90 (dd, *J* = 8.2, 2.2 Hz, 1H), 6.82 (d, *J* = 2.1 Hz, 1H), 6.45 (d, *J* = 8.2 Hz, 1H), 3.30 (s, 2H), 1.62–1.51 (m, 4H), 0.75 (t, *J*=7.5Hz,6H). GC-MS(EI,70eV):m/z (%)=209 $[M]^+$; tR = 14.63 min.

Benzyl 5-chlorospiro[indoline-3,4'-piperidine]-1'-carboxylate (**5h**). According to GP-D, a mixture of 4-chloro- phenylhydrazine salt **2b** (91 mg, 0.5 mmol) and 4-formyl-N- Cbz-piperidine **1c** (103 µL, 0.5 mmol) was treated with HCl (300 µL, 0.6 mmol) before $NaBH_4$ (144 mg, 3.82 mmol) was added. Yield: 89 mg (50%); yellowish liquid; Rf = 0.2 (H : E = 7 : 3). ^1H NMR (400 MHz, $CDCl_3$) δ 7.34–7.27 (m, 5H), 6.92 (dd, *J*=8.2,2.2Hz,1H),6.88 (d,*J*=2.1Hz,1H),6.47 (d,*J*= 8.2 Hz, 1H), 5.09 (s, 2H), 4.14–4.01 (m, 2H), 3.42 (s, 2H), 2.96–2.84 (m, 2H), 1.73–1.62 (m, 4H). GC-MS (EI, 70 eV): m/z (%) = 356 $[M]^+$; tR = 34.29 min. NMR data are in agreement with reported data. [7]

Benzyl 7-methylspiro[indoline-3,4'-piperidine]-1'-carboxylate (**5i**) According to GP-D, a mixture of o-tolylphenylhydrazine salt **2c** (80 mg, 0.5 mmol) and 4-formyl-N-Cbz-piperidine **1c** (103 µL, 0.5 mmol) was treated with HCl (300 µL, 0.6 mmol) before $NaBH_4$ (144 mg, 3.82 mmol)

was added. Yield: 78 mg (46%); yellowish liquid; Rf = 0.2 (H : E = 7 : 3). ^{1}H NMR (400 MHz, $CDCl_3$) δ 7.32–7.22 (m, 5H), 6.87–6.80 (m, 2H), 6.63 (t, *J* = 7.4 Hz, 1H), 5.09 (s, 2H), 4.16–4.00 (m, 2H), 3.43 (s, 2H), 3.05–2.85 (m, 2H), 2.06 (s, 3H), 1.78–1.61 (m, 4H). ^{13}C NMR (101 MHz, chloroform-d) δ 155.4, 148.9, 136.9, 135.5, 129.0, 128.5, 128.0, 127.9, 120.1, 119.3, 119.1, 77.4, 77.1, 76.7, 67.2, 55.9, 44.7, 41.3, 39.6, 35.8, 16.7. GC-MS (EI, 70 eV): m/z (%) = 336 $[M]^+$; tR = 27.11 min.

5a

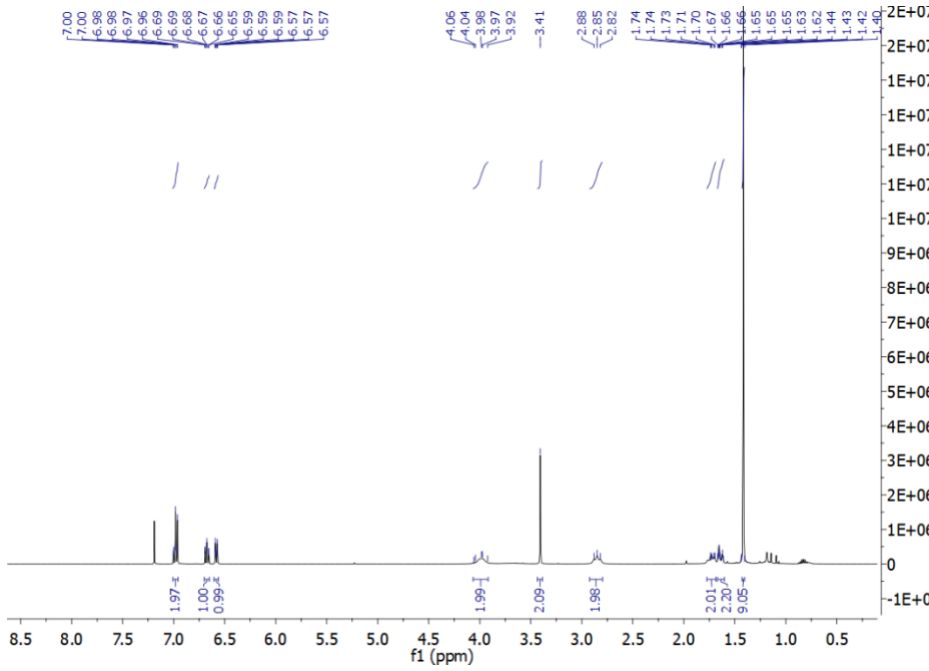

Supporting figure 1. ^{1}H NMR of compound **5a**

5b

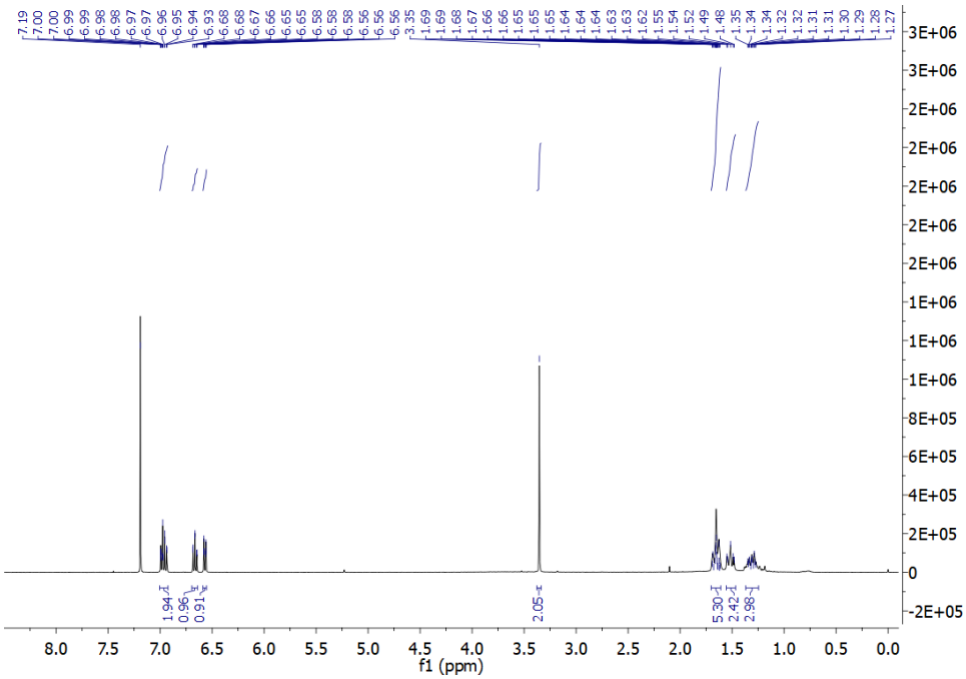

Supporting figure 2. ^{1}H NMR of compound **5b**

5c

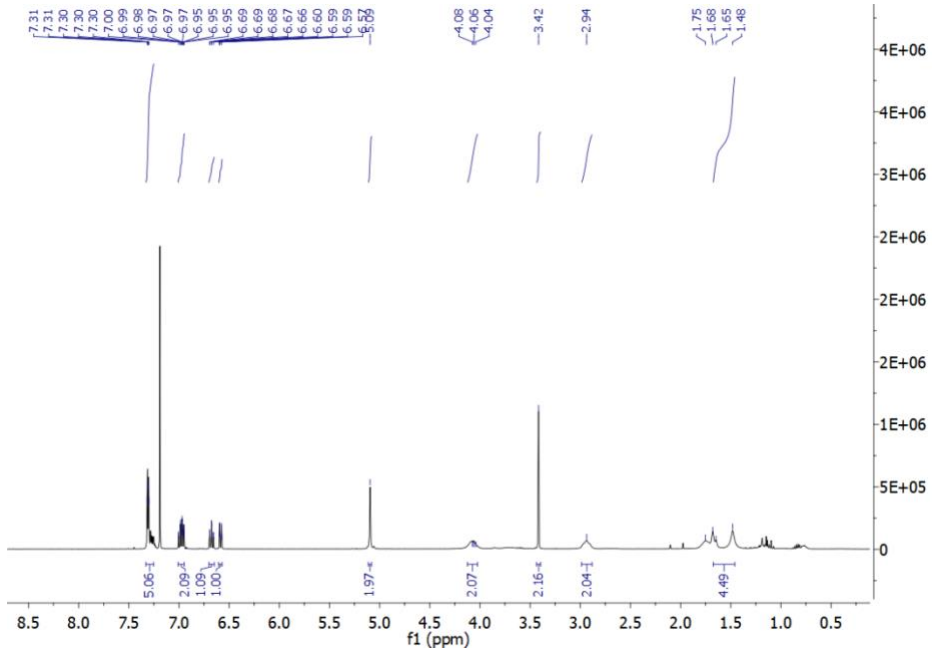

Supporting figure 3. ^{1}H NMR of compound **5c**

5d

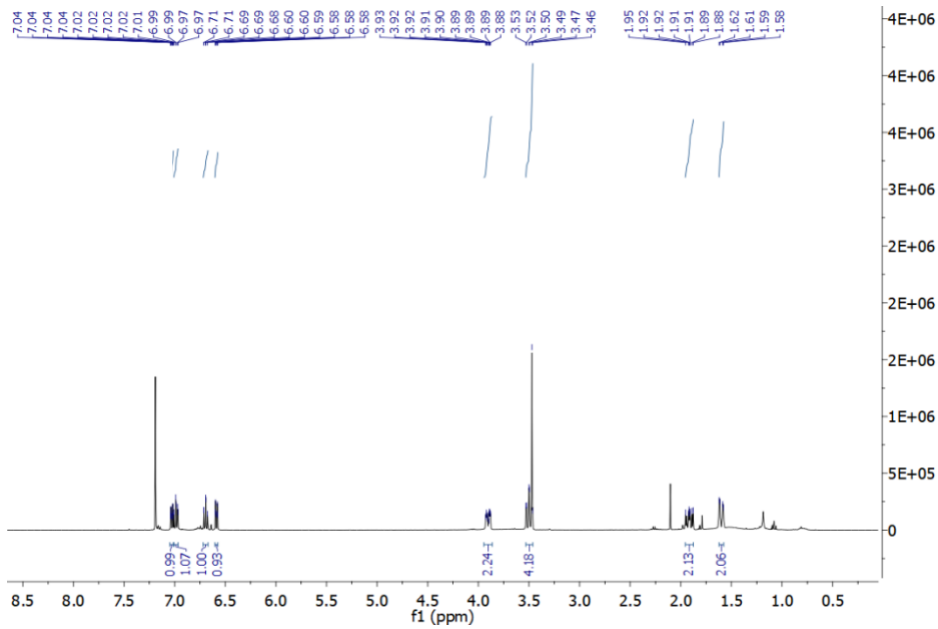

Supporting figure 4. ^{1}H NMR of compound **5d**

5e

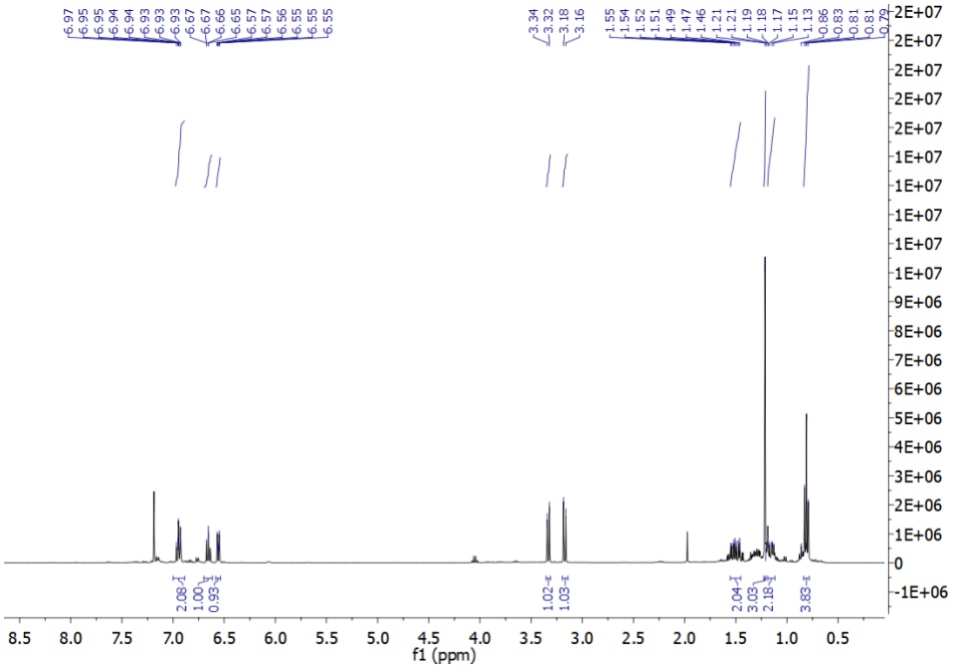

Supporting figure 5. ^{1}H NMR of compound **5e**

5f

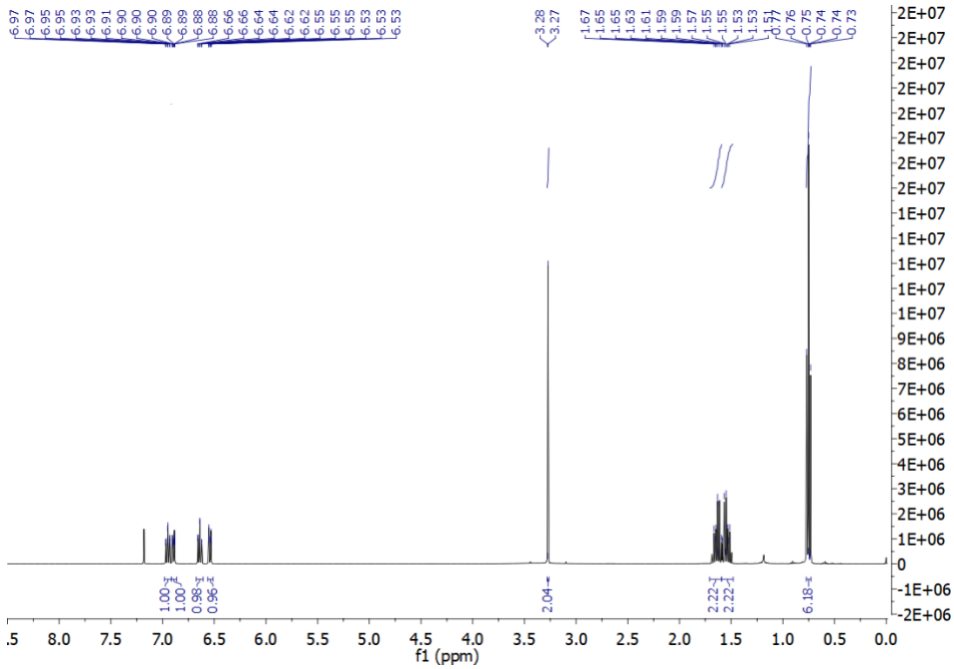

Supporting figure 6. ^{1}H NMR of compound **5f**

5g

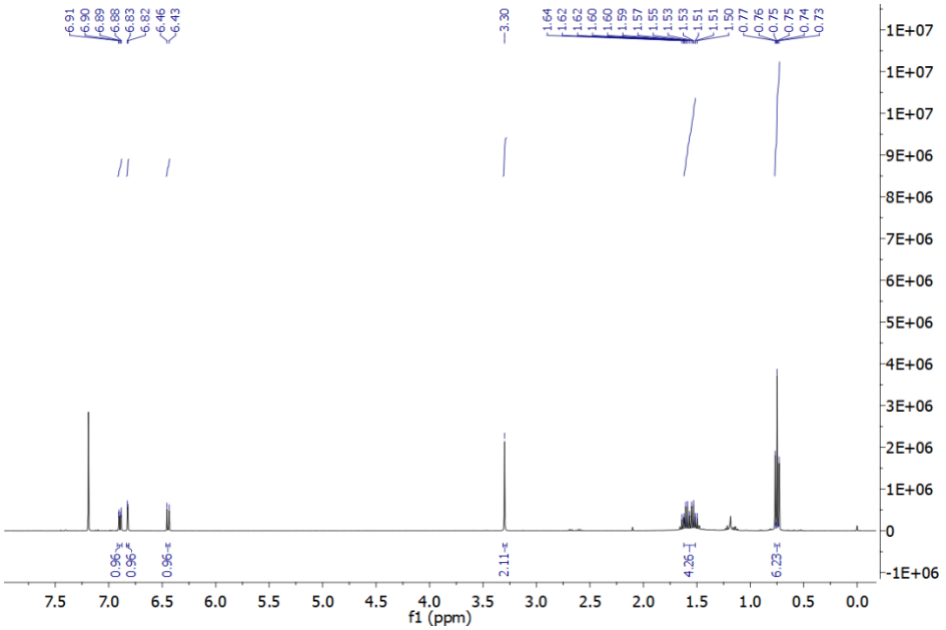

Supporting figure 7. ^{1}H NMR of compound **5g**

5h

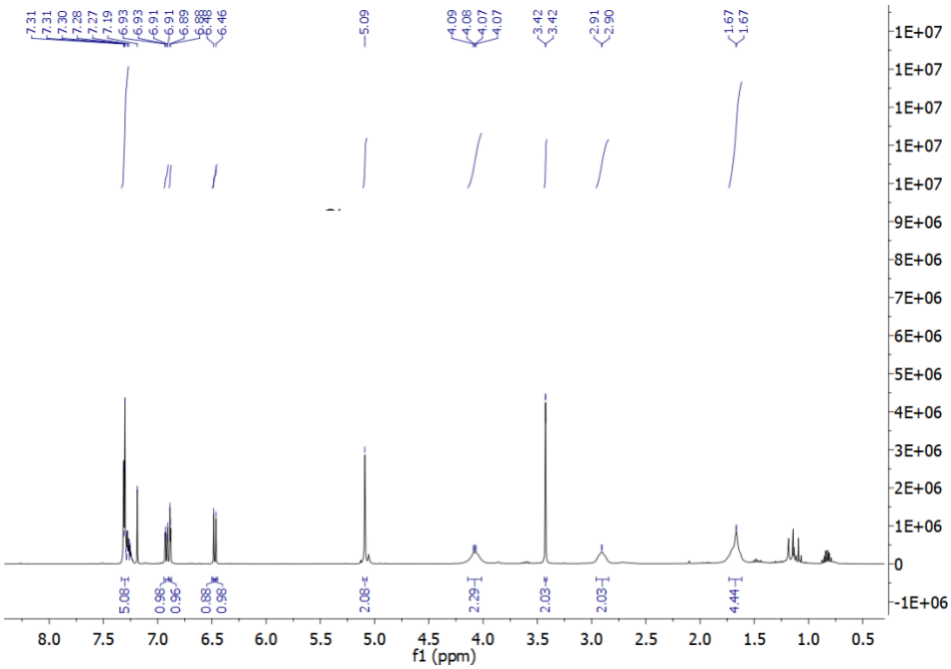

Supporting figure 8. ^{1}H NMR of compound **5h**

5i

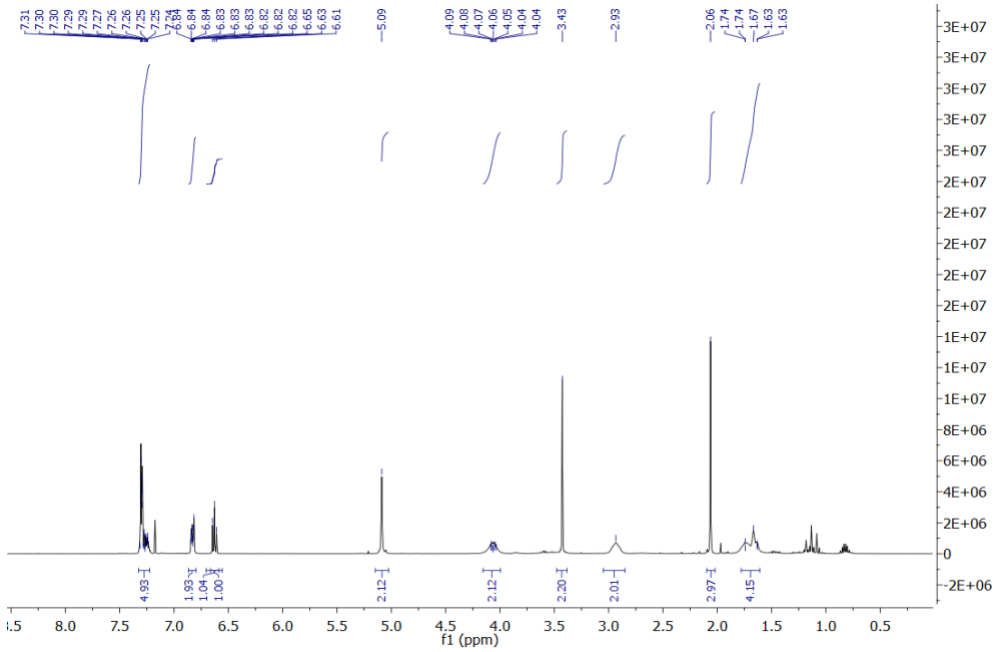

Supporting figure 9. ^{1}H NMR of compound **5i**

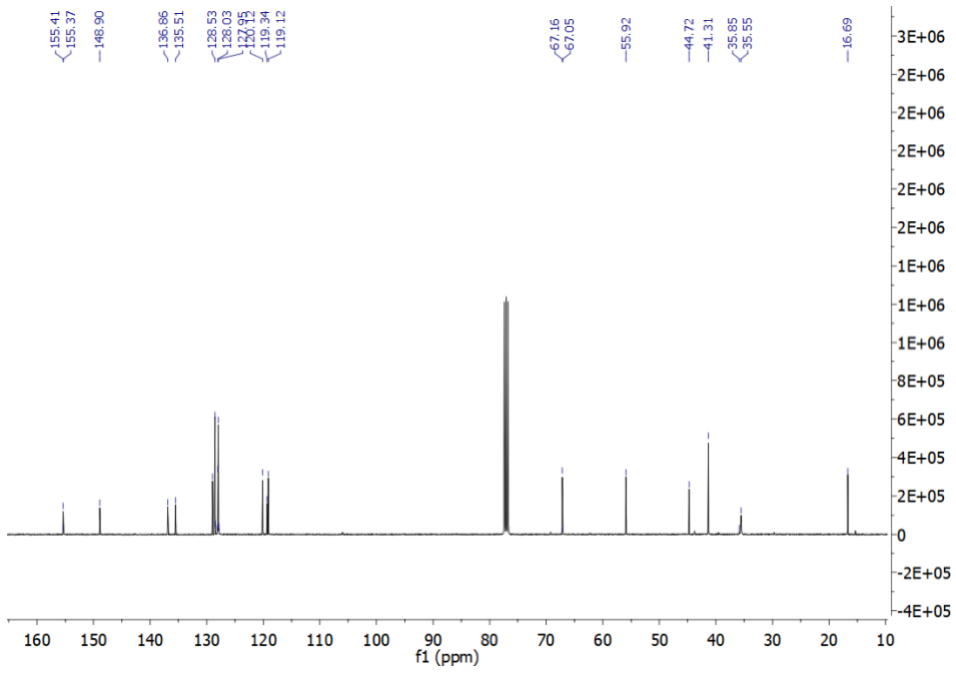

Supporting figure 9. ^{13}C NMR of compound **5i**

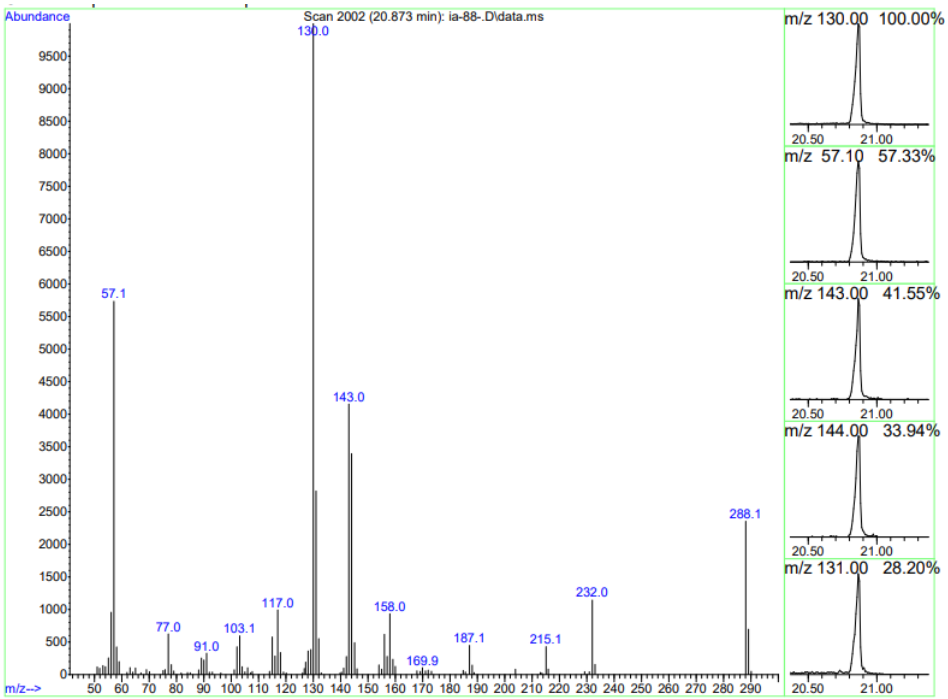

Supporting figure 10. GC-MS chromatogram of compound **5a**

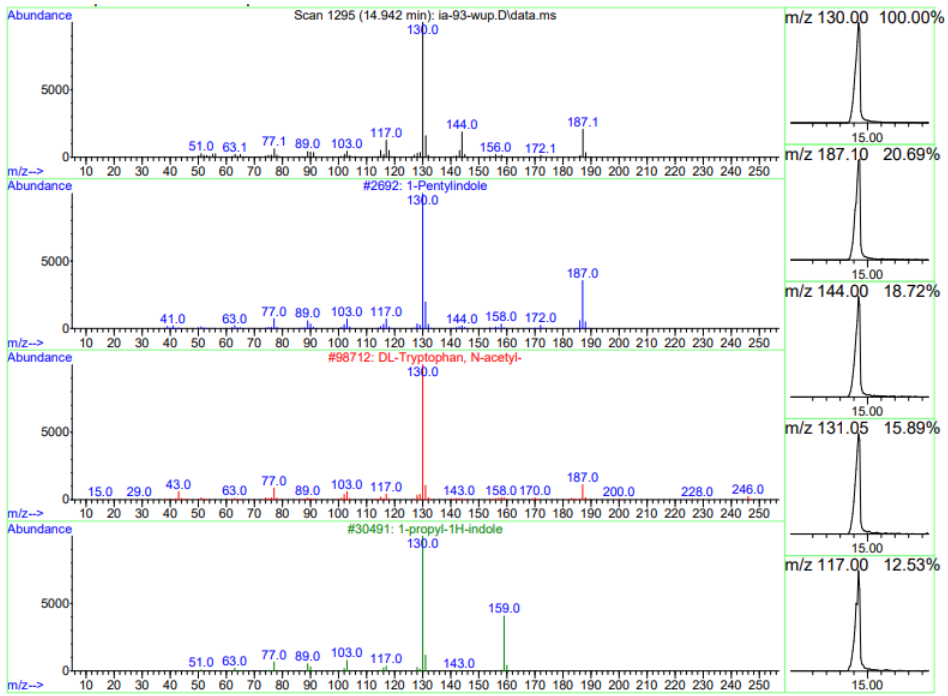

Supporting figure 11. GC-MS chromatogram of compound **5b**

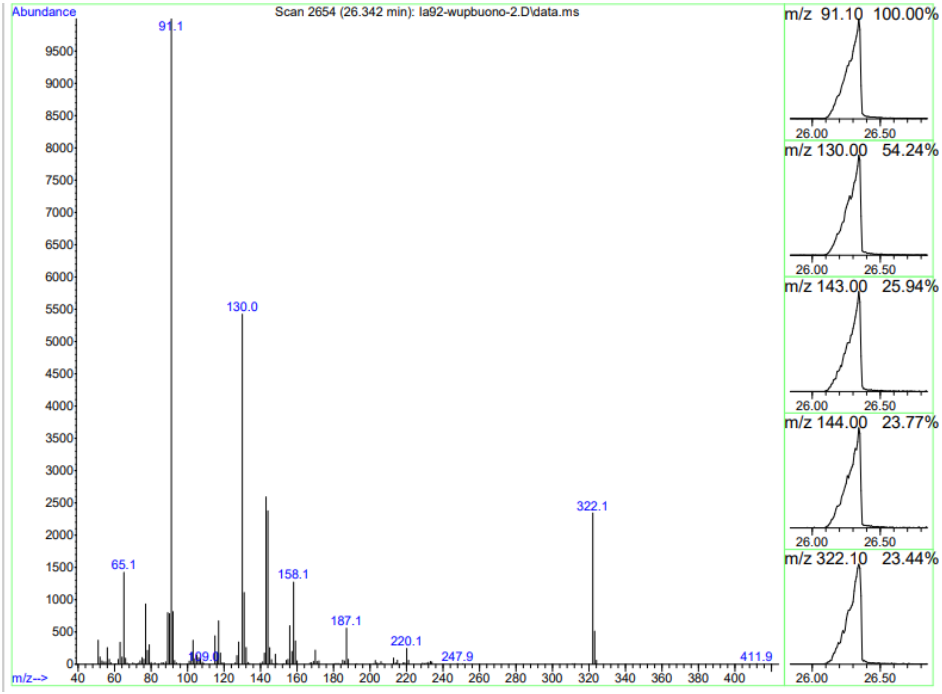

Supporting figure 12. GC-MS chromatogram of compound **5c**

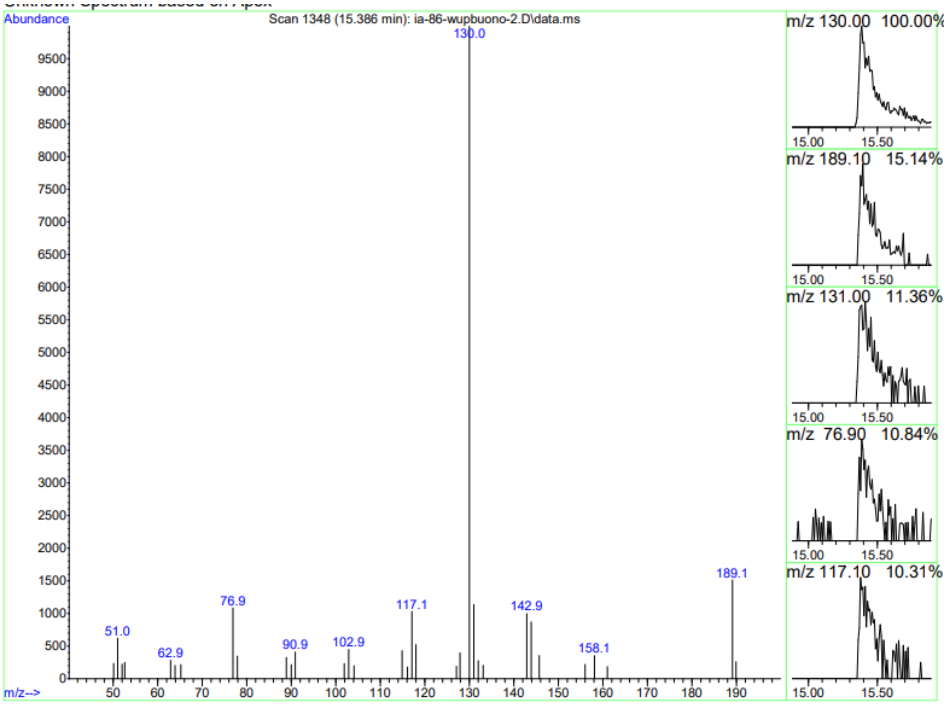

Supporting figure 13. GC-MS chromatogram of compound **5d**

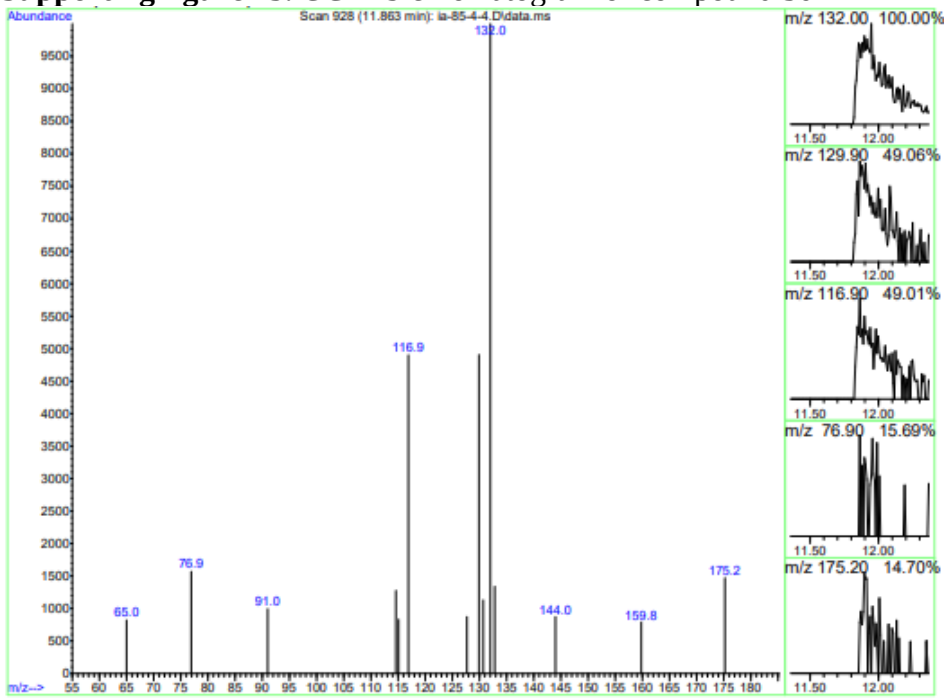

Supporting figure 14. GC-MS chromatogram of compound **5e**

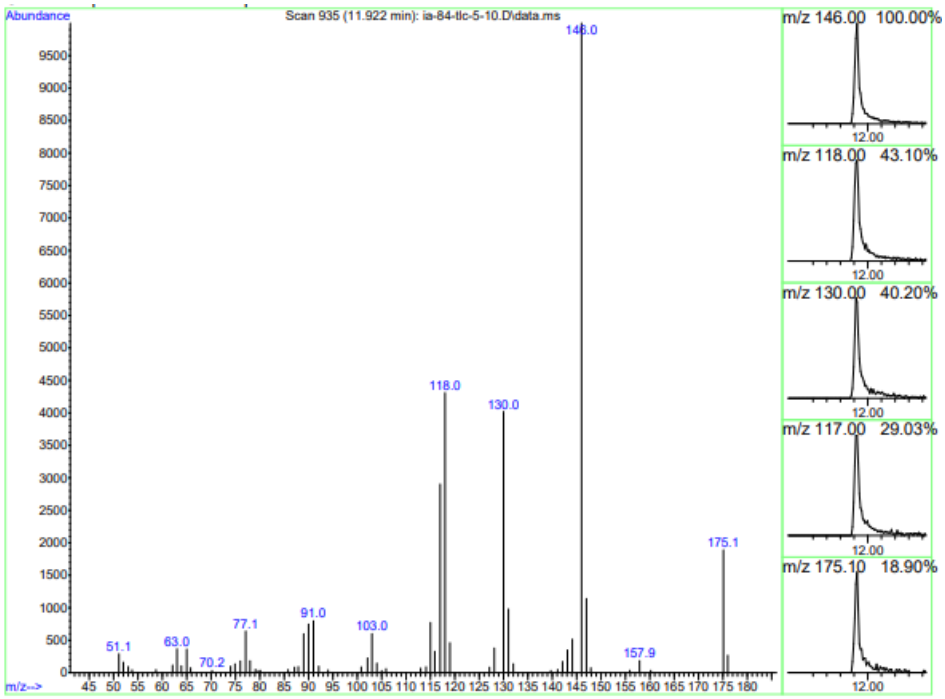

Supporting figure 15. GC-MS chromatogram of compound **5f**

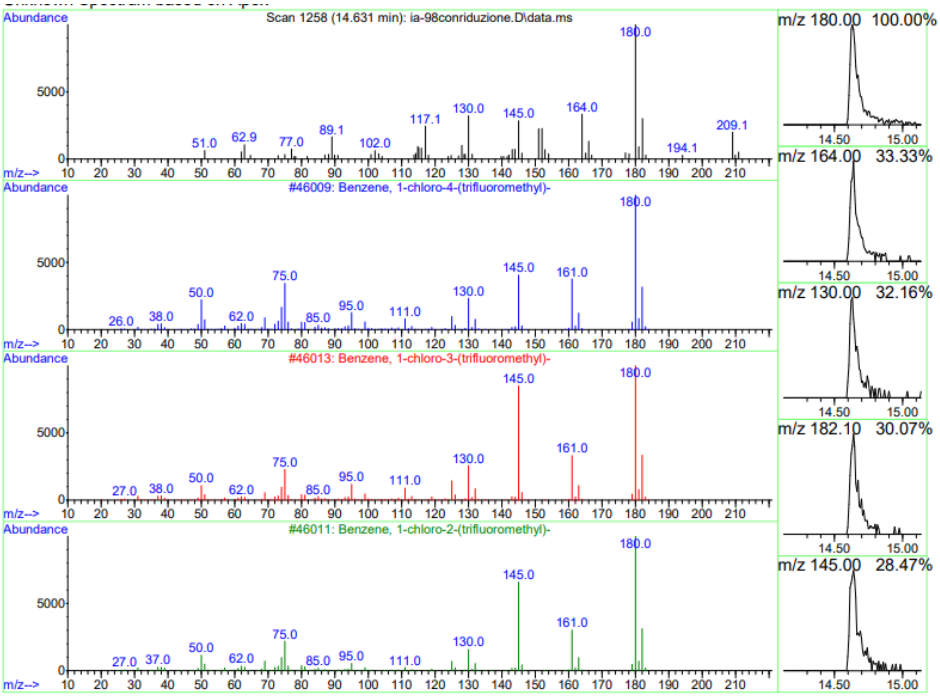

Supporting figure 16. GC-MS chromatogram of compound **5g**

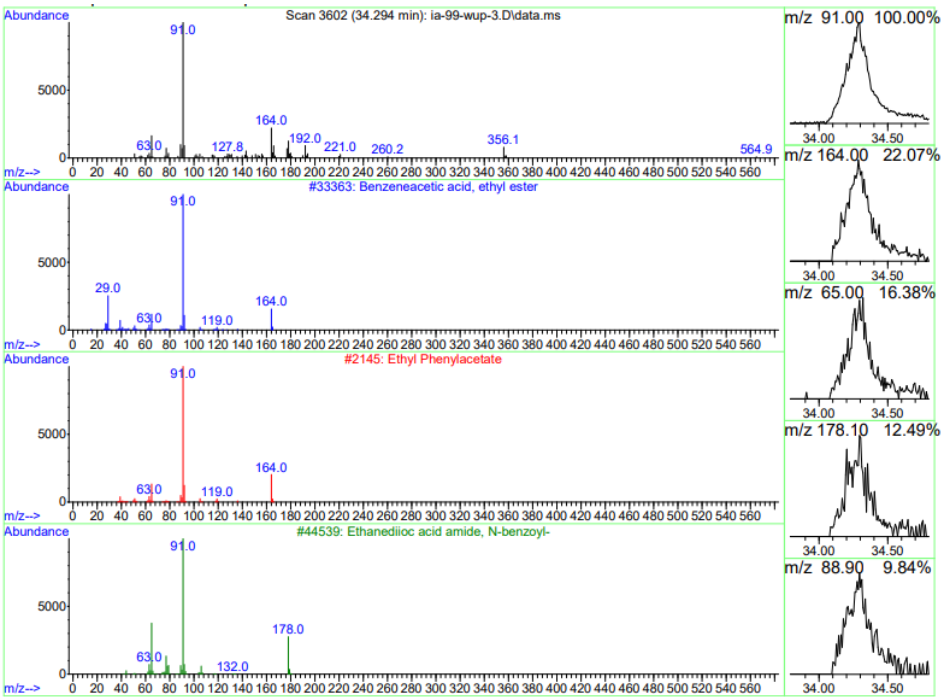

Supporting figure 17. GC-MS chromatogram of compound **5h**

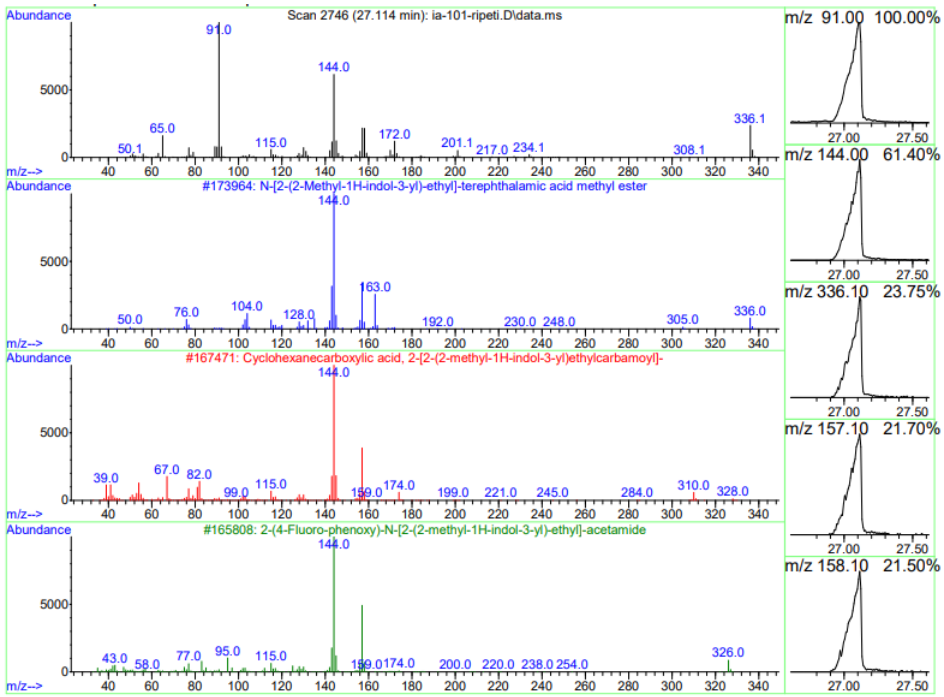

Supporting figure 18. GC-MS chromatogram of compound **5i**

References

(1) Schammel, A. W.; Boal, B. W.; Zu, L.; Mesganaw, T.; Garg, N. K. *Tetrahedron*, **2010**, 66, 4687–4695.
(2) Schammel, A. W.; Chiou, G.; Garg, N. K. *Org. Lett.*, **2012**, *14*, 4556-4559.
(3) Pagano, N.; Heil, M. L.; Cosford, N. D. *Synth. (Stuttg)* **2012**, *44*, 2537.
(4) Yu, J.; Xu, J.; Yu, Z.; Jin, Y.; Li, J.; Lv, Y. *J. Flow Chem* **2017**, *7*, 33.
(5) Alfano, A. I.; Zampella, A.; Novellino, E.; Brindisi, M.; Lange, H.; *Reac. Chem Eng.* **2020**, 5, 2091-2100.
(6) Suzuki, T.; Mate, N. A.; Adhikari, A. A.; Chisholm, J. D. *Molecules* **2019**, *24*.
(7) Lee, H.-S. K., Ko-hoon; Lim, Jin-Woo; Kim, Jae-Jyoung *BKCS* **2011**, *32*, 1083.
(8) Liddon, J. T. R.; Rossi-Ashton, J. A.; Taylor, R. J. K.; Unsworth, W. P. *Org. Lett.* **2018**, *20*, 3349.

Spiroindolenine-based peptidomimetic frameworks in continuous flow

4.1 Ugi-Joullièe MCR in continuous flow: sustainable synthesis of spiroindolenine-based peptidomimetics

Due to the well-established importance of peptidomimetics in medicinal chemistry and benefits generated from flow technology, including better mixing, higher heat and mass transfer, minimum consumption of solvents, higher yields and shorter times, we proposed a new protocol for the synthesis of peptidomimetics in continuous flow settings.

One of the drawbacks of peptides, as previously explained, is related to the potential of off-target effects caused by the rotatable bonds present in the structure. During the years, the design of new peptidomimetic structures is increasing adopting the conformational restriction concept, in order to overcome the problem associated to low selectivity and to mimic as much as possible the secondary structure of peptides. Among the conformationally restricted peptidomimetic structures, spirocyclic moieties are widely identified as useful tools for this purpose. Nowadays, the possibility of building spirocyclic constrained peptidomimetics, *via* multicomponent reactions (MCRs),[1] with decreased peptide-like features and improved drug-like properties is particularly attractive for medicinal chemistry researchers. MCRs are eco-friendly one-pot reactions taking place with three or more substrates and forming only one preeminent product.[2] MCRs can be seen as chemical strategies fully in line with the principles of eco-compatibility and eco-sustainability, which display crucial importance in modern chemistry. MCRs also have found routine application in the generation of libraries for biological screening, according to the principles of diversity-oriented synthesis (DOS) introduced by Schreiber.

The isocyanide-based multicomponent reactions (iMCRs) can be considered the crucial component of MCR armamentarium.

The classic Ugi-4CR, an isocyanide-based MCR, encompasses a condensation between a carbonyl compound (aldehyde or ketone), an amine derivative, a carboxylic acid and of course an isocyanide.[2,3]

The U-4CR is well-known as powerful method in organic synthesis for providing acyclic structures with a certain degree of complexity, although scarcely appealing from a medicinal chemistry point of view, due to the aforementioned potentially disadvantageous conformational flexibility. However, the implementation of intra-molecular Ugi-type reactions using bifunctional starting materials, like amino acids, oxoacids or cyclic imines, could lead to conformationally restricted peptidomimetic substructures potentially useful for pharmaceutical application.

In particular, the use of cyclic imine substrates, could lead to sterically constrained peptidomimetics endowed with improved bioavailability, stability and target selectivity. Due to the use of already condensed amines and aldehydes (*i.e* cyclic imines) the actual starting materials are reduced from 4 to 3; therefore, the reaction was named Joulliè-Ugi three-component. Scheme 1 shows the mechanism of Joulliè-Ugi three-component reaction.

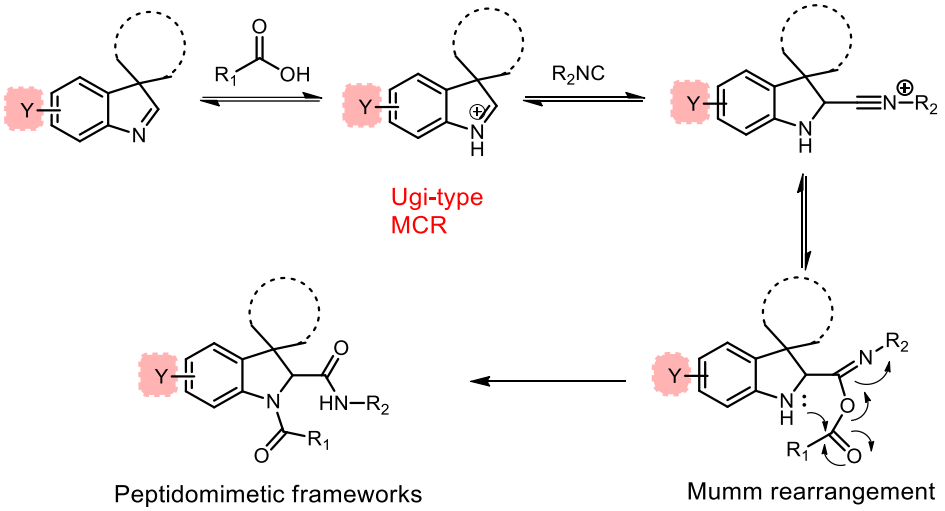

Scheme 1. JU-3CR mechanism. The first step involves the activation of preformed cyclic imine by carboxylic acid, achieving iminium intermediate. Then, an *in-situ* addition of isocyanide to the α carbon of the iminium ion produces nitrilium intermediate, followed by the addition of carboxylate, which undergoes a Mumm rearrangement to afford the product.

Compounds resulting from JU-3CR contain cyclic imines structural templates and thus may resemble proline-like constrained peptidomimetic moieties, extremely useful for the obtaining the desired conformational turns or for increasing the proteolytic stability of peptide-like derivatives (Figure 2).

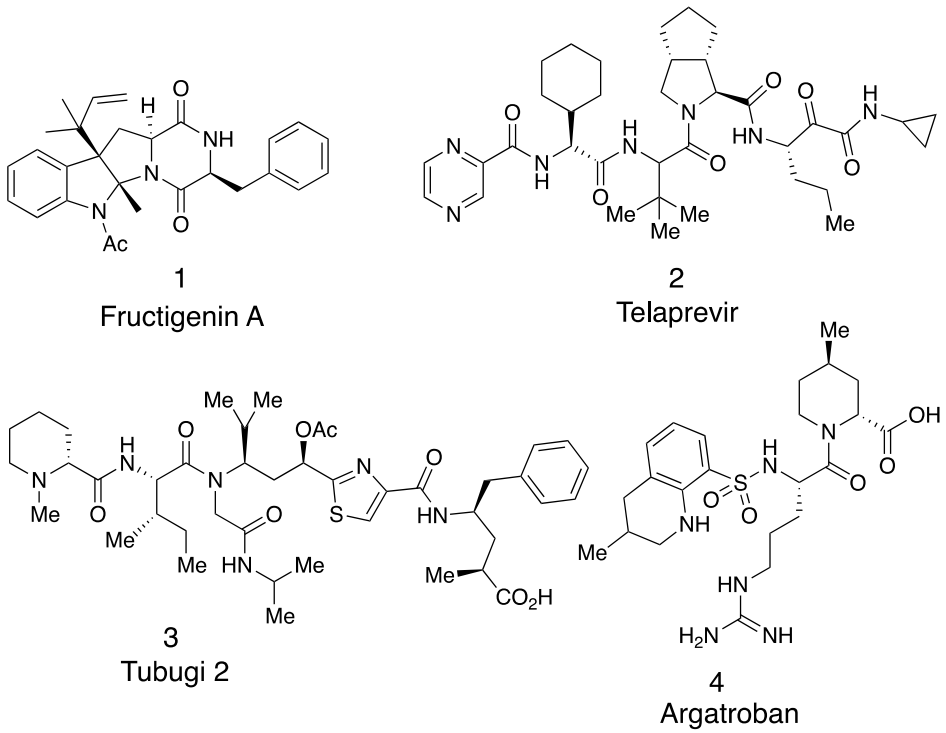

Figure 1. Medicinally relevant compounds obtained by the use of cyclic imines in Ugi-type reactions.[4,5,6]

In our quest towards development of sustainable protocols for the generation of peptidomimetic drug-like scaffolds under continuous flow conditions, we sought to investigate the reactivity of cyclic imines as substrates for the isocyanide-based MCRs. Having developed a reliable, green and sustainable flow-based route to generate (spiro)indolenines and (spiro)indolines, we decided to investigate the use of indolenines, as the cyclic amine substrates for a Joulliè-Ugi MCR, with the aim of quickly and efficiently achieve peptidomimetic frameworks.[7]

The (spiro)indolenine **5**, prepared in flow as reported above, was employed as the benchmark. Starting from there, we set out to explore different

isocyanides and amino acids for realizing structural variation in flow. We decided to functionalize the amine with three *N*- capped amino acid derivatives bearing different lateral chains and protecting groups and three isocyanide derivatives. In particular, we used Cbz-L-Ala, Cbz-L-Phe and Boc-L-PhG, with different electronic and steric properties, and we investigate the outcome -Boc and -Cbz protecting groups, which could also guarantee subsequent nitrogen functionalization at a later stage, *p*-Methoxyphenyl isocyanide, benzyl isocyanide and cyclohexyl isocyanide were explored by us in order to explore the different reactivities basically associated to steric and electronic features of the isocyanide component. Furthermore, we applied the methodology using trityl isocyanide prepared in house in the presence of and (*S*)-3-(acetylthio)-2-methylpropanoic acid, since this latter is an acid portion, bearing an acetyl capped thiol moiety, which is present in the drug captopril. Due the intrinsic instability associated to spiroindolenine **5**, we directly used it as MCR substrate without further purification after formation. In the preliminary batch investigation, spiroindolenine **5** was firstly dissolved in DCM (0.3 M) followed by the addition of the corresponding amino acid (**7a-c**) (1.0 eq) and isocyanide (**6a-c**) (1.0 eq) and the mixture was stirred in a sealed tube for 24-30 h at 50 °C. A library of 10 peptidomimetics (Table 1) was achieved in good yields ranging from 57% to 74% in form of their diastereomeric mixtures, after chromatographic purification. The diastereomeric mixtures were then separated through the use of reverse-phase HPLC using a PFP column (see Experimental Section for details).

Table 1. Ugi-Joullié products synthesized in batch mode.

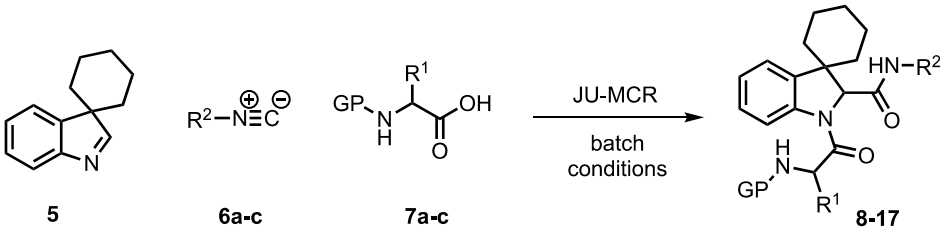

5 **6a-c** **7a-c** **8-17**

Entry	Products[a]	Yield (%)[d]
1	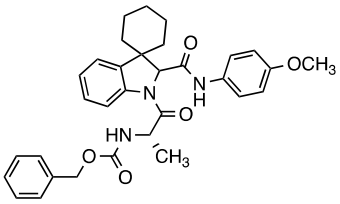	72
	(*S*,*S**)-**8** and (*S*,*R**)-**8**	
2	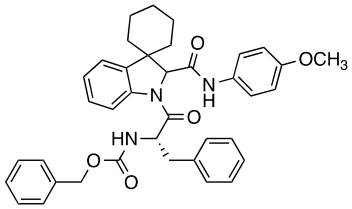	68
	(*S*,*S**)-**9** and (*S*,*R**)-**9**	
3	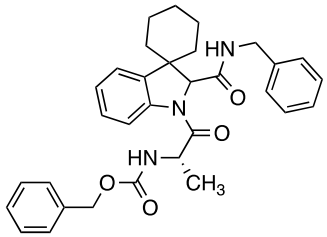	58
	(*S*,*S**)-**10** and (*S*,*R**)-**10** [b]	
4	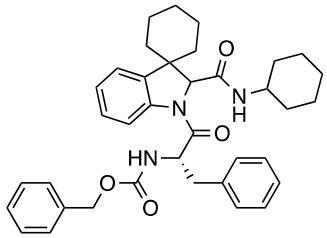	60
	(*S*,*S**)-**11** and (*S*,*R**)-**11** [b]	

5	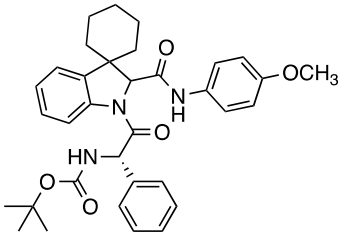 (*S*,*S**)-**12** and (*S*,*R**)-**12**	60
6	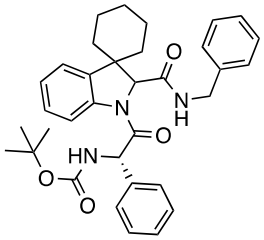 (*S*,*S**)-**13** and (*S*,*R**)-**13**	58
7	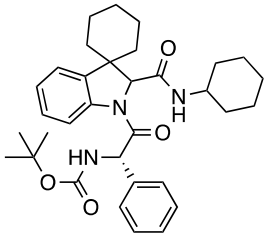 (*S*,*S**)-**14** and (*S*,*R**)-**14**	60
8	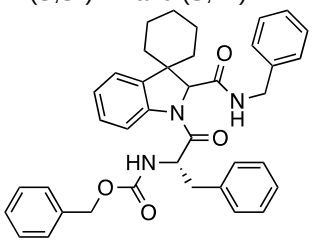 (*S*,R/*S*)-**15**	74
9	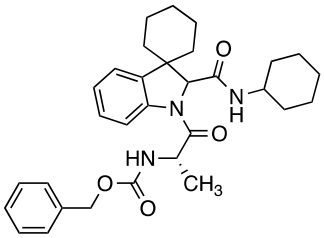 (*S*,R/*S*)-**16**	65

10	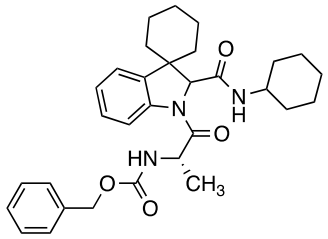 (*S*,R/S)-**16** [c]	62
11	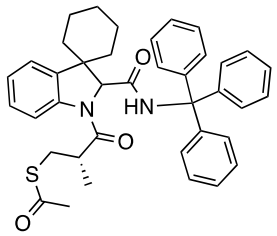 (*S*,*S**)-**17** and (*S*,*R**)-**17**	57

[a] Reactions conditions: Spiroindolenine **5** was dissolved in DCM (0.3 M) followed by the addition of the corresponding amino acid (1.0 eq) and isocyanide (1.0 eq). The reaction mixture was stirred for 30 h at 50 °C. [b] Reaction time: 24 hours; [c] Reactions conditions: Spiroindolenine **5** was dissolved in MeOH (0.3 M) followed by the addition of the corresponding amino acid (1.0 eq) and isocyanide (1.0 eq). The reaction mixture was stirred for 30 h at 50 °C. [d] Yield of the diastereomeric mixture after column chromatography as specified in the Experimental Section.

Based on the initial batch results, reliable flow conditions were elaborated in our rudimental set up, composed as followed: HPLC pumps, 1 mL sample loop, tubular reactor coil of 15 mL or 31 mL volume and a 100 psi (7 bar) BPR at the end of the line to regulate the pressure of the system. We screened a variety of reaction conditions, *i.e.* solvent, temperature, pressure and flow rate (Table 2). The best reaction conditions envisaged the use of ethanol as green solvent, a flow rate of 0.2 mL/min, corresponding to residence time of ~ 75 min and a temperature of 50 °C.

Table 2. Optimisation of reaction conditions in flow for the preparation of peptidomimetics.

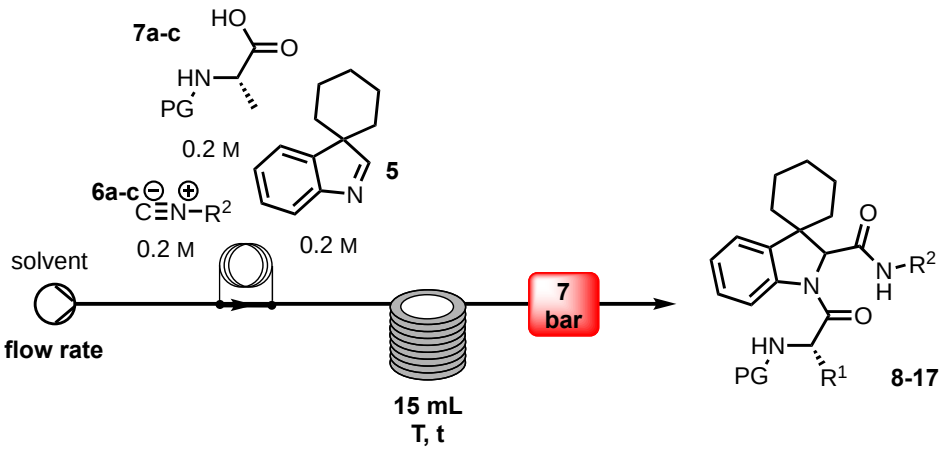

Entry[a]	Product	Residence time (min)	T (°C)	Yield (%) [b]	Output (g/h)
1	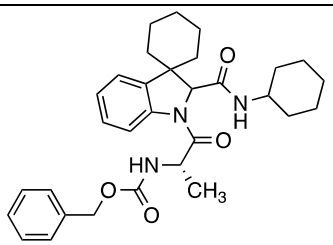 (*S*,R/S)-**16**	75	50	57	0.06
2	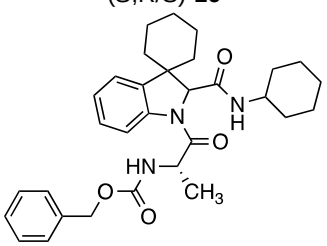 (*S*,R/S)-**16**	75	80	53	0.054
3	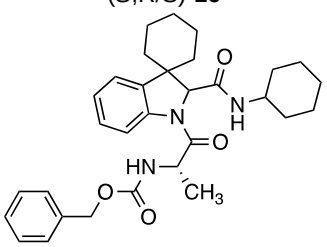 (*S*,R/S)-**16**	75	130	35	0.036

4[c]	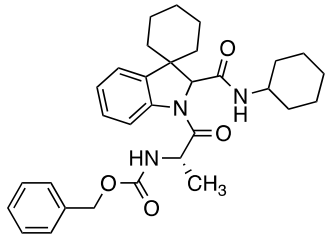 (*S*,R/S)-**16**	155	50	22	0.011
5[d]	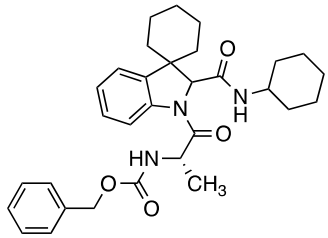 (*S*,R/S)-**16**	155	50	45	0.022
6[d]	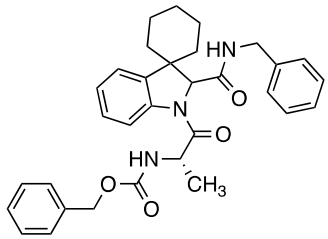 (*S*,*S**)-**10** and (*S*,*R**)-**10** [b]	75	50	54	0.056
7[d]	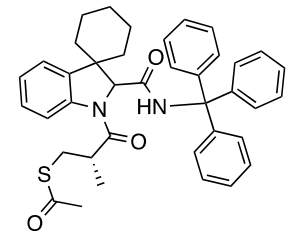 (*S*,*S**)-**17** and (*S*,*R**)-**17**	75	50	25[e]	0.032

[a] Reactions conditions: Spiroindolenine **5** was dissolved in MeOH (0.3 M) followed by the addition of the corresponding amino acid (1.0 eq) and isocyanide (1.0 eq). The reaction mixture was stirred for 75 min at 50 °C, with flow rate of 0.2 mL/min. [b] Isolated yield for the diastereomeric mixture after column chromatographic purification; [c] flow rate 0.1 mL/ min [d] ethanol as solvent; [e] The yield decreases in the protic solvent due to the competing Strecker-type reaction path involving trityl isocyanide as a suitable cyanide source; the same reaction using DCM as solvent provided a 47% yield.

The evidence that ethanol was well tolerated as solvent for the multicomponent reaction, prompted us to couple the indolenine formation step through Interrupted Fischer indolisation with the subsequent MCR protocol.

To remove both the excess of HCl and unreacted aldehyde, as reported in our first protocol detailed above, the reactor effluent spiroindolenine was passed through an in-line column packed with an excess of polymer-supported tris(2-aminoethyl)amine.

Parallelly, other two sample loops were loaded with the appropriate isocyanide and the amino acid in equimolar amounts. When the first drop of indolenine stream exited the column and entered in a subsequent glass mixing chip, the stream containing the carboxylic acid and the isocyanide was pumped with an overall flow rate of 0.4 mL/min. The exiting flow was monitored based on the predicted residence time and the color of the exiting stream. The MCR took place in a 16 mL tubular reactor at 50 °C then, in 80 min of residence time. Using ethanol as green solvent, four different peptidomimetics were realized (Table 3) in excellent overall yields for the diastereomeric mixtures.

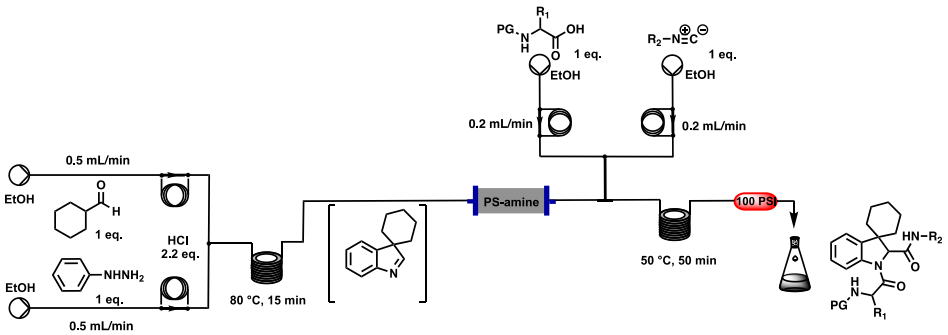

Table 3. Preparation of peptidomimetics in telescoped fashion.

Entry	Product	Time (min)	Yield (%)[a]	Output over two steps (mg/h)
1	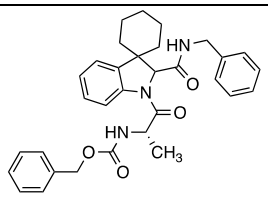 (*S*,*S**)-**10** and (*S*,*R**)-**10**	~101	46	0.039
2	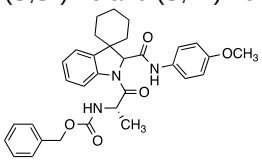 (*S*,*S**)-**8** and (*S*,*R**)-**8**	~101	51	0.038
3	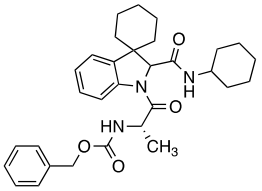 (*S*,R/S)-**16**	~101	56	0.048
4	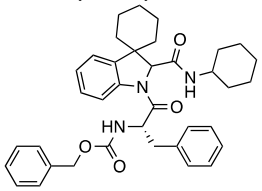 (*S*,*S**)-**23** and (*S*,*R**)-**23**	~101	47	0.045

[a] Isolated yield after column chromatography.

Only approx. 15% of the combined amount of solvent was necessary for the two batch processes and purifications of the first step done when applying the batch mode, and only 100 min were enough to complete the reaction, in comparison with the 24-48 h needed for the batch mode.

The generated compounds were against *S. epidermidis* to investigate the biofilm inhibition.

Biofilm formation is a major threat to public health, since biofilm-producing bacteria become extremely resistant to antibiotic therapy.[8] Biofilm formation has an enormous impact in terms of public health, causing infections associated to catheter, artificial prosthesis and other medical devices and generating skin, soft tissue and dental infections. In biofilm, the resistance mechanism is still unknown, although it seems clearly associated to multicellular pathways.[9-11]

Currently, no therapeutic options specifically aimed at inhibiting biofilm formation or disrupting mature biofilms are available.

First of all, in order to check whether our compounds were behaving as antimicrobial agents, the minimum inhibitory concentrations (MIC) were determined by broth microdilution assay, this analysis confirmed that none of the compounds showed antimicrobial potential. S*tafilococcus epidermidis* is an inhabitant of skin and the main responsible of nosocomial infections associated to medical devices.[12,13]

Biofilm inhibition of *S. epidermidis* was evaluated through the crystal violet assay and in particular three compounds were able to reduce biofilm formation by 20-25% at 100 μM concentration (Figure 2). The latter results are encouraging since infections due to biofilm are difficult to treat and foster further investigation and optimization for this class of compounds. Furthermore, a preliminary bioscreen in vitro was performed to establish the effects on human HaCaT cell survival, demonstrating good biocompatibility of all the assessed molecules whereas significant cytotoxic effects are detectable only at very high in vitro concentrations (Figure 3).

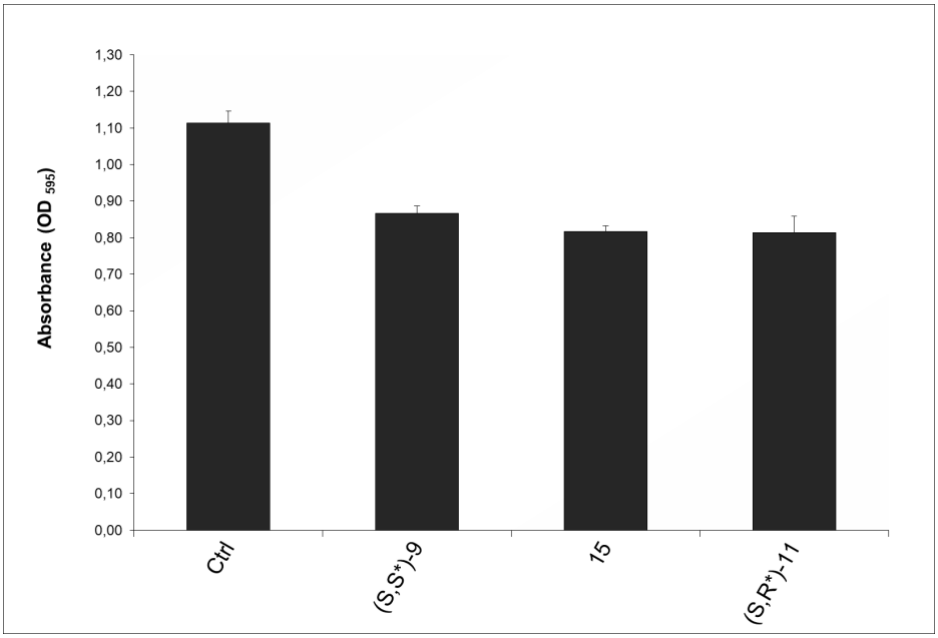

Figure 2. Effect of compounds *(S,S*)*-**9**, **15** and *(S,R,*)*-**11** on *S. epidermidis* biofilm reduction. Values represents the means ± standards deviations from three independent experiments. Control = DMSO treated cells (vehicle).

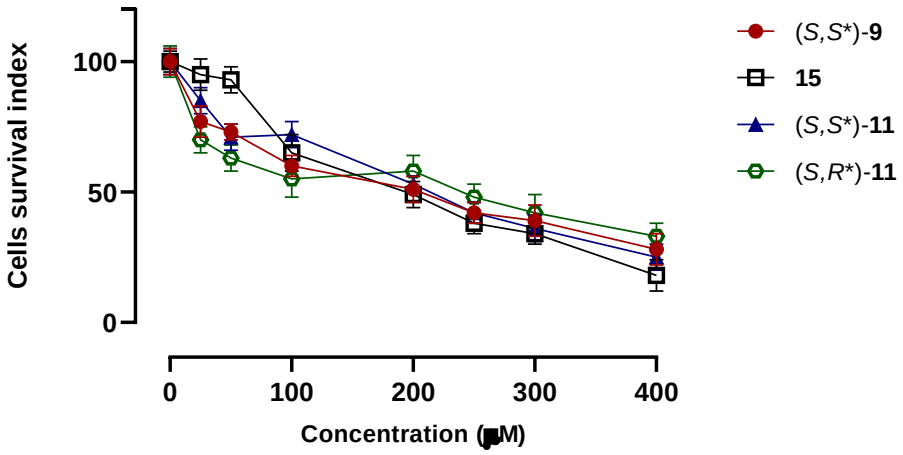

Figure 3. Cell survival index, evaluated by the MTT assay and live/dead cell ratio analysis. Human keratinocytes (HaCaT cells) were incubated for 48 with a range of concentrations (25→400 μM) of (*S*,*S**)-**9**, (*S*,*S**)-**11**, (*S*,*R**)-**11** and **15**. Results are expressed in lines graph as the percentage of cell survival index to untreated control cultures and are reported as mean ± SEM (*n*=4) of three independent experiments.

4.2 Experimental part

General comments

Unless otherwise specified, materials were purchased from commercial suppliers and used without further purification. TLC analysis was conducted using aluminum foil supported thin-layer silica gel chromatography plates (F254 indicator). Column chromatography was performed using 230–400 mesh, 60 Å pore diameter silica gel. For ^{1}H NMR and ^{13}C NMR measurements an accurately weighed amount of analyte (about 5.0–10.0 mg) was dissolved in 600 μL of deuterated chloroform ($CDCl_3$) or dimethyl sulfoxide (DMSO-d6). The mixture was transferred into a 5 mm NMR tube and the spectra were acquired on a Bruker Advance 400 MHz spectrometer by using the residual signal of the deuterated solvent as internal standard. Splitting patterns are described as singlet (s), doublet (d), triplet (t), quartet (q) and broad (br); the values of chemical shifts (δ) are given in ppm and coupling constants (J) in Hertz (Hz). NMR data were processed with MestreNova (Version 8.1.1, Mestrelab Research). ESI-MS spectra analysis was carried out on a mass spectrometer LTQ-XL. HPLC was performed with a Waters Model 510 pump equipped with Waters Rheodyne injector and a differential refractometer, model 401. Luna 5 μm PFP (2) 100 A HPLC Column 250 × 10 mm was employed. The purity of compounds was estimated to be greater than 95% by HPLC analysis. Optical rotation values were measured at room temperature operating at $\lambda = 589$ nm, corresponding to the sodium D line, and were determined in a Jasco P-200 (Jasco Europe s.r.l., Cremella, Italy) polarimeter using a microcell (1mg sensitivity) containing the compound dissolved in 1 mL of chloroform.

Continuous flow synthesis of spiroindolenine **5**

Chemical transformations in flow were realized using a self-made flow reactor: two Waters P510 HPLC pumps were connected each to a Rheodyne 9010 injection valves, each equipped with a 1 mL sample loop (SL) made from PTFE tubing and an injection port for disposable syringes. The injection valves were further connected via a T-piece to a coiled PTFE tubing of 15 mL volume. The coil was immersed in a silicone oil bath for controlling reaction temperatures. The tubular reactor finished into a back pressure regulator (BPR), which was either spring mechanism-based (6.7 bar) or simply a PEEK capillary of defined length (1.7 bar). Product containing exiting streams were collected directly in a flask. An aliquot of the collected phase was used for analysis by GC-MS. Reagents were prepared for loading into the sample loops according to one of the following this method: 0.25 mmol aldehyde+0.25 mmol $PhNHNH_2 \cdot HCl$ in 1 mL of EtOH, heated to 50 °C for 5 min prior to loading into the SL; SL B: (equiv.$^{-1}$) HCl in 1 mL of EtOH.

Spiro[cyclohexane-1,3'-indole] **5**. A mixture of phenylhydrazine salt (36.5 mg, 0.25 mmol) and cyclohexanecarboxaldehyde (30 μL, 0.25 mmol) was treated with HCl (150 μL, 0.3 mmol). Next, the reaction mixture was gradually poured into saturated aqueous $NaHCO_3$ (100 mL) and extracted with EtOAc (5 × 2 mL). Combined organic extracts were washed with brine, dried with Na_2SO_4, and used without purification. Yield: 58%; yellow solid; Rf=0.6 (H:E= 7 : 3). GC-MS (EI, 70 eV): m/z (%) = 187 $[M]^+$ tR = 14.94 min.

Synthesis of multicomponent products in batch (General procedure A)

Spiroindolenine **5** (0.54 mmol) was dissolved in DCM followed by the addition of the corresponding amino acid (**7a-c**) (1.0 eq) and isocyanide (**6a-c**) (1.0 eq). The reaction mixture was stirred for 24– 30 h at 50 °C. Then, DCM was evaporated under vacuum to achieve the crude residue that was subjected to column chromatography (SiO_2, corresponding eluent) and to HPLC to afford a diastereomeric mixture.

Synthesis of multicomponent products in flow (General procedure B)

Chemical transformations in flow were realized using a self-made flow reactor: a Waters P510 HPLC pump was connected to a Rheodyne 9010 injection valve, equipped with a 1 mL sample loop made from PTFE tubing and an injection port for disposable syringes. The injection valve was further connected to a coiled PTFE tubing of 15 mL volume. The coil was immersed in a silicone oil bath for controlling reaction temperatures. The tubular reactor finished into a mechanical back pressure regulator (BPR) of approx. 7 bar). Product containing exiting streams were collected directly in a flask.

A solution of spiroindolenine **5** (49.5 mg, 0.25 mmol), the suitable amino acid (0.25 mmol) and isocyanide (0.25 mmol) was prepared in MeOH (1 mL total solution volume). The flow reactor was heated to 80 °C MeOH was used as solvent at a total flow rate of 0.2 mL/ min to move the reaction mixture through the coil reactor for a residence time of 75 min.

Synthesis of multicomponent products in telescoped continuous flow (General procedure C)

The initial spiroindolenine formation step was performed analogously to the above reported conditions. Two HPLC pumps were connected to Rheodyne 9010 injection valves, each equipped with a 1 mL sample loop made from PTFE tubing and an injection port for disposable syringes. One sample loop was loaded with phenylhydrazine hydrochloride salt and cyclohexylcarbaldehyde (each 0.25 M in EtOH) and the other one with ethanolic HCl (0.3 M in EtOH). These two lines were joined by means of a T-piece that connected the injection part to a coiled PTFE tubing of 15 mL volume. The coil was immersed in a silicone oil bath for controlling reaction temperatures. This tubular reactor was followed by an Omnifit column reactor filled with an excess (in mmol) of polymer- supported tris(2-aminoethyl)amine. The exit of the column reactor was connected to one inlet of an effecting mixing chip (Sigma Aldrich glass microreactor LTF MR Lab MX) of 0.2 mL.

Two additional HPLC pumps were connected to two other six-port injection valves, each equipped with a 1 mL sample loop made from PTFE tubing and an injection port for disposable syringes, allowing for separate streams containing the appropriate amino acid (0.25 M ethanolic solution in sample loop) and isocyanide (0.25 M ethanolic solution in sample loop). The two streams were joined via a simple T-piece before being led via the second inlet port into the mixing chip. Mixing was achieved with an overall flow rate of 0.8 mL/min, realised by combination of 0.2 mL/min flow rate for the pumps furnishing acid and isonitrile, respectively, and a change of the overall flow rate of the spiroindolenine part to 0.4 mL/min

as soon as the spiroindolenine stream was about to reach the mixing chip, as indicated by the colouring of the tube content.

As soon as the fading colour of the solvent in the tubing indicated the completion of mixing, the MCR reaction was allowed to take place in a 16 mL tubular reactor held at 50 °C, by ultimately lowering the flow rate to 0.2 mL/min by switching off three of the four pumps.

The overall telescoped flow system was pressurised to 7 bar via a mechanical BPR. Product containing exiting streams were collected directly into a flask.

Compound characterization

Benzyl ((2S)-1-(2'-((4-methoxyphenyl)carbamoyl)spiro [cyclohexane-1,3'-indolin]-1'-yl)-1-oxopropan-2-yl)carbamate (**8**). According to general procedure A, a mixture of spiro[cyclohexane- 1,3'-indole] **5** (100 mg, 0.54 mmol), Z-L-alanine **7a** (120 mg, 0.54 mmol) and 4-methoxyphenyl isocyanide **6a** (71 mg, 0.54 mmol) was dissolved in DCM (2 mL) in a sealed tube at 50 °C for 30 hours. The crude product was purified by chromatography on silica gel with hexane/ EtOAc (7 : 3) to yield the single diastereoisomers. The products were subjected to HPLC with MeOH/H_2O (85 : 15) as the eluent (flow rate 3.00 mL/min) for purity determination. Total yield: 72 % (dr 1 : 1).

(S,S*)-8: yellowish solid; Rf = 0.45 (H : E = 7 : 3). ^{1}H NMR (400 MHz, DMSO-d6) δ 10.49 (s, 1H), 7.99 (d, 1H), 7.87 (d, 1H), 7.47 (d, 2H), 7.38–7.31 (m, 5H), 7.22 (d, 1H), 7.16 (t, 1H), 7.03 (t, 1H), 6.89 (d, 2H), 5.31 (s, 1H), 5.06 (d, 1H), 5.00 (d, 1H), 4.56 (t, 1H), 3.72 (s, 3H), 1.93–1.86 (m, 2H), 1.72–1.60 (m, 5H), 1.24 (s, 3H), 1.10 (d, J = 6.8 Hz, 3H). ^{13}C NMR (101 MHz, DMSO) δ 172.4, 167.2, 156.4, 156.2, 142.9, 141.1, 137.4,

131.6, 128.8 (2), 128.2, 128.1 (2), 127.4, 124.0, 122.5, 121.7 (2), 116.8, 114.5 (2), 70.2, 65.9, 55.6 (2), 48.8, 31.1, 30.0, 25.5, 23.2, 22.3, 16.8. ESI-MS m/z: $[M + H]^+$ 542. tR HPLC = 11.19 min. $[\alpha]^{20}_D$ = + 7.76 (c 0.3, $CHCl_3$).

(S,R)-**8***: yellowish solid; Rf = 0.35 (H : E = 7 : 3). ^{1}H NMR (400 MHz, DMSO-d6) δ 10.33 (s, 1H), 8.01 (d, *J*=8.0 Hz, 1H), 7.59 (d, *J*=7.4 Hz, 1H), 7.47–7.42 (m, 2H), 7.34–7.30 (m, 4H), 7.23–7.18 (m, 2H), 7.04 (d, *J* = 7.1 Hz, 1H), 6.89 (t, *J* = 9.0 Hz, 2H), 4.99–4.93 (m, 3H), 4.55–4.48 (m, 1H), 3.72 (s, 3H), 1.94–1.81 (m, 3H), 1.73–1.69 (m, 2H), 1.65–1.62 (m, 2H), 1.35 (d, *J* = 6.5 Hz, 3H), 1.24 (s, 3H). ^{13}C NMR (101 MHz, $CDCl_3$) δ 171.4, 166.4, 156.9, 155.4, 140.4, 139.7, 136.2, 129.5, 128.5 (3), 128.1 (3), 125.6, 123.1 (2), 122.9, 117.9, 114.0 (2), 71.2, 66.9, 55.4, 49.3, 39.5, 30.3, 29.7, 25.4, 22.7 (2), 18.6. ESI-MS m/z: $[M + H]^+$ 542; tR HPLC = 11.79 min. $[\alpha]^{20}_D$ = - 22.13 (c 0.3, CHCl3).

Benzyl((2S)-1-(2'-((4-methoxyphenyl)carbamoyl)spiro [cyclohexane-1,3'-indolin]-1'-yl)-1-oxo-3-phenylpropan-2-yl) carbamate (**9**). According to general procedure A, a mixture of spiro[cyclohexane-1,3'-indole] **5** (100 mg, 0.54 mmol), Z-L-Phenyl- alanine **7b** (161 mg, 0.54 mmol) and 4-methoxyphenyl isocyanide **6a** (71 mg, 0.54 mmol) was dissolved in DCM (2 mL) in a sealed tube at 50 °C for 30 hours. The crude product was purified by chromatography on silica gel with hexane/EtOAc (7 : 3) to yield the single diastereoisomers. The products were subjected to HPLC with MeOH/H2O (85 : 15) as the eluent (flow rate 3.00 mL/min) for purity determination. Total yield: 68 % (dr 1 : 1).

(S,S)-**9***: yellowish solid; Rf = 0.62 (H : E = 7 : 3). ^{1}H NMR (400 MHz, DMSO-d6) δ 10.64 (s, 1H), 8.03 (t, J = 7.6 Hz, 2H), 7.55 (d, *J* = 7.6 Hz, 2H), 7.35–7.25 (m, 6H), 7.20–7.06 (m, 7H), 6.92 (d, *J* = 7.9 Hz, 2H),

5.49 (s, 1H), 4.97 (s, 2H), 4.61 (s, 1H), 3.72 (s, 3H), 2.92–2.83 (m, 2H), 1.98–1.90 (m, 2H), 1.79–1.62 (m, 6H), 1.27–1.21 (m, 2H). ^{13}C NMR (101 MHz, $CDCl_3$) δ 169.9, 166.7, 156.7, 156.6, 140.9, 140.5, 136.0, 135.8, 130.2, 129.3 (2), 129.1, 128.5 (2), 128.2, 128.0 (2), 126.8, 125.2, 125.0, 124.9, 122.6, 121.6 (2), 117.7, 114.1 (2), 71.0, 67.3, 55.5, 54.8, 49.2, 39.5, 38.3, 30.3, 25.3, 23.2, 22.7. ESI-MS m/z: $[M + H]^+$ 618; tR HPLC = 22.22 min. $[\alpha]^{20}_D$ = + 23.93 (c 0.3, $CHCl_3$).

(S,R)-**9***: yellowish solid; Rf = 0.52 (H : E = 7 : 3).

^{1}H NMR (400 MHz, DMSO-d6) δ 10.30 (s, 1H), 8.08 (d, *J*=7.8 Hz, 1H), 7.58 (d, *J*=8.5 Hz,1H), 7.51 (d, *J*=8.5Hz, 1H), 7.42 (d, *J*=8.8Hz, 2H), 7.29 (d, *J*=9.3 Hz, 6H), 7.20–7.17 (m, 3H), 7.07–6.98 (m, 2H), 6.86 (d, *J* = 8.7 Hz,3H), 4.90–4.86 (m, 1H), 4.84 (s, 2H), 4.75 (d, *J* = 12.6 Hz, 1H), 3.70 (s, 3H), 3.03–2.95 (m, 2H), 1.89–1.79 (m, 2H), 1.71–1.61 (m, 6H), 1.37–1.27 (m, 2H).

^{13}C NMR (101 MHz, $CDCl_3$) δ 170.4, 166.3, 156.8, 155.2, 140.2, 140.0, 136.1, 135.5, 129.3 (2), 128.9 (2), 128.4 (4), 128.0 (3), 127.2 (2), 125.5, 122.8 (2), 117.7, 113.9 (2), 71.8, 66.9, 55.4, 54.9, 48.9, 39.7, 39.6, 30.6, 25.3, 23.1, 22.7.

ESI-MS m/z: $[M+H]^+$ 618; tR HPLC=23.54 min. $[\alpha]^{20}_D$ = + 2.63 (c 0.3, $CHCl_3$).

Benzyl((2S)-1-(2'-(benzylcarbamoyl)spiro[cyclohexane-1,3'-indo- lin]-1'-yl)-1-oxopropan-2-yl)carbamate (**10**).

According to general procedure A, a mixture of spiro[cyclohexane-1,3'-indole] **5** (100 mg, 0.54 mmol), Z-L-Alanine **7a** (161 mg, 0.54 mmol) and benzyl isocyanide **6b** (65 μL, 0.54 mmol) was dissolved in DCM (2 mL) in a sealed tube at 50 °C for 24 hours. The crude product was purified by chromatography on silica gel with hexane/EtOAc (7 : 3) and by HPLC

with MeOH/H_2O (82 : 18) as the eluent (flow rate 3.00 mL/min) to yield single diastereomers. Total yield: 58 % (dr 1 : 1)

(S,S)-**10***: yellowish solid; Rf=0.62 (H:E=7:3).

^{1}H NMR (400MHz, DMSO-d6) δ 8.98 (s, 1H), 7.99 (d, *J*=7.8 Hz, 1H), 7.56 (d, *J*=7.3 Hz, 1H), 7.42–7.38 (m, 3H), 7.31–7.23 (m, 7H), 7.19–7.15 (m, 2H), 7.03 (d, *J* = 7.1 Hz, 1H), 5.08 (q, *J* = 12.6 Hz, 2H), 4.89 (s, 1H), 4.57–4.48 (m, 1H), 4.38–4.31 (m, 1H), 4.25–4.18 (m, 1H), 1.75 (d, *J* = 13.4 Hz, 1H), 1.64–1.52 (m, 6H), 1.34–1.22 (m, 6H).

^{13}C NMR (101 MHz, DMSO) δ 171.7, 167.7, 155.8, 142.8, 141.1, 139.0, 137.5, 128.8 (2), 128.7 (2), 128.4 (2), 128.2, 128.1 (3), 127.4, 124.0, 122.1, 116.7, 68.3, 65.8, 49.2, 48.5, 43.1, 29.7, 25.6, 23.2, 22.2, 21.8, 18.7.

ESI-MS m/z: $[M + H]^+$ 526; tR HPLC = 18.79 min. $[\alpha]^{20}_D$ = - 34.50 (c 0.3, $CHCl_3$).

(S,R)-**10***: yellowish solid; Rf = 0.62 (H : E = 7 : 3).

^{1}H NMR (400 MHz, DMSO-d6) δ 9.08 (s, 1H), 7.95 (d, *J* = 7.9 Hz, 1H), 7.81 (d, *J* = 6.0 Hz, 1H), 7.35–7.31 (m, 6H), 7.30–7.27 (m, 3H), 7.22–7.10 (m, 3H), 7.01 (t, *J* = 7.3 Hz, 1H), 5.20 (s, 1H), 5.06–4.95 (m, 2H), 4.42–4.36 (m, 1H), 4.26 (d, *J* = 5.4 Hz, 2H), 1.80 (dd, *J* = 17.8, 10.0 Hz, 2H), 1.69–1.55 (m, 6H), 1.27–1.16 (m, 2H), 1.00 (d, *J* = 6.8 Hz, 3H).

^{13}C NMR (101 MHz, DMSO) δ 172.2, 168.5, 156.4, 142.7, 141.3, 139.1, 137.3, 128.8 (2), 128.7 (2), 128.6 (2), 128.3, 128.1 (2), 127.5, 127.3, 124.0, 122.3, 116.9, 69.7, 65.9, 48.6, 48.4, 43.0, 29.9, 25.5, 23.2, 22.3, 16.9 (2).

ESI-MS m/z: $[M+H]^+$ 526; tR HPLC = 20.79 min. $[\alpha]^{20}_D$ = + 9.63 (c 0.3, $CHCl_3$).

Benzyl((2S)-1-(2'-(cyclohexylcarbamoyl)spiro[cyclohexane-1,3'-indolin]-1'-yl)-1-oxo-3-phenylpropan-2-yl)carbamate (**11**).

According to general procedure A, a mixture of spiro[cyclohexane-1,3'-indole] **5** (100 mg, 0.54 mmol), Z-L-phenylalanine **7b** (161 mg, 0.54 mmol) and cyclohexyl isocyanide **6c** (66 μL, 0.54 mmol) was dissolved in DCM (2 mL) in a sealed tube at 50 °C for 24 hours. The crude product was purified by chromatography on silica gel with hexane/ EtOAc (8 : 2) and by HPLC with MeOH/H_2O (82 : 18) as the eluent (flow rate 3.00 mL/min) to yield single diastereomers. Total yield: 60% (dr 1:1).

(S,S)-**11***: yellowish solid; Rf = 0.51 (H : E = 7 : 3).

^{1}H NMR (400 MHz, DMSO-d6) δ 8.45 (d, *J* = 6.6 Hz, 1H), 7.99 (d, *J* = 7.8 Hz, 1H), 7.89 (d, *J* = 7.4 Hz, 1H), 7.34–7.24 (m, 10H), 7.21–7.19 (m, 1H), 7.15 (d, *J* = 7.5 Hz, 1H), 7.02 (t, *J* = 7.3 Hz, 1H), 5.27 (s, 1H), 4.96 (s, 2H), 4.69–4.61 (m, 1H), 3.46 (s, 1H), 2.90 (d, 1H), 2.76 (d, *J* = 12.9 Hz, 1H), 1.87–1.83 (m, 1H), 1.75–1.59 (m, 9H), 1.55–1.49 (m, 3H), 1.25–1.10 (m, 7H).

^{13}C NMR (101 MHz, DMSO) δ 171.1, 167.6, 156.7, 142.8, 141.5, 137.9, 137.2, 129.7 (2), 128.7 (2), 128.3 (2), 128.2, 128.0 (2), 127.3, 126.8, 124.0, 122.4, 116.9, 69.6, 65.9, 54.1, 48.6 (2), 36.4, 32.3, 31.9, 29.7, 25.6 (3), 24.9, 24.7, 23.3, 22.3.

ESI-MS m/z: $[M + H]^+$ 542; tR HPLC =18.87 min. $[\alpha]^{20}_D$ = + 19.78 (c 0.28, $CHCl_3$).

(S,R)-**11***: yellowish solid; Rf = 0.43 (H : E = 7 : 3).

^{1}H NMR (400 MHz, DMSO-d6) δ 8.34 (d, *J* = 7.1 Hz, 1H), 8.05 (d, *J* = 7.8 Hz, 1H), 7.37–7.24 (m, 11H), 7.15–7.10 (m, 2H), 6.99 (d, *J* = 6.9 Hz, 1H), 5.00 (s, 2H), 4.81–4.73 (m, 1H), 4.64 (s, 1H), 3.48 (s, 1H), 2.97 (d, *J* = 6.9 Hz, 2H), 1.83–1.76 (m, 2H), 1.73–1.58 (m, 10H), 1.27–1.12 (m, 7H), 1.02 (s, 1H).

^{13}C NMR (101 MHz, DMSO) δ 169.9, 166.5, 155.6, 142.7, 141.2, 137.4, 136.9, 129.8 (2), 128.7 (2), 128.6 (2), 128.2, 127.9 (2), 127.4, 126.9, 124.1,

122.3, 116.7, 69.4, 65.7, 54.5, 48.2, 48.1, 32.6 (2), 32.1(3), 29.8, 25.7 (3), 25.1, 24.9, 23.1, 22.4.

ESI-MS m/z: $[M + H]^+$ 542 HPLC=19.75 min. $[\alpha]^{20}_D$ = - 2.33 (c 0.3, $CHCl_3$).

tert-Butyl((1S)-2-(2'-((4-methoxyphenyl)carbamoyl)spiro [cyclohexane-1,3'-indolin]-1'-yl)-2-oxo-1-phenylethyl)carbamate (**12**). According to general procedure A, a mixture of spiro [cyclohexane-1,3'-indole] **5** (100 mg, 0.54 mmol), Boc-L-α-phenyl- glycine **7c** (136 mg, 0.54 mmol) and 4-metoxyphenyl isocyanide **6a** (71 mg, 0.54 mmol) was dissolved in DCM (2 mL) in a sealed tube at 50 °C for 30 hours. The crude product was purified by chromatography on silica gel with hexane/ EtOAc (8:2) and by HPLC with MeOH/H_2O (82 : 18) as eluent (flow rate 3.00 mL/min) to yield single diastereomers. Total yield: 60 % (dr 1 : 1).

(S,S)-**12***: yellowish solid; Rf = 0.43 (H : E = 7 : 3).

^{1}H NMR (400 MHz, DMSO-d6) δ 10.40 (s, 1H), 7.96 (d, *J* = 7.8 Hz, 1H), 7.69 (d, *J* = 6.9 Hz, 1H), 7.44 (d, *J* = 6.7 Hz, 2H), 7.33–7.30 (m, 2H), 7.25 (d, *J* = 7.4 Hz, 2H), 7.16 (d, *J*=7.4 Hz, 2H), 7.08 (t, *J*=7.3 Hz, 1H), 6.88 (d, *J*=8.6 Hz, 2H), 5.72 (d, *J* = 6.9 Hz, 1H), 5.55 (s, 1H), 3.76 (s, 3H), 2.04–1.83 (m, 4H), 1.77–1.65 (m, 6H), 1.44 (s, 9H).

^{13}C NMR (101 MHz, DMSO) δ 170.1, 166.4, 156.1, 156.1, 142.8, 141.5, 135.9, 131.4, 128.7 (2), 128.4 (2), 128.2, 127.3, 124.2, 122.4, 121.8(2), 117.2, 114.2 (2), 79.1, 70.2, 56.6, 55.6, 49.1, 29.7, 28.6 (3), 25.5 (2), 23.1, 22.5.

ESI-MS m/z: $[M+ H]^+$ 570; tR HPLC = 11.64 min. $[\alpha]^{20}_D$ = + 62.1 (c 0.3, $CHCl_3$).

(S,R)-**12***: yellowish solid; Rf = 0.38 (H : E = 7 : 3).

^{1}H NMR (400 MHz, Chloroform-d) δ 8.31 (d, J = 7.9 Hz, 1H), 7.49 (d, J = 6.5 Hz, 2H), 7.39– 7.35 (m, 2H), 7.30–7.27 (m, 2H), 7.22–7.12 (m, 4H), 6.80 (d, J = 8.9 Hz, 2H), 5.72–5.64 (m, 1H), 4.62 (s, 1H), 3.76 (s, 3H), 1.78 (d, J = 33.5 Hz, 6H), 1.65 (s, 1H), 1.57 (d, J = 9.8 Hz, 1H), 1.41 (s, 9H), 1.14 (d, J = 11.7 Hz, 2H).

^{13}C NMR (101 MHz, CDCl3) δ 169.1, 166.6, 157.0, 154.7, 140.4, 139.7, 135.9, 129.6, 129.4 (2), 128.9, 128.5, 128.2 (2), 125.6, 123.5 (2), 122.7, 117.8, 114.0 (2), 79.9, 70.2, 58.1, 55.5, 49.5, 39.6, 30.2, 28.3 (3), 25.1, 22.6, 22.1.

ESI-MS m/z: $[M + H]^{+}$ 570; tR HPLC = 12.26 min. $[\alpha]^{20}_{D}$ = + 28.31 (c 0.32, $CHCl_3$).

tert-Butyl((1S)-2-(2'-(benzylcarbamoyl)spiro[cyclohexane-1,3'-indolin]-1'-yl)-2-oxo-1-phenylethyl)carbamate (**13**). According to general procedure A, a mixture of spiro[cyclohexane-1,3'-indole] **5** (100 mg, 0.54 mmol), Boc-L-α-phenylglycine **7c** (136 mg, 0.54 mmol) and benzyl isocyanide **6b** (65 μL, 0.54 mmol) was dissolved in DCM (2 mL) in a sealed tube at 50°C for 30 hours. The crude product was purified by chromatography on silica gel with hexane/ EtOAc (85 : 15) and by HPLC with MeOH/H_2O (82 : 18) as the eluent (flow rate 3.00 mL/min) to yield single diastereomers. Total yield:58% (dr1:1).

(S,S*)-13: yellowish solid; Rf=0.48 (H:E=7:3).

^{1}H NMR (400MHz, DMSO-d6) δ 8.95 (s, 1H), 7.97 (d, *J* = 7.6 Hz, 1H), 7.79 (d, *J* = 7.3 Hz, 1H), 7.43–7.37 (m, 5H), 7.35–7.29 (m, 4H), 7.23–7.20 (m, 3H), 7.07 (t, *J*=7.3Hz, 1H), 5.67 (d, *J*=7.3Hz, 1H), 5.46 (s, 1H), 4.15 (d, *J*= 14.0 Hz, 1H), 3.89 (d, *J* = 13.9 Hz, 1H), 1.94–1.85 (m, 2H), 1.76 (d, *J* = 12.7 Hz, 1H), 1.69–1.57 (m, 6H), 1.44 (s, 9H), 1.31–1.29 (m, 1H).

^{13}C NMR (101 MHz, DMSO) δ 170.0, 168.1, 156.0, 142.7, 141.7, 138.8, 136.6, 128.6 (4), 128.5 (2), 128.5 (2), 128.2, 127.4, 127.2, 124.2, 122.2, 117.3, 79.0, 69.6, 56.3, 48.7, 43.0, 31.1, 29.6, 28.6 (3), 25.5, 23.2, 22.6. ESI-MS m/z: $[M + H]^+$ 554; tR HPLC = 17.93 min. $[\alpha]^{20}_D$ = + 85.33 (c 0.3, $CHCl_3$).

(S,R)-**13:*** yellowish solid; R = 0.39 (H : E = 7 : 3).

^{1}H NMR (400 MHz, DMSO-d6) δ 9.13 (s, 1H), 8.11 (d, *J* = 7.7 Hz, 1H), 7.57 (d, *J* = 6.4 Hz, 2H), 7.43–7.32 (m, 9H), 7.21 (d, *J* = 7.0 Hz, 1H), 7.16 (d, *J* = 6.4 Hz, 1H), 7.06 (t, *J*=13.4Hz, 1H), 5.53 (d, *J*=7.5Hz, 1H), 4.73 (s, 1H), 4.44–4.32 (m, 2H), 2.15 (s, 9H), 1.52–1.42 (m, 10H).

^{13}C NMR (101 MHz, DMSO) δ 169.0, 167.8, 155.1, 142.7, 140.7, 139.1, 137.3, 129.1 (2), 128.6 (4), 128.5, 128.2 (2), 127.5, 127.3, 124.3, 122.3, 116.7, 78.8, 68.6, 57.3, 48.6, 43.1, 31.1 (3), 28.6 (2), 25.3, 23.0, 22.1.

ESI-MS m/z: [M + H] + 554; tR HPLC = 18.92 min. $[\alpha]^{20}_D$ = + 49.47 (c 0.3, $CHCl_3$).

tert-Butyl((1S)-2-(2'-(cyclohexylcarbamoyl)spiro[cyclohexane-1,3'-indolin]-1'-yl)-2-oxo-1-phenylethyl)carbamate (**14**). According to general procedure A, a mixture of spiro[cyclohexane-1,3'-indole] **5** (100 mg, 0.54 mmol), Boc-L-α-phenylglycine **7c** (136 mg, 0.54mmol) and cyclohexyl isocyanide **6c** (66μL, 0.54mmol) was dissolved in DCM (2 mL) in a sealed tube at 50°C for 30 hours. The crude product was purified by chromatography on silica gel with hexane/ EtOAc (92 : 8) to yield the single diastereoisomers. The products were subjected to HPLC with MeOH/H_2O (85:15) as the eluent (flow rate 3.00 mL/min) for purity determination. Total yield: 60% (dr 1:1).

(S,S)-**14***: yellowish solid; Rf = 0.56 (H : E = 7 : 3).

^{1}H NMR (400 MHz, DMSO-d6) δ 8.51 (d, *J* = 7.6 Hz, 1H), 8.10 (d, *J* = 7.9 Hz, 1H), 7.59 (d, *J* = 7.1 Hz, 2H), 7.45–7.39 (m, 3H), 7.28 (d, *J* = 7.9 Hz, 1H), 7.23–7.15 (m, 2H), 7.05 (t, *J* = 7.4 Hz, 1H), 5.52 (d, *J* = 8.0 Hz, 1H), 4.73 (s, 1H), 3.67–3.59 (m, 1H), 1.86–1.62 (m, 10H), 1.44 (s, 9H), 1.35–1.18 (m, 8H), 0.96 (t, *J* = 18.9 Hz, 2H).

^{13}C NMR (101 MHz, DMSO) δ 169.2, 166.4, 154.9, 142.8, 140.9, 137.9, 128.9 (2), 128.6, 128.2 (2), 127.5, 124.2, 122.3, 116.5, 78.7, 68.9, 56.9, 48.4, 48.2, 32.6, 32.4, 29.7, 28.5 (4), 25.7, 25.4, 25.2, 25.1, 23.0, 21.9. ESI-MS m/z: $[M+H]^+$ 546; tR HPLC = 12.93 min. $[\alpha]^{20}_D$ = + 47.60 (c 0.3, $CHCl_3$).

(S,R)-**14***: yellowish solid; Rf=0.52 (H:E=7:3).

^{1}H NMR (400MHz, DMSO-d6) δ 8.42 (d, *J*=6.6 Hz, 1H), 7.93 (d, *J*=7.8 Hz, 1H), 7.73 (d, *J* = 7.4 Hz, 1H), 7.48–7.42 (m, 2H), 7.38–7.32 (m, 3H), 7.23–7.15 (m, 3H), 7.06 (t, *J* = 7.3 Hz, 1H), 5.70 (d, *J* = 7.5 Hz, 1H), 5.41 (s, 1H), 3.31– 3.24 (m, 1H), 1.82–1.60 (m, 10H), 1.43 (s, 9H), 1.32–1.28 (m, 2H), 1.20–1.12 (m, 7H).

^{13}C NMR (101 MHz, DMSO) δ 170.1, 167.0, 156.1, 142.8, 142.0, 136.6, 128.5, 128.4 (2), 128.2, 127.1, 124.21, 122.1, 117.2, 79.1, 69.5, 56.2, 48.7, 48.0, 32.2, 31.8, 29.6, 29.4, 28.5 (4), 25.6 (2), 24.8, 24.5, 23.4, 22.6.

ESI-MS m/z: [M + H] + 546; tR HPLC = 12.32 min. $[\alpha]^{20}_D$ = + 56.33 (c 0.3, $CHCl_3$).

Benzyl((2S)-1-(2'-(benzylcarbamoyl)spiro[cyclohexane-1,3'-indo- lin]-1'-yl)-1-oxo-3-phenylpropan-2-yl)carbamate (**15**). According to general procedure A, a mixture of spiro[cyclohexane-1,3'-indole] **5** (100 mg, 0.54 mmol), Z-L-Phenylalanine **7b** (161 mg, 0.54 mmol) and benzyl isocyanide **6b** (65 μL, 0,54 mmol) was dissolved in DCM (2 mL) in a sealed tube at 50°C for 30 hours. The crude product was purified by chromatography on

silica gel with hexane/ EtOAc (8 : 2) and by HPLC with MeOH/H_2O (88 : 12) as eluent (flow rate 3.00 mL/ min) to afford an inseparable mixture of diastereomers (74% total yield). Yellowish oil; Rf = 0.64 (H : E = 7 : 3).
^{1}H NMR (400 MHz, DMSO- d6) δ 9.06 (s, 1H), 8.97 (s, 1H), 8.08 (d, *J*=7.9 Hz, 1H), 8.02 (d, *J*= 7.8Hz, 1H), 7.93 (d, *J*=7.8Hz, 1H), 7.56 (d, *J*=8.4Hz, 1H), 7.35 (s, 2H), 7.30–7.21 (m, 25H), 7.21–7.17 (m, 4H), 7.15–7.12 (m, 2H), 7.06– 6.98 (m, 3H), 5.35 (s, 1H), 5.05 (s, 2H), 4.95 (s, 2H), 4.82 (d, *J* = 7.8 Hz, 1H), 4.71 (s, 1H), 4.63–4.56 (m, 1H), 4.41–4.33 (m, 2H), 4.13–4.01 (m, 2H), 2.98–2.88 (m, 3H), 2.76–2.69 (m, 1H), 1.84–1.74 (m, 3H), 1.64– 1.49 (m, 12H), 1.30–1.19 (m, 4H), 1.07–1.03 (m, 1H).
^{13}C NMR (101 MHz, DMSO) δ 171.2, 170.3, 168.7, 167.7, 156.6, 155.7, 142.6, 141.4, 141.1, 139.1, 138.7, 137.9, 137.6, 137.5, 137.2, 136.9, 129.8, 129.7, 128.7 (2), 128.7 (2), 128.7 (3), 128.7 (3), 128.6 (3), 128.5 (3), 128.4 (3), 128.2, 128.1, 128.0 (3), 127.5, 127.4, 127.4, 127.3, 126.9, 126.8, 124.2, 124.2, 122.4, 122.3, 117.1, 116.8, 69.7, 69.4, 65.9, 65.7, 54.4, 54.4, 48.6, 48.2, 43.4, 43.2, 39.2 (3), 36.5, 29.8, 29.7, 25.6, 25.5, 23.1 (2), 22.5, 22.3.
ESI-MS m/z: $[M + H]^+$ 602; tR HPLC = 14.51 min.

Benzyl((2S)-1-(2'-(cyclohexylcarbamoyl)spiro[cyclohexane-1,3'-indolin]-1'-yl)-1-oxopropan-2-yl)carbamate (**16**). According to general procedure A, a mixture of spiro[cyclohexane-1,3'-indole] **5** (100 mg, 0.54 mmol), Z-L-Alanine **7a** (120 mg, 0.54 mmol) and cyclohexyl isocyanide **6c** (66 μL, 0.54 mmol) was dissolved in DCM (2 mL) in a sealed tube at 50°C for 30 hours. The crude product was purified by chromatography on silica gel with hexane/ EtOAc (8:2) and by HPLC with MeOH/H_2O (85:15) as eluent (flow rate 3.00 mL/ min) to afford an inseparable mixture of diastereomers. Total yield: 65%; yellowish oil; Rf =0.51 (H:E=7:3).

^{1}H NMR (400 MHz, DMSO- d6) δ 8.53 (d, J = 7.6 Hz, 1H), 8.41 (d, J = 7.7 Hz, 1H), 7.99–7.92 (m, 2H), 7.82 (d, *J*=6.1Hz, 1H), 7.44 (d, *J*=7.5Hz, 1H), 7.38–7.31 (m, 9H), 7.18–7.11 (m, 5H), 7.02–6.98 (m, 2H), 5.12 (s, 1H), 5.05–4.95 (m, 4H), 4.79 (s, 1H), 4.51–4.43 (m, 2H), 3.57–3.50 (m, 2H), 1.87–1.80 (m, 4H), 1.74–1.62 (m, 19H), 1.55 (d, *J* = 11.5 Hz, 5H), 1.30 (d, *J* = 6.8 Hz, 4H), 1.26–1.19 (m, 9H), 1.14 (d, *J* = 6.9 Hz, 5H).

^{13}C NMR (101 MHz, DMSO) δ 172.3, 171.7, 167.4, 166.3, 156.4, 155.7, 142.9, 142.9, 141.5, 141.2, 137.5, 137.4, 128.8 (2), 128.7 (2), 128.2 (4), 128.1 (2), 127.3, 127.2, 123.9, 123.8, 122.2, 122.1, 116.7, 116.5, 69.5, 68.3, 65.8, 65.7, 49.2, 48.6, 48.3, 48.3, 47.9, 47.9, 32.7, 32.5, 32.4, 32.3, 31.1, 29.8, 29.7, 25.6 (2), 25.6 (2), 25.0, 24.8 (2), 24.7, 23.4, 23.3, 22.4, 22.2, 19.0, 17.1 (2).

ESI-MS m/z: $[M+H]^+$ 518; tR HPLC=12.47 min.

S-((2S)-2-methyl-3-oxo-3-(2'-(tritylcarbamoyl)spiro[cyclohexane- 1,3'-indolin]-1'-yl)propyl) ethanethioate (**17**). According to general procedure A, a mixture of spiro[cyclohexane-1,3'-indole] **5** (100 mg, 0.54 mmol), (S)-3-(acetylthio)-2-methylpropanoic acid **7d** (74 μL, 0.54 mmol) and triphenylmethyl (trityl) **6d** (159 mg, 0.59 mmol) was dissolved in DCM (2 mL) in a sealed tube at 50°C for 30 hours. The crude product was purified by chromatography on silica gel with hexane/ EtOAc (8 : 2) and by HPLC with MeOH/H_2O (85 : 15) as the eluent (flow rate 3.00 mL/min) to yield single diastereomers. Total yield: 57% (dr 1:1).

(S,S*)-23: yellowish solid; Rf = 0.58 (H : E = 7 : 3).

^{1}H NMR (700 MHz, Chloroform-d) δ 8.07 (d, *J* = 7.6 Hz, 1H), 7.12–7.09 (m, 8H), 7.07–7.00 (m, 5H), 6.97–6.92 (m, 5H), 6.71 (d, 1H), 4.57 (s, 1H), 3.27 (d, *J*= 16.6 Hz, 1H), 3.13 (q, *J* = 25.5, 7.4 Hz, 1H), 2.84 (d, 1H), 2.00

(s, 3H), 1.64–1.52 (m, 6H), 1.45–1.38 (m, 2H), 1.28 (d, *J* = 6.5 Hz, 3H), 1.20– 1.13 (m, 2H).

^{13}C NMR (176 MHz, Chloroform-d) δ 194.37, 172.33, 166.55, 143.07 (3), 139.36, 139.02, 127.63 (6), 127.12 (6), 126.85 (3), 125.96, 124.34, 121.46, 116.99, 69.75, 69.20, 48.44, 39.26, 37.80, 30.35, 29.54, 28.17, 24.34, 21.89, 21.39, 17.11. tR HPLC=14.95 min. $[\alpha]^{20}_{D}$ = + 12.63 (c 0.3, $CHCl_3$).

(S,R*)-23: yellowish solid; Rf = 0.58 (H : E = 7 : 3).

^{1}H NMR (700 MHz, Chloroform-d) δ 8.10 (d, J = 7.5 Hz, 1H), 7.17–7.13 (m, 12H), 7.01– 6.97 (m, 6H), 6.89 (d, 1H), 5.13 (s, 1H), 3.22 (dd, J = 13.4, 5.5 Hz, 1H), 2.91 (d, 1H), 2.79 (d, J = 11.5 Hz, 1H), 2.24 (s, 3H), 1.75–1.60 (m, 9H), 1.29–1.26 (m, 1H), 1.18 (d, J = 5.8 Hz, 3H).

^{13}C NMR (176 MHz, Chloroform-d) δ 196.41, 173.01, 167.61, 144.14 (3), 141.12, 140.42, 128.31 (6), 127.88 (6), 127.05 (4), 125.10, 122.42, 118.20, 71.33, 70.26, 49.37, 39.08, 38.81, 33.77, 30.63, 29.76, 25.55, 23.19, 22.88, 16.61. tR HPLC = 15.97 min. $[\alpha]^{20}_{D}$ = - 14.37 (c 0.3, $CHCl_3$).

Antibiotics and strains

Vancomycin, tobramycin, oxacillin, imipenem, and amphotericin B were purchased from Sigma-Aldrich (Milan, Italy). Staphylococcus aureus ATCC 43300, S. epidermidis ATCC 35984, Pseudomonas aeruginosa ATCC 27853, Klebsiella pneumoniae ATCC BAA-1705 (carbapenemase producer), and Candida albicans ATCC 90028 were obtained from the American Type Culture Collection (Rockville, MD).

Antimicrobial susceptibility testing Minimal inhibitory concentrations (MIC) of all the compounds were determined in Mueller- Hinton medium (MH) by the broth microdilution assay, following the procedure already described. The compounds were added to bacterial suspension in each well yielding a final cell concentration of 1 × 106 CFU/mL and a final

compound concentration ranging from 3.1 to 100 μM. Negative control wells were set to contain bacteria in Mueller-Hinton broth plus the amount of vehicle (DMSO) used to dilute each compound. Positive controls included vancomycin (2 μg/mL), tobramycin (1 and 4 μg/mL), oxacillin (2 and 10 μg/mL), and imipenem (4 and 8 μg/mL). The MIC was defined as the lowest concentration of drug that caused a total inhibition of microbial growth after 24 hours incubation time at 37 °C. Medium turbidity was measured by a microtiter plate reader (Bio-Rad mod 680, Milan, Italy) at 595 nm.

Candida albicans ATCC 90028 The antifungal activity of compounds 8–16 was determined using a standardized broth microdilution method (Clinical and Laboratory Standards Institute (CLSI) document M27-A2). Briefly, cell suspension was adjusted to 3× 103 CFU/mL in RPMI 1640 medium (Sigma) supplemented with 0.2% (w/v) glucose. One hundred microliter aliquots of these cell suspensions were dispensed into 96-well microtiter plates. Compounds were serially diluted using RPMI 1640 medium and added to the wells at a final concentration ranging from 3.1 to 100 μM, and the plate was incubated for 48 hours at 37 °C. Amphotericin B (2 μg/mL) was chosen as the positive control. All the tests were conducted at least three times using independent cell suspensions.

Biofilm formation assay

Biofilm formation was evaluated by measuring the ability of cells to adhere to sterile 96-well polystyrene flat-bottom microtiter plate (BD Falcon, Mississauga, Ontario Canada) as described previously. Briefly, a suspension of S. epidermidis (MH supplemented with 1% glucose) at the final density of 10^5 $CFUmL^{-1}$ was treated with compound (*S,S**)-15, (*S,R**)-17 and 15 at 100 μM. After 24 hours at 37°C, planktonic cells were removed, and the wells washed twice with phosphate-buffered saline

(PBS) and dried at 60 °C for 30 min. Crystal violet solution (150 mL at 0.1 %) was added to each well and the plates were incubated at room temperature for 30 min. The wells were then washed with PBS and discolored with 200 mL of 96 % ethanol for 20 min. Absorbance was measured at 595 nm using a microtiter plate reader. The percentage of biofilm mass reduction was calculated using the formula: [(Ac-At)/Ac] × 100, where Ac is the OD_{595} for control wells and At is OD_{595} in the presence of a compound.

Cell culture

HaCaT cells, an immortalized, nontumorigenic human keratinocyte cell line purchased from ATCC, were cultured in Dulbecco's modified Eagle's medium (DMEM; Invitrogen, Paisley, United Kingdom) containing high glucose (4.5g/L), supplemented with 10% fetal bovine serum (FBS; Cambrex, Verviers, Belgium), L-glutamine (2 mM; Sigma, Milan, Italy), penicillin (100 U/mL; Sigma), and streptomycin (100 mg/mL; Sigma) at 37 °C in a humidified 5 % CO2 atmosphere, according to ATCC recommendations.

In vitro bioscreens

The biological effects and cytotoxicity of *(S,S*)*-**9**, *(S,S*)*-**11**, *(S,R*)*-**11** and *(S,R/S)*-**15** were investigated through the estimation of a "cell survival index", arising from the combination of cell viability evaluation and automatic cell count. Cells were inoculated in 96- microwell culture plates at a density of 10^4 cells/well and allowed to grow for 24h. The medium was then replaced with fresh medium and cells were treated for further 48 h with a range of concentrations (25→400 μM) of *(S,S*)*-**9**, *(S,S*)*-**11**, *(S,R*)*-**11** and *(S,R/ S)*-**15**. DMSO was used as vehicle to solubilize

compounds under investigation to a final concentration of 100 mM. DMSO toxicity was evaluated in control cultures at a concentration ranging from 0.025 to 0.5% v/v (the same concentrations used in bioscreen experiments) to exclude interference with cell viability. Cell viability was evaluated by the MTT assay procedure, which measures the level of mitochondrial dehydrogenase activity using the yellow 3- (4,5-dimethyl-2-thiazolyl)-2,5-diphenyl-2H-tetrazolium bromide (MTT, Sigma) as substrate. The assay is based on the redox ability of living mitochondria to convert dissolved MTT into insoluble purple formazan. Briefly, after the treatments, the medium was removed, and the cells were incubated with 20 μL/well of a MTT solution (5 mg/mL) for 1 h in a humidified 5 % CO2 incubator at 37 °C. The incubation was stopped by removing the MTT solution and by adding 100 μL/well of DMSO to solubilize the formazan. Finally, the absorbance was monitored at 550 nm by using a microplate reader (iMark microplate reader, Bio-Rad, Milan, Italy). Cell number was determined by TC20 automated cell counter (Bio-Rad, Milan, Italy), providing an accurate and reproducible total count of cells and a live/dead ratio in one step by a specific dye (trypan blue) exclusion assay. Bio-Rad's TC20 automated cell counter uses disposable slides, trypan blue dye (0.4 % trypan blue dye w/v in 0.81 % sodium chloride and 0.06% potassium phosphate dibasic solution) and a CCD camera to count cells based on the analyses of captured images. Once the loaded slide is inserted into the slide port, the TC20 automatically focuses on the cells, detects the presence of trypan blue dye and provides the count. When cells are damaged or dead, trypan blue can enter the cell allowing living cells to be counted. Operationally, after treatments in 96-microwell culture plates, the medium was removed, and the cells were collected. Ten microliters of cell suspension, mixed with 0.4 % trypan blue solution at 1:1 ratio, were loaded

into the chambers of disposable slides. The results are displayed as total cell count (number of cells per ml). If trypan blue is detected, the instrument also accounts for the dilution and shows live cell count and percent viability. Total counts and live/dead ratio from random samples for each cell line were subjected to comparisons with manual hemocytometers in control experiments. The calculation of the concentration required to inhibit the net increase in the cell number and viability by 50% (IC_{50}) is based on plots of data (n = 4 for each experiment) and repeated three times (total n = 12). IC_{50} values were obtained by means of a dose response curve by nonlinear regression using a curve fitting program, GraphPad Prism 5.0, and are expressed as mean ± SEM (n=12) of five independent experiments.

Synthesis of *N*-trityl isocyanide

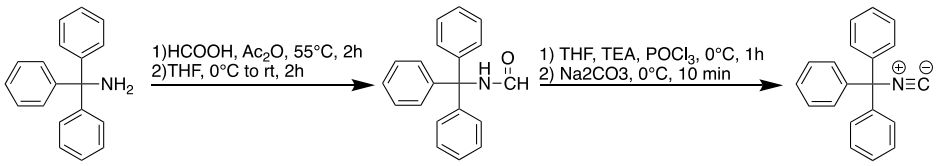

N-Trityl formamide

Formic acid (10.4 mmol, 2.7 equiv.) and acetic anhydride (8.85 mmol, 2.3 equiv.) are reacted in a dry flask at 55 °C for 2 h. The solution is transferred dropwise to a solution of trityl amine (3.85 mmol, 1 equiv.) in 7 mL THF (0.6 M) at 0 °C under N_2 atmosphere. The reaction mixture is heated to room temperature and stirred for 2 h. The reaction is quenched with saturated Na_2CO_3 solution and the aqueous layer is extracted with

AcOEt. The white solid is dried to afford the pure product. Yield: quantitative.

Trityl isocyanide

Trityl formamide (4.11 mmol, 1 equiv) and triethylamine (27.54 mol, 6.7 equiv) are dissolved in 7 mL THF (0.6 M) and cooled to 0 °C under N_2 atmosphere. Phosphorus oxychloride (6.99 mmol, 1.7 equiv) is added dropwise to reaction mixture and is stirred for 1 h. The solution is then transferred to an extraction funnel and washed with saturated $NaHCO_3$ solution and the aqueous layer is extracted with CH_2Cl_2. The product is purified by chromatography on silica gel column (95:5 Hex/AcOEt). Yield: 88%.

Table S1. In vitro antibacterial activity. MIC values (μM) for synthesized compounds against *Staphylococcus aureus, S. epidermidis, Pseudomonas aeruginosa, Klebsiella pneumoniae, Candida albicans.*

Compounds	*S.aureus* ATCC 43300	*S. epidermidis* ATCC 35984	*P. aeruginosa* ATCC 27853	*K.pneumoniae* ATCC BAA-1705	*Candida albicans ATCC 90028*
(S,S*)-8	>100	>100	>100	>100	>100
(S,R*)-8	>100	>100	>100	>100	>100
(S,S*)-9	>100	>100	>100	>100	>100
(S,R*)-9	>100	>100	>100	>100	>100
(S,S*)-10	>100	>100	>100	>100	>100
(S,R*)-10	>100	>100	>100	>100	>100
15	>100	>100	>100	>100	>100
16	>100	>100	>100	>100	>100
(S,S*)-11	>100	>100	>100	>100	>100
(S,R*)-11	>100	>100	>100	>100	>100
(S,S*)-12	>100	>100	>100	>100	>100
(S,R*)-12	>100	>100	>100	>100	>100
(S,S*)-13	>100	>100	>100	>100	>100
(S,R*)-13	>100	>100	>100	>100	>100
(S,S*)-14	>100	>100	>100	>100	>100
(S,R*)-14	>100	>100	>100	>100	>100
Oxacillin	10	2	NA	NA	NA
Vancomycin	2	2	NA	NA	NA
Tobramycin	1	1	4	4	NA
Imipenem	NT	NT	4	>8	NA
Amphotericin B	NA	NA	NA	NA	2

*NA= not applicable; NT= Not tested. For oxacillin, vancomycin, tobramycin and imipenem MIC values are expressed as μg/mL.

(S,S)*-**8**

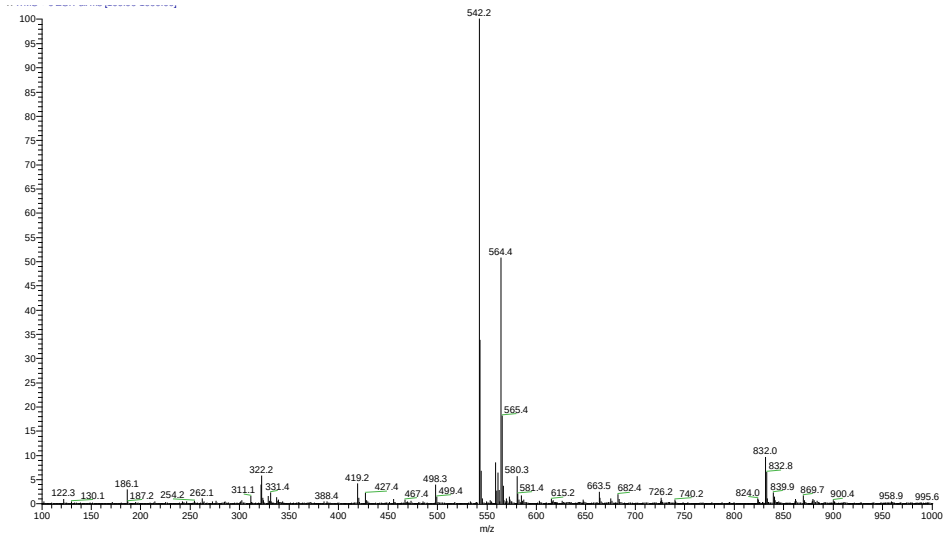

Supporting figure 1. ESI-MS of compound *(S,S*)*-**8**

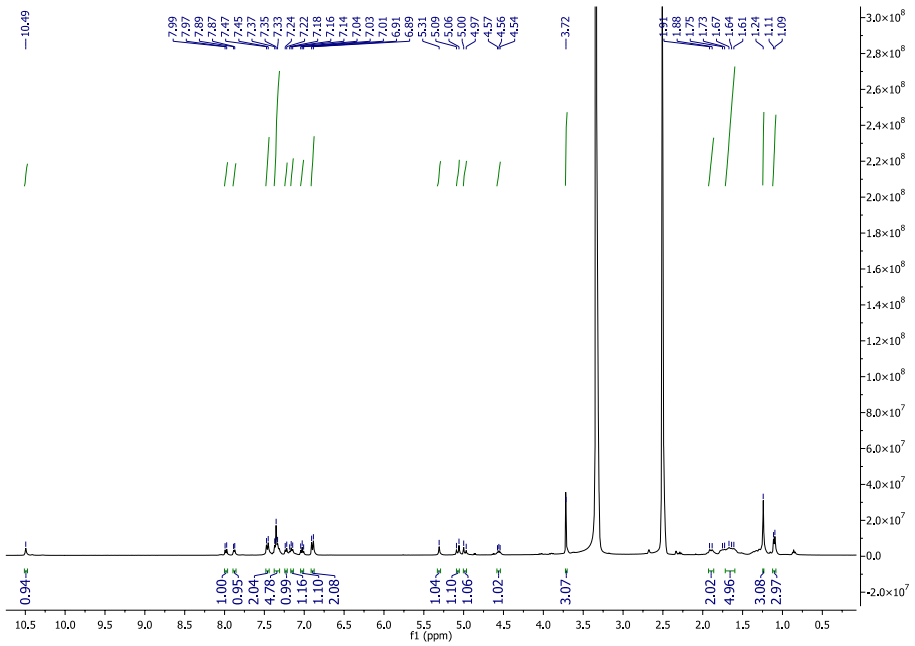

Supporting figure 2. ^{1}H NMR of compound *(S,S*)*-**8**

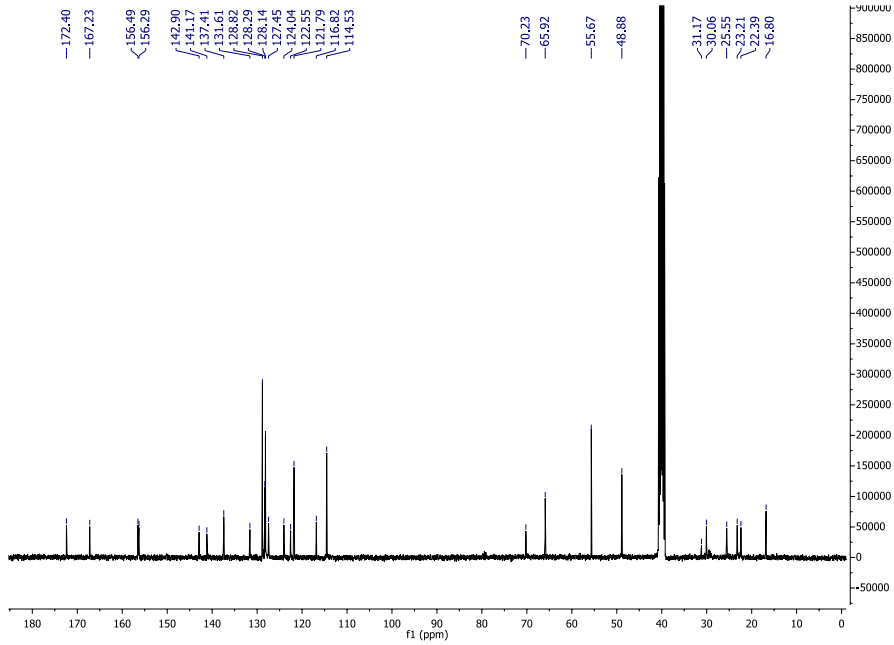

Supporting figure 3. ^{13}C NMR of compound *(S,S*)*-**8**

(S,R)*-**8**

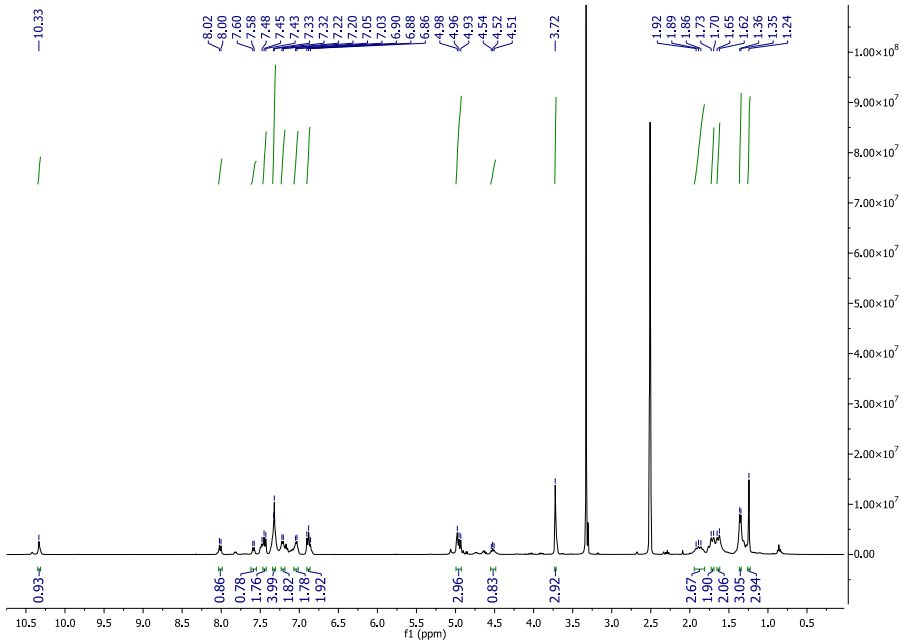

Supporting figure 4. ^{1}H NMR of compound *(S,R*)*-**8**

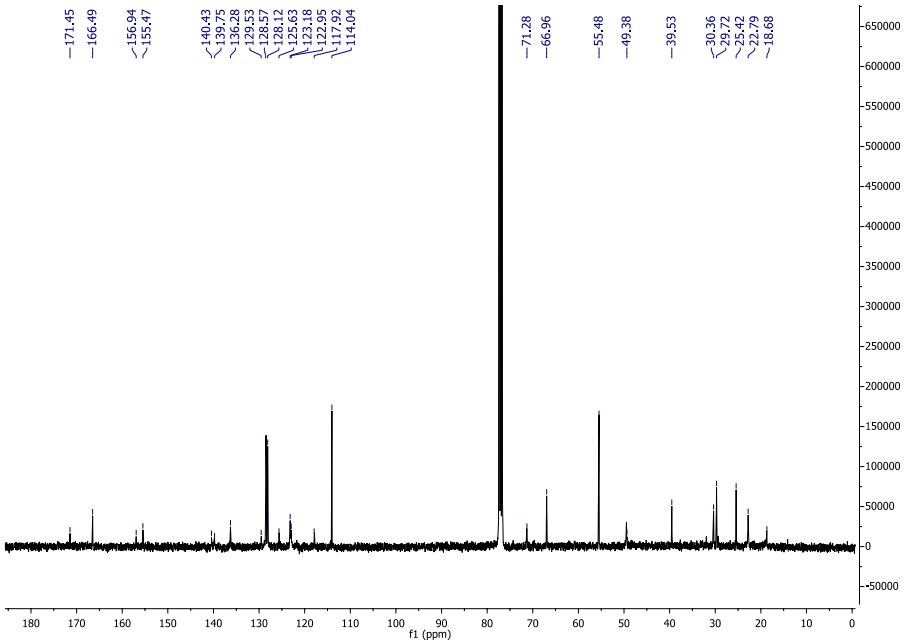

Supporting figure 5. ^{13}C NMR of compound *(S,R*)*-**8**

(S,S)*-**9**

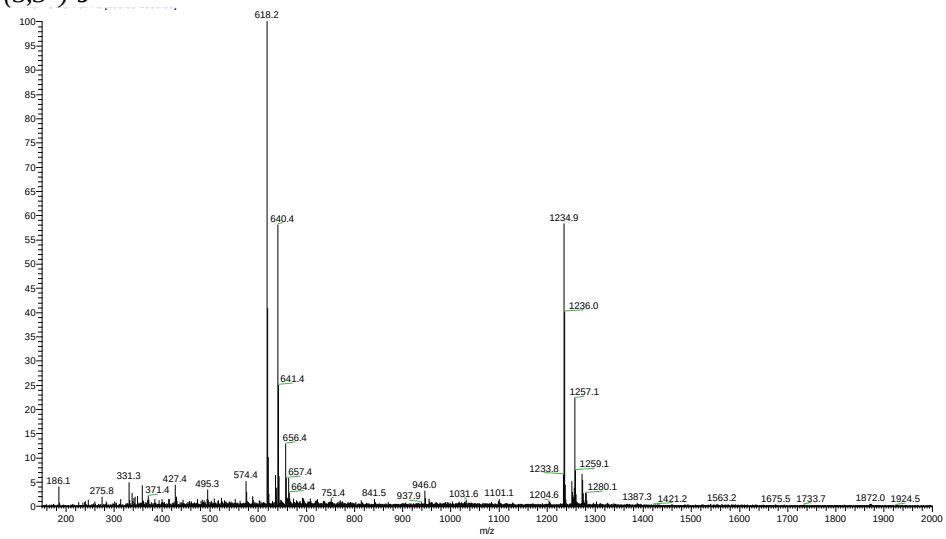

Supporting figure 6. ESI-MS of compound *(S,S*)*-**9**

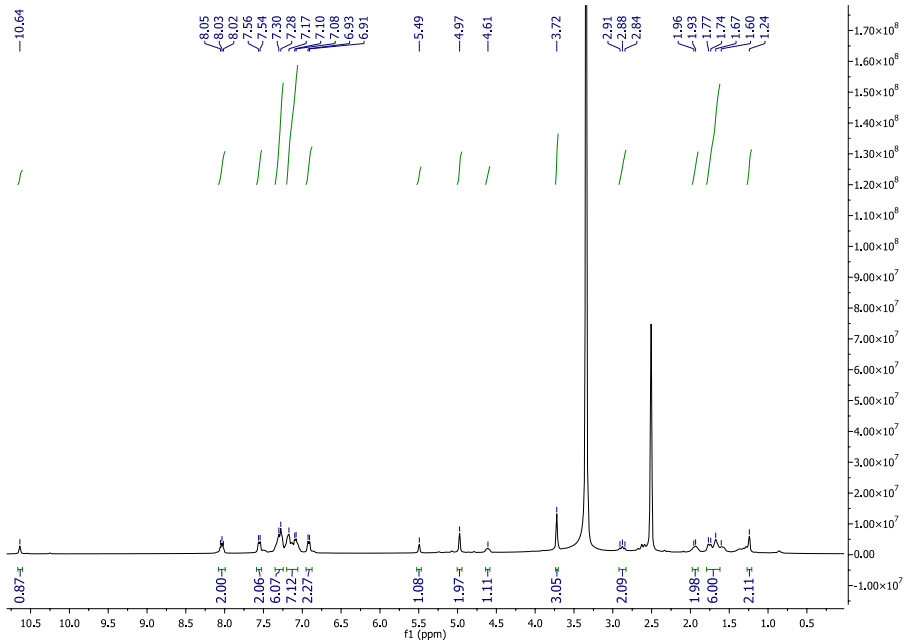

Supporting figure 7. ^{1}H NMR of compound *(S,S*)*-**9**

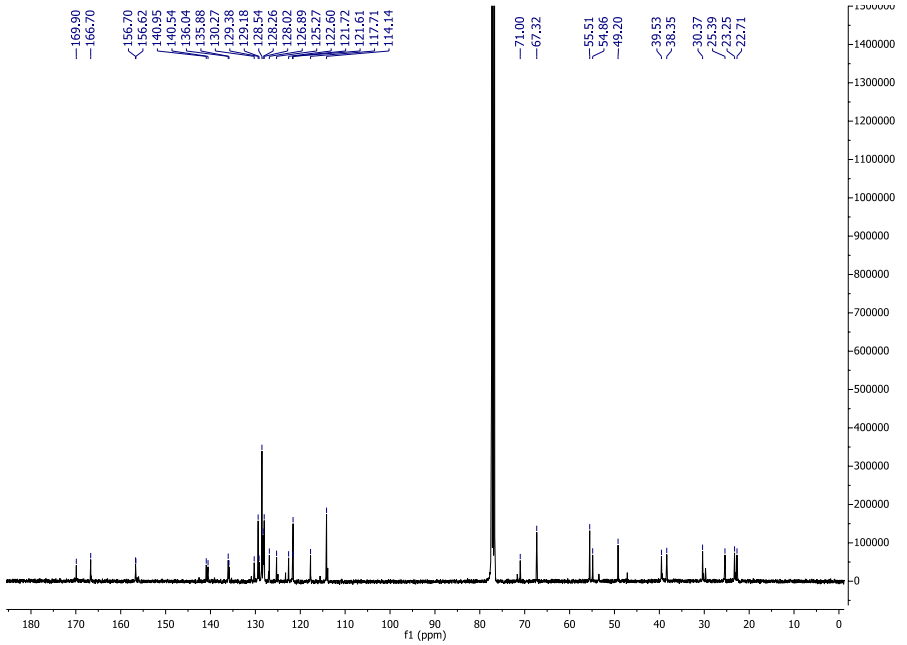

Supporting figure 8. ^{13}C NMR of compound *(S,S*)*-**9**

(S,R)*-**9**

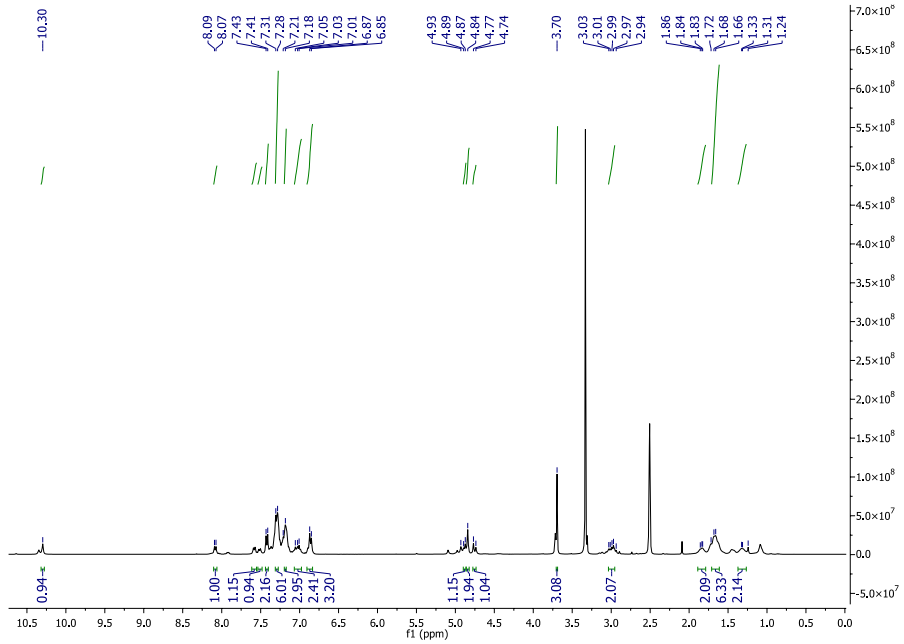

Supporting figure 9. ^{1}H NMR of compound *(S,R*)*-**9**

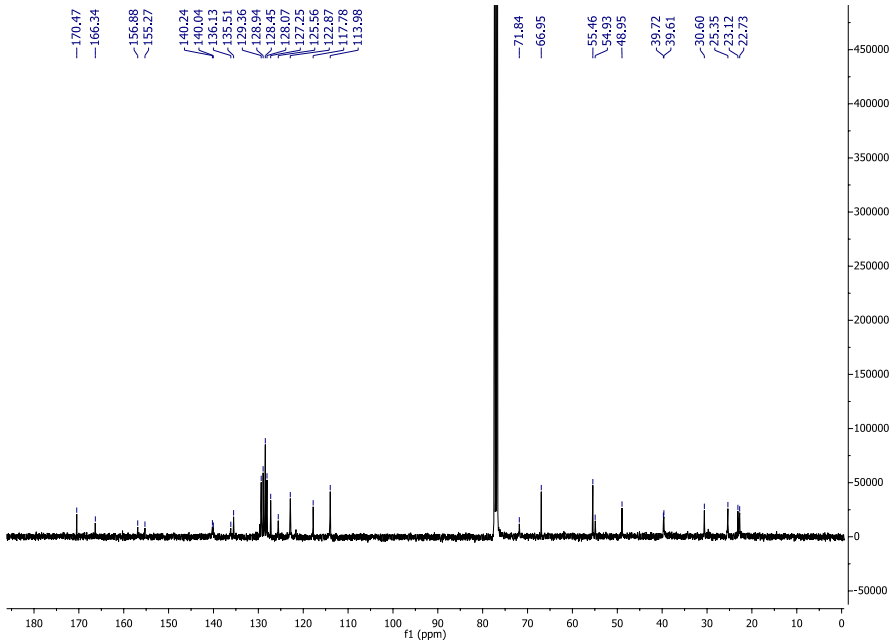

Supporting figure 10. ^{13}C NMR of compound *(S,R*)*-**9**

(S,S)*-**10**

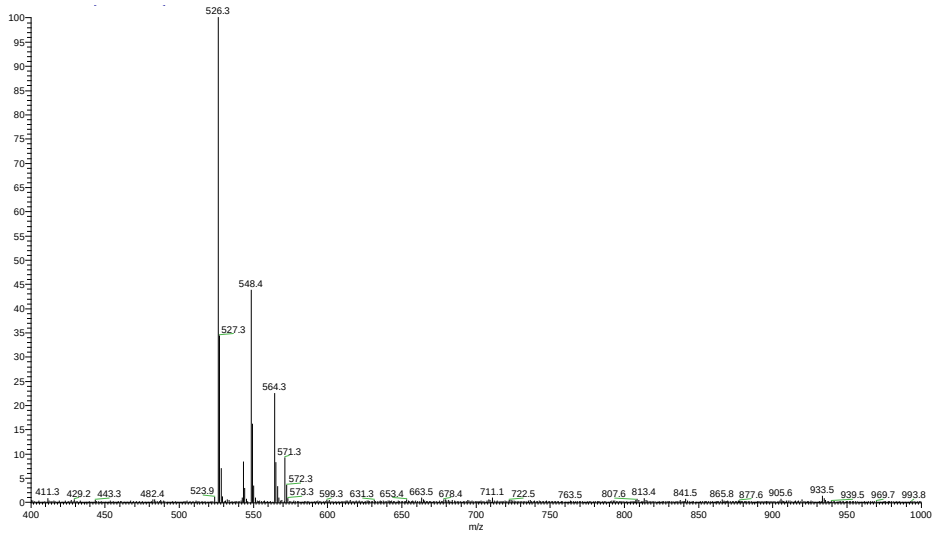

Supporting figure 11. ESI-MS of compound *(S,S*)*-**10**

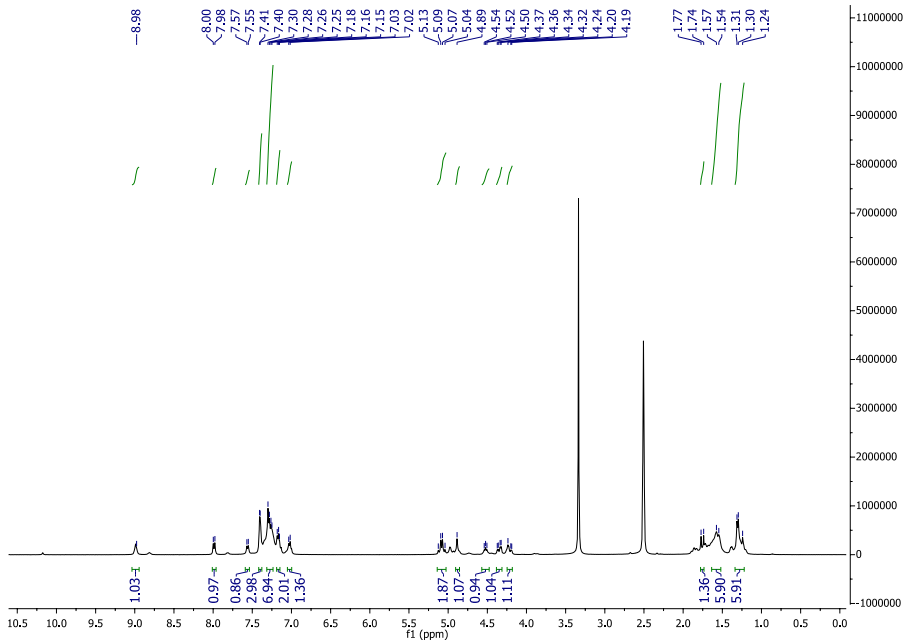

Supporting figure 12. ^{1}H NMR of compound *(S,S*)*-**10**

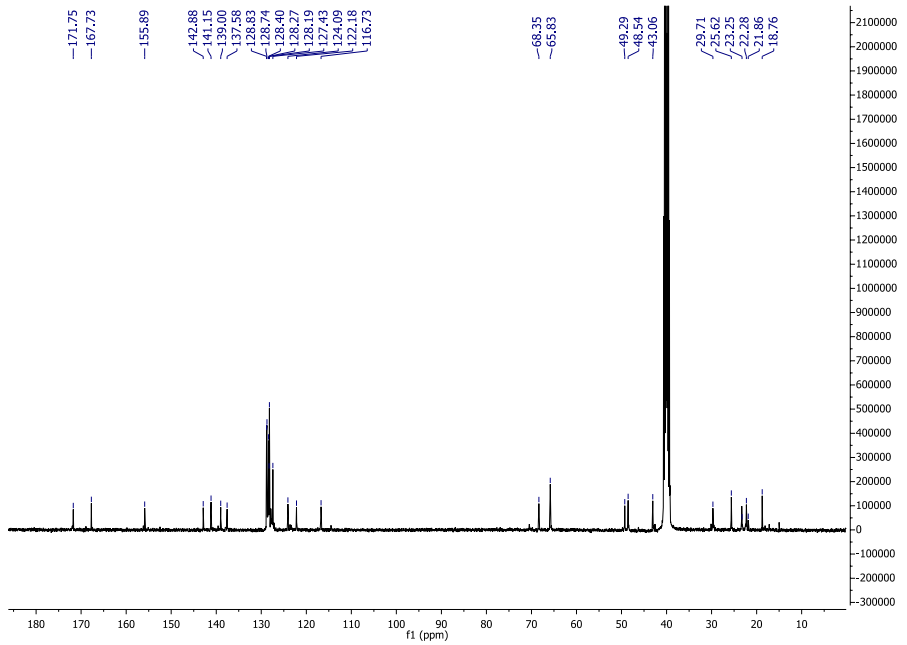

Supporting figure 13. ^{13}C NMR of compound *(S,S*)*-**10**

(S,R)*-**10**

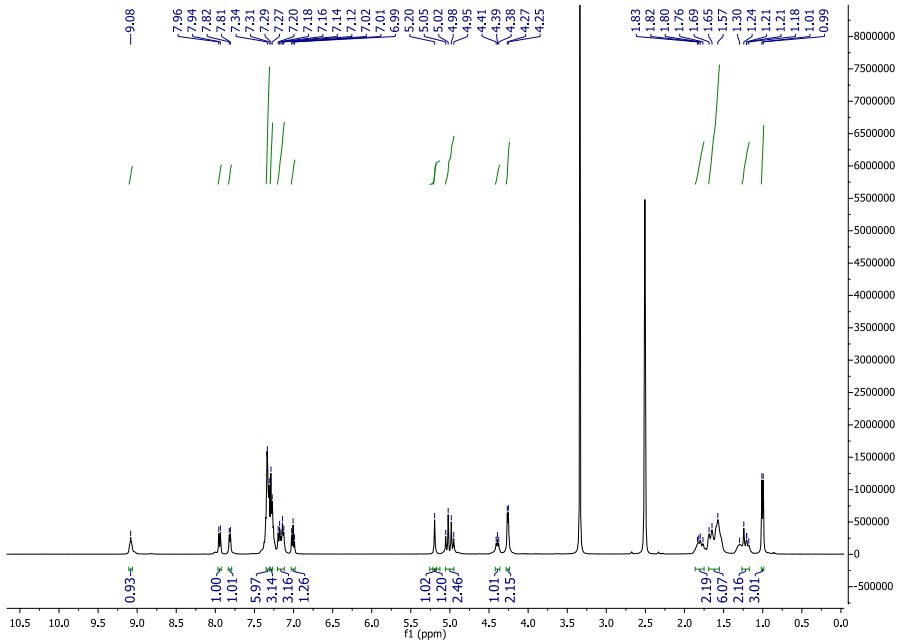

Supporting figure 14. ^{1}H NMR of compound *(S,R*)*-**10**

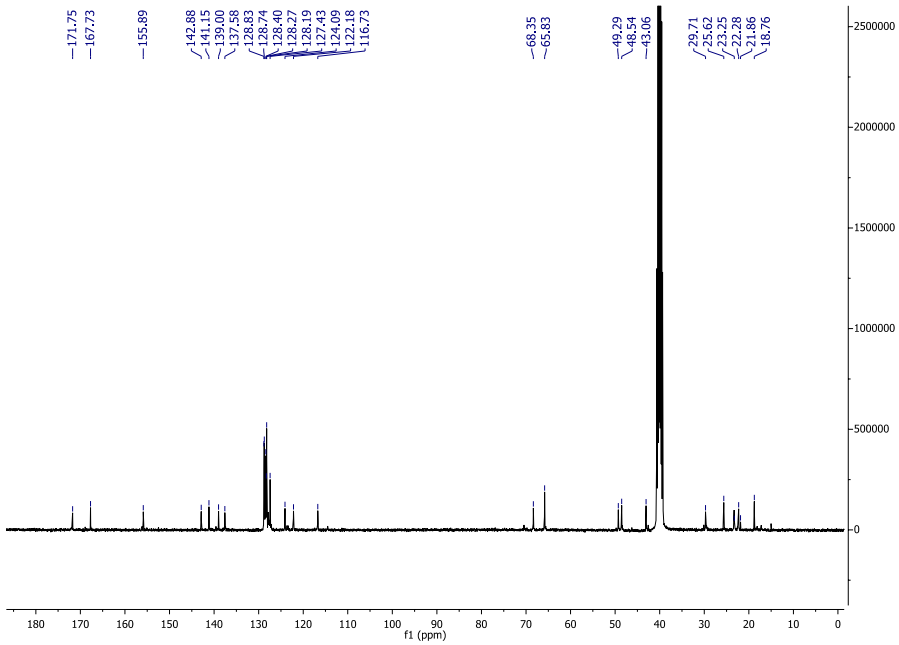

Supporting figure 15. ^{13}C NMR of compound *(S,R*)*-**10**

(S,S)*-**11**

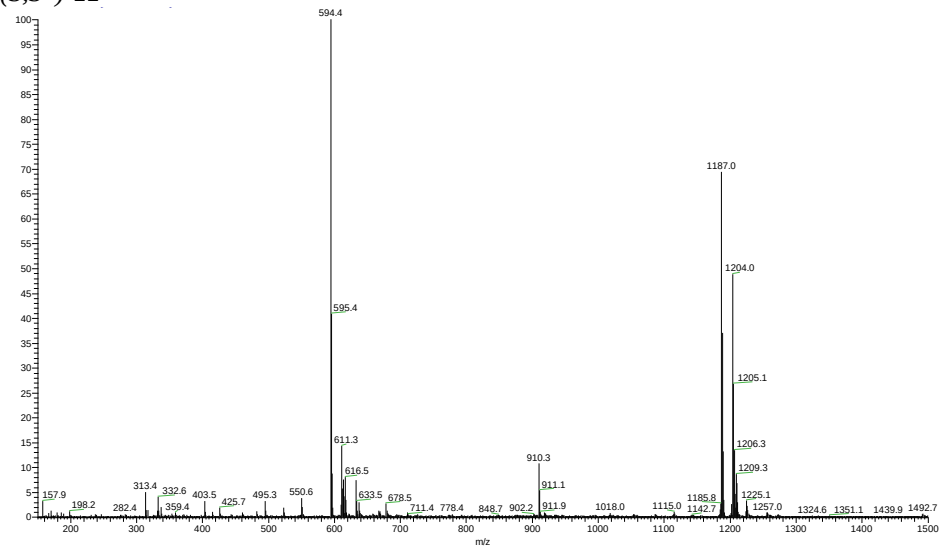

Supporting figure 16. ESI-MS of compound *(S,S*)*-**11**

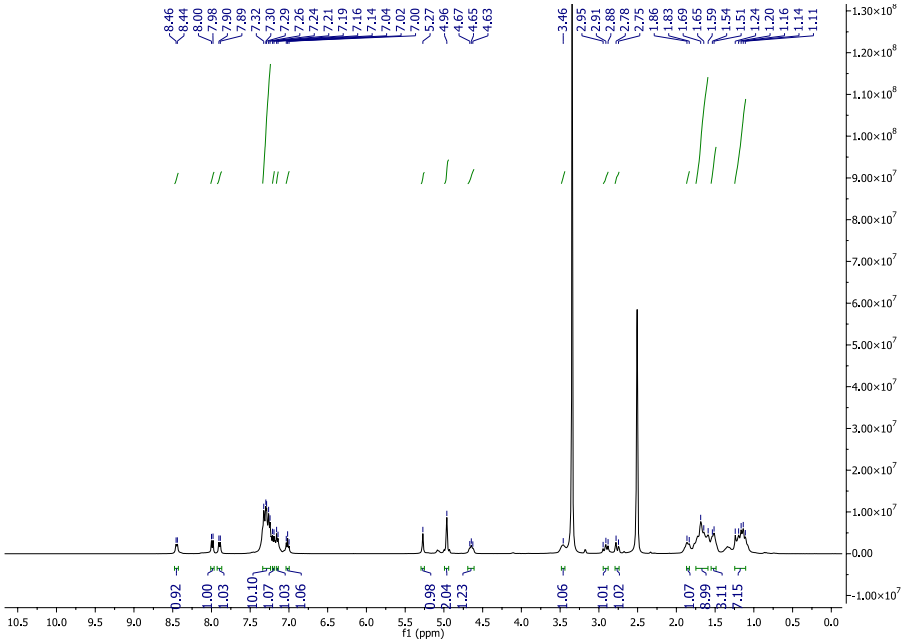

Supporting figure 17. ^{1}H NMR of compound *(S,S*)*-**11**

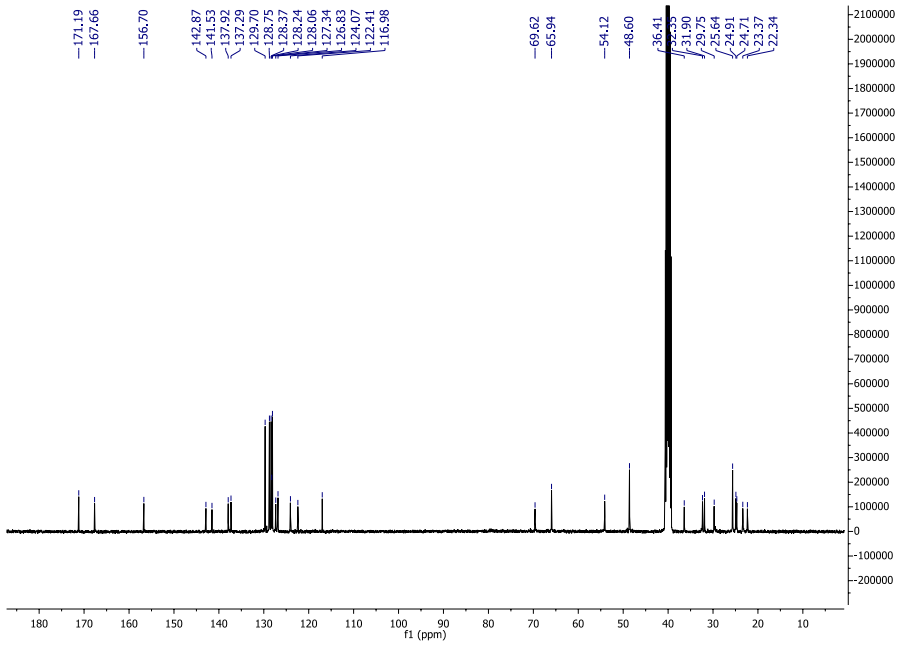

Supporting figure 18. ^{13}C NMR of compound *(S,S*)*-**11**

(S,R)*-**11**

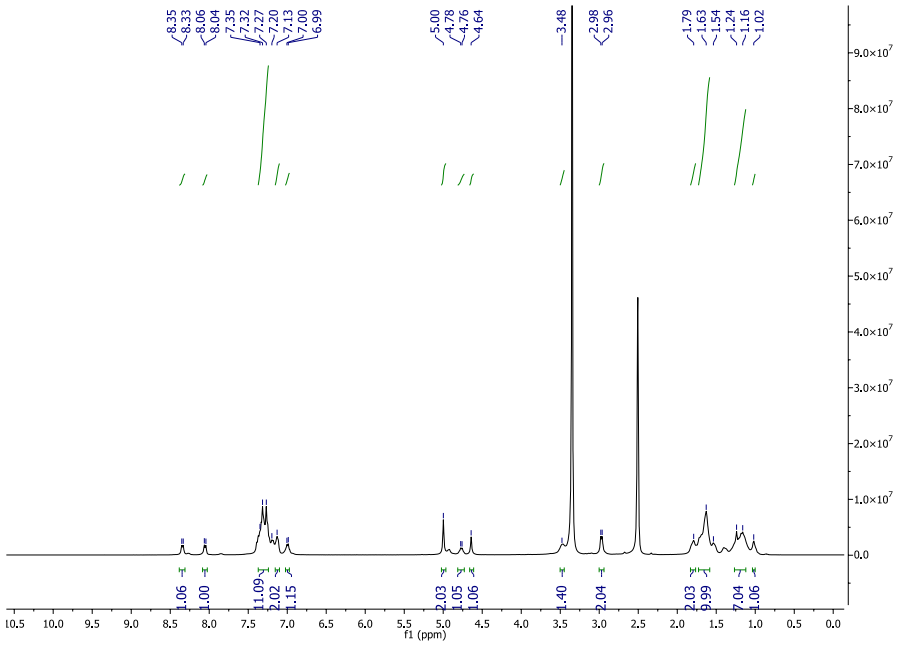

Supporting figure 19. ^{1}H NMR of compound *(S,R*)*-**11**

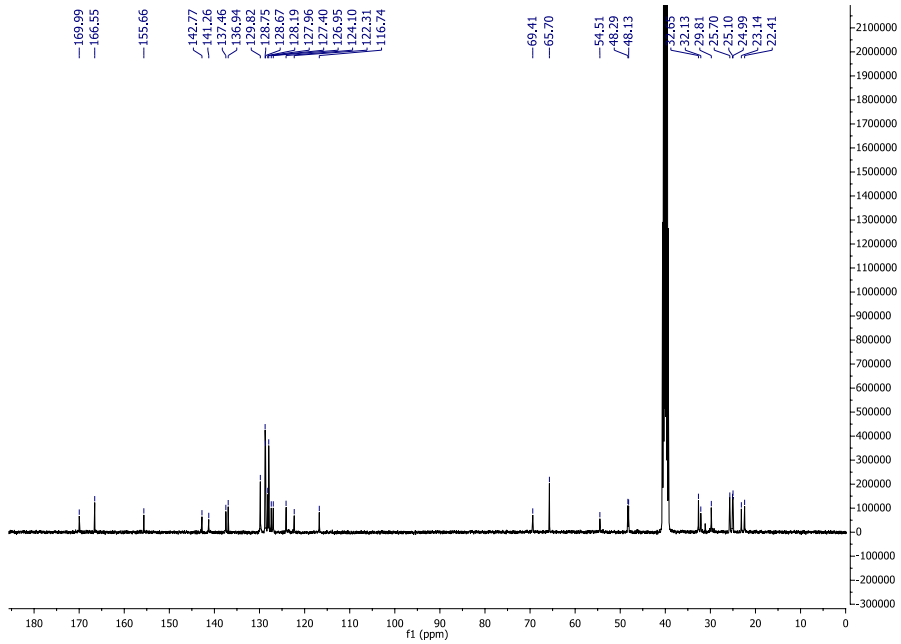

Supporting figure 20. ^{13}C NMR of compound *(S,R*)*-**11**

(S,S)*-**12**

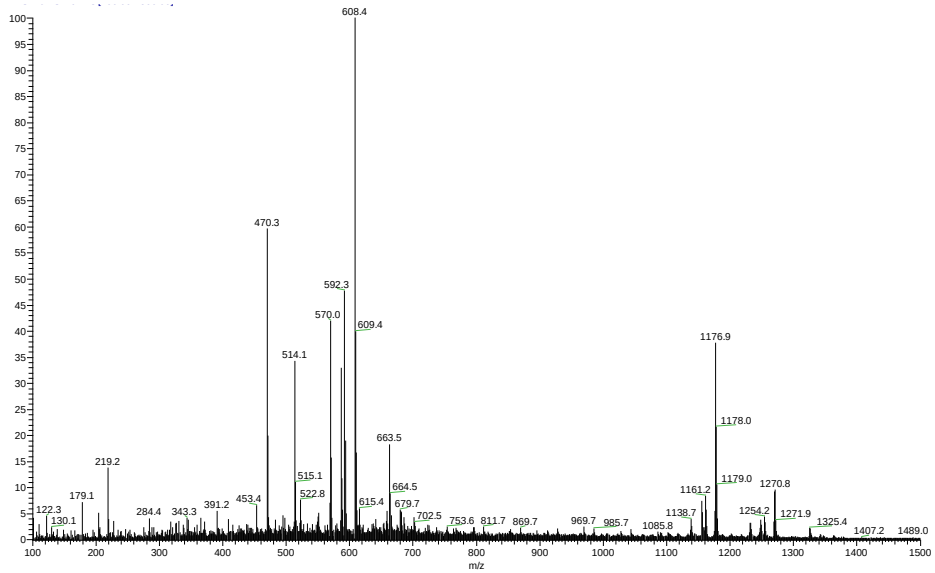

Supporting figure 21. ESI-MS of compound *(S,S*)*-**12**

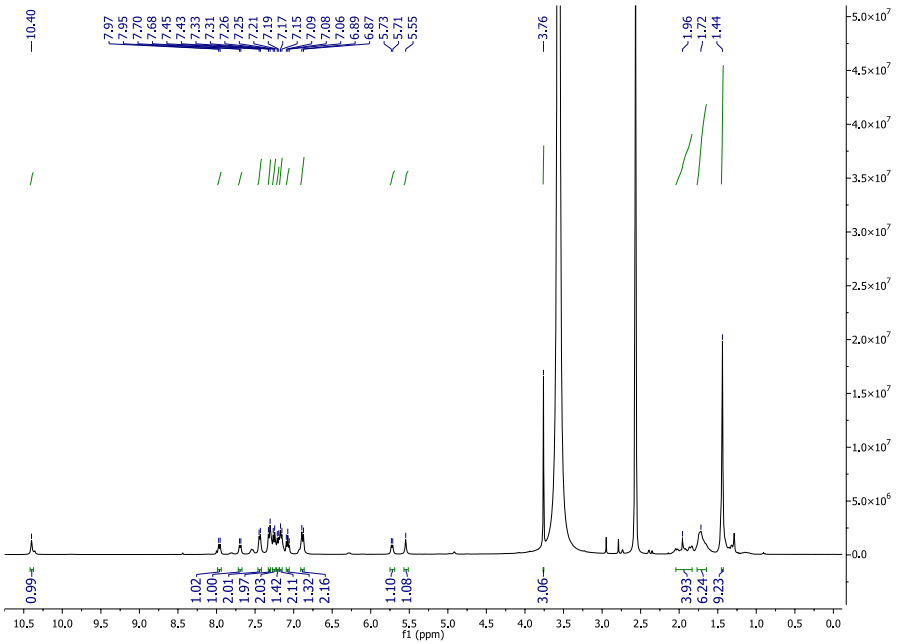

Supporting figure 22. ^{1}H NMR of compound *(S,S*)*-**12**

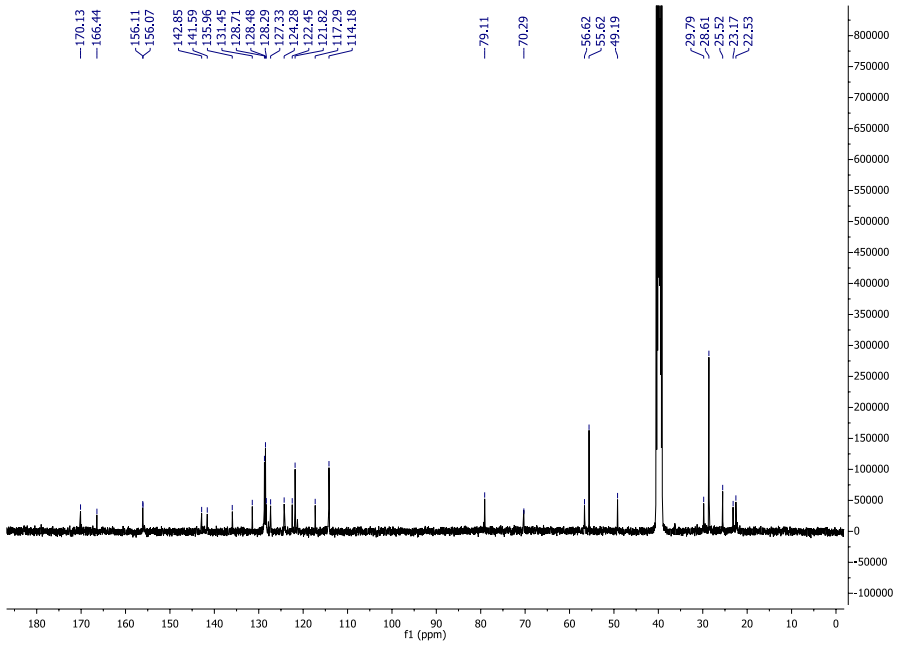

Supporting figure 23. ^{13}C NMR of compound *(S,S*)*-**12**

(S,R)*-**12**

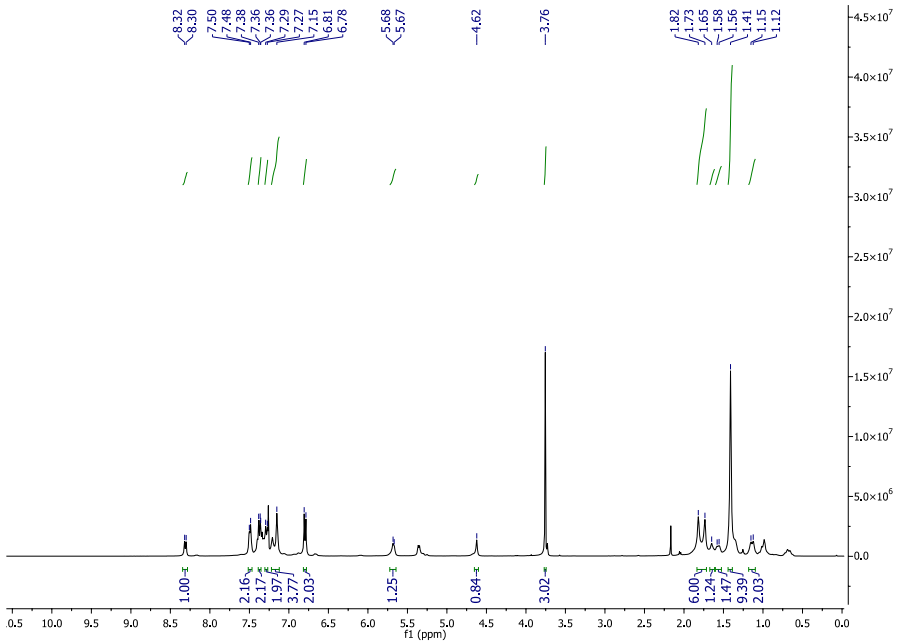

Supporting figure 24. ^{1}H NMR of compound *(S,R*)*-**12**

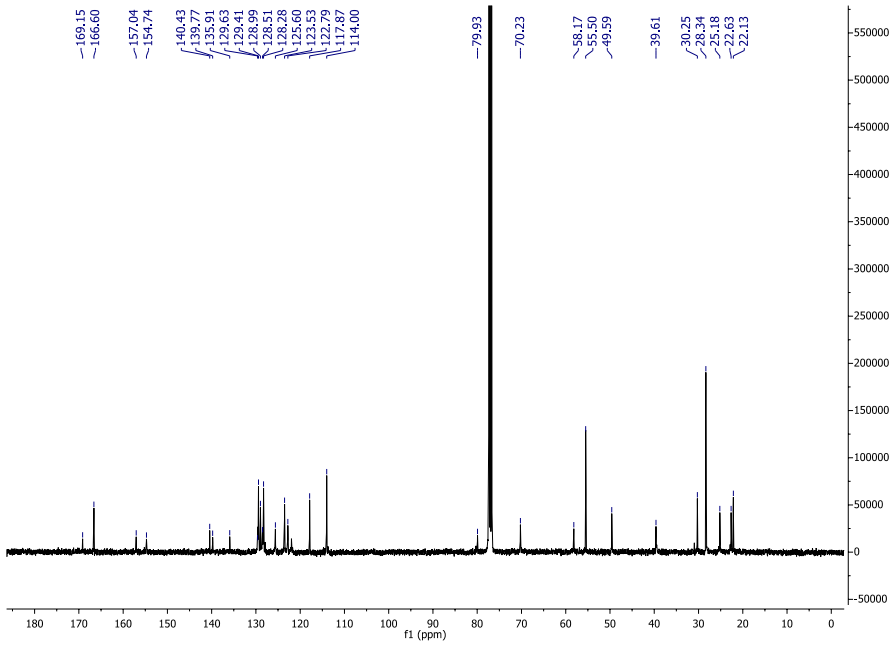

Supporting figure 25. ^{13}C NMR of compound *(S,R*)*-**12**

(S,S)*-**13**

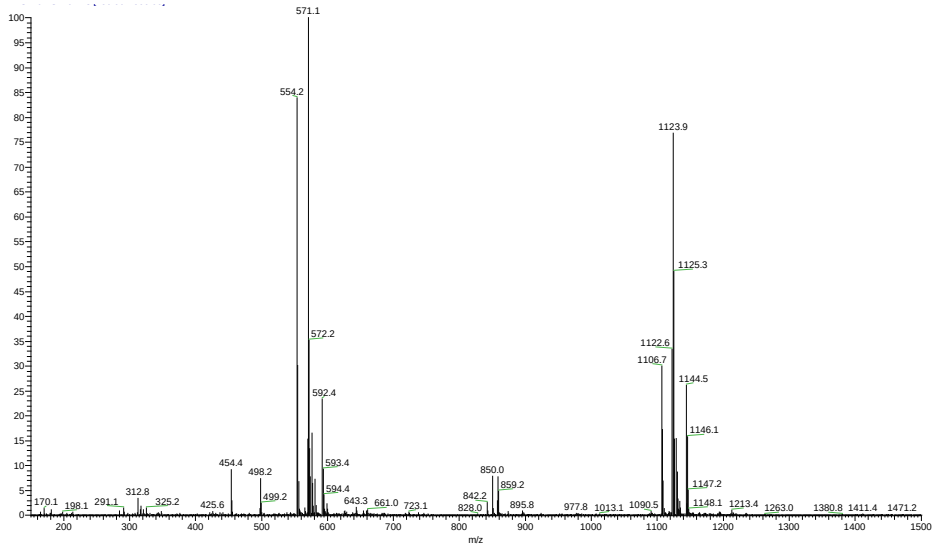

Supporting figure 26. ESI-MS of compound *(S,S*)*-**13**

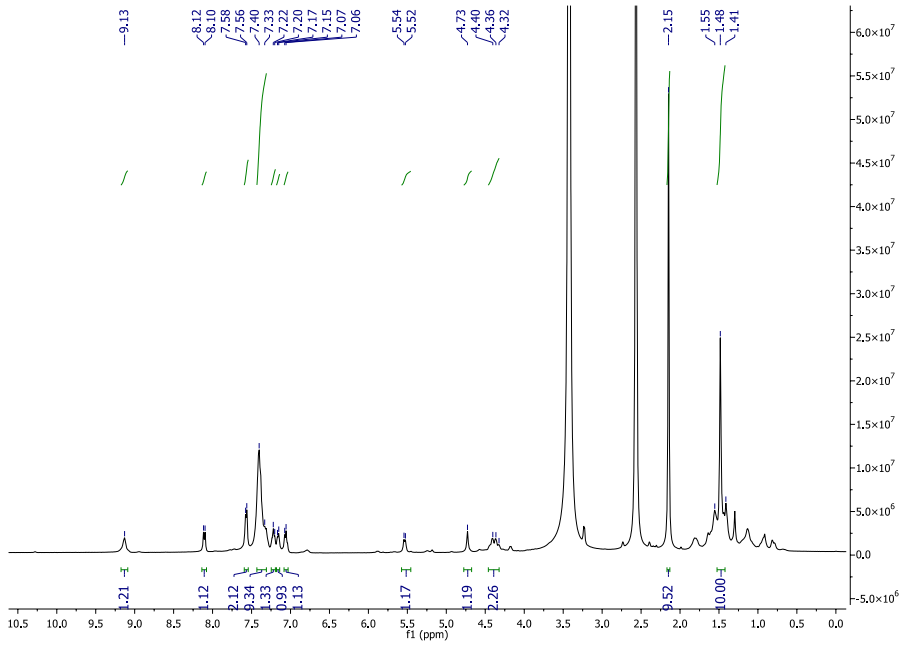

Supporting figure 27. ^{1}H NMR of compound *(S,S*)*-**13**

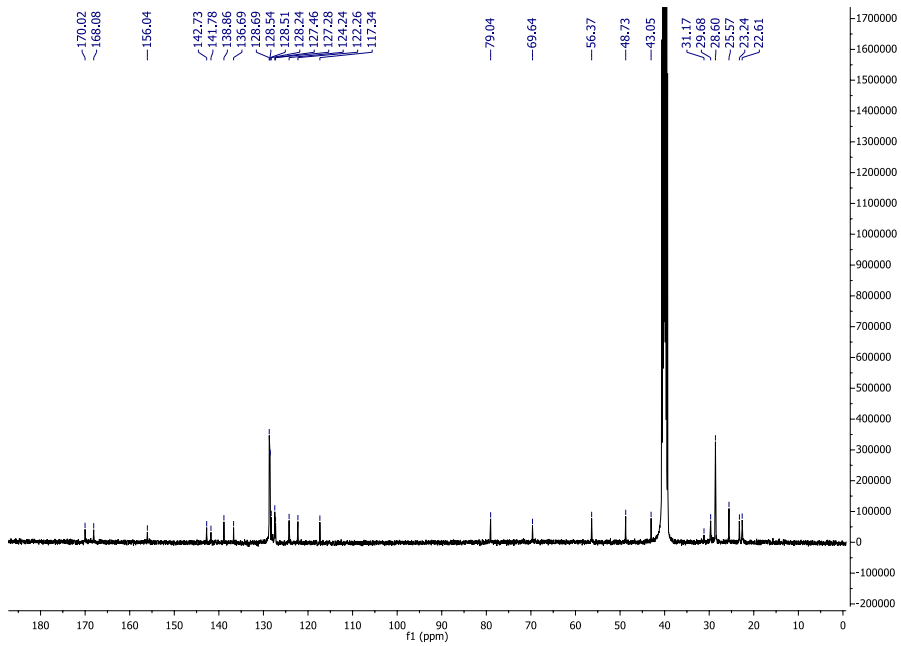

Supporting figure 28. ^{13}C NMR of compound *(S,S*)*-**13**

(S,R)*-**13**

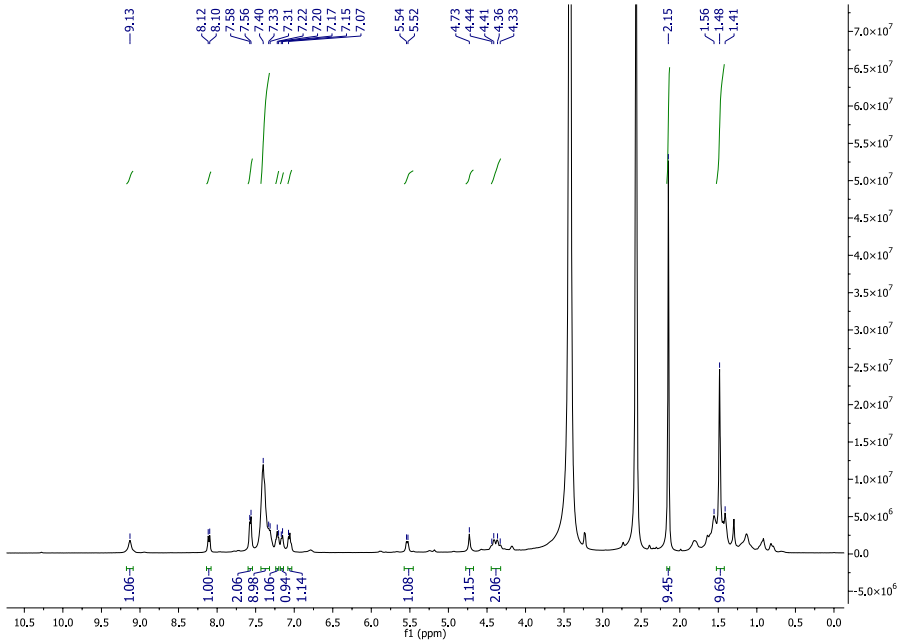

Supporting figure 29. ^{1}H NMR of compound *(S,R*)*-**13**

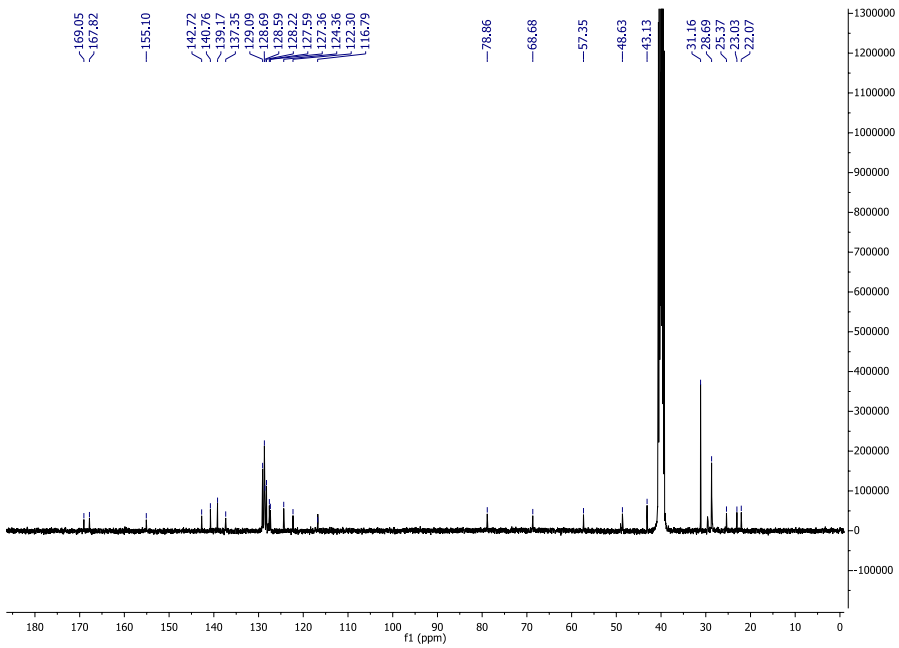

Supporting figure 30. ^{13}C NMR of compound *(S,R*)*-**13**

(S,S)*-**14**

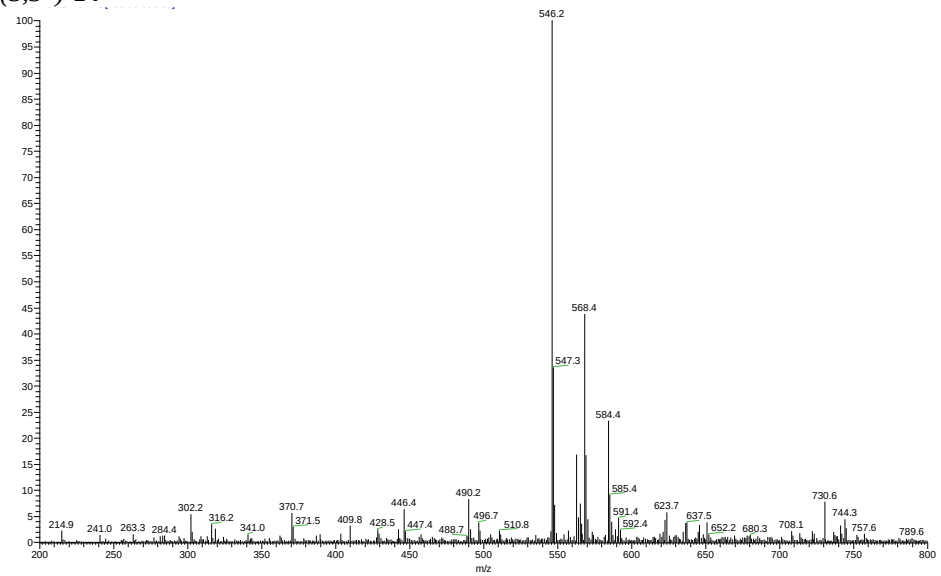

Supporting figure 31. ESI-MS of compound *(S,S*)*-**14**

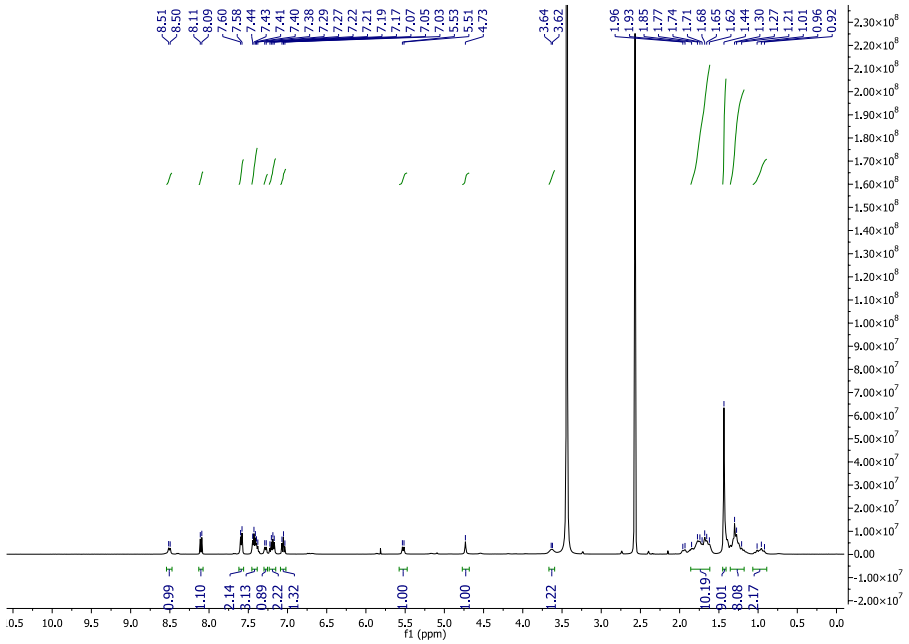

Supporting figure 32. ^{1}H NMR of compound *(S,S*)*-**14**

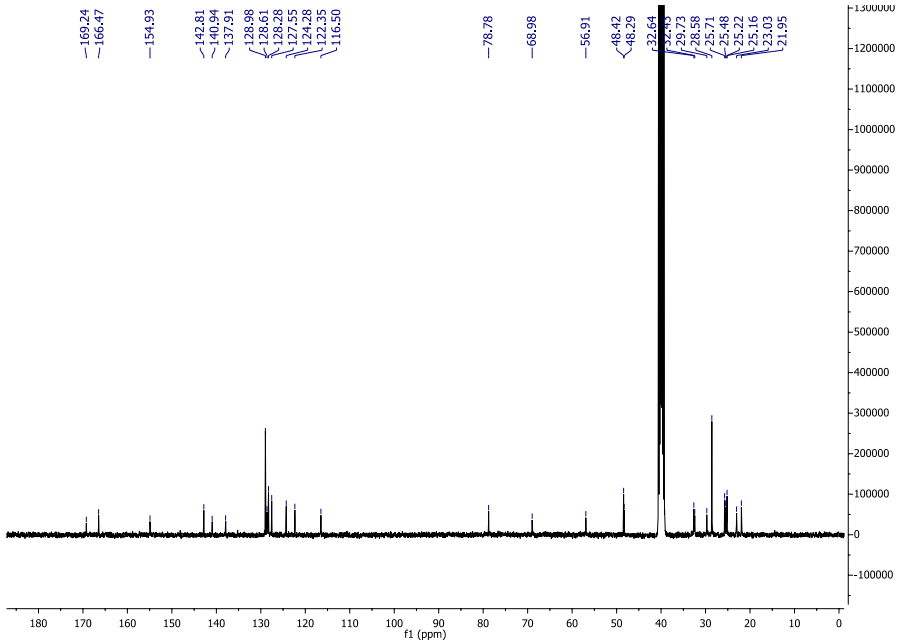

Supporting figure 33. ^{13}C NMR of compound *(S,S*)*-**14**

(S,R)*-**14**

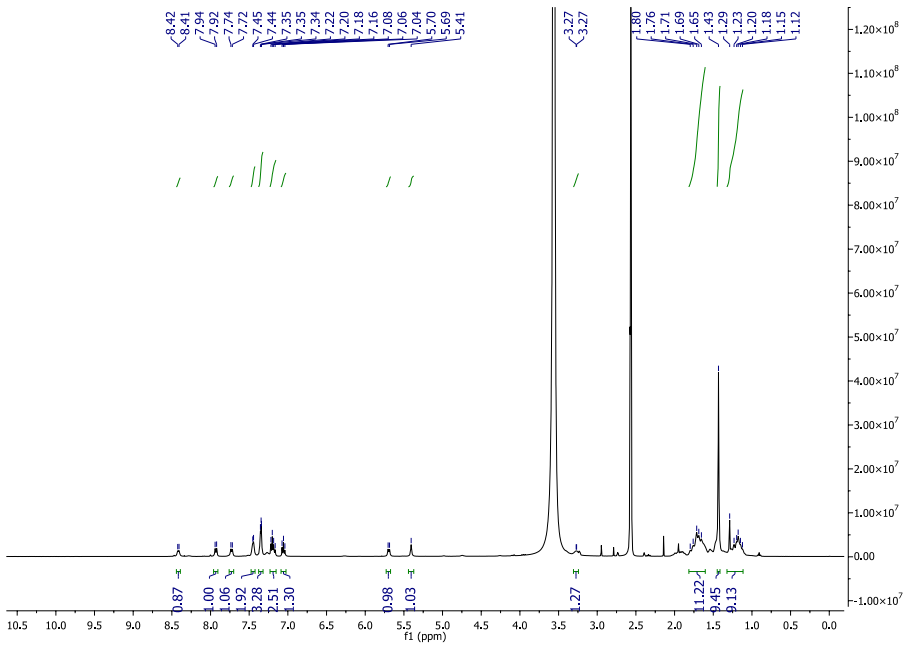

Supporting figure 34. ^{1}H NMR of compound *(S,R*)*-**14**

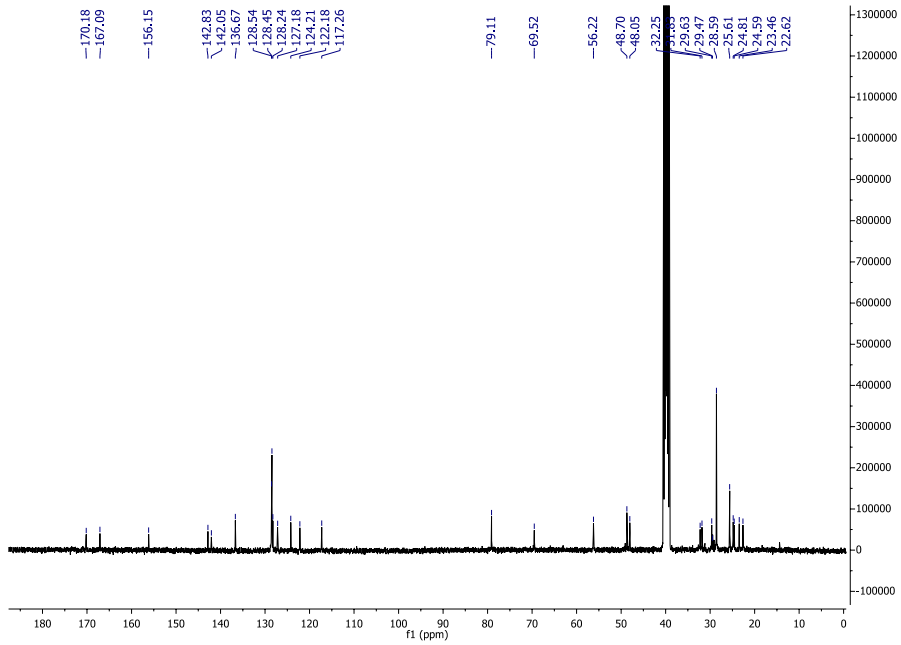

Supporting figure 35. ^{13}C NMR of compound *(S,R*)*-**14**

15

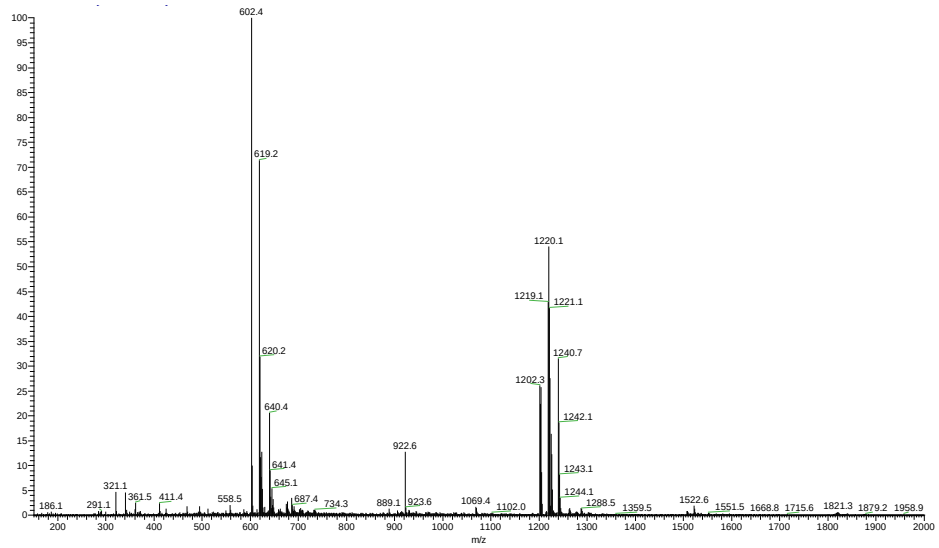

Supporting figure 36. ESI-MS of compound **15**

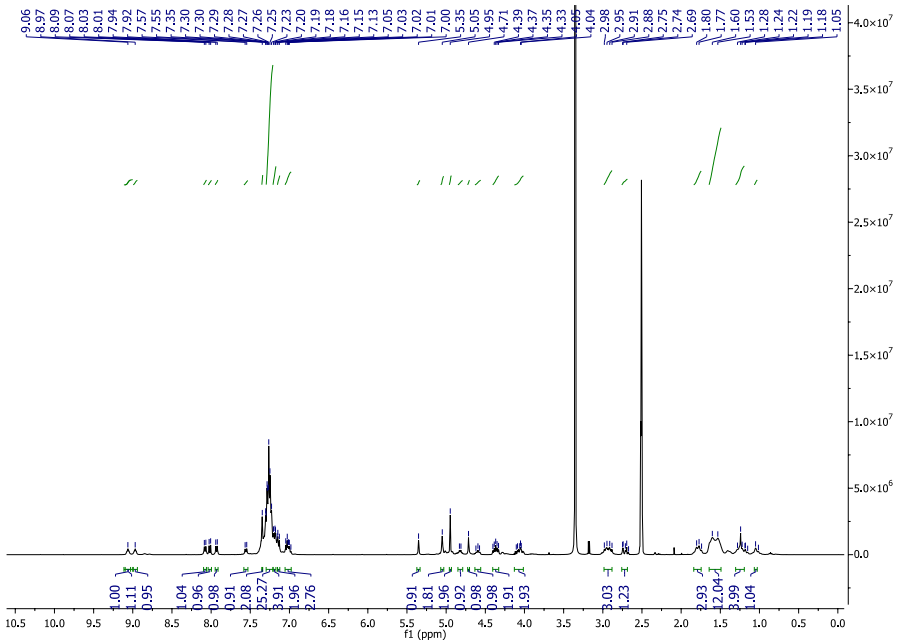

Supporting figure 37. ^{1}H NMR of compound **15**

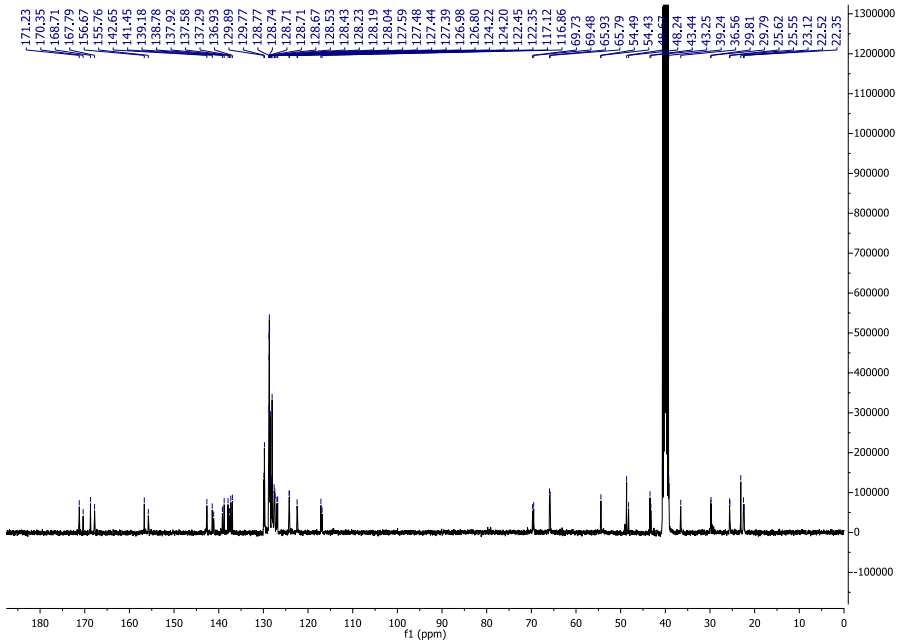

Supporting figure 38. ^{13}C NMR of compound **15**

16

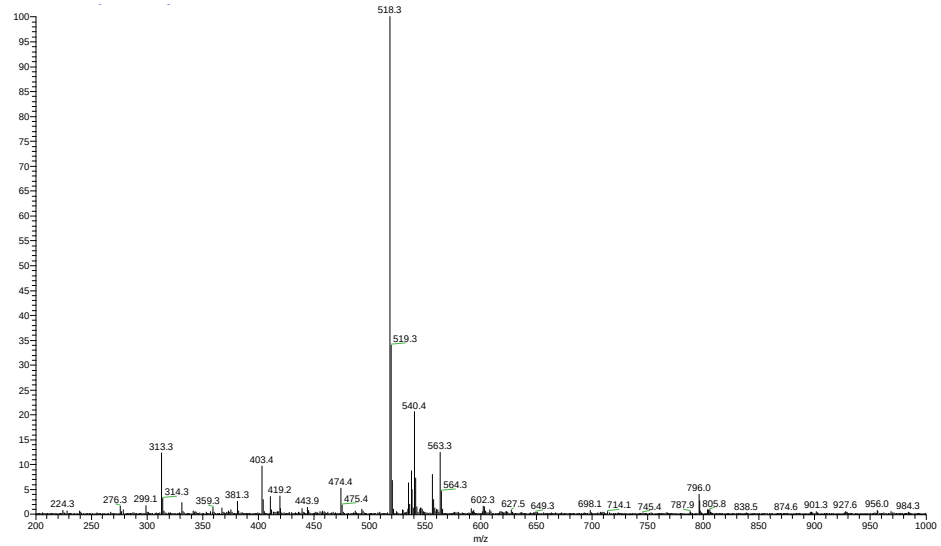

Supporting figure 39. ESI-MS of compound **16**

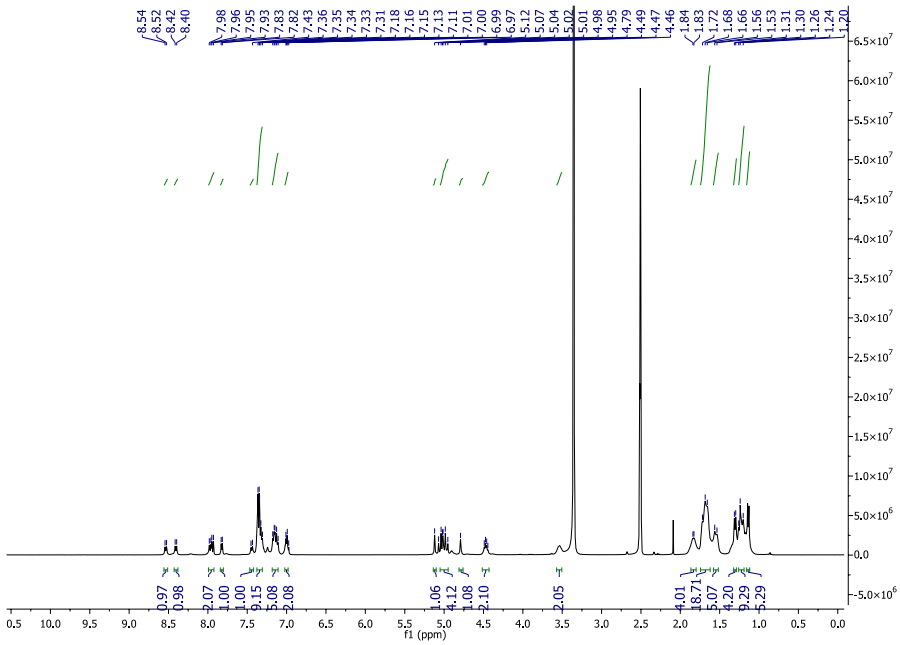

Supporting figure 40. ^{1}H NMR of compound **16**

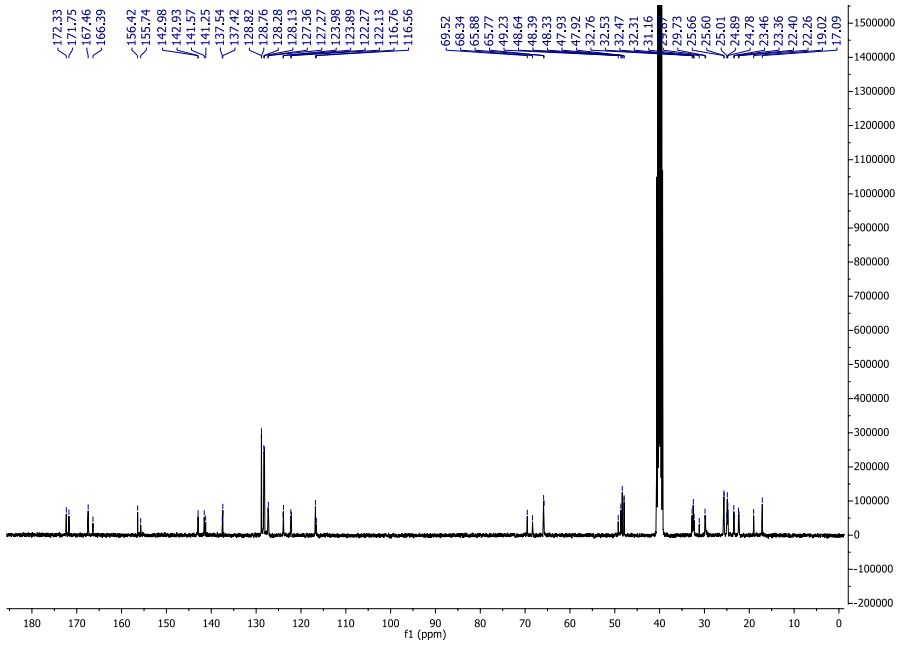

Supporting figure 41. ^{13}C NMR of compound **16**

(S,S)*-**17**

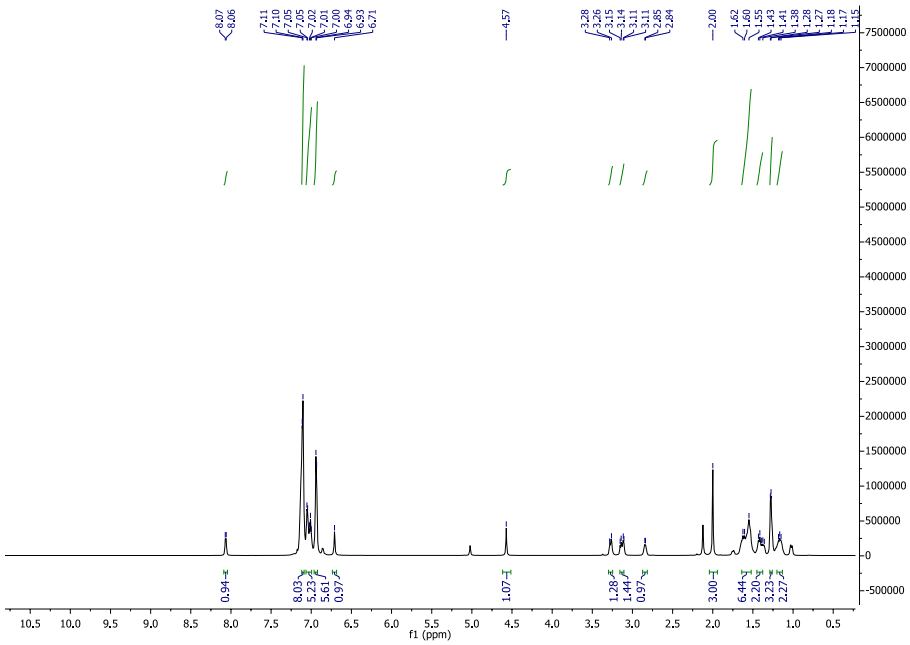

Supporting figure 41. ^{1}H NMR of compound *(S,S*)*-**17**

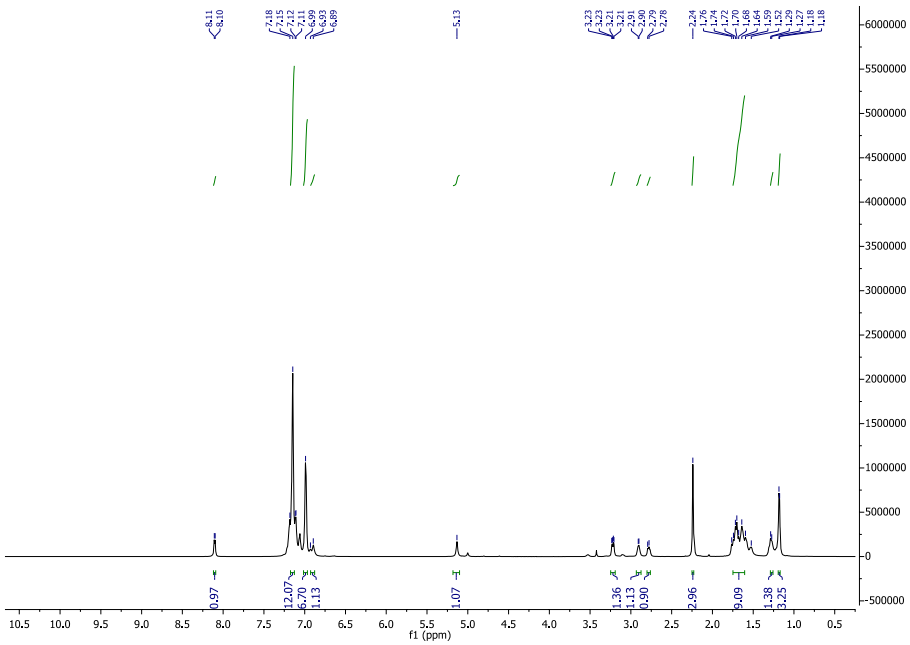

Supporting figure 42. ^{13}**C** NMR of compound *(S,S*)*-**17**

(S,R)*-**17**

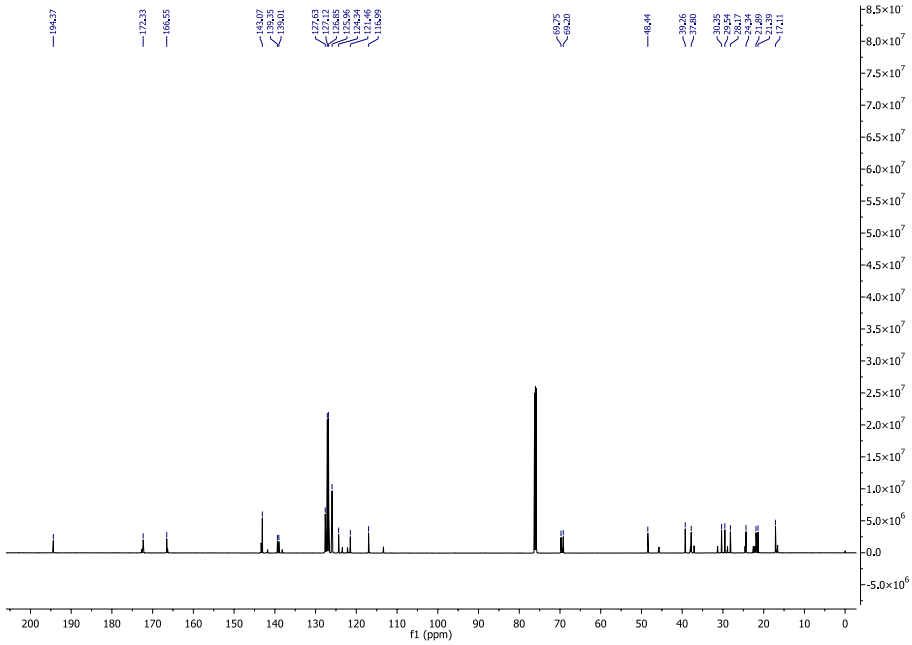

Supporting figure 43. ^{1}H NMR of compound *(S,R*)*-**17**

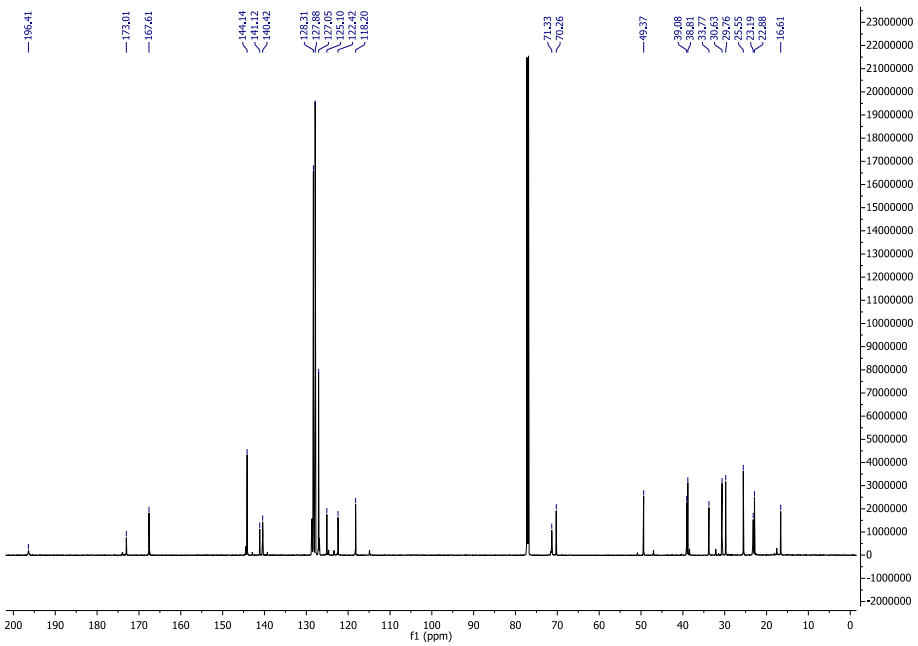

Supporting figure 44. ^{13}C NMR of compound *(S,R*)*-**17**

4.3 References

(1) Dömling, A. *Chem. Rev.* **2006**, *106*, 17.
(2) John, S. E.; Gulati, S.; Shankaraiah, N. *Org. Chem. Front.* **2021**, *8*, 4237.
(3) Shaabani, A.; Mohammadian, R.; Afshari, R.; Hooshmand, S. E.; Nazeri, M. T.; Javanbakht, S. *Mol. Divers.* **2021**, *25*, 1145.
(4) Pando,O.; Stark, S.; Denkert, A.; Porzel, A.; Preusentanz, R.; Wessjohann, L.A. *J. Am. Chem. Soc.* **2011**, *133*, 7692–7695.
(5) Dömling, A.; Beck, B.; Eichelberger, U.; Sakamuri, S.; Menon, S.; Chen, Q. Z.; Lu, Y.; Wessjohann, L. A. *Angew. Chem.* **2006**, *118*, 7393–7397.
(6) Van der Heijden, G.; van Schaik, T. B.; Mouarrawis, V.; de Wit, M. J.; Velde, C. M. V.; Ruijter, E.; Orru, R. V. *Eur. J. Org. Chem.* **2019**, *2019*, 5313–5325.
(7) Alfano, A. I.; Buommino, E.; Ferraro, M. G.; Irace, C.; Zampella, A.; Lange, H.; Brindisi, M. *ChemMedChem* **2021**, *16*, 3795.
(8) Flemming, H. C.; Wingender, J. *Nat. Rev. Microbiol.* **2010**, *8*, 623.
(9) Shrout, J. D.; Tolker-Nielsen, T.; Givskov, M.; Parsek, M. R. *MRS Bull* **2011**, *36*, 367.
(10) Fuqua, C.; Greenberg, E. P. *Nat. Rev. Mol. Cell. Biol.* **2002**, *3*, 685.
(11) Taga, M. E.; Bassler, B. L. *Proc Natl Acad Sci U S A* **2003**, *100 Suppl 2*, 14549.
(12) Kranjec, C.; Morales Angeles, D.; Torrissen Marli, M.; Fernandez, L.; Garcia, P.; Kjos, M.; Diep, D. B. *Antibiotics (Basel)* **2021**, *10*.
(13) Guzzo, F.; Scognamiglio, M.; Fiorentino, A.; Buommino, E.; D'Abrosca, B. *Molecules* **2020**, *25*.

Chapter 5

Enantiomerically pure spiroindolenine-based α-amino nitriles in continuous flow

5.1 Strecker reaction in continuous flow: enantioselective sustainable synthesis of spiroindoline-based compounds

As mentioned above, the first reported example of catalytic asymmetric Strecker dates back to 1996. Despite the great achievements and the impressive progress in the enantioselective Strecker reactions, the main examples are mainly focused on the transformation of acyclic aldimines and ketimines into enantiopure α-amino nitriles, while the catalytic asymmetric Strecker reactions with cyclic imines are barely studied.[1-8]

The first asymmetric hydrocyanation has been reported in 2000 by Jacobsen, providing the use of chiral 1,2-*trans*-diaminocyclohexane-based urea/Schiff base as the catalyst, followed by other two works reported in 2007 and 2010, exploiting trimethylsilyl or acetyl cyanides as cyanide sources.[9]

To the best of our knowledge, the first and only asymmetric cyanation of cyclic *(Z)*-aldimines stretch back to 2012, when Shao and Tian used ethyl cyanoformate as safer cyanide source with respect to the classic HCN or TMSCN, in the presence of Cinchona alkaloid-based thiourea catalyst at 10 °C to give final product. Despite the good yields and the excellent *ee.*, the reaction suffers from one problematic drawback in term of reaction time, since requiring 48-72 hours for starting material consumption.[10]

Obviously, the prolonged reaction time also clashes with the basic principles of green chemistry.

In the context of our interest towards sustainable flow-based approaches, we first decided to analyze the existing Strecker protocols in flow in the

literature. During this search, we could only find out three relevant examples.[11-13] Subsequently, taking advantage of our previous experience in handling metastable indolenines, and having developed a green and sustainable flow protocol for the synthesis of (spiro)indolenine templates, we decided to establish a flow-based organocatalytic Strecker protocol on cyclic *(Z)*-aldimines.

Using the (spiro)indolenine **2** as the benchmark, prepared in flow as described above, we first set out to reproduce the catalytic asymmetric batch protocol reported in the paper of 2012, in absence (Table 1, Entry 1), in presence of 10 mol% (Table 1, Entry 2) and 20 mol% of the cinchona based catalyst *(R)*-**1a**. (Table 1, Entry 3) at 10 °C in dichloroethane with the addition of 1.2 equiv. of methanol for 72 h. (Table 15) We registered in both cases a comparable outcome in terms enantiomeric ratios, namely 70:30 and 77:23 after separation by chiral HPLC was achieved with 10 mol% and 20 mol% and yield ≈ 95%.

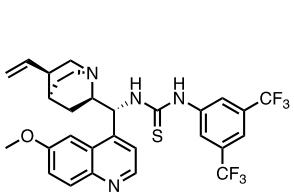

(R)-**1a**

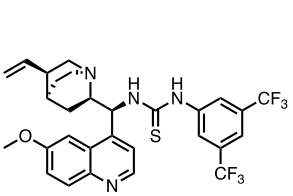

(S)-**1a**

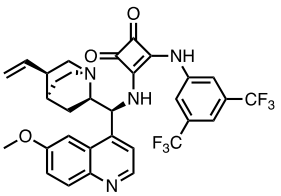

(S)-**1b**

Figure 1. Cinchona- based catalysts ***(R)***-1a, ***(S)***-1a and ***(S)***-1b.

Table 1. Basic screening of reaction conditions for the formation of compound **4** in batch.

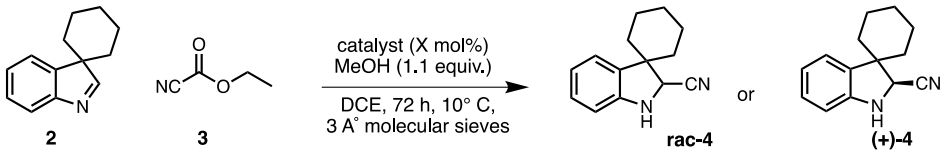

2 **3** **rac-4** **(+)-4**

Entry [a]	Equiv. of 26	Catalyst	Yield (%)[b]	*e.r.*[c]	Product
1	1.1	//	96	//	rac-**4**
2	1.1	**(*R*)-1a** (10 mol%)	94	70:30	(+)-**4**
3	1.1	**(*R*)-1a** (20 mol%)	93	77:23	(+)-**4**

[a] General procedure A with the suitable variations (see experimental part); [b] Isolated yield after column chromatography; [c] Enantioselectivity was determined by HPLC analysis on a chiral stationary phase (see supporting info).

With these batch results in hand, we shifted the reaction from the classical flask into a capillary reactor using a home-made flow system, consisted of conventional HPLC pump and a six-port Rheodyne injectors containing volume sample loop of 1 mL. A PTFE tubular reactor was immersed in a conventional water bath for changing the cooling needed for reaction, followed thus by a 7 bar back-pressure regulator (BPR) to maintain the control of the system.

On the basis of the batch reaction conditions, an exploration of key parameters allowed the identification of the reagent mixing mode, stoichiometry, the optimum solvent for the synthesis, temperature and reaction time. The initial investigation was dedicated to the screening of suitable solvents.

Table 2. Solvent screening in flow for asymmetric Strecker on compound **4.**

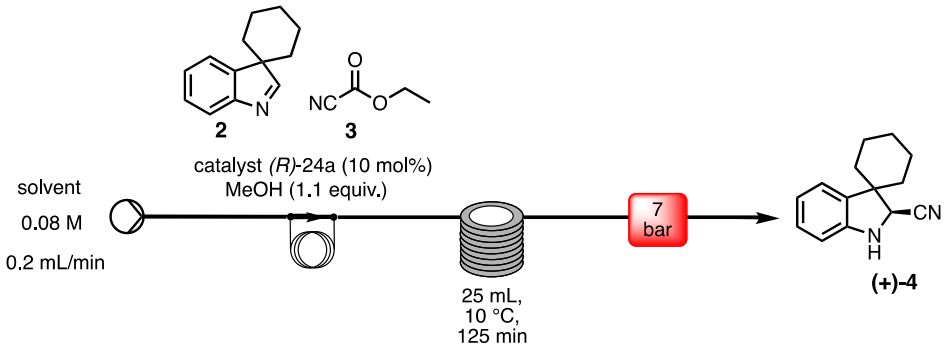

Entry[a]	Equiv. of 26	Solvent	Yield (%)[b]	*e.r.*[c]
1	1.1	DCE	87	75:25
2	1.1	DCM	53	82:18
3	1.1	EtOAc	8	n.d.
4	1.1	CPME	20	n.d.

[a] General procedure B with the suitable variations (see experimental part); [b] Isolated yield after column chromatography; [c] Enantioselectivity was determined by HPLC analysis on a chiral stationary phase (see Supporting Info).

Starting from our spiroindolenine **2**, ethyl cyanoformate **3**, 1.1 equiv. of MeOH, cinchona-based catalyst *(R)*-**1a** (10% mol), a focused exploration of solvents was carried out. The solution was injected with a flow rate of 0.2 mL/min for an overall residence time of 125 minutes at temperature of 10° C. The exiting stream was collected in a classic flask for further purification. Table 2 shows the representative results in terms of solvent screening.

In line with our batch investigation, we first tested the reaction outcome using 1,2-DCE and DCM, being "chlorinated solvents". (Table 2, Entries 1-2). Despite the good yield of the final product (87%), 1,2-DCE furnished the same enantiomeric ratio (*er*) with respect to the batch protocol (75:25). However, a slight increment in term of *er* was verified with DCM, but unfortunately a drop of yield of 30% was concomitantly registered. Taking into account our initial aim, to reach eco-sustainability and eco-compatibility, we switched from chlorinated solvents (quite toxics) to "greener" ones, choosing ethyl acetate and cyclopentylmethylether. Unfortunately, disappointing results have been obtained in both cases (Table 2, Entries 3-4) in terms of yield and *er*.

We then tried to identify the optimum cinchona-based catalyst as well as the catalyst and parallelly the suitable amount of ethyl cyanoformate to be employed, as reported in Table 3.

Table 3. Screening of catalysts.

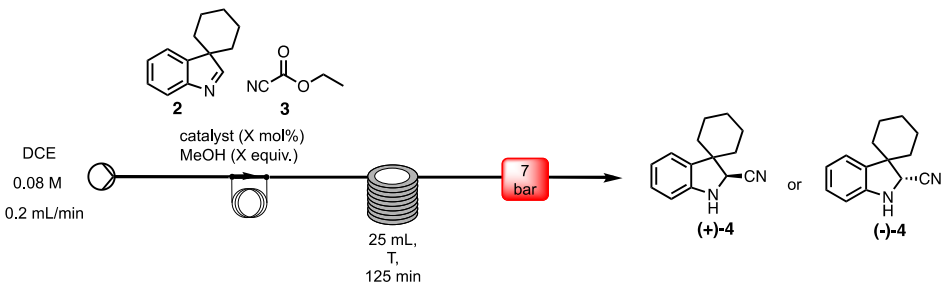

Entry[a]	Equiv. of 26	Catalyst	Yield (%)[b]	*e.r.*[c]	Product
1	1.1	**(*R*)-1a** 20 mol%	90	91:9	(+)-**4**
2	1.1	**(*R*)-1a** 40 mol%	82	95:5	(+)-**4**

3[d]	1.1	**(*R*)-1a** 10 mol%	70	93:7	(+)-**4**
4	**1.3**	**(*R*)-1a** 10 mol%	**93**	**95:5**	(+)-**4**
5	1.3	**(*R*)-1a** 5 mol%	92	90:10	(+)-**4**
6	1.3	**(*S*)-1a** 10 mol%	88	85:15	(-)-**4**
7[e]	1.3	**(*R*)-1a** 10 mol%	34	65:35	(+)-**4**
8[f]	1.3	**(*R*)-1a** 10 mol%	38	80:20	(+)-**4**
9	1.3	**(*S*)-1b** 10 mol%	92	92:8	(-)-**4**

[a] General procedure B with the suitable variations (see the experimental part); [b] Isolated yield after column chromatography; [c] Enantioselectivity was determined by HPLC analysis on a chiral stationary phase (see supporting info); [d]: The reaction mixture was stirred at 0 °C; [e]: The mixture was pressurized at 1.8 bar; [f] The reaction mixture was stirred at 0 °C with 1.8 bar of pressure at 0.1 mL/min.

First of all, increasing the catalyst *(R)*-**1a** loading from 10% mol to 20% mol up to a substoichiometric amount (40% mol) improved the enantiomeric ratio from 75:25 to 91:9 (Table 3, Entry 1) and 95:5 (Table 3, Entry 2), respectively. When the reaction was carried out at lower temperature (0° C), with 10% mol of catalyst, a satisfying enantiomeric excess was achieved; however, this result was accompanied by a significant yield drop (70%), (Table 3, Entry 3). The first successful outcome in terms of both *er* and yield was achieved when using 1.3 equiv. of ethyl cyanoformate instead 1.1 equiv., 10% mol of catalyst and temperature of 10 °C. We obtained 93% of yield and 95:5 of *er* (Table 3, Entry 4). With these gratifying conditions in hand, we tried to reduce the

catalyst loading from 10% mol to 5% mol, but a drop of 10% in term of *er* was highlighted. We attempted to apply the best conditions (Table 3, Entry 4) to the catalyst with opposite chirality with respect to *(R)*-**1a**, obtaining 88% yield and 85:15 *er* (Table 3, Entry 6). Changing the pressure of the system from 7 to only 1.8 bar, and working at both at 0 °C and 10 °C (Table 3, Entries 7 and 8, respectively), disappointing results were achieved. Finally, we performed an experiment with the squaramide-based catalyst *(S)*-**1b** at 10 mol %, which provided similar outcome. (Table 3, Entry 9).

Moreover, protic source seems necessary for the reaction, thus leading us to hypothesize a plausible mechanism for the reaction (Figure 2).

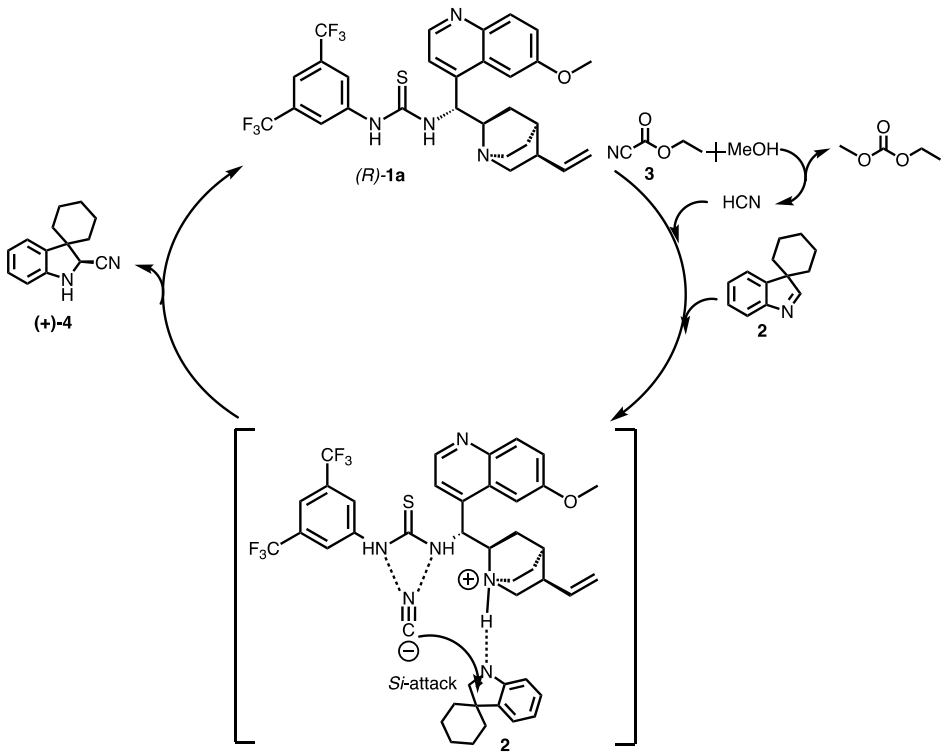

Figure 2. Proposed mechanism for the enantioselective Strecker on cyclic (*Z*)-aldimines using ethyl cyanoformate.

Ethyl cyanoformate in presence of an alcohol (R-OH) generates HCN during the reaction. The thiourea catalyst is responsible for the pre-orientation and the protonation of substrates acting as bifunctional organocatalyst. The free cyanide anion can be activated by the thiourea moiety of the catalyst, while the cyclic imine is activated upon formation of a hydrogen bond with the ammonium salt. The cyanide is directed to the *Si*-face of the imine, thus explain the enantioselective reaction outcome.

We thus opted for screening the nature of protic additive. (Table 4)

Table 4. Screening of alcohols.

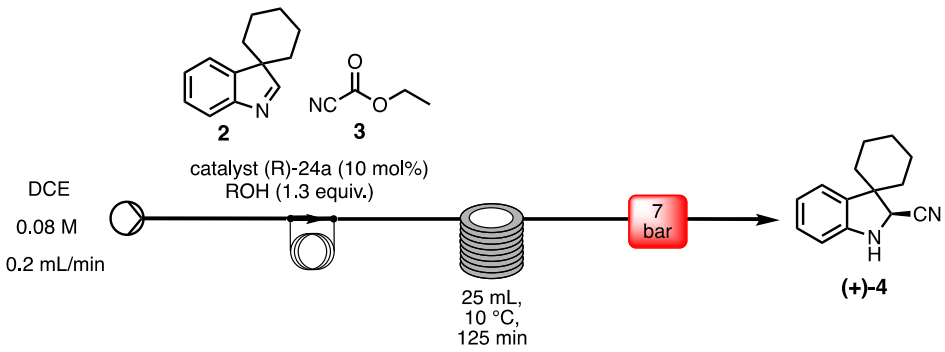

Entry[a]	Equiv. of 3	ROH[b]	Yield (%)[c]	*e.r.*[d]
1[e]	**1.3**	**MeOH**	**93**	**95**
2	1.3	//	8	92:8
3	1.3	EtOH	65	67:33
4	1.3	*i*PrOH	44	86:14

[a] General procedure B with the suitable variations (see Experimental); [b]: 1.3 equiv.; [c] Isolated yield after column chromatography; [d] Enantioselectivity determined by HPLC analysis on a chiral stationary phase (see Supporting Info); [e] Best result from Table 3, entry 4.

Starting from the best outcome that involves the use of methanol (Table 4, Entry 1), we perform the reaction in absence of any types of alcohols (Table 4, Entry 2), in presence of ethanol (Table 4, Entry 3) or isopropanol (Table 4, Entry 4). Unsatisfying results were achieved in all cases; however, in general, the reaction works better in presence of a protic additive.

Further investigations will be carried out interrogating the outcome of perfluorinated alcohols. Not only they represent an environmentally benign protic source, but they also display other favorable features, such as high polarity, low boiling point and strong hydrogen bond donating properties.[14,15]

Last, in view of our interest for the implementation of sustainable protocols, we tried to recover the organocatalyst, in order to reuse it. In a first trial, given the basic characteristics in the cinchona catalyst, we tried to employ the acidic resin Amberlyst 15 to catch the catalyst, as reported in the literature.[16] We just added a column reactor filled with sand and 1 mmol Amberlyst 15 at the end of the line. However, in the collected stream, no traces of product were detected, since the acidic resin also held back the Strecker product. In the second trial, we moved to bromotris(triphenylphosphine)copper(I), used as ligand for the thiourea functionality as reported in the literature, but again we obtained unsatisfactory results.[17]

The use of silica gel, because of intrinsic acid functionalities, and sand inverted the negative trend. This resulted in an in-line separation with the initially collected stream only containing the reaction product. Once all the product fractions were collected, the catalyst could be easily released by

flushing with ethyl acetate and methanol. The entire amount of the employed cinchona catalyst was recovered, and the purity was up to 95%, as determined by NMR analysis.

Reaction scope and versatility are currently under investigation in the laboratories where I performed my thesis work.

5.2 Experimental part

General comments

Unless otherwise specified, materials were purchased from commercial suppliers and used without further purification. TLC analysis was conducted using aluminum foil supported thin-layer silica gel chromatography plates (F254 indicator). Column chromatography was performed using 230–400 mesh, 60 Å pore diameter silica gel. For ^{1}H NMR and ^{13}C NMR measurements an accurately weighed amount of analyte (about 5.0–10.0 mg) was dissolved in 600 μL of deuterated chloroform ($CDCl_3$) or dimethyl sulfoxide (DMSO-d_6). The mixture was transferred into a 5 mm NMR tube and the spectra were acquired on a Bruker Advance 400 MHz spectrometer by using the residual signal of the deuterated solvent as internal standard. Splitting patterns are described as singlet (s), doublet (d), triplet (t), quartet (q) and broad (br); the values of chemical shifts (δ) are given in ppm and coupling constants (J) in Hertz (Hz). NMR data were processed with MestreNova (Version 8.1.1,

Mestrelab Research). ESI-MS spectra analysis was carried out on a mass spectrometer LTQ-XL.

High pressure liquid chromatography (HPLC) analyses were performed on was performed with a Waters Model 510 pump equipped with Waters Rheodyne injector and a differential refractometer, model 401, and an isostatic pump, using a chiral stationary phase column (Lux® 5µm Cellulose-1 Chiral HPLC Column, 250 x 4.6 mm) and the UV detection was monitored at 254 nm. The chiral HPLC methods were calibrated with the corresponding racemic mixtures.

Optical rotation values were measured at room temperature operating at λ = 589 nm, corresponding to the sodium D line, and were determined in a Jasco P-200 (Jasco Europe s.r.l., Cremella, Italy) polarimeter using a microcell (1 mg sensitivity) containing the compound dissolved in 1 mL of chloroform.

Synthesis of starting material

*Spiro[cyclohexane-1,3'-indole] (**2**) in flow and batch mode*

Synthesis in flow. Chemical transformations in flow were realized using a self-made flow reactor: one Waters P510 HPLC pumps were connected to a Rheodyne 9010 injection valve, equipped with a 1 mL sample loop made from PTFE tubing and an injection port for disposable syringe. The injection valve was further connected to a coiled PTFE tubing of 15 mL volume. The coil was immersed in a silicon oil bath for controlling reaction temperatures. The tubular reactor finished into a back pressure regulator (BPR), which was either spring mechanism-based (6.7 bar) or simply a PEEK capillary of defined length (1.7 bar). Product containing exiting streams were collected directly in a flask. Reagents were prepared

for loading into the sample loops (SL) according to the following method: 0.25 mmol aldehyde + 0.25 mmol $PhNHNH_2 \cdot HCl$ in 1 mL of EtOH, heated to 50 °C for 5 min prior to loading into the SL; SL B: 1.2 equiv. HCl in 1 mL of EtOH.

Synthesis in batch. A mixture of phenylhydrazine (HCl salt, 36.5 mg, 0.25 mmol) and cyclohexanecarboxaldehyde (30 µL, 0.25 mmol) was treated with HCl (150 µL, 0.3 mmol). Next, the reaction mixture was gradually poured into saturated aqueous $NaHCO_3$ (100 mL) and extracted with EtOAc (5 × 2 mL). Combined organic extracts were washed with brine, dried with Na_2SO_4, and used without purification.
Yield: 58%; yellow solid; R_f = 0.6 (H:E = 7:3).
GC-MS (EI, 70 eV): *m*/*z* (%) = 187 $[M]^+$ t_R = 14.94 min

*Synthesis of catalyst (S)-**1b**.*
The synthesis of catalyst ***(S)-1b*** was performed according to literature procedures.[18-20]

*Synthesis of Strecker product **4** in batch (General procedure A)*
To a flame dried reaction vial equipped with a magnetic stirring bar were added powdered 3 Å molecular sieves. The molecular sieves were thermally activated under vacuum for 30 min, and cooled to 10 °C under nitrogen. To the reaction vial were added cyclic (*Z*)-aldimine **25** (15 mg, 0.08 mmol), catalyst **24a** or **24b** (10 mol%), dry 1,2-dichloroethane (1.0 mL), ethyl cyanoformate **26** (9 µL, 1.1 equiv.), and methanol (5 µL, 1.1 equiv.). The resulting mixture was stirred at 10 °C for 72 h, and directly charged onto silica gel. Product **27** was isolated using petroleum ether/ethyl acetate (20/1~3/1) as eluent.

*Synthesis of Strecker product **4** in flow (General procedure B)*

Chemical transformations in flow were realized using a self-made flow reactor: a Waters P510 HPLC pump was connected to a Rheodyne 9010 injection valve, equipped with a 1 mL sample loop made from PTFE tubing and an injection port for disposable syringes. The injection valve was further connected to a coiled PTFE tubing of 25 mL volume. The coil was immersed in a water bath for controlling reaction temperatures. The tubular reactor finished into a mechanical back pressure regulator (BPR) of approx. 7 bar. Product containing exiting streams were collected directly in a flask.

A solution of spiroindolenine **2** (15 mg, 0.08 mmol), ethyl cyanoformate (9 µL, 1.3 equiv.), the suitable catalyst **1a** or **1b** (10 mol%) and methanol (5 µL, 1.3 equiv.) was prepared in 1,2-dichloroethane (1 mL total solution volume). The flow reactor was cooled to 10 °C using at a total flow rate of 0.2 mL/min to move the reaction mixture through the coil reactor for a residence time of 125 min.

NMR analyses

^{1}H NMR measurements. An accurately weighed amount of analyte (about 5.0 mg) was dissolved in 600 µL of deuterated chloroform ($CDCl_3$). The mixture was transferred into a 5 mm NMR tube. The spectra were acquired on a Bruker 400 MHz spectrometer using the standard Bruker zg sequence (32 scans at 20 °C). NMR data were processed with MestreNova (version 8.1.1, Mestrelab Research).

^{13}C NMR measurements. An accurately weighed amount of analyte (about 5.0 mg) was dissolved in 600 µL of deuterated chloroform ($CDCl_3$). The

mixture was transferred into a 5 mm NMR tube. The spectra were acquired on a Bruker 400 MHz spectrometer using the standard Bruker zgpg30 sequence (3072 scans at 20 °C). NMR data were processed with MestreNova (version 8.1.1, Mestrelab Research).

Compound characterization

Spiro[cyclohexane-1,3'-indoline]-2'-carbonitrile (rac-4)

^{1}H NMR (700 MHz, Chloroform-d) δ 7.01 (t, J = 7.3 Hz, 2H), 6.76 (t, J = 7.4 Hz, 1H), 6.61 (d, J = 7.9 Hz, 1H), 4.38 (s, 1H), 4.10 (s, 1H), 2.08 (d, J = 14.6 Hz, 1H), 1.90 (td, J = 13.9, 13.0, 3.7 Hz, 1H), 1.79 (dd, J = 11.0, 6.7 Hz, 1H), 1.73 (d, J = 12.9 Hz, 1H), 1.65 (d, J = 10.4 Hz, 2H), 1.34 (tt, J = 27.2, 12.1 Hz, 4H).

^{13}C NMR (176 MHz, Chloroform-*d*) δ 147.16, 135.03, 128.32, 122.88, 120.45, 119.53, 110.52, 57.12, 49.76, 35.50, 32.92, 25.36, 23.17.

(+)-4 was obtained as a white solid in 93% yield and 95% ee from a reaction catalyzed by **(*R*)-1a**. The er value was determined by chiral stationary phase HPLC analysis [Lux® 5µm Cellulose-1 Chiral HPLC Column, 250 x 4.6 mm], 1.0 mL/min, λ = 254 nm, tr (minor) = 15.1 min, tr (major) = 26.4 min]. $[\alpha]^{20}_{D}$ = + 37,38 (c 0.3, $CHCl_3$).

(-)-4 was obtained as a white solid in 92% yield and 95% *ee* from a reaction catalyzed by XC. The er value was determined by chiral stationary phase HPLC analysis [Lux® 5µm Cellulose-1 Chiral HPLC Column, 250 x 4.6 mm], 1.0 mL/min, λ = 254 nm, tr (minor) = 18.9 min, tr (major) = 37.7 min]. $[\alpha]^{20}_{D}$ = -43,63.0 (c 0.3, $CHCl_3$);

Spiro[cyclohexane-1,3'-indoline]-2'-carbonitrile (rac-4)

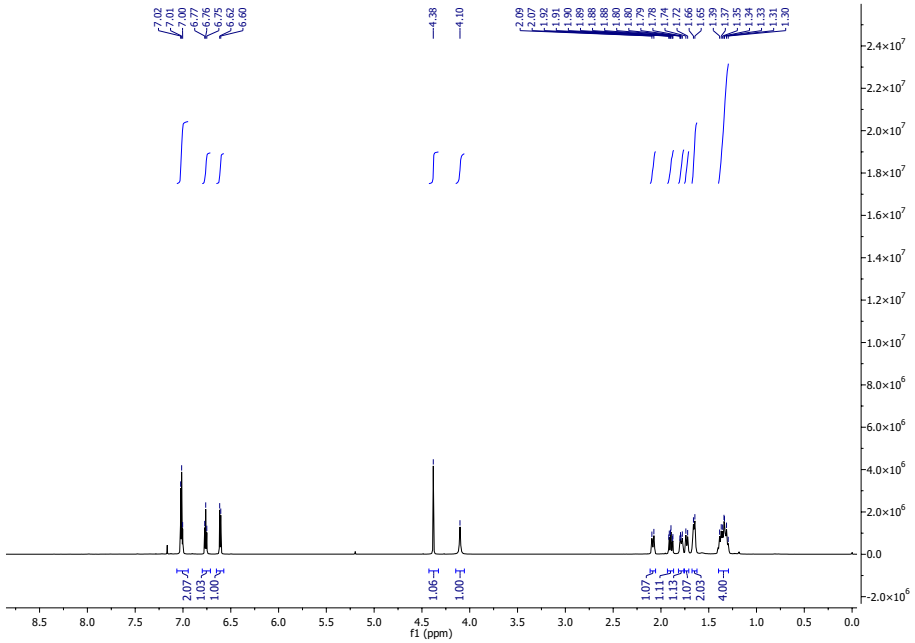

Supporting figure 1. ^{1}H NMR of compound **rac-4**

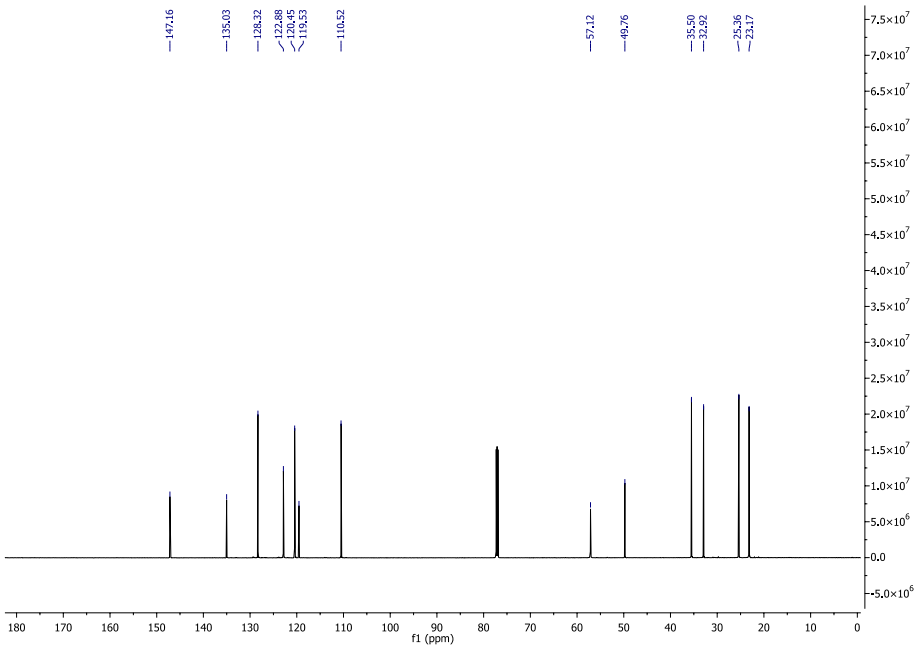

Supporting figure 2. ^{13}C NMR of compound **rac-4**

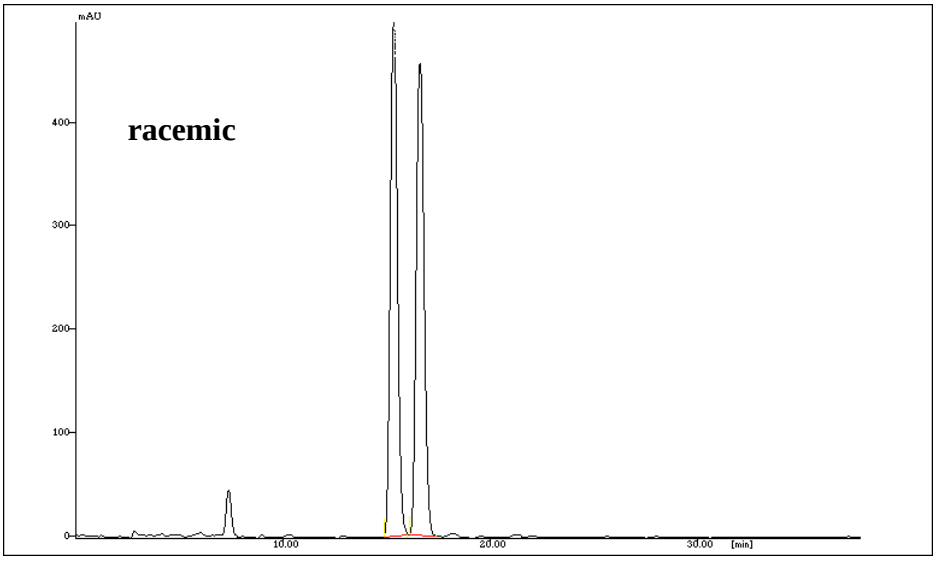

Supporting figure 3. HPLC chromatogram 1

Table 1, entry 1

Peak [a]	Time (min)	Area (mAU·s)	Area (%)
1	15.333	10330.25	49%
2	15.592	10489.50	51%

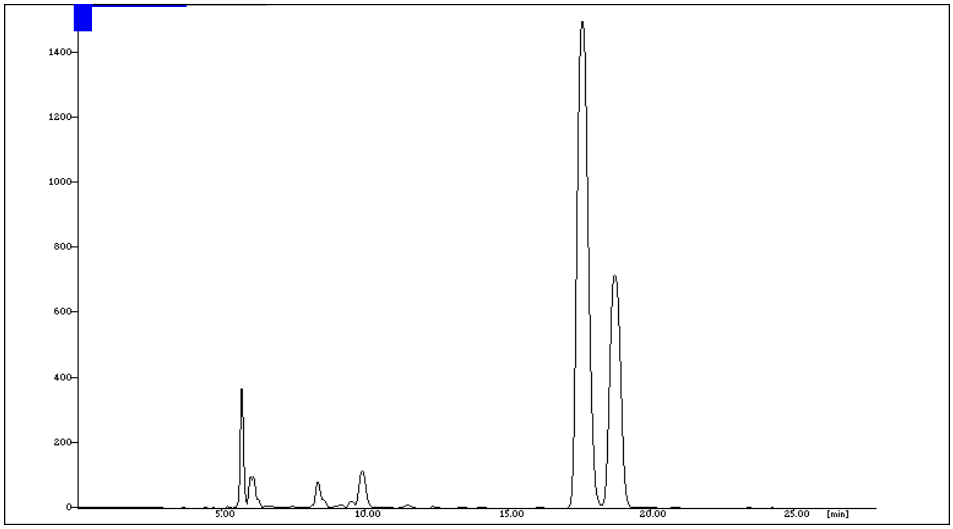

Supporting figure 4. HPLC chromatogram 2

Table 1, entry 2

Peak[a]	Time (min)	Area (mAU·s)	Area (%)
1	17.583	36171.25	69%
2	18.725	16247.17	30%

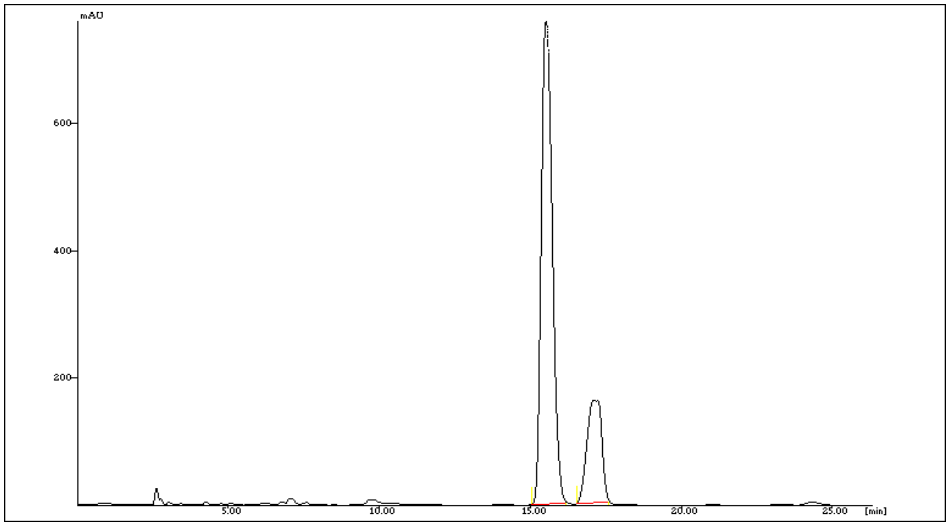

Supporting figure 5. HPLC chromatogram 3

Table 1, entry 3

Peak [a]	Time (min)	Area (mAU·s)	Area (%)
1	15.500	17493.50	
2	17.092	5094.50	

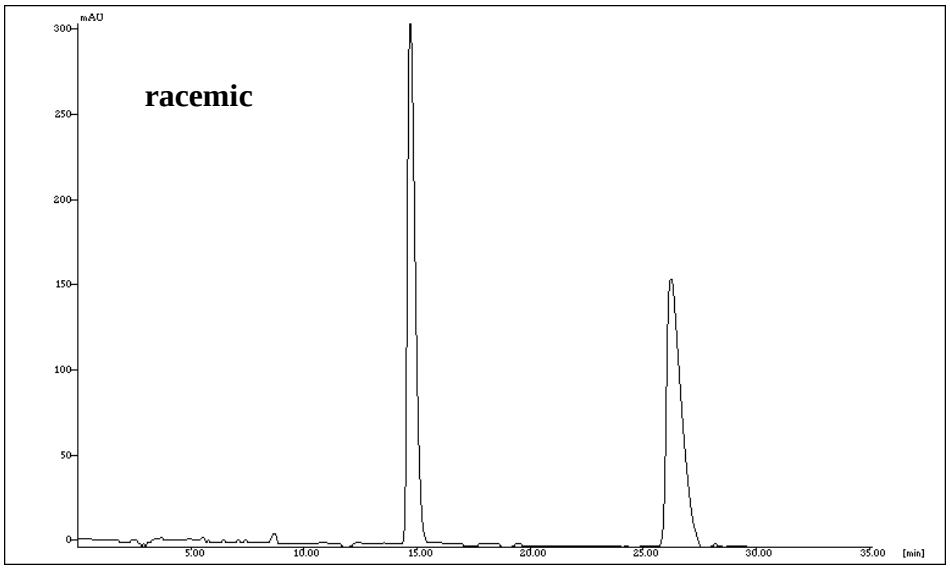

Supporting figure 6. HPLC chromatogram 4

Table 1, entry 1

Peak [a]	Time (min)	Area (mAU·s)	Area (%)
1	14.675	6326.686	49.12
2	26.183	6553.256	50.88

[a]: Lux® 5µm Cellulose-1 Chiral HPLC Column, 250 x 4.6 mm was used.

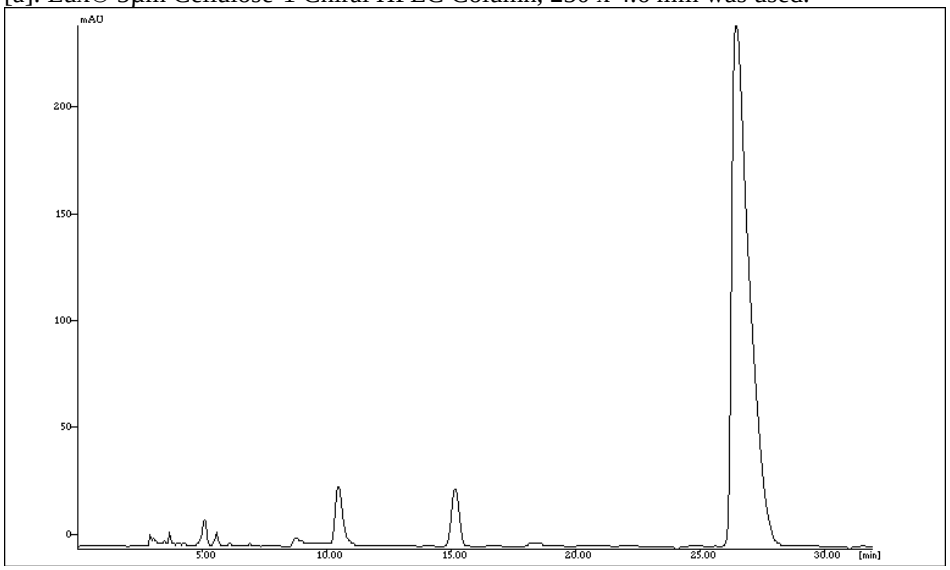

Supporting figure 7. HPLC chromatogram 5

Table 3, entry 4

Peak [a]	Time (min)	Area (mAU·s)	Area (%)
1	15.108	523.250	4.72
2	26.417	11074.500	95.50

[a] Lux® 5µm Cellulose-1 Chiral HPLC Column, 250 x 4.6 mm was used.

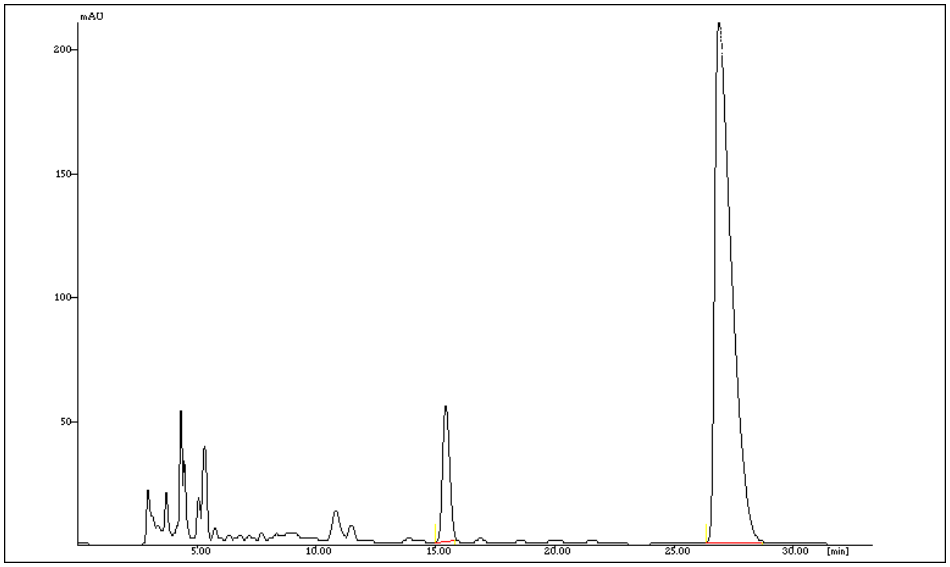

Supporting figure 8. HPLC chromatogram 6

Table 3, entry 1

Peak [a]	Time (min)	Area (mAU·s)	Area (%)
1	15.392	969.08	9%
2	26.850	9601.50	91%

[a] Lux® 5µm Cellulose-1 Chiral HPLC Column, 250 x 4.6 mm was used.

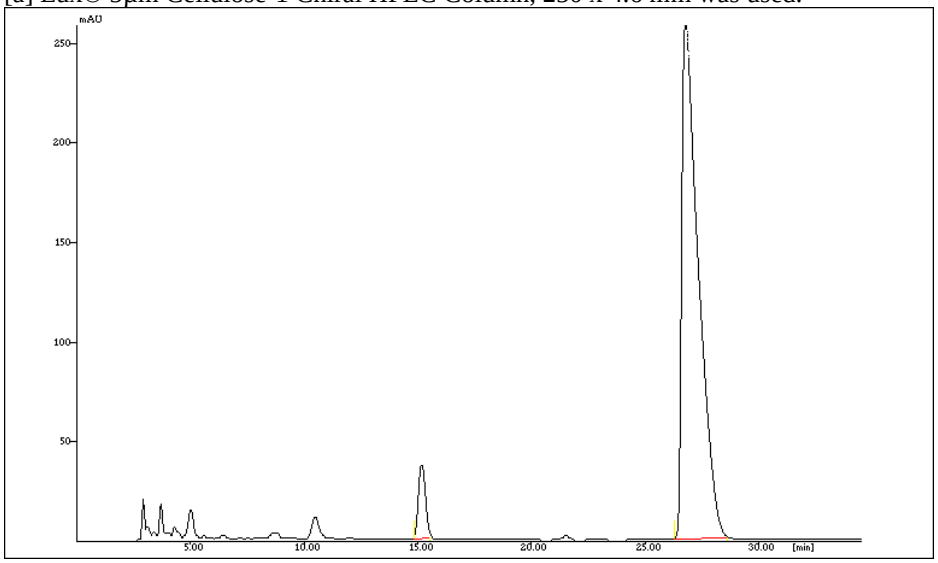

Supporting figure 9. HPLC chromatogram 7

Table 3, entry 2

Peak [a]	Time (min)	Area (mAU·s)	Area (%)
1	15.133	692.75	5%
2	26.750	12356.50	95%

[a] Lux® 5µm Cellulose-1 Chiral HPLC Column, 250 x 4.6 mm was used.

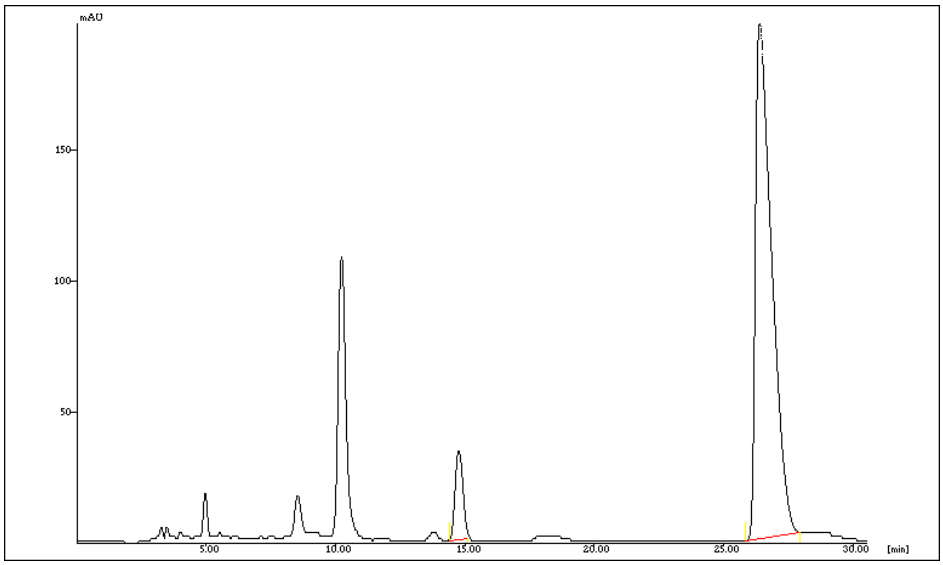

Supporting figure 10. HPLC chromatogram 8

Table 3, entry 3

Peak [a]	Time (min)	Area (mAU·s)	Area (%)
1	14.717	620.25	7%
2	26.367	8049.29	93%

[a] Lux® 5µm Cellulose-1 Chiral HPLC Column, 250 x 4.6 mm was used.

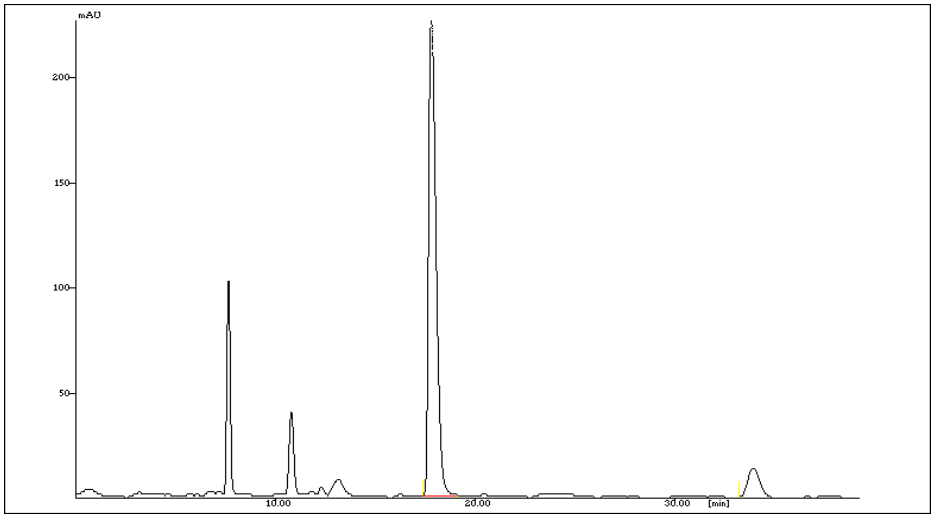

Supporting figure 11. HPLC chromatogram 9

Table 3, entry 9

Peak [a]	Time (min)	Area (mAU·s)	Area (%)
1	18.983	6249.750	92%
2	37.717	589.000	8%

[a] Lux® 5µm Cellulose-1 Chiral HPLC Column, 250 x 4.6 mm was used.

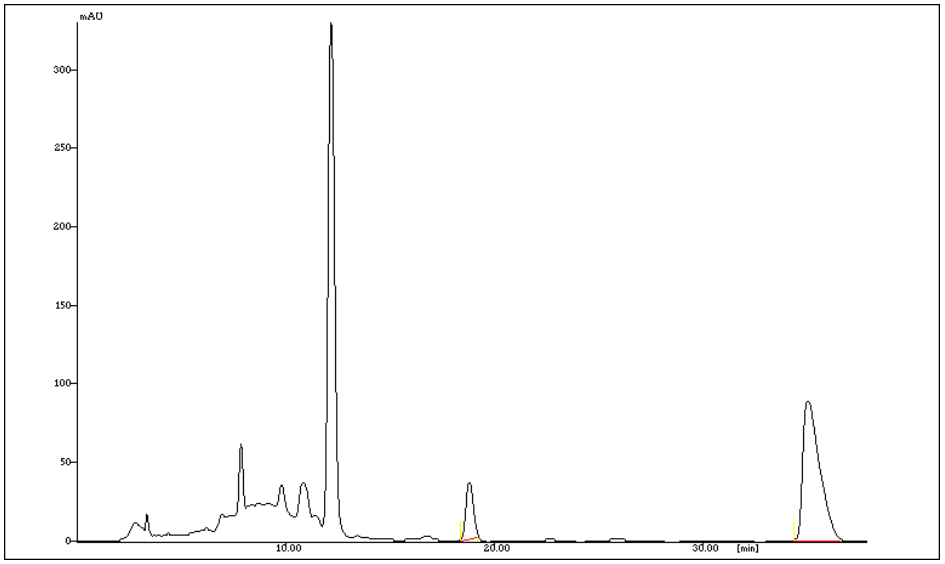

Supporting figure 12. HPLC chromatogram 10

Table 4, entry 4

Peak [a]	Time (min)	Area (mAU·s)	Area (%)
1	18.758	772.00	14%
2	34.983	4677.00	86%

[a] Lux® 5µm Cellulose-1 Chiral HPLC Column, 250 x 4.6 mm was used.

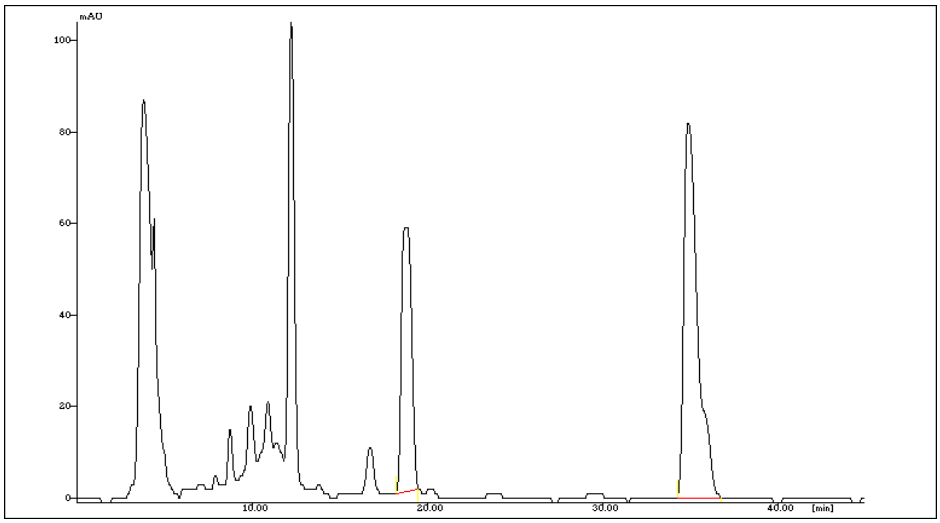

Supporting figure 13. HPLC chromatogram 11

Table 4, entry 3

Peak [a]	Time (min)	Area (mAU·s)	Area (%)
1	18.650	2074.93	33%
2	34.842	4150.00	67%

[a] Lux® 5µm Cellulose-1 Chiral HPLC Column, 250 x 4.6 mm was used.

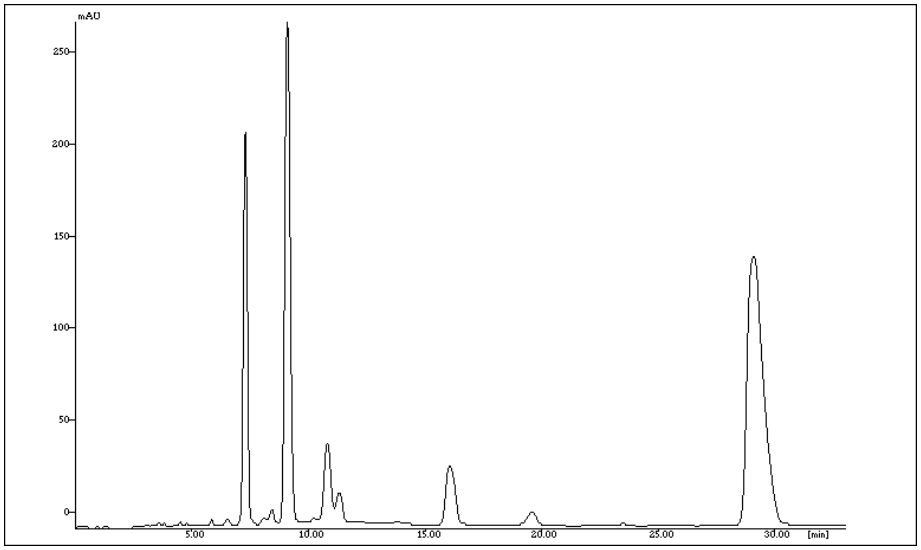

Supporting figure 14. HPLC chromatogram 12

Table 3, entry 5

Peak	Time (min)	Area (mAU·s)	Area (%)
1	16.017	764.00	10%
2	29.050	6592.00	90%

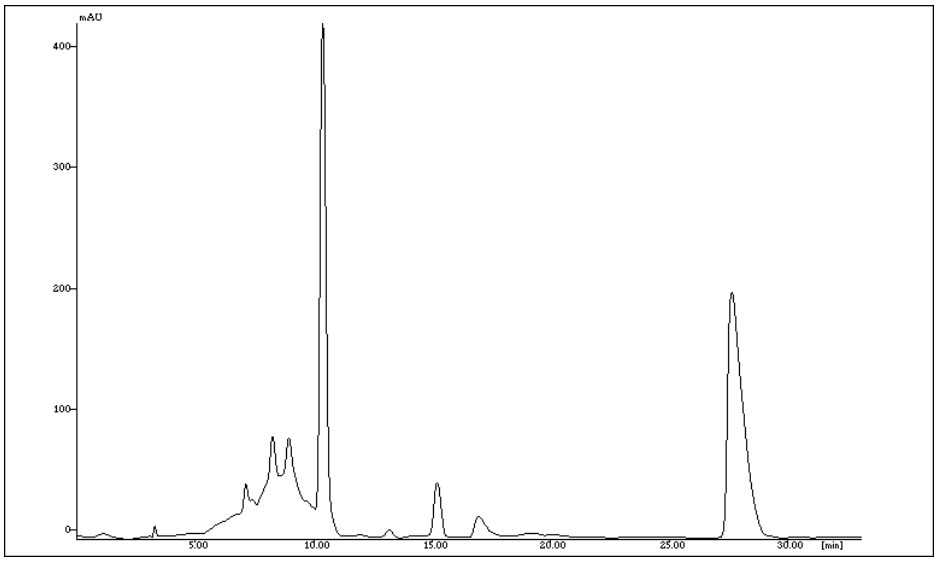

Supporting figure 15. HPLC chromatogram 13

Table 4, entry 2

Peak [a]	Time (min)	Area (mAU·s)	Area (%)
1	15.175	732.75	8%
2	27.600	8263.25	92%

[a] Lux® 5µm Cellulose-1 Chiral HPLC Column, 250 x 4.6 mm was used.

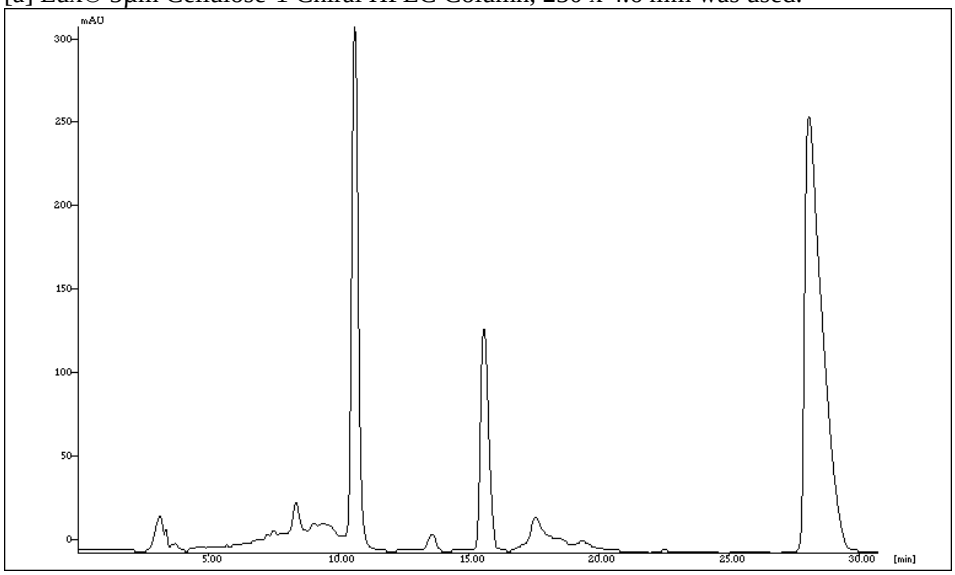

Supporting figure 16. HPLC chromatogram 14

Table 2, entry 2

Peak [a]	Time (min)	Area (mAU·s)	Area (%)
1	15.558	2505.25	18%
2	28.050	11322.04	82%

[a] Lux® 5µm Cellulose-1 Chiral HPLC Column, 250 x 4.6 mm was used.

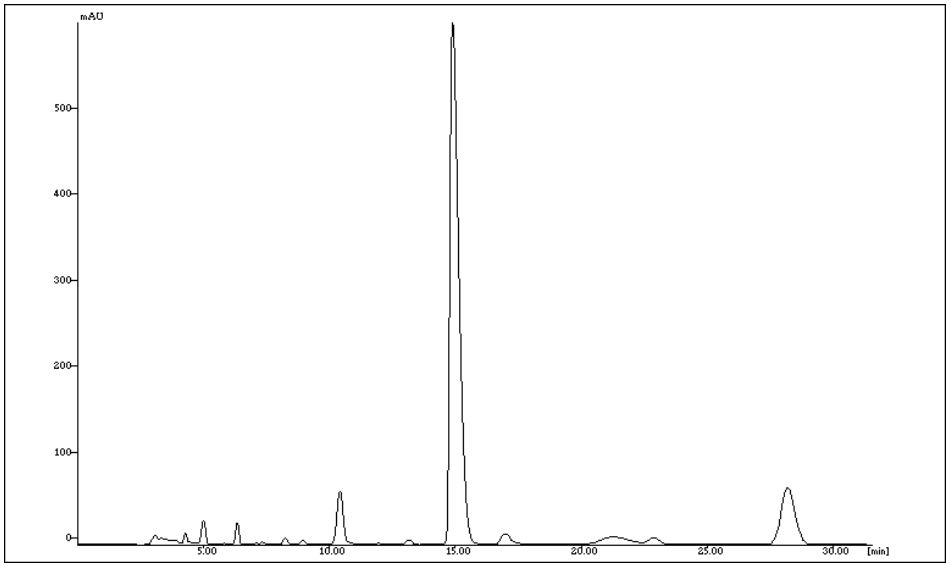

Supporting figure 17. HPLC chromatogram 15

Table 3, entry 6

Peak	Time (min)	Area (mAU·s)	Area (%)
1	14.867	13137.50	85%
2	28.158	2269.50	15%

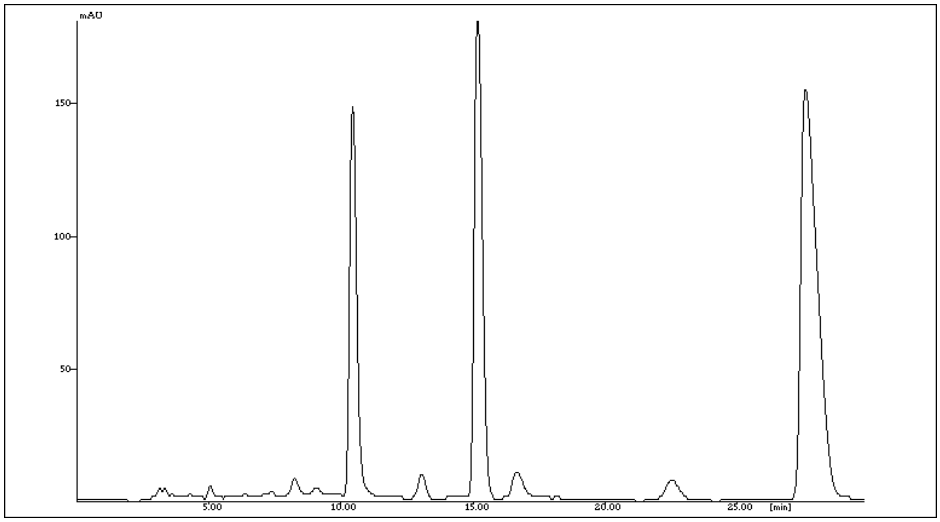

Supporting figure 18. HPLC chromatogram 16

Table 3, entry 7

Peak	Time (min)	Area (mAU·s)	Area (%)
1	15.150	3376.68	35%
2	27.550	6244.00	65%

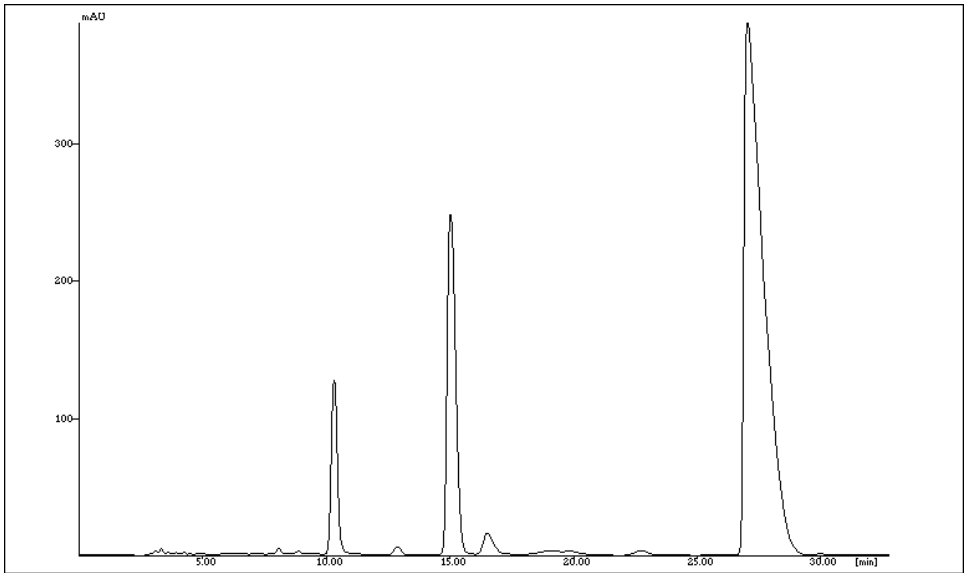

Supporting figure 19. HPLC chromatogram 17

Table 3, entry 8

Peak	Time (min)	Area (mAU·s)	Area (%)
1	14.992	5064.68	20%
2	27.000	20087.00	80%

References

(1) Pan, S. C.; List, B. *Chem Asian J* **2008**, *3*, 430.
(2) Zuend, S. J.; Coughlin, M. P.; Lalonde, M. P.; Jacobsen, E. N. *Nature* **2009**, *461*, 968.
(3) Karimi, B.; Maleki, A. *Chem. Commun. (Camb)* **2009**, 5180.
(4) Hatano, M.; Hattori, Y.; Furuya, Y.; Ishihara, K. *Org. Lett.* **2009**, *11*, 2321.
(5) Seayad, A. M.; Ramalingam, B.; Yoshinaga, K.; Nagata, T.; Chai, C. L. *Org. Lett.* **2010**, *12*, 264.
(6) Kaur, P.; Pindi, S.; Wever, W.; Rajale, T.; Li, G. *J. Org. Chem.* **2010**, *75*, 5144.
(7) Huang, J.; Liu, X.; Wen, Y.; Qin, B.; Feng, X. *J. Org. Chem.* **2007**, *72*, 204.
(8) Zhang, G. W.; Zheng, D. H.; Nie, J.; Wang, T.; Ma, J. A. *Org Biomol Chem* **2010**, *8*, 1399.
(9) Sigman, M. S.; Vachal, P.; Jacobsen, E. N. *Angew. Chem. Int. Ed. Engl.* **2000**, *39*, 1279.
(10) Shao, Y. D.; Tian, S. K. *Chem. Commun. (Camb)* **2012**, *48*, 4899.
(11) Wiles, C.; Watts, P. *Eur. J. Org. Chem.* **2008**, *2008*, 5597.
(12) Ushakov, D. B.; Gilmore, K.; Kopetzki, D.; McQuade, D. T.; Seeberger, P. H. *Angew. Chem. Int. Ed. Engl.* **2014**, *53*, 557.
(13) Seayad, A. M.; Ramalingam, B.; Chai, C. L.; Li, C.; Garland, M. V.; Yoshinaga, K. *Chemistry* **2012**, *18*, 5693.
(14) Neimann, K.; Neumann, R. *Org Lett.* **2000**, 2, 18, 2861-2863.
(15) Bhattacharya, T.; Ghosh, A.; Maiti, D. *Chem. Sci.* **2021**, 12, 3857.
(16) Carlone, A.; Bernardi, L.; McCormack, P.; Warr, T.; Oruganti, S.; Cobley, C. J. *Org. Process Res. De.v* **2021**, *25*, 2795.
(17) Saeed, A.; Larik, F. A.; Jabeen, F.; Mehfooz, H.; Ghumro, S. A.; El-Seedi, H. R.; Ali, M.; Channar, P. A.; Ashraf, H. *Russ J. Gen. Chem+* **2018**, *88*, 541.
(18) Vakulya, B.; Varga, S.; Csampai, A.; Soos, T. *Org. Lett.* **2005**, *7*, 1967.
(19) Yang, W.; Du, D. M. *Org Lett* **2010**, *12*, 5450.
(20) Badiola, E.; Fiser, B.; Gomez-Bengoa, E.; Mielgo, A.; Olaizola, I.; Urruzuno, I.; Garcia, J. M.; Odriozola, J. M.; Razkin, J.; Oiarbide, M.; Palomo, C. *J. Am. Chem. Soc.* **2014**, *136*, 17869.

Chapter 6

Indolenine-based MBL inhibitors

6.1 New MBL inhibitors in batch and continuous flow: synthesis of broad-spectrum compounds

As mentioned in the previous paragraphs, both Captopril isomers (**1** and **2**) displayed activity in the micromolar range towards various MBL isoforms. Our rational design starts from the need to synthetize molecules that are able to establish as high as possible number of interactions in the active site of MBL. Our work was then focused on the synthesis of derivatives inspired by captopril in order to improve the inhibitory activity against MBL, decreasing off-target interaction and whenever possible employing sustainable continuous flow methodologies. The rational design of our compounds started from the NDM-1 isoform, since the activity of both isomers of captopril is well described on this MBL Our aim, in particular, in addition to maintaining the thiol portion essential for interaction with the zinc atoms, was to maximize other interactions in the enzymatic pocket, in particular hydrogen bonds and hydrophobic interactions. Figure 1 shows the binding of NMD-1 with L-Captopril (PDB 4EXS).

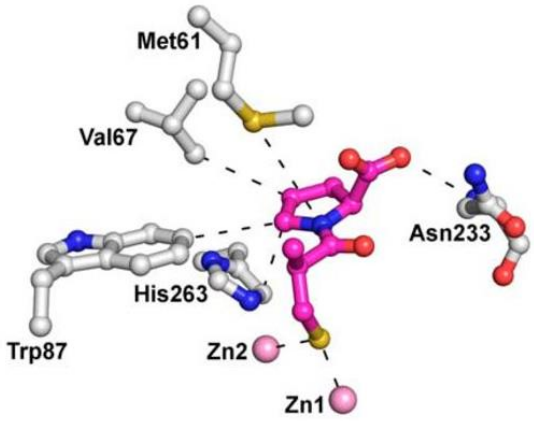

Figure 1. X-ray structure of L-captopril in complex with NDM-1. Zinc ions are represented by pink spheres, L-captopril is in magenta and the residues interacting with captopril are represented as gray sticks. Hydrogen bonds, zinc coordination bonds, and hydrophobic interactions are shown as thin black dashes.[1]

The rational design of our compounds started from the evidence of the activity of both isomers of captopril. The general scheme of the rational design of the new NDM-1 inhibitors and general structures 1 and 2 are shown in Figure 2.

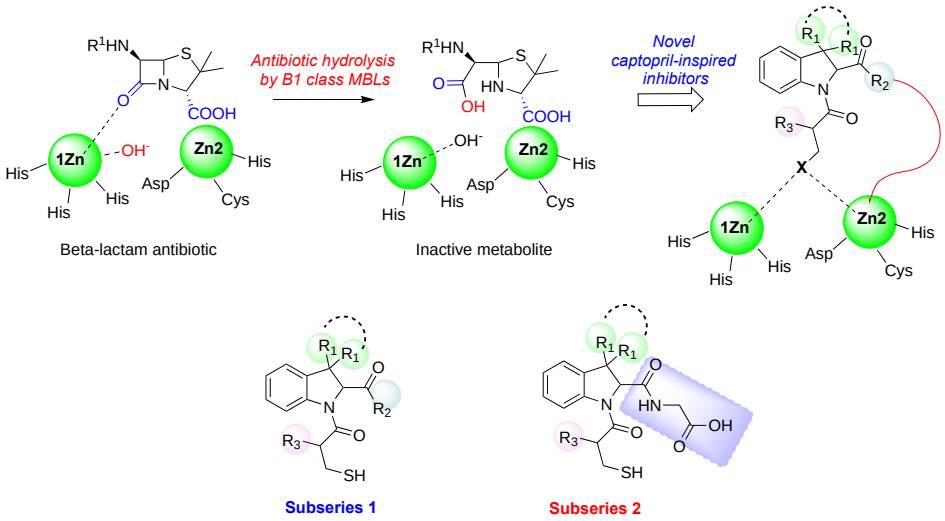

Figure 2. General scheme of the rational design of new NDM-1 inhibitors.

We have developed in our lab two different series of compounds, as showed in Figure 3.

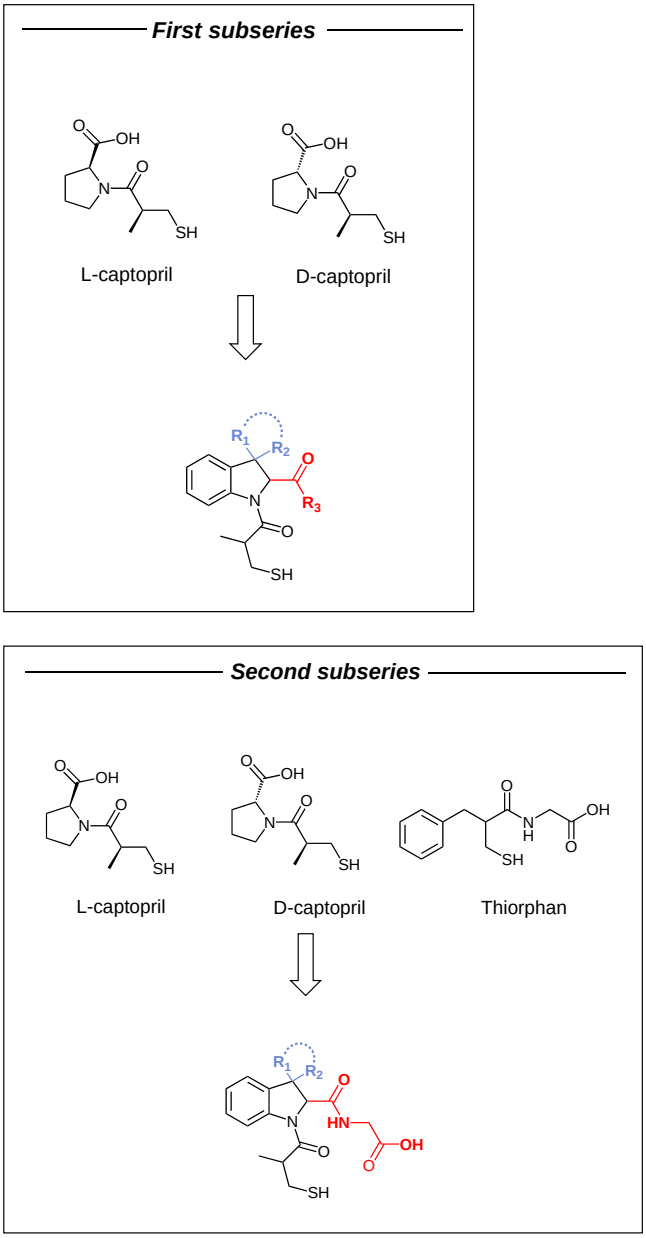

Figure 3. General structures of first and second subseries.

In compounds belonging to subseries 1, we have replaced the pyrrolidine framework of captopril drug with an indolenine moiety, thus potentially increasing the possibility to establish additional π–π or cation-π

interaction within the active site of the enzyme. The insertion of a spirocyclohexyl framework, or two methyl/ethyl groups on 3-position was also performed with the aim of increasing hydrophobic interactions with the active site. The third structural modification, aiming at potentially minimizing interactions with ACE-2 enzyme, like the most of already existent captopril carboxylic derivatives, was performed on 2-position of the indoline system, by replacing the carboxylic acid with a carboxamide moiety.

In subseries 2, our design followed a merging approach between captopril and thiorphan structures; accordingly, the glycyl amide moiety of thiorphan was inserted in 2-postion of the indoline ring.

Scheme **1** shows the synthesis of the final compounds **8a-f**.

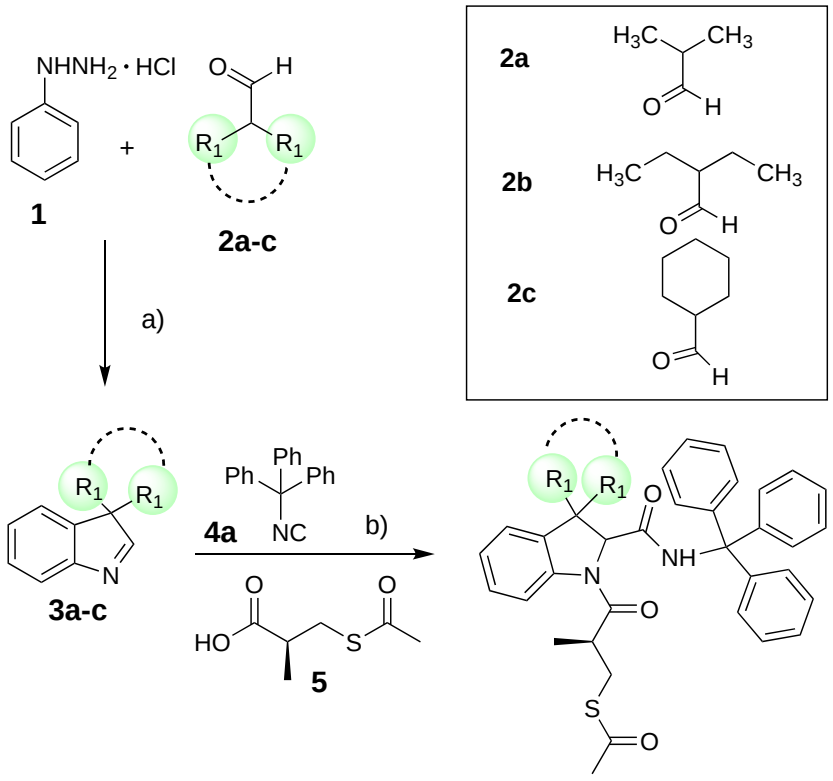
NHNH2 · HCl
1
2a-c
2a
2b
2c
a)
3a-c
4a
b)
5
(S,R*)-6a, (S,S*)-6a
(S,R*)-6b, (S,S*)-6b
(S,R*)-6c, (S,S*)-6c
c)
d)
8a-f
(S,R*)-7a, (S,S*)-7a
(S,R*)-7b, (S,S*)-7b
(S,R*)-7c, (S,S*)-7c

Scheme 1. Synthesis of compounds **8a-f**

The key intermediates **6a-c** were synthetized through a Joulliè Ugi multicomponent reaction starting from indolenine **3a-c**, prepared as described above, in the presence of trityl isocyanide **4a**, and of (*S*)-3-(acetylthio)-2-methylpropanoic acid **5** (a fragment present in the side chain of captopril), in DCM at 50 °C. After 12 h, the compounds **6a-c** were obtained in form of diasteroisomeric mixtures in approximately 1:1 *dr* (as determined by HPLC and NMR analysis). After separation of diastereomeric mixture through HPLC, the reaction with trifluoroacetic acid in dichloromethane at room temperature allowed the deprotection of trityl group on primary amides **7a-c**. Last reaction step involved the hydrolysis of thioester with 2 N sodium hydroxide in tetrahydrofuran, furnishing final compounds **8a-f**.

Scheme 2 shows the synthesis of compounds belonging to subseries 2.

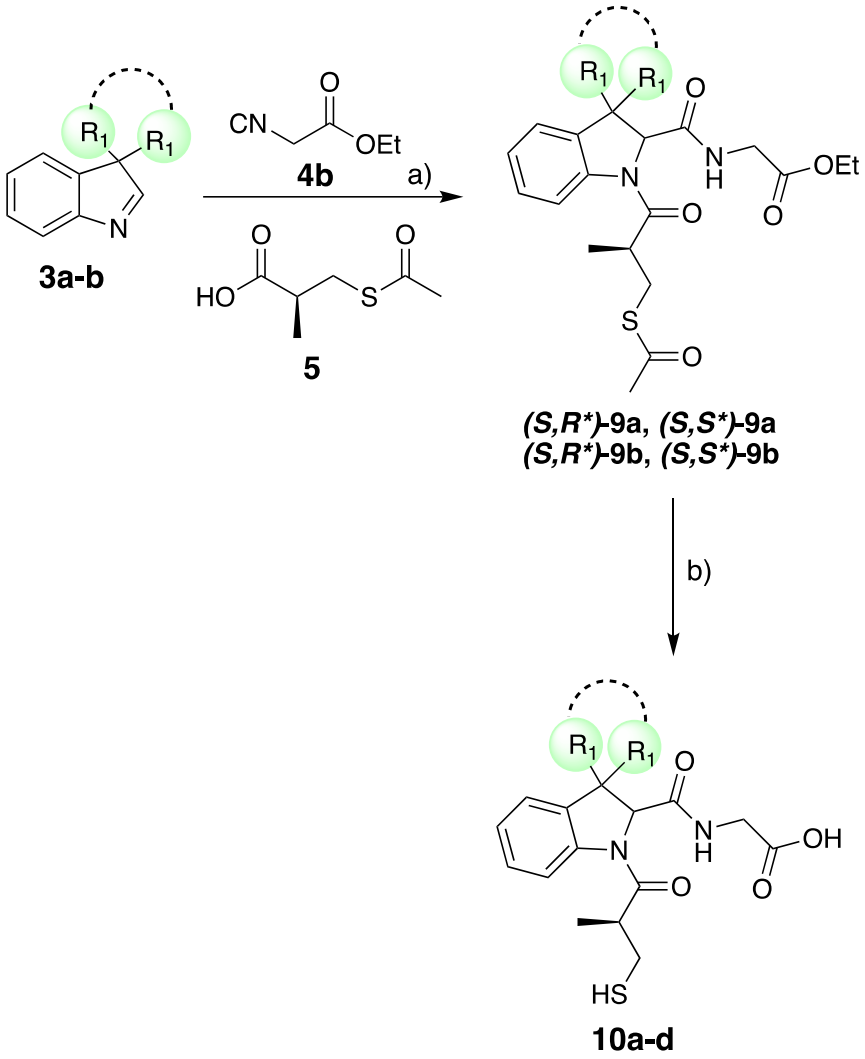

Scheme 2. Synthesis of compounds **10a-d**

In this series of compounds, the Joullié-Ugi multicomponent step was performed in the presence of the commercially available ethyl isocyanoacetate **4b**, indolenine **3a-b** and again acid **5**. After the separation of diastereomeric mixture by reverse phase HPLC, alkaline hydrolysis of the ethyl ester and thioester functionalities provided products **10a-d** in high yields and no detectable epimerization events.

Furthermore, having already developed a procedure in telescoped mode for synthetizing the multicomponent products, we applied the method to the other key intermediates, achieving comparable yields over two steps with respect to the batch synthesis (see supporting material), but avoiding, in this case, the isolation of spiroindolenine intermediates and saving 95% of batch time (**6a-c and 9a-b**) (Figure 15).

A)

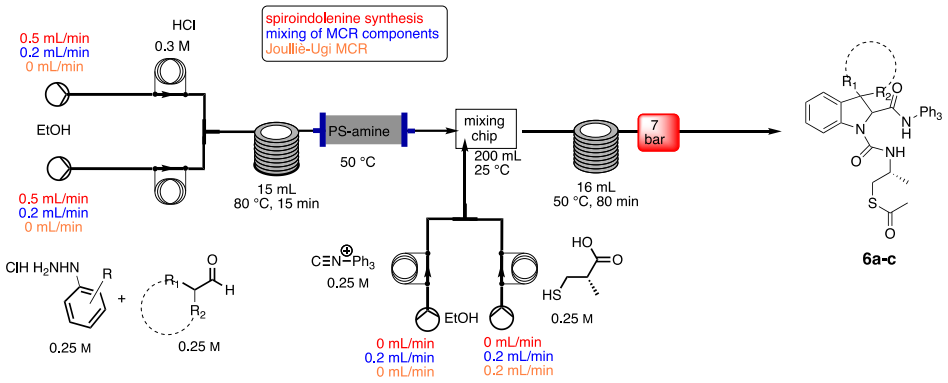

B)

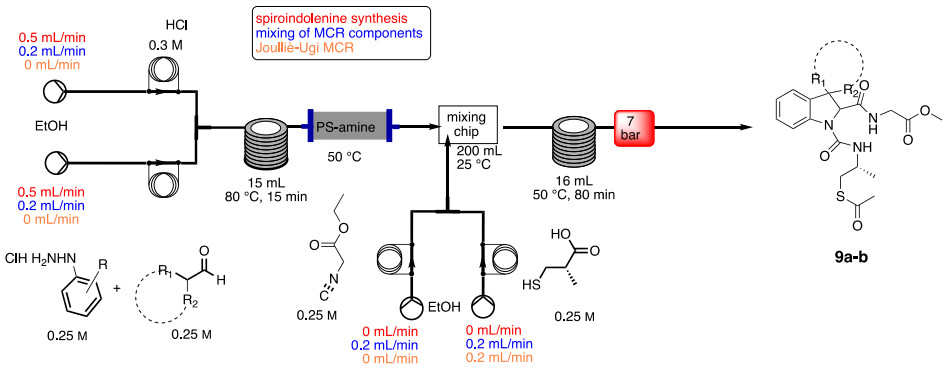

Figure 15. Telescoped approach for key intermediates A) **6a-c** B) **9a-b**.

In collaboration with Eugen Proschak and Thomas Wichelhaus, at the Goethe University of Frankfurt, our compounds have been tested to evaluate the activity firstly on NDM-1. The best inhibitors on NDM-1,

were tested also on other two clinically relevant MBL isoforms, namely VIM-1 and IMP-7.

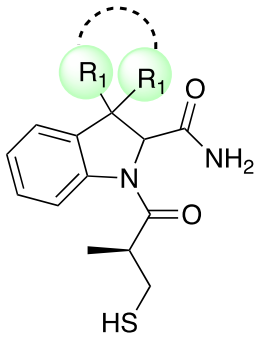

8a-f

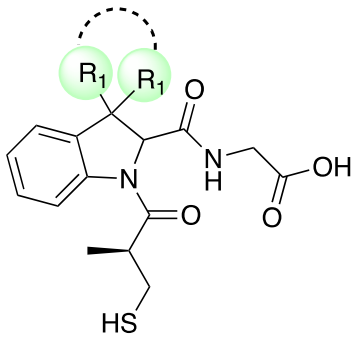

10a-d

Cmpd	**Structure**	IC_{50} NDM-1 (μM)	IC_{50} VIM-1 (μM)	IC_{50} IMP-7 (μM)
8a	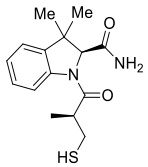	17.9	-	-
8b	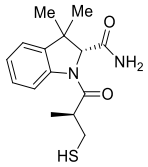	4.08	0.7	1.79
8c	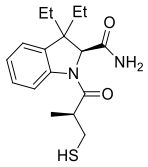	8.41	-	-

8d	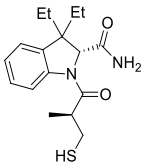	3.46	0.4	3.29
8e	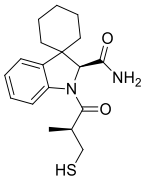	7.42	-	-
8f	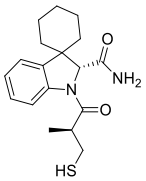	4.78	-	-
10a	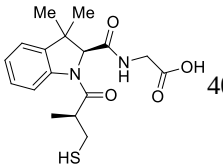	40	-	-
10b	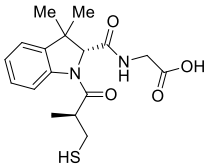	8	7.36	8.62
10c	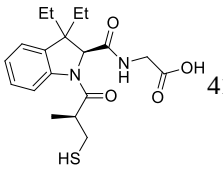	41	-	-
10d	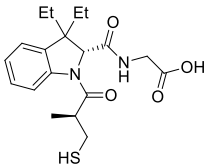	10	-	-

(S,S)*-**7a**	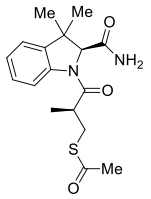	N.A.	-	-
(S,R)*-**7b**	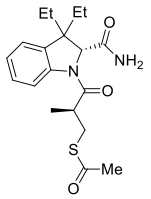	N.A.	-	-
(S,S)*-**7c**	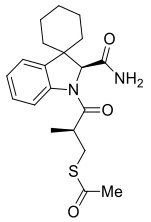	N.A.	-	-

Table 3. Biological activity on NDM-1, VIM-1 and IMP-7.

IC_{50} values were determined in a kinetic fluorescence-based in vitro assay as described previously.[2] All compounds were preincubated with the protein for 30 min before addition of the substrate.[3]

Most of our compounds showed improved inhibition profile on NDM-1 with respect to L-captopril and D-captopril. Compounds **8b** and **8d** have demonstrated a broad-spectrum inhibition profile, with sub micromolar activity on VIM-1. As expected, compounds *(S,S*)*-**7a**, *(S,R*)*-**7b** and *(S,S*)*-**7c** containing the capping acetyl moiety on the thiol group were inactive, confirming the importance of the free thiol moiety for interaction within NDM-1 active site.

Stereochemistry at 2 positions moderately influenced moderately the activity of the first set of newly conceived compounds, with a general

preference for R stereochemistry at the 2-position, in line with the trend observed for L- and D- captopril isomers.

Future structural optimization, beyond improving *in vitro* activity, will aim at maintaining the broad-spectrum profile.
Studies of co-crystallization of inhibitors with NDM-1 and VIM-1 isoforms and cellular studies in synergy with beta-lactam antibiotics are currently ongoing.

6.2 Experimental part

General comments

Unless otherwise specified, materials were purchased from commercial suppliers and used without further purification. TLC analysis was conducted using aluminum foil supported thin-layer silica gel chromatography plates (F254 indicator). Column chromatography was performed using 230–400 mesh, 60 Å pore diameter silica gel. For ^{1}H NMR and ^{13}C NMR measurements an accurately weighed amount of analyte (about 5.0 - 10.0 mg) was dissolved in 600 µL of dimethyl sulfoxide (DMSO-d_6). The mixture was transferred into a 5 mm NMR tube and the spectra were acquired on a Bruker Advance 400 MHz spectrometer by using the residual signal of the deuterated solvent as internal standard. Splitting patterns are described as singlet (s), doublet (d), triplet (t), quartet (q) and broad (br); the values of chemical shifts (δ) are given in ppm and coupling constants (*J*) in Hertz (Hz). NMR data were processed with MestreNova (Version 8.1.1, Mestrelab Research). ESI-MS spectra analysis was carried out on a mass spectrometer LTQ-XL. HPLC was performed with a Waters Model 510 pump equipped with Waters Rheodyne injector and a differential refractometer, model 401. Luna 5µm PFP (2) 100A HPLC Column 250 x 10 mm was employed.

Continuous flow synthesis of indolenine 3a-c

Chemical transformations in flow were realized using a self-made flow reactor: two Waters P510 HPLC pumps were connected each to a Rheodyne 9010 injection valves, each equipped with a 1 mL sample loop (SL) made from PTFE tubing and an injection port for disposable syringes. The injection valves were further connected *via* a T-piece to a coiled PTFE tubing of 15 mL volume. The coil was immersed in a silicone oil bath for controlling reaction temperatures. The tubular reactor finished into a back

pressure regulator (BPR), which was either spring mechanism-based (6.7 bar) or simply a PEEK capillary of defined length (1.7 bar). Product containing exiting streams were collected directly in a flask. An aliquot of the collected phase was used for analysis by GC-MS. Reagents were prepared for loading into the sample loops according to one of the following this method: 0.25 mmol aldehyde + 0.25 mmol $PhNHNH_2$•HCl in 1 mL of EtOH, heated to 50 ºC for 5 min prior to loading into the SL; SL B: (equiv.-1) HCl in 1 mL of EtOH.

3,3-Dimethyl-3*H*-indole **39a**, 3,3-Diethyl-3*H*-indole **39b** Spiro[cyclohexane-1,3'-indole **39c** were synthetized in according to previous reported procedure.[4]

Synthesis of multicomponent key intermediate in batch (General procedure A)

Following the reported procedure in literature [4], indolenine **3a-c** (3 mmol) were dissolved in DCM (0.3 M) followed by the addition of the corresponding amino acid (1.0 eq) and isocyanide (1.0 eq). The reaction mixture was stirred for 24-30 h at 50 °C. Then, DCM was evaporated under vacuum to achieve the crude residue that was subjected to column chromatography (SiO_2, corresponding eluent) and to HPLC to afford a diastereomeric mixture.

Synthesis of multicomponent products in flow (General procedure B)

Chemical transformations in flow were realized using a self-made flow reactor: Waters P510 HPLC pump were connected to a Rheodyne 9010 injection valve, equipped with a 1 mL sample loop made from PTFE tubing and an injection port for disposable syringes. The injection valve was further connected to a coiled PTFE tubing of 15 mL volume. The coil

was immersed in a silicone oil bath for controlling reaction temperatures. The tubular reactor finished into a mechanical back pressure regulator (BPR) of approx. 7 bar. Product containing exiting streams were collected directly in a flask.

A solution of indolenine **3a-c** (0.25 mmol), the suitable amino acid (1 equiv.) and isocyanide (1 equiv.) was prepared in EtOH (1 mL total solution volume). The flow reactor was heated to 80 °C. EtOH was used as solvent at a total flow rate of 0.2 mL/min to move the reaction mixture through the coil reactor for a residence time of 75 min.

Synthesis of acetylated products in batch (General procedure C)

The multicomponent intermediate key was dissolved in DCM/TFA 1:1 and the reaction was stirred overnight at room temperature. The mixture was washed with $NaHCO_3$ and extracted with DCM. The solvent was evaporated under vacuum and the reaction was purified by chromatography on silica gel.

Synthesis of final products in batch (General procedure D)

Then the intermediate was dissolved in THF/NaOH (1:3, 0.5 mL/1.5 mL) and the reaction was stirred for 2 hours at room temperature. The mixture was quenched with HCl 2N and extracted with ethyl acetate. Then, solvent was evaporated under vacuum and the reaction was purified by chromatography on silica gel to afford the final products.

6a

According to general procedure A, a mixture of 3,3-Dimethyl-3*H*-indole **3a**, (351 mg, 2.42 mmol), 3-(acetylthio)-2-methylpropanoic acid **5** (242 µL, 2.66 mmol) and tritylisocyanide **4a** (716 mg, 2.66 mmol) was dissolved in DCM (5 mL) in a sealed tube at 50 °C for 30 hours. The crude product was purified by chromatography on silica gel with hexane/ EtOAc (85:15) to yield the diastereomeric mixture. The racemic products were subjected to HPLC with MeOH/H_2O (85:15) as the eluent (flow rate 3.00 mL/min) for obtain pure diastereomers. Total yield: 26% (*dr* 1:1).

(S,S)*-**6a**

Yellowish solid; Rf = 0.38 (H/E 7:3)

^{1}H NMR (700 MHz, DMSO-d_6) δ 9.27 (s, 1H), 7.90 (d, *J* = 8.0 Hz, 1H), 7.30 – 7.26 (m, 15H), 6.97 (m, 3H), 4.98 (s, 1H), 3.15 (dt, *J* = 13.6, 6.3 Hz, 2H), 2.89 (h, *J* = 6.8 Hz, 1H), 2.29 (s, 5H), 1.29 (d, *J* = 6.9 Hz, 4H), 1.24 (s, 4H), 1.16 (s, 3H).

^{13}C NMR (176 MHz, DMSO-d_6) δ 195.85, 168.50, 144.64, 129.16, 128.85, 128.00, 127.74, 126.97, 126.72, 71.24, 44.92, 31.58, 31.10, 29.49, 29.17, 20.41, 18.25.

tR HPLC: 12.57 min

(S,R)*-**6a**

Yellowish solid; Rf = 0.38 (H/E 7:3)

^{1}H NMR (700 MHz, DMSO-d_6) δ 9.18 (s, 1H), 7.94 (d, *J* = 8.0 Hz, 1H), 7.28 (m, 10H), 7.22 – 7.15 (m, 3H), 7.14 – 7.06 (m, 2H), 7.05 (d, *J* = 7.3 Hz, 1H), 6.99 – 6.92 (m, 2H), 4.98 (s, 1H), 3.09 (dd, *J* = 13.4, 6.2 Hz, 1H), 3.02 (dd, *J* = 13.3, 7.5 Hz, 1H), 2.81 – 2.75 (m, 2H), 2.39 (s, 2H), 1.27 (s, 3H), 1.24 (s, 3H), 1.00 (d, *J* = 3.9 Hz, 3H).

^{13}C NMR (176 MHz, DMSO-d_6) δ 195.55, 172.86, 168.70, 144.73, 142.26, 140.88, 128.84, 128.04, 127.46, 126.97, 124.10, 121.93, 116.75, 72.39, 70.37, 45.12, 38.42, 33.22, 31.96, 31.14, 29.49, 21.51, 17.69.
tR HPLC: 11.49 min

(S,S)-**7a***

According to procedure C, ***(S,S*)*-6a** (90 mg, 0.15 mmol) was dissolved in DCM/TFA 1:1 (4.5 mL/4.5 mL) and the reaction was stirred overnight at room temperature. The mixture was washed with $NaHCO_3$ and extracted with DCM. Then, solvent was evaporated under vacuum and the reaction was purified by chromatography on silica gel with hexane/ EtOAc (1:1) to yield product as yellowish solid. Yield: 54% (27 mg). Rf = 0.17 (H/E 1:1)
^{1}H NMR (700 MHz, DMSO-d_6) δ 8.08 (d, *J* = 8.0 Hz, 1H), 7.78 (s, 1H), 7.38 (s, 1H), 7.19 (d, *J* = 7.4 Hz, 2H), 7.16 (t, *J* = 7.7 Hz, 1H), 7.02 (t, *J* = 7.4 Hz, 1H), 4.58 (s, 1H), 3.04 (dd, *J* = 13.2, 5.8 Hz, 1H), 2.99 (dd, *J* = 13.2, 8.6 Hz, 1H), 2.75 (dq, *J* = 12.7, 6.2 Hz, 1H), 2.33 (s, 3H), 1.32 (d, *J* = 18.2 Hz, 6H), 1.08 (d, *J* = 6.6 Hz, 3H).
^{13}C NMR (176 MHz, DMSO) δ 195.00, 173.05, 170.37, 141.86, 140.08, 127.25, 123.71, 121.85, 116.26, 72.57, 43.16, 38.25, 32.69, 31.92, 30.55, 22.23, 17.13.

8a

According to procedure D, *(S,S*)*-**7a** (20 mg, 0.06 mmol) was dissolved in THF/NaOH (1:3, 0.5 mL/1.5 mL) and the reaction was stirred for 2 hours at room temperature. The mixture was quenched with HCl 2N and extracted with ethyl acetate. Then, solvent was evaporated under vacuum and the reaction was purified by chromatography on silica gel with hexane/

EtOAc 4:6 to yield the product as yellowish solid. Yield: 57% (10 mg). Rf = 0.37 (DCM/MeOH 95:5).

^{1}H NMR (700 MHz, DMSO-d_6) δ 8.11 (d, J = 8.0 Hz, 1H), 7.77 (s, 1H), 7.41 (s, 1H), 7.20 (d, J = 7.3 Hz, 1H), 7.17 (t, J = 7.4 Hz, 1H), 7.02 (t, J = 7.4 Hz, 1H), 4.81 (s, 1H), 2.73 (dt, J = 12.7, 7.5 Hz, 2H), 2.62 – 2.58 (m, 1H), 2.37 (t, J = 8.0 Hz, 1H), 1.34 (d, J = 22.8 Hz, 6H), 1.07 (d, J = 6.1 Hz, 3H).

^{13}C NMR (176 MHz, DMSO-d_6) δ 173.92, 142.44, 140.61, 124.04, 122.27, 116.71, 72.90, 43.62, 42.60, 32.48, 28.62, 22.78, 17.71.

MS (ESI) m/z calc. $[M+H]^+$ $C_{15}H_{21}N_2O_2S_+$: 293.4; found: 293.19.

(S,R)*-**7a**

According to procedure C, *(S,R*)*-**6a** (65 mg, 0.11 mmol) was dissolved in DCM/TFA 1:1 (4 mL/4 mL) and the reaction was stirred overnight at room temperature. The mixture was washed with $NaHCO_3$ and extracted with DCM. Then, solvent was evaporated under vacuum and the reaction was purified by chromatography on silica gel with hexane/ EtOAc (6:4) to yield product as yellowish solid. Yield:80% (29 mg). Rf = 0.18 (H/E 4:6).

^{1}H NMR (700 MHz, DMSO-d_6) δ 8.05 (d, J = 8.0 Hz, 1H), 7.69 (s, 1H), 7.29 (s, 1H), 7.19 – 7.14 (m, 2H), 7.01 (d, J = 7.3 Hz, 1H), 4.51 (s, 1H), 3.02 (dd, J = 13.2, 5.6 Hz, 1H), 2.96 (dd, J = 13.2, 8.3 Hz, 1H), 2.67 (dq, J = 13.7, 6.8 Hz, 1H), 2.30 (s, 3H), 1.33 (s, 3H), 1.28 (s, 3H), 1.20 (d, J = 6.9 Hz, 3H).

^{13}C NMR (176 MHz, DMSO-d_6) δ 195.60, 173.38, 170.59, 142.45, 140.38, 127.66, 124.12, 122.23, 116.58, 72.29, 43.64, 39.09, 32.30, 31.68, 30.95, 22.46, 18.21.

8b

According to procedure D, *(S,R*)*-**7a** (29 mg, 0.09 mmol) was dissolved in THF/NaOH (1:3, 0.5 mL/1.5 mL) and the reaction was stirred for 2 hours at room temperature. The mixture was quenched with HCl 2N and extracted with ethyl acetate. Then, solvent was evaporated under vacuum and the reaction was purified by chromatography on silica gel with hexane/ EtOAc 4:6 to yield the product as yellowish solid. Yield: 33% (8.6 mg). Rf = 0.23 (H/E 2:8).

^{1}H NMR (700 MHz, DMSO-d_6) δ 8.07 (d, *J* = 8.0 Hz, 1H), 7.77 (s, 1H), 7.41 (s, 1H), 7.18 (d, *J* = 7.3 Hz, 1H), 7.17 – 7.14 (m, 1H), 7.03 – 7.00 (m, 1H), 4.57 (s, 1H), 2.76 (dt, *J* = 13.6, 7.0 Hz, 2H), 2.61 – 2.58 (m, 1H), 2.16 – 2.12 (m, 1H), 1.32 (d, *J* = 37.0 Hz, 6H), 1.20 (d, *J* = 6.7 Hz, 3H).

^{13}C NMR (176 MHz, DMSO-d_6) δ 173.23, 170.50, 142.01, 139.89, 127.17, 123.57, 116.13, 71.96, 43.16, 42.25, 31.87, 30.69, 26.85, 22.12, 17.10.

MS (ESI) m/z calc. $[M+H]^+$ $C_{15}H_{21}N_2O_2S_+$: 293.4; found: 293.19.

6b

According to general procedure A, a mixture of 3,3-Diethyl-3*H*-indole **3b**, (100 mg, 0.69 mmol), 3-(acetylthio)-2-methylpropanoic acid **5** (70 µ, 0.76 mmol) and tritylisocyanide **4a** (205 mg, 0.76 mmol) was dissolved in DCM (5 mL) in a sealed tube at 50 °C for 30 hours. The crude product was purified by chromatography on silica gel with hexane/ EtOAc (85:15) to yield the diastereomeric mixture. The racemic products were subjected to HPLC with MeOH/H_2O (85:15) as the eluent (flow rate 3.00 mL/min) for obtain pure diastereomers. Total yield: 47% (*dr* 1:1).

(S,S)*-**6b**

Orange solid; Rf = 0.4 (H/E 7:3)

^{1}H NMR (700 MHz, DMSO-d_6) δ 9.01 (s, 1H), 7.93 – 7.88 (m, 1H), 7.24 (m, 16H), 6.98 – 6.91 (m, 3H), 5.07 (d, *J* = 8.3 Hz, 1H), 3.18 (dd, *J* = 9.4, 5.2 Hz, 2H), 3.09 (d, *J* = 7.0 Hz, 1H), 2.20 (dd, *J* = 31.3, 9.1 Hz, 4H), 1.34 – 1.22 (m, 6H), 0.74 (dd, *J* = 33.6, 7.4 Hz, 3H).

^{13}C NMR (176 MHz, DMSO-d_6) δ 195.66, 144.83, 144.52, 129.14, 128.79, 127.99, 127.75, 126.97, 126.83, 123.47, 117.20, 70.13, 51.88, 31.51, 31.02, 29.82, 21.78, 18.54, 17.82, 10.03, 7.68.

tR HPLC: 20.83 min

(S,R)*-**6b**

Orange solid; Rf = 0.4 (H/E 7:3)

^{1}H NMR (700 MHz, DMSO-d_6) δ 8.93 (s, 1H), 7.92 (d, *J* = 7.9 Hz, 1H), 7.32 – 7.25 (m, 8H), 7.22 (m, 7H), 7.12 – 7.09 (t, 1H), 7.06 (d, *J* = 7.2 Hz, 1H), 6.97 – 6.93 (t, 1H), 5.19 (s, 1H), 3.06 (d, *J* = 6.5 Hz, 2H), 2.94 (dq, *J* = 13.9, 7.5, 6.7 Hz, 1H), 2.33 (s, 3H), 1.74 (tt, *J* = 14.1, 7.1 Hz, 2H), 1.56 – 1.49 (m, 2H), 0.93 (dd, *J* = 16.9, 9.6 Hz, 4H), 0.67 (t, *J* = 7.2 Hz, 3H).

^{13}C NMR (176 MHz, DMSO-d_6) δ 199.59 172.43, 168.52, 144.64, 129.15, 128.79, 128.10, 127.80, 127.09, 123.62, 123.55, 117.16, 71.42, 70.42, 52.16, 32.94, 31.03, 30.69, 23.45, 17.14, 10.22, 8.08.

tR HPLC: 17.86 min

(S,S)*-**7b**

According to procedure C, *(S,S*)*-**6b** (100 mg, 0.18 mmol) was dissolved in DCM/TFA 1:1 (4 mL/4 mL) and the reaction was stirred overnight at room temperature. The mixture was washed with $NaHCO_3$ and extracted with DCM. Then, solvent was evaporated under vacuum and the reaction

was purified by chromatography on silica gel with hexane/ EtOAc (6:4) to yield product as yellowish solid. Yield:86% (56 mg). Rf = 0.28 (H/E 6:4).
^{1}H NMR (700 MHz, DMSO-d_6) δ 8.10 (d, *J* = 7.9 Hz, 1H), 7.79 (s, 1H), 7.43 (s, 1H), 7.16 (t, *J* = 7.6 Hz, 1H), 7.12 (d, *J* = 7.3 Hz, 1H), 7.02 (t, *J* = 7.3 Hz, 1H), 4.64 (s, 1H), 3.01 (d, *J* = 7.0 Hz, 2H), 2.81 (q, *J* = 6.6 Hz, 1H), 2.31 (s, 3H), 1.93 (dq, *J* = 14.4, 6.9 Hz, 1H), 1.71 (dt, *J* = 14.6, 7.0 Hz, 1H), 1.62 (ddt, *J* = 20.5, 13.7, 6.8 Hz, 2H), 1.09 (d, *J* = 6.3 Hz, 3H), 0.92 (t, *J* = 7.3 Hz, 3H), 0.68 (t, *J* = 7.1 Hz, 3H).
^{13}C NMR (176 MHz, DMSO-d_6) δ 194.87, 172.93, 170.65, 143.02, 136.95, 127.17, 123.32, 123.21, 116.33, 70.41, 50.63, 38.38, 33.20, 32.58, 30.52, 25.36, 17.32, 9.29, 7.85.

8c

According to procedure D, *(S,S*)*-**7b** (48 mg, 0.13 mmol) was dissolved in THF/NaOH (1:3, 0.5 mL/1.5 mL) and the reaction was stirred for 2 hours at room temperature. The mixture was quenched with HCl 2N and extracted with ethyl acetate. Then, solvent was evaporated under vacuum and the reaction was purified by chromatography on silica gel with hexane/ EtOAc 1:1 to yield the product as yellowish solid. Yield: 32% (8.6 mg). Rf = 0.41 (H/E 4:6).
^{1}H NMR (700 MHz, DMSO-d_6) δ 8.12 (d, *J* = 8.0 Hz, 1H), 7.77 (s, 1H), 7.47 (s, 1H), 7.16 (t, *J* = 7.7 Hz, 1H), 7.11 (d, *J* = 7.3 Hz, 1H), 7.01 (t, *J* = 7.3 Hz, 1H), 4.82 (s, 1H), 2.83 (dq, *J* = 12.8, 6.4 Hz, 1H), 2.70 (dt, *J* = 12.7, 9.0 Hz, 1H), 2.58 (ddd, *J* = 12.9, 7.5, 4.6 Hz, 1H), 2.32 (t, *J* = 8.3 Hz, 1H), 1.94 (dt, *J* = 14.6, 7.3 Hz, 1H), 1.70 (dq, *J* = 14.7, 7.3 Hz, 1H), 1.64 (q, *J* = 7.2 Hz, 2H), 1.06 (d, *J* = 6.6 Hz, 3H), 0.96 (t, *J* = 7.4 Hz, 3H), 0.68 (t, *J* = 7.3 Hz, 3H).

^{13}C NMR (176 MHz, DMSO-d_6) δ 173.39, 170.84, 143.06, 137.19, 123.32, 123.04, 116.33, 70.64, 50.57, 42.14, 32.78, 30.71, 28.06, 25.09, 17.51, 9.37, 7.93.

MS (ESI) m/z calc. $[M+H]^+$ $C_{17}H_{25}N_2O_2S^+$: 321.45; found: 321.16.

(S,R)*-**7b**

According to procedure C, *(S,R*)*-**6b** (95 mg, 0.17 mmol) was dissolved in DCM/TFA 1:1 (4 mL/4 mL) and the reaction was stirred overnight at room temperature. The mixture was washed with $NaHCO_3$ and extracted with DCM. Then, solvent was evaporated under vacuum and the reaction was purified by chromatography on silica gel with hexane/ EtOAc (6:4) to yield product as yellowish solid. Yield:65% (35 mg). Rf = 0.28 (H/E 6:4).

^{1}H NMR (700 MHz, DMSO-d_6) δ 8.12 (d, *J* = 8.0 Hz, 1H), 7.78 (s, 1H), 7.39 (s, 1H), 7.23 (t, *J* = 7.6 Hz, 1H), 7.17 (d, *J* = 7.3 Hz, 1H), 7.07 (t, *J* = 7.4 Hz, 1H), 4.61 (s, 1H), 3.08 (dd, *J* = 13.1, 5.5 Hz, 1H), 3.02 (dd, *J* = 13.2, 8.4 Hz, 1H), 2.82 (dq, *J* = 13.6, 6.7 Hz, 1H), 2.00 (tt, *J* = 10.8, 5.5 Hz, 1H), 1.76 – 1.67 (m, 2H), 1.59 (dq, *J* = 14.5, 7.3 Hz, 1H), 1.25 (d, *J* = 6.8 Hz, 3H), 1.03 (t, *J* = 7.4 Hz, 3H), 0.71 (t, *J* = 7.3 Hz, 3H).

^{13}C NMR (176 MHz, DMSO-d_6) δ 195.56, 173.18, 170.74, 143.41, 137.65, 128.24, 123.78, 116.73, 70.79, 51.01, 38.99, 32.77, 31.81, 30.97, 24.78, 18.20, 9.79, 8.22.

8d

According to procedure D, *(S,R*)*-**7b** (35 mg, 0.10 mmol) was dissolved in THF/NaOH (1:3, 0.5 mL/1.5 mL) and the reaction was stirred for 2 hours at room temperature. The mixture was quenched with HCl 2N and extracted with ethyl acetate. Then, solvent was evaporated under vacuum and the reaction was purified by chromatography on silica gel with hexane/

EtOAc 1:1 to yield the product as yellow solid. Yield: 21% (9 mg). Rf = 0.41 (H/E 4:6).

^{1}H NMR (700 MHz, DMSO-d_6) δ 8.08 (d, *J* = 8.0 Hz, 1H), 7.79 (s, 1H), 7.45 (s, 1H), 7.16 (t, *J* = 7.5 Hz, 1H), 7.11 (d, *J* = 7.3 Hz, 1H), 7.01 (t, *J* = 7.3 Hz, 1H), 4.60 (s, 1H), 2.75 (dt, *J* = 13.6, 7.2 Hz, 1H), 2.69 (dq, *J* = 12.7, 6.2 Hz, 1H), 2.47 (dd, *J* = 13.2, 7.2 Hz, 1H), 2.12 (t, *J* = 8.1 Hz, 1H), 1.95 (dt, *J* = 14.4, 7.2 Hz, 1H), 1.66 (ddt, *J* = 27.6, 14.0, 7.1 Hz, 3H), 1.56 (dq, *J* = 14.3, 7.3 Hz, 1H), 1.19 (d, *J* = 6.6 Hz, 3H), 0.97 (t, *J* = 7.3 Hz, 3H), 0.65 (t, *J* = 7.2 Hz, 3H).

^{13}C NMR (176 MHz, DMSO-d_6) δ 173.52, 171.17, 127.63, 123.77, 123.53, 116.77, 70.91, 51.04, 42.50, 32.94, 27.50, 25.01, 17.55, 9.81, 8.25.

MS (ESI) m/z calc. $[M+H]^+$ $C_{17}H_{25}N_2O_2S^+$: 321.45; found: 321.16.

The spectra of *(S,R*)*-**6c**, *(S,S*)*-**6c** are reported in our previous paper.[5]

(S,S)*-**7c**

According to procedure C, *(S,S*)*-**6c** (215 mg, 0.34 mmol) was dissolved in DCM/TFA 1:1 (4.5 mL/4.5 mL) and the reaction was stirred overnight at room temperature. The mixture was washed with $NaHCO_3$ and extracted with DCM. Then, solvent was evaporated under vacuum and the reaction was purified by chromatography on silica gel with hexane/ EtOAc (6:4) to yield product as yellow solid. Yield: 78% (95 mg). Rf = 0.19 (H/E 6:4)

^{1}H NMR (700 MHz, DMSO-d_6) δ 8.21 (d, *J* = 7.9 Hz, 1H), 8.06 (s, 1H), 7.59 (s, 1H), 7.38 (d, *J* = 7.4 Hz, 1H), 7.33 (t, *J* = 7.6 Hz, 1H), 7.20 (t, *J* = 7.4 Hz, 1H), 5.01 (s, 1H), 3.28 – 3.23 (m, 1H), 3.20 (q, *J* = 9.4, 8.0 Hz, 2H), 2.50 (s, 3H), 1.84 (m, 8H), 1.56 – 1.46 (m, 2H), 1.29 (d, *J* = 6.0 Hz, 3H).

^{13}C NMR (176 MHz, DMSO-d_6) δ 194.78, 172.73, 170.09, 142.12, 140.86, 127.02, 123.61, 121.96, 116.54, 69.42, 47.40, 37.93, 32.46, 30.51, 29.53, 25.07, 22.69, 21.89, 17.37 (2).

8e

According to procedure D, *(S,S*)*-**7c** (35 mg, 0.10 mmol) was dissolved in THF/NaOH (1:3, 0.5 mL/1.5 mL) and the reaction was stirred for 2 hours at room temperature. The mixture was quenched with HCl 2N and extracted with ethyl acetate. Then, solvent was evaporated under vacuum and the reaction was purified by chromatography on silica gel with hexane/ EtOAc 6:4 to yield the product as yellow solid. Yield: 38% (25 mg). Rf = 0.56 (H/E 4:6).

^{1}H NMR (700 MHz, DMSO-d_6) δ 8.11 (d, *J* = 7.9 Hz, 1H), 7.93 (s, 1H), 7.50 (s, 1H), 7.26 (d, *J* = 7.3 Hz, 1H), 7.20 (t, *J* = 7.7 Hz, 1H), 7.06 (t, *J* = 7.7 Hz, 1H), 5.05 (s, 1H), 3.11 – 3.05 (m, 1H), 2.76 (dt, *J* = 13.0, 9.3 Hz, 1H), 2.67 (ddd, *J* = 12.9, 7.8, 5.0 Hz, 1H), 2.42 (t, *J* = 8.4 Hz, 1H), 1.98 – 1.91 (m, 1H), 1.86 – 1.80 (m, 2H), 1.79 – 1.70 (m, 4H), 1.62 (dt, *J* = 13.1, 3.5 Hz, 2H), 1.41 – 1.34 (m, 1H), 1.14 (d, *J* = 6.6 Hz, 3H).
^{13}C NMR (176 MHz, DMSO-d_6) δ 173.68, 170.78, 142.68, 141.42, 127.43, 122.42, 116.92, 69.82, 47.88, 42.13, 30.11, 28.55, 25.54, 23.30, 22.39, 18.00 (2).
MS (ESI) m/z calc. $[M+H]^+$ $C_{18}H_{25}N_2O_2S^+$: 333.46; found: 333.16

(S,R)*-**7c**

According to procedure C, *(S,R*)*-**6c** (200 mg, 0.325 mmol) was dissolved in DCM/TFA 1:1 (4.5 mL/4.5 mL) and the reaction was stirred overnight at room temperature. The mixture was washed with $NaHCO_3$ and extracted with DCM. Then, solvent was evaporated under vacuum and the reaction

was purified by chromatography on silica gel with hexane/ EtOAc (6:4) to yield product as yellowish solid. Yield: 60% (72 mg). Rf = 0.19 (H/E 6:4)
^{1}H NMR (700 MHz, DMSO-d_6) δ 7.99 (d, *J* = 7.9 Hz, 1H), 7.87 (s, 1H), 7.30 (s, 1H), 7.17 (d, *J* = 7.4 Hz, 1H), 7.13 (t, *J* = 7.7 Hz, 1H), 6.99 (t, *J* = 7.2 Hz, 1H), 4.72 (s, 1H), 3.03 (dd, *J* = 13.2, 5.5 Hz, 1H), 2.98 (dd, *J* = 13.1, 8.6 Hz, 1H), 2.89 (dq, *J* = 13.7, 6.8 Hz, 1H), 2.31 (s, 3H), 1.92 – 1.79 (m, 2H), 1.74 (d, *J* = 12.6 Hz, 2H), 1.70 – 1.61 (m, 4H), 1.55 (t, *J* = 14.2 Hz, 2H), 1.19 (d, *J* = 6.8 Hz, 3H).
^{13}C NMR (176 MHz, DMSO-d_6) δ 195.53, 173.14, 170.19, 142.67, 127.43, 124.00, 122.33, 116.79, 69.05, 47.86, 39.16, 31.72, 30.99, 29.93, 25.60, 23.23, 22.25, 18.64 (2).

8f

According to procedure D, *(S,R*)*-**7c** (72 mg, 0.20 mmol) was dissolved in THF/NaOH (1:3, 1.2 mL/3.5 mL) and the reaction was stirred for 2 hours at room temperature. The mixture was quenched with HCl 2N and extracted with ethyl acetate. Then, solvent was evaporated under vacuum and the reaction was purified by chromatography on silica gel with hexane/ EtOAc 6:4 to yield the product as yellowish solid. Yield: 33% (20 mg). Rf = 0.56 (H/E 4:6).
^{1}H NMR (700 MHz, DMSO-d_6) δ 8.08 (d, *J* = 8.0 Hz, 1H), 8.06 (d, *J* = 8.0 Hz, 1H), 8.03 (s, 1H), 8.01 (s, 1H), 7.52 (s, 1H), 7.48 (s, 1H), 7.24 (d, *J* = 7.3 Hz, 2H), 7.19 (t, *J* = 7.7 Hz, 2H), 7.06 (t, *J* = 7.3 Hz, 2H), 4.85 (s, 1H), 4.83 (s, 1H), 3.16 (dd, *J* = 12.8, 7.7 Hz, 1H), 3.14 – 3.08 (m, 1H), 2.90 (dq, *J* = 13.6, 6.8 Hz, 2H), 2.87 – 2.80 (m, 2H), 2.55 – 2.51 (m, 1H), 2.19 (t, *J* = 8.2 Hz, 1H), 1.94 (dt, *J* = 15.7, 8.4 Hz, 2H), 1.87 – 1.78 (m, 5H), 1.79 – 1.68 (m, 8H), 1.66 – 1.55 (m, 5H), 1.30 (d, *J* = 6.5 Hz, 3H), 1.26 (d, *J* = 6.7 Hz, 3H).

^{13}C NMR (176 MHz, DMSO-d_6) δ 173.42, 170.53, 142.72, 142.68, 141.18, 141.16, 127.44, 123.99, 123.95, 122.36, 116.85, 69.27, 69.14, 47.92, 47.89, 42.52, 41.79, 39.01, 30.00, 29.95, 27.40, 25.69, 25.58, 23.27, 23.21, 22.35, 18.49, 18.01.

MS (ESI) m/z calc. $[M+H]^+$ $C_{18}H_{25}N_2O_2S^+$: 333.46; found: 333.16

((*S,S)*-**9a**, *(S,R)*-**9a**)

According to general procedure A, a mixture of 3,3-Dimethyl-3*H*-indole **3a**, (150 mg, 1.03 mmol), 3-(acetylthio)-2-methylpropanoic acid **5** (103 µL, 1.33 mmol) and ethyl isocyanoacetate **4b** (124 µL, 1.33 mmol) was dissolved in DCM (5 mL) in a sealed tube at 50 °C for 30 hours. The crude product was purified by chromatography on silica gel with hexane/ EtOAc (85:15) to yield the diastereomeric mixture. The racemic products were subjected to HPLC with MeOH/H_2O (65:35) as the eluent (flow rate 3.00 mL/min) for obtain pure diastereomers. Total yield: 32% (*dr* 1:1). tR HPLC: 22.35; tR HPLC: 24.36.

^{1}H NMR (600 MHz, DMSO-d_6) δ 8.78 (d, *J* = 26.8 Hz, 2H), 8.07 (t, *J* = 8.8 Hz, 2H), 7.22 – 7.14 (m, 4H), 7.07 – 6.99 (m, 2H), 4.72 (s, 1H), 4.63 (s, 1H), 4.11 – 4.07 (m, 4H), 3.87,(m, 4H), 3.04 (m, 3H), 2.96 (m, 3H), 2.34 (s, 6H), 1.36 – 1.29 (m, 12H), 1.20 – 1.18 (m, 6H), 1.12 (d, *J* = 7.1 Hz, 6H).

10a

According to procedure D, *(S,S*)*-**9a** (75 mg, 0.18 mmol) was dissolved in THF/NaOH (1:3, 1.2 mL/3.5 mL) and the reaction was stirred for 2 hours at room temperature. The mixture was quenched with HCl 2N and extracted with ethyl acetate. Then, solvent was evaporated under vacuum and the reaction was purified by chromatography on silica gel with DCM/

MeOH 9:1 to yield the product as white solid. Yield: 37% (23 mg). Rf = 0.37 (DCM/MeOH 8:2 + formic acid).

^{1}H NMR (700 MHz, DMSO-d_6) δ 10.22 (s, 1H), 8.59 (s, 1H), 8.10 (d, *J* = 7.9 Hz, 1H), 7.20 – 7.14 (m, 2H), 7.02 (t, *J* = 7.5 Hz, 1H), 4.96 (s, 1H), 3.78 – 3.69 (m, 2H), 2.83 – 2.76 (m, 1H), 2.69 (dt, *J* = 18.3, 9.1 Hz, 1H), 2.58 (dt, *J* = 13.0, 6.7 Hz, 1H), 2.40 (t, *J* = 8.2 Hz, 1H), 1.32 (s, 3H), 1.24 (s, 3H), 1.02 (d, *J* = 6.5 Hz, 3H).

^{13}C NMR (101 MHz, DMSO-d_6) δ 174.06, 168.93, 168.90, 142.42, 127.60, 124.03, 122.25, 116.74, 72.74, 44.06, 42.47, 32.41, 29.46, 28.77, 22.56, 17.79.

MS (ESI) m/z calc. $[M+H]^+$ $C_{17}H_{23}N_2O_4S^+$: 351.43; found: 351.14.

10 b

According to procedure D, *(S,R*)*-**9 a** (61 mg, 0.15 mmol) was dissolved in THF/NaOH (1:3, 1.0 mL/3.0 mL) and the reaction was stirred for 2 hours at room temperature. The mixture was quenched with HCl 2N and extracted with ethyl acetate. Then, solvent was evaporated under vacuum and the reaction was purified by chromatography on silica gel with DCM/ MeOH 9:1 to yield the product as white solid. Yield: 98% (49 mg). Rf = 0.27 (DCM/MeOH 8:2 + formic acid).

^{1}H NMR (700 MHz, DMSO-d_6) δ 10.28 (s, 1H), 8.50 (s, 1H), 8.15 – 8.11 (m, 1H), 7.22 (dt, *J* = 14.6, 7.1 Hz, 2H), 7.10 – 7.05 (m, 1H), 4.79 (s, 1H), 3.79 – 3.67 (m, 2H), 3.06 (dd, *J* = 13.1, 6.4 Hz, 1H), 2.84 – 2.75 (m, 2H), 2.73 (dt, *J* = 13.6, 7.0 Hz, 2H), 1.37 (t, *J* = 7.6 Hz, 6H), 1.31 – 1.26 (m, 3H).

^{13}C NMR (176 MHz, DMSO-d_6) δ 174.05, 168.51, 142.46, 140.52, 127.64, 124.07, 116.62, 72.43, 55.40, 49.07, 42.71, 32.35, 27.58, 22.46, 17.59.

MS (ESI) m/z calc. $[M+H]^+$ $C_{17}H_{23}N_2O_4S^+$: 351.43; found: 351.14.

9b

According to general procedure A, a mixture of 3,3-Diethyl-3*H*-indole **3b**, (320 mg, 1.85 mmol), 3-(acetylthio)-2-methylpropanoic acid **5** (186 µL, 2.04 mmol) and ethyl isocyanoacetate **4b** (223 µL, 2.04 mmol) was dissolved in DCM (5 mL) in a sealed tube at 50 °C for 30 hours. The crude product was purified by chromatography on silica gel with hexane/ EtOAc (9:1) to yield the diastereomeric mixture. The racemic products were subjected to HPLC with MeOH/H_2O (85:15) as the eluent (flow rate 3.00 mL/min) for obtain pure diastereomers. Total yield: 23% (*dr* 1:1).

(S,S)-**9b**

Yellow solid; Rf = 0.28 (H/E 7:3)

^{1}H NMR (400 MHz, DMSO-d_6) δ 8.75 (s, 1H), 8.06 (d, *J* = 7.9 Hz, 1H), 7.22 – 7.09 (m, 2H), 7.02 (t, *J* = 7.6 Hz, 1H), 4.68 (s, 1H), 4.09 (q, *J* = 7.1 Hz, 2H), 3.91 (dd, *J* = 17.4, 5.5 Hz, 1H), 3.78 (dd, *J* = 17.4, 5.6 Hz, 1H), 2.97 (d, *J* = 6.9 Hz, 2H), 2.74 (q, *J* = 6.7 Hz, 1H), 2.30 (s, 3H), 1.61 (ddq, *J* = 49.5, 14.6, 6.8 Hz, 4H), 1.19 (t, *J* = 6.6 Hz, 6H), 0.94 (t, *J* = 7.2 Hz, 3H), 0.66 (t, *J* = 7.2 Hz, 3H).

^{13}C NMR (101 MHz, DMSO-d_6) δ 195.75, 173.28, 169.41, 127.68, 123.81, 123.65, 116.75, 70.68, 60.97, 51.40, 41.24, 32.59, 31.86, 30.92, 24.66, 14.51, 9.74, 8.21.

(S,R)-**9b**

Yellow solid; Rf = 0.28 (H/E 7:3)

^{1}H NMR (400 MHz, DMSO-d_6) δ 8.79 (s, 1H), 8.09 (d, *J* = 8.1 Hz, 1H), 7.18 (t, *J* = 7.6 Hz, 1H), 7.13 (d, *J* = 7.3 Hz, 1H), 7.03 (t, *J* = 7.5 Hz, 1H), 4.78 (s, 1H), 4.09 (dtt, *J* = 10.8, 7.3, 3.7 Hz, 2H), 3.86 (t, *J* = 5.4 Hz, 2H),

3.01 (d, *J* = 6.8 Hz, 2H), 2.85 (dq, *J* = 13.6, 6.5 Hz, 1H), 2.32 (s, 3H), 1.91 (dq, *J* = 14.9, 7.4 Hz, 1H), 1.71 – 1.59 (m, 3H), 1.18 (t, *J* = 7.1 Hz, 3H), 1.05 (d, *J* = 6.5 Hz, 3H), 0.89 (t, *J* = 7.4 Hz, 3H), 0.70 (t, *J* = 7.2 Hz, 3H).
^{13}C NMR (101 MHz, DMSO-d_6) δ 195.75, 169.62, 137.49, 123.83, 123.76, 116.98, 70.90, 60.98, 51.52, 41.29, 33.20, 33.07, 30.98, 25.28, 17.82, 14.52, 9.64, 8.30.

10c

According to procedure D, *(S,S*)*-**9b** (50 mg, 0.11 mmol) was dissolved in THF/NaOH (1:3, 1.5 mL/4.5 mL) and the reaction was stirred for 2 hours at room temperature. The mixture was quenched with HCl 2N and extracted with ethyl acetate. Then, solvent was evaporated under vacuum and the reaction was purified by chromatography on silica gel with DCM/ MeOH 9:1 to yield the product as yellow solid. Yield: 95% (40 mg). Rf = 0.32 (DCM/MeOH 8:2 + formic acid).
^{1}H NMR (400 MHz, DMSO-d_6) δ 8.48 (s, 1H), 8.12 (d, *J* = 7.9 Hz, 1H), 7.17 (t, *J* = 7.6 Hz, 1H), 7.11 (t, *J* = 7.5 Hz, 1H), 7.02 (t, *J* = 7.3 Hz, 1H), 5.00 (s, 1H), 3.71 (s, 2H), 2.69 – 2.62 (m, 1H), 2.57 (dd, *J* = 12.7, 7.3 Hz, 1H), 2.44 – 2.30 (m, 1H), 1.66 (tt, *J* = 14.4, 7.4 Hz, 4H), 1.01 (d, *J* = 6.4 Hz, 3H), 0.91 (d, *J* = 7.3 Hz, 3H), 0.69 (t, *J* = 7.3 Hz, 3H).
^{13}C NMR (101 MHz, DMSO-d_6) δ 174.02, 169.29, 162.78, 143.44, 137.80, 127.59, 123.80, 123.52, 116.85, 71.07, 51.33, 36.25, 32.96, 31.24, 25.27, 18.06, 9.68, 8.36.
MS (ESI) m/z calc. $[M+H]^+$ $C_{19}H_{27}N_2O_4S^+$: 379.49; found: 379.07.

10d

According to procedure D, *(S,R*)*-**9b** (45 mg, 0.11 mmol) was dissolved in THF/NaOH (1:3, 1.5 mL/4.5 mL) and the reaction was stirred for 2

hours at room temperature. The mixture was quenched with HCl 2N and extracted with ethyl acetate. Then, solvent was evaporated under vacuum and the reaction was purified by chromatography on silica gel with DCM/ MeOH 9:1 to yield the product as yellow solid. Yield: 97% (37 mg). Rf = 0.32 (DCM/MeOH 8:2 + formic acid).

^{1}H NMR (400 MHz, DMSO-d_6) δ 8.43 (s, 1H), 8.07 (d, J = 7.6 Hz, 1H), 7.20 – 7.13 (m, 1H), 7.11 (d, J = 6.6 Hz, 1H), 7.02 (d, J = 7.1 Hz, 1H), 4.82 (s, 1H), 3.73 (s, 2H), 2.99 (d, J = 9.6 Hz, 1H), 2.79 – 2.64 (m, 2H), 1.69 – 1.61 (m, 2H), 1.57 (dd, J = 13.9, 7.6 Hz, 2H), 1.20 (s, 3H), 0.94 (s, 4H), 0.66 (t, J = 6.8 Hz, 3H).

^{13}C NMR (101 MHz, DMSO-d_6) δ 173.60, 143.45, 137.78, 127.57, 123.77, 123.51, 116.74, 70.80, 51.24, 32.78, 29.49, 27.67, 17.76, 9.72, 8.23.

MS (ESI) m/z calc. $[M+H]^+$ $C_{19}H_{27}N_2O_4S^+$: 379.49; found: 379.07.

(S,S)*-**6a**

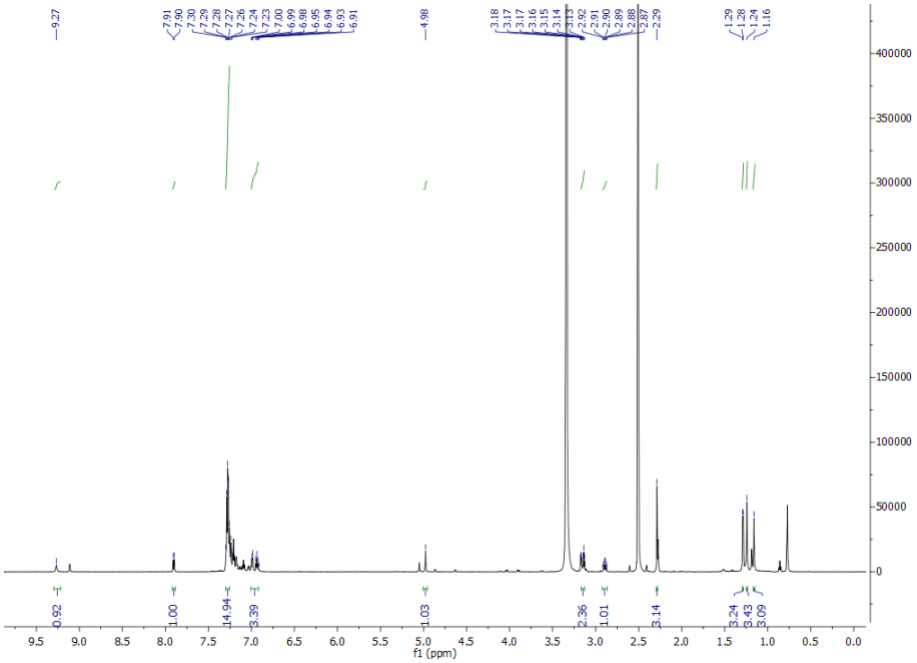

Supporting figure 1. ^{1}H NMR of compound *(S,S*)*-**6a**

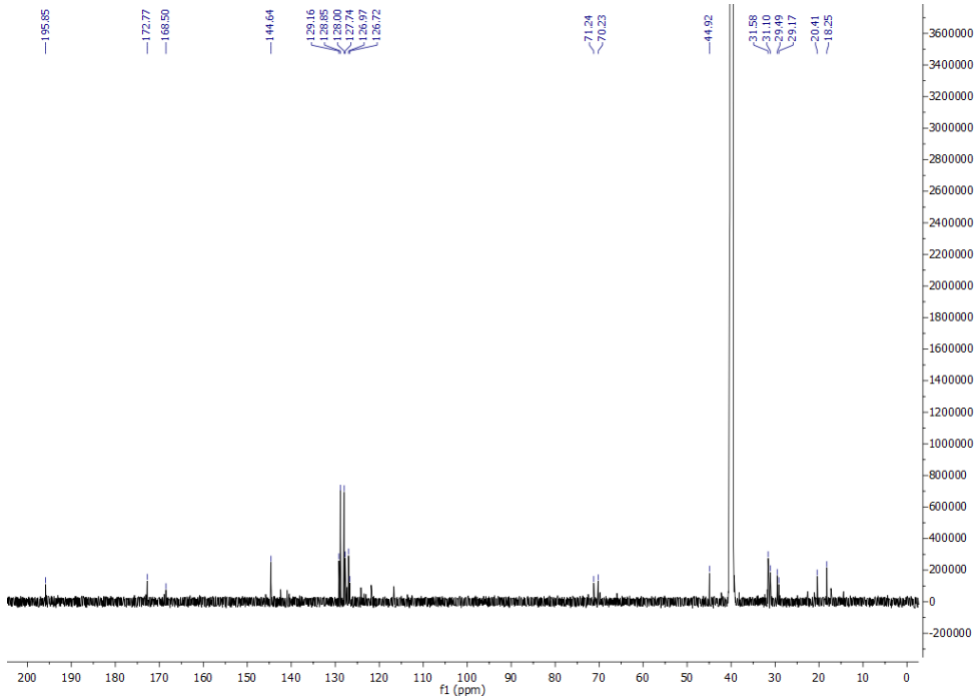

Supporting figure 2. ^{13}C NMR of compound *(S,S*)*-**6a**

(S,R)*-**6a**

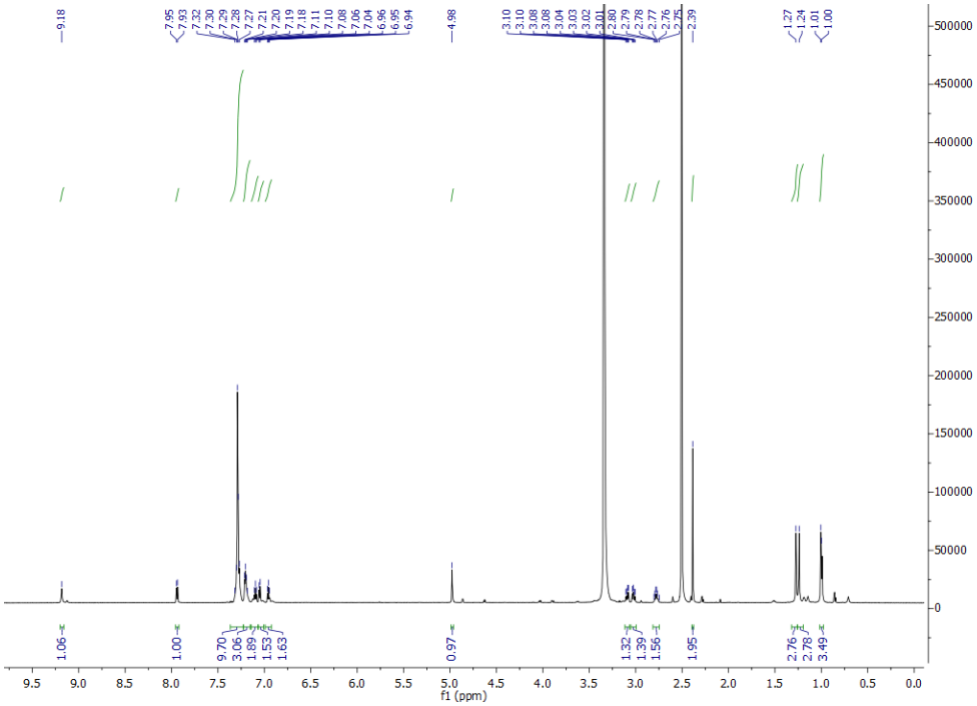

Supporting figure 3. ^{1}H NMR of compound *(S,R*)*-**6a**

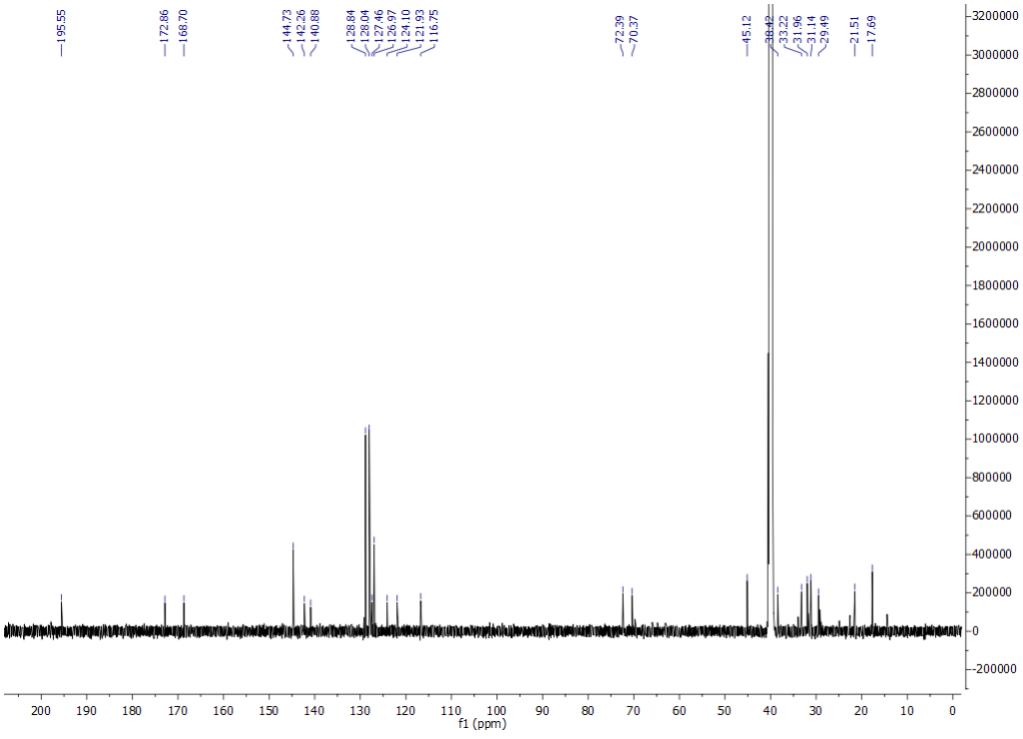

Supporting figure 4. ^{13}C NMR of compound *(S,R*)*-**6a**

(S,S)*-**7a**

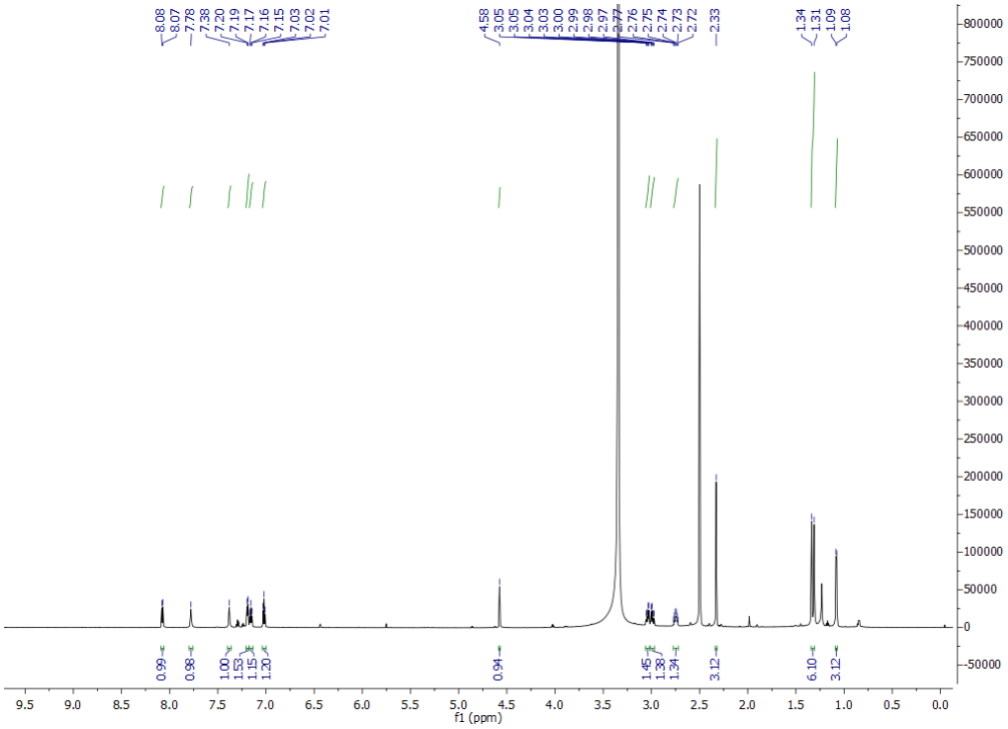

Supporting figure 5. ^{1}H NMR of compound *(S,S*)*-**7a**

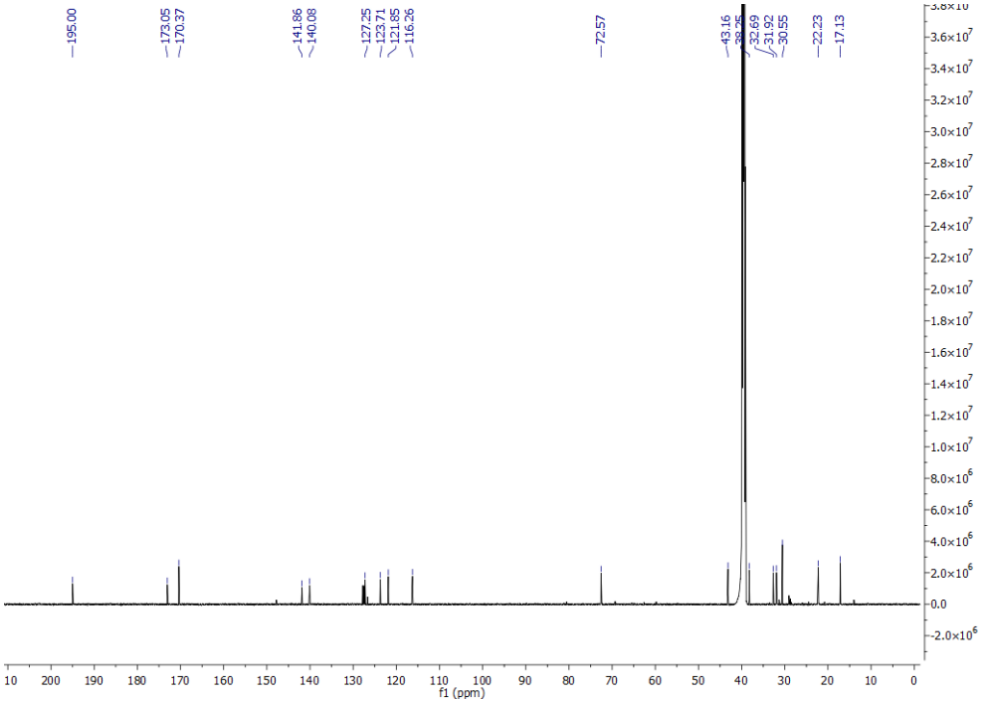

Supporting figure 6. ^{13}C NMR of compound *(S,S*)*-**7a**

8a

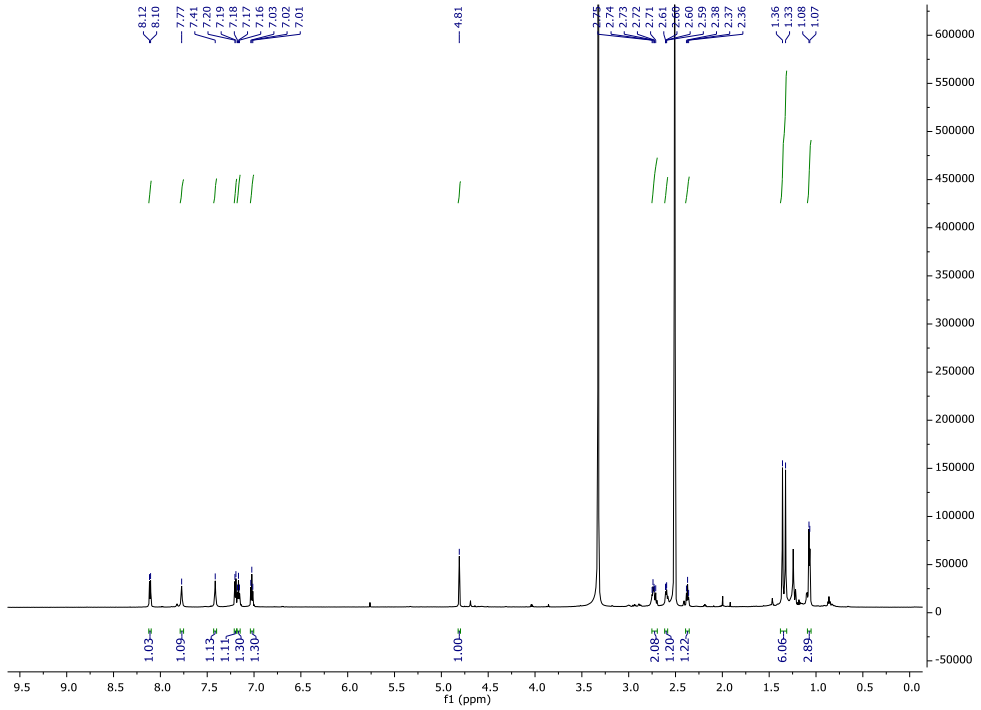

Supporting figure 7. ^{1}H NMR of compound **8a**

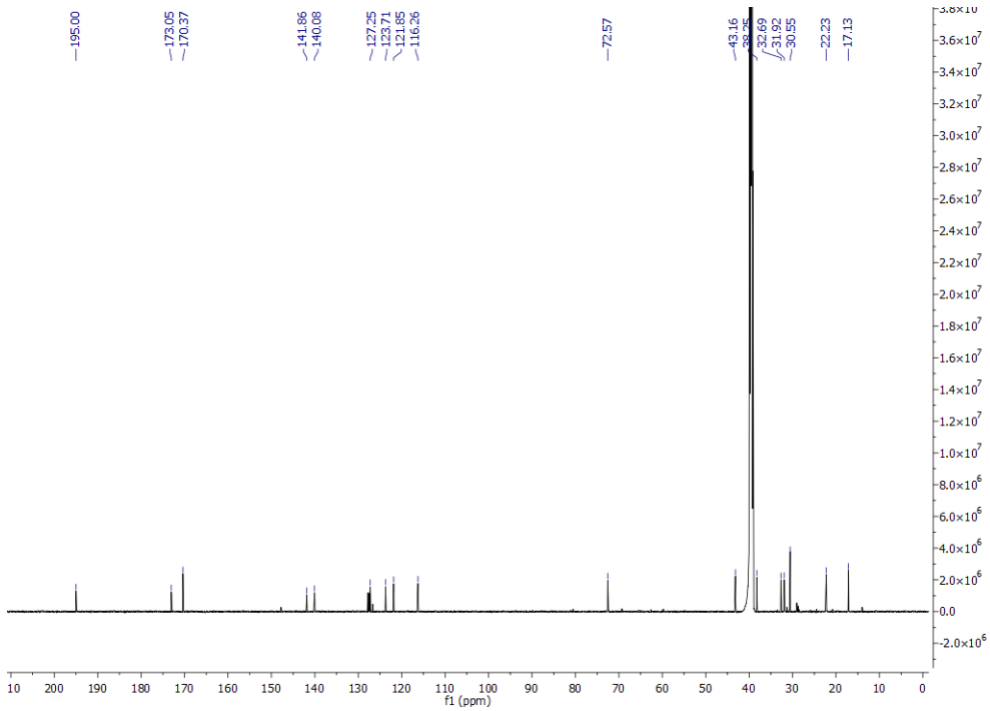

Supporting figure 8. ^{13}C NMR of compound **8a**

(S,R)*-**7a**

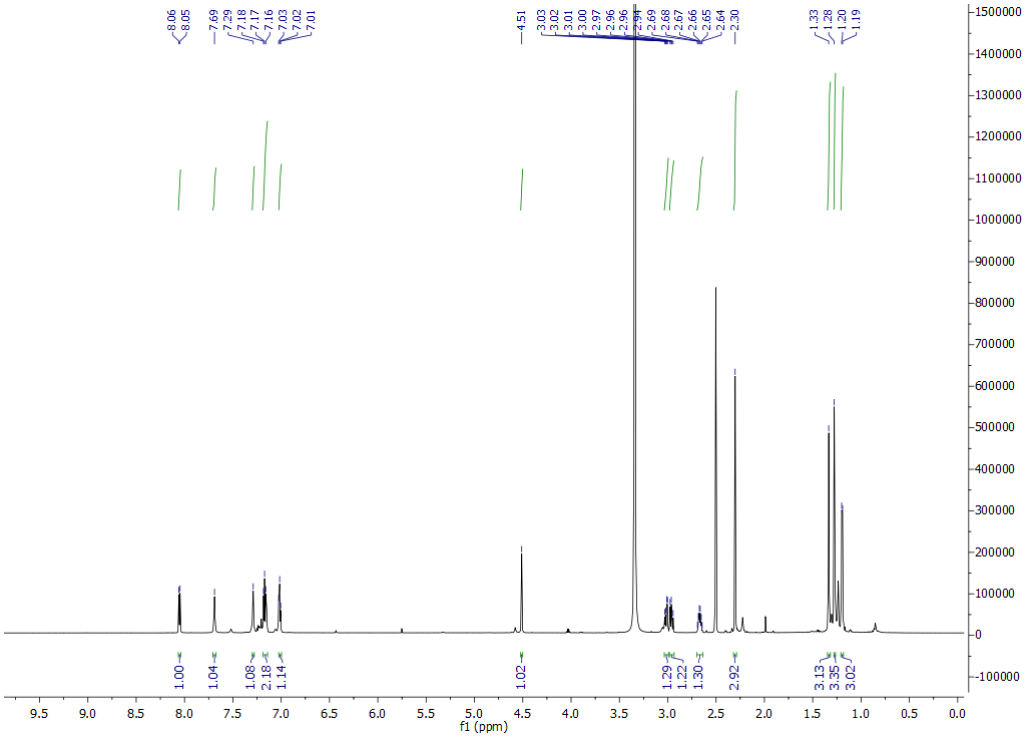

Supporting figure 9. ^{1}H NMR of compound *(S,R*)*-**7a**

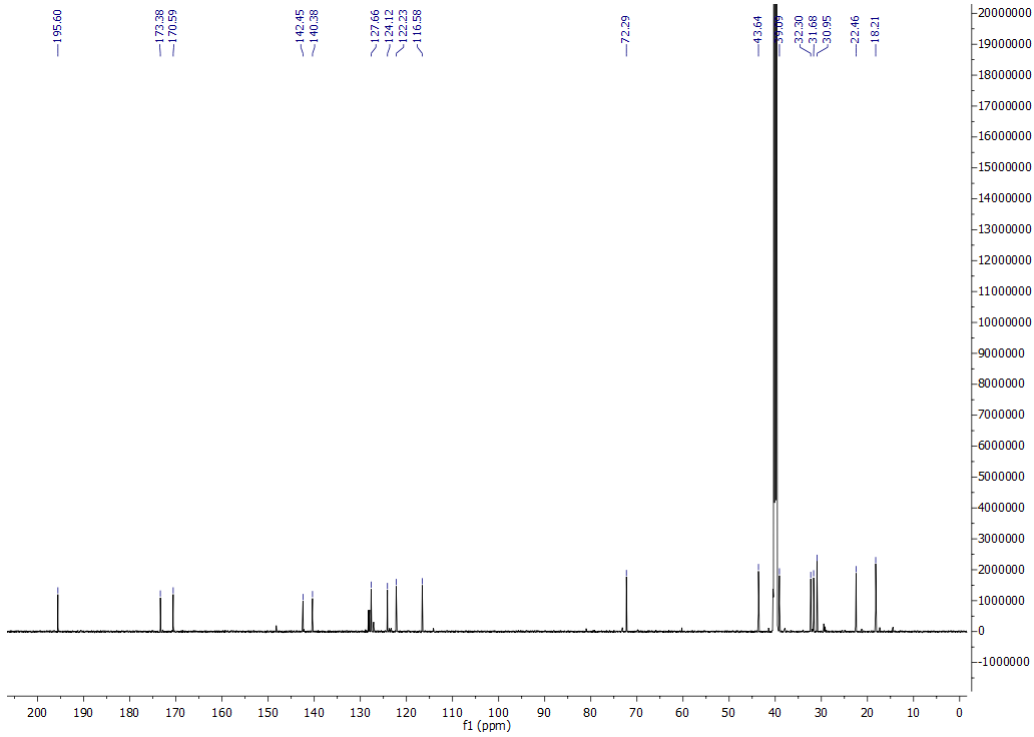

Supporting figure 10. ^{13}C NMR of compound *(S,R*)*-**7a**

8b

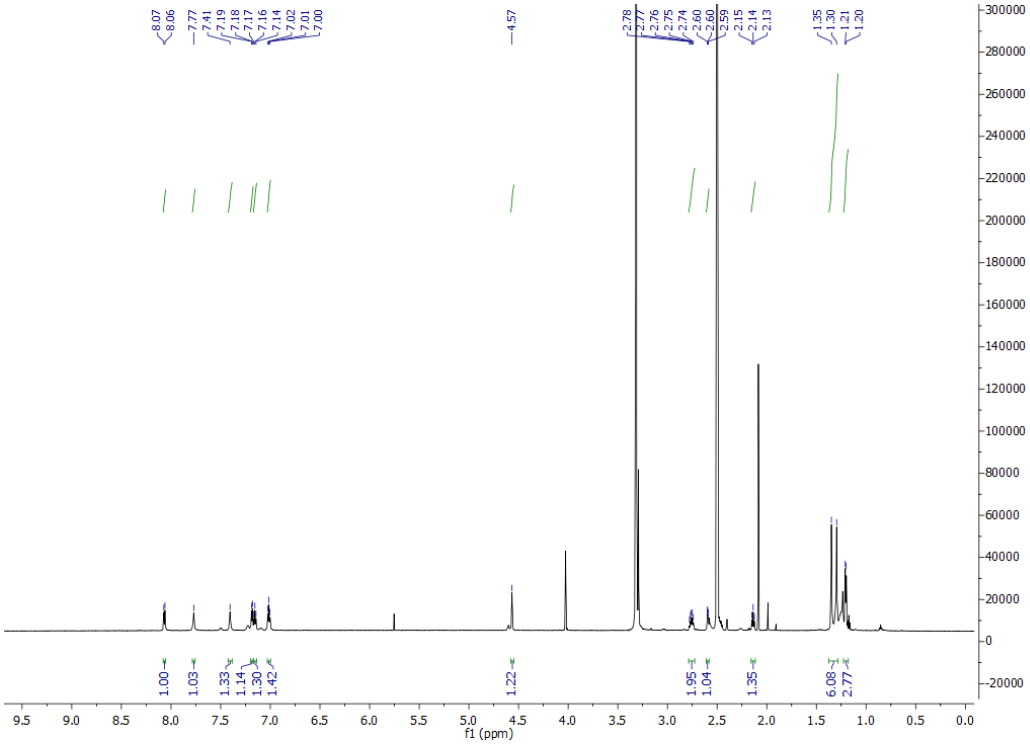

Supporting figure 11. ^{1}H NMR of compound **8b**

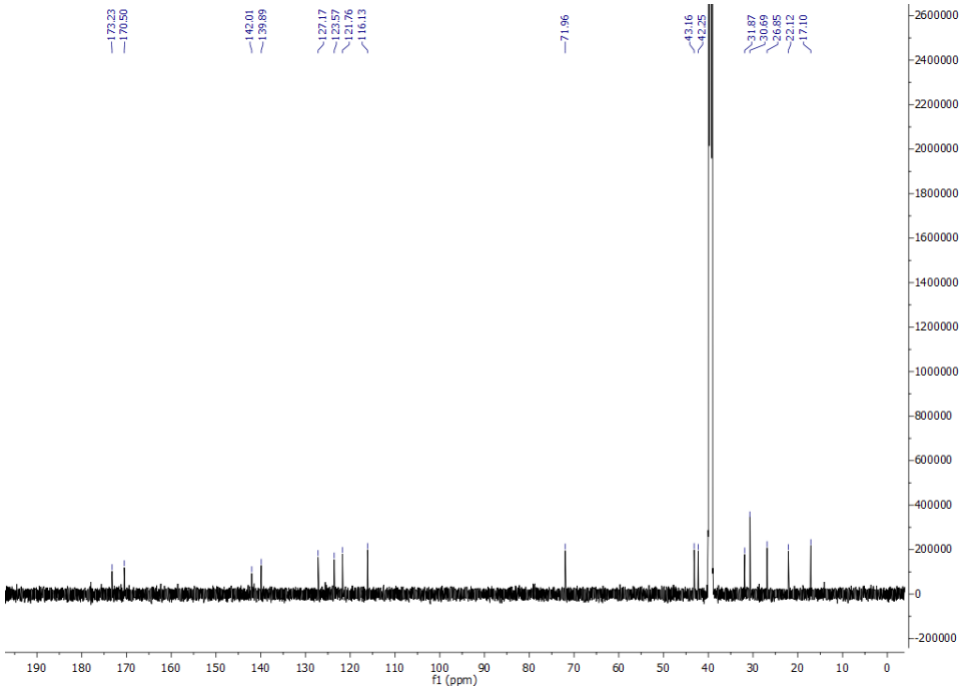

Supporting figure 12. ^{13}C NMR of compound *(S,R*)*-**8b**

(S,S)*-**6b**

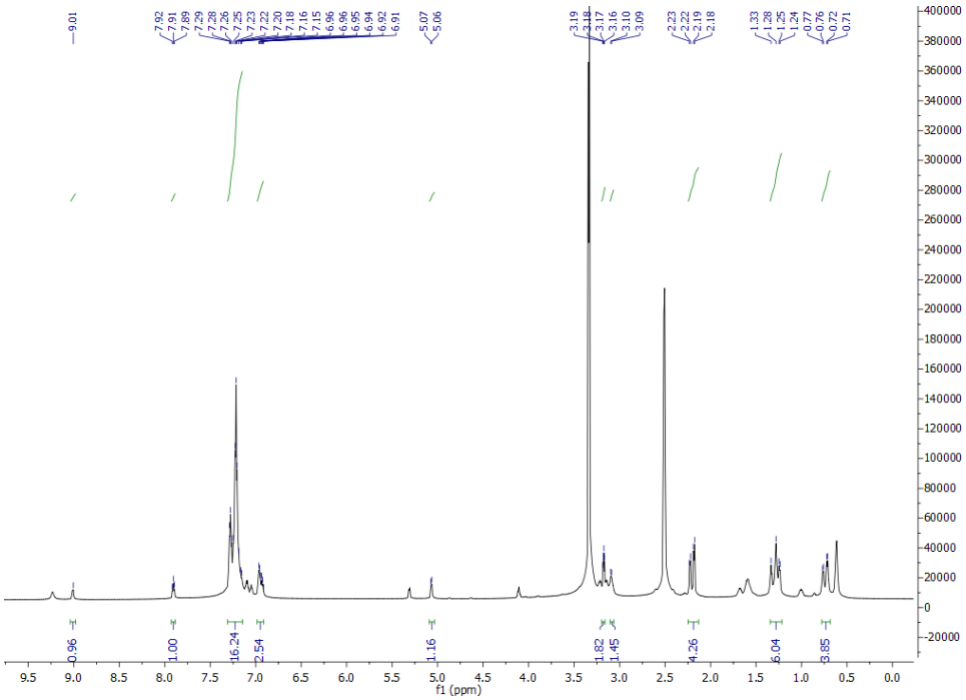

Supporting figure 13. ^{1}H NMR of compound *(S,S*)*-**6b**

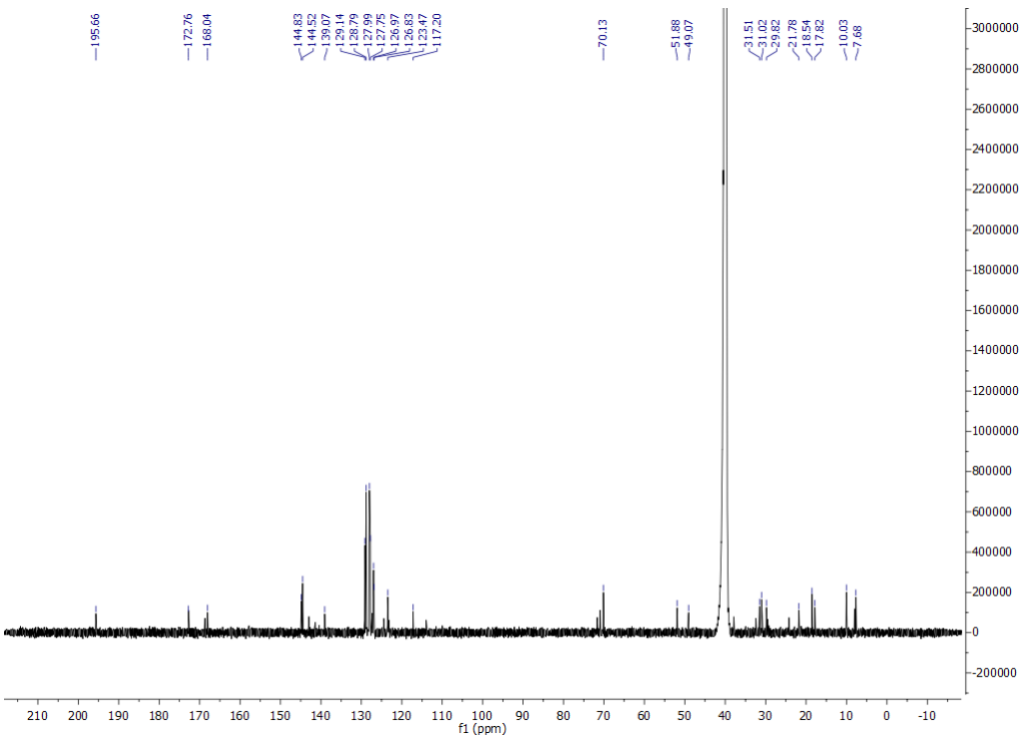

Supporting figure 14. ^{13}C NMR of compound *(S,S*)*-**6b**

(S,R)*-**6 b**

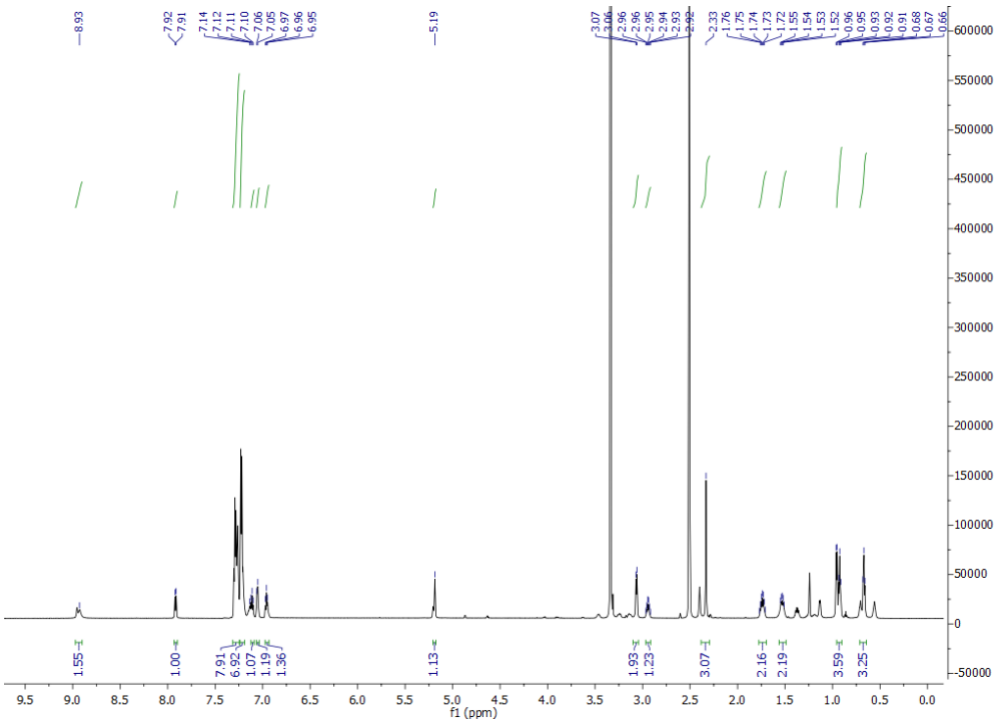

Supporting figure 15. ^{1}H NMR of compound *(S,R*)*-**6b**

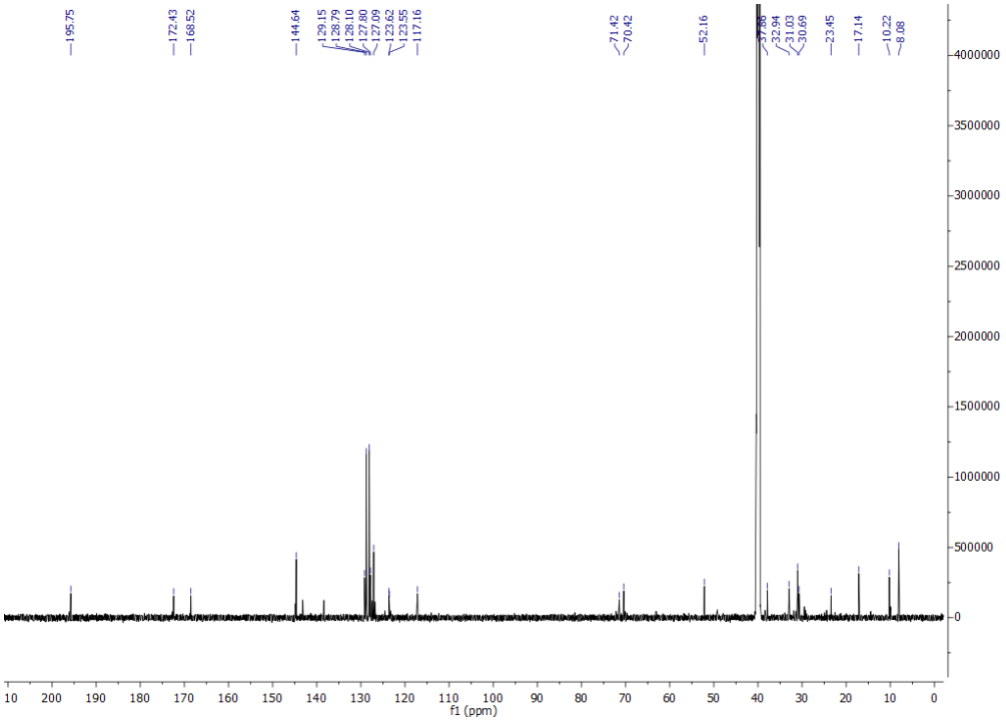

Supporting figure 16. ^{13}C NMR of compound *(S,R*)*-**6b**

(S,S)*-**7b**

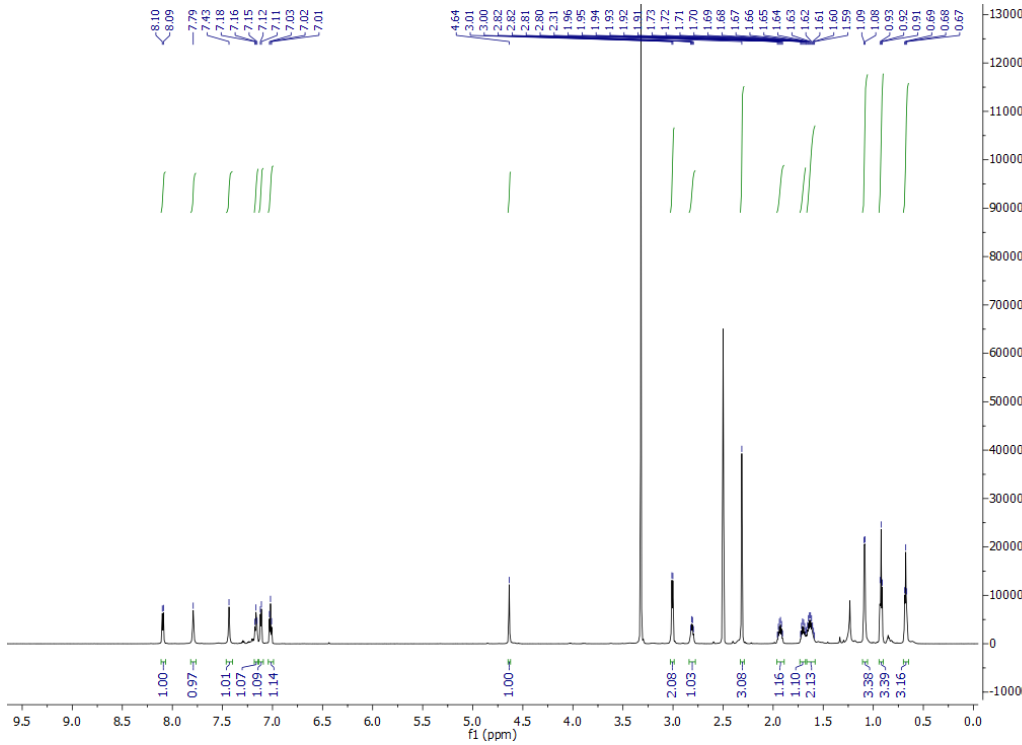

Supporting figure 17. ^{1}H NMR of compound *(S,S*)*-**7b**

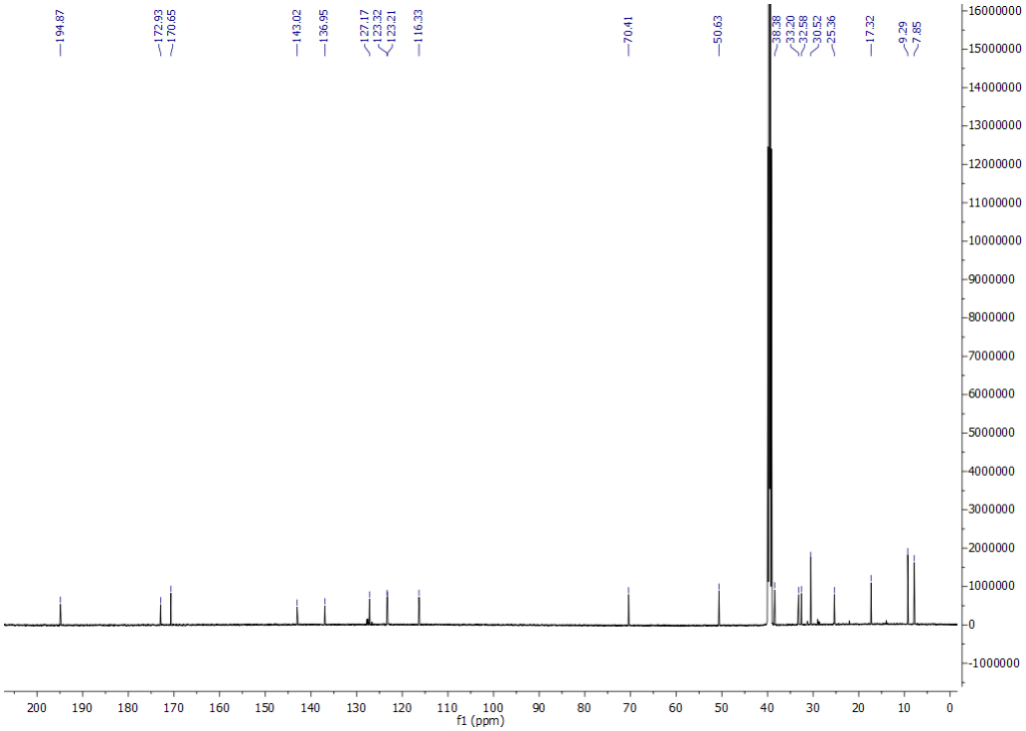

Supporting figure 18. ^{13}C NMR of compound *(S,S*)*-**7b**

8c

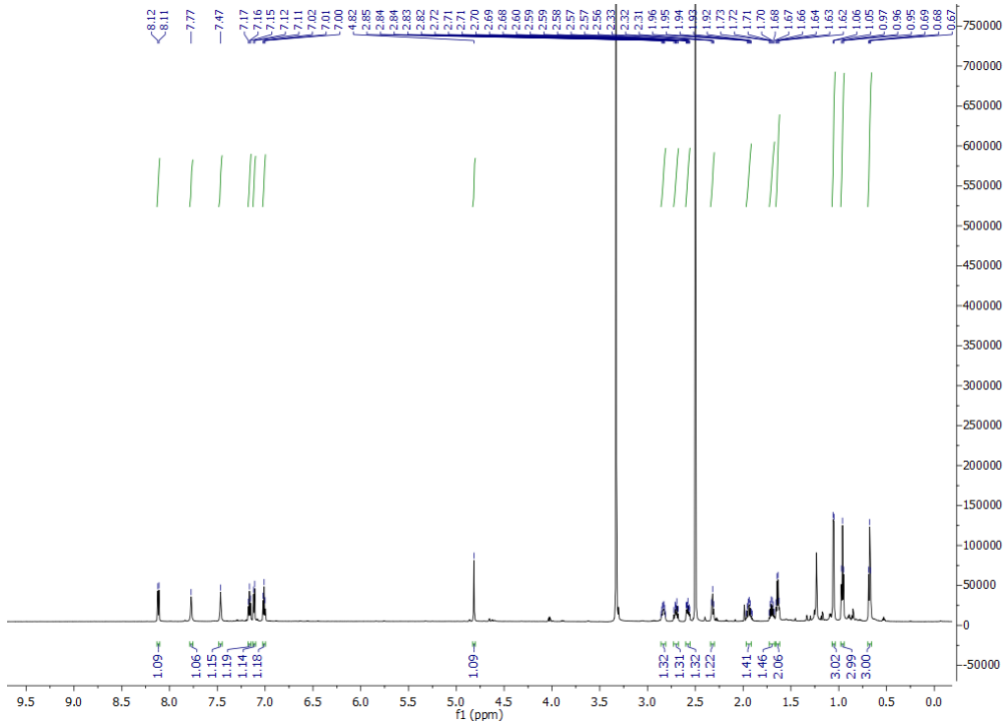

Supporting figure 19. ^{1}H NMR of compound **8c**

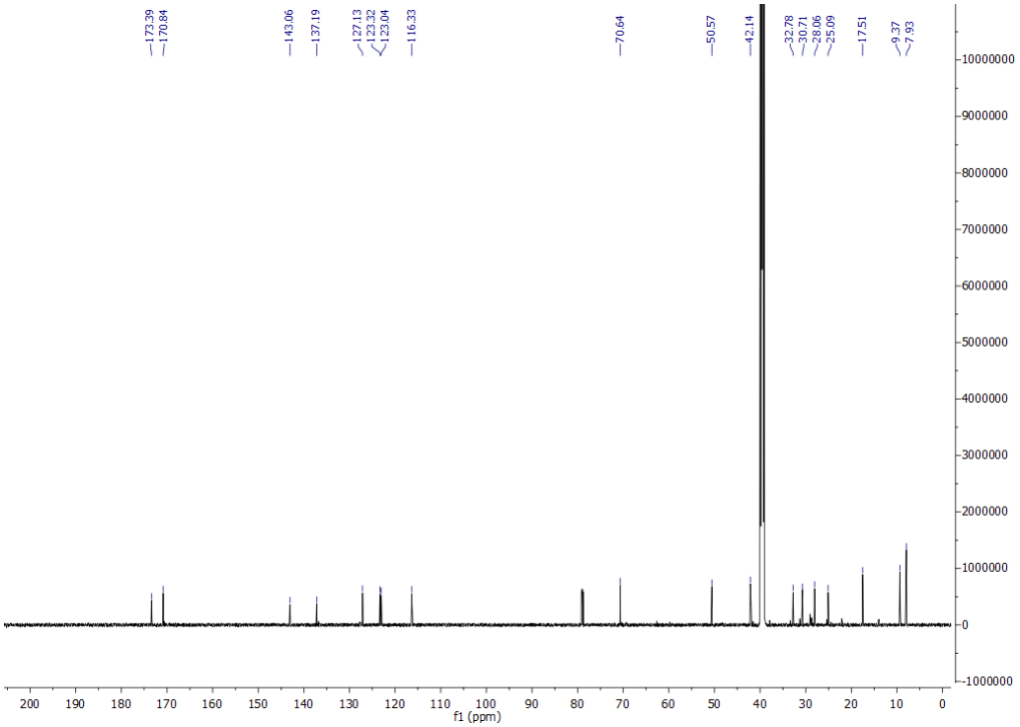

Supporting figure 20. ^{13}C NMR of compound **8c**

(S,R)*-**7b**

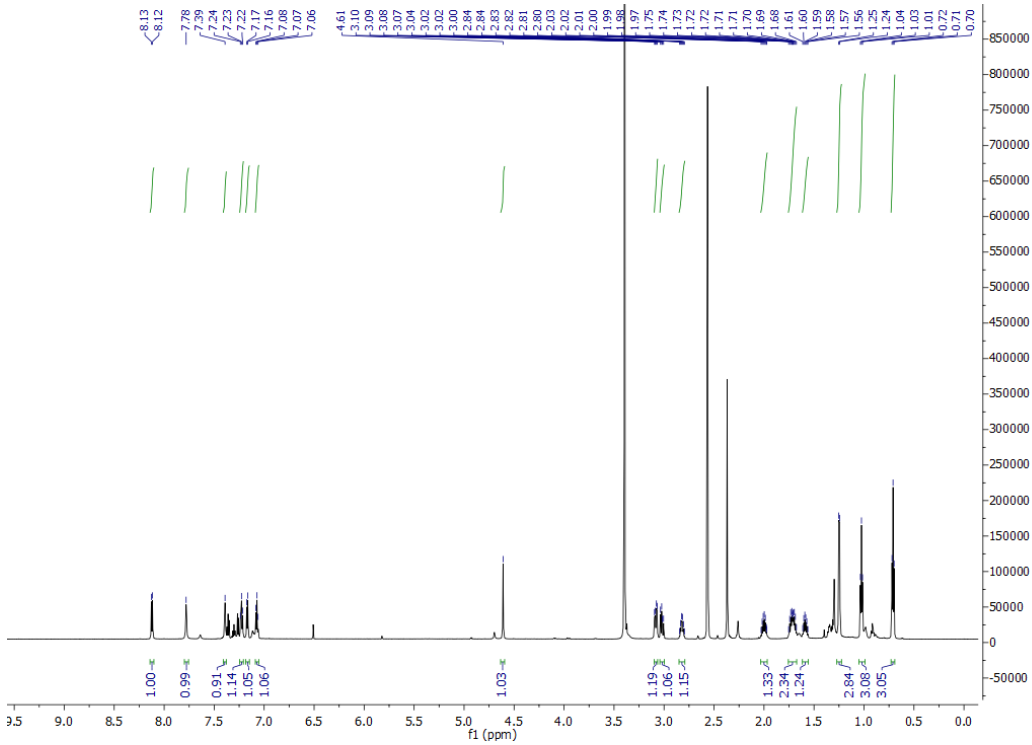

Supporting figure 21. ^{1}H NMR of compound *(S,R*)*-**7b**

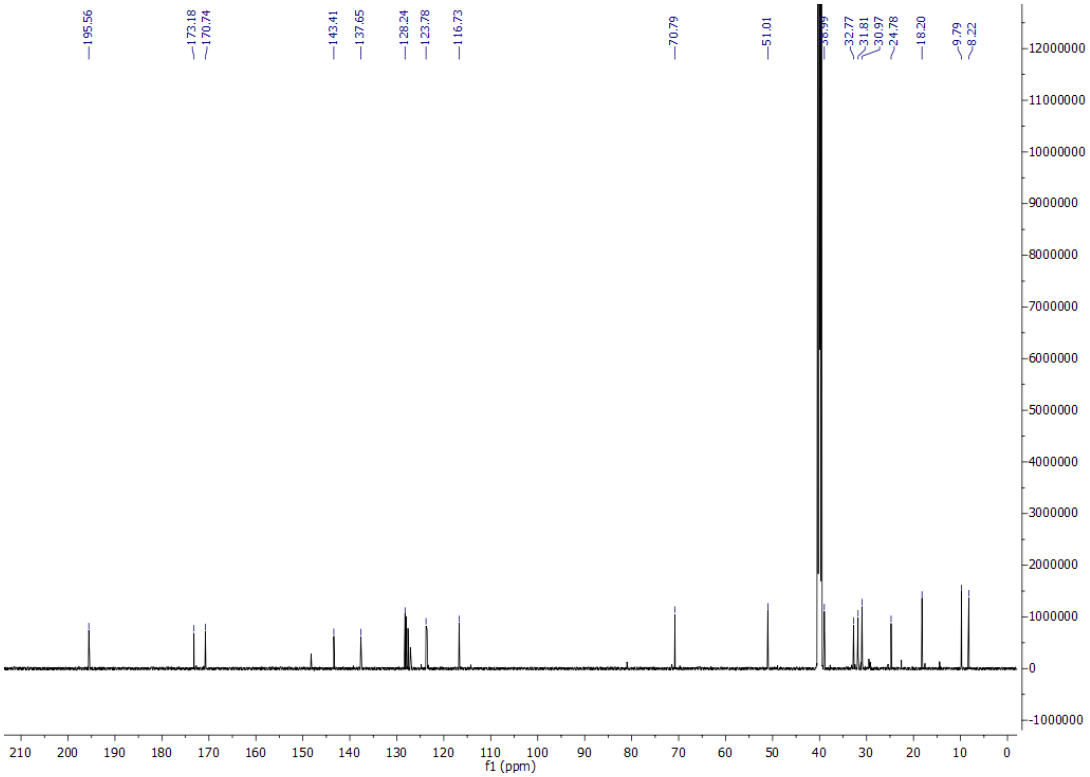

Supporting figure 22. ^{13}C NMR of compound *(S,R*)*-**7b**

8d

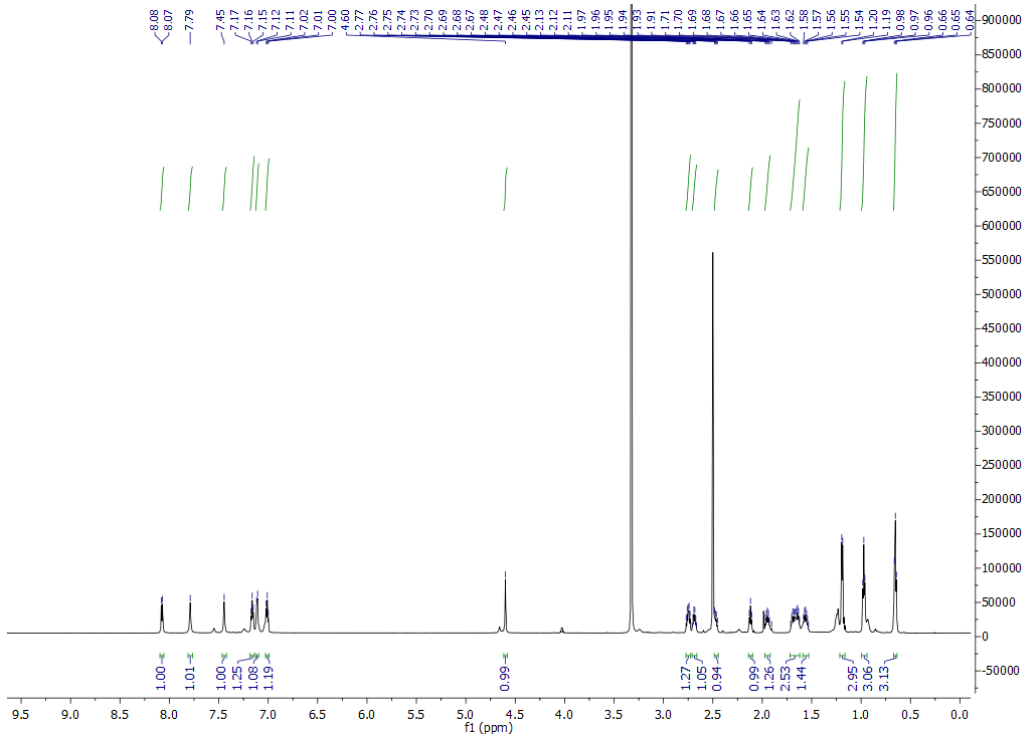

Supporting figure 23. ^{1}H NMR of compound **8d**

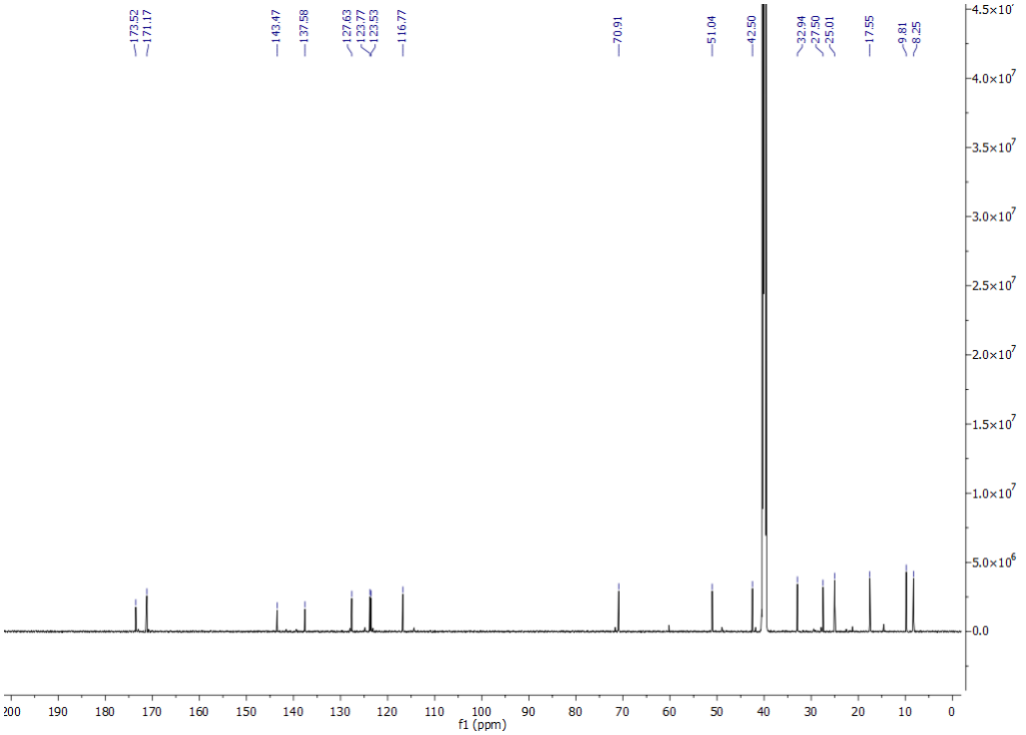

Supporting figure 24. ^{13}C NMR of compound **8d**

(*S*,*S**)-**7c**

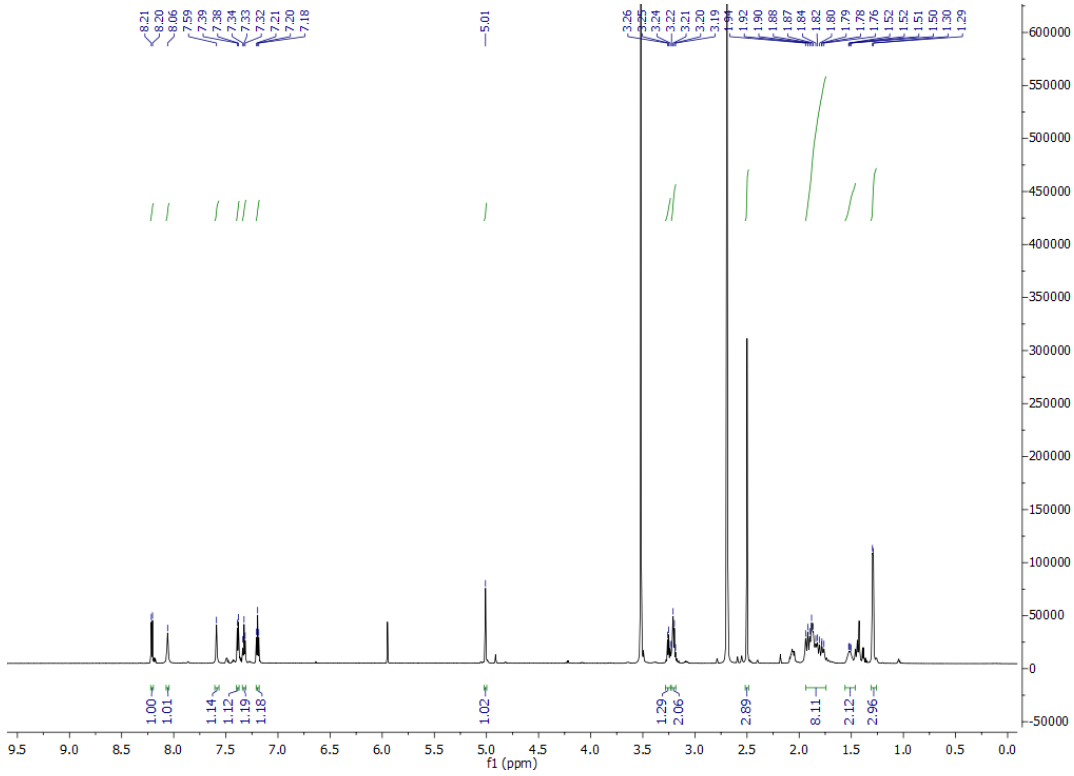

Supporting figure 25. ^{1}H NMR of compound *(S,S*)*-**7c**

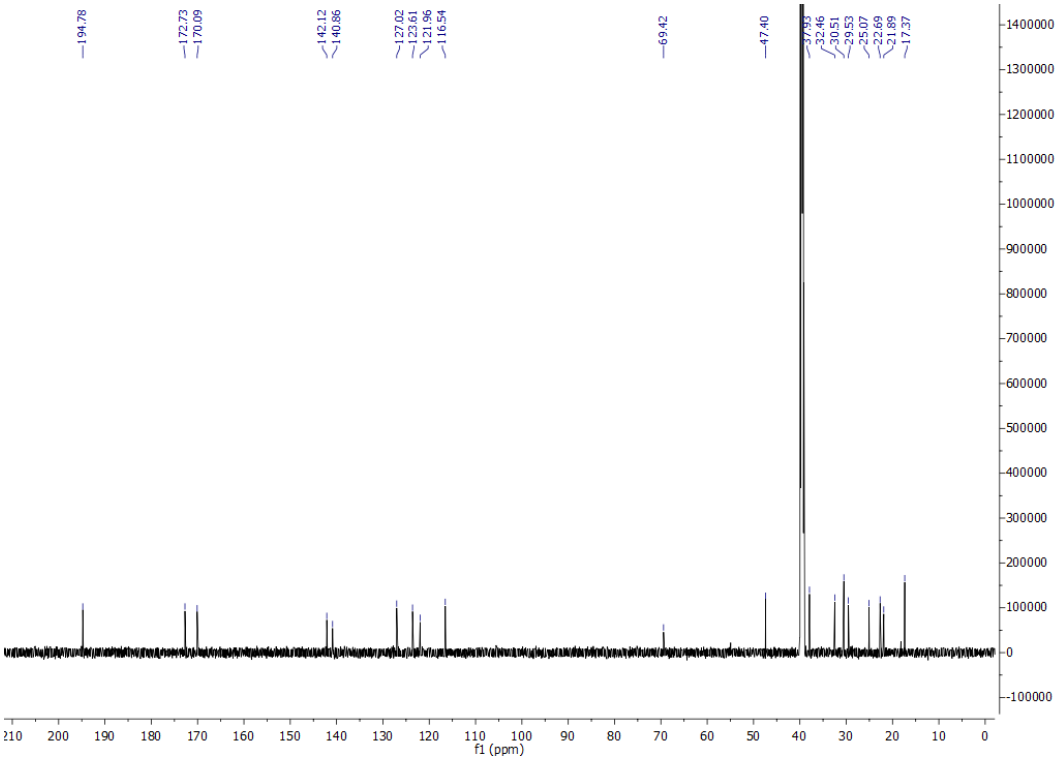

Supporting figure 26. ^{13}C NMR of compound *(S,S*)*-**7c**

8e

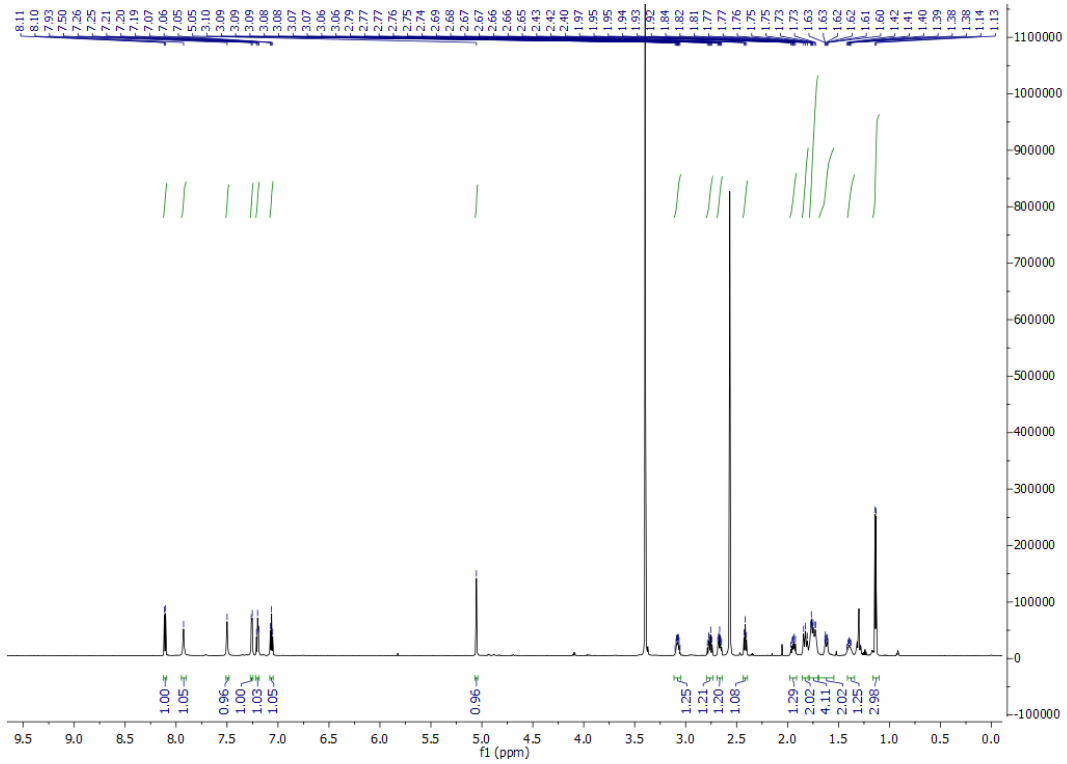

Supporting figure 27. ^{1}H NMR of compound **8e**

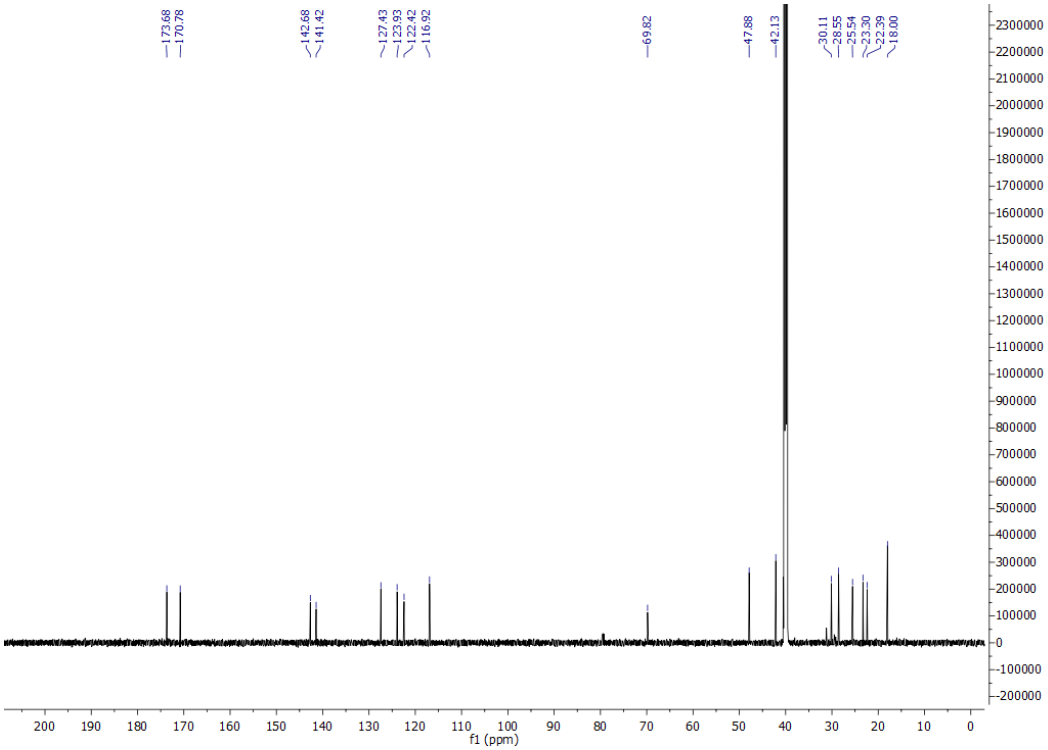

Supporting figure 28. ^{13}C NMR of compound **8e**

(S,R)*-**7c**

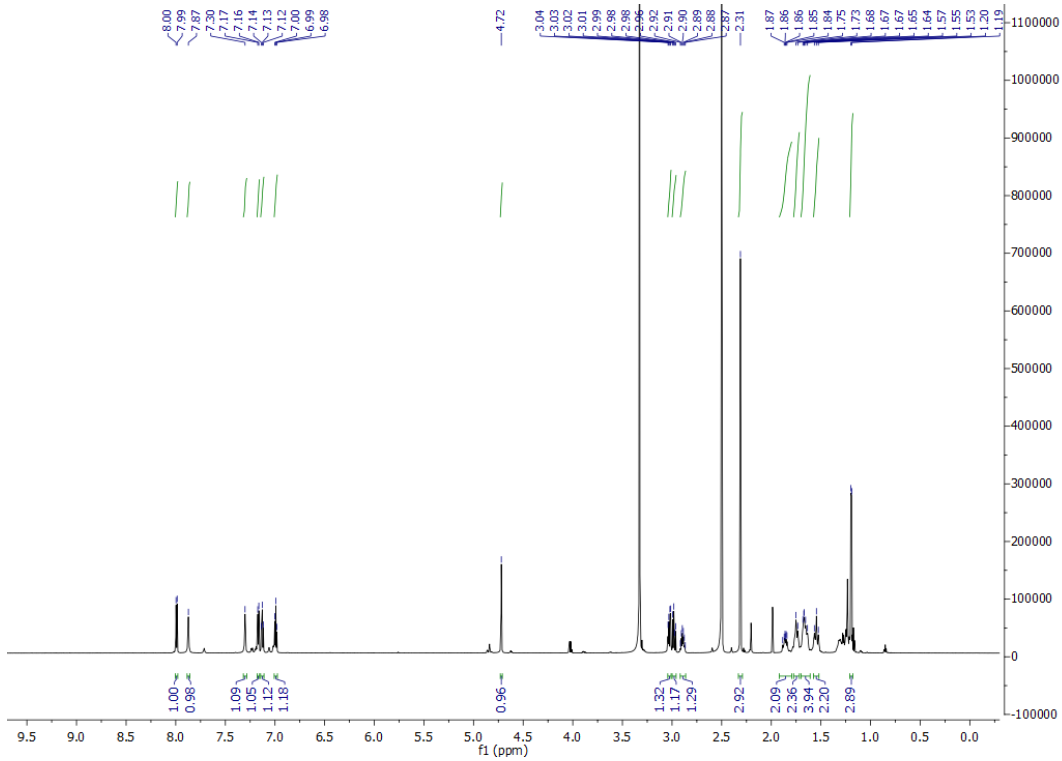

Supporting figure 29. ^{1}H NMR of compound *(S,R*)*-**7c**

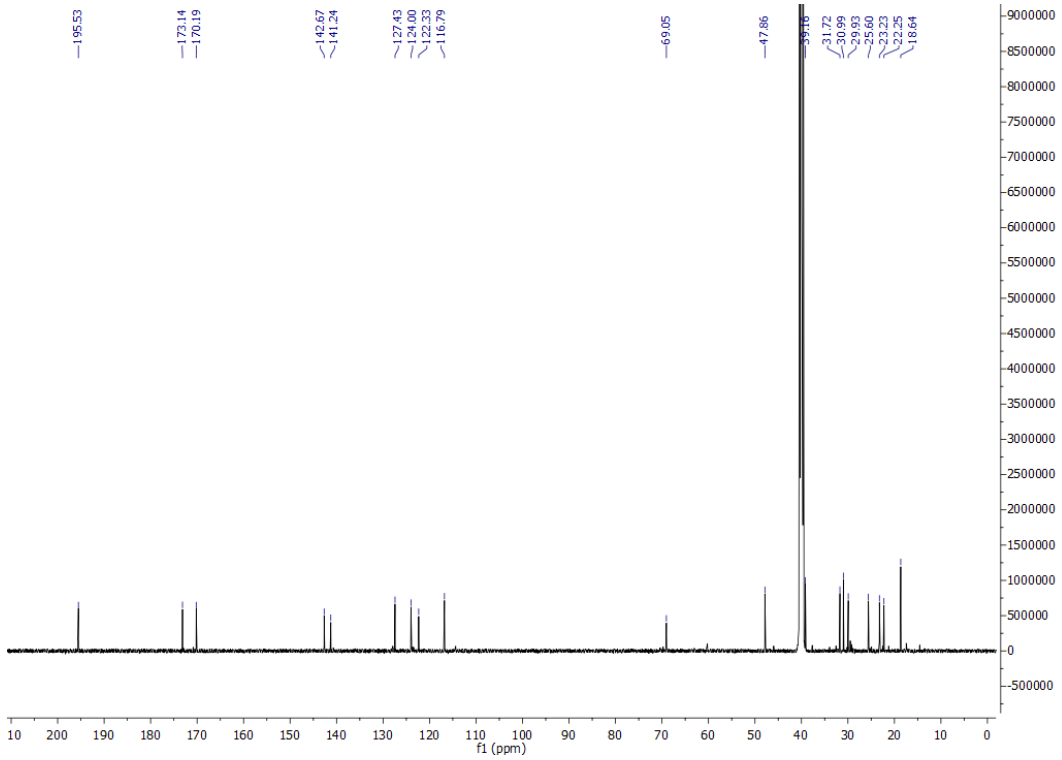

Supporting figure 30. ^{13}C NMR of compound *(S,R*)*-**7c**

8f

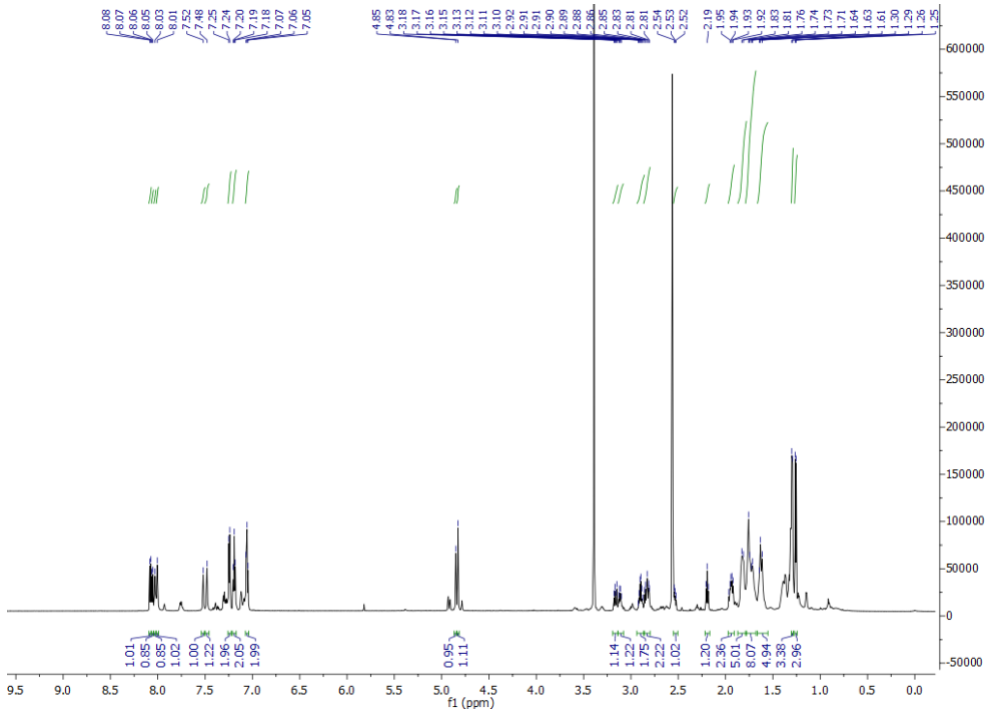

Supporting figure 31. ^{1}H NMR of compound **8f**

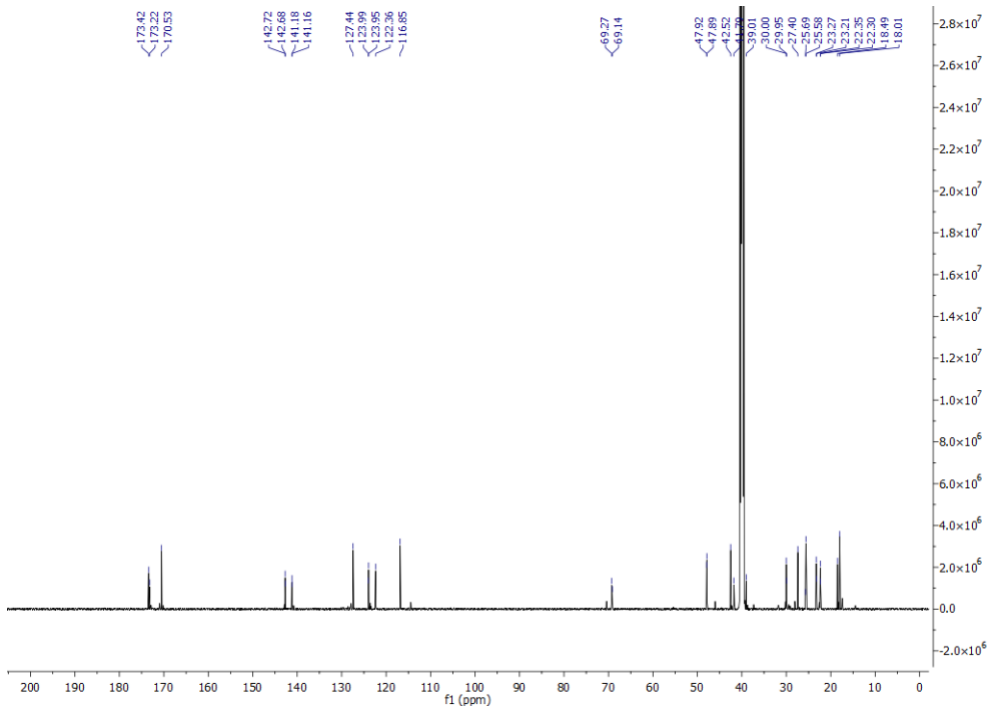

Supporting figure 32. ^{13}C NMR of compound **8f**

(*(S,S*)*-**9a**, *(S,R*)*-**9a**)

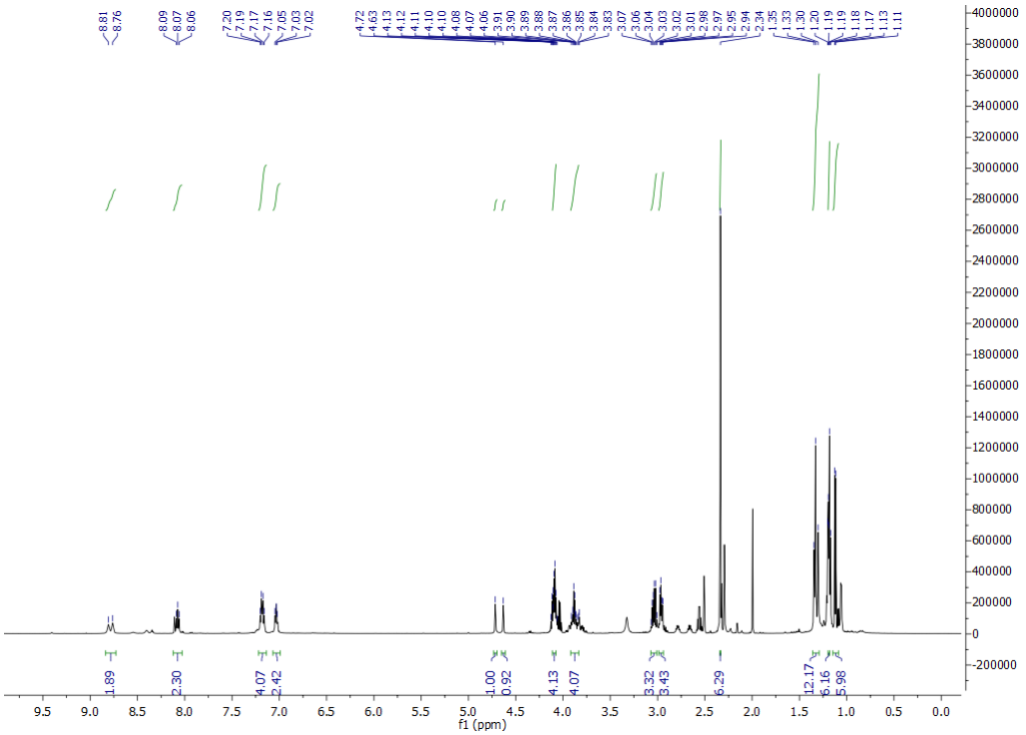

Supporting figure 33. ^{1}H NMR of compound *(S,S*)*-**9a**, *(S,R*)*-**9a**

10a

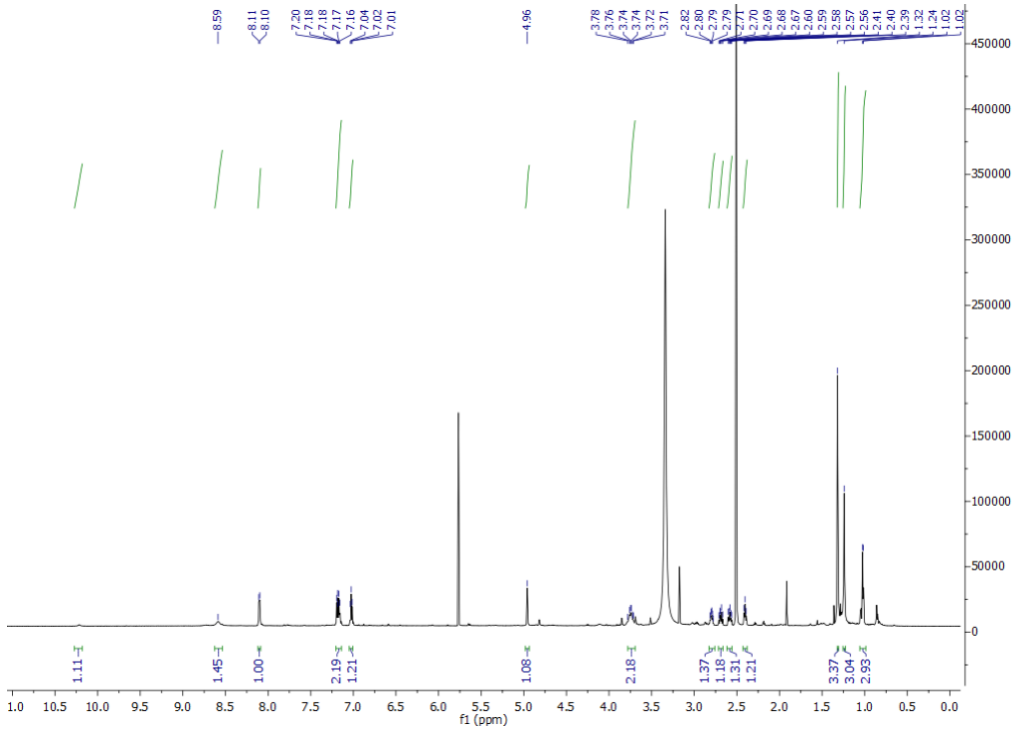

Supporting figure 34. ^{1}H NMR of compound **10a**

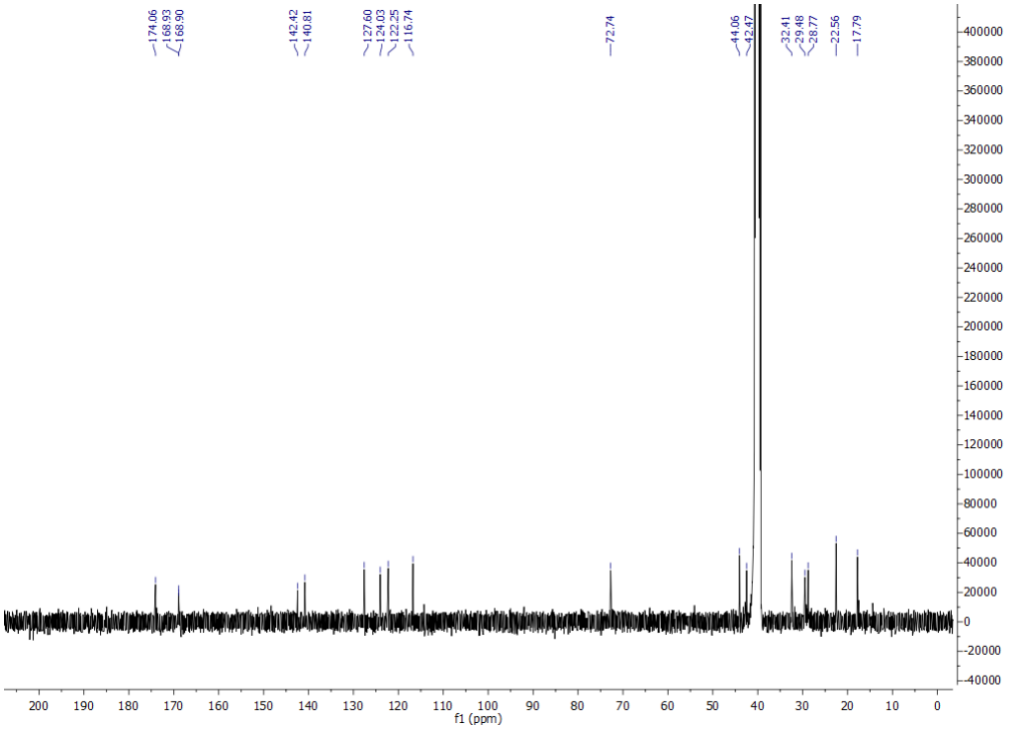

Supporting figure 35. ^{13}C NMR of compound **10a**

10b

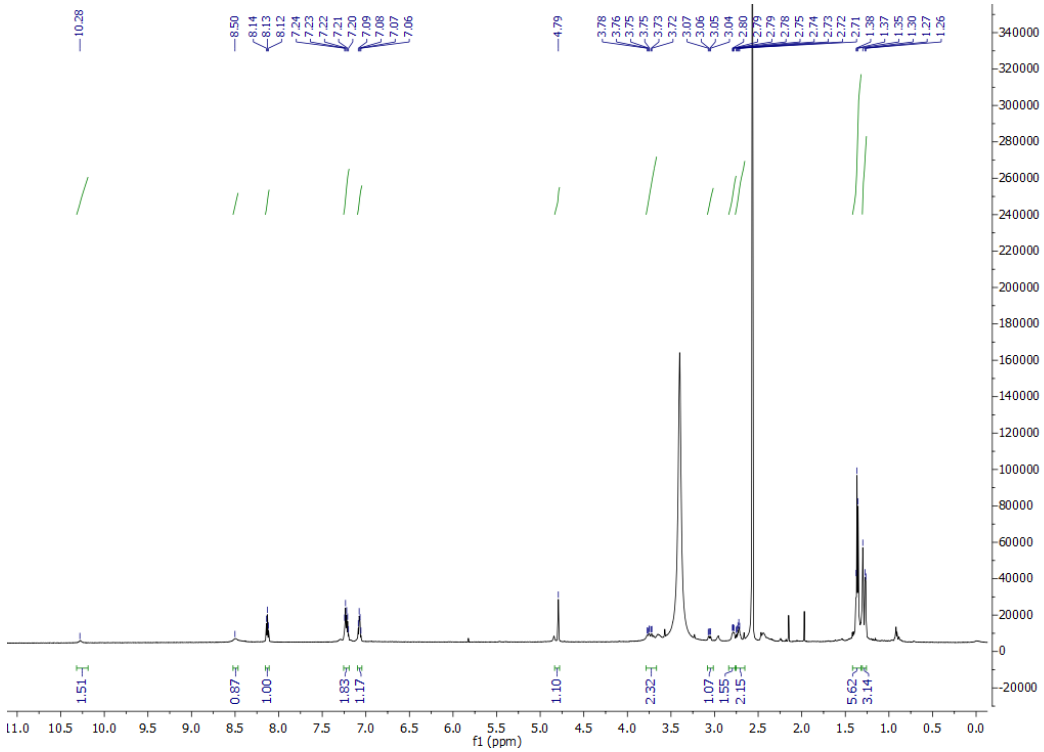

Supporting figure 36. ^{1}H NMR of compound **10b**

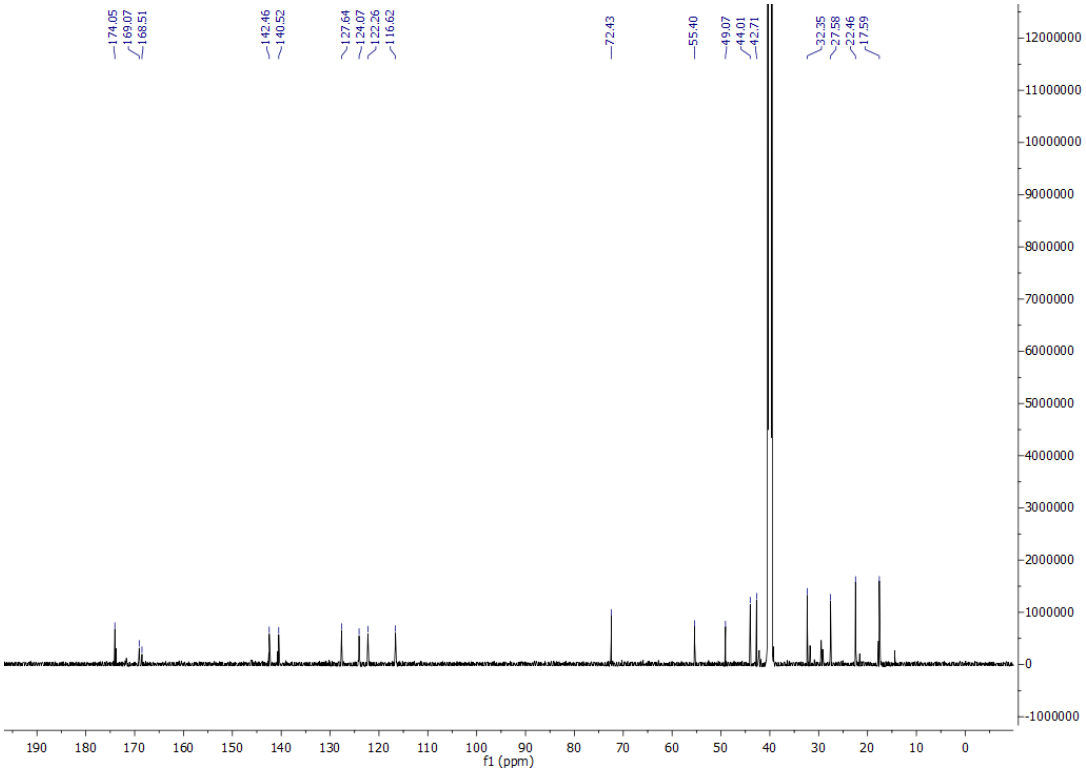

Supporting figure 37. ^{13}C NMR of compound **10b**

(S,S)*-**9b**

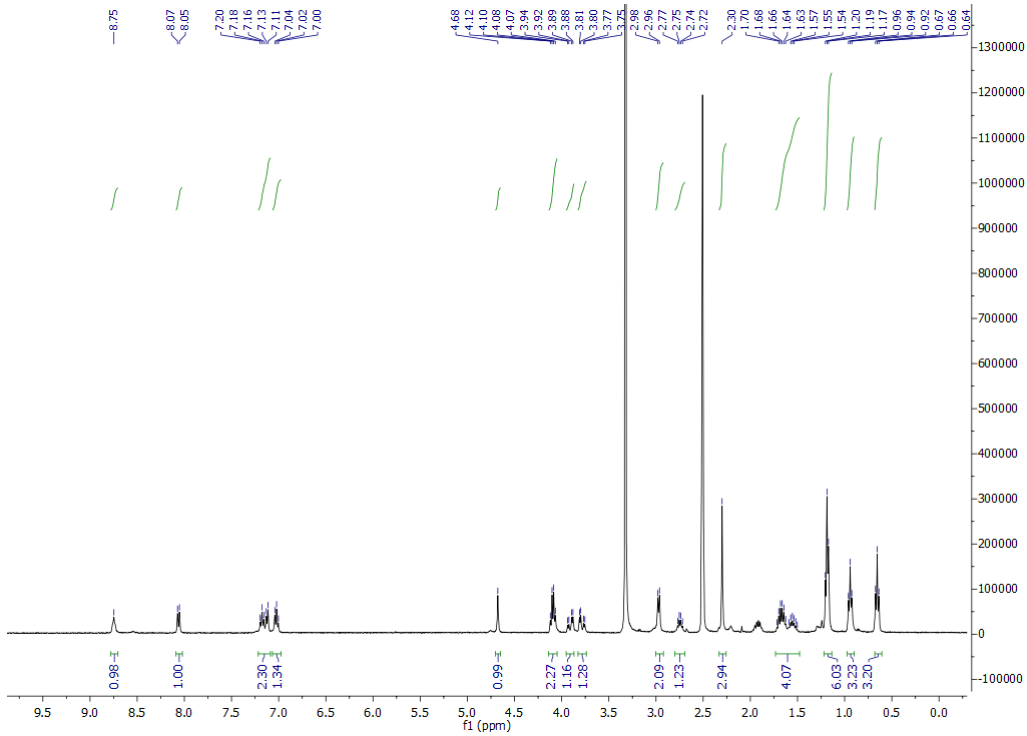

Supporting figure 38. ^{1}H NMR of compound *(S,S*)*-**9b**

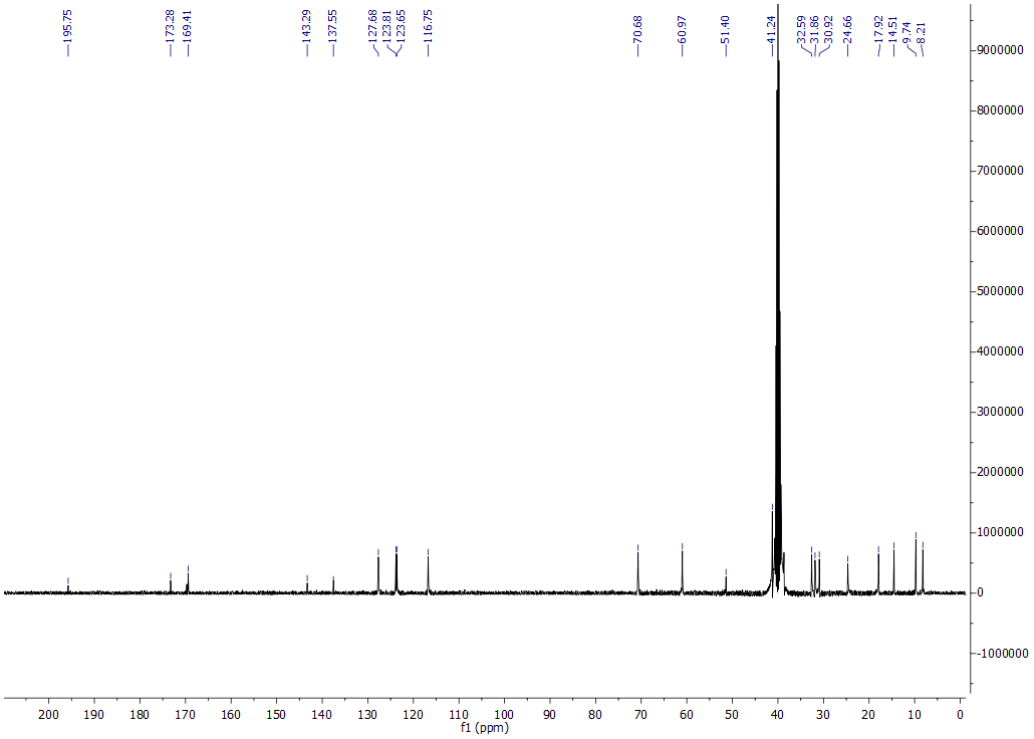

Supporting figure 39. ^{13}C NMR of compound *(S,S*)*-**9b**

(S,R)*-**9b**

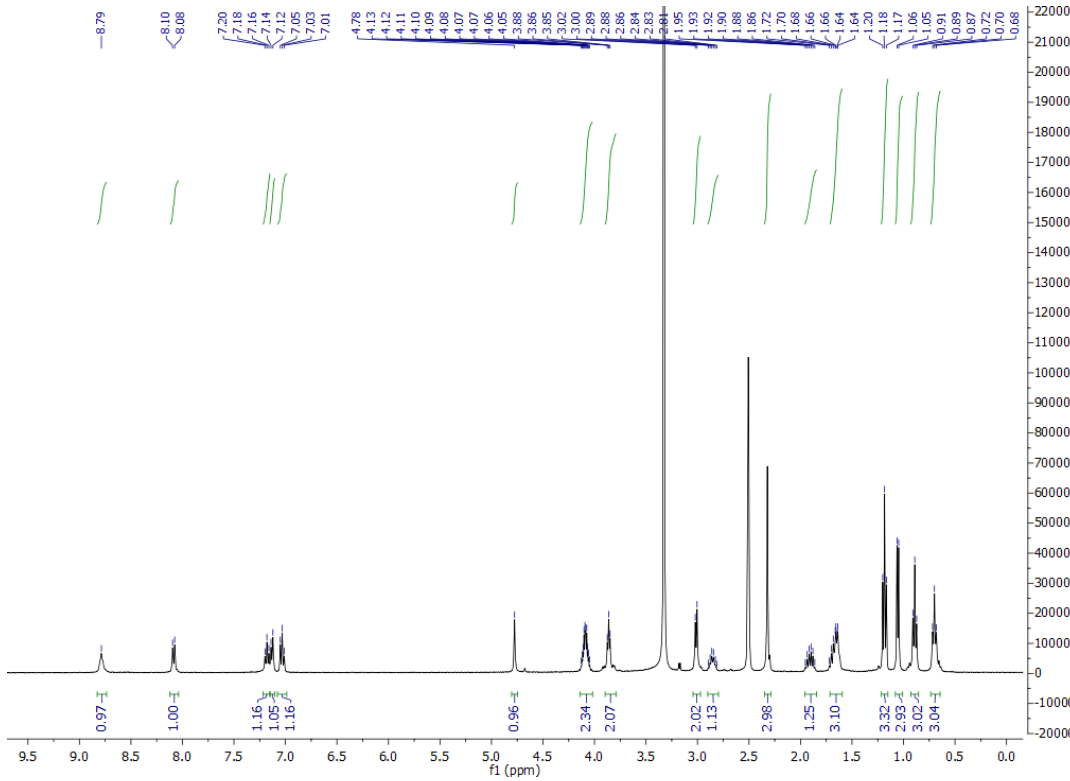

Supporting figure 40. ^{1}H NMR of compound *(S,R*)*-**9b**

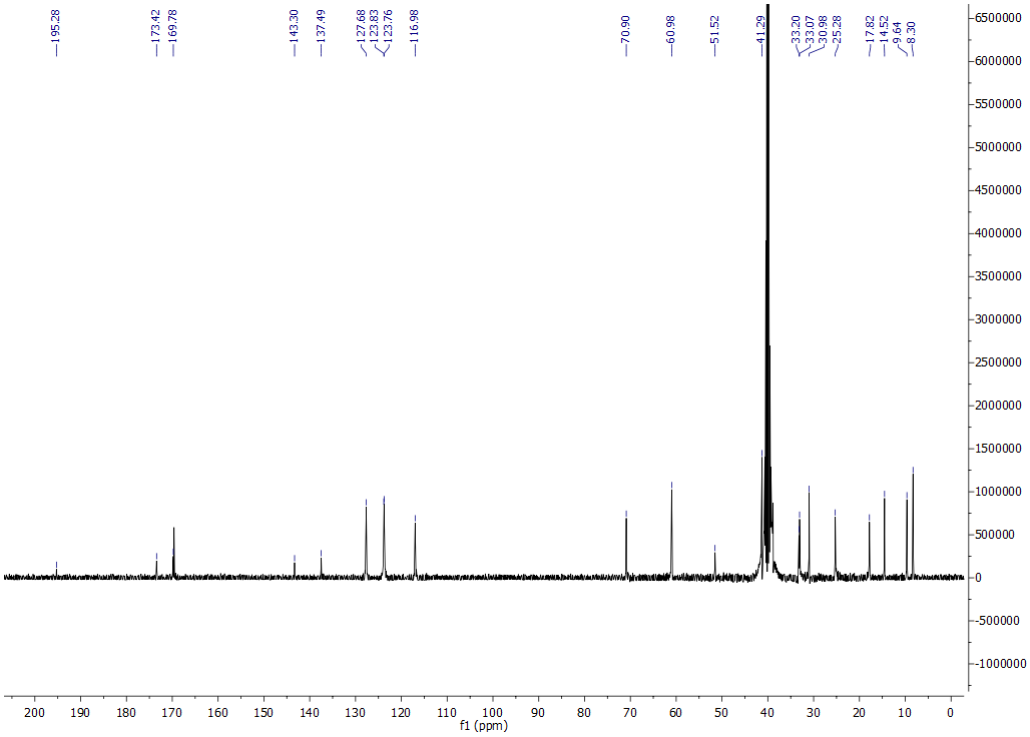

Supporting figure 41. ^{13}C NMR of compound *(S,R*)*-**9b**

10c

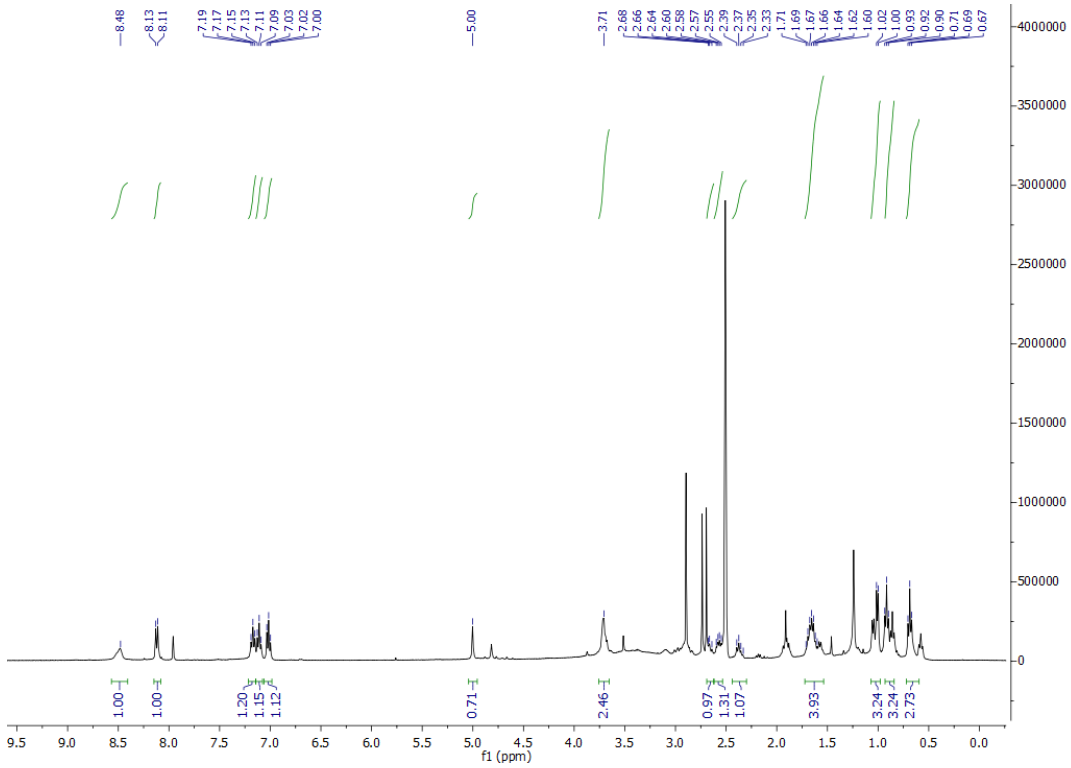

Supporting figure 42. ^{1}H NMR of compound **10c**

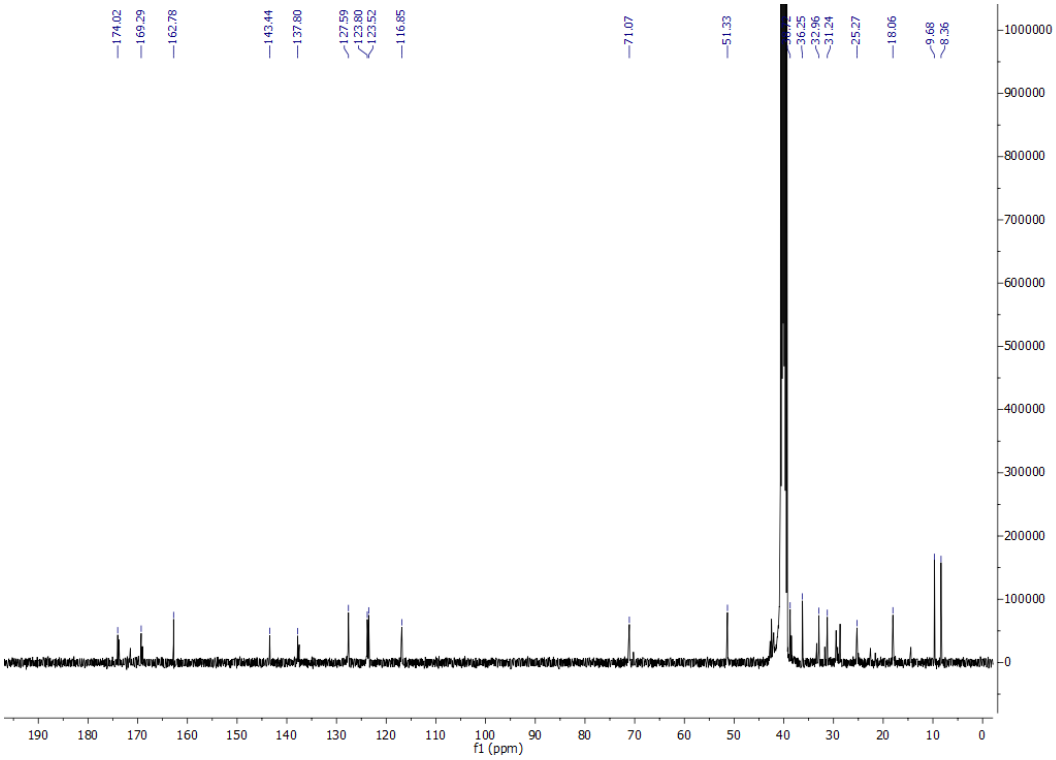

Supporting figure 43. ^{13}C NMR of compound **10c**

10d

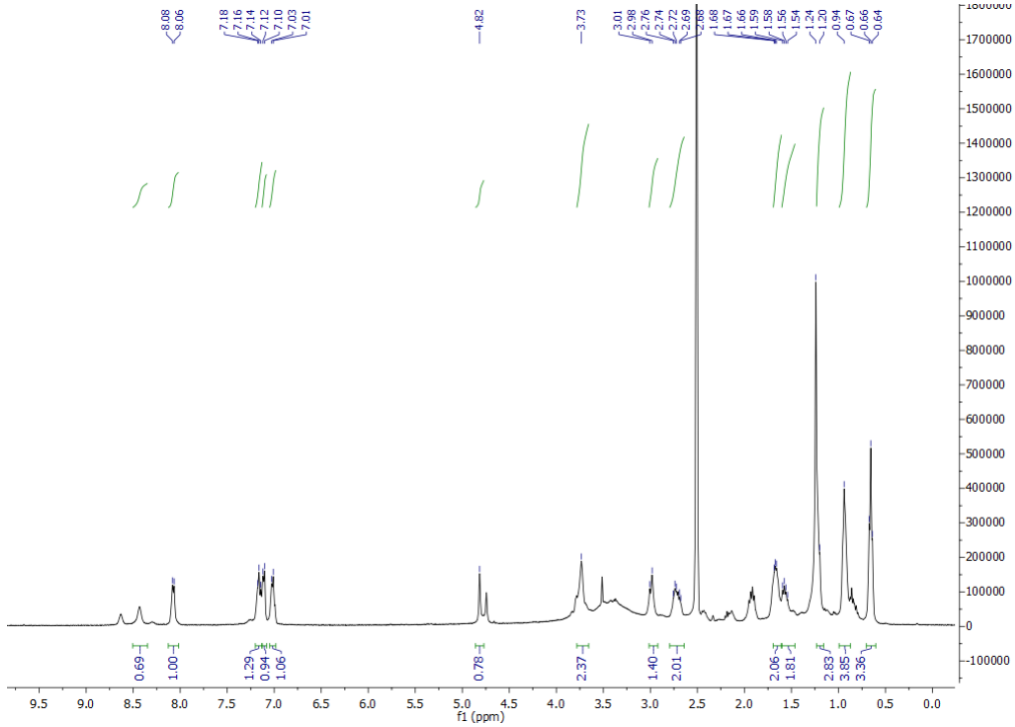

Supporting figure 44. ^{1}H NMR of compound **10d**

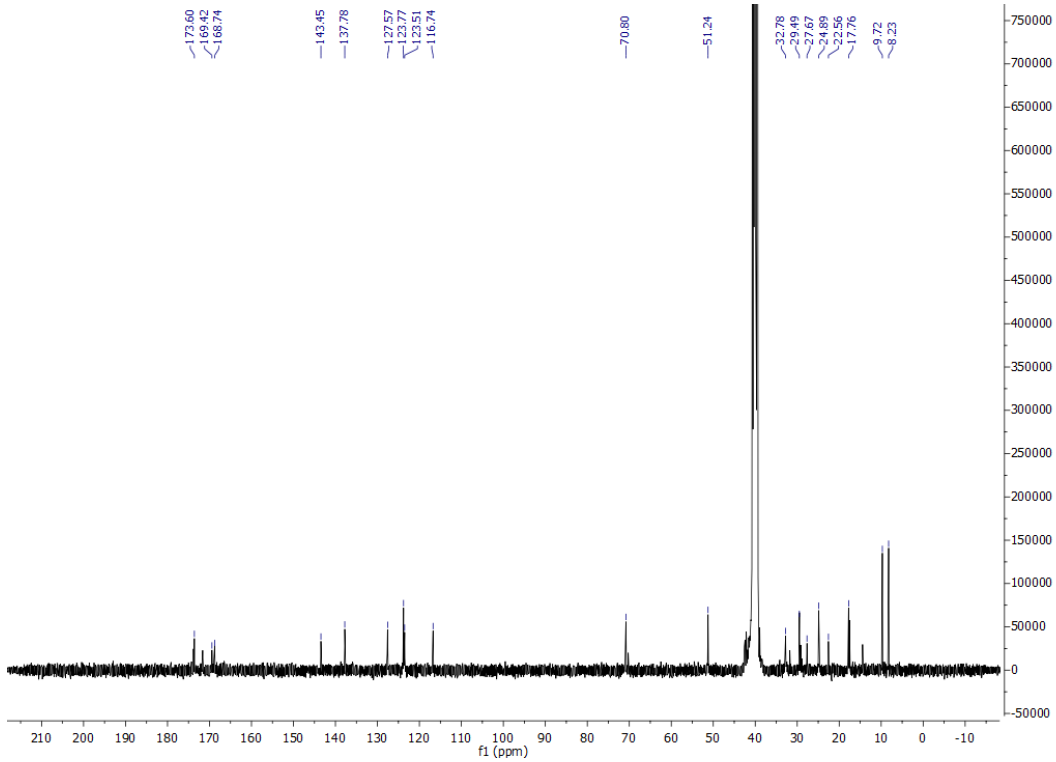

Supporting figure 45. ^{13}C NMR of compound **10d**

References

(1) Brem, J.; van Berkel, S. S.; Zollman, D.; Lee, S. Y.; Gileadi, O.; McHugh, P. J.; Walsh, T. R.; McDonough, M. A.; Schofield, C. *Antimicrob Agents Chemother* **2015**, *60*, 1, 142-50.

(2) Worthington, R. J.; Melander, C. *J. Org. Chem.* **2013**, *78*, 4207.

(3) Klingler, F. M.; Wichelhaus, T. A.; Frank, D.; Cuesta-Bernal, J.; El-Delik, J.; Muller, H. F.; Sjuts, H.; Gottig, S.; Koenigs, A.; Pos, K. M.; Pogoryelov, D.; Proschak, E. *J. Med. Chem.* **2015**, *58*, 3626.

(4) Alfano, A.I.; Zampella, A.; Novellino, E.; Brindisi, M.; Lange, H.; *Reac. Chem Eng.* **2020**, 5, 2091-2100.

(5) Alfano, A. I.; Buommino, E.; Ferraro, M. G.; Irace, C.; Zampella, A.; Lange, H.; Brindisi, M. *ChemMedChem* **2021**, *16*, 3795.

Chapter 7

Flow chemistry applied to photocatalysis (Noël research group)

7.1 Photochemically induced Halogen Atom Transfer

Alkene functionality displays a carbon-carbon double bond (C=C) and it represents one of the most abundant functional groups in nature. The low cost of these feedstock compounds allowed them to be widely utilized in olefin functionalization reactions.[1]

Radical chemistry has been proved during the last 40 years to be one of the main straightforward methods for olefin functionalization towards the production of pharmaceuticals and agrochemicals.[2] Before the awakening of new technologies in chemical engineering.[3-5], the radical chemistry has been underused by chemists because of toxic reagents or initiators and high temperature often required.

Carbon free-radicals generated in radical chemistry, are nucleophilic and can be trapped by various electrophiles. Reductive addition of carbon-centered radicals to electron withdrawing olefins, known as Giese reaction, represents the first radical protocol for the functionalization of olefins (Scheme 1). [6,7]

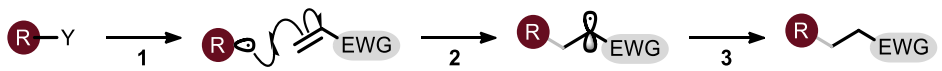

Scheme 1. Mechanism of the Giese reaction.[6,7]

The formation of an alkyl radical generated from different starting materials and with different mechanism (Scheme 1, step 1) allows to subsequent radical addition to the olefin functional group (Scheme 1, step

2). Then, once the free radical is in place, a halogen atom transfer provides the formation of the final products.[8]

In the first step of Giese reaction, but more generally in all radical reactions, the carbon radical can be generated starting from different sources and processes, as already mentioned above, like the Figure 1 exemplifies.

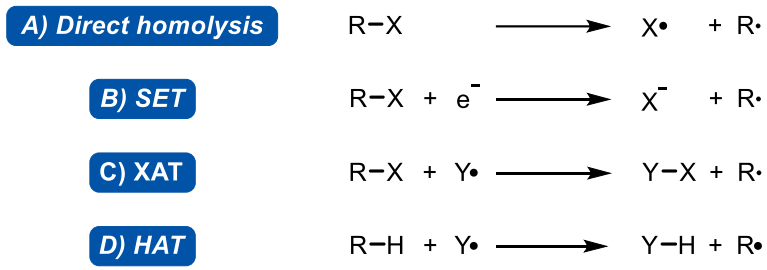

Figure 1. A) Direct homolysis; B) Single electron transfer; C) Halogen atom transfer; D) Hydrogen atom transfer.[9,10]

In the direct homolysis,[11] the R-X bond cleaves homolytically and a carbon-radical is formed (A). Alternatively, during a SET (single electron transfer), the reduction of an organic halide causes a mesolytic cleavage (B).[12] Consequently, a carbon-radical and a negatively charged halide ion are formed. Furthermore, during XAT (halogen atom transfer) process, a halogen abstractor forms a bond with the halogen of a R-X bond, allowing the cleavage and formation of a carbon-radical (C).[13] Lastly, during HAT (hydrogen atom transfer) a radical is formed, after the abstraction of a hydrogen atom by a photocatalyst or an abstractor radical (D).[9]

When the Giese reaction was discovered, organotin hydrides were commonly used for the generation of alkyl radicals.[14]

Scheme 2 shows a classic radical mechanism, with AIBN as initiator, tributyltin hydride and heat.

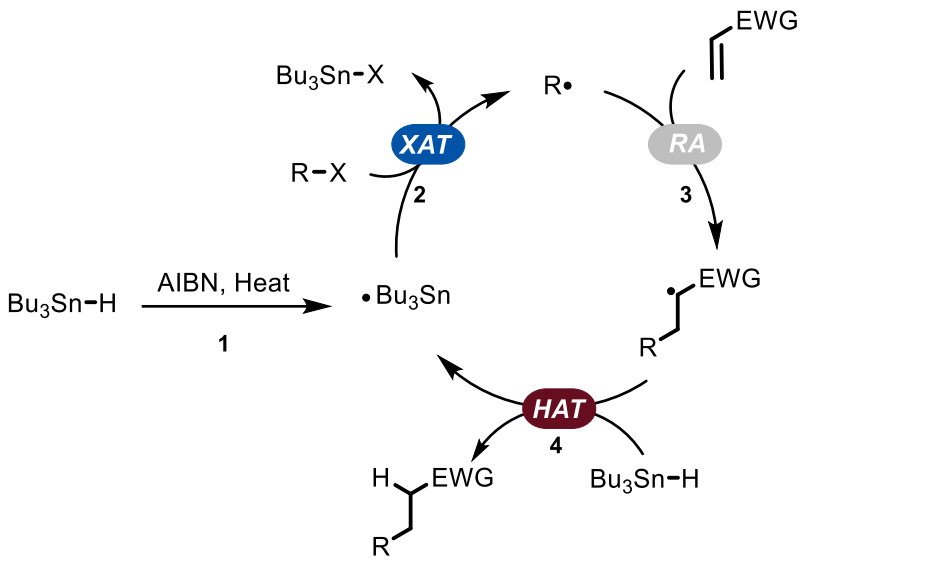

EWG = Electron withdrawing group (e.g. CO_2R, COR, CN . . .)

Scheme 2. Radical mechanism with organotin hydrides.[14]

AIBN and the use of high temperatures allow the formation of an organotin radical (Scheme 2, step 1), that promotes the XAT process in order to generate an alkyl carbon-centered radical (Scheme 2, step 2). The latter undergoes to a radical trap by electron withdrawing olefin, achieving the bond formation between the olefin and the alkyl radical (Scheme 2, step 3). Finally, the last step involves the HAT process, in which a hydrogen atom is abstracted from an organotin hydride molecule achieving the final product.

Certainly, the reaction is a radical chain, having AIBN as radical initiator, that could initiate infinite cycles, also proved by the quantum yield.[15]

$$\Phi\ (\lambda) = \frac{mol\ of\ product\ formed}{mol\ of\ photons\ absorbed}$$

Quantum yield is the ratio between the number of photons emitted and the number of photons absorbed. The quantum yield is reported as a decimal fraction between 0 and 1. When quantum yield >1 the involved mechanism is a radical chain; on the contrary, quantum yield <1 indicates a closed catalytic cycle.

The radical chain mechanism with organotin hydride involves two different processes: XAT and HAT. The rate and the selectivity are determined by polar effects in both cases, that take place surrounding the transition state. In the HAT case, the polar effects are opposite to the XAT one. In fact, the alkyl group (R) in HAT process requires a partial positive charge and the radical a partial negative charge, contrarily to what happens for XAT.

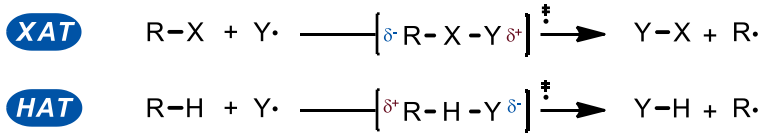

Scheme 3. XAT and HAT reactions.

The need for novel greener and more sustainable reactions, implied a reduced use of organotin hydrides undergoes, due to their high intrinsic toxicity and harsh temperature required, that is certainly not in agreement with the twelve principles of green chemistry.

A valid and more sustainable alternative to organotin hydrides in radical formation was discovered by the group of Chatgilialoglu which proposed the use of tris(trimethylsilyl)silane (TTMS).[16]
The silyl radical generated from HAT reaction on TTMS, can behave as the starting material for further XAT reaction, achieving a stronger bond between silicon and halogen atom.

Another issue in terms of sustainability was represented by the initiator AIBN, required for radical generation. Fortunately, this problem has been overcome by the emergence of photolysis.
Photolysis is a type of chemical reaction involving the splitting from compounds into smaller units upon light absorbance. In contrast to thermal decomposition, photolysis can be performed under mild reaction conditions.
The energy required for cleaving a specific bond by photolysis is equal to its BDE. In the specific case of TTMS, the BDE is 79 kcal/mol.

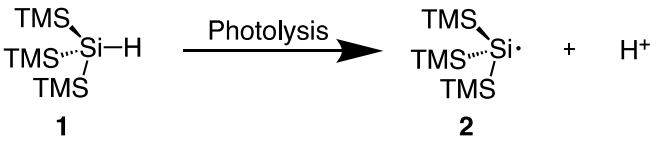

1 **2**

Scheme 4. Photolysis TTMS

During my PhD I had the chance to spent 6 months working in the laboratory of flow-chemistry directed by Professor Timothy Noël, University of Amsterdam. During this time, I worked on project dealing with the study and application of Giese reaction, generating the initial radical by photolysis of the TTMS. The aim was the development of a

simple and straightforward protocol for hydroalkylation of an electron poor olefin with unactivated alkyl bromides.

The optimization was previously tuned in Noël research group, and I was involved on the follow up and scope expansion within this project.

First of all, a screening of solvents, concentrations, light wavelengths, temperatures ed equivalents (Tables 1 and 2) was carried out on cyclohexyl bromide (**4**), a secondary alkyl bromide, and 2-benzylidenemalononitrile (**3**), used as model compounds, in the presence of TTMS. The mixture was flowed in a commercially available Vapourtec reactor, equipped with a 365 nm UV-A lamp.

Table 1. Optimization of the solvent and concentration.

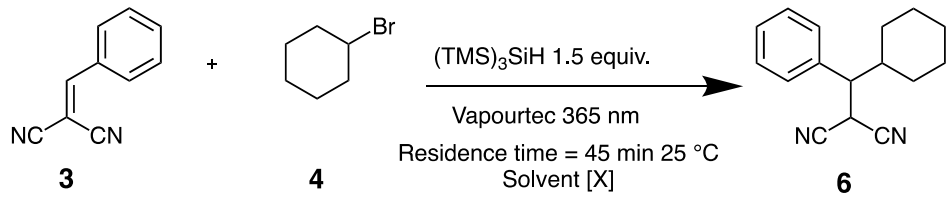

Entry	Solvent	Concentration	Yield (%)
1	MeCN	0.1	7
2	MeCN	0.5	4
3	TFT	0.1	7

4	TFT	0.5	7
5	HFIP	0.1	21
6	Acetone	0.5	7
7	DCM	0.5	7
8	*i*PrOH	0.1	11
10	THF	0.1	8

Table 2. Optimization of the light source, residence time and temperature.

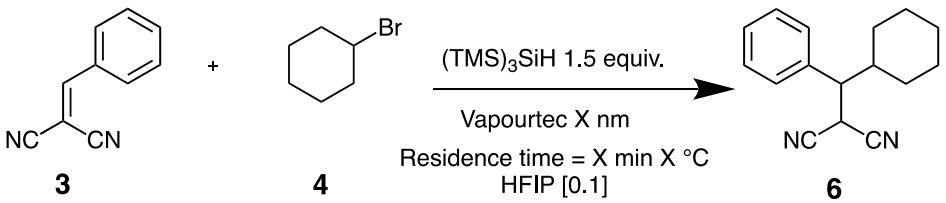

Entry	Light Wavelength	Temperature	τ	Yield (%)
1	365 nm	25	45	21
2	365 nm	25	120	62
3	365 nm	40	45	70
4	405 nm	40	45	27
5	405 nm	25	45	7

6	Dark	50	45	6
7	365 nm	40	60	73
8	365 nm	40	120	73

After a huge optimization (further entries are not present in the tables) the best solvent for the secondary alkyl bromide turned out to be HFIP. The reaction was carried out at 40 °C for 120 min with 1.1 equiv. of TTMS. The use of a standard check valve before the coil in order to ensure the flow in one direction and the back pressure of 2.8 bar at the end of the coil to maintain the pressure of all system, has been necessary.

In order to explore the scope of alkyl bromide, parallelly, a tiny optimization was carried out using 1-bromopropane (**4**), a primary alkyl bromide, as model compound. (Table 3) As primary test, 60 minutes of residence time and 40 °C as temperature were used. Under these conditions (Table 3, Entry 1), the product 2-(1-phenylbutyl)malononitrile (**6**) was obtained with decent results (53% NMR yield, 70% conv.) During the reaction, silyl bromide I is formed as co-product and the direct silylation of the olefin forms side-product II.

Table 3. Optimization with primary alkyl bromide. NMR yields are calculated using TCE as external standard.

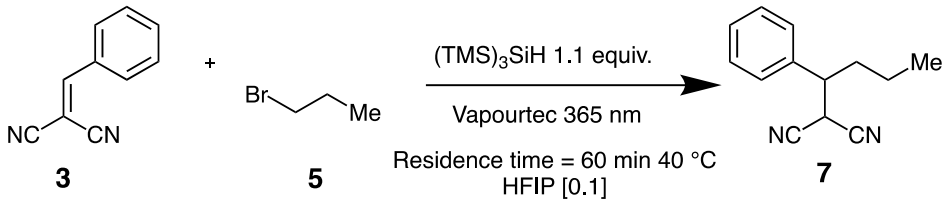

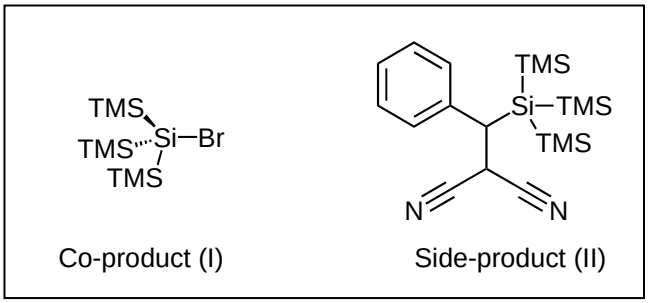

Entry	Variation	Conversion %	**7** NMR yield (%)	**II** NMR yield (%)
1	-	70	53	0%
2	90 min	85	61	4
3	120 min	98	62	11
4	120 min, 1 equiv. of TTMS	93	62	7
5	120 min, 5 equiv. of 5	98	47	12
6	20 min, 850 W	72	21	5
7	120 min, 0.2 M	94	50	15
8	120 min, 0.5 M	64	38	17

The residence time was then increased from 60 minutes to 90 and 120 minutes, leading to an overall improvement in term of yield and conversion (Table 3, Entries 2 and 3). Despite the entry 3 shows nearly full conversion, the product yield remained almost the same with respect to entry 2. Established that 120 minutes could be a good residence time,

we aimed at optimizing other parameters. Unfortunately, disappointing results with respect to the entry 3 were achieved in all other entries, upon modification of equivalents, residence times and concentration (Table 3, Entries 4-8). 1,1,3,3,3-Hexafluoro-2-propanol or HFIP is one of "unconventional solvents". It is corrosive and inflammable, but it is emerging as green and sustainable deep eutectic solvent. (DES). Is quite common the use of HFIP-based aqueous biphasic solvents (ABSs) for microextraction of components from beverages, recycle of food wastes and separation of natural product. [17]

Utilizing the conditions described in entry 3, the scope of primary alkyl bromides has been investigated. (Figure 3).

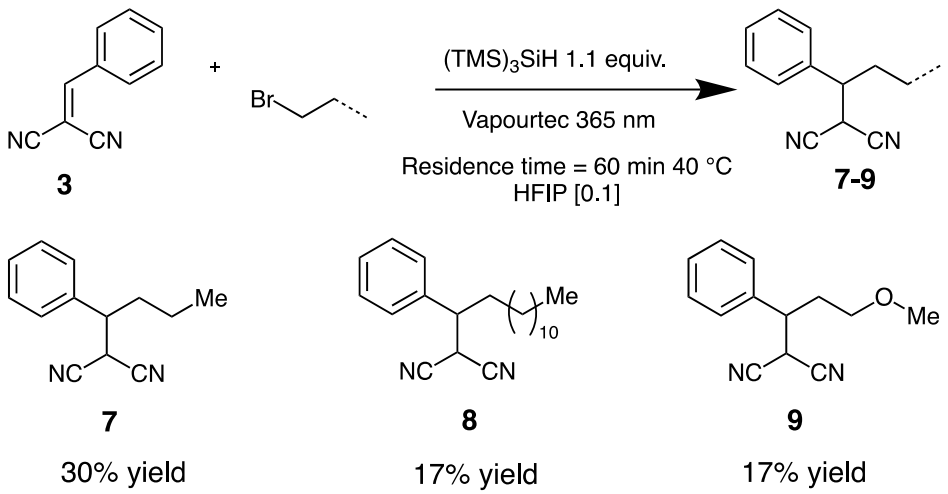

Figure 3. First investigation of primary alkyl bromides.

As figure 3 highlighted, against our expectations, a low NMR yield was obtained when other primary alkyl bromides were tested.

Then, we decided to perform a re-finetuning of the reaction conditions, replacing HFIP with acetonitrile, which, beyond being a greener solvent, led to an improved 65% NMR yield and to a nearly full conversion on the model substrate in 120 minutes (Table 4, Entry 1).

Table 4. Further optimization of primary alkyl bromide.

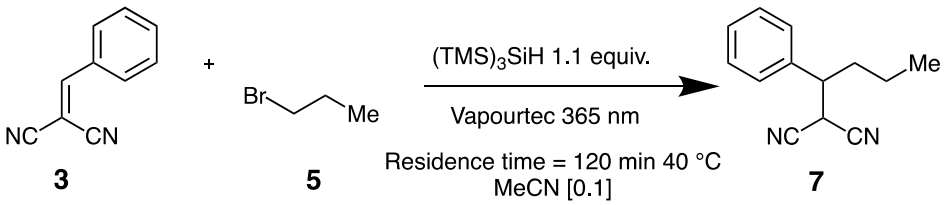

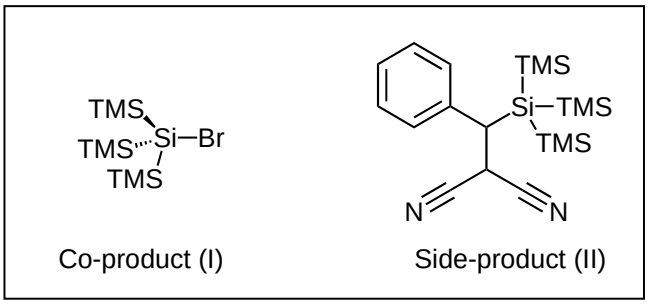

Entry	Variation	Conversion %	**7** NMR yield (%)	**II** NMR yield (%)
1	-	97	65	13
2	90 min	88	64	12
3	2.0 equiv. of 2,6 lutidine	81	43	8

Reducing the time to 90 minutes or adding 2.0 equivalents of 2,6-lutidine, no improvement in term of yield was achieved (Table 4, Entries 2 and 3). In this way, compound **7** was achieved with 65% NMR yield (see below).

Whit the optimized conditions in hands for primary and secondary alkyl bromides, the outcome of tertiary bromides was also interrogated.

Then, we moved to olefins scope, adjusting the conditions for each type of substrates, screening carbonyls, sulfones, amides, and phosphorus containing functional groups.
The overall scope is shown in Figures 4 and 5. A library of 22 compounds, on 5 mmol scale, was generated with yields ranging between 40% and 80%, after chromatographic purification.

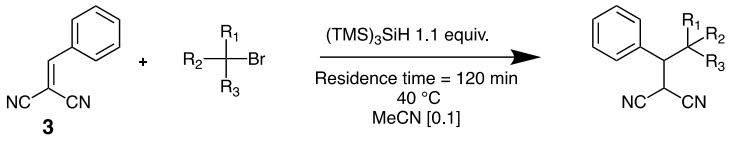

Primary alkyl bromide

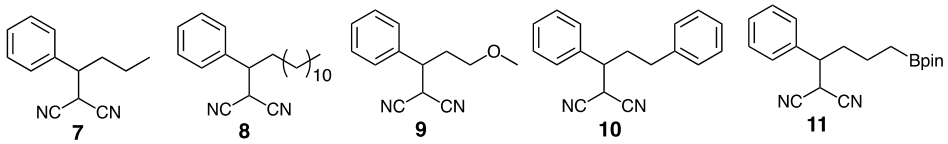

Secondary alkyl bromide

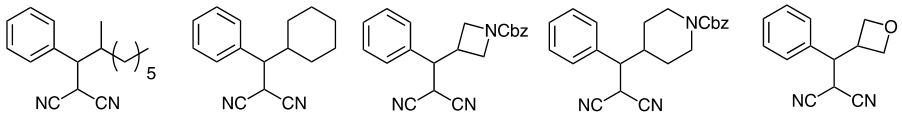

Tertiary alkyl bromide

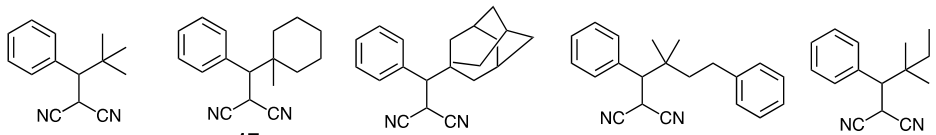

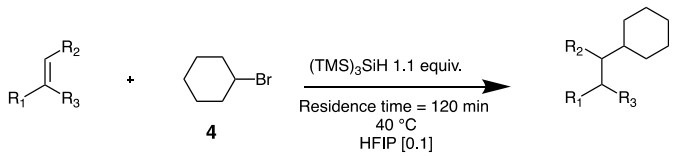

Carbonyl, sulfone, amide

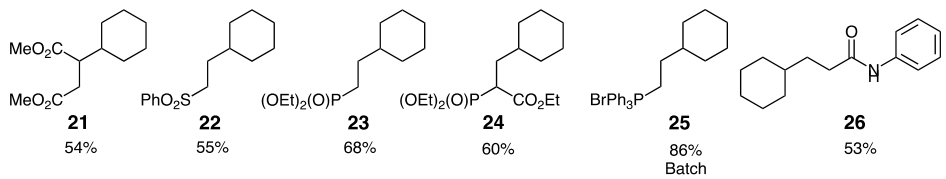

Figure 4. Overall scope

Regarding the substituent effects, all the alkyl bromides (primary, secondary and tertiary) show great activity. Compounds **9** and **15**, containing an oxygen in the structure, gave a lower yield with respect to the ones containing nitrogen. In the compound **12**, two different diasteroisomers were observed, without any kind of selectivity. The lower yield in all the alkyl bromide scoped was achieved with compound **19**, probably due to the longer chain and the bulky aromatic group. About the olefins scope, moderate to good yields were observed in all compounds; the only issue is related to compound **25**, that showed low conversion (45%) with the flow setup, leading us to switch the protocol from flow to batch. Further studies involving the synthesis of natural products and drug-like compounds are ongoing in the Noël

research group.

We decided to use compound **24** for further functionalization, in particular for successive HWE olefination, previously explored in Noël research group.[18] We focused our attention to the introduction of aromatic aldehydes in the second step, without purification of the first intermediate. (27-29)

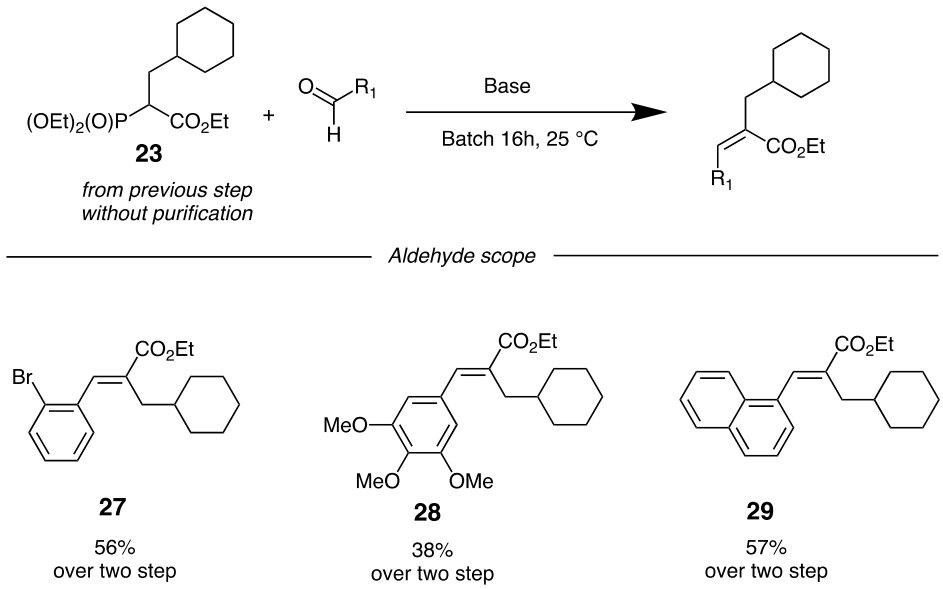

Figure 5. HWE

Moreover, exploiting the advantages of flow chemistry in term of scaling up, we further investigated the scaling up potential of the protocol by increasing the dimension of the reactor coil. A solution of benzylidenemalononitrile (5.00 mmol) *tert*-butyl bromide and $(TMS)_3SiH$ was run in a 20 mL PFA coil (internal diameter 2.0 mm, external diameter 3.0 mm) and product **6** was obtained with 71% yield.

About the mechanism of photocatalytic cycle (Figure 6), studies are still ongoing in the Noël research lab, but a plausible mechanism can be hypothesized, based on the photolytic cleavage of TTMS. In the first step, the Si-H bond is homoltically cleaved by photolysis (Figure 6, step 1). Upon formation of the radical, a XAT step takes place forming a more stable Si-Br bond and prompting the formation of a radical on the alkyl compound (Figure 5, step 2). Consequently, the alkyl radical is trapped by electron-poor olefin, allowing the formation of another radical (Figure 5,

step 3). Lastly, the hydrogen of TTMS molecule is abstracted through HAT reaction (Figure 5, step 4). The latter step enables the propagation of the radical process, justifying the radical chain.

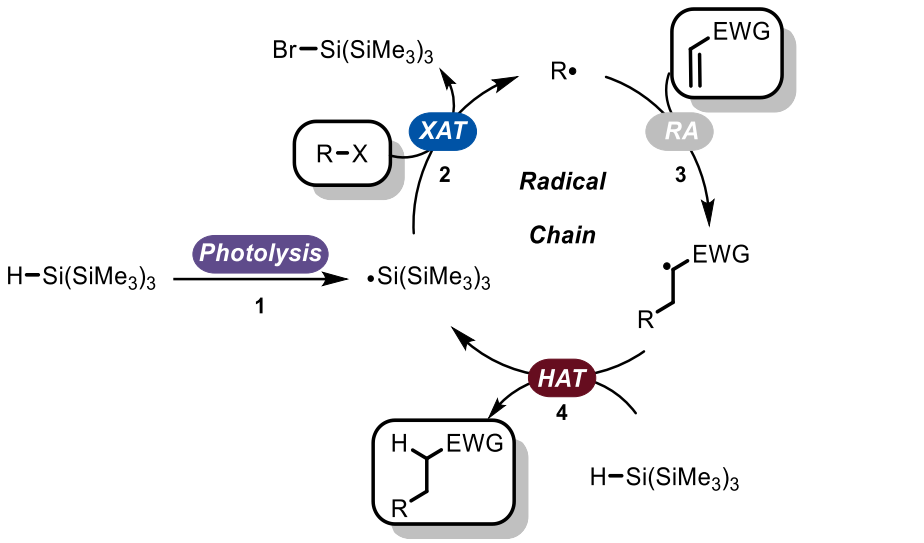

Figure 6. Proposed mechanism of Giese reaction

For further studies, systematic measurements of the absorption properties of all the components of the reaction have been conducted (Figure 7).

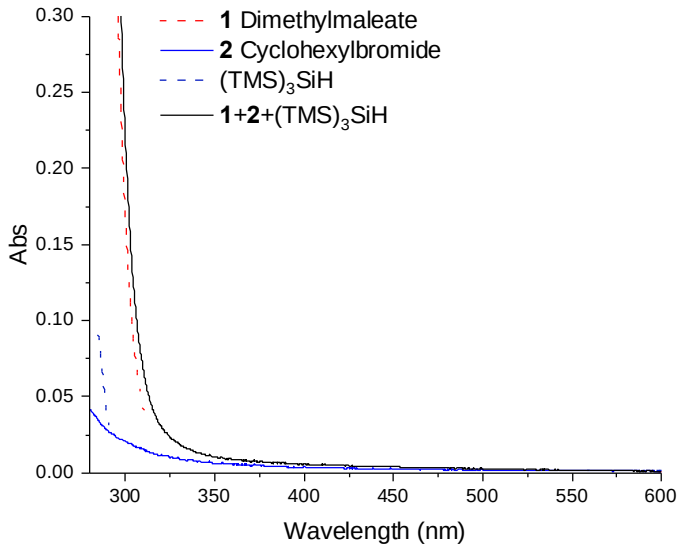

Figure 7. Absorption spectrum.

Figure 7 highlighted similar absorption of both the alkyl bromide and the tris(trimethylsilyl)silane at 365 nm. As a result of the similarity in absorbance, the photolysis of the alkyl bromide should also be taken into account with regards to the mechanism. Further studies, as mentioned above, are still ongoing.

7.1.1 Experimental Part

General information

^{1}H (300 and 400 MHz), ^{13}C (75 and 101 MHz) and ^{19}F (282 and 376 MHz) spectra were recorded at ambient temperature using Bruker AV 300-I, AV 400. ^{1}H NMR spectra are reported in parts per million (ppm) downfield relative to $CDCl_3$ (7.26 ppm) and all ^{13}C NMR spectra are reported in ppm relative to $CDCl_3$ (77.16 ppm) unless stated otherwise. The multiplicities of signals are designated by the following abbreviations: s (singlet), d (doublet), t (triplet), q (quartet), m (multiplet), dd (doublet of doublets), dt (doublet of triplets), td (triplet of doublets), ddd (doublet of doublet of doublets). Coupling constants (J) are reported in hertz (Hz). NMR data was processed using the MestReNova 14 software package. High resolution mass spectra (HRMS) were collected on an AccuTOF LC, JMS-T100LP Mass spectrometer (JEOL, Japan) or on an AccuTOF GC v 4g, JMS-T100GCV Mass spectrometer (JEOL, Japan). Disposable syringes were purchased from Laboratory Glass Specialist. Syringe pumps were purchased from Chemix Inc. model Fusion 200 Touch. Product isolation was performed manually, using silica (P60, SILICYCLE). TLC analysis was performed using Silica on aluminum foils TLC plates (F254, SILICYCLE) with visualization under ultraviolet light (254 nm and 365 nm) or appropriate TLC staining (Potassium Permanganate). Organic solutions were concentrated under reduced pressure on a Büchi rotary evaporator (in vacuo at 40 ºC, ~5 mbar).

UV-Vis spectra were recorded with a double beam spectrophotometer Shimadzu UV2700 equipped with a deuterium lamp (190-350 nm), a halogen lamp (330-900 nm) and a photomultiplier (Hamamatsu R928). Measurements were performed in a quartz cuvette (optical path: 1 cm). All

spectra were recorded in CH_3CN (solvent cutoff: 190 nm) in quartz cuvettes (optical path: 1 cm) with a bandwidth of 5 nm and a data pitch of 1 nm.

Luminescence spectra were recorded with a Horiba Fluorolog-3 equipped with a 450W Xenon lamp and a photomultiplier (Hamamatsu R636). Measurements were performed in a quartz cuvette (optical path: 1 cm) sealed with a rubber septum. The solution was bubbled with N_2 for 10 minutes before irradiation at 362 nm (A = 0.1). The slits of the excitation monochromator were kept at 10 nm, while those of the emission monochromator at 5 nm. Integration time was 0.1 s, each spectrum is an average of 2 acquisitions with a data pitch of 1 nm. A long-pass filter was used to minimize the intensity of the Raman band. The nature of the latter was verified by observing its shift by changing the excitation wavelength (data not shown).

Nanosecond transient absorptions were recorded with an in-house assembled setup. An excitation wavelength of 319 nm was used. The excitation wavelength of 319 nm was generated using a tunable Nd:YAG-laser system (NT342B, Ekspla) comprising the pump laser (NL300) with harmonics generators (SHG, THG) producing 355 nm to pump an optical parametric oscillator (OPO) with SHG connected in a single device. The laser system was operated at a repetition rate of 5 Hz with a pulse length of 5 ns. The probe light running at 10 Hz was generated by a high-stability short arc xenon flash lamp (FX-1160, Excelitas Technologies) using a modified PS302 controller (EG&G). Using a 50/50 beam splitter, the probe light was split equally into a signal beam and a reference beam and focused on the entrance slit of a spectrograph (SpectraPro-150, Princeton Instruments) with a grating of 150 ln/mm blaze at 500nm. The probe beam (A = 1 mm^2) was passed through the sample cell and orthogonally

overlapped with the excitation beam on a 1 mm × 1 cm area. The excitation energy was recorded by measuring the excitation power at the back of an empty sample holder. In order to correct for fluctuations in the flash lamp spectral intensity, the reference was used to normalize the signal. Both beams were recorded simultaneously using a gated intensified CCD camera (PI-MAX3, Princeton Instruments) which has an adjustable gate of minimal 2.9 ns (20 ns were used). Two delay generators (DG535 and DG645, Stanford Research Systems, Inc.) were used to time the excitation pulse, and to change the delay of the flash lamp and gate of the camera during the experiment. The setup was controlled by an in-house written Labview program.

For the reactions performed in batch, we have used a homemade, 3D-printed reactor. The reactor was designed to fit reaction vials and to be equipped with a Kessil lamp. The reactor was designed in Adobe Inventor 2021 with 4 different parts. The lid (100mm x 12mm) is designed to host up to 8 reactions vials and holds the Kessil lamp in the center (Figure S1A). The box is designed with holes to allow the air flow to escape the reactor and keep the temperature stable (Figure S1B), as measured by an external thermometer. A reflector is situated underneath the lamp and reflects the photons inside the box to have a light distribution as homogeneous as possible (Figure S1C). A fan is glued on the bottom to provide an air flow while keeping light from escaping the system. Finally, the stirring plate adapter (Figure S1D) was added to fix the system on a stirring plate and provide homogeneous stirring (Figure S1E). It also spaces the reflector from the plate to ensure a continuous air flow from the top to the bottom of the system. All the inside surfaces were covered with reflective tape. An overview of the assembled reactor is shown in Figure S2.

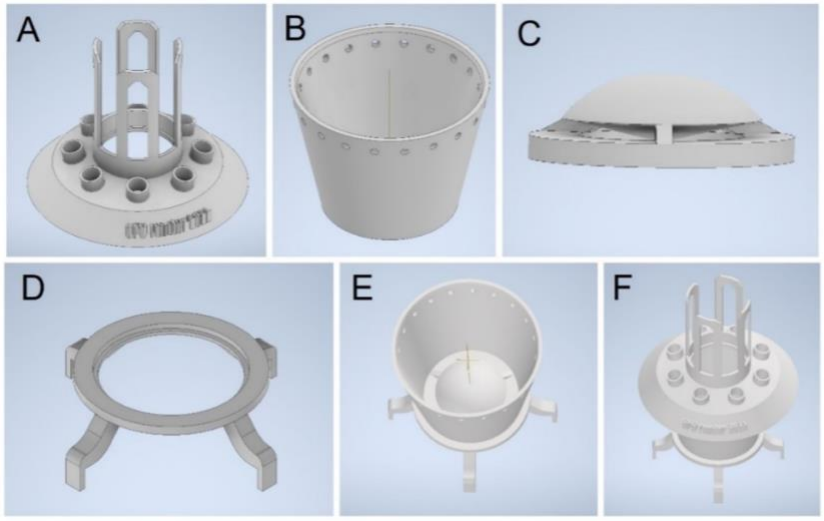

Figure S1 Overview of the 3D-printed reactor.

Figure S2 Pictures of the assembled reactor equipped with a Kessil lamp (365 nm).

For reaction performed in flow, a Vapourtec device with a UV-150 photochemical reactor was used, equipped with 16 W 365 nm LED. The temperature of the photochemical chamber was kept constant at 40 °C.



For the scale-up the set up was the same except for the coil, that has been replaced by a two layers coil (V = 20 mL, internal diameter 2.0 mm, external diameter 3.0 mm).

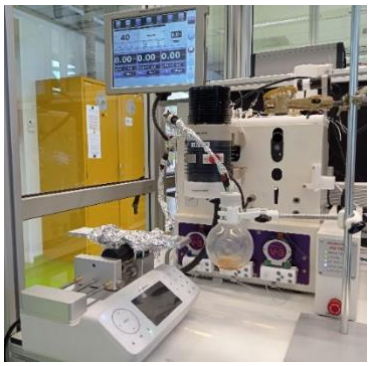

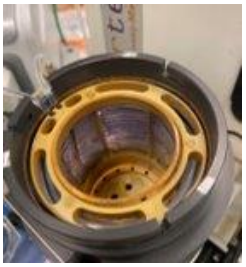

General procedure A

To a flame-dried nitrogen-purged screw-capped vial, fitted with a rubber septum, charged with the electron poor olefin (0.5 mmol, 1 equiv.) in HFIP (5 mL, 0.1 M), the alkyl bromide derivative (1.25 mmol, 2.5 equiv.) and

$(TMS)_3SiH$ (170 μL, 0.550 mmol, 1.1 equiv.) were added. Subsequently, the solution was sparged with nitrogen for 30 seconds and the reaction vessel was sealed with parafilm. This solution was taken with a 6 mL syringe (12.4 mm inner diameter), positioned on a syringe pump and connected to a Vapourtec UV-150 reactor, equipped with a 10 mL PFA coil prefilled with CH_3CN (internal diameter 1.3 mm, external diameter 1.6 mm), and with a check valve and a back-pressure regulator (2.8 psi) as shown in Figure S3. The solution was pumped, unless differently specified, with a total flow rate of 0.083 mL min^{-1} and collected at the end of the reactor. The solvent of the resulting reaction mixture was removed under reduced pressure and purification by flash column chromatography on silica gel gave the corresponding products in the stated yield.

General procedure B

To a flame-dried nitrogen-purged screw-capped vial, fitted with a rubber septum, charged with the electron poor olefin (0.5 mmol, 1 equiv.) in dry CH_3CN (5 mL, 0.1 M), the alkyl bromide derivative (1.25 mmol, 2.5 equiv.) and $(TMS)_3SiH$ (170 μL, 0.550 mmol, 1.1 equiv.) were added. Subsequently, the solution was sparged with nitrogen for 30 seconds and the reaction vessel was sealed with parafilm. This solution was taken with a 6 mL syringe (12.4 mm inner diameter), positioned on a syringe pump and connected to a Vapourtec UV-150 reactor, equipped with a 10 mL PFA coil prefilled with CH_3CN (internal diameter 1.3 mm, external diameter 1.6 mm), and with a check valve and a back-pressure regulator (2.8 psi) as shown in Figure S3. The solution was pumped, unless differently specified, with a total flow rate of 0.083 mL min^{-1} and collected at the end of the reactor. The solvent of the resulting reaction mixture was removed under reduced pressure and purification by flash column

chromatography on silica gel gave the corresponding products in the stated yield.

General procedure C

To a flame-dried nitrogen-purged screw-capped vial, fitted with a rubber septum, charged with the electron poor olefin (0.5 mmol, 1 equiv.) in dry CH_3CN (5 mL, 0.1 M), the alkyl bromide derivative (1.25 mmol, 2.5 equiv.), $(TMS)_3SiH$ (170 μL, 0.550 mmol, 1.1 equiv.) and 2,6-lutidine (116 μL, 1.00 mmol, 2.0 equiv.) were added. Subsequently, the solution was sparged with nitrogen for 30 seconds and the reaction vessel was sealed with parafilm. This solution was taken with a 6 mL syringe (12.4 mm inner diameter), positioned on a syringe pump and connected to a Vapourtec UV-150 reactor, equipped with a 10 mL PFA coil prefilled with CH_3CN (internal diameter 1.3 mm, external diameter 1.6 mm), and with a check valve and a back-pressure regulator (2.8 psi) as shown in Figure S3. The solution was pumped, unless differently specified, with a total flow rate of 0.083 mL min^{-1} and collected at the end of the reactor. The solvent of the resulting reaction mixture was removed under reduced pressure and purification by flash column chromatography on silica gel gave the corresponding products in the stated yield.

General Procedure D (Fed batch)

To a flame-dried nitrogen-purged screw-capped vial, fitted with a rubber septum, charged with the electron poor olefin (0.5 mmol, 1 equiv.) in dry CH_3CN (5 mL, 0.1 M), the alkyl bromide derivative (1.25 mmol, 2.5 equiv.) and $(TMS)_3SiH$ (170 μL, 0.550 mmol, 1.1 equiv.) were added. Subsequently, the solution was sparged with nitrogen for 30 seconds and the reaction vessel was sealed with parafilm. This solution was taken with

a 6 mL syringe (12.4 mm inner diameter), positioned on a syringe pump and connected to a Vapourtec UV-150 reactor, equipped with a 10 mL PFA coil prefilled with CH_3CN (internal diameter 1.3 mm, external diameter 1.6 mm), and with a check valve and a back-pressure regulator (2.8 psi). The solution was pumped, unless differently specified, with a total flow rate of 0.083 mL min^{-1}.

Parallelly, in an oven-dried vial an aldehyde derivative (1.5 mmol, 3 equiv.) was dissolved in dry THF (250 μL) under inert atmosphere. Before the first drop of the outflow of the photoreactor entered in contact with the aldehyde solution, LiOtBu 1 M in dry THF (1.50 mL, 1.5 mmol, 3 equiv.) was added. After the whole reaction mixture reached the vial, the solution was kept stirring at room temperature for the indicated time. The solvent of the resulting reaction mixture was removed under reduced pressure and purification by flash column chromatography on silica gel gave the corresponding products in the stated yield.

General procedure for the scale up

To an oven dried flask, fitted with a rubber septum, charged with benzylidenemalononitrile (770.8 mg, 5.00 mmol, 1 equiv.) in CH_3CN (50 mL, 0.1 M), tert-butyl bromide (1.4 ml, 12.50 mmol, 2.5 equiv.) and $(TMS)_3SiH$ (1.70 ml, 5.500 mmol, 1.1 equiv.) were added. Subsequently, the solution was sparged with nitrogen for less than 1 minute and the vessel was sealed with parafilm. This solution was taken with a 50 mL syringe (28.9 mm inner diameter), positioned on a syringe pump and connected to Vapourtec UV-150 equipped with a 20 mL PFA coil prefilled with CH_3CN (internal diameter 2.0 mm, external diameter 3.0 mm), and with a check valve and a back-pressure regulator (2.8 psi). The solution was pumped with a total flow rate of 0.166 mL min^{-1} and collected at the end of the

reactor. The solvent of the resulting reaction mixture was removed under reduced pressure and purification by flash column chromatography on silica gel (100% pentane to pentane 8:2 Et_2O) to afford product **6** (755 mg, 71% yield) as a colourless oil.

Compounds characterization

2-(cyclohexyl(phenyl)methyl)malononitrile (**6**) Prepared according to general procedure A, using cyclohexyl bromide (154 µL, 1.25 mmol, 2.5 equiv.) and benzylidenemalononitrile (77.1 mg, 0.5 mmol, 1 equiv.). The crude mixture was purified by flash column chromatography (100% pentane to pentane 9:1 Et_2O, two consecutive runs) to afford product **6** (86 mg, 72% yield) as a colorless oil. The spectroscopic data are consistent with those reported previously.[19]

^{1}H NMR (400 MHz, Chloroform-d) δ 7.45 – 7.34 (m, 3H), 7.34 – 7.28 (m, 2H), 4.19 (d, J = 5.5 Hz, 1H), 2.89 (dd, J = 9.8, 5.5 Hz, 1H), 2.02 (dtd, J = 14.5, 11.2, 3.4 Hz, 1H), 1.93 (dt, J = 12.3, 3.3 Hz, 1H), 1.87-1.80 (m, 1H), 1.73 – 1.61 (m, 2H), 1.53 – 1.42 (m, 1H), 1.37 (tt, J = 12.8, 3.6 Hz, 1H), 1.29 – 0.99 (m, 3H), 0.90 – 0.75 (m, 1H).

^{13}C NMR (101 MHz, Chloroform-d) δ 136.7, 129.1, 128.7, 128.3, 112.3, 112.0, 52.3, 39.2, 31.2, 30.6, 27.1, 25.9, 25.8, 25.7.

2-(1-phenylbutyl)malononitrile (**7**)

Prepared according to procedure B, using 1-bromopropane (154 mg, 1.25 mmol, 2.5 equiv) and benzylidenemalononitrile (77.1 mg, 0.5 mmol, 1 equiv.). The crude mixture was purified by flash column chromatography (pentane 100% to pentane 9:1 Et_2O) to afford **7** (61.5 mg, 62% yield) asa pale yellow oil. The spectroscopic data are consistent with those reported previously.[20]

^{1}H NMR (400 MHz, Chloroform-d) δ 7.46 – 7.27 (m, 5H), 3.87 (d, J = 6.3 Hz, 1H), 3.29 – 3.14 (m, 1H), 2.06 – 1.92 (m, 2H), 1.36 – 1.18 (m, 2H), 0.93 (t, J = 7.4 Hz, 3H).
^{13}C NMR (101 MHz, Chloroform-d) δ 136.8, 129.3, 128.9, 127.8, 111.94, 111.92, 46.4, 34.2, 30.3, 20.2, 13.6.

2-(1-phenyltridecyl)malononitrile (**8**)

Prepared according to procedure B, using 1-bromodocecane (312 mg, 1.25 mmol, 2.5 equiv.) and benzylidenemalononitrile (77.1 mg, 0.5 mmol, 1 equiv.). The crude mixture was purified by flash column chromatography (toluene 100% to toluene 9:1 pentane) to afford **8** (82.7 mg, 50% yield) as a pale yellow oil. This compound was previously unreported.
^{1}H NMR (400 MHz, Chloroform-d) δ 7.44 – 7.33 (m, 3H), 7.34 – 7.28 (m, 2H), 3.87 (d, J = 6.2 Hz, 1H), 3.24 – 3.13 (m, 1H), 2.06 – 1.92 (m, 2H), 1.35 – 1.18 (m, 20H), 0.88 (t, J = 6.7 Hz, 3H).
^{13}C NMR (101 MHz, Chloroform-d) δ 136.97, 129.42, 129.00, 127.96, 112.06, 46.75, 32.24, 32.04, 30.40, 29.84, 29.75, 29.67, 29.59, 29.47, 29.38, 29.26, 27.09, 22.82, 14.26.
HRMS (FI) m/z calcd for: C22H32N2 324.2565, found 324.2565.

2-(3-methoxy-1-phenylpropyl)malononitrile (**9**)

Prepared according to procedure C, using 1-bromo-2-methoxyethane (174 mg, 1.25 mmol, 2.5 equiv.) and benzylidenemalononitrile (77.1 mg, 0.5 mmol, 1 equiv.). The crude mixture was purified by flash column chromatography (pentane 100% to pentane 8:2 Et_2O) to afford **9** (50.3 mg, 46% yield) as a pale yellow oil. This compound was previously unreported.

^{1}H NMR (400 MHz, Chloroform-d) δ 7.46 – 7.36 (m, 3H), 7.36 – 7.29 (m, 2H), 4.25 (d, J = 6.0 Hz, 1H), 3.50 – 3.41 (m, 2H), 3.33 – 3.23 (m, 4H), 2.39 – 2.26 (m, 1H), 2.19 – 2.06 (m, 1H).

^{13}C NMR (101 MHz, Chloroform-d) δ 136.7, 129.2, 128.9, 127.9, 112.2, 112.0, 69.5, 58.8, 44.0, 32.2, 29.7.

HRMS (FI) m/z calcd for: C13H14N2O 214.1106, found 214.1106.

2-(1,3-diphenylpropyl)malononitrile (**10**)

Prepared according to procedure B, using (2-bromoethyl)benzene (231 mg, 1.25 mmol, 2.5 equiv.) and benzylidenemalononitrile (77.1 mg, 0.5 mmol, 1 equiv.). The crude mixture was purified by flash column chromatography (pentane 100% to pentane 9:1 Et_2O) to afford **10** (81.1 mg, 63% yield) as a pale yellow oil. This compound was previously unreported.

^{1}H NMR (300 MHz, Chloroform-d) δ 7.68 – 7.27 (m, 10H), 4.03 (d, J = 6.2 Hz, 1H), 3.43 – 3.30 (m, 1H), 2.91 – 2.75 (m, 1H), 2.71 – 2.60 (m, 1H), 2.59 – 2.47 (m, 2H).

^{13}C NMR (75 MHz, Chloroform-d) δ 139.9, 136.2, 129.5, 129.1, 128.7, 128.4, 128.0, 126.5, 111.8, 111.7, 45.6, 33.5, 32.7, 30.4.

HRMS (FI) m/z calcd for: C18H16N2 260.1313, found 260.1313.

2-(3-bromopropyl)-4,4,5,5-tetramethyl-1,3,2-dioxaborolane (**11**)

Prepared according to procedure B, using 2-(3-bromopropyl)-4,4,5,5-tetramethyl-1,3,2-dioxaborolane (311 mg, 1.25 mmol, 2.5 equiv.) and benzylidenemalononitrile (77.1 mg, 0.5 mmol, 1 equiv.). The crude mixture was purified by flash column chromatography (pentane 100% to pentane 9:1 Et_2O) to afford **11** (85.0 mg, 52% yield) as a pale yellow oil. This compound was previously unreported.

^{1}H NMR (300 MHz, Chloroform-d) δ 7.46 – 7.34 (m, 3H), 7.34 – 7.26 (m, 2H), 3.89 (d, J = 6.1 Hz, 1H), 3.33 – 3.14 (m, 1H), 2.08 – 1.95 (m, 2H), 1.47 – 1.18 (m, 13H), 0.89 – 0.71 (m, 2H).

^{13}C NMR (75 MHz, Chloroform-d) δ 136.8, 129.2, 128.8, 127.9, 112.0, 111.9, 83.2, 46.4, 34.3, 30.2, 24.9, 24.8, 21.4.

HRMS (FI) m/z calcd for: C19H25BN2O2: 304.2009, found: 324.2013.

2-(2-methyl-1-phenyloctyl)malononitrile (**12**)

Prepared according to general procedure A, using 2-bromooctane (219 µL, 1.25 mmol, 2.5 equiv.) and benzylidenemalononitrile (77.1 mg, 0.5 mmol, 1 equiv.). The crude mixture was purified by flash column chromatography (pentane 95:5 Et2O to pentane 92:8 Et_2O) to afford a mixture of diastereomers **12A** and **12B** in a 1:1 ratio (91 mg, 68% total yield) as a colorless oil. These compounds were previously unreported.

Diastereomer A

^{1}H NMR (400 MHz, Chloroform-d) δ 7.45 – 7.34 (m, 3H), 7.34 – 7.25 (m, 2H), 4.18 (d, J = 6.7 Hz, 1H), 3.01 (dd, J = 8.6, 6.8 Hz, 1H), 2.29 – 2.18 (m, 1H), 1.54 – 1.45 (m, 1H), 1.45 – 1.27 (m, 8H), 1.25 – 1.11 (m, 1H), 0.94 – 0.86 (m, 3H), 0.81 (d, J = 6.7 Hz, 3H).

^{13}C NMR (101 MHz, Chloroform-d) δ 136.3, 129.1, 128.7, 128.4, 112.2, 111.9, 51.6, 34.7, 34.3, 31.8, 29.3, 27.4, 26.4, 22.6, 16.4, 14.1.

HRMS (FD) m/z calcd for C18H24N2: 268.1939; found: 268.1932.

Diastereomer B

^{1}H NMR (400 MHz, Chloroform-d) δ 7.46-7.35 (m, 3H), 7.34 - 7.28 (m, 2H), 4.17 (d, J = 5.4 Hz, 1H), 2.90 (dd, J = 10.1, 5.4 Hz, 1H), 2.30 - 2.15 (m, 1H), 1.28 – 1.14 (m, 8H), 1.12 (m, 4H), 0.97 (m, 1H), 0.83 (t, J = 7.1 Hz, 3H).

^{13}C NMR (101 MHz, Chloroform-d) δ 136.7, 129.1, 128.8, 128.3, 112.2, 111.9, 52.3, 34.7, 33.4, 31.6, 29.1, 27.8, 26.2, 22.5, 17.4, 14.3.
HRMS (GC-FI) m/z calcd for C18H24N2: 268.1939; found: 268.1947.

benzyl 3-(2,2-dicyano-1-phenylethyl)azetidine-1-carboxylate (**13**)

Prepared according to general procedure A, using benzyl 3-bromoazetidine-1-carboxylate (203 mg, 0.750 mmol, 2.5 equiv.) and benzylidenemalononitrile (46.3 mg, 0.3 mmol, 1 equiv.). The crude mixture was purified by flash column chromatography (pentane 95:5 acetone to pentane 8:2 acetone) to afford product **13** (54 mg, 52% yield) as a colorless oil. This compound was previously unreported.
^{1}H NMR (400 MHz, Chloroform-d) δ 7.46 – 7.27 (m, 10H), 5.07 (s, 2H), 4.36 (t, J = 8.5 Hz, 1H), 4.02 (dd, J = 9.1, 5.6 Hz, 1H), 3.96 (t, J = 8.8 Hz, 1H), 3.90 (d, J = 5.7 Hz, 1H), 3.54 – 3.45 (m, 2H), 3.39 – 3.27 (m, 1H).
^{13}C NMR (101 MHz, Chloroform-d) δ 156.1, 136.3, 134.4, 129.6, 129.5, 128.6, 128.2, 128.1, 127.9, 111.3, 111.2, 66.9, 50.0, 31.3, 31.0, 28.2.
HRMS (GC-EI) m/z calcd for C21H19N3O2: 345.1477; found: 345.1488.

benzyl 4-(2,2-dicyano-1-phenylethyl)piperidine-1-carboxylate (**14**)

Prepared according to general procedure A, using benzyl 4-bromo-1-piperidinecarboxylate (271 µL, 1.25 mmol, 2.5 equiv.) and benzylidenemalononitrile (77.1 mg, 0.5 mmol, 1 equiv.). The crude mixture was purified by flash column chromatography (pentane 9:1 Et_2O to pentane 7:3 Et2O) to afford product **14** (114 mg, 61% yield) as a colorless oil. This compound was previously unreported.
^{1}H NMR (400 MHz, Chloroform-d) δ 7.47 – 7.27 (m, 10H), 5.11 (s, 2H), 4.32 (brs, 1H), 4.21-4.05 (m, 2H), 2.90 (dd, J = 9.9, 5.3 Hz, 2H), 2.71 (brs,

1H), 2.27 – 2.12 (m, 1H), 1.88 (d, J = 12.6 Hz, 1H), 1.46 – 1.37 (m, 1H), 1.37-1.19 (m, 1H), 1.12 – 1.01 (m, 1H).

^{13}C NMR (101 MHz, Chloroform-d) δ 155.0, 136.6, 135.8, 129.4, 129.2, 128.5, 128.2, 128.1, 127.9, 111.8, 111.7, 67.2, 51.6, 43.7, 43.5, 37.9, 27.0.

HRMS (GC-EI) m/z calcd for C23H23N3O2: 373.1790; found: 373.1795.

2-(oxetan-3-yl(phenyl)methyl)malononitrile (**15**) Prepared according to general procedure C, using 3-bromooxetane (150 µL, 1.25 mmol, 2.5 equiv.) and benzylidenemalononitrile (77.1 mg, 0.5 mmol, 1 equiv.). The crude mixture was purified by flash column chromatography (pentane 95:5 acetone to pentane 8:2 acetone) to afford product **15** (51 mg, 48% yield) as a colorless oil. This compound was previously unreported.

^{1}H NMR (400 MHz, Chloroform-d) δ 7.49 – 7.35 (m, 3H), 7.30 – 7.25 (m, 2H), 5.01 (t, J = 6.7 Hz, 1H), 4.74 (t, J = 6.1 Hz, 1H), 4.62 (t, J = 7.0 Hz, 1H), 4.21 (t, J = 6.3 Hz, 1H), 3.88 – 3.72 (m, 3H).

^{13}C NMR (101 MHz, Chloroform-d) δ 134.5, 129.6, 129.5, 127.8, 111.2, 75.7, 74.7, 49.9, 37.1, 28.3.

HRMS (GC-FI) m/z calcd for C13H12N2O: 212.0950; found: 212.0960.

2-(2,2-dimethyl-1-phenylpropyl)malononitrile (**16**)

Prepared according to general procedure B, using tert-butyl bromide (140 µL, 1.25 mmol, 2.5 equiv.) and benzylidenemalononitrile (77.1 mg, 0.5 mmol, 1 equiv.). The crude mixture was purified by flash column chromatography (pentane 99:1 Et_2O to pentane 8:2 Et_2O) to afford product **16** (72 mg, 68% yield) as a colorless oil. The spectroscopic data are consistent with those reported previously.[21]

^{1}H NMR (400 MHz, Chloroform-d) δ 7.41 – 7.37 (m, 5H), 4.22 (d, J = 5.7 Hz, 1H), 3.01 (d, J = 5.7 Hz, 1H), 1.11 (s, 9H).

^{13}C NMR (101 MHz, Chloroform-d) δ 136.3, 129.3, 128.7, 128.6, 113.2, 113.1, 56.8, 34.9, 28.5, 25

2-((1-methylcyclohexyl)(phenyl)methyl)malononitrile (**17**)

Prepared according to general procedure B, using 1-bromo-1-methylcyclohexane (221 mg, 1.25 mmol, 2.5 equiv.), and benzylidenemalononitrile (77.1 mg, 0.5 mmol, 1 equiv.). The crude mixture was purified by flash column chromatography (pentane 99:1 Et_2O to pentane 9:1 Et_2O) to afford product **17** (57 mg, 45% yield) as a colorless oil. The spectroscopic data are consistent with those reported previously.[22]

^{1}H NMR (400 MHz, Chloroform-d) δ 7.45 – 7.35 (m, 5H), 4.25 (d, J = 5.4 Hz, 1H), 3.06 (d, J = 5.3 Hz, 1H), 1.65 – 1.20 (m, 10H), 1.16 (s, 3H).

^{13}C NMR (75 MHz, Chloroform-d) δ 135.7, 129.7, 128.6, 128.6, 113.4, 113.2, 56.8, 37.3, 36.8, 36.6, 25.7, 24.2, 21.8, 21.4, 20.3.

2-(((3r,5r,7r)-adamantan-1-yl)(phenyl)methyl)malononitrile (**18**)

Prepared according to general procedure B, using 1-bromoadamantane (269 mg, 1.25 mmol, 2.5 equiv.) and benzylidenemalononitrile (77.1 mg, 0.5 mmol, 1 equiv.) but with a residence time of 180 min. The crude mixture was purified by flash column chromatography (pentane 99:1 Et2O to pentane 9:1 Et2O) to afford product **18** (78 mg, 54% yield) as a white solid. The spectroscopic data are consistent with those reported previously.[23]

^{1}H NMR (400 MHz, Chloroform-d) δ 7.45 – 7.33 (m, 5H), 4.24 (d, J = 5.3 Hz, 1H), 2.81 (d, J = 5.3 Hz, 1H), 2.07 – 1.99 (m, 3H), 1.75 – 1.56 (m, 12H).

^{13}C NMR (101 MHz, Chloroform-d) δ 135.3, 129.7, 128.6, 128.5, 113.5, 113.3, 58.0, 40.4, 36.5, 36.4, 28.4, 23.8.

2-(2,2-dimethyl-1,4-diphenylbutyl)malononitrile (**19**)

Prepared according to general procedure B, using (3-bromo-3-methylbutyl)benzene (284 mg, 1.25 mmol, 2.5 equiv.), and benzylidenemalononitrile (77.1 mg, 0.5 mmol, 1 equiv.). The crude mixture was purified by flash column chromatography (pentane 95:5 Et_2O to pentane 8:2 Et_2O) to afford product **19** (60 mg, 40% yield) as a colorless oil. This compound was previously unreported.

^{1}H NMR (400 MHz, Chloroform-d) δ 7.46 – 7.35 (m, 5H), 7.30 – 7.21 (m, 2H), 7.21 – 7.13 (m, 1H), 7.12 – 7.05 (m, 2H), 4.20 (d, J = 5.5 Hz, 1H), 3.14 (d, J = 5.5 Hz, 1H), 2.69 – 2.51 (m, 2H), 1.69 – 1.56 (m, 2H), 1.24 (s, 3H), 1.12 (s, 3H).

^{13}C NMR (101 MHz, Chloroform-d) δ 141.7, 135.8, 129.6, 128.9, 128.8, 128.6, 128.3, 126.1, 113.2, 113.1, 55.4, 43.3, 37.6, 30.3, 25.4, 25.3, 24.9.

HRMS (GC-EI) m/z calcd for C21H22N2: 302.1783; found: 302.1783.

2-(2,2-dimethyl-1-phenylbutyl)malononitrile (**20**)

Prepared according to general procedure C, using 2-bromo-2-methylbutane (189 mg, 1.25 mmol, 2.5 equiv.), and benzylidenemalononitrile (77.1 mg, 0.5 mmol, 1 equiv.). The crude mixture was purified by flash column chromatography (pentane 98:2 Et_2O to pentane 8:2 Et_2O) to afford product **20** (72 mg, 64% yield) as a pale yellow oil. The spectroscopic data are consistent with those reported previously.[24]

^{1}H NMR (400 MHz, Chloroform-d) δ 7.44 – 7.33 (m, 5H), 4.21 (d, J = 5.4 Hz, 1H), 3.08 (d, J = 5.4 Hz, 1H), 1.47 – 1.31 (m, 2H), 1.13 (s, 3H), 1.00 (s, 3H), 0.90 (t, J = 7.4 Hz, 3H).

^{13}C NMR (101 MHz, Chloroform-d) δ 136.0, 129.6, 128.7, 128.6, 113.3, 113.1, 55.1, 37.5, 33.4, 24.8, 24.7, 24.5, 8.1.

Dimethyl 2-cyclohexylsuccinate (**21**)

Prepared according to general procedure A, using cyclohexyl bromide (154 µL, 1.25 mmol, 2.5 equiv.) and dimethyl maleate (62.6 µL, 0.5 mmol, 1 equiv.). The crude mixture was purified by flash column chromatography (pentane 99:1 Et_2O to pentane 9:1 Et_2O) to afford product **21** (62 mg, 54% yield) as a colorless oil. The spectroscopic data are consistent with those reported previously.[25]

^{1}H NMR (400 MHz, Chloroform-d) δ 3.68 (s, 3H), 3.65 (s, 3H), 2.77 – 2.66 (m, 2H), 2.50 – 2.39 (m, 1H), 1.77 – 1.68 (m, 2H), 1.68 – 1.52 (m, 4H), 1.28 – 0.93 (m, 5H).

^{13}C NMR (101 MHz, Chloroform-d) δ 175.6, 173.6, 52.3, 52.2, 47.6, 40.5, 33.8, 31.2, 30.7, 26.9, 26.7.

((2-cyclohexylethyl)sulfonyl)benzene (**22**)

Prepared according to general procedure A, using cyclohexyl bromide (154 µL, 1.25 mmol, 2.5 equiv.) and (vinylsulfonyl)benzene (91.1 mg, 0.5 mmol, 1 equiv.). The crude mixture was purified by flash column chromatography (hexane 99:1 Et_2O to hexane 8:2 Et_2O) to afford product **22** (71 mg, 53% yield) as a colorless oil. The spectroscopic data are consistent with those reported previously.[26]

^{1}H NMR (400 MHz, Chloroform-d) δ 7.93 – 7.86 (m, 2H), 7.69 – 7.61 (m, 1H), 7.56 (dd, J = 8.4, 7.0 Hz, 2H), 3.12 – 3.05 (m, 2H), 1.71 – 1.57 (m, 7H), 1.32 – 1.03 (m, 4H), 0.92 – 0.78 (m, 2H).

^{13}C NMR (101 MHz, Chloroform-d) δ 141.3, 135.6, 131.3, 130.1, 56.4, 38.7, 34.8, 31.6, 28.3, 28.0.

diethyl (2-cyclohexylethyl)phosphonate (**23**)

Prepared according to general procedure A, using cyclohexyl bromide (154 µL, 1.25 mmol, 2.5 equiv.) and diethyl vinylphosphonate (77.1 µL, 0.5 mmol, 1 equiv.). The crude mixture was purified by flash column chromatography (CH_2Cl_2 95:5 EtOAc to CH_2Cl_2 7:3 EtOAc) to afford product **23** (84 mg, 68% yield) as a colorless oil. The spectroscopic data are consistent with those reported previously.[27]

^{1}H NMR (400 MHz, Chloroform-d) δ 4.17 – 3.99 (m, 4H), 1.78 – 1.59 (m, 7H), 1.47 (m, 2H), 1.31 (t, J = 7.0 Hz, 6H), 1.28 – 1.09 (m, 4H), 0.94 – 0.80 (m, 2H).

^{13}C NMR (101 MHz, Chloroform-d) δ 61.4 (d, J = 6.5 Hz), 38.3 (d, J = 16.8 Hz), 32.8, 29.6 (d, J = 5.1 Hz), 26.5, 26.2, 23.2 (d, J = 140.5 Hz), 16.5 (d, J = 6.0 Hz).

^{31}P NMR (162 MHz, Chloroform-d) δ 33.37 (tp, J = 17.4, 8.7 Hz).

Ethyl 3-cyclohexyl-2-(diethoxyphosphoryl)propanoate (**24**)

Prepared according to general procedure B, using cyclohexyl bromide (154 µL, 1.25 mmol, 2.5 equiv.) and ethyl 2-(diethoxyphophoryl)acrylate (118 mg, 0.5 mmol, 1 equiv.) The crude mixture was purified by flash column chromatography (pentane 6:4 EtOAc) to afford product **24** (96 mg, 60% yield) as a colorless oil. The spectroscopic data are consistent with those reported previously.

^{1}H NMR (400 MHz, Chloroform-d) δ 4.24 – 4.06 (m, 6H), 3.05 (ddd, J = 23.1, 11.5, 3.4 Hz, 1H), 1.94 (m, 1H), 1.76 – 1.57 (m, 6H), 1.33 – 1.10 (m, 13H), 0.98 – 0.77 (m, 2H).

^{13}C NMR (101 MHz, Chloroform-d) δ 169.63 (d, J = 5.0 Hz), 62.91 – 62.61 (m), 61.37, 43.42 (d, J = 130.6 Hz), 36.45 (d, J = 14.1 Hz), 34.19 (d,

J = 5.0 Hz), 32.85 (d, J = 155.8 Hz), 26.48, 26.17 (d, J = 13.5 Hz), 16.49 (dd, J = 6.0, 2.6 Hz), 14.26.

^{31}P NMR (162 MHz, Chloroform-d) δ 23.57.

Bromo(2-cyclohexylethyl)triphenyl-λ5-phosphane (**25**)

To a flame-dried nitrogen-purged screw-capped vial, fitted with a rubber septum, charged with the triphenyl(vinyl)phosphonium bromide (185 mg, 0.5 mmol, 1 equiv.) in CH_3CN (5 mL, 0.1 M), cyclohexyl bromide (154 µL, 1.25 mmol, 2.5 equiv.) and $(TMS)_3SiH$ (170 µL, 0.550 mmol, 1.1 equiv.) were added. Subsequently, the solution was sparged with nitrogen for 30 seconds and the reaction vessel was sealed with parafilm. The vial was then placed in a 3D-printed photoreactor (see Figure S2) using a Kessil Lamp (390 nm, 100% intensity) as light source and irradiated overnight. The solvent of the resulting reaction mixture was removed under reduced pressure and purification by crystallization (pentane 20:1 MeOH) affords product **25** (190 mg, 84% yield) as a yellowish solid. This compound was previously unreported.

^{1}H NMR (400 MHz, Chloroform-d) δ 7.77 (m, 9H), 7.67 (m, 6H), 3.59 (td, J = 12.7, 7.1 Hz, 2H), 1.75 (dd, J = 12.8, 3.4 Hz, 2H), 1.65 – 1.40 (m, 6H), 1.25 – 1.11 (m, 2H), 1.04 (m, 1H), 0.87 – 0.74 (m, 2H).

^{13}C NMR (101 MHz, Chloroform-d) δ 135.14 (d, J = 3.0 Hz), 133.90 – 133.21 (m), 130.58 (d, J = 12.5 Hz), 118.23 (d, J = 86.0 Hz), 37.90 (d, J = 14.5 Hz), 32.76, 29.62, 26.22, 25.85, 20.78 (d, J = 50.3 Hz).

^{31}P NMR (162 MHz, CDCl3) δ 24.96.

HRMS (LC-UV-ESI) m/z calcd for C26H30BrP: 373.2085; found 373.2093.

3-cyclohexyl-N-phenylpropanamide (**26**)

Prepared according to general procedure A, using cyclohexyl bromide (154 µL, 1.25 mmol, 2.5 equiv.) and *N*-phenylacrylamide (73.6 µL, 0.5 mmol, 1 equiv.). The crude mixture was purified by flash column chromatography (pentane 50:2.5 Et_2O to pentane 50:20 Et_2O) to afford product **26** (61 mg, 53% yield) as a white solid. The spectroscopic data are consistent with those reported previously.[28]

^{1}H NMR (400 MHz, Chloroform-d) δ 7.51 (d, J = 8.0 Hz, 2H), 7.31 (t, J = 7.8 Hz, 2H), 7.17 – 7.05 (m, 2H), 2.41 – 2.32 (m, 2H), 1.79 – 1.66 (m, 4H), 1.63 (q, J = 7.3 Hz, 3H), 1.36 – 1.07 (m, 4H), 1.00 – 0.86 (m, 2H).

^{13}C NMR (101 MHz, Chloroform-d) δ 171.8, 138.0, 129.0, 124.1, 119.8, 37.3, 35.3, 33.1, 33.0, 26.5, 26.2.

methyl (E)-3-(2-bromophenyl)-2-(cyclohexylmethyl)acrylate (**27**)

Prepared according to general procedure D, using cyclohexyl bromide (154 µL, 1.25 mmol, 2.5 equiv.), ethyl 2-(diethoxyphophoryl)acrylate (118 mg, 0.5 mmol, 1 equiv.) and 2-bromobenzaldehyde (197 µL, 1.50 mmol, 3.0 equiv.) Only one of the possible diastereomer, with E configuration, was detected via ^{1}H NMR of the reaction crude (the NOESY spectrum is reported below). The crude mixture was purified by flash column chromatography (Pentane 98:2 EtOAc) to afford product **27** (98 mg, 56% yield) as a colorless oil. This compound was previously unreported.

^{1}H NMR (300 MHz, Chloroform-d) δ 7.65 – 7.58 (m, 2H), 7.34 – 7.24 (m, 3H), 4.29 (q, J = 7.1 Hz, 2H), 2.30 (d, J = 7.0 Hz, 2H), 1.65 – 1.55 (m, 5H), 1.35 (t, J = 7.1 Hz, 3H), 1.19 – 0.97 (m, 3H), 0.80 – 0.62 (m, 2H).

^{13}C NMR (101 MHz, CDCl3) δ 168.34, 138.85, 136.98, 134.41, 132.77, 130.38, 129.37, 127.16, 124.05, 60.98, 37.55, 34.69, 33.22 (2), 26.48, 26.37 (2), 14.42.

HRMS (GC-EI) m/z calcd for 350.0881; found 350.0874

methyl (E)-2-(cyclohexylmethyl)-3-(3,4,5-trimethoxyphenyl)acrylate (**28**)

Prepared according to general procedure D, using cyclohexyl bromide (154 µL, 1.25 mmol, 2.5 equiv.), ethyl 2-(diethoxyphophoryl)acrylate (118 mg, 0.5 mmol, 1 equiv.) and 3,4,5-trimethoxybenzaldehyde (294 mg, 1.50 mmol, 3.0 equiv.). Only one of the possible diastereomer, with E configuration, was detected via ^{1}H NMR of the reaction crude (the NOESY spectrum is reported below). The crude mixture was purified by flash column chromatography (Pentane 98:2 EtOAc) to afford product **28** (68 mg, 38% yield) as a colorless oil. This compound was previously unreported.

^{1}H NMR (400 MHz, Chloroform-d) δ 7.58 (s, 1H), 6.64 (s, 2H), 4.27 (q, J = 7.1 Hz, 2H), 3.88 (s, 3H), 3.87 (s, 6H), 2.53 (d, J = 7.1 Hz, 2H), 1.64 (m, 8H), 1.35 (t, J = 7.1 Hz, 3H), 1.16 (m, 3H).

^{13}C NMR (101 MHz, Chloroform-d) δ 139.01, 132.40, 131.43, 106.84, 106.82, 60.97, 60.81, 56.13, 38.25, 34.63, 33.46, 26.42, 26.38, 26.38, 14.34.

HRMS (GC-EI) m/z calcd for 362.2093; found 362.2085

Methyl (E)-2-(cyclohexylmethyl)-3-(naphthalen-1-yl)acrylate (**29**)

Prepared according to general procedure D, using cyclohexyl bromide (154 µL, 1.25 mmol, 2.5 equiv.), ethyl 2-(diethoxyphophoryl)acrylate (118 mg, 0.5 mmol, 1 equiv.) and 1-naphtaldehyde (81.5 µL, 1.50 mmol, 3.0 equiv.) Only one of the possible diastereomer, with E configuration, was detected via ^{1}H NMR of the reaction crude (the NOESY spectrum is reported below). The crude mixture was purified by flash column

chromatography (Pentane 98:2 EtOAc) to afford product **29** (92 mg, 57% yield) as a colorless oil. This compound was previously unreported.

^{1}H NMR (400 MHz, Chloroform-d) δ 8.12 (s, 1H), 7.92 – 7.85 (m, 2H), 7.82 (d, J = 8.2 Hz, 1H), 7.54 – 7.45 (m, 3H), 7.36 (d, J = 7.0 Hz, 1H), 4.34 (q, J = 7.1 Hz, 2H), 2.33 (d, J = 7.0 Hz, 2H), 1.61 – 1.50 (m, 5H), 1.40 (t, J = 7.1 Hz, 3H), 1.08 (m, 2H), 0.89 (m, 2H), 0.72 – 0.58 (m, 2H).

^{13}C NMR (101 MHz, Chloroform-d) δ 168.63, 138.12, 135.19, 133.78, 133.54, 131.64, 128.56, 128.31, 126.31, 126.22, 126.17, 125.30, 125.09, 60.91, 37.49, 35.13, 33.23, 26.41, 26.34, 14.48, 14.26.

HRMS (GC-EI) m/z calcd for 322.1933; found 322.1936.

6

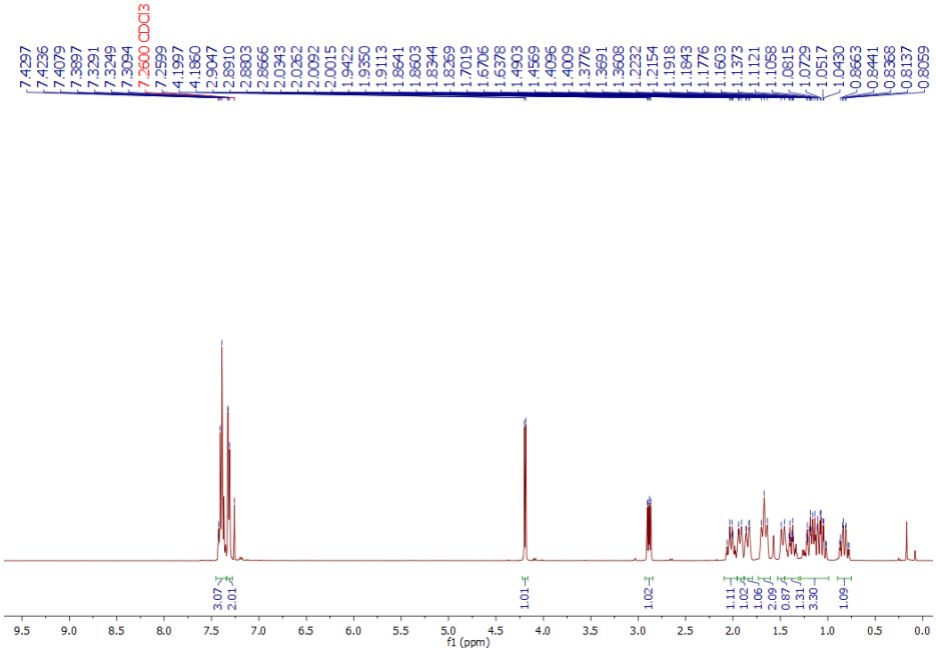

Supporting figure 1. ^{1}H NMR of compound **6**

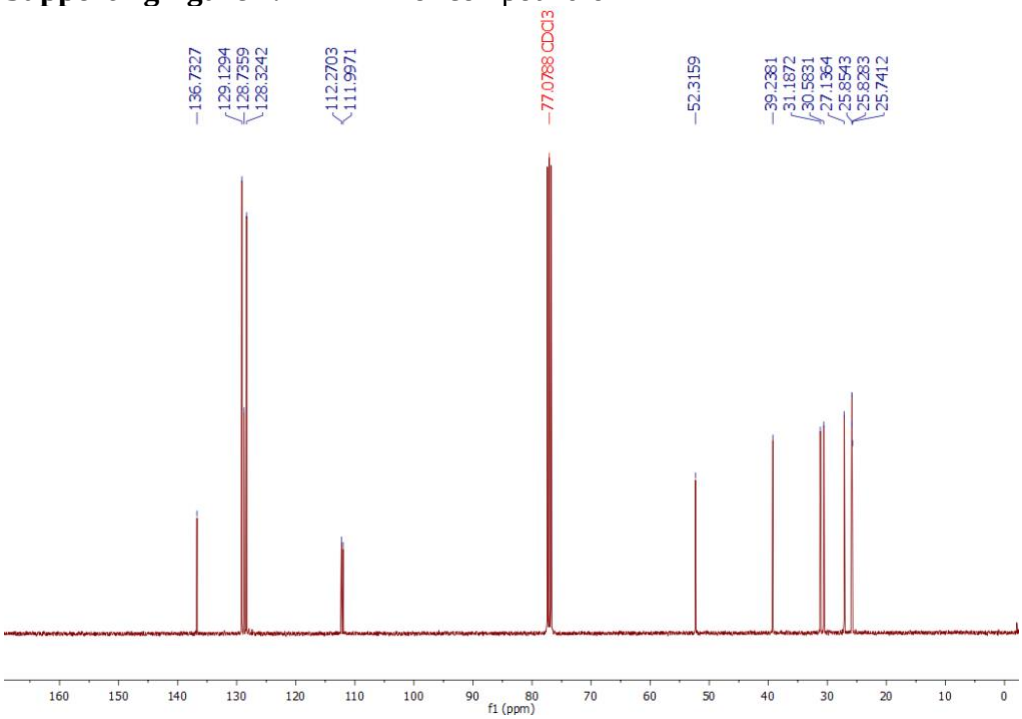

Supporting figure 2. ^{13}C NMR of compound **6**

7

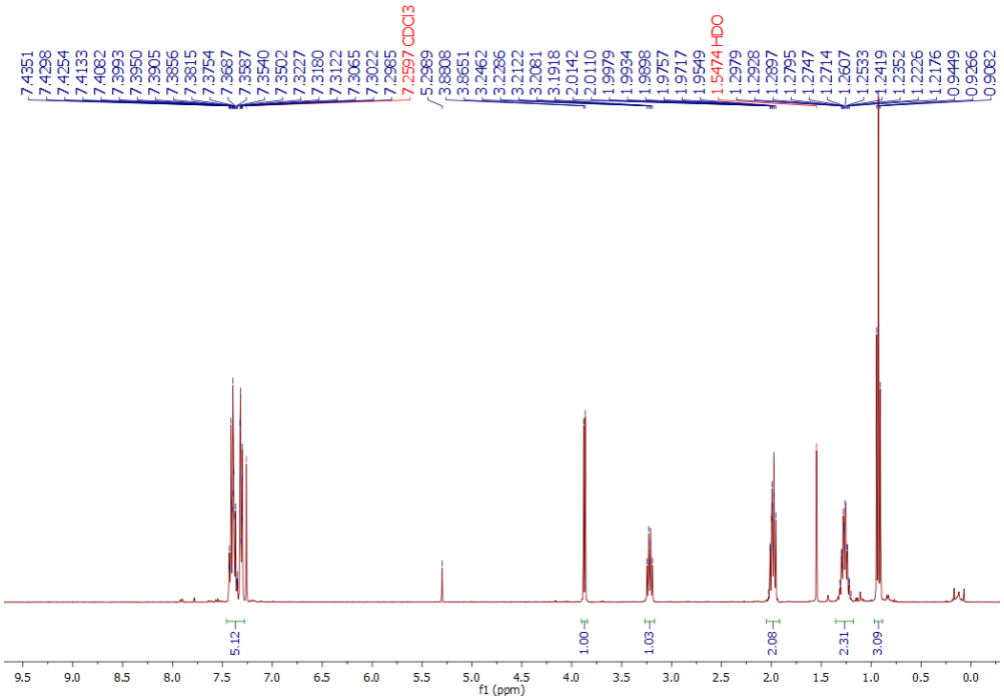

Supporting figure 3. ^{1}H NMR of compound **7**

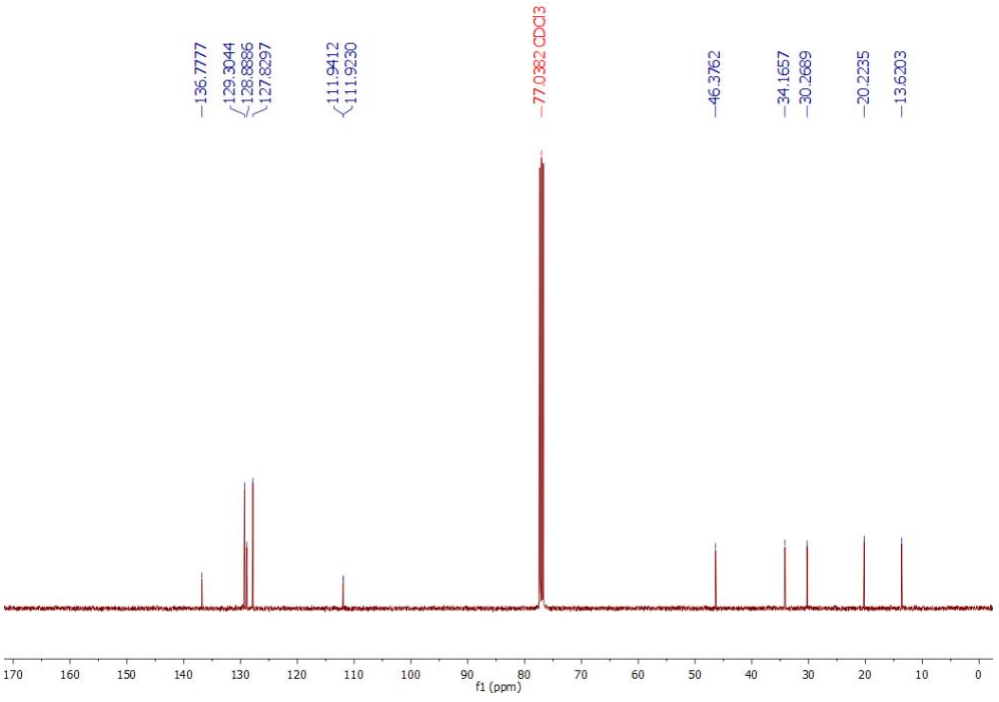

Supporting figure 4. ^{13}C NMR of compound **7**

8

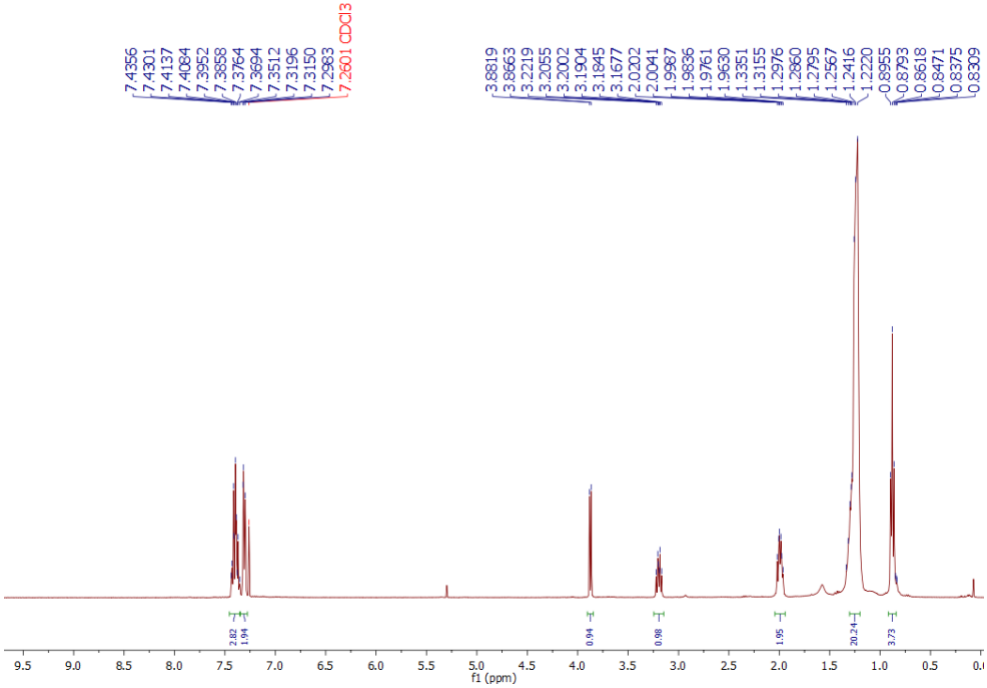

Supporting figure 5. ^{1}H NMR of compound **8**

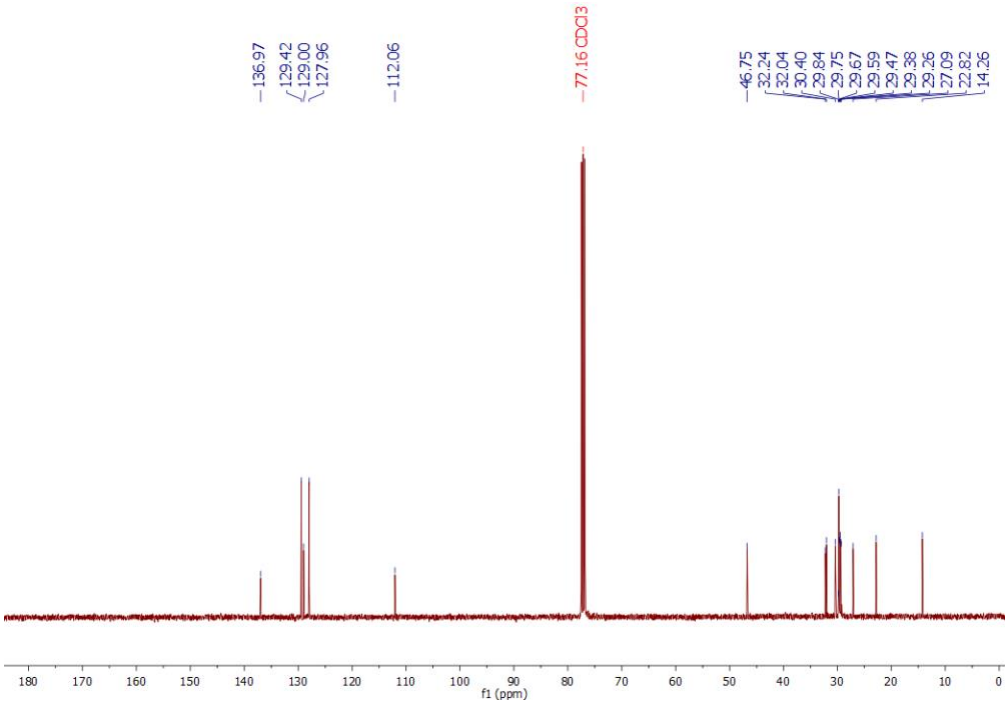

Supporting figure 6. ^{13}C NMR of compound **8**

9

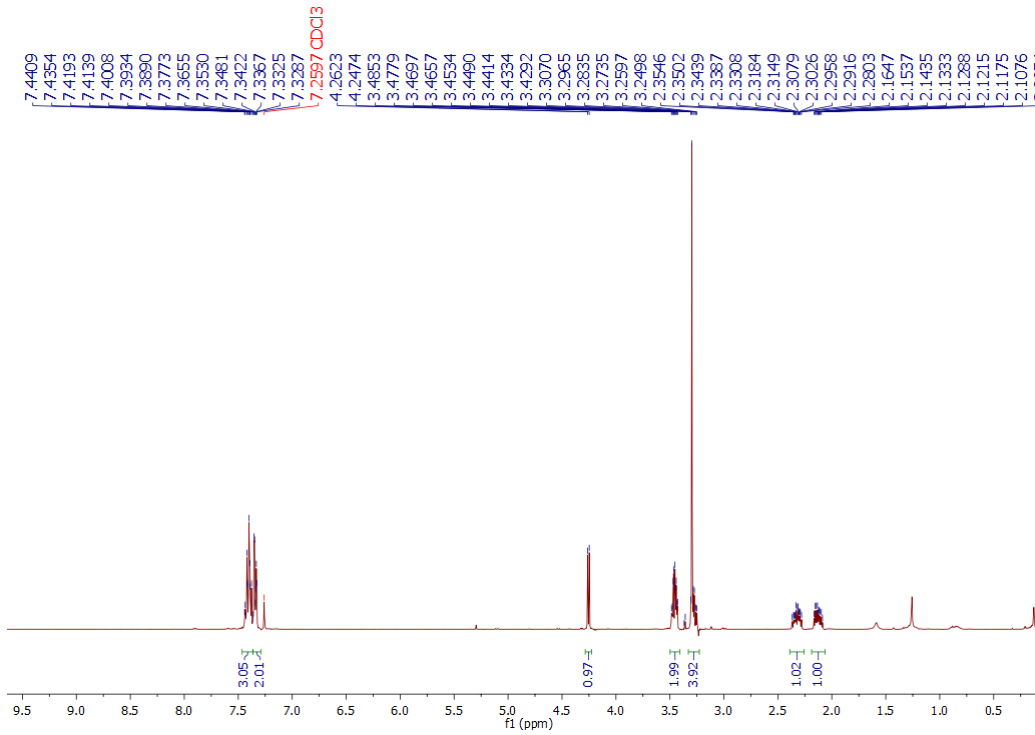

Supporting figure 7. ^{1}H NMR of compound **9**

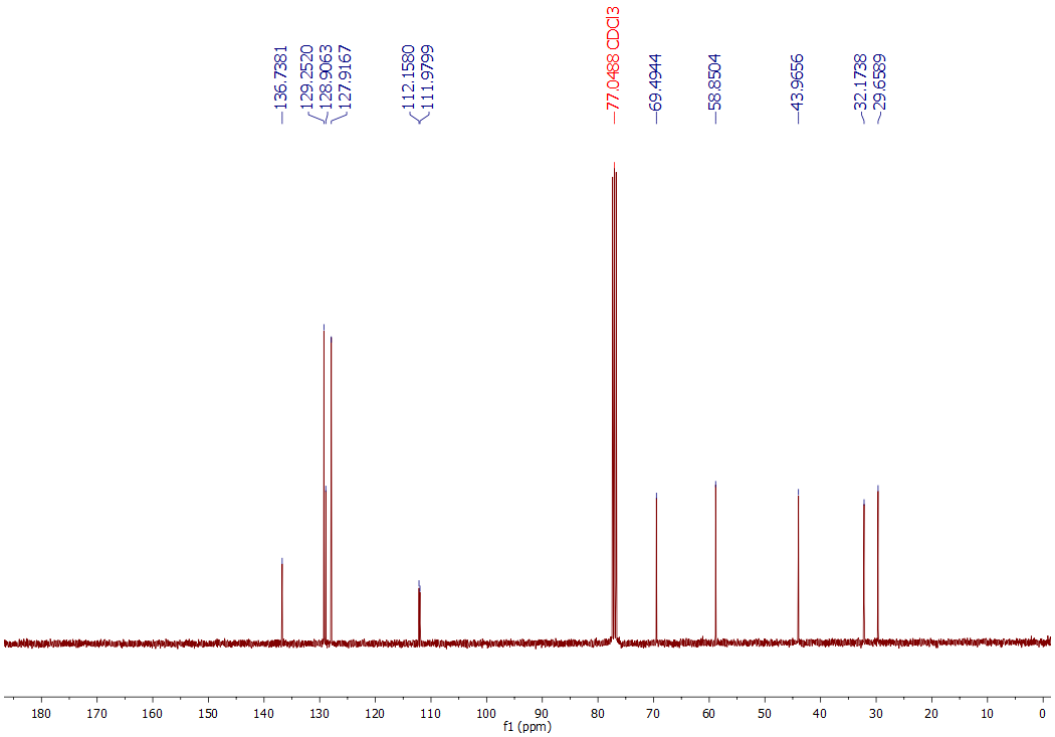

Supporting figure 8. ^{13}C NMR of compound **9**

10

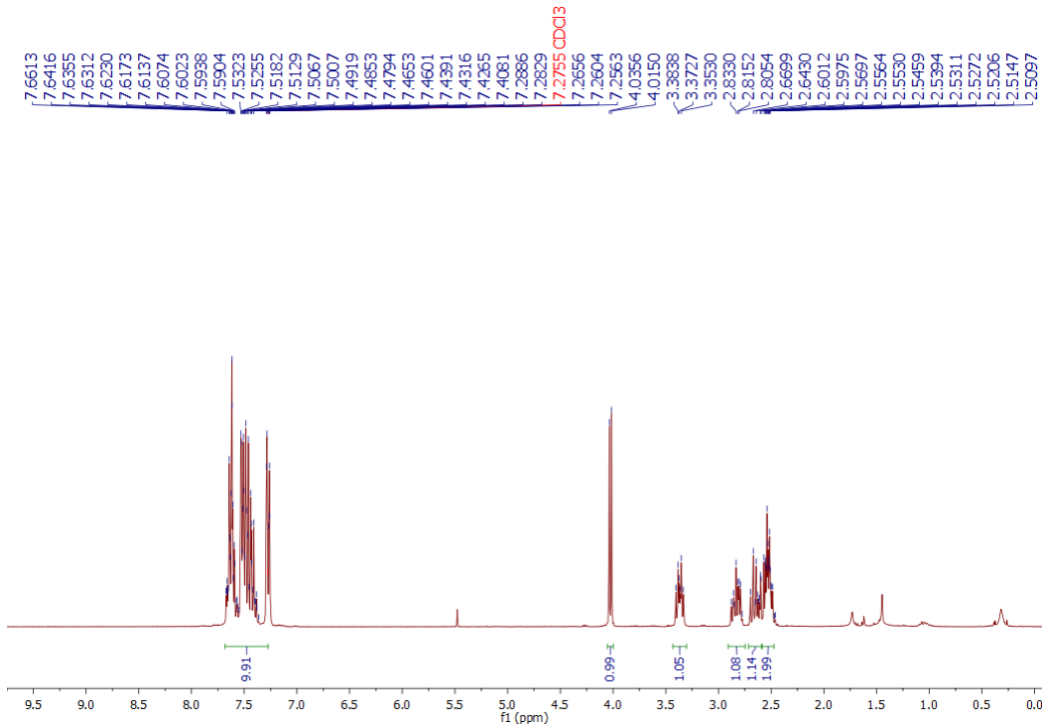

Supporting figure 9. ^{1}H NMR of compound **10**

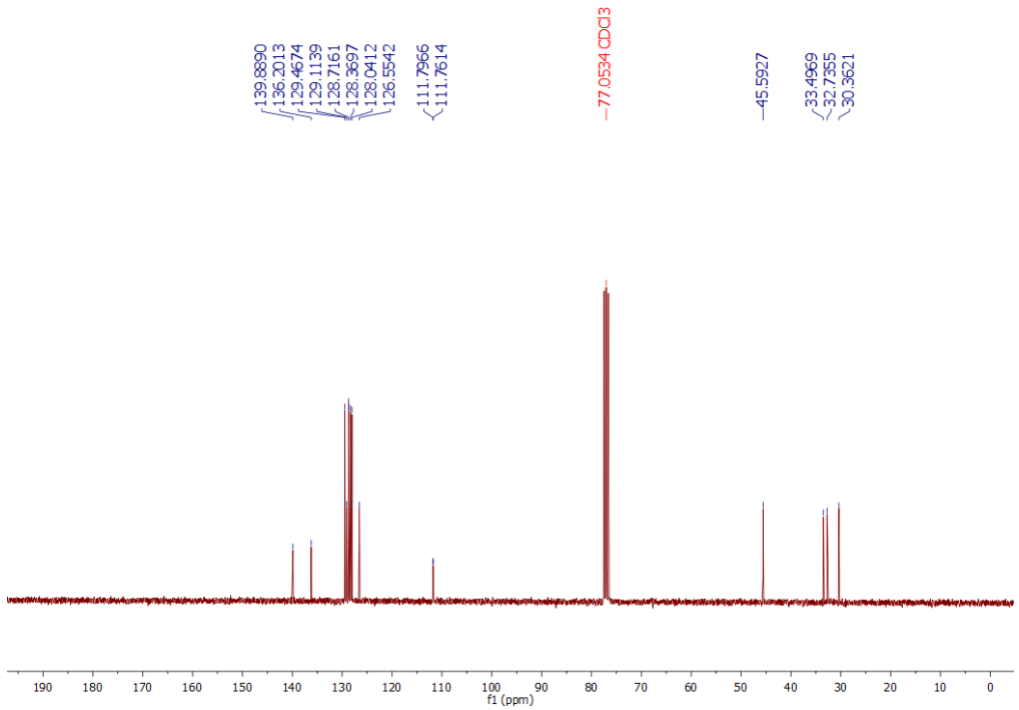

Supporting figure 10. ^{13}C NMR of compound **10**

11

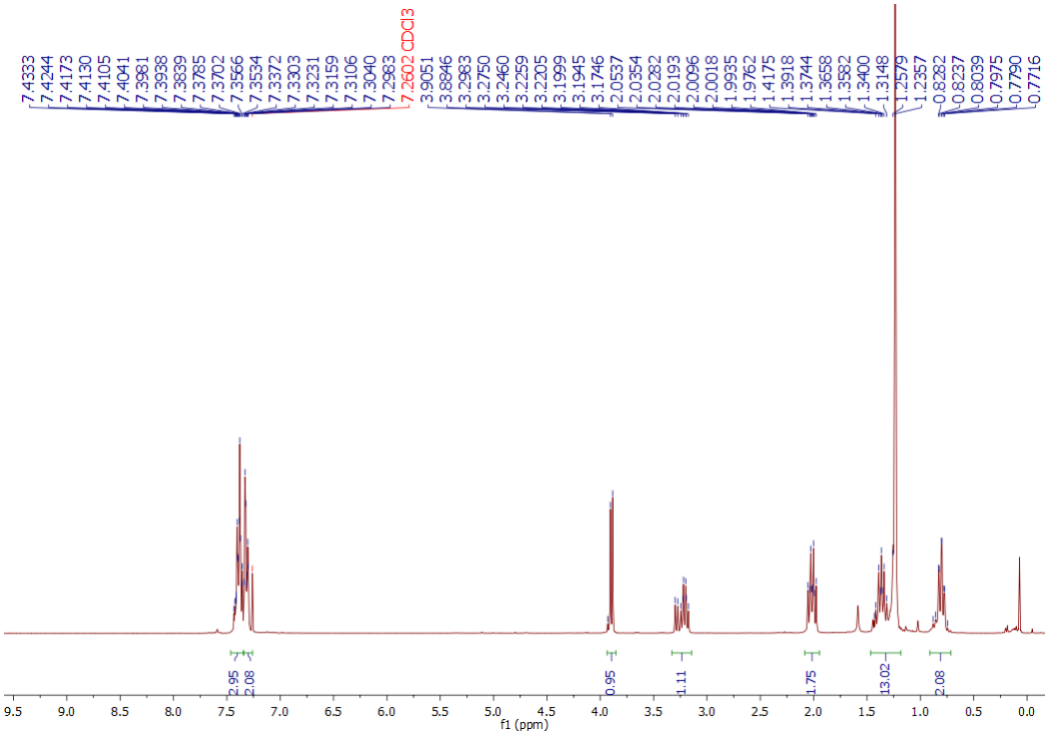

Supporting figure 11. ^{1}H NMR of compound **11**

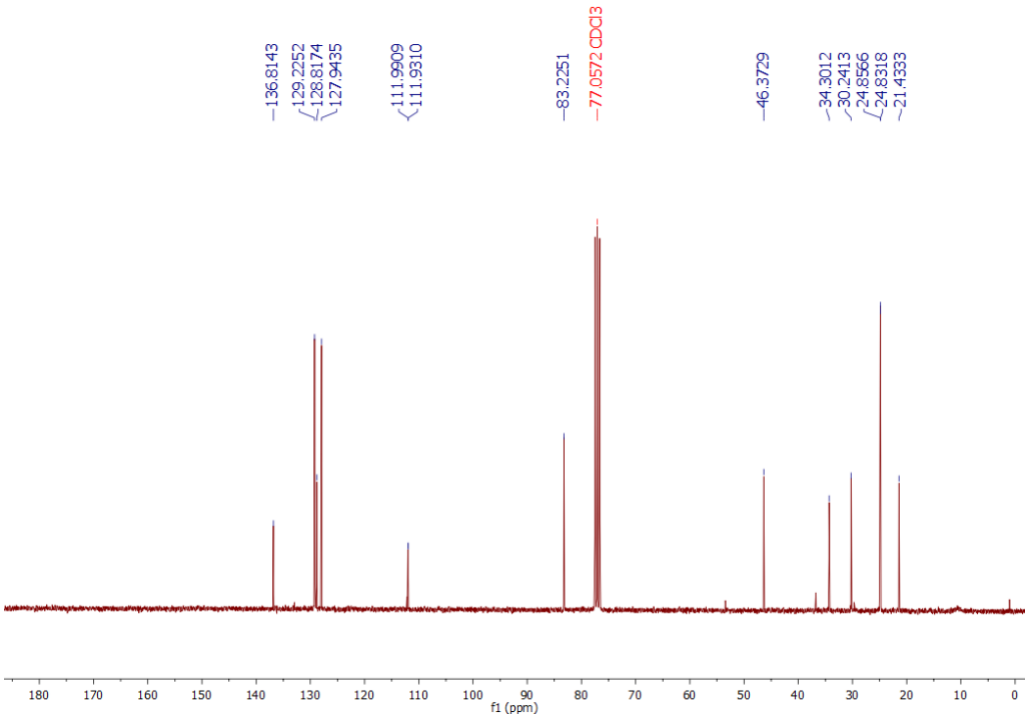

Supporting figure 12. ^{13}C NMR of compound **11**

12A

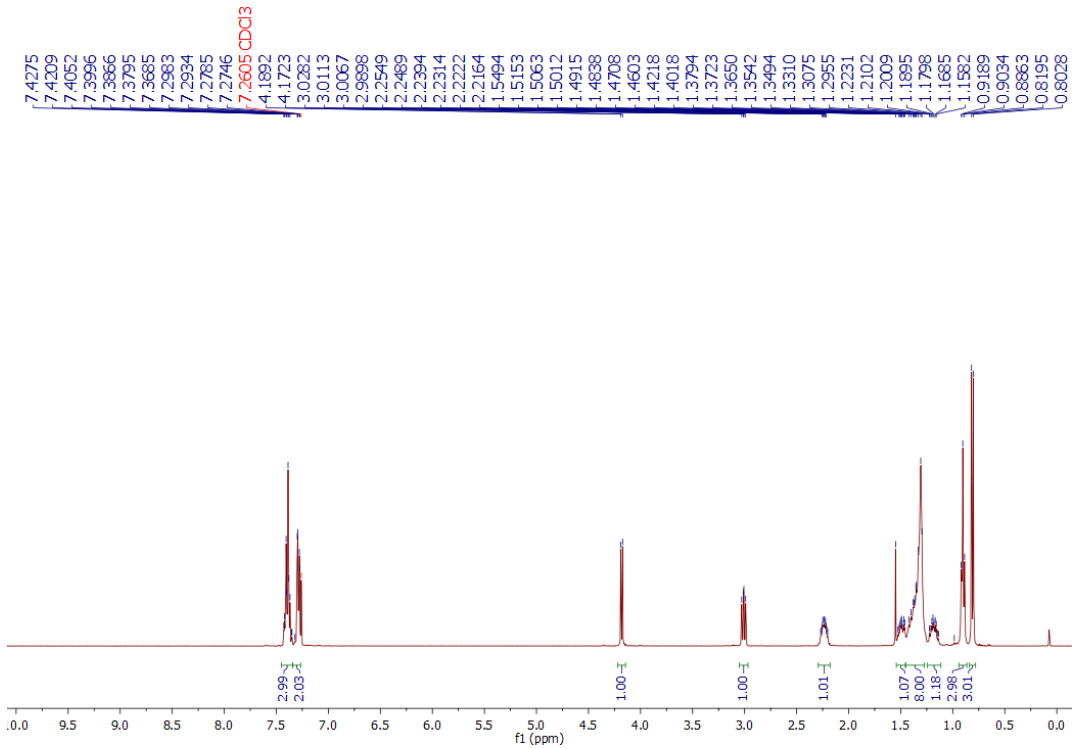

Supporting figure 13. ^{1}H NMR of compound **12A**

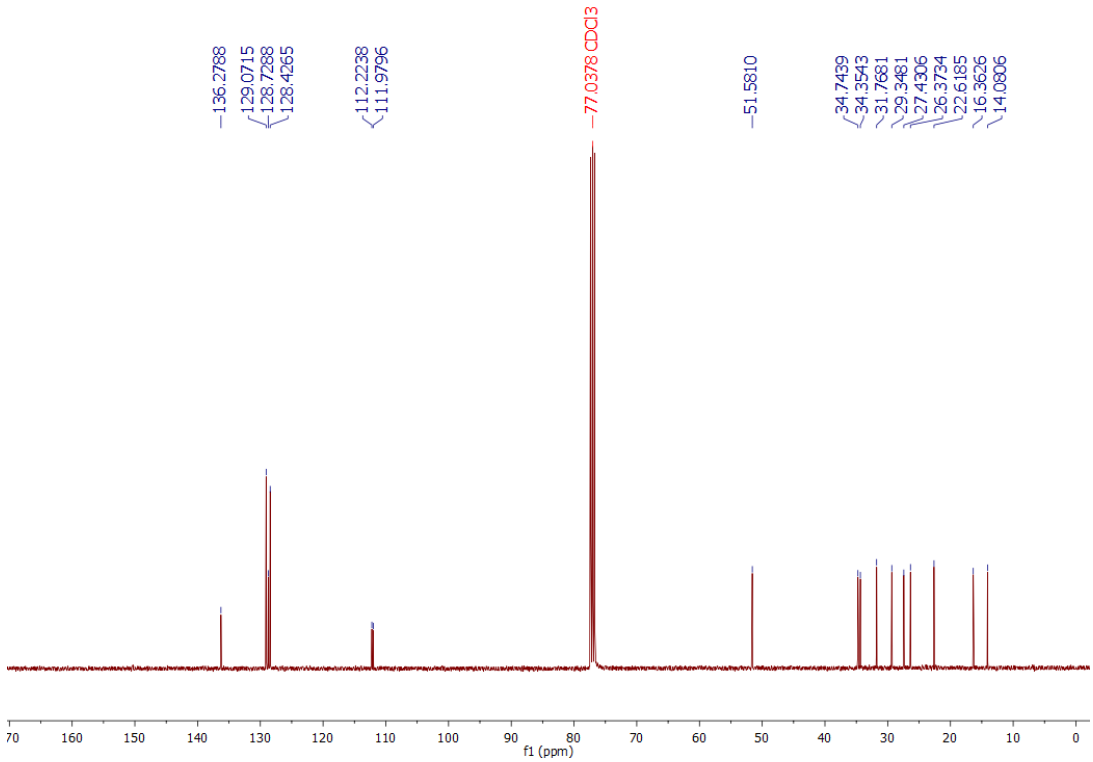

Supporting figure 14. ^{13}C NMR of compound **12A**

12B

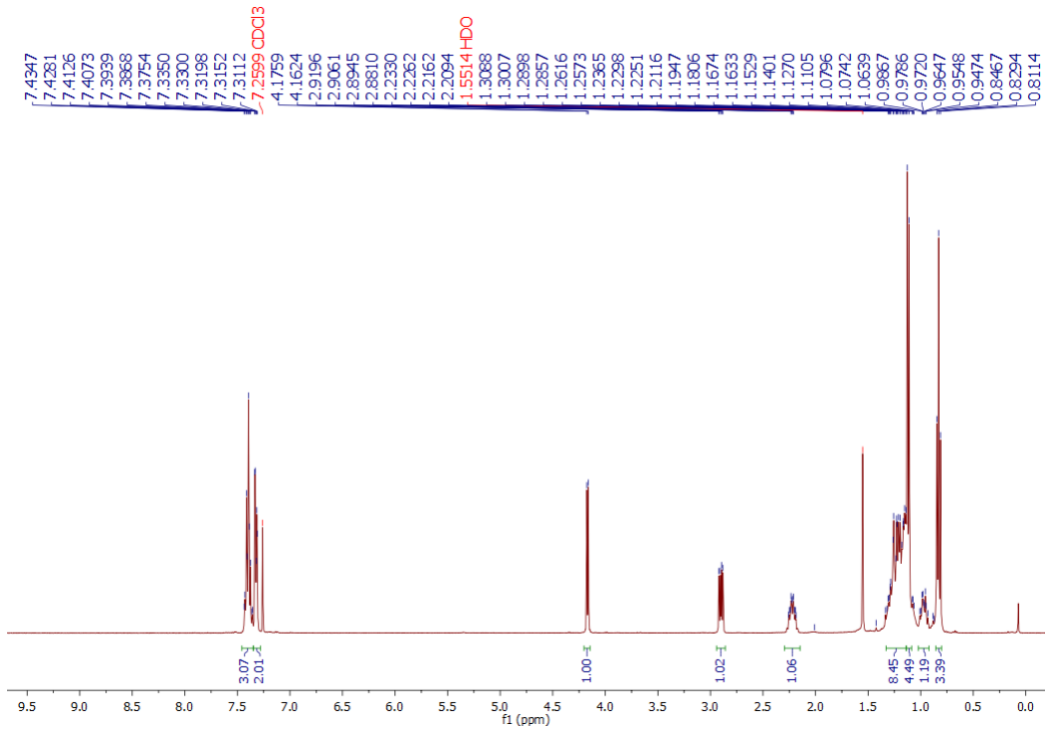

Supporting figure 15. ^{1}H NMR of compound **12B**

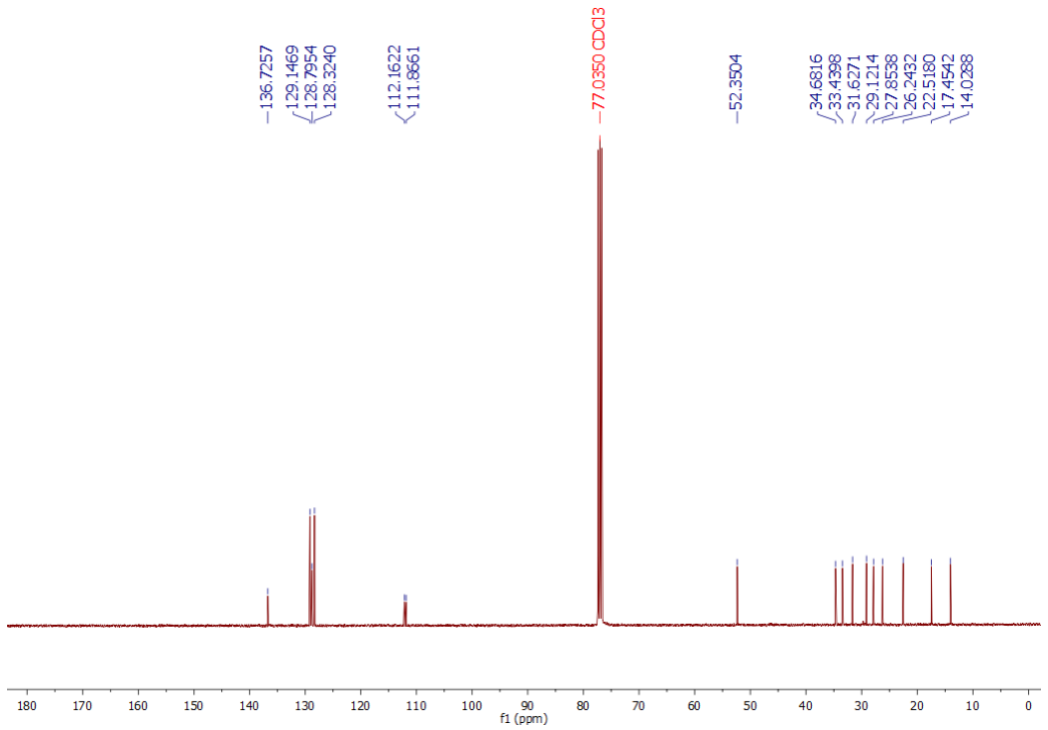

Supporting figure 16. ^{13}C NMR of compound **12B**

13

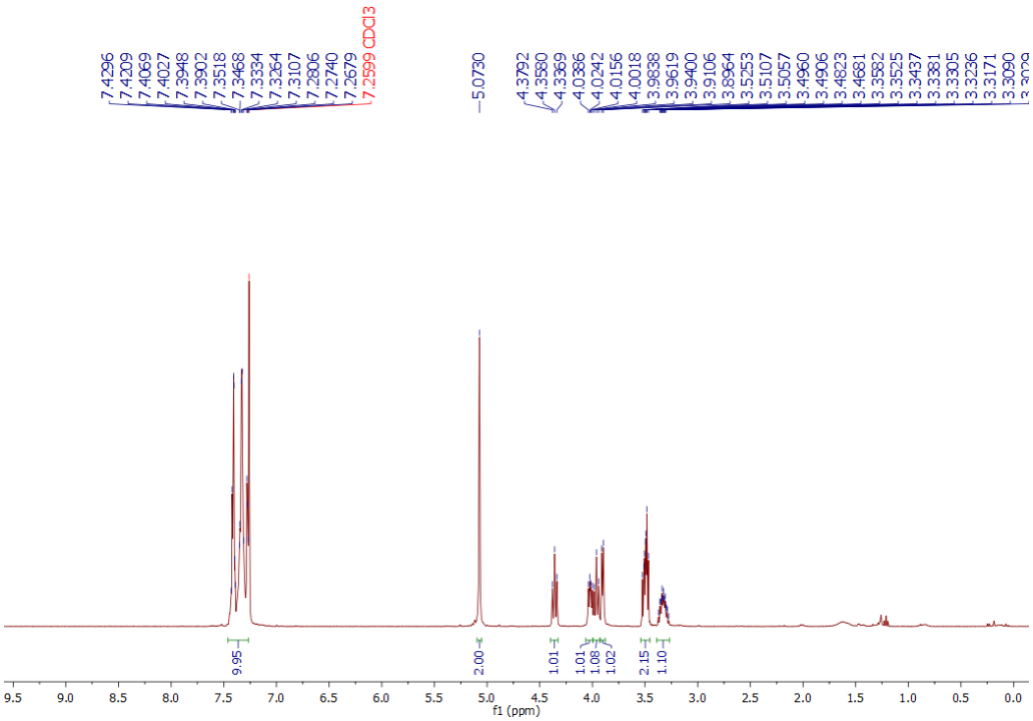

Supporting figure 17. ^{1}H NMR of compound **13**

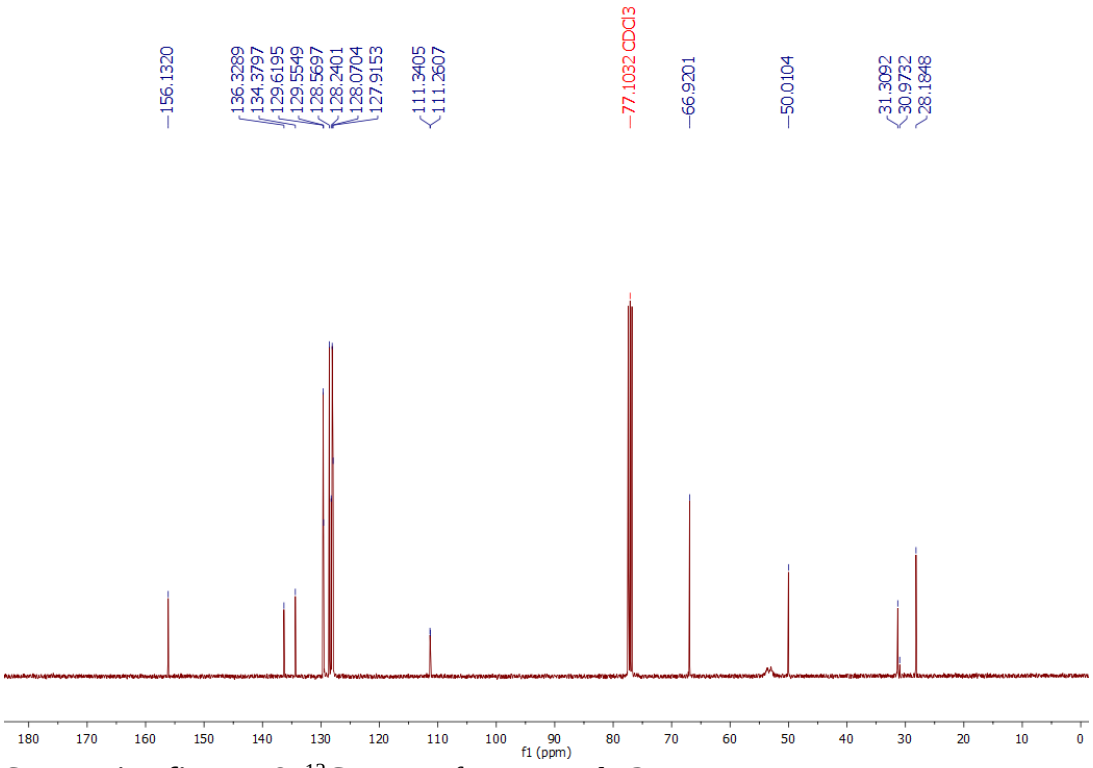

Supporting figure 18. ^{13}C NMR of compound **13**

14

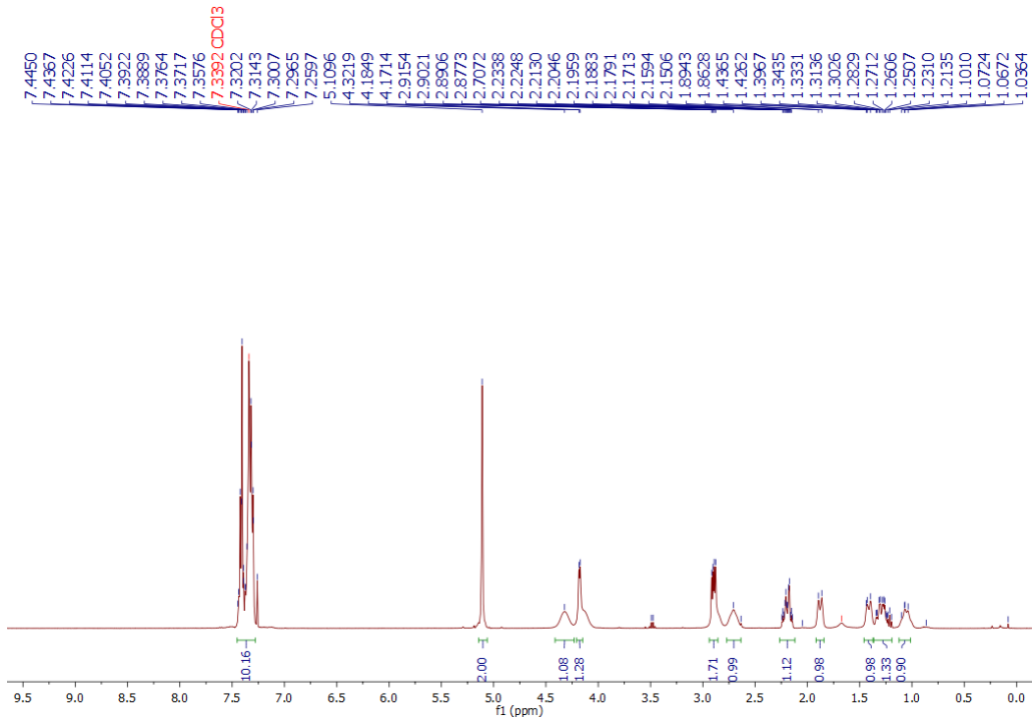

Supporting figure 19. ^{1}H NMR of compound **14**

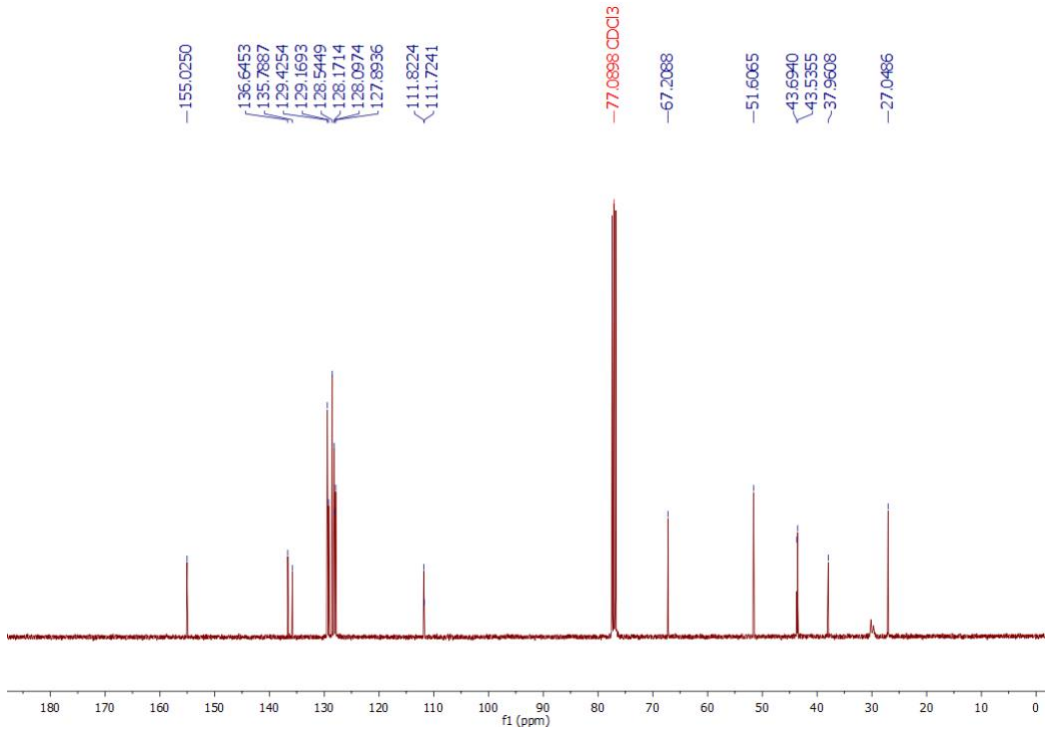

Supporting figure 20. ^{13}C NMR of compound **14**

15

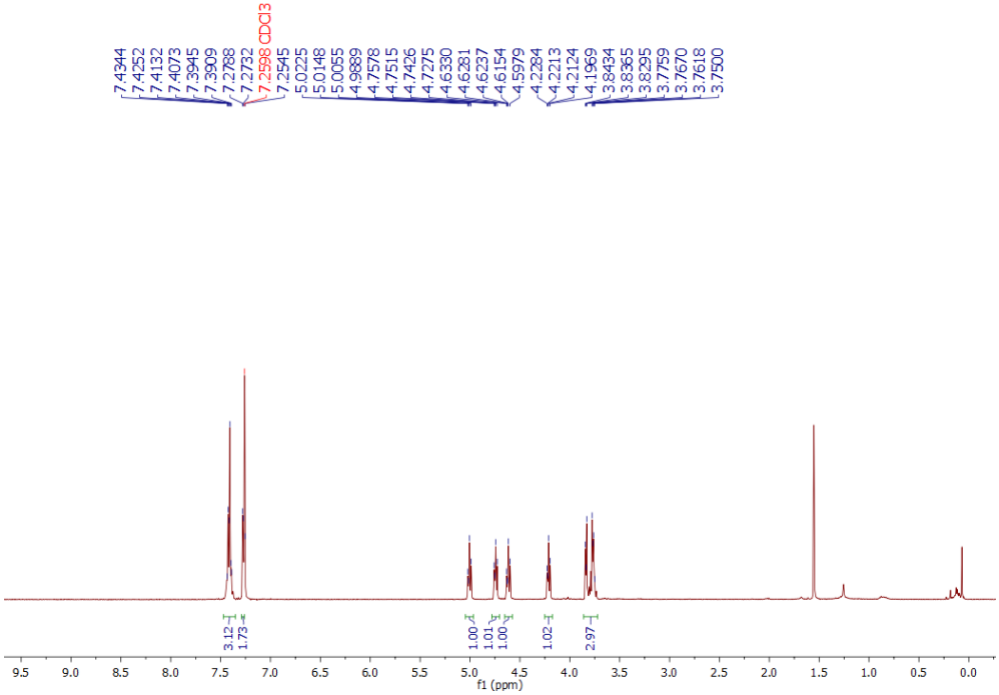

Supporting figure 21. ^{1}H NMR of compound **15**

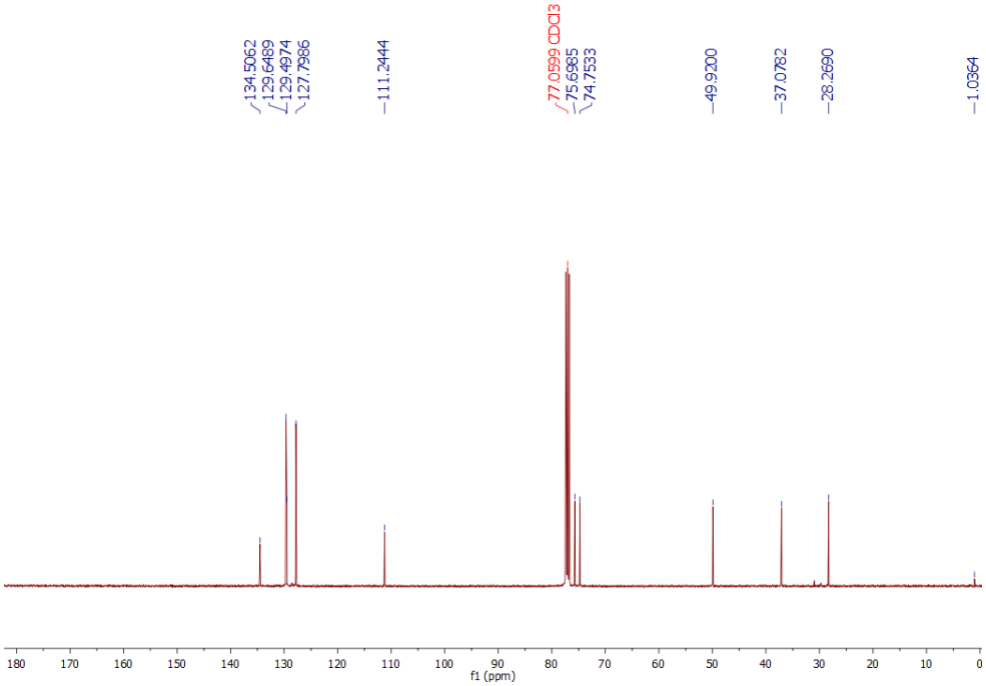

Supporting figure 22. ^{13}C NMR of compound **15**

16

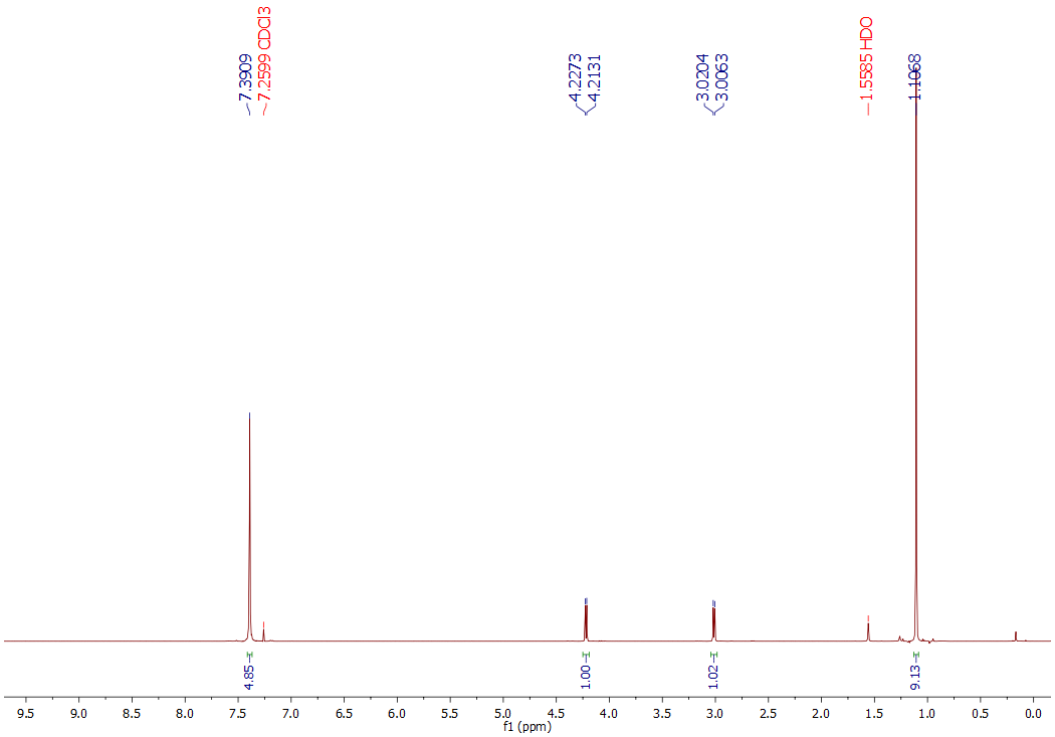

Supporting figure 23. ^{1}H NMR of compound **16**

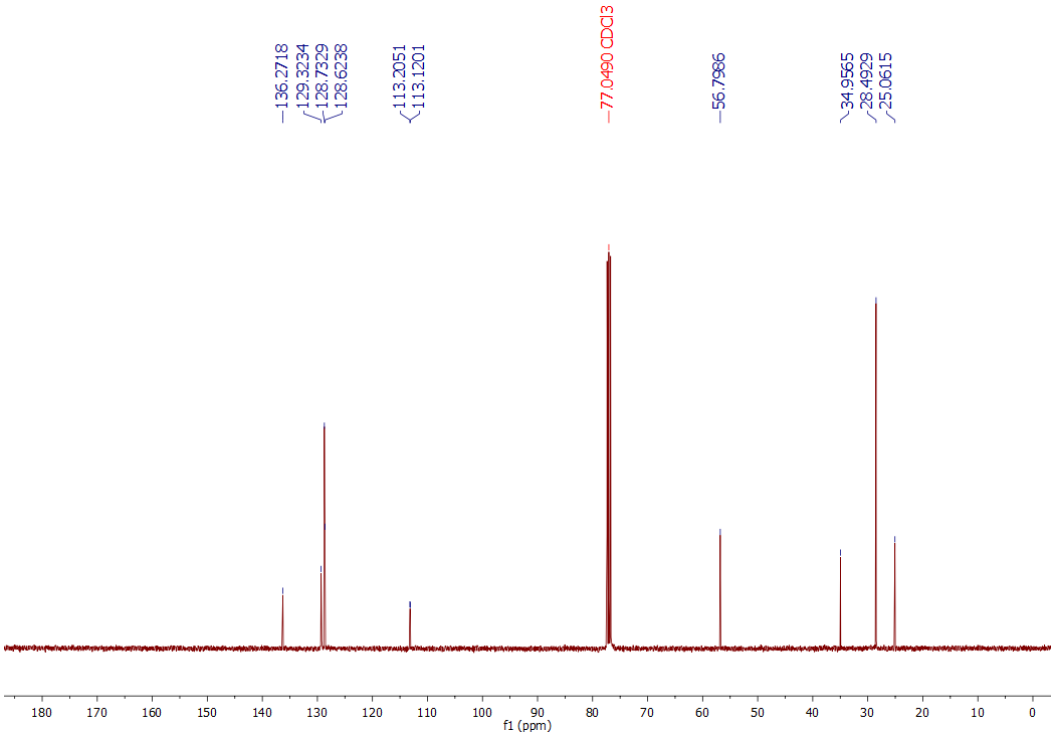

Supporting figure 24. ^{13}C NMR of compound **16**

17

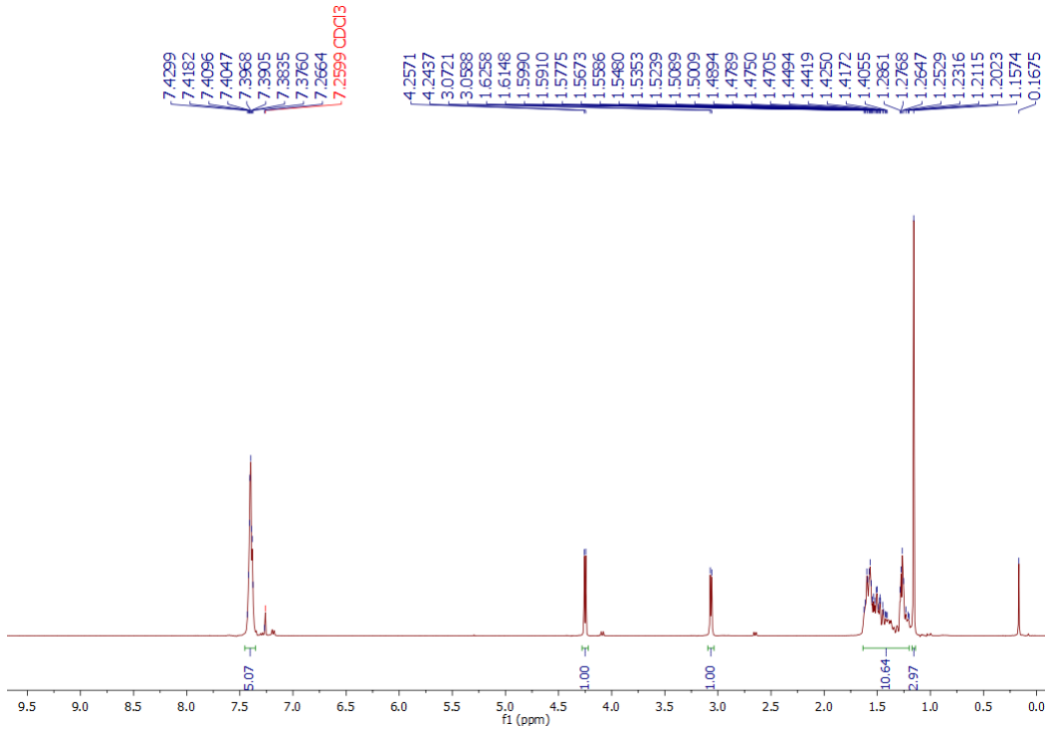

Supporting figure 25. ^{1}H NMR of compound **17**

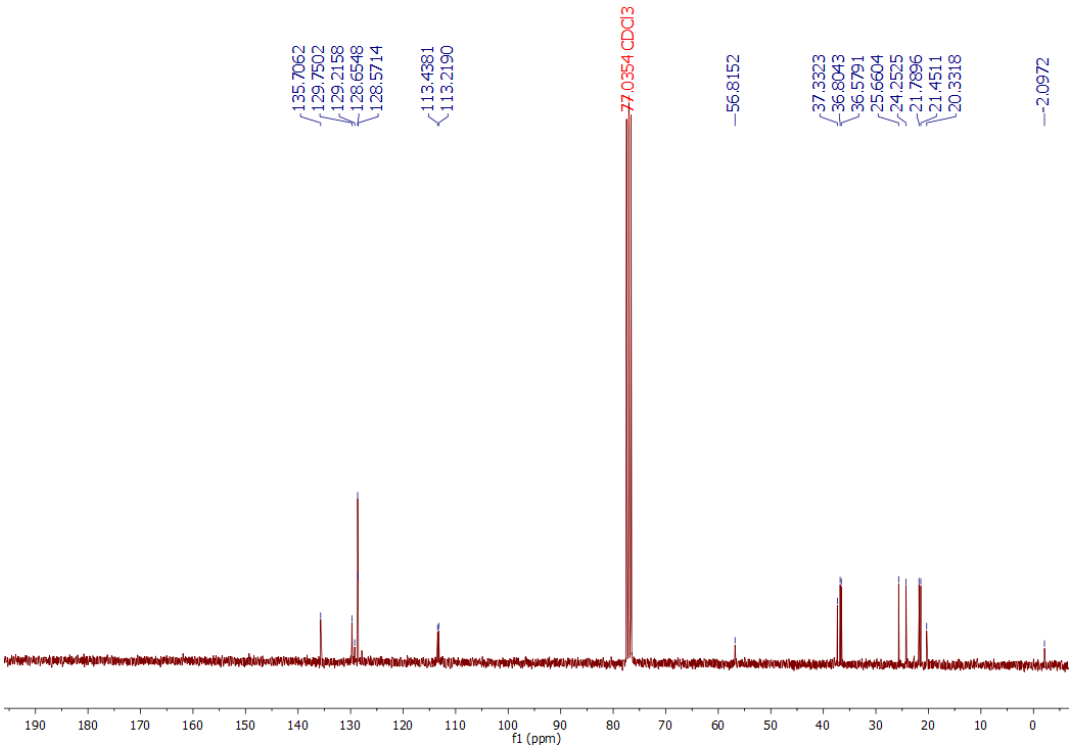

Supporting figure 26. ^{13}C NMR of compound **17**

18

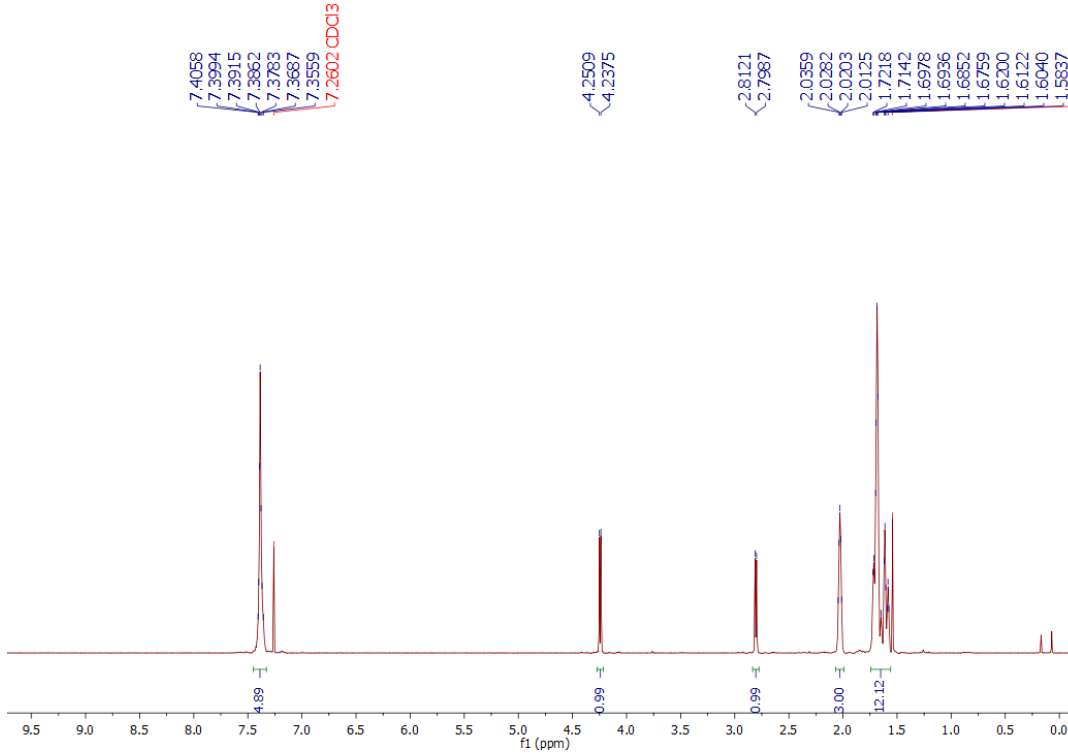

Supporting figure 27. ^{1}H NMR of compound **18**

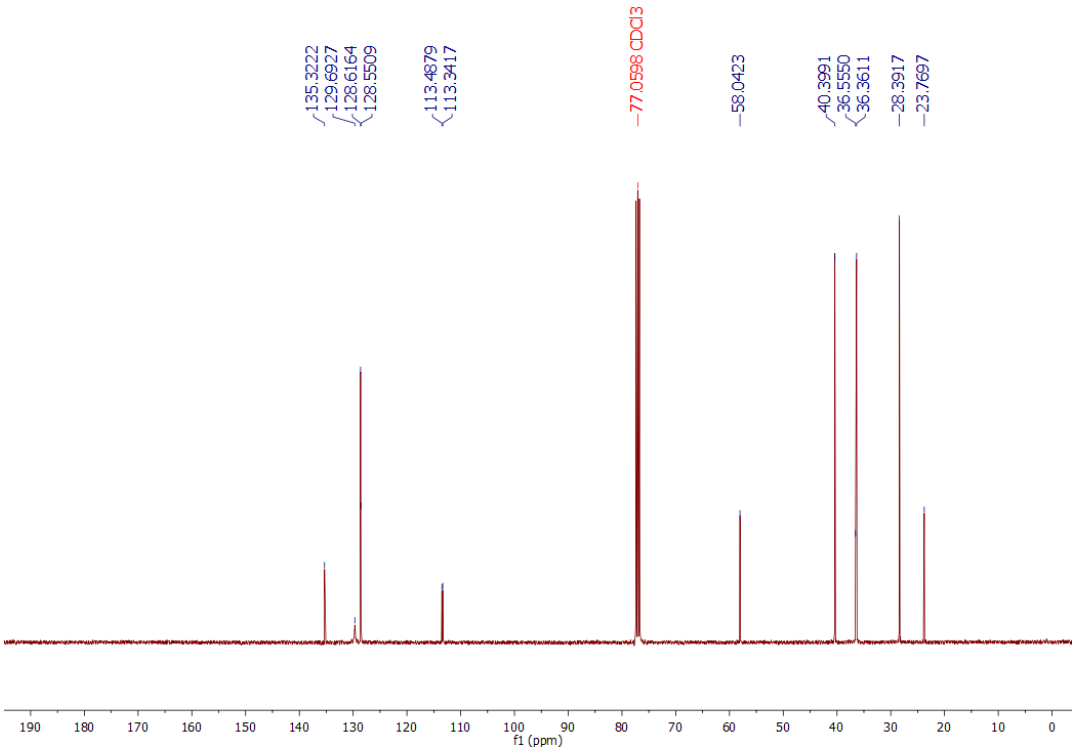

Supporting figure 28. ^{13}C NMR of compound **18**

19

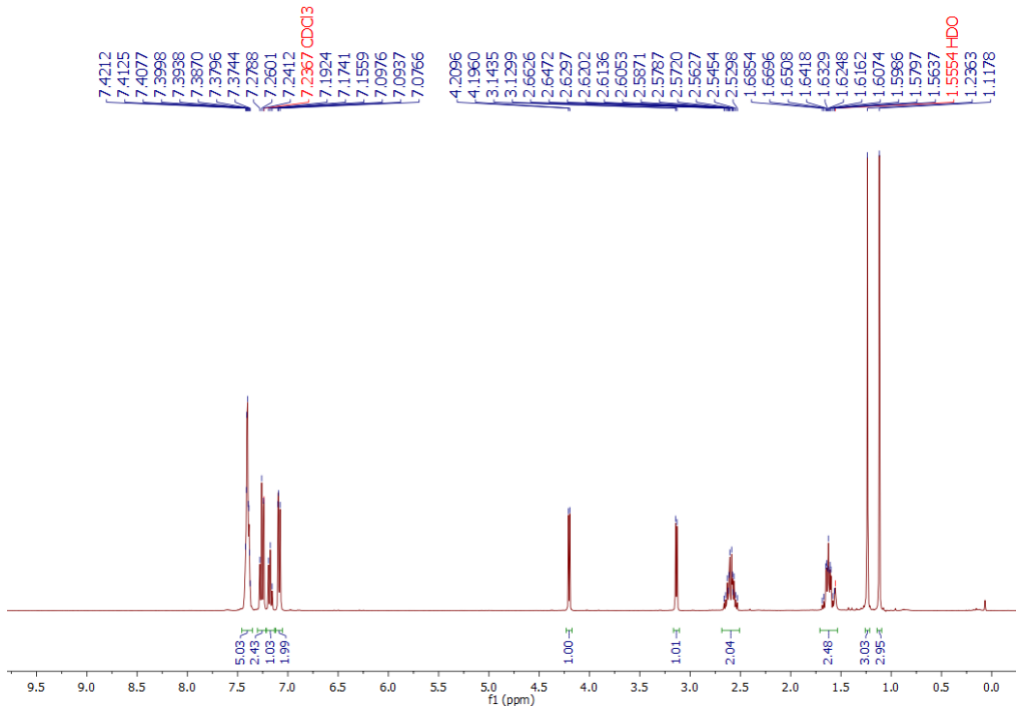

Supporting figure 29. ^{1}H NMR of compound **19**

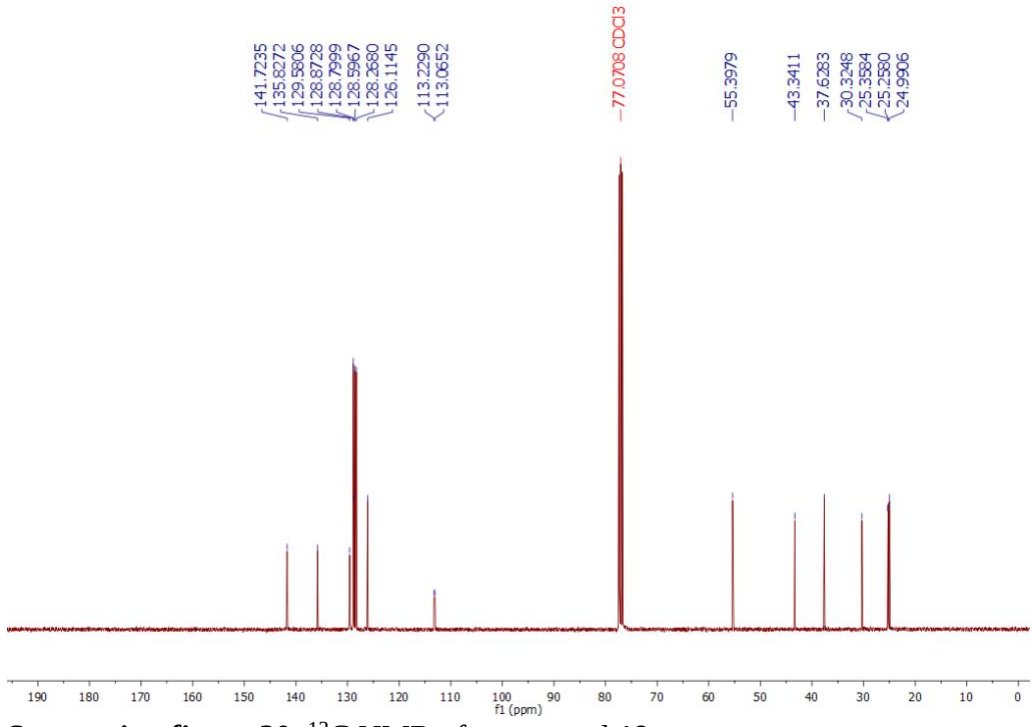

Supporting figure 30. ^{13}C NMR of compound **19**

20

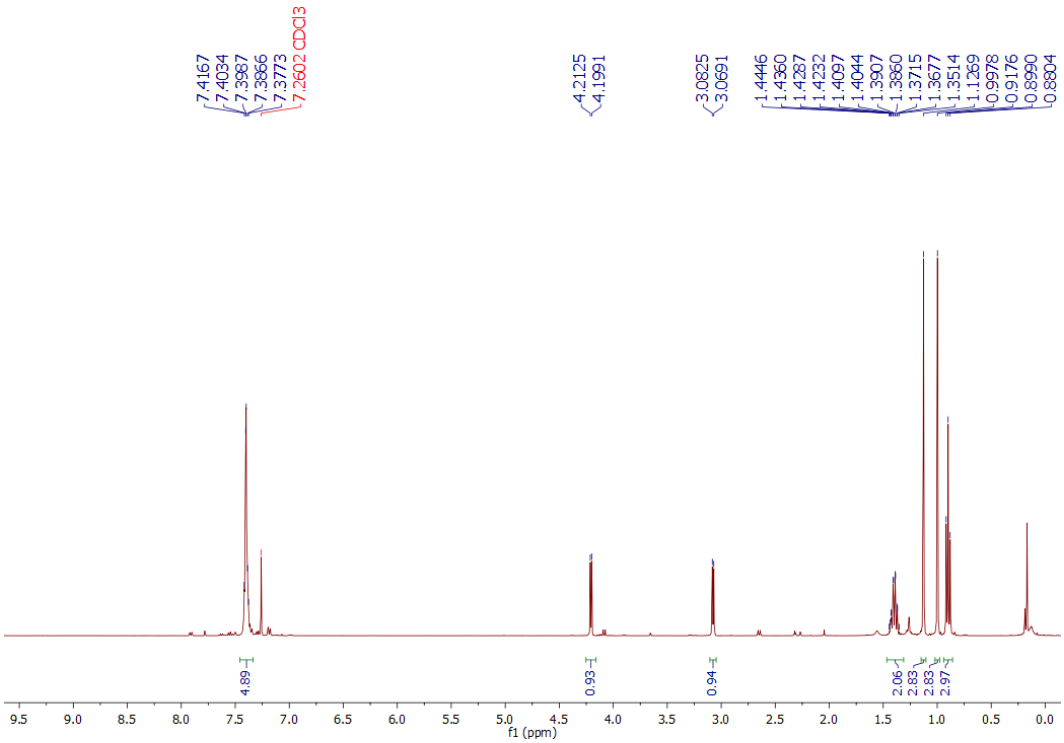

Supporting figure 31. ^{1}H NMR of compound **20**

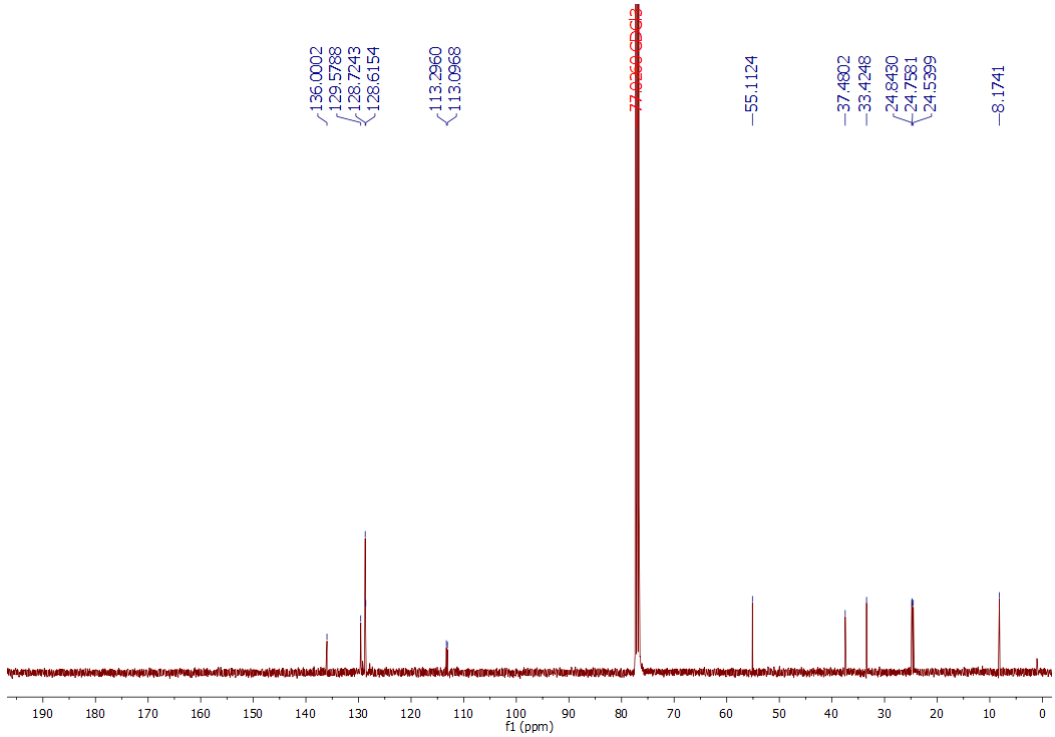

Supporting figure 32. ^{13}C NMR of compound **20**

21

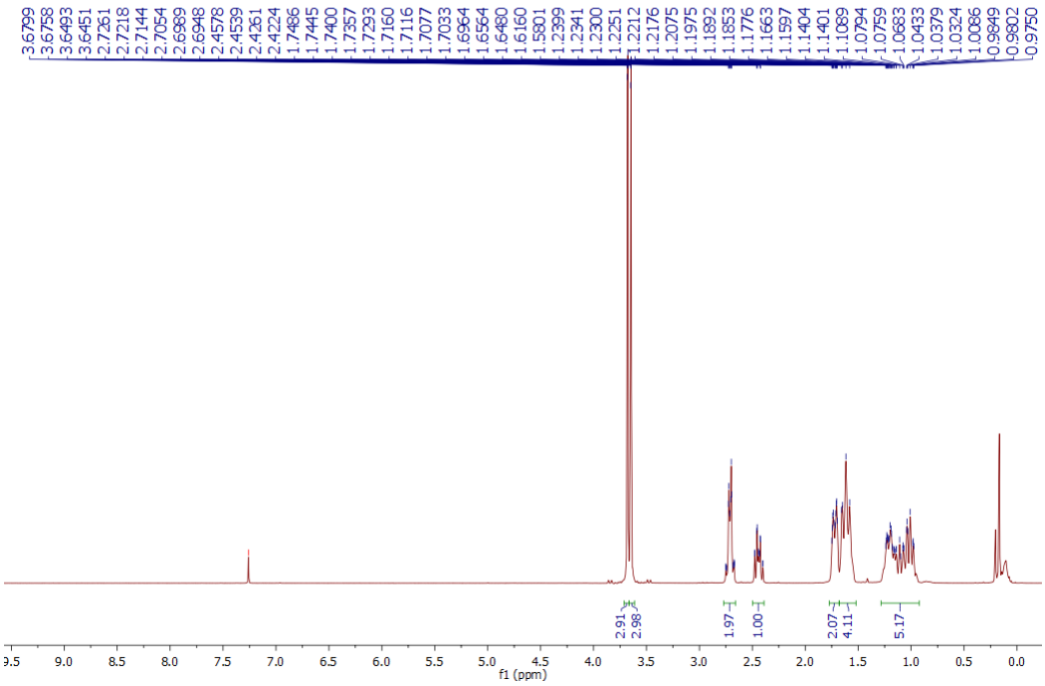

Supporting figure 33. ^{1}H NMR of compound **21**

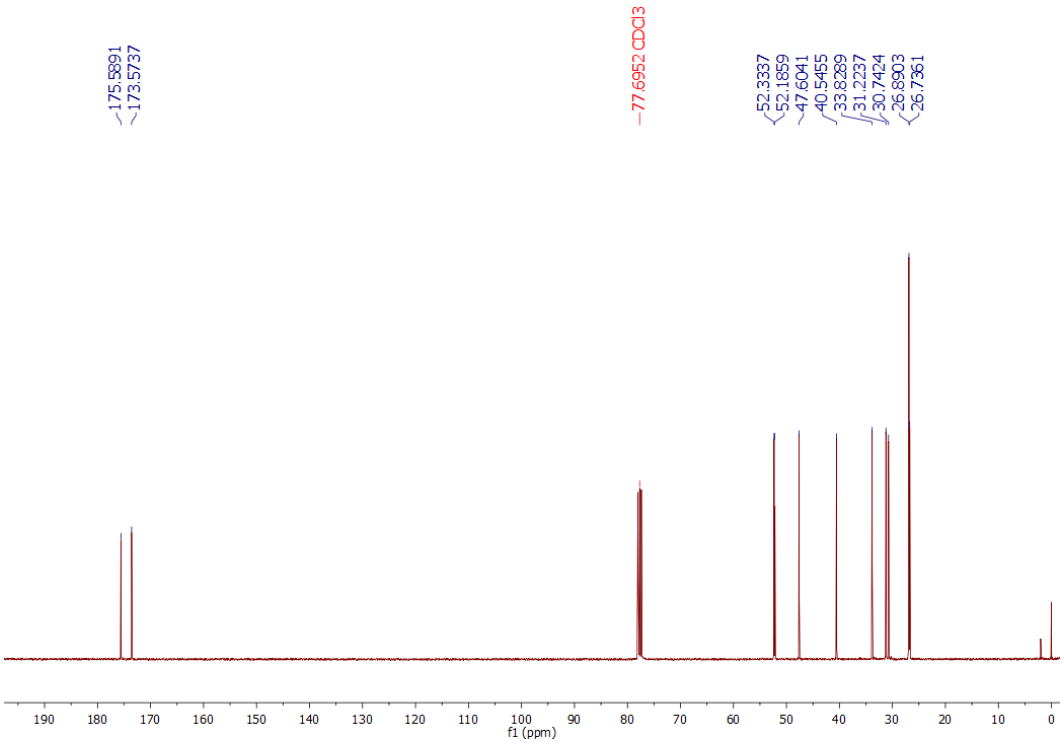

Supporting figure 34. ^{13}C NMR of compound **21**

22

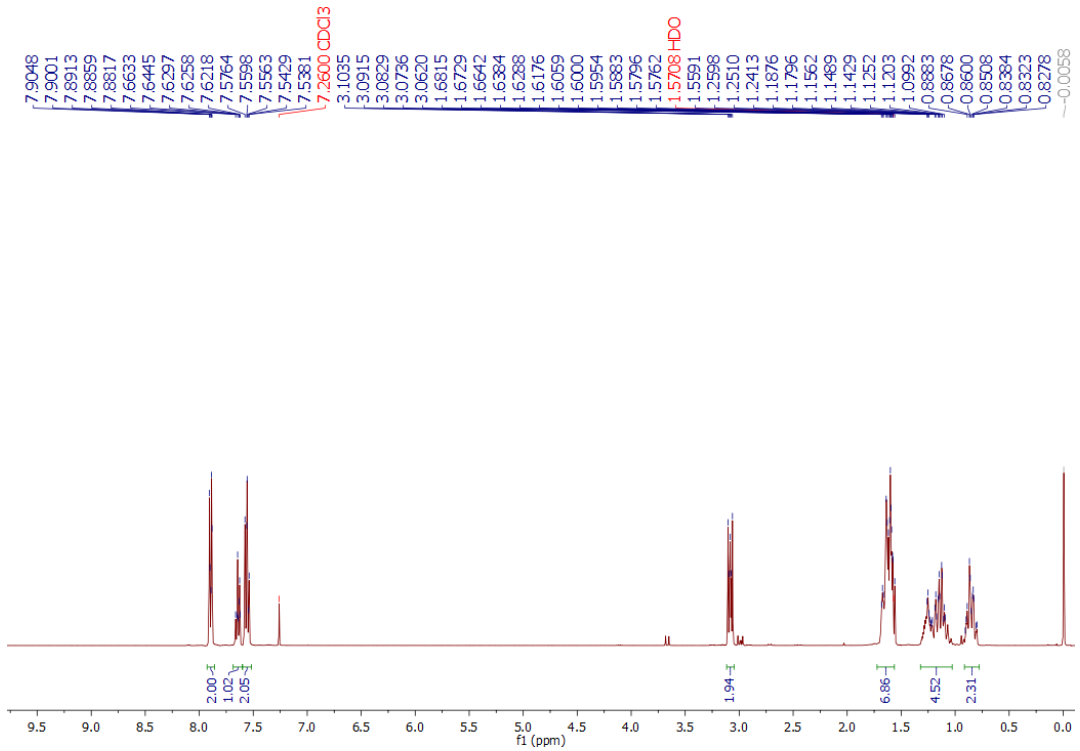

Supporting figure 35. ^{1}H NMR of compound **22**

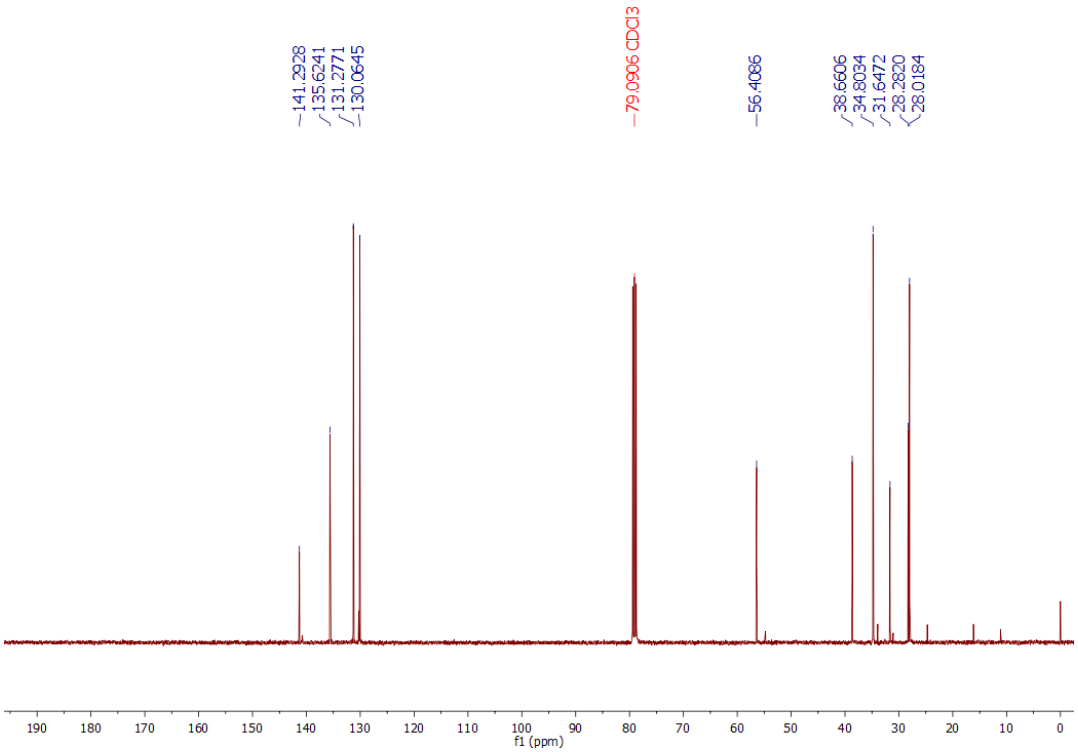

Supporting figure 36. ^{13}C NMR of compound **22**

23

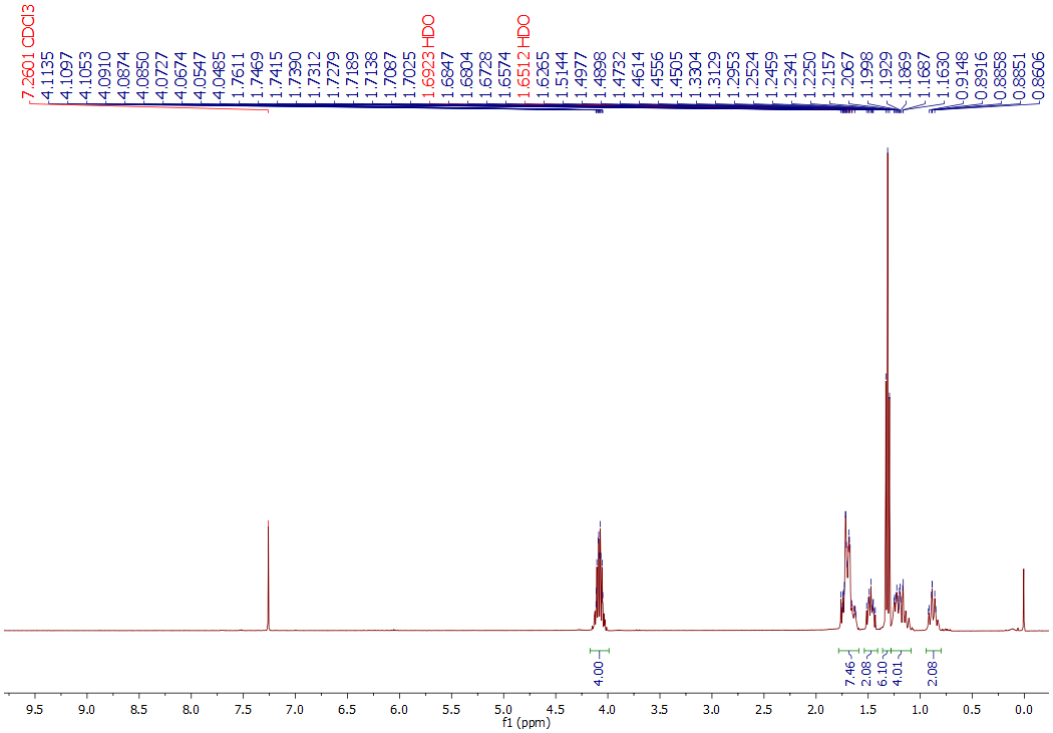

Supporting figure 37. ^{1}H NMR of compound **23**

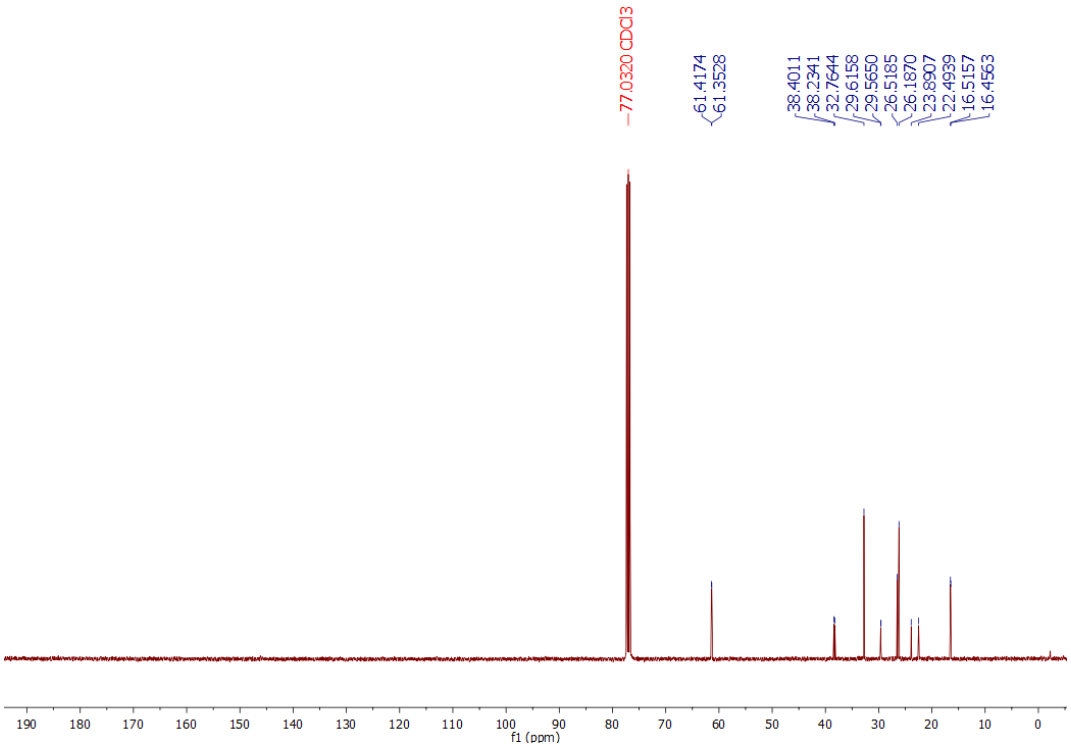

Supporting figure 38. ^{13}C NMR of compound **23**

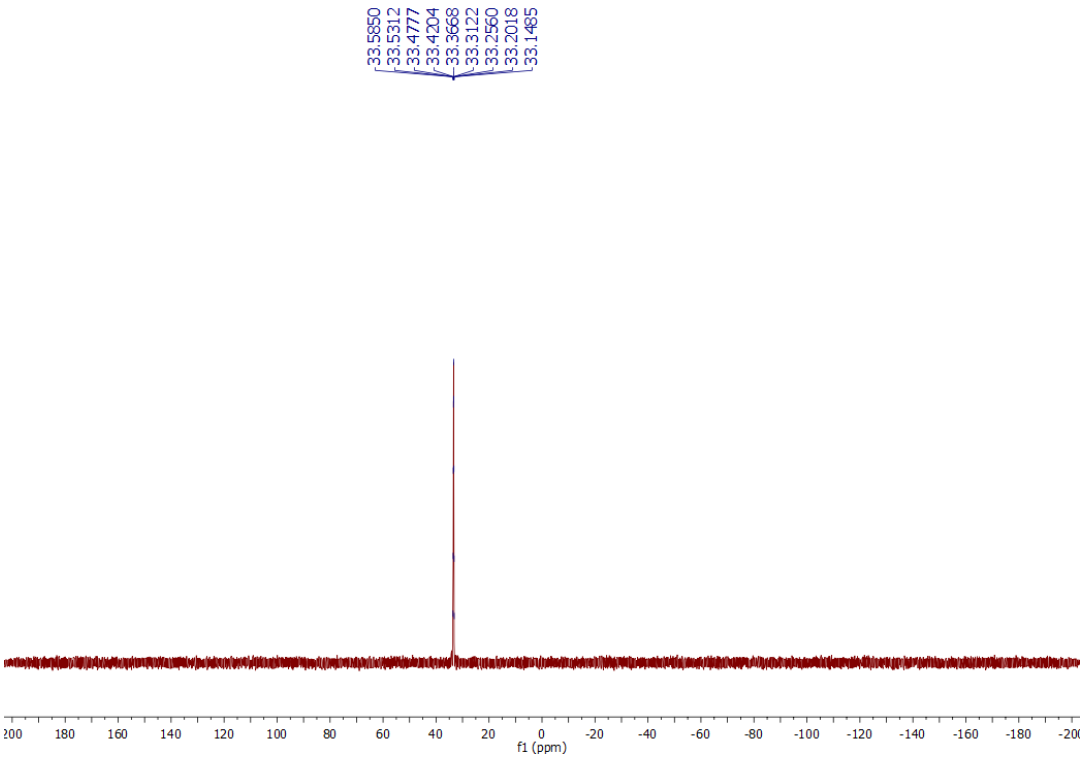

Supporting figure 39. ^{31}P NMR of compound **23**

24

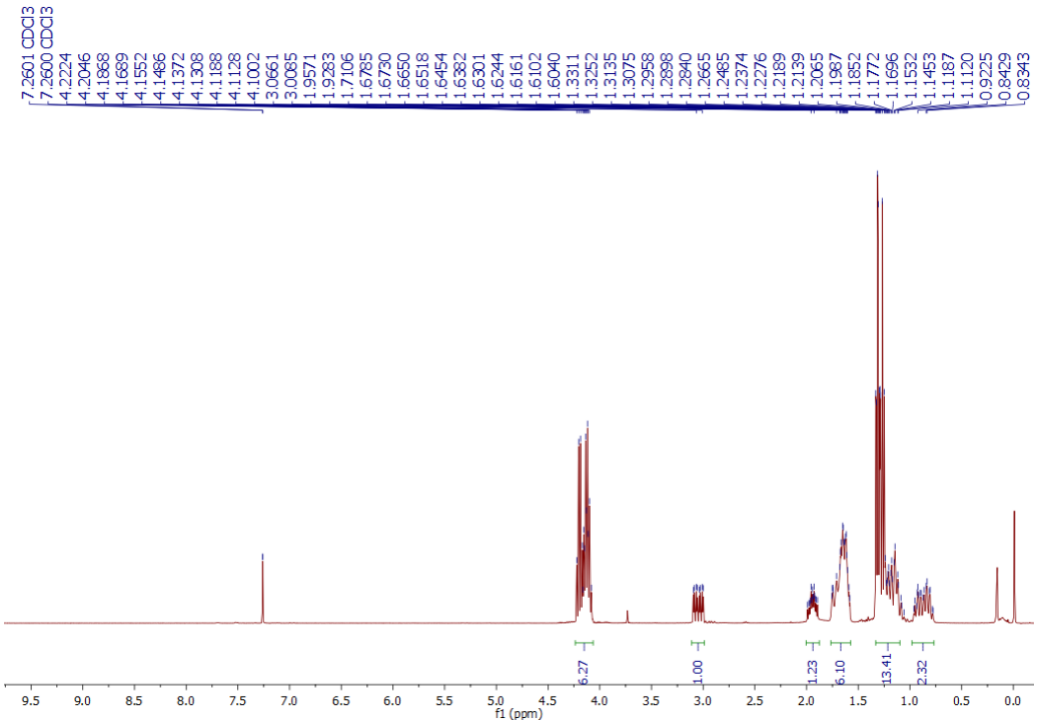

Supporting figure 40. ^{1}H NMR of compound **24**

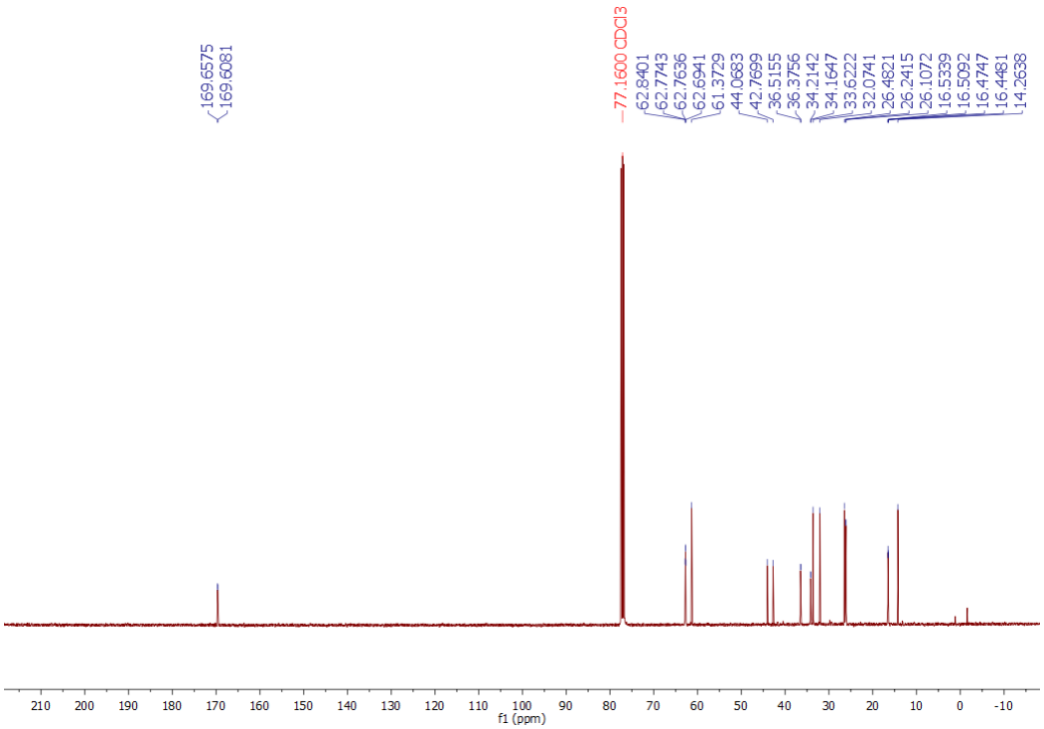

Supporting figure 41. ^{13}C NMR of compound **24**

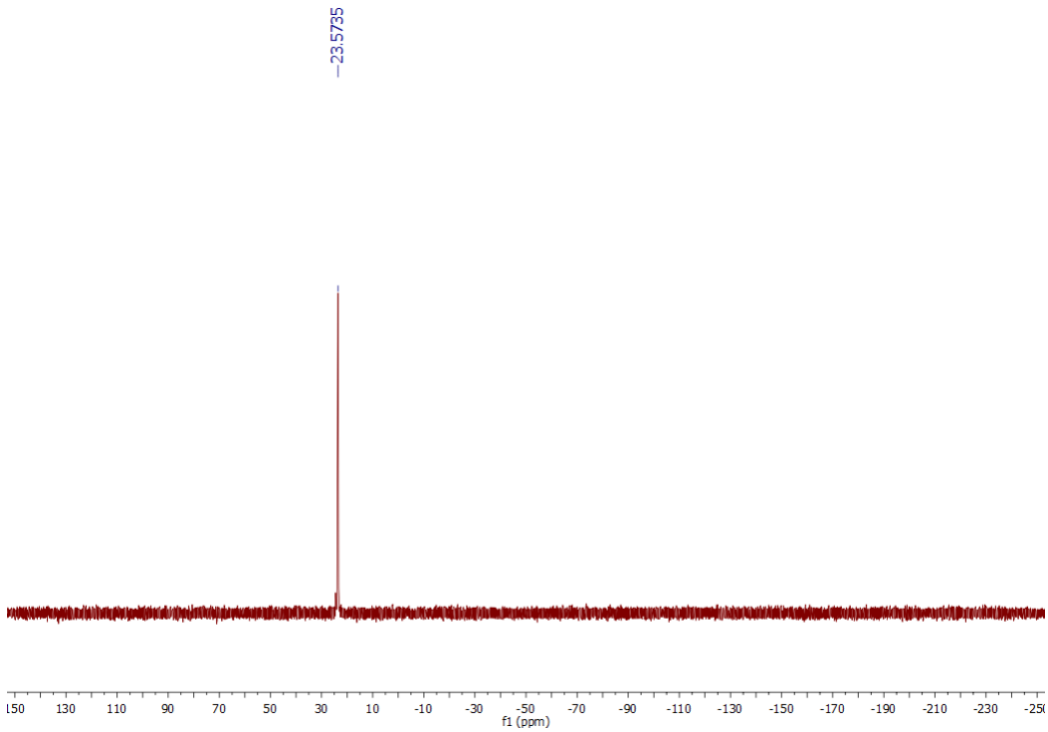

Supporting figure 42. ^{31}P NMR of compound **24**

25

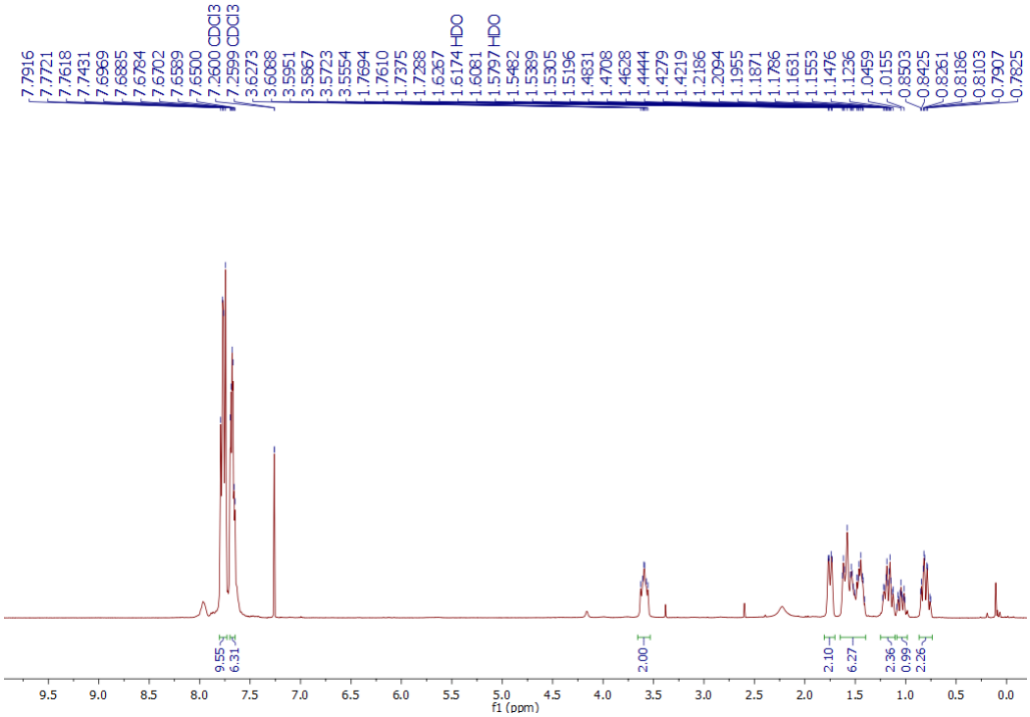

Supporting figure 43. ^{1}H NMR of compound **25**

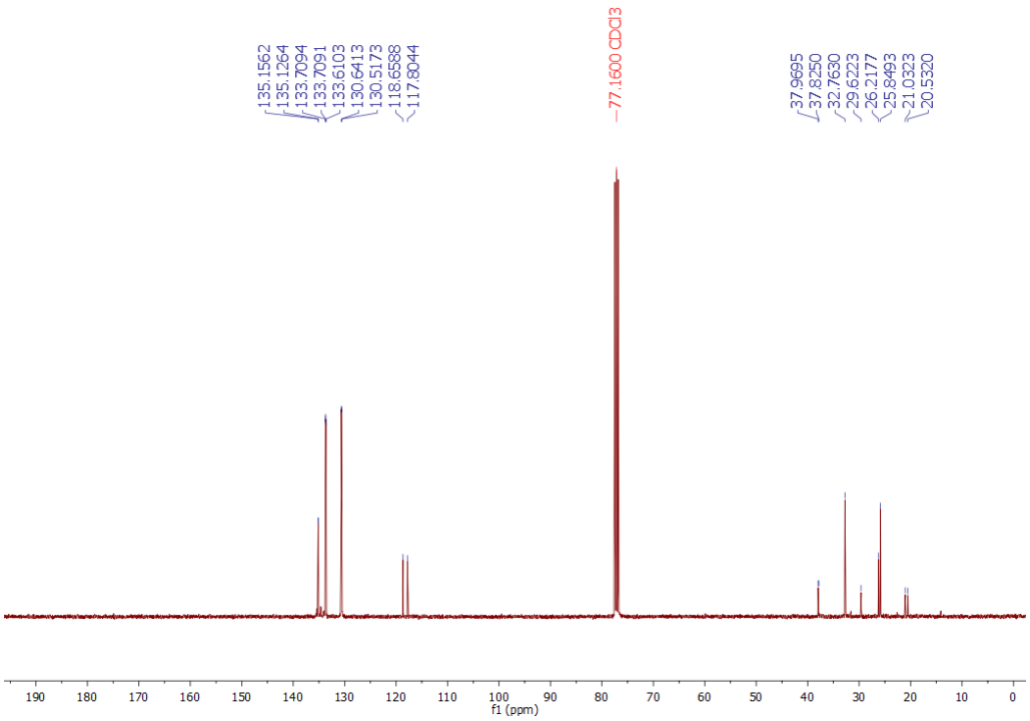

Supporting figure 44. ^{13}C NMR of compound **25**

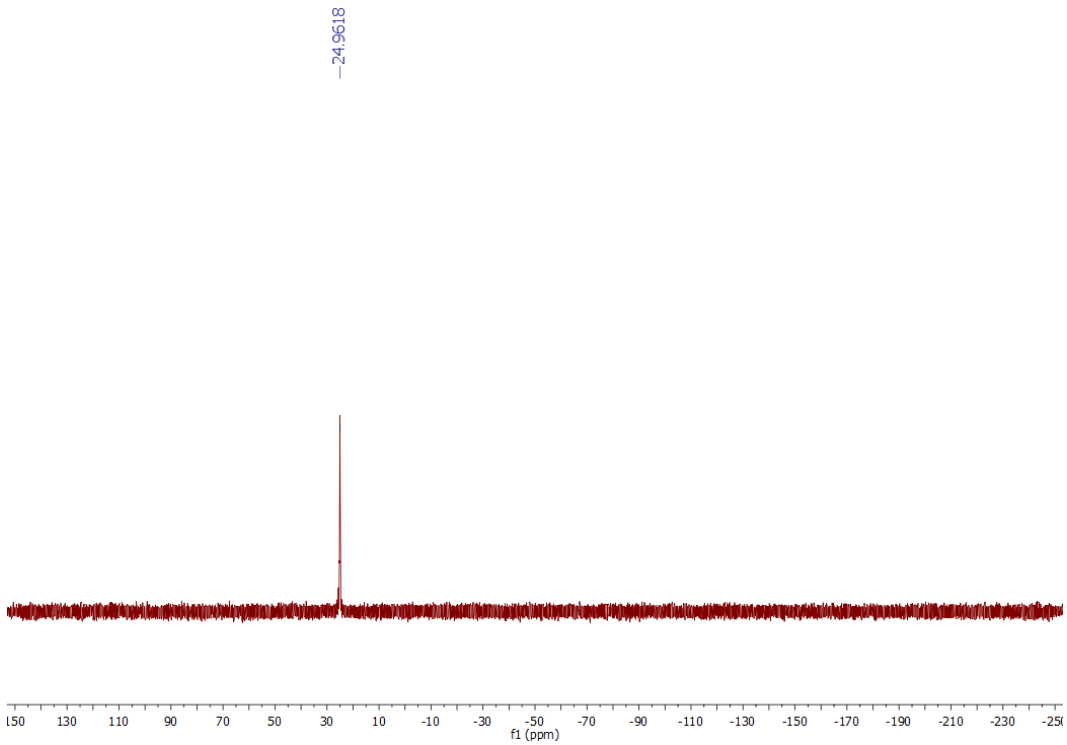

Supporting figure 45. ^{31}P NMR of compound **25**

26

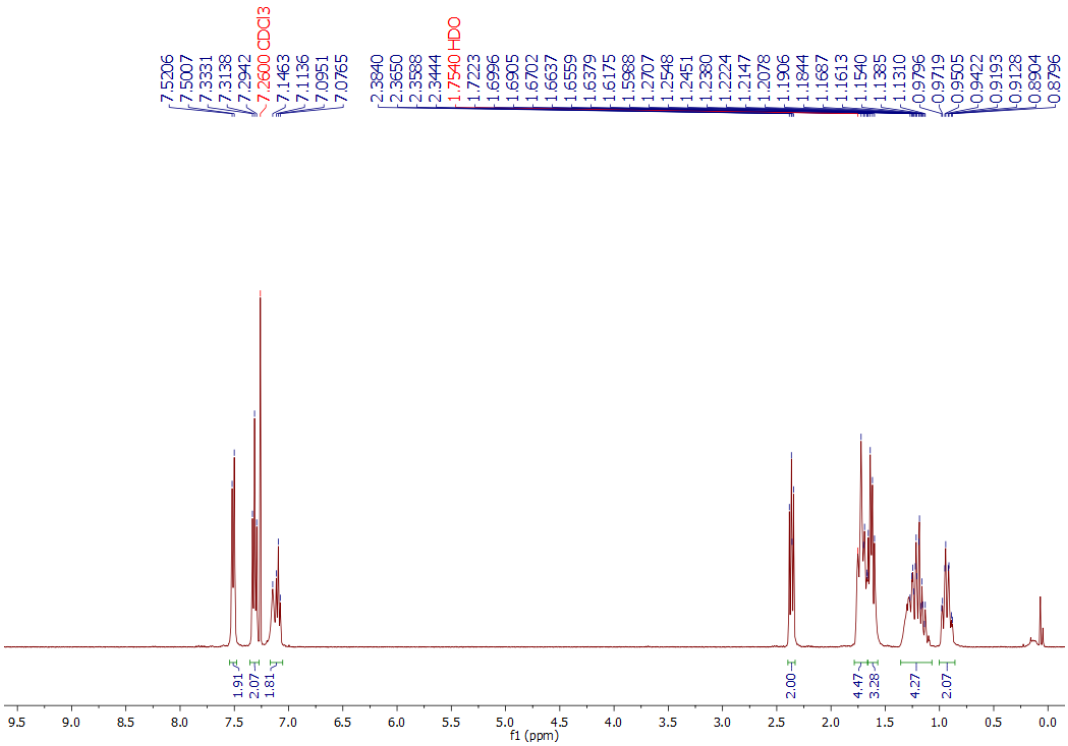

Supporting figure 46. ^{1}H NMR of compound **26**

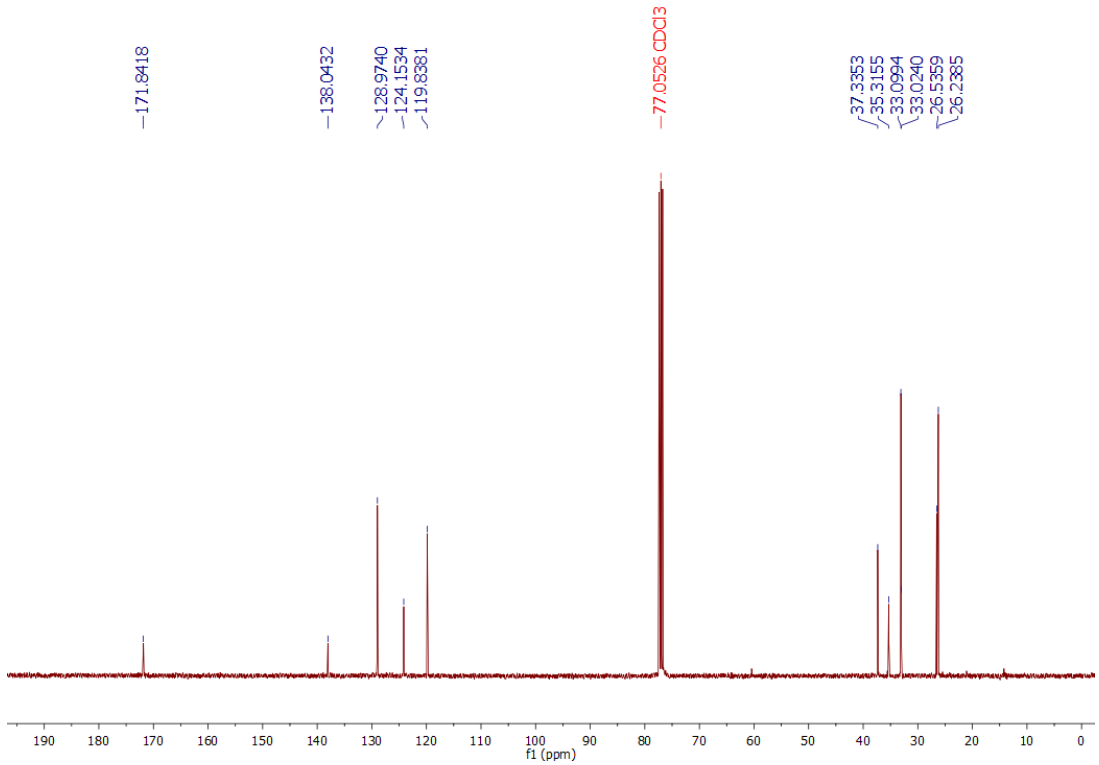

Supporting figure 47. ^{13}C NMR of compound **26**

27

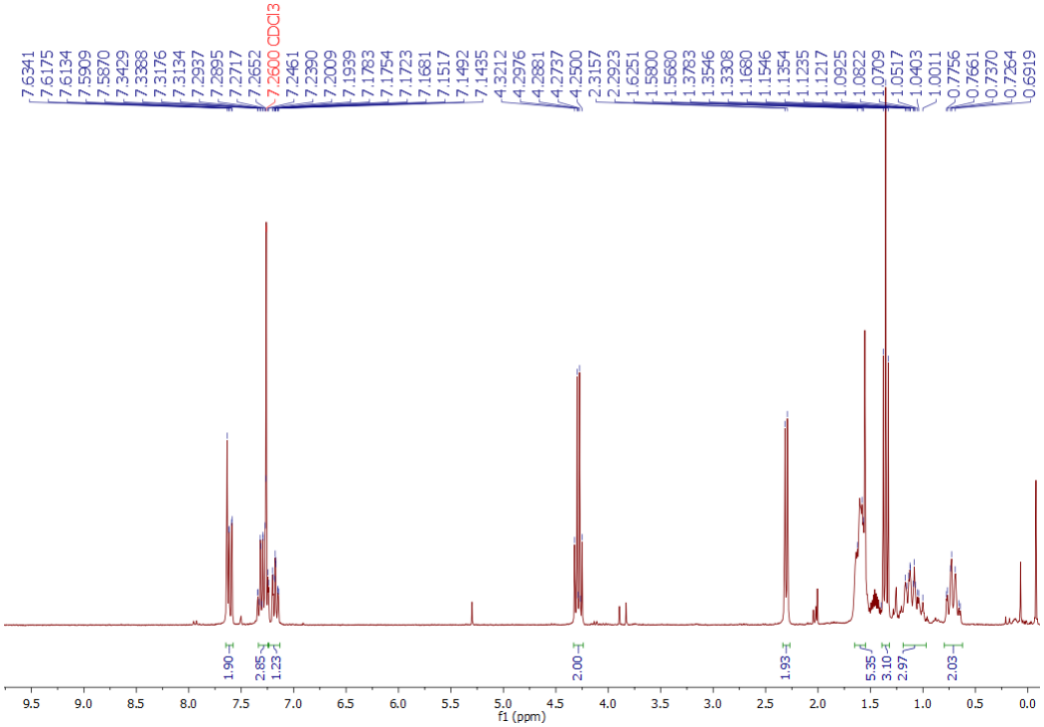

Supporting figure 48. ^{1}H NMR of compound **27**

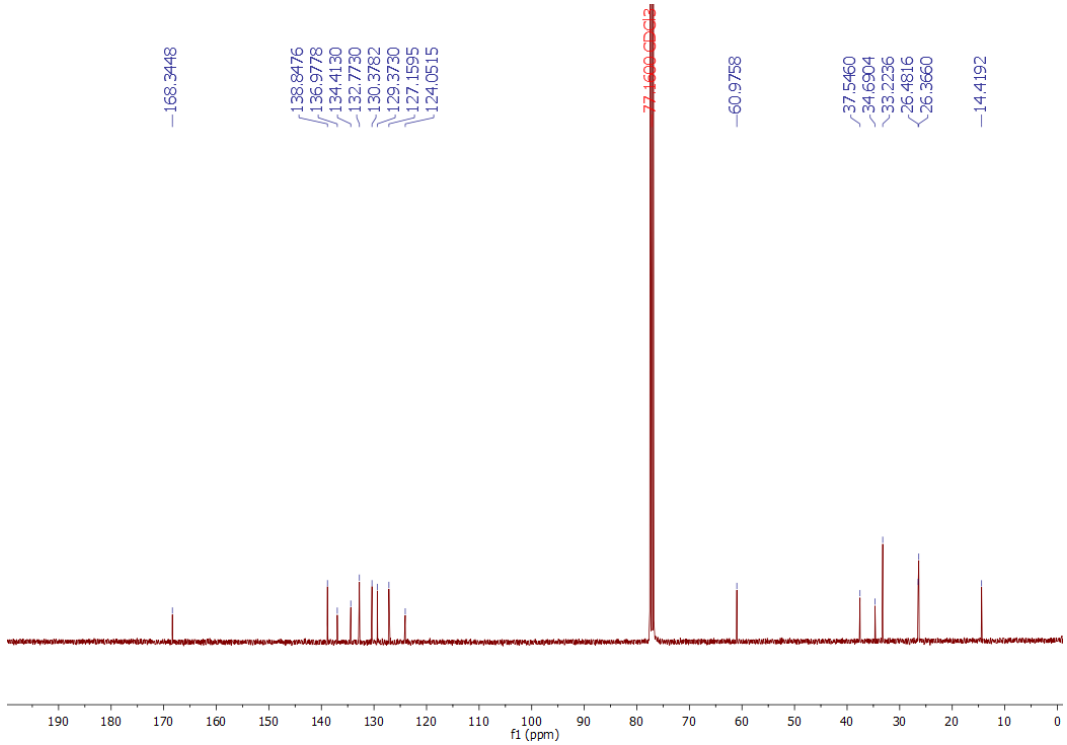

Supporting figure 49. ^{13}C NMR of compound **27**

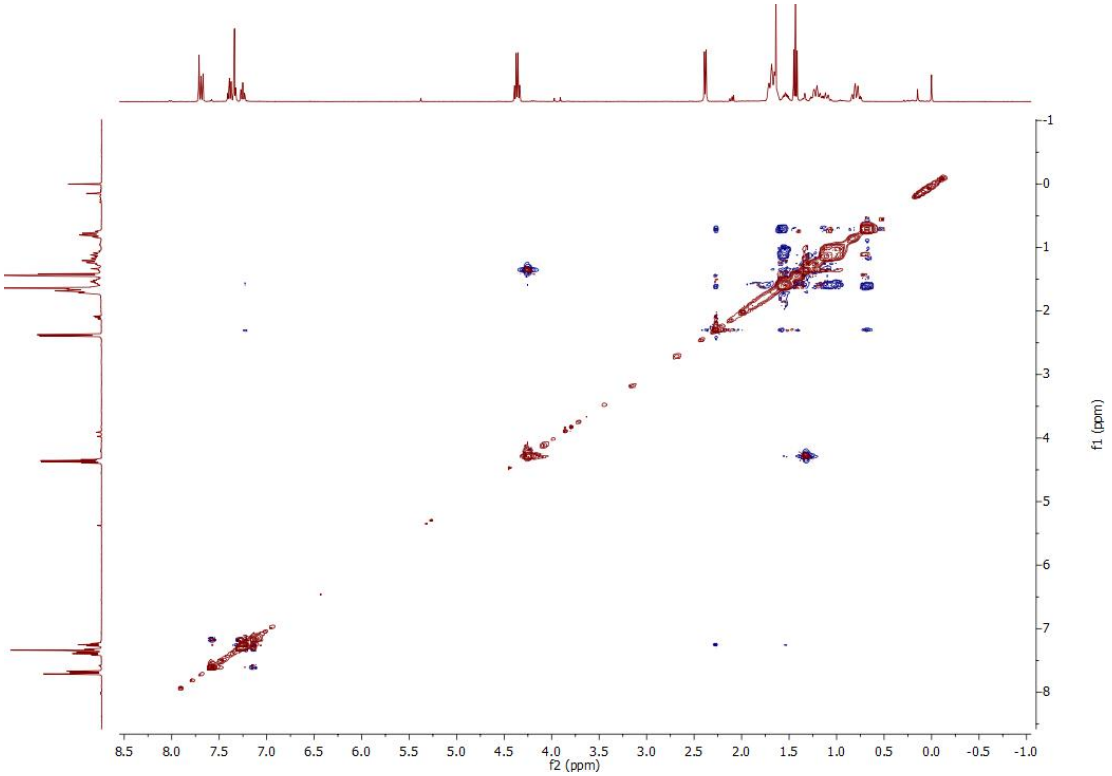

Supporting figure 50. NOESY NMR of compound **27**

28

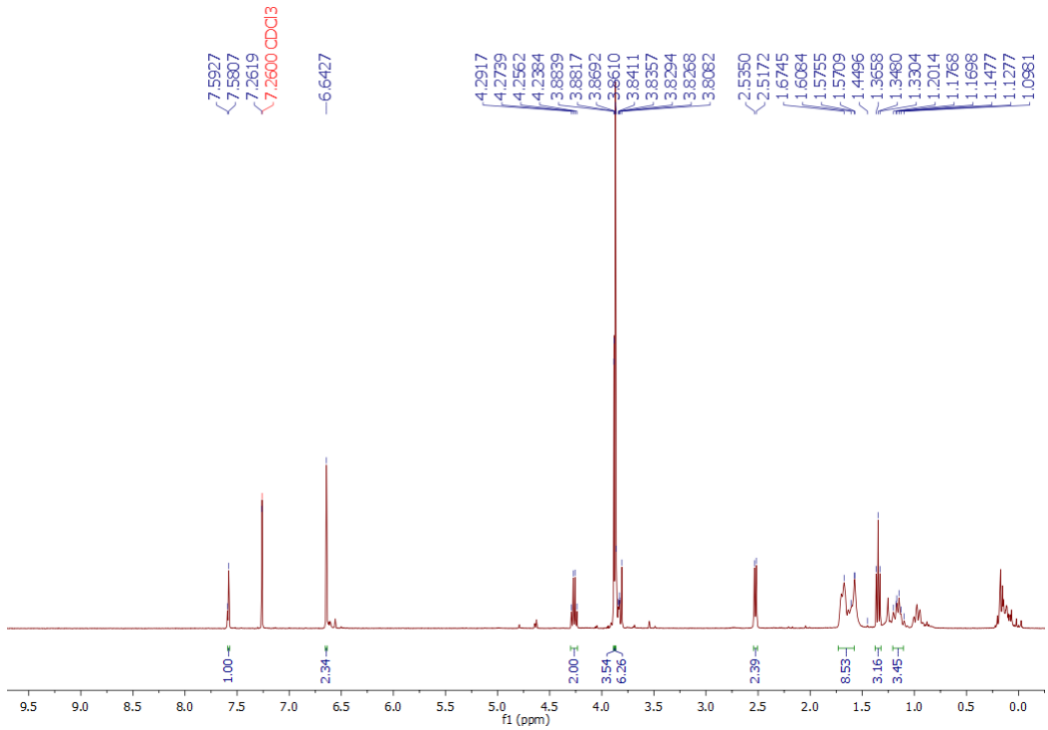

Supporting figure 51. ^{1}H NMR of compound **28**

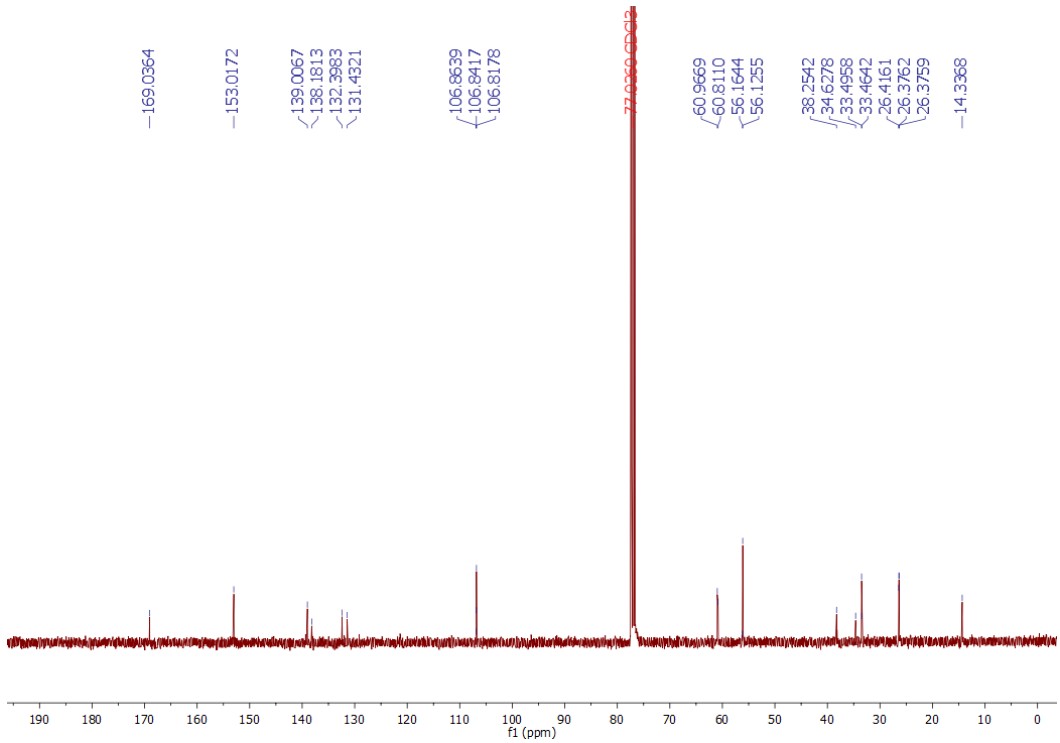

Supporting figure 52. ^{13}C NMR of compound **28**

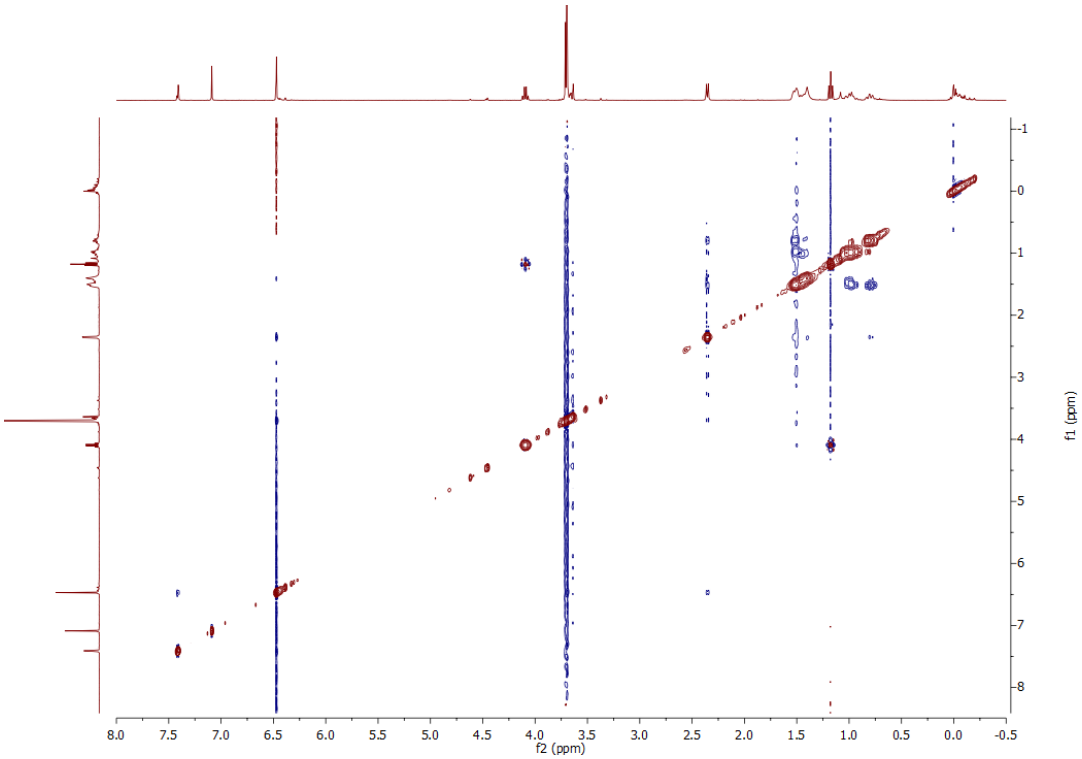

Supporting figure 53. NOESY NMR of compound **28**

29

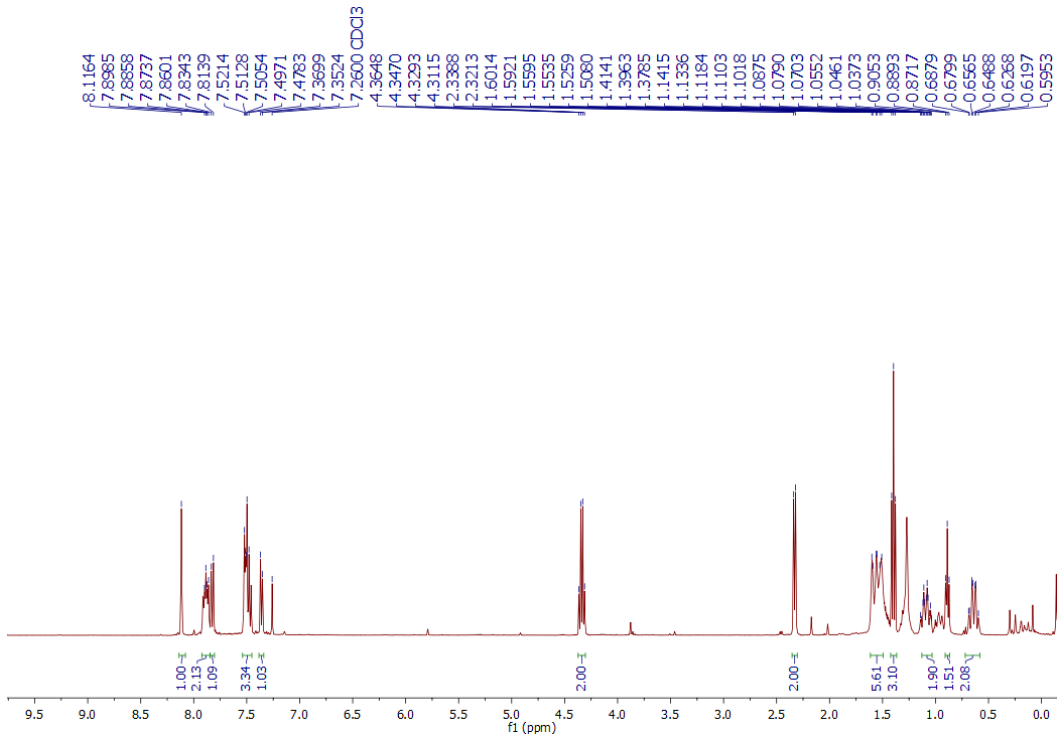

Supporting figure 54. ^{1}H NMR of compound **29**

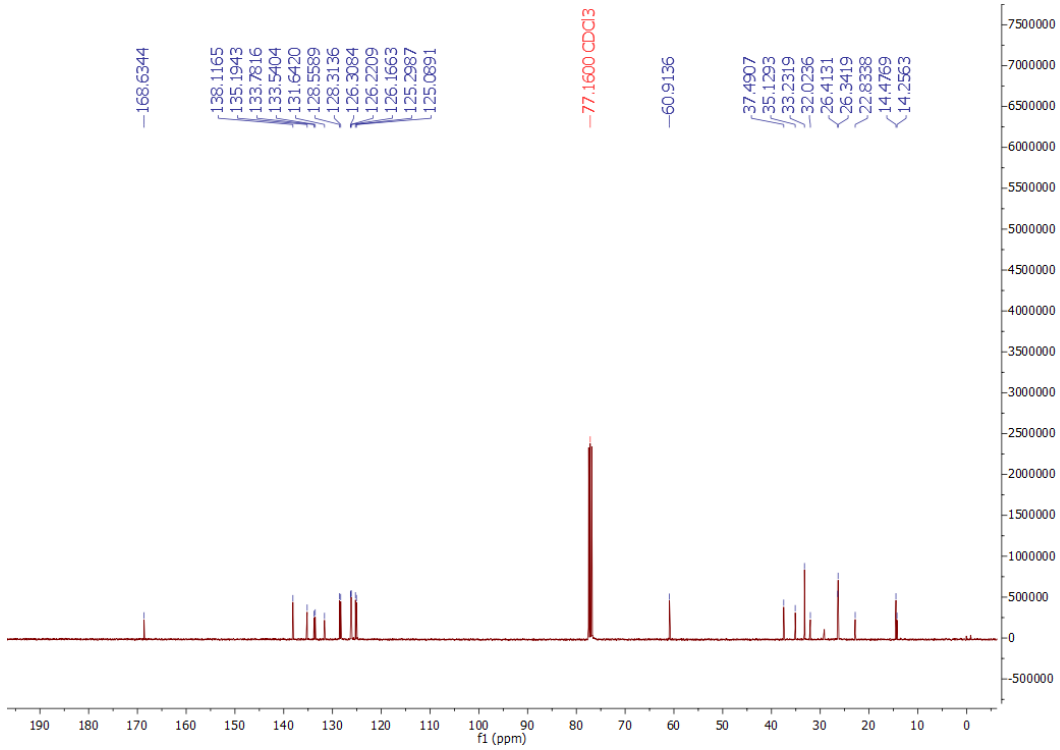

Supporting figure 55. ^{13}C NMR of compound **29**

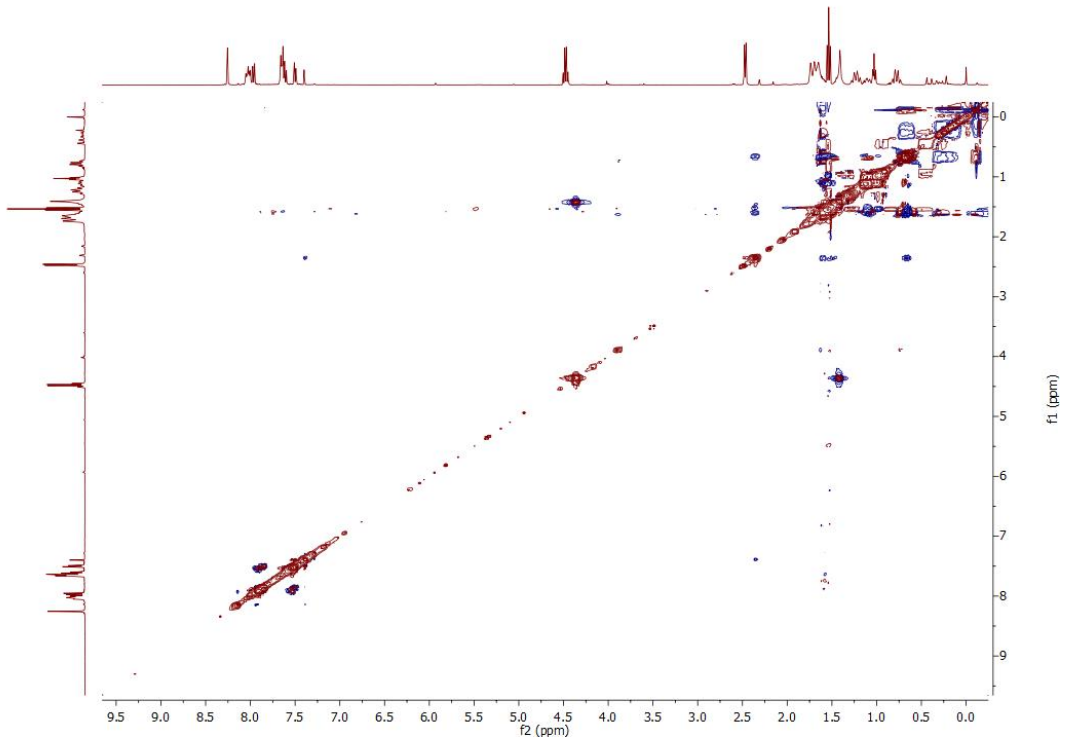

Supporting figure 56. NOESY NMR of compound **29**

References

(1) McDonald, R. I.; Liu, G.; Stahl, S. S. *Chem Rev* **2011**, *111*, 2981.
(2) Yan, M.; Lo, J. C.; Edwards, J. T.; Baran, P. S. *J Am Chem Soc* **2016**, *138*, 12692.
(3) Shaw, M. H.; Twilton, J.; MacMillan, D. W. *J Org Chem* **2016**, *81*, 6898.
(4) Yuan, Y.; Yang, J.; Lei, A. *Chem Soc Rev* **2021**, *50*, 10058.
(5) Buglioni, L.; Raymenants, F.; Slattery, A.; Zondag, S. D. A.; Noel, T. *Chem Rev* **2022**, *122*, 2752.
(6) Giese, B. *Angewandte chemie international edition* **1983**, *22*, 753.
(7) Giese, B.; Gonzàlez-Gomez, J. A.; Witzel, T. *Angewandte Chemie International Edition in English* **1984**, *23*, 69.
(8) Kitcatt, D. M.; Nicolle, S.; Lee, A. L. *Chem Soc Rev* **2022**, *51*, 1415.
(9) Capaldo, L.; Ravelli, D.; Fagnoni, M. *Chem Rev* **2022**, *122*, 1875.
(10) Julia, F.; Constantin, T.; Leonori, D. *Chem Rev* **2022**, *122*, 2292.
(11) Kimura, K.; Nagakura, S. *Spectrochimica Acta* **1961**, *17*, 166.
(12) Zhang, N.; Samanta, S. R.; Rosen, B. M.; Percec, V. *Chem Rev* **2014**, *114*, 5848.
(13) Kuivila, H. G.; Menapace, L. W. *Journal of Organic Chemistry* **1963**, *28*, 2165.
(14) Kuivila, H. G. *Accounts of chemical research* **1968**, *1*, 299.
(15) Buzzetti, L.; Crisenza, G. E. M.; Melchiorre, P. *Angew Chem Int Ed Engl* **2019**, *58*, 3730.
(16) Chatgilialoglu, C.; Griller, D.; Lesage, M. **1988**, *53*, 3641.
(17) Bhattacharya, T.; Ghosh, A.; Maiti, D. *Chem. Sci.*, **2021**,*12*, 3857-3870.
(18) Capaldo, L.; Bonciolini, S.; Pulcinella, A.; Nuno, M.; Noel, T. *Chem Sci* **2022**, *13*, 7325.
(19) Deng, H. P.; Zhou, Q.; Wu, J. *Angew Chem Int Ed Engl* **2018**, *57*, 12661.
(20) Jin, Y.; Zhang, Q.; Wang, L.; Wang, L.; Meng, C.; Duan, C. *Green chemistry* **2021**, *23*, 6984.
(21) Li, J.; Lear, M. J.; Hayashi, Y. *Chemistry* **2021**, *27*, 5901.
(22) Feng, G.; Wang, X.; Jin, J. *European Journal of Organic Chemistry* **2019**, *2019*, 6728.
(23) Zhang, K.; Chang, L.; An, Q.; Wang, X.; Zuo, Z. *J Am Chem Soc* **2019**, *141*, 10556.
(24) Xu, Q. H.; Wei, L. P.; Xiao, B. *Angew Chem Int Ed Engl* **2022**, *61*, e202115592.

(25) de Pedro Beato, E.; Spinnato, D.; Zhou, W.; Melchiorre, P. *J Am Chem Soc* **2021**, *143*, 12304.
(26) Xue, F.; Wang, F.; Liu, J.; Di, J.; Liao, Q.; Lu, H.; Zhu, M.; He, L.; He, H.; Zhang, D.; Song, H.; Liu, X. Y.; Qin, Y. *Angew Chem Int Ed Engl* **2018**, *57*, 6667.
(27) Li, Q.; Dai, P.; Tang, H.; Zhang, M.; Wu, J. *Chem Sci* **2022**, *13*, 9361.
(28) Geant, P.; Mohamed, B. S.; Périgaud, C.; Peyrottes, S.; Uttaro, JP.; Mathé, C. *New Journal of Chemistry* **2016**, *40*, 5318.

Chapter 8

Conclusions & Perspectives

In conclusion, during the three years of my PhD work, my research efforts were devoted toward the development of continuous flow protocols for the generation of different privileged scaffolds with potential medicinal chemistry application. Among the emerging new technologies aimed at implementing eco-compatible and more sustainable synthetic processes, flow chemistry represents one of the most promising and with a huge potential. The first objective of the PhD activity was the development of a green and sustainable protocol for the synthesis of 3,3-disubstituted (spiro)indolenines through an interrupted Fischer indolisation reaction. Capitalizing on this developed flow chemistry protocol for the synthesis of spiroindolenines, we subsequently decided to exploit cyclic imines as the substrates for the generation of peptidomimetic frameworks through a Ugi-Joulliè multicomponent reaction (MCR). We were also able to implement a telescoped approach, allowing to produce in continuous flow the indolenine substrate, followed by the MCR step, finally leading to the target peptidomimetic compound. The conceived methodology allowed to use only 15% of the solvent amount required for the batch counterpart and reducing the reaction times by more than 90%. Moreover, some of derivatives showed promising antibiofilm properties, reducing biofilm formation by 20-25% at 100 μM concentration. Further investigation and optimization for this class of peptidomimetic frameworks will be carried out in the next future.

The PhD project also involved the investigation of organocatalytic approaches, exploiting continuous flow technology. More in detail, starting from our developed indolenine templates, we were able to develop

a flow-based methodology for enantioselective Strecker reaction. The highly enantioselective outcome for cyclic *(Z)*-aldimines (95%) was guaranteed by the use of a thiourea cinchona-based catalyst. Further optimization of the methodology and scope broadening for the proposed methodology are currently ongoing in our lab.

Finally, I recently developed indoline-based metallo beta lactamase inhibitors (MBL), inspired by the structure of the drug Captopril. A multistep synthesis, involving two steps carried out in continuous flow, allowed the generation of a focused library of compounds in high yields and optical purities, thus guaranteeing fast structure-activity relationships studies. Some of the newly conceived compounds displayed broad-spectrum inhibition profile against three of the most clinically relevant MBLs, namely NDM-1, VIM-1 and IMP-7.

In conclusion, this PhD project aimed at demonstrating that medicinal chemistry can strongly benefit from the synergy between continuous flow and sustainable chemical processes.